TRANSMEMBRANE TRANSPORTERS

RECEPTOR BIOCHEMISTRY AND METHODOLOGY

SERIES EDITORS

David R. Sibley
Molecular Neuropharmacology Section
Experimental Therapeutics Branch
NINDS
National Institutes of Health
Bethesda, Maryland

Recent Volumes in Series

Receptor Localization: Laboratory Methods and Procedures
Marjorie A. Ariano, *Volume Editor*

Identification and Expression of G Protein-Coupled Receptors
Kevin R. Lynch, *Volume Editor*

Structure–Function Analysis of G Protein-Coupled Receptors
Jürgen Wess, *Volume Editor*

Regulation of G Protein-Coupled Receptor Function and Expression
Jeffrey L. Benovic, *Volume Editor*

Genetic Manipulation of Receptor Expression and Function
Domenico Accili, *Volume Editor*

Transmembrane Transporters
Michael W. Quick, *Volume Editor*

Founding Series Editors
J. Craig Venter Len C. Harrison

TRANSMEMBRANE TRANSPORTERS

Edited by

Michael W. Quick, Ph.D.

Department of Neurobiology
University of Alabama at Birmingham School of Medicine
Birmingham, AL

A JOHN WILEY & SONS, INC., PUBLICATION

Library of Congress Cataloging in Publication Data is available.

ISBN 0-471-06513-7

Printed in the United States of America

10 9 8 7 6 5 4 3 2 1

CONTENTS

SERIES PREFACE

The activation of cell surface receptors serves as the initial step in many important physiological pathways, providing a mechanism for circulating hormones or neurotransmitters to stimulate intracellular signaling pathways. Over the past 10–15 years, we have witnessed a new era in receptor research, arising from the application of molecular biology to the field of receptor pharmacology. Receptors can be classified into families on the basis of similar structural and functional characteristics, with significant sequence homology shared among members of a given receptor family. By recognizing parallels within a receptor family, our understanding of receptor-mediated signaling pathways is moving forward with increasing speed. The application of molecular biological tools to receptor pharmacology now allows us to consider the receptor—ligand interaction from the perspective of the receptor as a complement to the classic approach of probing the binding pocket from the perspective of the ligand.

Against this background, the newly launched Receptor Biochemistry and Methodology series will focus on advances in molecular pharmacology and biochemistry in the receptor field and their application to the elucidation of the mechanism of receptor-mediated cellular processes. The previous version of this series, published in the mid-1980s, focused on the methods used to study membrane-bound receptors at that time. Given the rapid advances in the field over the past decade, the new series will focus broadly on molecular and structural approaches to receptor biology. In this series, we interpret the term receptor broadly, covering a large array of signaling molecules including membrane-bound receptors, transporters, and ion channels, as well as intracellular steroid receptors. Each volume will focus on one aspect of receptor biochemistry and will contain chapters covering the basic biochemical and pharmacological properties of the various receptors, as well as short reviews covering the theoretical background and strategies underlying the methodology. We hope that the series will provide a valuable overview of the status of the receptor field in the late 1990s, while also providing information that is of practical utility for scientists working at the laboratory bench. Ultimately, it is our hope that this series, by

pulling together molecular and biochemical information from a diverse array of receptor fields, will facilitate the integration of structural and functional insights across receptor families and lead to a broader understanding of these physiologically and clinically important proteins.

DAVID R. SIBLEY

PREFACE

In the broadest sense, transmembrane transporters might be defined as any integral membrane protein designed to move molecules across biological membranes. Defined as such, transmembrane transporters likely are present in all subcellular compartments of all cells of all organisms, and they perform a myriad of diverse functions such as acquisition of nutrients, regulation of metabolite concentrations, removal of toxins, maintenance of ionic and chemical gradients, and secretion of macromolecules and nucleic acids. In other words, transmembrane transporters are the components of life itself.

Biochemical characterization and functional analysis of substrate flux over the previous half century led to the cloning of the first transporters less than 20 years ago. Few would have predicted how intriguing this family of proteins would be. As the new century begins, we are faced with a number of exciting questions: What is the structure of the various classes of transporters, and how does that structure map onto functional properties of the protein? What are the mechanisms by which transporters translocate their substrates? What does the cellular and subcellular distribution of the transporter tell us about its functional roles? What are the initial triggers and signal transduction cascades that mediate the regulation of transporter expression and function? What are the roles of transporters in shaping the behavior of organisms? What diseases are associated with transporter dysfunction, and how can transporters be targeted as a therapeutic tool? Answers to these questions are emerging with the help of a wide array of experimental techniques. The purpose of this book is to provide the reader with a state-of-the-molecule update on what we know about transmembrane transporters from many leaders in the field, and the methodological approaches they use to further our understanding of these molecules.

I hope this volume serves a number of purposes for readers. For those new to the field of transporter biology, I hope that the text serves to give you an idea of the multiple approaches used to study transporters and, more importantly, to pique your interest in these molecules. For those of you who study these proteins, I hope that the conceptual and methodological approaches that are presented in these pages inform your own research. To try to accomplish these goals, each chapter is arranged in the following manner: First,

authors of each chapter, where appropriate, will give an overview of the important biological questions that are presently being considered in their field. Next, scientific approaches to address these questions are presented. These approaches include not only benchtop protocols, but they also address conceptual frameworks, specific examples of the types of data one obtains using these approaches, and pitfalls related to these techniques. Of course, the transmembrane transporter field is much too large to be adequately encompassed in one book. So, authors have provided annotations to papers that they believe are of interest to readers who wish to delve deeper into these issues.

The 16 chapters of this volume were chosen in order to provide readers with information across a diverse array of topics and approaches. To provide a framework for thinking about transporters in general, Chapter 1 deals with characterizing transporter families. As in many fields of biology, genetic approaches to understanding transmembrane transporters are a powerful tool; Chapters 2 through 5 describe such approaches in yeast, flies, mice, and humans. Chapters 6 and 7 provide information regarding the use of expression strategies to understand function and regulation of transport. As mentioned above, an important question in the field is how functional aspects of transport map onto transporter structure. Although experiments designed to obtain high-resolution transporter structure are still in their infancy, approaches involving chemical modification, peptide mapping, and proteomics are revealing important answers to these structural questions. Chapters 8 through 11 present information of these topics. Lastly, the importance of transporters lies in what they do, and so information is presented regarding functional aspects of transporter biology. These studies include examining unitary properties of substrate translocation using high-resolution electrophysiological approaches (Chapters 12–14), imaging (Chapter 15), and modeling (Chapter 16).

I thank all authors for their expert contributions to this volume. The idea for a volume in the *Receptor Biochemistry and Methodology Series* on transmembrane transporters came from the series editor, David Sibley. I also thank Dave, as well as Luna Han of John Wiley and Sons, Inc., for their suggestions and patience. I am very grateful to Heather Ryals for her expert editorial assistance. I sincerely hope that this volume will be both informative and useful for scientists in the field of transporter biology, and for readers interested in learning about this important class of signaling molecules.

MICHAEL W. QUICK
Birmingham, AL

CONTRIBUTORS

ALEXANDRA R. BELOUS, Departments of Pharmacology and Psychiatry, Center for Molecular Neuroscience, Vanderbilt University School of Medicine, Nashville, TN, USA

RANDY D. BLAKELY, Departments of Pharmacology and Psychiatry, Center for Molecular Neuroscience, Vanderbilt University School of Medicine, Nashville, TN, USA

ECKHARD BOLES, Institut fuer Mikrobiologie, Heinrich-Heine-Universitat, Dusseldorf, Germany

MARTIN G. BURG, Department of Biomedical and Health Sciences, Grand Valley State University, Allendale, MI, USA

ROBERT J. CORMIER, Departments of Psychiatry and Neurobiology, Washington University School of Medicine, St. Louis, MO, USA

SCOTT L. DEKEN, Department of Neurobiology, University of Alabama at Birmingham School of Medicine, Birmingham, AL, USA

BARBARA DEMENEIX, CNRS UMR, Museum National d'Hisoire Naturelle, Paris, France

VÉRONIQUE FABRE, INSERM, Faculte de Medecine, Paris, France

JON D. GAFFANEY, Department of Biochemistry and Molecular Biology, University of North Dakota School of Medicine and Health Sciences, Grand Forks, ND, USA

AURELIO GALLI, Department of Pharmacology, University of Texas at San Antonio, Health Science Center, San Antonio, TX, USA

MICHEL HAMON, INSERM, Faculte de Medecine, Paris, France

MATHEW V. JONES, Department of Physiology, University of Wisconsin-Madison, Madison, WI, USA

SARA R. JONES, Department of Physiology and Pharmacology, Wake Forest University School of Medicine, Winston-Salem, NC, USA

H. RONALD KABACK, Howard Hughes Medical Institute, Departments of Physiology and Microbiology, Immunology and Molecular Genetics, and the Molecular Biology Institute, University of California at Los Angeles, Los Angeles, CA, USA

KRISTOPHER M. KAHLIG, Department of Pharmacology, University of Texas Health Sciences Center at San Antonio, San Antonio, TX, USA

RONALD S. KAPLAN, Department of Biochemistry and Molecular Biology, Finch University of Health Sciences, The Chicago Medical School, North Chicago, IL, USA

MICHAEL P. KAVANAUGH, Vollum Institute, Oregon Health and Sciences University, Portland, OR, USA

HANK F. KUNG, Departments of Radiology and Pharmacology, University of Pennsylvania School of Medicine, Philadelphia, PA, USA

MEI-PING KUNG, Department of Radiology, University of Pennsylvania School of Medicine, Philadelphia, PA, USA

H. PETER LARSSON, Neurological Sciences Institute, Oregon Health and Science University, Portland, OR, USA

JOHANNES LE COUTRE, Nestlé Research Center, Bioscience Department, Lausanne, Switzerland

MARGARET J. LOWE, Department of Biochemistry and Molecular Biology, University of North Dakota School of Medicine and Health Sciences, Grand Forks, ND, USA

MARIE-PASCALE MARTRES, INSERM, Faculté de Médecine, Créteil, France

STEVEN MENNERICK, Departments of Psychiatry and Neurobiology, Washington University School of Medicine, St. Louis, MO, USA

LINDA S. OVERSTREET, The Vollum Institute, Oregon Health Sciences University, Portland, OR, USA

WILLIAM L. PAK, Department of Biological Sciences, Purdue University, West Lafayette, IN, USA

MICHAEL W. QUICK, Department of Neurobiology, University of Alabama at Birmingham School of Medicine, Birmingham, AL, USA

GARY RUDNICK, Department of Pharmacology, Yale University School of Medicine, New Haven, CT, USA

MILTON H. SAIER, JR., Department of Biology, University of California at San Diego, La Jolla, CA, USA

CHRISTINE SAUNDERS, Department of Biochemistry, University of Texas Health Sciences Center at San Antonio, San Antonio, TX, USA

YVONNE SCHMITZ, Departments of Neurology and Psychiatry, College of Physicians and Surgeons, Columbia University; Department of Neuroscience, New York State Psychiatric Institute, New York, NY, USA

DAVID SULZER, Departments of Neurology and Psychiatry, College of Physicians and Surgeons, Columbia University; Department of Neuroscience, New York State Psychiatric Institute, New York, NY, USA

ANASTASSIOS V. TZINGOUNIS, Vollum Institute, Oregon Health and Science University, Portland, OR, USA

ROXANNE A. VAUGHAN, Department of Biochemistry and Molecular Biology, University of North Dakota School of Medicine and Health Sciences, Grand Forks, ND, USA

DAN WANG, Department of Neurobiology, University of Alabama at Birmingham School of Medicine, Birmingham, AL, USA

GARY L. WESTBROOK, The Vollum Institute and Department of Neurology, Oregon Health Sciences University, Portland, OR, USA

JULIAN P. WHITELEGGE, The Pasarow Mass Spectrometry Laboratory, Departments of Psychiatry and Biobehavioral Sciences, Chemistry and Biochemistry and The Neuropsychiatric Institute, University of California, Los Angeles, CA, USA

CHARLES F. ZORUMSKI, Departments of Psychiatry and Neurobiology, Washington University School of Medicine, St. Louis, MO, USA

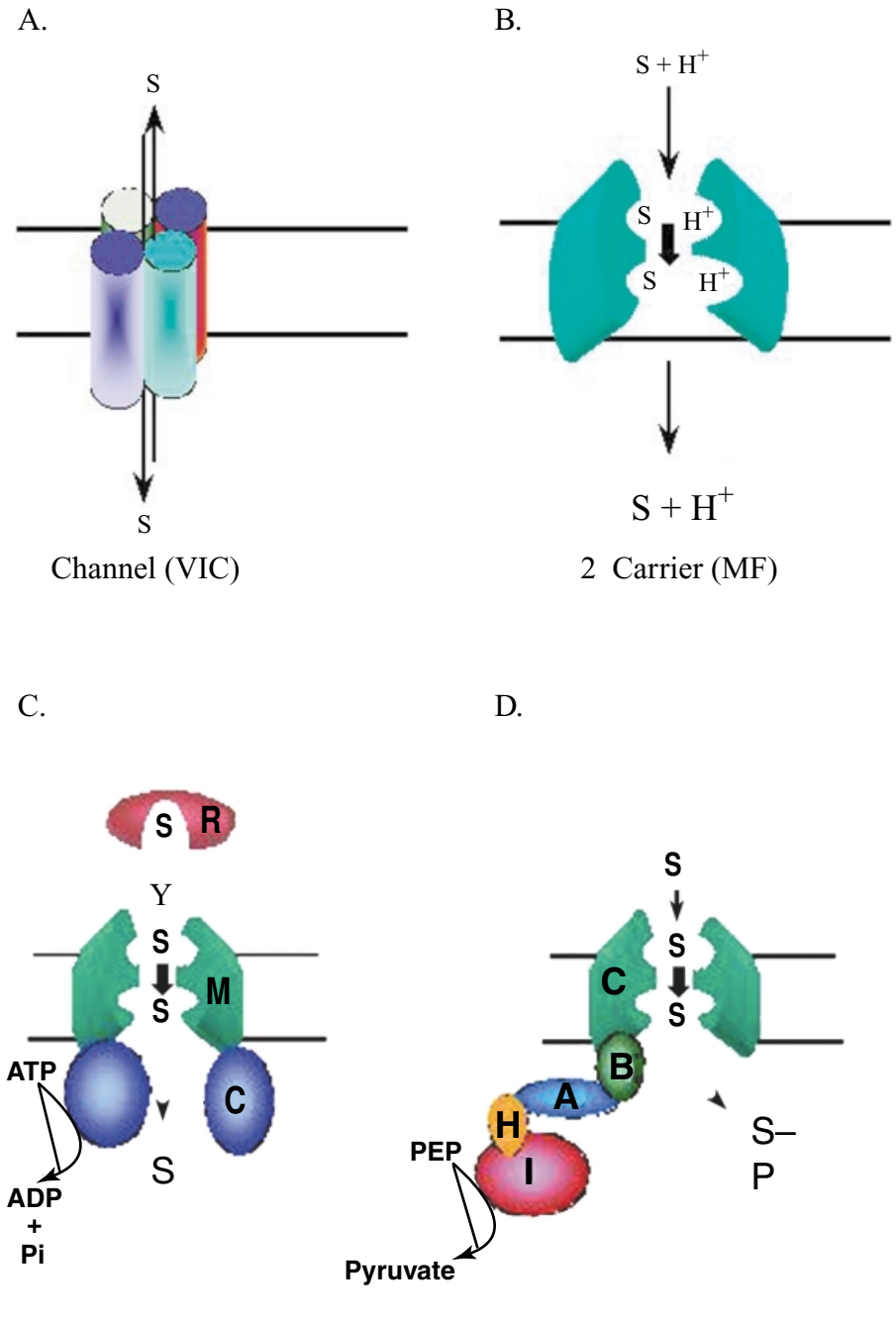

Figure 1.1. Schematic depiction of the four major types of transporters found in living organisms. For full caption, see page 4.

Transmembrane Transporters, Edited by Michael Quick
ISBN 0-471-06513-7

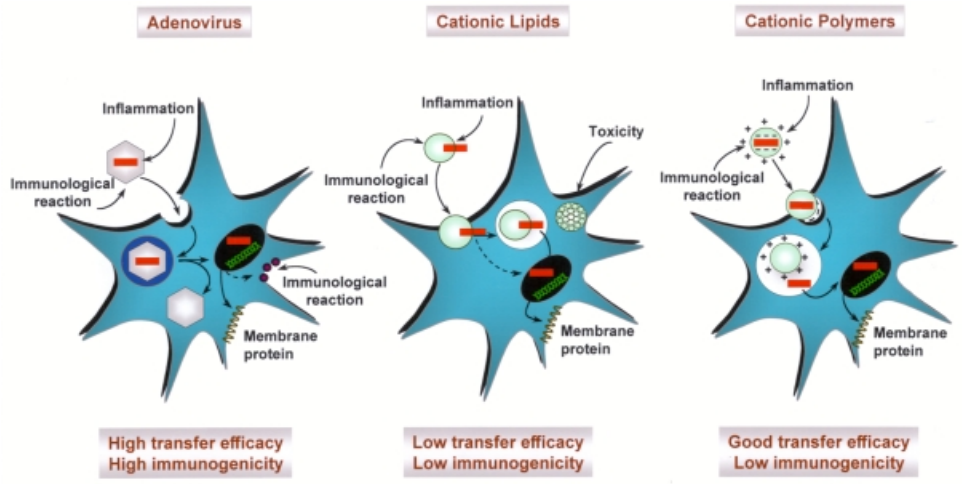

Figure 6.1. Schematic representation of various techniques of gene transfer into cells. Adapted from Crystal (1995).

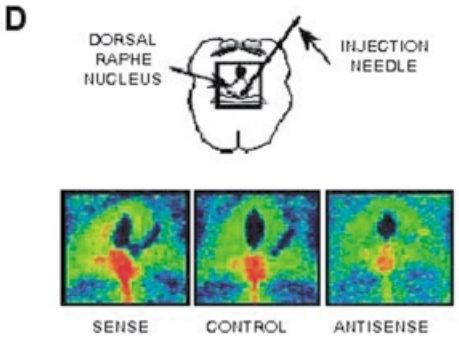

Figure 6.2. D) Autoradiographic labeling of SERT in the dorsal raphe nucleus 3 days post-injection of sense (sense) or nonrecombinant plasmid (control) or 7 days after administration of the short antisense plasmid (antisense). Increasing OD values corresponded from blue, green, yellow to red. From Fabre, et al., 2000b, copyright 2000, Society for Neuroscience.

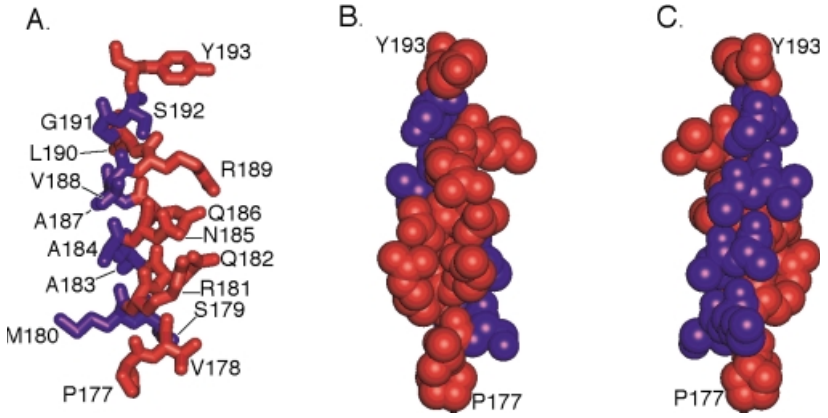

Figure 9.4. Graphical representation of residues 177–193 within TMDIV colored on the basis of reactivity toward the MTS reagents. For full caption, see page 155.

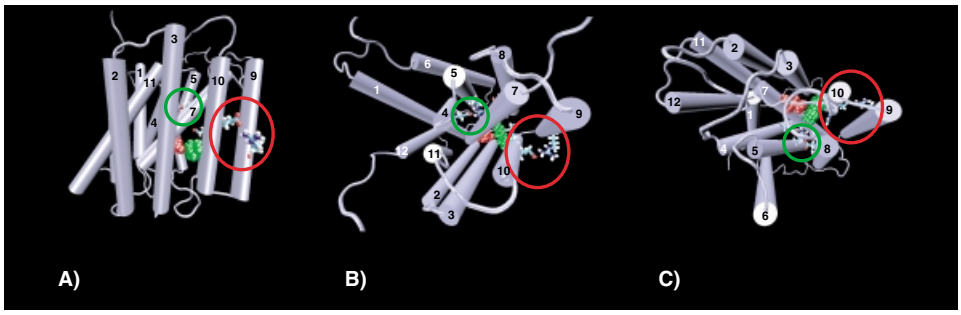

Figure 11.6. Helix packing model of lac permease (**A**) sideview with cytoplasmic side on top, (**B**) cytoplasmic view, and (**C**) periplasmic view. The D240/K319 salt bridge, shown in red and green, is located between the residues involved in proton translocation (E325 and R302 encircled in red) and the residues involved in substrate binding (E126 and R144 encircled in green). The additional irreplaceable residues E269 and H322 are obstructed by the helices.

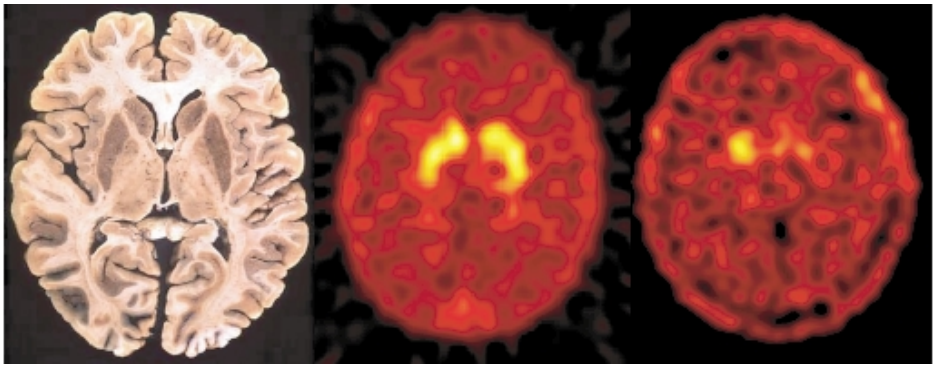

Figure 15.3. Transaxial, SPECT images of human brain at 3 h post-i.v. injection of 20 mCi of [^{99m}Tc]TRODAT-1 for normal and parkinsonian subject, respectively. In the normal subject, a high accumulation of [^{99m}Tc]TRODAT-1 was observed in caudate and putamen, where dopamine transporters are concentrated, whereas the parkinsonian patient (right) displayed a dramatic decreased uptake in this region of the brain. A comparable post-mortem brain section of a normal human is displayed on the left.

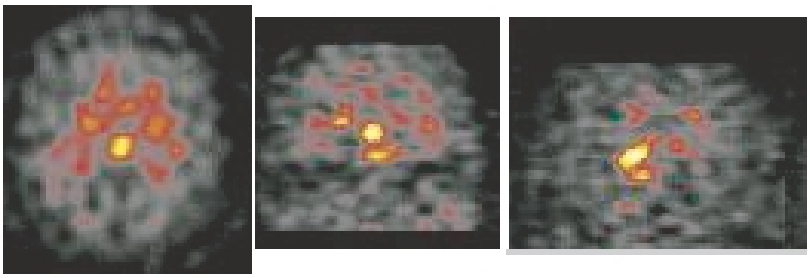

Figure 15.5. SPECT images of a normal subject's brain at 5 h after injection of [^{123}I]ADAM.

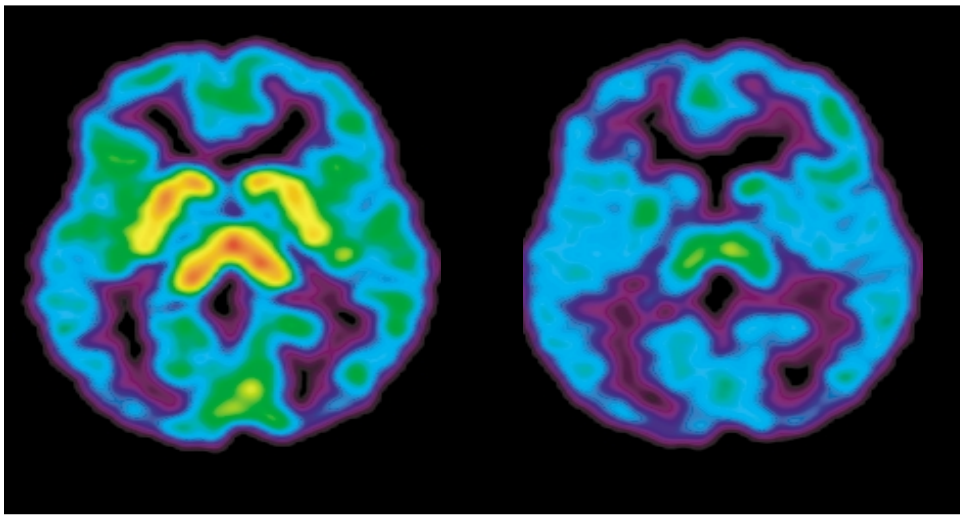

Figure 15.6. PET imaging of SERT in the normal human brain. Effects of citalopram on [^{11}C]DASB PET scan with a treatment of 20 mg citalopram/day for four weeks. Images represent summated frames normalized to mean summated cerebellum values (PET images kindly provided by the courtesy of Dr. Sylan Houle, University of Toronto).

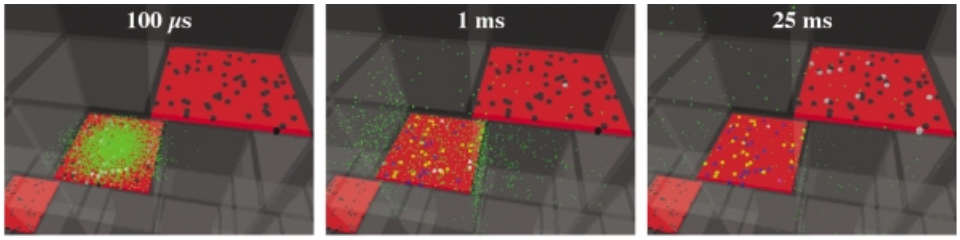

Figure 16.7. The simulated tissue consisted of GABA-impermeable cubes 320 nm in length, representing cell membranes (gray). The extracellular space exists *between* the cubes and was 15 nm wide. For full caption, see page 271

CHAPTER 1

FAMILIES OF TRANSPORTERS AND THEIR CLASSIFICATION

MILTON H. SAIER, JR.

1.1 SUMMARY

Thirty completely sequenced genomes of bacteria, archaea, and eukaryotes have been surveyed for the presence of genes that encode homologues of known solute transport proteins. These analyses and others have revealed the presence of more than 300 families of sequence-related transporters and putative transporters. All such proteins have been classified according to a system that we call transporter classification (TC). In this summary chapter, the main features of this system are described and the families are presented in tabular form. Detailed information concerning these families and their constituent transporters is available in our database (*TCDB.ucsd.edu*).

1.2 INTRODUCTION

Biological organisms consist of cells built of proteins, carbohydrates, lipids, and nucleic acids. Virtually all of the catalytic activities of the cell are performed by proteins. About one-third of the proteins of a cell are embedded in biological membranes, and about one-third of these function to catalyze the transport of molecules from one side of the membrane to the other (Paulsen et al. 1998a,b; 2000). Although many of these proteins couple their vectorial reactions to changes in cellular energy state, others catalyze the vectorial process without expending energy.

1.3 THE TC SYSTEM

Our research group has undertaken the task of classifying biological transmembrane molecular transport systems (Saier 1999). In the proposed classification system, each functionally dissimilar transporter is classified by a five-digit TC number. The first of these digits (a number) refers to the class, as determined by the mode of transport and energy coupling mechanism; the second (a letter) refers to the subclass, determined by the type of transporter and the energy coupling mechanism; the third (a number) refers to the family

Transmembrane Transporters. Edited by Michael Quick

ISBNs: 0-471-06517 (Hardcover); 0-471-43404-3 (Electronic)

or superfamily; the fourth (a number) refers to a phylogenetic cluster within the family (or a family within the superfamily); and the fifth (a number) refers to the substrate specificities of the individual permeases. Thus, the number 2.A.1.4.5 refers to a secondary carrier (2.A) of the major facilitator superfamily (MFS; 2.A.1); in the fourth family of the MFS, called the organophosphate:P_i antiporter (OPA) family (2.A.1.4), with a specificity for glucose-6-P (2.A.1.4.5). The example selected to illustrate this particular TC number is the microsomal glucose-6-P transporter (glycogen storage or Gierke's disease protein) of humans. The entire TC system can be found in our database and related software, and information is available on our web*site (http://www-biology.ucsd.edu/~msaier/transport/*). The genome analyses on which this system was originally based can be found within the same website and was prepared and organized by my colleague, Dr. Ian Paulsen, currently at the Institute for Genomic Research (TIGR) Rockville, MD, (Paulsen et al. 1998a,b; 2000). This website presents representative multiple alignments, phylogenetic trees, and other analyses for some of the families included within the TC systems.

Classification according to permease type and energy source is outlined in Table 1.1. Figure 1.1 depicts in schematic form the major types of transporters found in nature. The main classes and subclasses will be discussed below. Classes 1–5 represent defined class-

Table 1.1. Classes and subclasses of transporters according to the TC system[a]

1. Channels/Pores
   - 1.A α-Type channels
   - 1.B β-Barrel porins
   - 1.C Pore-forming toxins (proteins and peptides)
   - 1.D Nonribosomally synthesized channels
2. Electrochemical Potential-driven Transporters
   - 2.A Porters (uniporters, symporters, antiporters)
   - 2.B Non-ribosomally synthesized porters
   - 2.C Ion-gradient-driven energizers
3. Primary Active Transporters
   - 3.A *P-P*-bond hydrolysis-driven transporters
   - 3.B Decarboxylation-driven transporters
   - 3.C Methyltransfer-driven transporters
   - 3.D Oxidoreduction-driven transporters
   - 3.E Light absorption-driven transporters
4. Group Translocators
   - 4.A Phosphotransfer-driven group translocators
5. Transmembrane Electron Flow Systems
   - 5.A Two-electron carriers
   - 5.B One-electron carriers
8. Accessory Factors Involved in Transport
   - 8.A Auxiliary transport proteins
9. Incompletely Characterized Transport Systems
   - 9.A Recognized transporters of unknown biochemical mechanism
   - 9.B Putative but uncharacterized transport proteins
   - 9.C Functionally characterized transporters lacking identified sequences

[a]This system of classification has been approved by the transporter nomenclature committee of the International Union of Biochemistry and Molecular Biology. No assignment has been made for categories 6–7. These will be reserved for novel types of transporters, yet to be discovered, that do not fall within categories 1–5.

es of transporters; class 8 is for auxiliary transport proteins, and class 9 is for ill-defined and putative transporters. Classes 7 and 8 are not currently used and will be reserved for new, yet to be discovered, types of transporters.

1.3.1. Channel-Type Transporters

Transmembrane channel proteins of this class are found ubiquitously in the membranes of all types of organisms, from bacteria to higher eukaryotes. Transport systems of this type catalyze facilitated diffusion (by an energy-independent process) by passage through a transmembrane aqueous pore or channel without evidence for a carrier-mediated mechanism. These channel proteins usually consist of either α-helical spanners or β-strands that form barrel-like structures. Class 1 channels include a) α-helical type channels; b) β-barrel type channels; c) protein and peptide toxins that form channels in cells other than the ones that synthesize the proteins; d) other channels, including "depsipeptides," which are not made by ribosome-mediated messenger RNA translation; and holins, a subclass of class 1.A that functions specifically in bacterial cell lysis.

1.3.2. Carrier-Type Transporters

Transport systems are included in this class if they use a carrier-mediated process to catalyze uniport (a single species is transported by facilitated diffusion), antiport (two or more species are transported in opposite directions in a tightly coupled process coupled only to chemiosmotic energy), and/or symport (two or more species are transported together in the same direction in a tightly coupled process coupled only to chemiosmotic energy). Large protein carriers are placed into subclass 2.A; depsipeptide carriers comprise subclass 2.B; and chemiosmotic energizers of transport represent subclass 2.C.

1.3.3. Primary Active Transporters

These transport systems consist of several types; subclass 3.A includes pyrophosphate bond hydrolysis-driven active transporters. Transport systems are included in this subclass if they hydrolyze pyrophosphate or the terminal pyrophosphate bond in adenosine trisphosphate (ATP) or another nucleoside triphosphate to drive the active uptake and/or extrusion of a solute or solutes. The transport protein may or may not be phosphorylated transiently, but the substrate is not phosphorylated; subclass 3.B includes decarboxylation-driven active transporters. Transport systems that drive solute (e.g., ion) uptake or extrusion by decarboxylation of a cytoplasmic substrate (a single family) are included in this class. Subclass 3.C consists of methyltransfer-driven active transporters. A single characterized family of multicomponent transporters currently falls into this category, the Na^+-transporting methyltetrahydromethanopterin:coenzyme M methyltransferases of archaea. Subclass 3.D consists of oxidoreduction-driven active transporters. Transport systems that drive transport of a solute (e.g., an ion) energized by the flow of electrons (or hydride ions) from a reduced substrate to an oxidized substrate are included in this class. Finally, subclass 3.E includes light-driven active transporters. Transport systems that use light energy to drive transport of a solute (e.g., an ion) are included in this last subclass.

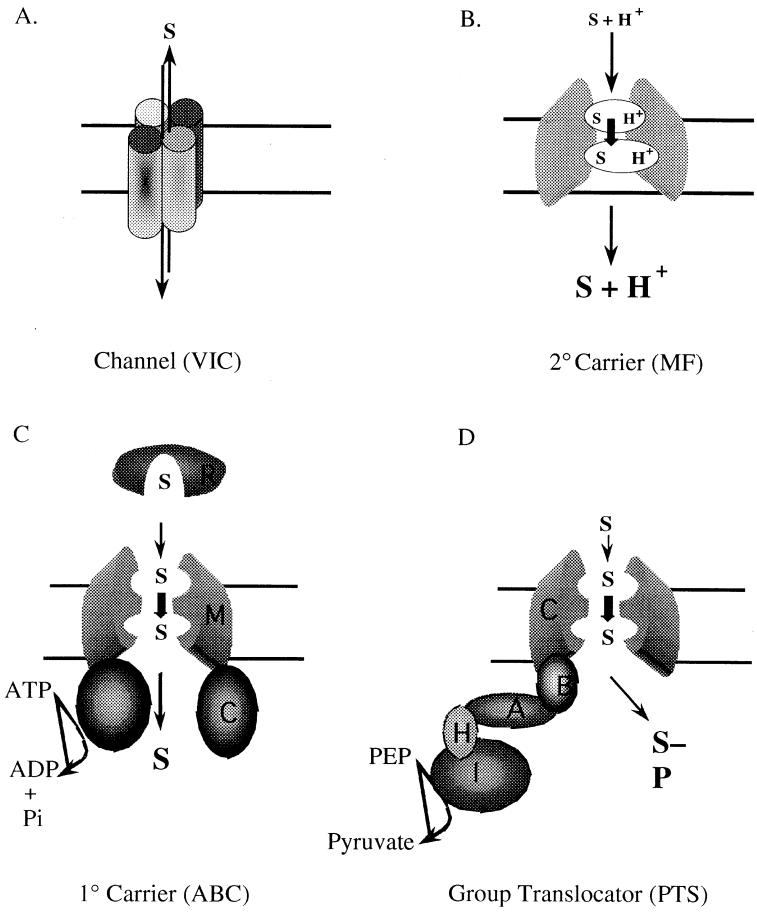

Figure 1.1. Schematic depiction of the four major types of transporters found in living organisms. **A)** Channels (usually oligomeric). A voltage-gate ion channel (VIC) family member (TC 1.A.1) is represented. The tetrameric channel allows solute, S, to flow freely across the membrane without energy coupling. **B)** Secondary carriers (usually monomeric or dimeric). A major facilitator superfamily (MFS) porter (TC 2.A.1) is depicted. A functionally dimeric (heterodimeric or homodimeric) carrier utilizes both domains for solute (and cation) recognition. Most secondary carriers have both domains fused in a single polypeptide chain. One or more conformational changes allow alternative binding conformers. Solute is accumulated in accordance with the electrochemical gradients of the solutes transported. A solute:proton symport mechanism is portrayed, but solute uniport, solute:proton antiport, or solute:solute antiport may, instead of or in addition to symport, be catalyzed by secondary carriers. **C)** Primary active transporters (usually multidomain and multicomponent). An ATP-binding cassette (ABC) superfamily uptake permease (TC 3.A.1) is shown. The functionally dimeric (homo or heterodimeric) pump allows active transport of solute into (or out of) the cell against a large concentration gradient. A single extracellular receptor (R) feeds solute into the dimeric membrane channel (M), and solute transport is energized by ATP hydrolysis, which is catalyzed by the cytoplasmic dimeric ATPase (C). **D)** Group translocators (always multidomain). A phosphoenolpyruvate (PEP)-dependent phosphotransferase system (PTS) superfamily group translocator (TC 4.A.1) is presented. The functionally dimeric (homodimeric) membrane transporter, (Enzyme IIC (C), is energized by a series of phosphoryl transfer reactions sequentially catalyzed by Enzyme I (I), HPr (H), Enzyme IIA (A), and Enzyme IIB (B). The sugar substrate is phosphorylated during transport. (See color insert.)

Table 1.2. Families of Transport Proteins

1.A. α-Type Channels
- 1.A.1 The Voltage-gated Ion Channel (VIC) Superfamily
- 1.A.2 The Animal Inward Rectifier K^+ Channel (IRK-C) Family
- 1.A.3 The Ryanodine-Inositol 1,4,5-triphosphate Receptor Ca^{2+} Channel (RIR-CaC) Family
- 1.A.4 The Transient Receptor Potential Ca^{2+} Channel (TRP-CC) Family
- 1.A.5 The Polycystin Cation Channel (PCC) Family
- 1.A.6 The Epithelial Na^+ Channel (ENaC) Family
- 1.A.7 ATP-gated Cation Channel (ACC) Family
- 1.A.8 The Major Intrinsic Protein (MIP) Family
- 1.A.9 The Ligand-gated Ion Channel (LIC) Family of Neurotransmitter Receptors
- 1.A.10 The Glutamate-gated Ion Channel (GIC) Family of Neurotransmitter Receptors
- 1.A.11 The Chloride Channel (ClC) Family
- 1.A.12 The Organellar Chloride Channel (O-ClC) Family
- 1.A.13 The Epithelial Chloride Channel (E-ClC) Family
- 1.A.14 The Nonselective Cation Channel-1 (NSCC1) Family
- 1.A.15 The Nonselective Cation Channel-2 (NSCC2) Family
- 1.A.16 The Yeast Stretch-Activated, Cation-Selective, Ca^{2+} Channel, Mid1 (Mid1) Family
- 1.A.17 The Chloroplast Outer Envelope Solute Channel (CSC) Family
- 1.A.18 The Chloroplast Envelope Anion Channel-forming Tic110 (Tic110) Family
- 1.A.19 The Influenza Virus Matrix-2 Channel (M2-C) Family
- 1.A.20 The gp91^{phox} Phagocyte NADPH Oxidase-associated Cytochrome b_{558} (CytB) H^+-channel Family
- 1.A.21 The Bcl-2 (Bcl-2) Family
- 1.A.22 The Large Conductance Mechanosensitive Ion Channel (MscL) Family
- 1.A.23 The Small Conductance Mechanosensitive Ion Channel (MscS) Family
- 1.A.24 The Gap Junction-forming Connexin (Connexin) Family
- 1.A.25 The Gap Junction-forming Innexin (Innexin) Family
- 1.A.26 The Plant Plasmodesmata (PPD) Family
- 1.A.27 The Phospholemman (PLM) Family
- 1.A.28 The Urea Transporter (UT) Family
- 1.A.29 The Urea/Amide Channel (UAC) Family
- 1.A.30 The H^+- or Na^+-translocating Bacterial MotAB Flagellar Motor / ExbBD Outer Membrane Transport Energizer (Mot/Exb) Superfamily
  - 1.A.30.1 The H^+- or Na^+-translocating Bacterial Flagellar Motor (Mot) Family
  - 1.A.30.2 The TonB-ExbB-ExbD / TolA-TolQ-TolR (Exb) Family of Energizers for Outer Membrane Receptor (OMR)-Mediated Active Transport
- 1.A.31 The Annexin (Annexin) Family
- 1.A.32 The Type B Influenza Virus NB Channel (NB-C) Family
- 1.A.33 The Cation Channel-forming Heat Shock Protein-70 (Hsp70) Family
- 1.A.34 The Envelope Virus E1 Channel (EVE1-C) Family
- 1.A.35 The Metal Ion Transporter (MIT) Family
- 1.A.36 The Intracellular Chloride Channel (ICC) Family

1.B. β-Barrel Porins
- 1.B.1 The General Bacterial Porin (GBP) Family
- 1.B.2 The Chlamydial Porin (CP) Family
- 1.B.3 The Sugar Porin (SP) Family
- 1.B.4 The *Brucella-Rhizobium* Porin (BRP) Family
- 1.B.5 The *Pseudomonas* OprP Porin (POP) Family
- 1.B.6 The OmpA-OmpF Porin (OOP) Family
- 1.B.7 The *Rhodobacter* PorCa Porin (RPP) Family

(continues)

Table 1.2. Families of Transport Proteins *(continued)*

1.B.8 The Mitochondrial and Plastid Porin (MPP) Family
1.B.9 The FadL Outer Membrane Protein (FadL) Family
1.B.10 The Nucleoside-specific Channel-forming Outer Membrane Porin (Tsx) Family
1.B.11 The Outer-Membrane Fimbrial Usher Porin (FUP) Family
1.B.12 The Autotransporter (AT) Family
1.B.13 The Alginate Export Porin (AEP) Family
1.B.14 The Outer-Membrane Receptor (OMR) Family
1.B.15 The Raffinose Porin (RafY) Family
1.B.16 The Short-chain Amide and Urea Porin (SAP) Family
1.B.17 The Outer-Membrane Factor (OMF) Family
1.B.18 The Outer Membrane Auxiliary (OMA) Protein Family
1.B.19 The Glucose-selective OprB Porin (OprB) Family
1.B.20 The Two-Partner Secretion (TPS) Family
1.B.21 The OmpG Porin (OmpG) Family
1.B.22 The Outer Bacterial Membrane Secretin (Secretin) Family
1.B.23 The Cyanobacterial Porin (CBP) Family
1.B.24 The Mycobacterial Porin (MBP) Family
1.B.25 The Outer Membrane Porin (Opr) Family
1.B.26 The Cyclodextrin Porin (CDP) Family
1.B.27 The *Helicobacter* Outer Membrane Porin (HOP) Family
1.B.28 The Plastid Outer Envelope Porin of 24 kDa (OEP24) Family
1.B.29 The Plastid Outer Envelope Porin of 21 kDa (OEP21) Family
1.B.30 The Plastid Outer Envelope Porin of 16 kDa (OEP16) Family
1.B.31 The *Campylobacter jejuni* Major Outer Membrane Porin (MomP) Family
1.B.32 The Fusobacterial Outer Membrane Porin (FomP) Family
1.B.33 The *Vibrio* Chitoporin/Neisserial Porin (VC/NP) Family
1.B.34 The Corynebacterial Porin (PorA) Family

1.C. Pore-forming Toxins
1.C.1 The Channel-forming Colicin (Colicin) Family
1.C.2 The Channel-forming δ–Endotoxin Insecticidal Crystal Protein (ICP) Family
1.C.3 The α-Hemolysin Channel-forming Toxin (αHL) Family
1.C.4 The Aerolysin Channel-forming Toxin (Aerolysin) Family
1.C.5 The Channel-forming ε-Toxin (ε-toxin) Family
1.C.6 The Yeast Killer Toxin K1 (YKT-K1) Family
1.C.7 The Diphtheria Toxin (DT) Family
1.C.8 The Botulinum and Tetanus Toxin (BTT) Family
1.C.9 The Vacuolating Cytotoxin (VacA) Family
1.C.10 The Pore-forming Haemolysin E (HlyE) Family
1.C.11 The Pore-forming RTX Toxin (RTX-toxin) Family
1.C.12 The Cholesterol-binding, Thiol-Activated Cytolysin (TAC) Family
1.C.13 The Channel-forming Leukocidin Cytotoxin (Ctx) Family
1.C.14 The Cytohemolysin (CHL) Family
1.C.15 The Whipworm Stichosome Porin (WSP) Family
1.C.16 The Magainin (Magainin) Family
1.C.17 The Cecropin (Cecropin) Family
1.C.18 The Melittin (Melittin) Family
1.C.19 The Defensin (Defensin) Family
1.C.20 The Nisin (Nisin) Family
1.C.21 The Lacticin 481 (Lacticin 481) Family
1.C.22 The Lactococcin A (Lactococcin A) Family
1.C.23 The Lactocin S (Lactocin S) Family

Table 1.2. Families of Transport Proteins *(continued)*

1.C.24 The Pediocin (Pediocin) Family
1.C.25 The Lactococcin G (Lactococcin G) Family
1.C.26 The Lactacin X (Lactacin X) Family
1.C.27 The Divergicin A (Divergicin A) Family
1.C.28 The AS-48 (AS-48) Family
1.C.29 The Plantaricin EF (Plantaricin EF) Family
1.C.30 The Plantaricin JK (Plantaricin JK) Family
1.C.31 The Channel-forming Colicin V (Colicin V) Family
1.C.32 The Amphipathic Peptide Mastoparan (Mastoparan) Family
1.C.33 The Cathilicidin (Cathilicidin) Family
1.C.34 The Tachyplesin (Tachyplesin) Family
1.C.35 The Amoebapore (Amoebapore) Family
1.C.36 The Bacterial Type III-Target Cell Pore (IIITCP) Family
1.C.37 The Lactococcin 972 (Lactococcin 972) Family
1.C.38 The Pore-forming Equinatoxin (Equinatoxin) Family
1.C.39 The Complement Protein C9 (CPC9) Family
1.C.40 The Bactericidal Permeability–Increasing Protein (BPIP) Family
1.C.41 The Tripartite Haemolysin BL (HBL) Family
1.C.42 The Channel-forming *Bacillus anthrax* Protective Antigen (BAPA) Family
1.C.43 The Earthworm Lysenin Toxin (Lysenin) Family
1.C.44 The Plant Thionine (PT) Family
1.C.45 The Plant Defensin (PD) Family
1.C.46 The C-type Natriuretic Peptide (CNP) Family
1.C.47 The Insect Defensin (Insect Defensin) Family
1.C.48 The Prion Peptide Fragment (PPF) Family
1.C.49 The Cytotoxic Amylin (Amylin) Family
1.C.50 The Amyloid β-Protein Peptide (AβPP) Family
1.C.51 The Pilosulin (Pilosulin) Family
1.C.52 The Dermaseptin (Dermaseptin) Family
1.C.53 The Bacteriocin AS-48 Cyclic Polypeptide (Bacteriocin AS-48) Family
1.C.54 The Shiga Toxin B-Chain (ST-B) Family
1.C.55 The Agrobacterial VirE2 Target Host Cell Membrane Anion Channel (VirE2) Family
1.C.56 The *Pseudomanas syringae* HrpZ Target Host Cell Membrane Cation Channel (HrpZ) Family
1.C.57 The Clostridial Cytotoxin (CCT) Family
1.C.58 The Microcin E492 (Microcin E492) Family

1.D. Nonribosomally synthesized Channels
1.D.1 The Gramicidin A (Gramicidin A) Channel Family
1.D.2 The Syringomycin Channel-forming (Syringomycin) Family
1.D.3 The Syringopeptin Channel-Forming (Syringopeptin) Family
1.D.4 The Tolaasin Channel-forming (Tolaasin) Family
1.D.5 The Alamethicin Channel-forming (Alamethicin) Family
1.D.6 The Complexed Poly 3-Hydroxybutyrate Ca^{2+} Channel (cPHB-CC) Family
1.D.7 The Beticolin (Beticolin) Family
1.D.8 The Saponin (Saponin) Family
1.D.9 The Polyglutamine Ion Channel (PG-IC) Family
1.D.10 The Ceramide-forming Channel (Ceramide) Family

1.E. Holins
1.E.1 The P21 Holin S (P21 Holin) Family
1.E.2 The λ Holin S (λ Holin) Family

(continues)

Table 1.2. Families of Transport Proteins *(continued)*

1.E.3 The P2 Holin TM (P2 Holin) Family
1.E.4 The LydA Holin (LydA Holin) Family
1.E.5 The PRD1 Holin M (PRD1 Holin) Family
1.E.6 The T7 Holin (T7 Holin) Family
1.E.7 The HP1 Holin (HP1 Holin) Family
1.E.8 The T4 Holin (T4 Holin) Family
1.E.9 The T4 Immunity Holin (T4 Immunity Holin) Family
1.E.10 The *Bacillus subtilis* ϕ29 Holin (ϕ29 Holin) Family
1.E.11 The ϕ11 Holin (ϕ11 Holin) Family
1.E.12 The ϕAdh Holin (ϕAdh Holin) Family
1.E.13 The ϕU53 Holin (ϕU53 Holin) Family
1.E.14 The LrgA Holin (LrgA Holin) Family
1.E.15 The ArpQ Holin (ArpQ Holin) Family
1.E.16 The Cph1 Holin (Cph1 Holin) Family
1.E.17 The BlyA Holin (BlyA Holin) Family
1.E.18 The *Lactococcus lactis* Phage r1t Holin (r1t holin) Family
1.E.19 The *Clostridium difficile* TcdE Holin (TcdE Holin) Family

2.A. Porters (Uniporters, Symporters and Antiporters)
2.A.1 The Major Facilitator Superfamily (MFS)
2.A.1.1 The Sugar Porter (SP) Family
2.A.1.2 The Drug: H^+ Antiporter-1 (12 Spanner) (DHA1) Family
2.A.1.3 The Drug: H^+ Antiporter-1 (14 Spanner) (DHA2) Family
2.A.1.4 The Organophosphate: P_i Antiporter (OPA) Family
2.A.1.5 The Oligosaccharide:H^+ Symporter (OHS) Family
2.A.1.6 The Metabolite: H^+ Symporter (MHS) Family
2.A.1.7 The Fucose: H^+ Symporter (FHS) Family
2.A.1.8 The Nitrate/Nitrite Porter (NNP) family
2.A.1.9 The Phosphate: H^+ Symporter (PHS) Family
2.A.1.10 The Nucleoside: H^+ Symporter (NHS) Family
2.A.1.11 The Oxalate:Formate Antiporter (OFA) Family
2.A.1.12 The Sialate:H^+ Symporter (SHS) Family
2.A.1.13 The Monocarboxylate Porter (MCP) Family
2.A.1.14 The Anion:Cation Symporter (ACS) Family
2.A.1.15 Aromatic Acid:H^+ Symporter (AAHS) Family
2.A.1.16 The Siderophore-Iron Transporter (SIT) Family
2.A.1.17 The Cyanate Porter (CP) Family
2.A.1.18 The Polyol Porter (PP) Family
2.A.1.19 The Organic Cation Transporter (OCT) Family
2.A.1.20 The Sugar Efflux Transporter (SET) Family
2.A.1.21 The Drug:H^+ Antiporter-3 (12 Spanner) (DHA3) Family
2.A.1.22 The Vesicular Neurotransmitter Transporter (VNT) Family
2.A.1.23 The Conjugated Bile Salt Transporter (BST) Family
2.A.1.24 The Unknown Major Facilitator-1 (UMF1) Family
2.A.1.25 The Peptide-Acetyl-Coenzyme A Transporter (PAT) Family
2.A.1.26 The Unknown Major Facilitator-2 (UMF2) Family
2.A.1.27 The Phenyl Propionate Permease (PPP) Family
2.A.1.28 The Unknown Major Facilitator-3 (UMF3) Family
2.A.1.29 The Unknown Major Facilitator-4 (UMF4) Family
2.A.1.30 The Putative Abietane Diterpenoid Transporter (ADT) Family
2.A.1.31 The Nickel Resistance (Nre) Family
2.A.1.32 The Putative Aromatic Compound/Drug Exporter (ACDE) Family

Table 1.2. Families of Transport Proteins *(continued)*

2.A.1.33 The Putative YqgE Transporter (YqgE) Family
2.A.1.34 The Feline Leukemia Virus Subgroup C Receptor (FLVCR) Family
2.A.1.35 The Fosmidomycin Resistance (Fsr) Family
2.A.1.36 The Acriflavin-sensitivity (YnfM) Family
2.A.1.37 The Putative Short-chain Fatty Acid Porter (AtoE) Family
2.A.2 The Glycoside-Pentoside-Hexuronide (GPH):Cation Symporter Family
2.A.3 The Amino Acid-Polyamine-Organocation (APC) Family
2.A.3.1 The Amino Acid Transporter (AAT) Family
2.A.3.2 The Basic Amino Acid/Polyamine Antiporter (APA) Family
2.A.3.3 The Cationic Amino Acid Transporter (CAT) Family
2.A.3.4 The Amino Acid/Choline Transporter (ACT) Family
2.A.3.5 The Ethanolamine Transporter (EAT) Family
2.A.3.6 The Archaeal/Bacterial Transporter (ABT) Family
2.A.3.7 The Glutamate:GABA Antiporter (GGA) Family
2.A.3.8 The L-type Amino Acid Transporter (LAT) Family
2.A.3.9 The Spore Germination Protein (SGP) Family
2.A.3.10 The Yeast Amino Acid Transporter (YAT) Family
2.A.4 The Cation Diffusion Facilitator (CDF) Family
2.A.5 The Zinc (Zn^{2+})-Iron (Fe^{2+}) Permease (ZIP) Family
2.A.6 The Resistance-Nodulation-Cell Division (RND) Superfamily
2.A.6.1 The Heavy Metal Efflux (HME) Family
2.A.6.2 The (Largely Gram-negative Bacterial) Hydrophobe/Amphiphile Efflux-1 (HAE1) Family
2.A.6.3 The Putative Nodulation Factor Exporter (NFE) Family
2.A.6.4 The SecDF (SecDF) Family
2.A.6.5 The (Gram-positive Bacterial Putative) Hydrophobe/Amphiphile Efflux-2 (HAE2) Family
2.A.6.6 The Eukaryotic (Putative) Sterol Transporter (EST) Family
2.A.6.7 The (Largely Archaeal Putative) Hydrophobe/Amphiphile Efflux-3 (HAE3) Family
2.A.7 The Drug/Metabolite Transporter (DMT) Superfamily
2.A.7.1 The 4 TMS Small Multidrug Resistance (SMR) Family
2.A.7.2 The 5 TMS Bacterial/Archaeal Transporter (BAT) Family
2.A.7.3 The 10 TMS Drug/Metabolite Exporter (DME) Family
2.A.7.4 The Plant Drug/Metabolite Exporter (P-DME) Family
2.A.7.5 The Glucose/Ribose Porter (GRP) Family
2.A.7.6 The L-Rhamnose Transporter (RhaT) Family
2.A.7.7 The Chloramphenicol-Sensitivity Protein (RarD) Family
2.A.7.8 The *Caenorhabditis elegans* ORF (CEO) Family
2.A.7.9 The Triose-phosphate Transporter (TPT) Family
2.A.7.10 The UDP-N-Acetylglucosamine:UMP Antiporter (UAA) Family
2.A.7.11 The UDP-Galactose:UMP Antiporter (UGA) Family
2.A.7.12 The CMP-Sialate:CMP Antiporter (CSA) Family
2.A.7.13 The GDP-Mannose:GMP Antiporter (GMA) Family
2.A.7.14 The Plant Organocation Permease (POP) Family
2.A.8 The Gluconate:H^+ Symporter (GntP) Family
2.A.9 The Cytochrome Oxidase Biogenesis (Oxa1) Family
2.A.10 The 2-Keto-3-Deoxygluconate Transporter (KDGT) Family
2.A.11 The Citrate-Mg^{2+}:H^+ (CitM)–Citrate-Ca^{2+}:H^+ (CitH) Symporter (CitMHS) Family
2.A.12 The ATP:ADP Antiporter (AAA) Family

(continues)

Table 1.2. Families of Transport Proteins *(continued)*

2.A.13 The C_4-Dicarboxylate Uptake (Dcu) Family
2.A.14 The Lactate Permease (LctP) Family
2.A.15 The Betaine/Carnitine/Choline Transporter (BCCT) Family
2.A.16 The Telurite-resistance/Dicarboxylate Transporter (TDT) Family
2.A.17 The Proton-dependent Oligopeptide Transporter (POT) Family
2.A.18 The Amino Acid/Auxin Permease (AAAP) Family
2.A.19 The Ca^{2+}:Cation Antiporter (CaCA) Family
2.A.20 The Inorganic Phosphate Transporter (PiT) Family
2.A.21 The Solute:Sodium Symporter (SSS) Family
2.A.22 The Neurotransmitter:Sodium Symporter (NSS) Family
2.A.23 The Dicarboxylate/Amino Acid:Cation (Na^+ or H^+) Symporter (DAACS) Family
2.A.24 The Citrate:Cation Symporter (CCS) Family
2.A.25 The Alanine or Glycine:Cation Symporter (AGCS) Family
2.A.26 The Branched Chain Amino Acid:Cation Symporter (LIVCS) Family
2.A.27 The Glutamate:Na^+ Symporter (ESS) Family
2.A.28 The Bile Acid:Na^+ Symporter (BASS) Family
2.A.29 The Mitochondrial Carrier (MC) Family
2.A.30 The Cation-Chloride Cotransporter (CCC) Family
2.A.31 The Anion Exchanger (AE) Family
2.A.32 The Silicon Transporter (Sit) Family
2.A.33 The NhaA Na^+:H^+ Antiporter (NhaA) Family
2.A.34 The NhaB Na^+:H^+ Antiporter (NhaB) Family
2.A.35 The NhaC Na^+:H^+ Antiporter (NhaC) Family
2.A.36 The Monovalent Cation:Proton Antiporter-1 (CPA1) Family
2.A.37 The Monovalent Cation:Proton Antiporter-2 (CPA2) Family
2.A.38 The K^+ Transporter (Trk) Family
2.A.39 The Nucleobase:Cation Symporter-1 (NCS1) Family
2.A.40 The Nucleobase:Cation Symporter-2 (NCS2) Family
2.A.41 The Concentrative Nucleoside Transporter (CNT) Family
2.A.42 The Hydroxy/Aromatic Amino Acid Permease (HAAAP) Family
2.A.43 The Lysosomal Cystine Transporter (LCT) Family
2.A.44 The Formate-Nitrite Transporter (FNT) Family
2.A.45 The Arsenite-Antimonite (ArsB) Efflux Family
2.A.46 The Benzoate:H^+ Symporter (BenE) Family
2.A.47 The Divalent Anion:Na^+ Symporter (DASS) Family
2.A.48 The Reduced Folate Carrier (RFC) Family
2.A.49 The Ammonium Transporter (Amt) Family
2.A.50 The Glycerol Uptake (GUP) Family
2.A.51 The Chromate Ion Transporter (CHR) Family
2.A.52 The Ni^{2+}-Co^{2+} Transporter (NiCoT) Family
2.A.53 The Sulfate Permease (SulP) Family
2.A.54 The Mitochondrial Tricarboxylate Carrier (MTC) Family
2.A.55 The Metal Ion (Mn^{2+}-iron) Transporter (Nramp) Family
2.A.56 The Tripartite ATP-independent Periplasmic Transporter (TRAP-T) Family
2.A.57 The Equilibrative Nucleoside Transporter (ENT) Family
2.A.58 The Phosphate:Na^+ Symporter (PNaS) Family
2.A.59 The Arsenical Resistance-3 (ACR3) Family
2.A.60 The Organo Anion Transporter (OAT) Family
2.A.61 The C_4-dicarboxylate Uptake C (DcuC) Family
2.A.62 The NhaD Na^+:H^+ Antiporter (NhaD) Family
2.A.63 The Monovalent Cation (K^+ or Na^+):Proton Antiporter-3 (CPA3) Family

Table 1.2. Families of Transport Proteins *(continued)*

2.A.64 The Twin Arginine Targeting (Type V Secretory Pathway) (Tat) Family
2.A.65 The Bilirubin Transporter (BRT) Family
2.A.66 The Multi-Antimicrobial Extrusion (MATE) Family
2.A.67 The Oligopeptide Transporter (OPT) Family
2.A.68 The p-Aminobenzoyl-glutamate Transporter (AbgT) Family
2.A.69 The Auxin Efflux Carrier (AEC) Family
2.A.70 The Malonate:Na^+ Symporter (MSS) Family
2.A.71 The Folate-Biopterin Transporter (FBT) Family
2.A.72 The K^+ Uptake Permease (KUP) Family
2.A.73 The Inorganic Carbon (HCO_3^-) Transporter (ICT) Family
2.A.74 The 4 TMS Multidrug Endosomal Transporter (MET) Family
2.A.75 The L-Lysine Exporter (LysE) Family
2.A.76 The Resistance to Homoserine/Threonine (RhtB) Family
2.A.77 The Cadmium Resistance (CadD) Family
2.A.78 The Branched Chain Amino Acid Exporter (LIV-E) Family
2.A.79 The Threonine/Serine Exporter (ThrE) Family
2.A.80 The Tricarboxylate Transporter (Tct) Family

2.B Nonribosomally Synthesized Porters
2.B.1 The Valinomycin Carrier (Valinomycin) Family
2.B.2 The Monensin (Monensin) Family
2.B.3 The Nigericin (Nigericin) Family
2.B.4 The Macrotetrolide Antibiotic (MA) Family
2.B.5 The Macrocyclic Polyether (MP) Family
2.B.6 The Ionomycin (Ionomycin) Family

2.C Ion-gradient-driven Energizers
2.C.1 he TonB-ExbB-ExbD/TolA-TolQ-TolR (TonB) Family of Auxiliary Proteins for Energization of Outer Membrane Receptor (OMR)-mediated Active Transport

3.A *P-P*-bond-hydrolysis-driven Transporters
3.A.1 The ATP-binding Cassette (ABC) Superfamily

ABC-type Uptake Permeases (All from Prokaryotes—Bacteria and Archaea)
3.A.1.1 The Carbohydrate Uptake Transporter-1 (CUT1) Family
3.A.1.2 The Carbohydrate Uptake Transporter-2 (CUT2) Family
3.A.1.3 The Polar Amino Acid Uptake Transporter (PAAT) Family
3.A.1.4 The Hydrophobic Amino Acid Uptake Transporter (HAAT) Family
3.A.1.5 The Peptide/Opine/Nickel Uptake Transporter (PepT) Family
3.A.1.6 The Sulfate Uptake Transporter (SulT) Family
3.A.1.7 The Phosphate Uptake Transporter (PhoT) Family
3.A.1.8 The Molybdate Uptake Transporter (MolT) Family
3.A.1.9 The Phosphonate Uptake Transporter (PhnT) Family
3.A.1.10 The Ferric Iron Uptake Transporter (FeT) Family
3.A.1.11 The Polyamine/Opine/Phosphonate Uptake Transporter (POPT) Family
3.A.1.12 The Quaternary Amine Uptake Transporter (QAT) Family
3.A.1.13 The Vitamin B_{12} Uptake Transporter ($VB_{12}T$) Family
3.A.1.14 The Iron Chelate Uptake Transporter (FeCT) Family
3.A.1.15 The Manganese/Zinc/Iron Chelate Uptake Transporter (MZT) Family
3.A.1.16 The Nitrate/Nitrite/Cyanate Uptake Transporter (NitT) Family
3.A.1.17 The Taurine Uptake Transporter (TauT) Family
3.A.1.18 The Putative Cobalt Uptake Transporter (CoT) Family
3.A.1.19 The Thiamin Uptake Transporter (ThiT) Family
3.A.1.20 The *Brachyspira* Iron Transporter (BIT) Family

(continues)

Table 1.2. Families of Transport Proteins *(continued)*

3.A.1.21 The Yersiniabactin Fe^{3+} Uptake Transporter (YbtPQ) Family
3.A.1.22 The Nickel Uptake Transporter (NiT) Family
ABC-type Efflux Permeases (Bacterial)
3.A.1.101 The Capsular Polysaccharide Exporter (CPSE) Family
3.A.1.102 The Lipooligosaccharide Exporter (LOSE) Family
3.A.1.103 The Lipopolysaccharide Exporter (LPSE) Family
3.A.1.104 The Teichoic Acid Exporter (TAE) Family
3.A.1.105 The Drug Exporter (DrugE1) Family
3.A.1.106 The Lipid Exporter (LipidE) Family
3.A.1.107 The Putative Heme Exporter (HemeE) Family
3.A.1.108 The β-Glucan Exporter (GlucanE) Family
3.A.1.109 The Protein-1 Exporter (Prot1E) Family
3.A.1.110 The Protein-2 Exporter (Prot2E) Family
3.A.1.111 The Peptide-1 Exporter (Pep1E) Family
3.A.1.112 The Peptide-2 Exporter (Pep2E) Family
3.A.1.113 The Peptide-3 Exporter (Pep3E) Family
3.A.1.114 The Probable Glycolipid Exporter (DevE) Family
3.A.1.115 The Na^+ Exporter (NatE) Family
3.A.1.116 The Microcin B17 Exporter (McbE) Family
3.A.1.117 The Drug Exporter-2 (DrugE2) Family
3.A.1.118 The Microcin J25 Exporter (McjD) Family
3.A.1.119 The Drug/Siderophore Exporter-3 (DrugE3) Family
3.A.1.120 The Drug Resistance ATPase-1 (Drug RA1) Family
3.A.1.121 The Drug Resistance ATPase-2 (Drug RA2) Family
ABC-type Efflux Permeases (Mostly Eukaryotic)
3.A.1.201 The Multidrug Resistance Exporter (MDR) Family
3.A.1.202 The Cystic Fibrosis Transmembrane Conductance Exporter (CFTR) Family
3.A.1.203 The Peroxysomal Fatty Acyl CoA Transporter (FAT) Family
3.A.1.204 The Eye Pigment Precursor Transporter (EPP) Family
3.A.1.205 The Pleiotropic Drug Resistance (PDR) Family
3.A.1.206 The a-Factor Sex Pheromone Exporter (STE) Family
3.A.1.207 The Conjugate Transporter-1 (CT1) Family
3.A.1.208 The Conjugate Transporter-2 (CT2) Family
3.A.1.209 The MHC Peptide Transporter (TAP) Family
3.A.1.210 The Heavy Metal Transporter (HMT) Family
3.A.1.211 The Cholesterol/Phospholipid/Retinal (CPR) Flippase Family
3.A.1.212 The Mitochondrial Peptide Exporter (MPE) Family
3.A.2 The H^+- or Na^+-translocating F-type, V-type and A-type ATPase (F-ATPase) Superfamily
3.A.3 The P-type ATPase (P-ATPase) Superfamily
3.A.4 The Arsenite-Antimonite (ArsAB) Efflux Family
3.A.5 The Type II (General) Secretory Pathway (IISP) Family
3.A.6 The Type III (Virulence-related) Secretory Pathway (IIISP) Family
3.A.7 The Type IV (Conjugal DNA-Protein Transfer or VirB) Secretory Pathway (IVSP) Family
3.A.8 The Mitochondrial Protein Translocase (MPT) Family
3.A.9 The Chloroplast Envelope Protein Translocase (CEPT or Tic-Toc) Family
3.A.10 The H^+-translocating Pyrophosphatase (H^+-PPase) Family
3.A.11 The Bacterial Competence-related DNA Transformation Transporter (DNA-T) Family
3.A.12 The Septal DNA Translocator (S-DNA-T) Family

Table 1.2. Families of Transport Proteins *(continued)*

3.A.13 The Filamentous Phage Exporter (FPhE) Family
3.A.14 The Fimbrilin/Protein Exporter (FPE) Family
3.B. Decarboxylation-driven Active Transporters
3.B.1 The Na^+-transporting Carboxylic Acid Decarboxylase (NaT-DC) Family
3.C. Methyl-transfer-driven Transporters
3.C.1 The Na^+-transporting Methyltetrahydromethanopterin:Coenzyme M Methyltransferase (NaT-MMM) Family
3.D. Oxidoreduction-driven Active Transporters
3.D.1 The Proton-translocating NADH Dehydrogenase (NDH) Family
3.D.2 The Proton-translocating Transhydrogenase (PTH) Family
3.D.3 The Proton-translocating Quinol:Cytochrome *c* Reductase (QCR) Superfamily
3.D.4 The Proton-translocating Cytochrome Oxidase (COX) Superfamily
3.D.5 The Na^+-translocating NADH:Quinone Dehydrogenase (Na-NDH) Family
3.D.6 The Putative Ion (H^+ or Na^+)-translocating NADH:Ferredoxin Oxidoreductase (NFO) Family
3.D.7 The H_2:Heterodisulfide Oxidoreductase (HHO) Family
3.D.8 The Na^+- or H^+-Pumping Formyl Methanofuran Dehydrogenase (FMF-DH) Family
3.D.9 The H^+-translocating $F_{420}H_2$ Dehydrogenase ($F_{420}H_2DH$) Family
3.E. Light-driven Active Transporters
3.E.1 The Ion-Translocating Microbial Rhodopsin (MR) Family
3.E.2 The Photosynthetic Reaction Center (PRC) Family
4.A. Phosphoryl-transfer-driven Group Translocators
4.A.1 The PTS Glucose–Glucoside (Glc) Family
4.A.2 The PTS Fructose–Mannitol (Fru) Family
4.A.3 The PTS Lactose–N,N'-Diacetylchitobiose-β-glucoside (Lac) Family
4.A.4 The PTS Glucitol (Gut) Family
4.A.5 The PTS Galactitol (Gat) Family
4.A.6 The PTS Mannose–Fructose–Sorbose (Man) Family

1.3.4. PEP-Dependent, Phosphoryl Transfer-Driven Group Translocators

Transport systems of the bacterial phosphoenolpyruvate:sugar phosphotransferase system (PTS) are included in this class. The product of the reaction, derived from extracellular sugar, is a cytoplasmic sugar–phosphate. Thus, group translocators are different from other transporters in that they modify their substrates during transport.

1.3.5. Transmembrane Electron Flow Systems

Systems that catalyze electron flow across a biological membrane, from donors localized to one side of the membrane to acceptors localized to the other side, are grouped into TC category 5. These systems contribute to or subtract from the membrane potential, depending on the direction of electron flow. They are therefore important to cellular energetics.

1.3.8. Auxiliary Transport Proteins

Proteins that in some way facilitate transport across one or more biological membrane(s), but do not themselves participate directly in transport, are included in this class. These

proteins always function in conjunction with one or more transport proteins. They may provide a function connected with energy coupling to transport, play a structural role in complex formation, serve a regulatory function, or provide a function related to biogenesis or stability of transporters.

1.3.9. Transporters of Unknown Classification

Class 9 transporters fall into subclasses 9.A, B, and C. Recognized transport protein families are grouped in subclass 9.A when their mode of transport or energy coupling mechanism is unknown. They will be classified elsewhere (i.e., classes 1–5) when the transport process and energy coupling mechanism become characterized. These families include at least one member for which a transport function has been established. Putative transporters in which no family member is an established transporter are grouped in subclass 9.B. Putative transport protein families are grouped under this number and will either be classified elsewhere when the transport function of a member becomes established or be eliminated from the TC classification system if the proposed transport function is disproven. These families include at least one member for which a transport function has been suggested, but evidence for such a function is not yet compelling. Functionally characterized transporters for which sequence data are lacking are placed in subclass 9.C. Transporters of particular physiological significance are included in this category, even though a family assignment cannot be made. They will be transferred to another category when their sequences become available.

1.4 FAMILIES OF TRANSPORT SYSTEMS

Table 1.2 lists all of the currently recognized families of well-characterized transporters. The table includes classes 1–4, but classes 5, 8, and 9 are omitted for the purpose of brevity. For these latter classes, the interested reader is referred to our database. Families within the major superfamilies are also listed in Table 1.2.

Channel-type transporters of class 1 include a variety of types, including channel-forming proteins and peptides that generally form transmembrane α-helix-lined pores (subclass 1.A), β-barrel type porins (subclass 1.B), channel-forming toxins (subclass 1.C), nonproteinaceous channels (subclass 1.D), and holins (subclass 1.E).

Carrier-type transporter proteins of class 2, subclass 2.A, include uniporters, symporters, and antiporters. This subclass of transporters is the largest within the TC system. Some of these families are large superfamilies, and the largest is the MFS, (TC 2.A.1; Pao et al., 1998; Saier et al., 1999). The MFS consists of 37 currently recognized families, each specific for a distinct group of substrates (Table 1.2).

Other superfamilies under TC classification 2 are the amino acid-polyamine-organocation (APC) superfamily (TC 2.A.3; Jack et al., 2000), with 10 currently recognized constituent families; the resistance-nodulation-cell division (RND) superfamily (TC 2.A.6; Tseng et al., 1999), with 7 recognized families; and the drug/metabolite transporter (DMT) superfamily (TC 2.A.7; Jack et al., 2001), with 14 families. Although the APC superfamily is concerned primarily with amino acid uptake (Jack et al., 2000), the RND superfamily appears to be concerned primarily with drug, heavy metal, and lipid efflux (Tseng et al., 1999), and the DMT superfamily transports a large variety of drugs and

metabolites both in prokaryotes and in eukaryotic organelles (Jack et al., 2001). Many other families represented under TC subclass 2.A include transporters that function in the maintenance of cellular ionic homeostasis, in the uptake of essential nutrients and in the efflux of metabolites and toxic substances. Other subclasses of class 2 include peptide and depsipeptide carriers (2.B) and chemiosmotic energizers (2.C).

TC class 3 includes all primary active transporters. As noted above, there are five subclasses in class 3 (see Table 1.1). Most important are the ATP- or pyrophosphate hydrolysis-driven transporters (subclass 3.A). TC family 3.A.1 is the ATP-binding cassette (ABC) superfamily with more than 50 recognized families (Table 1.2). However, 13 other large families are found under TC classification 3.A. These include the F-type ATPases (TC 3.A.2), which interconvert chemiosmotic and chemical energy and the P-type ion-transporting ATPases (TC 3.A.3), such as the Na^+,K^+-ATPase of mammals. Various families of protein secretion systems, a family of DNA uptake systems (TC 3.A.11), and a family of pyrophosphate-hydrolysis driven H^+ pumps (TC 3.A.10) are also included under TC 3.A. Other chemically driven, electron flow-driven, and light-driven transporters are included within TC class 3 (Table 1.2).

TC class 4 includes the permeases of the phosphoenolpyruvate (PEP)-dependent, sugar-transporting PTS. The PTS is at present the only recognized group-translocating system. This bacterial-specific system includes six families. Like most of the primary active transporters, each PTS permease is a composite of proteins or protein domains. Although one of these domains functions to transport sugar substrates across the membrane, the other PTS constituents function to couple transport to substrate phosphorylation. Group translocating systems thus modify their substrates during transport. Like some of the proteins of TC class 3, the permeases of TC class 4 are true enzymes in the classical sense, even though they catalyze vectorial reactions. We have proposed that the transporter and enzyme domains of these complex systems evolved independently (see Saier and Tseng, 1999; Saier, 2000b; Saier, 2001).

The above-described categories include all of the currently recognized, well-characterized transport systems with established energy coupling mechanisms. However, many supposed transporters are insufficiently well characterized to be included in one of these classes. They are therefore given a TC classification number that indicates their degree of incomplete characterization. TC classes 9 and 8 include putative permeases and auxiliary permease proteins, respectively. An important aspect of the structure, sequence, or function of the putative permeases in class 9 is not known. Although these categories are listed in Table 1.1, the families tabulated under classes 8 and 9 are not included in Table 1. 2 (see Saier, 2000a, and our database for descriptions of these families).

1.5 PERSPECTIVE

Many years ago, the Enzyme Commission (EC) established a system for the classification of enzymes, but the system did not (and still does not) include most permease proteins that function to facilitate vectorial reactions. The TC system has been designed to correct this deficiency, and it has been adopted recently by the International Union of Biochemistry and Molecular Biology (IUBMB), the scientific organization that maintains the EC system. Although modifications and improvements will be incorporated continuously, it seems clear that the TC system in its present form provides a framework for the comprehensive evaluation and conceptualization of all transporter types. It has been designed for

the classification of all transporters existing in living organisms, those currently recognized as well as those yet to be discovered.

We hope that this short chapter provides readers with sufficient exposure to the TC system to examine our database and websites for more detailed information. In this way, we hope that the maze of transport data, which is expanding in magnitude at a rapid rate, primarily due to genome sequencing and functional genomic efforts of many scientists, can be placed into a rational framework for intellectual conceptualization and evaluation.

ACKNOWLEDGMENTS

I am particularly grateful to Ian Paulsen for his invaluable contributions and stimulating discussions. Matthew Moreno generously provided depictions of the four types of transporters found in nature (Figs. 1.1A–D). Additionally, I wish to thank Milda Simonaitis, Jackie Richardson, Monica Mystry, Yolanda Anglin, and Mary Beth Hiller for their assistance in the preparation of this manuscript. Work in the author's laboratory was supported by National Institute of Health (Bethesda, MD) grants GM55434 and GM64368 from the National Institute of General Medical Sciences, as well as by the M.H. Saier, Sr., Research Fund.

ANNOTATED REFERENCES

Jack DL, Paulsen IT, Saier MH Jr (2000): The APC superfamily of transporters specific for amino acids, polyamines and organocations. Microbiology 146:1797–1814.

Jack DL, Yang N, Saier MH Jr (2001): The drug/metabolite transporter superfamily. Eur J Biochem 268:3620–3639.

This article defines a novel porter superfamily and uses modern techniques to classify the proteins into families.

Pao SS, Paulsen IT, Saier MH Jr (1998): The major facilitator superfamily. Microbiol Mol Biol Rev 62:1–32.

This review classifies families within the MFS and exemplifies the phylogenetic techniques that are used for this purpose.

Paulsen IT, Nguyen L, Sliwinski MK, Rabus R, Saier MH Jr (2000): Microbial genome analyses: comparative transport capabilities in eighteen prokaryotes. J Mol Biol 301:75–100.

This research article uses semiautomated software to identify and characterize all recognizable transport proteins encoded within a number of microbial genomes.

Paulsen IT, Sliwinski MK, Nelissen B, Goffeau A, Saier MH Jr (1998b): Unified inventory of established and putative transporters encoded within the complete genome of *Saccharomyces cerevisiae*. FEBS Lett 430:116–125.

Paulsen IT, Sliwinski MK, Saier MH Jr (1998a): Microbial genome analyses: global comparisons of transport capabilities based on phylogenies, bioenergetics and substrate specificities. J Mol Biol 277:573–592.

Saier MH Jr (1998): Molecular phylogeny as a basis for the classification of transport proteins from bacteria, archaea, and eukarya. In Poole RK (ed): Advances in Microbial Physiology. San Diego: Academic Press, pp 81–136.

Saier MH Jr (1999): Genome archeology leading to the characterization and classification of transport proteins. Curr Opin Microbiol 2:555–561.

Saier MH Jr (2000a): A functional/phylogenetic classification system for transmembrane solute transporters. Microbiol Mol Biol Rev 64:354–411.

This compendium provides the most comprehensive description of the Transporter Classification System available in hard copy to date.

Saier MH Jr (2000b): Vectorial metabolism and the evolution of transport systems. J Bacteriol 182:5029–5035.

This article, as well as the one of Saier and Tseng (1999), summarizes evidence for the evolutionary pathways taken for the appearance of transporter types found in living organisms.

Saier MH Jr (2001): Evolution of transport proteins. In Setlow JK (ed): Genetic Engineering. Principles and Methods, Vol. 23. New York: Kluwer Academic/Plenum Publishers, pp 1–10.

Saier MH Jr, Beatty JT, Goffeau A, Harley KT, Heijne WHM, Huang S-C, Jack DL, Jahn PS, Lew K, Liu J, Pao SS, Paulsen IT, Tseng T-T, Virk PS (1999): The major facilitator superfamily. J Mol Microbiol Biotechnol 1:257–279.

Saier MH Jr, Tseng T-T (1999): Evolutionary origins of transmembrane transport systems. In Broome-Smith JK, Baumberg S, Stirling CJ, Ward FB (eds): Transport of Molecules Across Microbial Membranes, Symposium 58, Society for General Microbiology. Cambridge, UK: Cambridge University Press, pp 252–274.

Tseng T-T, Gratwick KS, Kollman J, Park D, Nies DH, Goffeau A, Saier MH Jr (1999): The RND permease superfamily: an ancient, ubiquitous and diverse family that includes human disease and development proteins. J Mol Microbiol Biotechnol 1:107–125.

CHAPTER 2

YEAST AS A MODEL SYSTEM FOR STUDYING GLUCOSE TRANSPORT

ECKHARD BOLES

2.1 INTRODUCTION

The classical human interest in the budding yeast *Saccharomyces cerevisiae*, a lower unicellular eukaryote, stems from its well-known role in the preparation of wine, beer, and bread. Nevertheless, over the past decades attention has focused on some additional functions for *S. cerevisiae*, such as in the expression of foreign proteins for research, industrial, or medical use or as a scientific model organism. Advances in yeast genetics and molecular biology techniques have made *S. cerevisiae* an excellent choice for the characterization of general metabolic and regulatory processes.

A unique property of *S. cerevisiae* is its high specialization for converting certain sugars to ethanol and carbon dioxide. However, this yeast cannot use a very wide range of sugars. The preferred carbon sources of *S. cerevisiae* are glucose, mannose, and fructose. Other carbon sources are galactose; disaccharides, such as sucrose or maltose; and also nonsugar carbon sources, such as ethanol or acetate. *S. cerevisiae* can deal with an extremely broad range of glucose concentrations higher than 1.5 M, as in drying fruits down to micromolar concentrations. This extremely broad range of glucose concentrations seems to set specific demands to the transport system as that which is exposed directly to such extreme environmental conditions. Moreover, glucose is not only the preferred carbon and energy source for *S. cerevisiae*, but it also acts as a regulator of several aspects of cell growth and metabolism. Yeast cells can rapidly adapt both transport and metabolism to changing glucose availability by exchanging various transporters with different kinetic properties at the plasma membrane and by several kinds of regulatory and metabolic devices. *S. cerevisiae* has developed a multilayered regulatory system to ensure coordination between the supply of sugars in the environment and the enzymatic fittings of the cells: a) it senses the extracellular concentration of sugars and adapts its sugar transport activity accordingly, and b) sugar transport activity determines the flux of sugars into the cell, subsequently generating intracellular signals for further regulatoy processes (Özcan et al., 1996a; Ronne, 1995; Boles et al., 1996, 1997; Thevelein and de Winde 1999).

S. cerevisiae transports hexoses exclusively by facilitated diffusion. As the sequence of the yeast genome was being completed, altogether 18 different genes—*HXT1–HXT17* and *GAL2*—were identified, which encode proteins that belong to the yeast hexose transporter family (Fig. 2.1) (Kruckeberg, 1996). Such a large number of hexose transporters

Transmembrane Transporters. Edited by Michael Quick

ISBNs: 0-471-06517 (Hardcover); 0-471-43404-3 (Electronic)

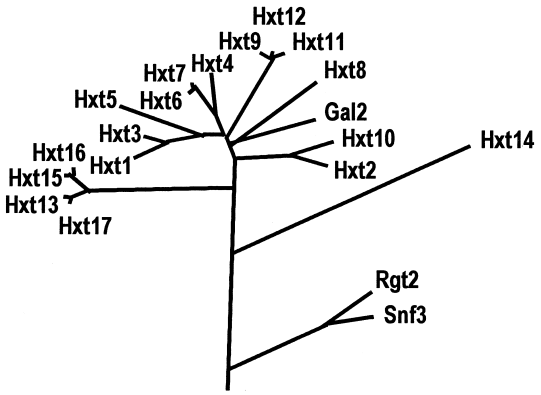

Figure 2.1. The hexose transporter family of *S. cerevisiae* (including the glucose sensors).

were unexpected for a unicellular organism. Therefore, the central question concerning research on glucose transport in yeast is obvious: Why has *S. cerevisiae* evolved such a large family of hexose transporters? More specifically: Do all these genes encode functional hexose transporters? Do these transporters differ in specificity or kinetics? How are the genes regulated? How are the proteins regulated? Are there even more transporters able to mediate uptake of hexose? Moreover, as yeast cells provide a convenient tool for the expression and characterization of heterologous proteins, this raises the question: How can we use yeast efficiently to explore sugar transporter sequences discovered during systematic sequencing of genomes?

This review is confined largely to recent developments in the field of yeast sugar transport. Reviews that cover the older literature (Lagunas, 1993; Bisson et al., 1993; Weusthuis et al., 1994), a review describing the structural similarities of the yeast hexose transporter proteins (Kruckeberg, 1996), and two reviews dealing with details on the molecular genetics of yeast hexose transport and its regulation (Boles and Hollenberg, 1997; Özcan and Johnston, 1999) are available.

2.2 CONSTRUCTION OF A YEAST STRAIN UNABLE TO TAKE UP HEXOSES

The yeast proteome contains at least 320 predicted or established membrane transport proteins, including the protein subunits of the mitochondrial and vacuolar H^+-ATPases (Paulsen et al., 1998; van Belle and André, 2001). Most yeast transporters belong to families comprising 2 to 35 proteins. For instance, the yeast genome contains 34 genes encoding proteins of the sugar transporter superfamily, including the hexose transporters (Hxt), the maltose transporters inositol and glycerophosphoinositol transporters, a high-affinity phosphate transporter, two glucose sensors, and some as-yet-uncharacterized proteins. Within the transporter families, some proteins exhibit nearly identical properties and others recognize the same compounds but with different affinities; others have developed different specificities, or the expression of the corresponding genes is differently regulated. A difficulty during analysis of multigene transporter families with genetic approaches is that they include proteins with overlapping substrate specificities. Thus, in order to

block uptake of a certain compound, it is often necessary to destroy multiple genes in the same yeast strain.

The first step toward a functional analysis of a yeast protein is the complete deletion of the corresponding gene on the chromosome (null mutant) by using the one-step gene replacement method (Orr-Weaver et al., 1981). However, mutants deficient in any of the *HXT* genes turned out not to have clearly detectable growth phenotype. Therefore, to characterize all the proteins of the highly redundant Hxt family, we decided to delete all the *HXT* genes successively in one and the same yeast strain (Wieczorke et al., 1999). Polymerase chain reaction (PCR)-generated deletion cassettes, consisting of a marker gene flanked by short homology regions to the target locus, are a convenient method for deleting genes in *S. cerevisiae* (Baudin et al., 1993; Wach et al., 1994). After transformation of these cassettes into yeast, homologous recombination between the flanking regions and the corresponding chromosomal regions results in a deletion of the gene and the simultaneous integration of the marker gene. However, as the number of marker genes is limited, we had to use a marker rescue system. This consisted of a *kanMX* geneticin resistance marker flanked by two *loxP* sites (Güldener et al., 1996). After successful deletion of the target gene, the *kanMX* marker gene could be removed by transforming the yeast cells with a plasmid expressing a bacteriophage P1 Cre-recombinase gene. Thus, this system allowed a repeated use of the *kanMX* marker gene. Another convenient feature was that six *HXT* genes are arranged in two clusters, each comprising three genes (*HXT5–1–4* and *HXT3–6–7*). In these cases, the complete clusters could be deleted, each with a single *kanMX* cassette.

We deleted the *HXT* genes successively, starting from *HXT17*, and proceeded until only the *HXT3–6–7* cluster remained (Wieczorke et al., 1999). A yeast strain containing only these three *HXT* genes did not exhibit any growth defects on media with glucose, fructose, or mannose. Only after the additional deletion of the *HXT3–6–7* gene cluster and the *GAL2* galactose permease gene, the cells of this so-called "*hxt*-null strain" were no longer able to grow with hexoses as the sole carbon source. Growth on maltose, which is taken up by an independent transport system, was indistinguishable from the wild-type strain under a lot of different conditions, indicating that none of the *HXT* genes fulfills an essential function other than in hexose transport. In another yeast strain with a different genetic background, deletion of only the genes *HXT1–7* and *GAL2* was enough to block growth of the yeast cells with hexoses (Reifenberger et al., 1995). This demonstrates that the Hxt encoded by *HXT1–7* and *GAL2* are the major transporters of yeast.

The large number of hexose transporters does not allow one to distinguish between the kinetics of individual transporters in a wild-type strain. Indeed, based on glucose transport kinetics obtained with *S. cerevisiae* wild-type strains, it was thought for a long time that *S. cerevisiae* contains only two kinetically distinct systems, a high-affinity system with a Km of about 1–2 mM, which is repressed by high extracellular glucose concentrations, and a more or less constitutive system with a Km of about 25–45 mM (Boles and Hollenberg, 1997). However, the *hxt*-null strain offered the possibility to re-introduce into its genome individual transporter genes and to determine the kinetics of the corresponding proteins with whole cell radioactive uptake assays (Reifenberger et al., 1997). Re-introduction of *HXT1* and *HXT3* resulted in yeast strains exhibiting only very low affinities for glucose uptake, indicating that *HXT1* and *HXT3* encode low-affinity transporters. *HXT2*-only and *HXT4*-only strains exhibited some intermediate affinities, and *HXT6*-only and *HXT7*-only strains had the highest affinities. All these strains also could take up fructose and mannose with lower affinities but not galactose, indicating that all of the main glu-

cose transporters of *S. cerevisiae* could take up glucose, fructose, and mannose. Expression of the *GAL2* gene in the *hxt*-null strain mediated high-affinity uptake of galactose, as well as of glucose.

In the case of expression of *HXT1–4* and *HXT6–7* in the *hxt*-null strain, a single copy of the genes under control of their own promoters was enough to restore uptake of and growth on glucose. In order to mediate significant hexose uptake by the other Hxt proteins (Hxt5, Hxt8–17), their corresponding genes had to be overexpressed in the *hxt*-null strain on multicopy plasmids under control of stronger promoters (Wieczorke et al., 1999). Nevertheless, all of them—except Hxt12 (a pseudogene)—could transport hexoses. Obviously, however, they differ slightly with respect to their hexose specificities and kinetics.

Although no growth on glucose and no measureable glucose uptake activity could be detected, determination of the glucose consumption rate in the *hxt1–17 gal2* multiple deletion strain showed that, after growth on maltose, this strain still exhibited a glucose consumption rate of about 30% that of the wild-type rate. As glucose consumption ceased after about 15 h, the results indicated that *S. cerevisiae* possesses even more proteins that are able to transport glucose and are repressed in the presence of glucose. With overexpression of all of the remaining 16 sugar transporter genes of *S. cerevisiae* in the *hxt*-null strain, three proteins of the maltose transporter subfamily (Agt1, Ydl247, and Yjr160) could transport glucose, but not fructose or mannose. The corresponding genes were repressed by glucose. Additional deletion of all three genes in the *hxt1–17 gal2* mutant strain, resulting in the so-called "complete *hxt*-null strain," led to the complete loss of the ability to consume glucose (Wieczorke et al., 1999).

The two proteins Snf3 and Rgt2 also belong to the sugar transporter family of yeast and are closely related to the hexose transporters (Fig. 2.1). However, they act as glucose sensors and cannot transport glucose (see below). Surprisingly, after deletion of the *SNF3* gene in the complete *hxt*-null strain, the cells regained their ability to grow slowly on glucose, fructose, and mannose, at least at high concentrations (Wieczorke et al., 1999). Also, after overexpression of the Mth1 or Std1 genes, which are involved in the glucose induction pathway (see below), the *hxt*-null cells could grow on glucose (S. Krampe and E. Boles, unpublished). These observations, together with the finding that no other protein of the sugar transporter family could restore growth to the *hxt*-null strain after overproduction, indicate that at least one still-unknown protein exists in yeast that does not belong to the sugar transporter family but is able to take up glucose.

2.3 GLUCOSE SENSING AND SIGNALING

Glucose is a global metabolic regulator in yeast. It controls the expression of many genes involved in carbohydrate utilization at the level of transcription (Gancedo, 1998; Boles et al., 1997), and it induces the inactivation of several enzymes by posttranscriptional mechanisms (Holzer, 1989). The availability of glucose is first detected at the plasma membrane. Unlike bacterial cells that can sense glucose during transport and phosphorylation by the phosphotransferase system (Postma et al., 1993), yeast cells express two glucose transporter homologues, Snf3 and Rgt2, at their cell surface to sense glucose availability and concentration, and to transduce a signal for the transcriptional induction of other glucose transporters (Fig. 2.2) (Özcan et al., 1996a; 1998). Like all members of the yeast sugar transporter family, Snf3 and Rgt2 contain 12 putative membrane-spanning regions

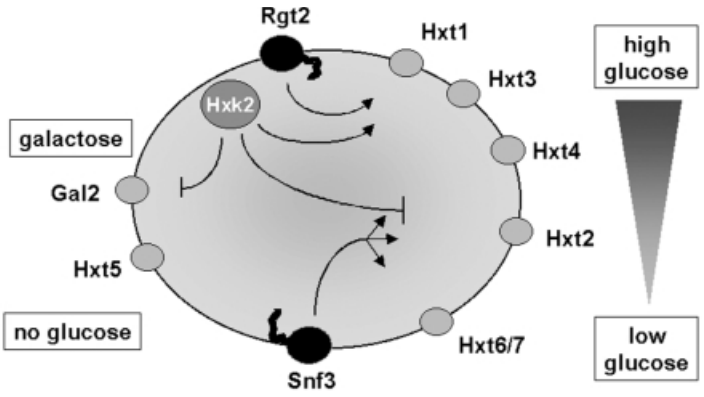

Figure 2.2. Schematic model of the function and regulation of the main hexose transporters of *S. cerevisiae*. Snf3 and Rgt2 are glucose sensors and activate a glucose-specific signaling pathway. Hxk2 (hexokinase II) is involved in the general glucose repression pathway and an *HXT1*-specific glucose induction pathway.

but, unlike the other members of this family, they possess unusually long additional sequences at their C-termini, which are predicted to be cytoplasmic. The C-terminal domains of Snf3 and Rgt2 mediate the signaling function of the proteins (Vagnoli et al., 1998; Özcan et al., 1998). Deletion of the extensions leads to a loss of sensor function.

Snf3 appears to be a sensor of low levels of glucose, which regulates mainly expression of high-affinity glucose transporters, and Rgt2 appears to be a sensor of high concentrations of glucose, which regulates expression of low-affinity glucose transporters (Fig. 2.2). Consequently, induction of high-affinity transporter Hxt2 by low levels of glucose is abolished in a *snf3* mutant, and induction of low-affinity transporter Hxt1 by high levels of glucose is strongly reduced in an *rgt2* mutant. Additionally, Snf3 is required at high levels of glucose for repression of the high-affinity transporters Hxt2, 6, and 7 (Vagnoli et al., 1998; Liang and Gaber, 1996). Dominant mutant forms of both Rgt2 and Snf3 have been identified, which signal in the complete absence of glucose (Özcan et al., 1996a). Despite the homology of Snf3 and Rgt2 to glucose permeases, neither of them can mediate significant glucose transport (Özcan et al., 1998; S. Dlugai and E. Boles, unpublished).

From these results the glucose sensors appear to function as two interacting domains: the C-terminal extensions that are required for the transmission of the glucose signal and the membrane-spanning domain that is necessary for glucose recognition. It is not known how the sensors recognize the glucose. Probably, the sensors act like receptors, which, on binding of glucose to the membrane-spanning domain, undergo a conformational shift to the C-terminus that might interact with proteins involved in transduction of the glucose signal.

Recently two proteins, Mth1 and Std1, have been detected to interact with the glucose sensors in the yeast two-hybrid system (Schmidt et al., 1999; Lafuente et al., 2000; Schulte et al., 2000). Interestingly, these proteins have also been shown to be partially localized within the nucleus and to interfere with the operation of the RNA polymerase II. It has been proposed that these proteins transduce the glucose signal from the plasma membrane to the nucleus. Other components known so far to be involved in glucose-induced

signal transduction are Rgt1, which acts as the transcriptional regulator of *HXT* gene expression (Özcan et al., 1996b), and a ubiquitin-conjugating enzyme complex (SCF^{Grr1}), which includes the F-box protein Grr1, Skp1, and Cdc53 (Özcan and Johnston, 1995; Li and Johnston, 1997; Skowyra et al., 1997). Rgt1 is a zinc cluster protein that binds directly to the promoters of the *HXT* genes. Rgt1 is a repressor of *HXT* genes in cells that grow without glucose and is a transcriptional activator of *HXT1* in cells that grow on high levels of glucose. It also has a neutral role in the presence of low levels of glucose. The SCF^{Grr1} complex is required for regulation of Rgt1 activity. Mth1 and Std1, as well as SCF^{Grr1}, act upstream of Rgt1 and downstream of the glucose sensors, but there is no clear epistatic relationship between Mth1/Std1 and SCF^{Grr1} (R. Wieczorke and E. Boles, unpublished).

2.4 PROPERTIES OF THE YEAST HEXOSE TRANSPORTERS

The main hexose transporters of yeast are encoded by genes *HXT1–7* and *GAL2* (Fig. 2.2). These proteins do not only differ with respect to their kinetic properties but are also expressed differentially in response to glucose. Indeed, five different kinds of transcriptional regulation can be distinguished: repression in the absence of glucose, induction by low levels of glucose, induction by high levels of glucose, induction by glucose but independent of the concentration, and repression by high levels of glucose (Boles and Hollenberg, 1997; Özcan and Johnston, 1999). Moreover, the insertion and removal of the proteins into the plasma membrane is regulated under certain conditions (Krampe et al., 1998; Kruckeberg et al., 1999). The expression pattern of the different Hxt proteins is consistent with their function as low-, intermediate-, or high-affinity transporters. *S. cerevisiae* cells express only those glucose transporters appropriate for the amount of extracellular glucose available (Fig. 2.2).

Most of the data on the kinetics of glucose transport mediated by the individual Hxt proteins were obtained by their expression in the *hxt*-null mutant. It has been argued that these values might not necessarily reflect the in vivo functions of these Hxt transporters. For instance, the affinities of some of the Hxt proteins might be modulated by their interaction with other transporters. However, a recent comparison of the expression of the individual *HXT* genes in a yeast wild-type strain grown under various conditions with the glucose transport kinetics of the same cultures revealed a broad agreement with the transport kinetics deduced in previous studies on single-*HXT* strains (Diderich et al., 1999).

Hxt1 is a glucose transporter with an extremely low affinity. In an Hxt1-only strain, its Km value was calculated to be about 100 mM (Reifenberger et al., 1997). In agreement with this, transcription of *HXT1* in a wild-type strain was associated with expression of low-affinity glucose transport. *HXT1* is strongly induced by high extracellular glucose concentrations but not by galactose, maltose, or ethanol. The transcript level increases with increasing glucose concentrations up to 200 mM. Carbon source-dependent expression of *HXT1* is controlled by at least two different signal transduction pathways: the Rgt2-dependent glucose induction pathway and another as yet unknown pathway, which requires the hexokinase II protein (Fig. 2.2) (Özcan and Johnston, 1999).

Hxt2: Surprisingly, glucose uptake kinetics of a *hxt*-null strain expressing only *HXT2* were dependent on the growth conditions of the cell (Reifenberger et al., 1997). After growth on 100 mM glucose, the Km value for glucose was about 10 mM. In contrast, after growth on low glucose concentrations the Hxt2-only strain displayed biphasic kinetics

with a high-affinity component (Km=1.5 mM) and a low-affinity component (Km = 60 mM). It is possible that the affinity of Hxt2 is modulated depending on the external glucose concentrations. Consistent with the finding of a high-affinity component, Hxt2 could restore growth of a *hxt*-null strain even on 5 mM glucose (Reifenberger et al., 1995). *HXT2* is induced only by low levels of glucose. It is repressed in the presence of high concentrations of glucose by Mig1, a DNA-binding repressor of many glucose-repressed genes (Özcan and Johnston, 1996). It is also repressed in the absence of glucose by the Rgt1 transcriptional repressor. *HXT2* expression increases only when cells are shifted from high to low glucose media, but not when approaching low glucose concentrations at the end of a batch-culture that started with 100 mM glucose. This finding indicates that expression requires both a low glucose concentration and exponentially growing cells.

Hxt3 is a low-affinity glucose transporter with a Km of about 60 mM; in wild-type cells, its transcription correlates with a substantial low-affinity transport component. Depending on the growth conditions and the strain background, *HXT3* expression was found to be either dependent on glucose but independent of its concentration (Özcan and Johnston, 1995) or, like *HXT1*, it increases with increasing glucose concentrations (Diderich et al., 1999).

Hxt4 has a moderately low affinity for glucose (Km about 9 mM). Contradictory results have been found in different studies concerning *HXT4* transcriptional regulation. In one study, the *HXT4* gene has been described as being induced by low levels of glucose but completely repressed at high levels, similar to *HXT2* (Özcan and Johnston, 1995). In another study, *HXT4* was induced only by elevated glucose concentrations, like *HXT1* (Diderich et al., 1999). DeRisi et al. (1997) detected *HXT4* mRNA late in fermentative growth and on glucose exhaustion. In our strains, *HXT4* is induced by glucose but independent of its concentration.

Hxt5 is expressed only in glucose-deprived cells or under a variety of starvation and stress conditions (Diderich et al., 1999; J. Becker and E. Boles, unpublished). It has an intermediate affinity for glucose and seems to be used to ensure that the yeast cells can utilize glucose rapidly as soon as it becomes available.

Hxt6 and Hxt7 are a pair of highly related glucose transporters. They are induced by low concentrations of glucose and are strongly repressed at higher concentrations. Transcriptional induction is under control of the Snf3-Mth1-SCF^{Grr1}-Rgt1 signaling pathway (Schulte et al., 2000). However, in contrast to all other Hxt, they exhibit a high basal expression level also during growth on alternative carbon sources. Transcription of *HXT7* is much stronger than that of *HXT6*. Both transporters are high-affinity glucose transporters (Km=1–2 mM) (Reifenberger et al., 1997). In agreement with this, *HXT7* was highly expressed in a wild-type strain under conditions that displayed a high-affinity kinetic component.

Gal2 is the yeast galactose permease, and its expression is induced by galactose and repressed by glucose. Nevertheless, it can transport galactose as well as glucose (Reifenberger et al., 1997). Galactose induction is under control of the Gal1/3-Gal80-Gal4 signaling pathway, which is activated directly by binding of intracellular galactose to Gal1 or Gal3 (Zenke et al., 1996; Sil et al., 1999).

Hxt8–17: With the exception of Hxt12, all of these transporters can transport hexoses (Wieczorke et al., 1999). However, under normal physiological conditions they are only very poorly transcribed. Therefore, it is reasonable to assume that they are involved in only very specific functions or that hexoses are not their true substrates. Hxt9 and 11 are

somehow involved in the pleiotropic drug-resistance mechanism and are induced by the Pdr1 and 3 transcription factors (Nourani et al., 1997). Hxt10 is one of 19 yeast genes coinduced by treatment of cells with antimycin and in a mutant lacking total mitochondrial genome (Epstein et al., 2001). *HXT1*3 is repressed by glucose via Mig1 and Mig2 (Lutfiyya et al., 1998). *HXT14* is induced some hours after transfer to sporulation medium during the completion of meiotic prophase (Chu et al., 1998).

What is the reason for such an extreme redundancy of hexose transporter genes in a unicellular organism? *S. cerevisiae* possesses glucose transporters with high, intermediate, low, and very low affinity. It could be argued that constitutive expression of one high-affinity, high-capacity glucose transporter should be enough to fulfill all the requirements of glucose uptake under any conditions. However, such an assumption seems not to be true. It has been shown that in yeast cells exhibiting only high-affinity glucose transport, at high extracellular glucose concentrations, the intracellular free glucose causes a significant inhibition of glucose uptake, which thereby reduces the glucose influx by up to 50% (Teusink et al., 1998). Consistent with these considerations, an *hxt*-null strain constitutively expressing only the high-affinity transporter Hxt7 exhibited significantly reduced growth rates at high glucose concentrations (S. Krampe and E. Boles, unpublished). Instead, at any specific extracellular glucose concentration, yeast cells express only those transporters with kinetic properties appropriate for this concentration. The maximal rate of glucose transport is fairly constant in cells taken from various time points of a batch culture started with 100 mM glucose and only the affinity for glucose changes (Walsh et al., 1994). Based on the expression profile of the different glucose transporters with different kinetic properties, it seems that yeast cells try to avoid running their glucose transport at its maximal rate. This would ensure that glucose uptake is always directly dependent on the extracellular glucose concentration. This seems to be especially important in view of the observation that glucose influx also performs some regulatory functions (Reifenberger et al., 1997; Boles et al., 1997; Thevelein and de Winde, 1999).

However, even those regulatory and kinetic constraints would not explain the existence of more than 18 hexose transporters. Noteworthy, eight of the *HXT* genes (*HXT8*, *9*, *11–13*, *15–17*) are in or adjacent to the subtelomeric regions of their chromosomes (Kruckeberg, 1996). Thus, the high levels of recombination and gene duplication at subtelomeric regions may explain their abundance. It is a common feature of many genes involved in carbon metabolism that they occur as families distributed in subtelomeric positions in multiple chromosomes. Moreover, it has been observed that under certain conditions—as in a continuous, glucose-limited environment—yeast cells still increased their number of glucose transporter genes. Analysis of a population of yeast cells that underwent 450 generations of glucose-limited growth revealed the occurrence of multiple tandem duplications involving the *HXT6* and *7* loci (Brown et al., 1998). Thus, some of the yeast glucose transporter genes might represent only surplus genes that have evolved and can be used under some extreme conditions.

2.5 YEAST *HXT*-MUTANTS AS A HETEROLOGOUS EXPRESSION SYSTEM

Heterologous expression of membrane transporters from animal cells, humans, parasites, plants, or microorganisms, in an easily usable expression system, could be a powerful tool to study function, structure, and pharmacological properties. It could also be used to de-

velop high-throughput screening assays for identifying specific agonists or antagonists of these proteins among the molecules present in libraries of chemical compounds. The yeast *S. cerevisiae* provides such a useful system, as it is easy to handle and grows fast and also because its physiology is well known and its molecular biology and genetics are well established. We have already used the yeast *hxt*-null strain to clone and characterize sugar transporters from other organisms, such as mammals, parasites, plants, and other yeasts.

2.6 GLUCOSE TRANSPORTERS FROM *PICHIA STIPITIS*

We have used the *hxt*-null strain to clone sugar transporters of the xylose-utilizing yeast *Pichia stipitis* (Weierstall et al., 1999). A DNA library from genomic DNA of *P. stipitis* was constructed and transformed into the *S. cerevisiae hxt*-null strain, which is unable to take up and to grow on glucose as the sole carbon source. First, uptake of the gene library plasmids was selected on medium without uracil (as the plasmids carried the *URA3*-selectable marker gene) and with maltose as a permissive carbon source. The transformants were replica plated onto selective medium with 2% glucose. After some days of incubation at 30°C, several colonies that could grow on glucose appeared. The plasmids were re-isolated out of the transformants, further characterized, and sequenced. Using this strategy, we finally were able to clone and characterize three different glucose transporters, *SUT1–3*, from *P. stipitis*.

2.7 MAMMALIAN GLUCOSE TRANSPORTERS

We have also used the *hxt*-null strain to characterize the mammalian GLUT1 glucose transporter (Wieczorke, 2001). First, we found that expression of GLUT1 did not support growth of the *hxt*-null strain on glucose. However, we observed that, after prolonged incubation on a glucose medium of the GLUT1 transformants suppressor, colonies appeared that obviously had become able to take up and consume glucose. Possible reasons for the restoration of growth on glucose could be a) a mutation in the GLUT1 sequence that converts GLUT1 into a functional glucose transporter in yeast; b) a mutation in the yeast genome that eliminates an inhibitory effect on functional GLUT1 expression in yeast; or c) a mutation in the yeast genome that converts an endogenous yeast protein into a glucose transporter or induces expression of an unknown silent glucose transporter. To distinguish among these three possiblities, some of the GLUT1 suppressor mutants were grown in nonselective yeast extract-peptone maltose medium for more than 15 generations. All the cells, which had lost their plasmids, could no longer grow on media containing glucose as the carbon source, which indicated that former growth was dependent on GLUT1. The GLUT1 plasmids were re-isolated out of the suppressor mutants, amplified in *E. coli*, and transformed back into the original *hxt*-null strain. Some of them could confer growth on glucose to all the transformants, indicating that they contain mutations in the GLUT1 sequences that convert GLUT1 into a functional glucose transporter in yeast. We observed that, in one of the mutant strains that had lost its plasmids, all the transformants regained the ability to grow on glucose after re-transformation of the original wild-type GLUT1 plasmid, which indicated that the strain contained a mutation in its genome that eliminated the inhibitory effect on func-

tional GLUT1 expression. This strain could then be used to characterize the kinetic and pharmacological properties of GLUT1, by using simple growth assays as well as sugar uptake experiments with radiolabeled sugars.

We found that all of the mammalian glucose transporters, GLUT1–GLUT5, GLUT11, and SGLT1, could not directly restore hexose uptake or growth of the *hxt*-null strain on hexoses. For some of them, we have also already isolated yeast mutant strains in which the inhibitory function on functional expression was eliminated. However, several plant hexose transporters, the THT1 glucose transporter of the mammalian form of African trypanosomes, and several hexose transporters from other yeast species were functional in the yeast *hxt*-null strain without any additional mutations and could restore growth on glucose.

2.8 STRATEGIES FOR CHARACTERIZING SUGAR TRANSPORTER-HOMOLOGOUS SEQUENCES

As described above, the *hxt*-null strain should be a valuable tool for cloning and characterizing sugar transporters from a variety of different organisms. This can be accomplished, as in the case of *P. stipitis*, with cDNA or genomic DNA libraries. Alternatively, we have optimized a new method we call "recombination-cloning," which allows a very fast and simple characterization of any sugar transporter-related sequence discovered during systematic sequencing of genomes (Fig. 2.3).

This method takes advantage of the very efficient mechanisms for homologous recombination in yeast. A yeast expression vector with a strong and carbon source-independent promoter (e.g., *ADH1*, *PGK1*, *MET25*, $HXT7^{(1–392)}$,…) is linearized with one or two restriction enzymes between the promoter and terminator sequences. It should be stressed here that the yeast *GAL* promoters, as present in many commercially available plasmids, should not be used to clone heterologous glucose transporter genes, as these promoters must be induced with galactose and are repressed by glucose. Both processes are dependent on the uptake of the sugars. The coding region of the putative sugar transporter gene is amplified by PCR from DNA libraries, genomic DNA, or by reverse transcriptase (RT)-PCR directly from RNA. The primers (55- to 60-mer oligonucleotides) should have the following features: From 5′ to 3′, the first primer has 35–40 nucleotides homologous to the promoter region on the plasmid from –40/35 to –1, followed by 20 nucleotides of sequence derived from the beginning of the coding region of the transporter gene, including the start codon. The second primer (from 5′ to 3′) has 35–40 nucleotides homologous to the complementary sequence of the beginning of the termination region, followed by 20 nucleotides complementary to the end of the coding region of the transporter gene, including the stop codon. Thus, the resulting PCR product contains the entire coding region flanked on both sites by 35 to 40 bp of DNA sequences identical to the sequences on the ends of the linearized plasmid.

The linearized plasmid is transformed into the *hxt*-null strain, together with the PCR-amplified sugar transporter cassette, and cells are plated onto selective media (selecting for the plasmid marker) with 2% maltose. Normally, the linearized plasmid will be degraded rapidly in the yeast cells. However, if homologous recombination occurs between the ends of the PCR product and the ends of the plasmid, the plasmid will be repaired, enabling growth of the cells on the selective medium and placing the transporter gene under control of the yeast promoter/terminator on the plasmid. The transformants can then be

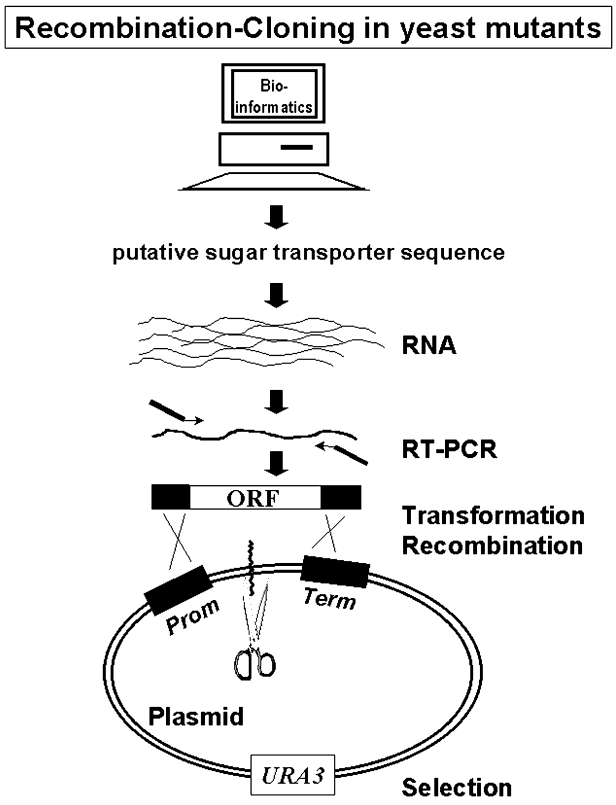

Figure 2.3. Flow diagram for recombination cloning in yeast mutants.

replica plated on media with different concentrations (0.1–5%) of glucose, fructose, mannose, galactose, and even sucrose (as sucrose can be metabolized by intracellular invertase activities but is not taken up by the *hxt*-null strain, it is even possible to select for sucrose transporters). If most of the transformants can grow on one or all of the various hexose media plates, the heterologous gene most likely encodes a sugar transporter. If all the transformants do not grow on hexoses, it is still possible that the transporter is not functional in yeast, such as GLUT1. In this case, several transformants should be mixed and subject to a sublethal mutagenic dose of UV-light and selected for the occurrence of suppressor colonies on the various hexose media (see below; Fig. 2.4).

In any case, if yeast transformants appear to grow on hexose media, it is absolutely necessary to characterize the plasmids after re-isolation and also to characterize the plasmid-cured yeast strains as described above for *P. stipitis SUT1–3* and mammalian GLUT1.

2.9 PROTOCOL

General yeast genetic and molecular biology methods are described in Guthrie and Fink (1991). The complete *hxt*-null strain EBY.VW4000 (Wieczorke et al., 1999), a suitable

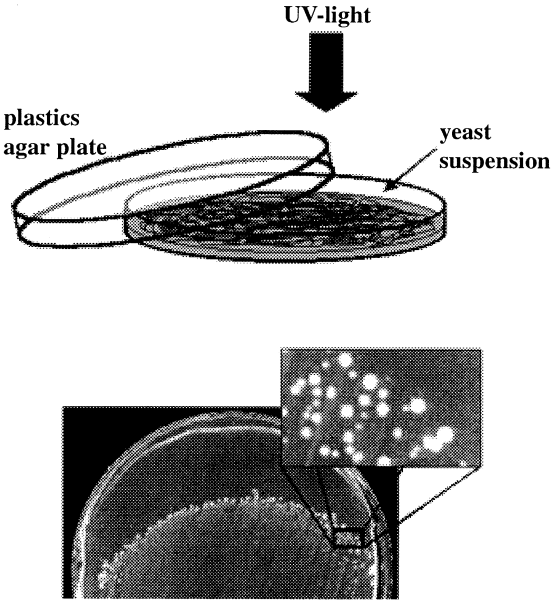

Figure 2.4. Schematic illustration of the selection of yeast suppressor mutants by UV-light. In the lower part, GLUT1 transformants of the *hxt*-null strain are shown, which were plated on 2% glucose medium, irradiated with UV-light for 15 min, and incubated at 30°C for 5 days.

yeast expression vector and an *HXT*-control plasmid, can be obtained on request by the author.

A) Preparation of PCR-cassette and linearized vector

1. Generate by PCR the transporter gene cassette with short flanking homology to the promoter and terminator regions of the yeast expression vector. Purify the PCR fragment after agarose gel electrophoresis or by using a PCR-product purification system.
2. Digest a yeast expression vector with one or two restriction enzymes cutting between the promoter and terminator sequences. If there are overhanging sequences left between the restriction enzyme cutting site and the short flanking homology regions, these will be removed automatically by homologous recombination in yeast. Purify the linearized vector after agarose gel electrophoresis.

B) *S. cerevisiae* transformation (modified from Gietz and Woods, 1994)

1. Inoculate a 5 ml YPM (see "Media and Solutions" below) preculture of the *hxt*-null strain from some yeast colonies on an agar plate and grow overnight at 30°C. This preculture can be stored at 4°C up to 3 months.
2. Determine the cell density of the preculture by measuring the optical density at 600 nm (dilutions should be made above an OD_{600nm} of 0.5).

3. Inoculate a 50 ml YPM culture with an OD_{600nm} ~0.02, and grow cells at 30°C until an OD_{600nm} of about 0.5–1 (usually overnight).
4. Collect cells by centrifugation at 1,500 g for 5 min in 50 ml tubes.
5. Resuspend the pellet in 20 ml of sterile water, and centrifuge again at 1,500 g for 5 min.

During this period, prepare 2 ml of 100 mM LiAc from 1 M LiAc stock solution and denature sheared salmon testes carrier DNA by boiling for 10 min and immediately placing on ice.

6. Resuspend the pellet in 1 ml of the freshly prepared 100 mM LiAc solution, and transfer the suspension into a 1.5 ml reaction tube.
7. Centrifuge at 5,000 g for 5 min, remove the supernatant, and resuspend the cells in 0.5 ml of the freshly prepared 100 mM LiAc solution.
8. Pipette 50 µl aliquots of the yeast suspension into sterile 1.5 ml reaction tubes, centrifuge at 5,000 g for 5 min, and remove the supernatants.
9. Add 240 µl 50% (w/v) PEG3350, 36 µl 1 M LiAc, and 5 µl of carrier DNA (10 µg/µl) to the yeast cells.
10. Add 0.1–0.5 µg linearized plasmid, between 1–5 µg of the PCR-DNA and sterile water (altogether 70 µl) to the yeast cells.
11. Vortex each tube for about 1 min (the yeast pellet should be resolved completely).
12. Incubate the cells at 30°C for 30 min.
13. Heat shock the transformation tubes at 42°C for 20 min.
14. Centrifuge the transformation tubes at 5000 rpm for 5 min, remove the PEG/LiAc supernatant with a pipette, and resuspend the cells in 1 ml sterile water.
15. Centrifuge again at 5000 rpm for 5 min, remove the supernatant, and resuspend the cells in 100 µl sterile water.
16. Plate the suspension on agar plates containing selective YNB (see "Media and Solutions" below) medium with 1% maltose.
17. Incubate plates at 30°C for 2–3 days.

It is recommended that controls include one transformation tube without any DNA, one tube with only the linearized plasmid, one tube with the empty plasmid, and one tube with a yeast *HXT*-control plasmid. Normally 0–10 colonies will appear on the control plate with only the linearized vector, and 50–1000 colonies will appear on the vector/PCR-DNA plate. No colonies should appear on the water control plates.

Media and Solutions

- YPM: 1% yeast extract, 2% bactopeptone, and 1% maltose.
- YNB selective medium: 0.67% Difco yeast nitrogen base, supplemented with 0.1 mM adenine; 0.2 mM arginine and tryptophan; 0.3 mM histidine, methionine, phenylalanine, and tyrosine; 0.4 mM isoleucine and lysine; and 0.5 mM threonine; leucine, uracil, and valine, but omit the plasmid-selective marker supplement, pH 6.2, plus carbon source.
- For agar plates, add 1.5–2% agar.
- 1 M LiAc.

- 50% (w/v) PEG3350.
- Carrier DNA (10 μg/μl): weigh out 1 g of high-molecular-weight DNA (deoxyribonucleic acid sodium salt type III from salmon testes) into 100 ml of TE buffer (10 mM Tris-HCl, pH 8.0, and 1.0 mM ethylene diamine tetraacetate [EDTA]). Disperse the DNA into solution by drawing it up and down repeatedly in a 10 ml pipette. Mix vigorously on a magnetic stirrer overnight at 4°C. Aliquot the DNA and store it at –20°C.

C) Growth Tests

Replica plate the transformants onto various selective hexose-media agar plates (glucose, mannose, fructose, galactose, sucrose; suggested concentrations, 2 g/l and 20 g/l final concentration). An agar plate can be replica plated successively at least on five additional agar plates.

Incubate the replica plated hexose-media plates for up to 4 days at 30°C. If several transformants appear to grow compared with the transformants containing the empty plasmid, purify some of them from background by streaking out cells on selective maltose-media plates growing into single separated colonies. Replica plate again on hexose-media plates in order to confirm the previous results. For further experiments (e.g., re-isolation of the plasmids, …) take colonies from the corresponding maltose plates only and grow them only in selective maltose medium. This procedure is absolutely necessary in order to avoid the selection of secondary-site mutations accelerating growth on hexose media.

In case no transformants grow on hexose-media plates, mix several transformants and plate them on new hexose-media plates. To induce mutations, open the lid of the agar plate about halfway and irradiate with UV-light for about 10–15 min as shown in Fig. 2.4. Incubate the plates at 30°C for about 7–10 days. Suppressor colonies will appear mainly at the border between those areas getting lethal doses of UV-light and those in the shadow of the lid.

D) Analysis of the Plasmids

As re-isolation of plasmids from yeast cells yields only very low amounts of DNA, which are insufficient for further analysis, re-isolated plasmid DNA must first be transformed into *E. coli* cells and isolated in larger quantities from the bacterial cells. All of the common yeast plasmids are yeast-*E. coli* shuttle plasmids. Re-isolation of plasmids from yeast cells can be performed under the same standard protocols as used for *E. coli* cells, but first the yeast cell walls must be broken by adding 2/3 volumes of glass beads (diameter 0.45 mm) to a collected yeast suspension and by vigorously shaking for 5 min (Boles and Zimmermann, 1993). The amplified plasmids should be transformed back into the *hxt*-null strain or the plasmid-cured mutant strains and should confer growth to all transformants on the corresponding hexose-media plates.

ACKNOWLEDGMENTS

I am indebted to my co-workers K. Freidel, S. Krampe, R. Wieczorke, S. Dlugai, T. Weierstall, F. Schulte, J. Becker, T. Hamacher, and J. Makuc, who contributed to the

work performed in my lab. I thank C.P. Hollenberg for his kind support. This article is dedicated to the memory of M. Ciriacy, who initiated the work on yeast hexose transporters in the laboratory in Duesseldorf. Work in my laboratory is supported by funds from the European Commission, the Bundesministerium fuer Bildung und Forschung, the Deutsche Forschungsgemeinschaft, the Internationale Brachet Stiftung, and Aventis Pharma Deutschland GmbH.

ANNOTATED REFERENCES

Baudin A, Ozier-Kalogeropoulos O, Denouel A, Lacroute F, Cullin C (1993): A simple and efficient method for direct gene deletion in *Saccharomyces cerevisiae*. Nucleic Acids Res 21:3329–3330.

Bisson LF, Coons DM, Kruckeberg AL, Lewis DA (1993): Yeast sugar transporters. Crit Rev Biochem Mol Biol 28:259–308.

Boles E, Hollenberg CP (1997): The molecular genetics of hexose transport in yeasts. FEMS Microbiol Rev 21:85–111.

Boles E, Müller S, Zimmermann FK (1996): A multi-layered sensory system controls yeast glycolytic gene expression. Mol Microbiol 19:641–642.

Boles E, Zimmermann FK (1993): *Saccharomyces cerevisiae* phosphoglucose isomerase and fructose bisphosphate aldolase can be replaced functionally by the corresponding enzymes of *Escherichia coli* and *Drosophila melanogaster*. Curr Genet 23:187–191.

Boles E, Zimmermann FK, Thevelein JM (1997): Metabolic signals. In Zimmermann FK, Entian KD (eds): Yeast sugar metabolism: Biochemistry, genetics, biotechnology and applications. Lancaster, PA: Technomic, pp 379–407.

Brown CJ, Todd KM, Rosenzweig RF (1998): Multiple duplications of yeast hexose transport genes in response to selection in a glucose-limited environment. Mol Biol Evol 15:931–942.

Chu S, DeRisi JL, Eisen M, Mulholland J, Botstein D, Brown PO, Herskowitz I (1998): The transcriptional program of sporulation in budding yeast. Science 282:699–705.

DeRisi JL, Iyer VR, Brown PO (1997): Exploring the metabolic and genetic control of gene expression on a genomic scale. Science 278:680–686.

Diderich JA, Schepper M, van Hoek P, Luttik MA, van Dijken JP, Pronk JT, Klaassen P, Boelens HF, de Mattos MJ, van Dam K, Kruckeberg AL (1999): Glucose uptake kinetics and transcription of *HXT* genes in chemostat cultures of *Saccharomyces cerevisiae*. J Biol Chem 274:15350–15359.

This work relates glucose uptake kinetics of *S. cerevisiae* wild-type cells under various defined conditions to the transcription of all 20 members of the yeast hexose transporter (*HXT*) gene family. A consistent relationship was observed between the expression of individual *HXT* genes, glucose uptake kinetics of the individual transporters, and glucose transport kinetics of wild-type cells. This paper is of special interest as it evaluates the functional role of individual hexose transporters in their wild-type context.

Epstein CB, Waddle JA, Hale W 4th, Dave V, Thornton J, Macatee TL, Garner HR, Butow RA (2001): Genome-wide responses to mitochondrial dysfunction. Mol Biol Cell 12:297–308.

Gancedo JM (1998): Yeast carbon catabolite repression. Microbiol Mol Biol Rev 62:334–361.

Gietz RD, Woods RA (1994): High efficiency transformation with lithium acetate. In Johnston JR (ed): Molecular Genetics of Yeast: A Practical Approach. Oxford: IRL Press, pp 121-134.

Güldener U, Heck S, Fielder T, Beinhauer J, Hegemann JH (1996): A new efficient gene disruption cassette for repeated use in budding yeast. Nucleic Acids Res 24:2519-2524.

Guthrie C, Fink GR (1991): Methods in Enzymology: Guide to Yeast Genetics and Molecular Biology, Vol. 194. San Diego: Academic Press, Inc.

Holzer H (1989): Proteolytic catabolite inactivation in *Saccharomyces cerevisiae*. Revis Biol Celular 21:305–319.

Krampe S, Stamm O, Hollenberg CP, Boles E (1998): Catabolite inactivation of the high-affinity hexose transporters Hxt6 and Hxt7 of *Saccharomyces cerevisiae* occurs in the vacuole after internalization by endocytosis. FEBS Lett 441:343–347.

Kruckeberg AL (1996): The hexose transporter family of *Saccharomyces cerevisiae*. Arch Microbiol 166:283–292.

Kruckeberg AL, Ye L, Berden JA, van Dam K (1999): Functional expression, quantification and cellular localization of the Hxt2 hexose transporter of *Saccharomyces cerevisiae* tagged with the green fluorescent protein. Biochem J 339:299–307.

Lafuente MJ, Gancedo C, Jauniaux JC, Gancedo JM (2000): Mth1 receives the signal given by the glucose sensors Snf3 and Rgt2 in *Saccharomyces cerevisiae*. Mol Microbiol 35:161–172.

Lagunas R (1993): Sugar transport in *Saccharomyces cerevisiae*. FEMS Microbiol Rev 10:229–242.

Li FN, Johnston M (1997): Grr1 of *Saccharomyces cerevisiae* is connected to the ubiquitin proteolysis machinery through Skp1: Coupling glucose sensing to gene expression and the cell cycle. EMBO J 16:5629–5638.

Liang H, Gaber RF (1996): A novel signal transduction pathway in *Saccharomyces cerevisiae* defined by Snf3-regulated expression of *HXT6*. Mol Biol Cell 7:1953–1966.

Lutfiyya LL, Iyer VR, DeRisi JL, DeVit MJ, Brown PO, Johnston M (1998): Characterization of three related glucose repressors and genes they regulate in *Saccharomyces cerevisiae*. Genetics 150:1377–1391.

Nourani A, Wesolowski-Louvel M, Delaveau T, Jacq C, Delahodde A (1997): Multiple-drug-resistance phenomenon in the yeast *Saccharomyces cerevisiae*: Involvement of two hexose transporters. Mol Cell Biol 17:5453–5460.

Orr-Weaver TL, Szostak JW, Rothstein RJ (1981): Yeast transformation: A model system for the study of recombination. Proc Natl Acad Sci USA 78:6354–6358.

Özcan S, Dover J, Johnston M (1998): Glucose sensing and signaling by two glucose receptors in the yeast *Saccharomyces cerevisiae*. EMBO J 17:2566–2573.

Özcan S, Dover J, Rosenwald AG, Wölfl S, Johnston M (1996a): Two glucose transporters in *Saccharomyces cerevisiae* are glucose sensors that generate a signal for induction of gene expression. Proc Natl Acad Sci USA 93:12428–12432.

Two members of the yeast glucose transporter family were shown to function as glucose sensors rather than glucose transporters. One of them, Snf3, appears to be a sensor of low concentrations of glucose and may be responsible for the induction of high-affinity glucose transporters. The other one, Rgt2, functions as a sensor for high concentrations of glucose and regulates induction of low-affinity glucose transporters. This paper is of particular interest as it provides the first demonstration of a new kind of eukaryotic nutrient sensor.

Özcan S, Johnston M (1995): Three different regulatory mechanisms enable yeast hexose transporter (*HXT*) genes to be induced by different levels of glucose. Mol Cell Biol 15:1564–1572.

Four of the main hexose transporter genes of *S. cerevisiae*, *HX1-HXT4*, were shown to be regulated by three different mechanisms: i) induction by high glucose concentrations, ii) induction by low glucose concentrations and repression at high glucose levels, and iii) induction by glucose independent of sugar concentration. Components of the signal transduction pathways were identified, and a model for glucose-regulated gene expression was proposed.

Özcan S, Johnston M (1996): Two different repressors collaborate to restrict expression of the yeast glucose transporter genes *HXT2* and *HXT4* to low levels of glucose. Mol Cell Biol 16:5536–5545.

Özcan S, Johnston M (1999): Function and regulation of yeast hexose transporters. Microbiol Mol Biol Rev 63:554–569.

Özcan S, Leong T, Johnston M (1996b): Rgt1p of *Saccharomyces cerevisiae*, a key regulator of glucose-induced genes, is both an activator and a repressor of transcription. Mol Cell Biol 16:6419–6426.

Paulsen IT, Sliwinski MK, Nelissen B, Goffeau A, Saier MH Jr. (1998): Unified inventory of established and putative transporters encoded within the complete genome of *Saccharomyces cerevisiae*. FEBS Lett 430:116–125.

Postma PW, Lengeler JW, Jacobson GR (1993): Phosphoenolpyruvate: Carbohydrate phosphotransferase systems of bacteria. Microbiol Rev 57:543–594.

Reifenberger E, Boles E, Ciriacy M (1997): Kinetic characterization of individual hexose transporters of *Saccharomyces cerevisiae* and their relation to the triggering mechanisms of glucose repression. Eur J Biochem 245:324–333.

Various yeast strains, each expressing only one of the major hexose transporters of *S. cerevisiae*, were used to determine the glucose uptake kinetics of the individual transporters. These could be grouped into three kinds of transporters: those with a very low affinity (Hxt1, 3), intermediate affinity (Hxt2, 4) and high affinity (Hxt6, 7). Moreover, it was shown that the glucose transporters themselves are not directly involved in the mechanisms of glucose-regulated gene expression.

Reifenberger E, Freidel K, Ciriacy M (1995): Identification of novel *HXT* genes in *Saccharomyces cerevisiae* reveals the impact of individual hexose transporters on glycolytic flux. Mol Microbiol 16:157–167.

Ronne H (1995): Glucose repression in fungi. Trend Genet 11:12–17.

Schmidt MC, McCartney RR, Zhang X, Tillman TS, Solimeo H, Wolfl S, Almonte C, Watkins SC (1999): Std1 and Mth1 proteins interact with the glucose sensors to control glucose-regulated gene expression in *Saccharomyces cerevisiae*. Mol Cell Biol 19:4561–4571.

Schulte F, Wieczorke R, Hollenberg CP, Boles E (2000): The *HTR1* gene is a dominant negative mutant allele of *MTH1* and blocks Snf3- and Rgt2-dependent glucose signaling in yeast. J Bacteriol 182:540–542.

Sil AK, Alam S, Xin P, Ma L, Morgan M, Lebo CM, Woods MP, Hopper JE (1999): The Gal3p-Gal80p-Gal4p transcription switch of yeast: Gal3p destabilizes the Gal80p-Gal4p complex in response to galactose and ATP. Mol Cell Biol 19:7828–7840.

Skowyra D, Craig KL, Tyers M, Elledge SJ, Harper JW (1997): F-box proteins are receptors that recruit phosphorylated substrates to the SCF ubiquitin-ligase complex. Cell 91:209–219.

Teusink B, Diderich JA, Westerhoff HV, van Dam K, Walsh MC (1998): Intracellular glucose concentration in derepressed yeast cells consuming glucose is high enough to reduce the glucose transport rate by 50%. J Bacteriol 180:556–562.

Thevelein JM, de Winde JH (1999): Novel sensing mechanisms and targets for the cAMP-protein kinase A pathway in the yeast *Saccharomyces cerevisiae*. Mol Microbiol 33:904–918.

Vagnoli P, Coons DM, Bisson LF (1998): The C-terminal domain of Snf3p mediates glucose-responsive signal transduction in *Saccharomyces cerevisiae*. FEMS Microbiol Lett 160:31–36.

van Belle D, André B (2001): A genomic view of yeast membrane transporters. Curr Opin Cell Biol 13:389–398.

Wach A, Brachat A, Pohlmann R, Philippsen P (1994): New heterologous modules for classical or PCR-based gene disruptions in *Saccharomyces cerevisiae*. Yeast 10:1793–1808.

Walsh MC, Smits HP, Scholte M, van Dam K (1994): Affinity of glucose transport in *Saccharomyces cerevisiae* is modulated during growth on glucose. J Bacteriol 176:953–958.

Weierstall T, Hollenberg CP, Boles E (1999): Cloning and characterization of three genes (*SUT1-3*) encoding glucose transporters of the yeast *Pichia stipitis*. Mol Microbiol 31:871–883.

Three glucose transporter genes from the yeast *P. stipitis* were cloned and characterized by heterologous expression in an *S. cerevisiae* strain unable to take up glucose due to the deletion of its main glucose transporter genes. This paper is of special interest because it describes how an *S. cerevisiae* hexose transport-deficient yeast strain can be used to clone and characterize glucose transporters from other organisms.

Weusthuis RA, Pronk JT, van den Broek PJ, van Dijken JP (1994): Chemostat cultivation as a tool for studies on sugar transport in yeasts. Microbiol Rev 58:616–630.

Wieczorke R (2001): Molekulargenetische und physiologische Untersuchungen zur Funktion von *FGY1* bei der heterologen Expression von Glukosetransportern in der Hefe *Saccharomyces cerevisiae*. Ph.D. thesis, Heinrich-Heine-Universität Düsseldorf.

Wieczorke R, Krampe S, Weierstall T, Freidel K, Hollenberg CP, Boles E (1999): Concurrent knock-out of at least 20 transporter genes is required to block uptake of hexose in *Saccharomyces cerevisiae*. FEBS Lett 464:123–128.

This paper describes the construction of a yeast strain completely deficient in the uptake of hexoses. Twenty different transporters were identified in *S. cerevisiae* that could mediate the uptake of hexoses across the plasma membrane. Targeted deletion of all the corresponding genes resulted in a yeast strain unable to consume glucose and grow on glucose as the sole carbon source. This strain provides a valuable tool for the cloning and characterization of hexose transporters from other organisms.

Zenke FT, Engles R, Vollenbroich V, Meyer J, Hollenberg CP, Breunig KD (1996): Activation of Gal4p by galactose-dependent interaction of galactokinase and Gal80p. Science 272:1662–1665.

CHAPTER 3

NEUROTRANSMITTER TRANSPORTERS OF *DROSOPHILA*

MARTIN G. BURG AND WILLIAM L. PAK

3.1 INTRODUCTION

In this chapter, we will consider neurotransmitter transporters (NTTs) identified in *Drosophila*. Neurotransmitter transporters are located on the plasma membranes of neurons and glia in the synaptic region, and they regulate the duration of synaptic activity by removing transmitters released into the synaptic cleft.

NTTs fall into two distinct multigene superfamilies: a) excitatory amino acid transporters and b) Na^+/Cl^--dependent transporters. The members of the first superfamily include transporters of such excitatory amino acids as glutamate and aspartate, and of certain neutral amino acids, whereas the members of the second superfamily include transporters of γ-aminobutyric acid, serotonin, dopamine, norepinephrine, epinephrine, glycine, proline, taurine, betaine, and creatine (Shafqat et al., 1993). Members of each superfamily have sequence homology with each other but not with members of the other superfamily. The membrane topology also differs between members of the two superfamilies. The first family is thought to have 8–12 putative transmembrane domains (TMDs), whereas all known members of the second family have 12 TMDs.

Before 1994, all molecularly characterized NTTs were mammalian. Because *Drosophila* offers the possibility of molecular genetic dissection of the transport process, several investigators have turned to *Drosophila* to isolate and characterize *Drosophila* homologues of mammalian NTTs. Two NTTs of each superfamily have now been cloned in *Drosophila* by cDNA cloning, which takes advantage of interspecies homology, and were characterized functionally by expressing in cell lines and/or *Xenopus* oocytes. However, in vivo functions have not been determined for any of these. Perhaps the most important reason for using *Drosophila* is that it is one of the few organisms that offer the possibility of carrying out "forward genetics." That is, one can isolate mutants with appropriate phenotypes first and then isolate the genes and gene products corresponding to the mutants. One infers the in vivo functions of the proteins from the mutant phenotypes. Potentially, such an approach would allow one to determine both the molecular structure of the protein and its presumptive function in vivo. Moreover, the approach can identify a novel class of proteins because no a priori assumption is made about the nature of the proteins in cloning the genes. There have been two examples of NTTs identified by a forward genetic approach in *Drosophila.* Both are members of the Na+/Cl^--dependent transporter superfamily. One of these, Blot, appears to have its main function outside the nervous

Transmembrane Transporters. Edited by Michael Quick

ISBNs: 0-471-06517 (Hardcover); 0-471-43404-3 (Electronic)

system. The other one, *RosA/Ine*, however, was identified because of the profound effects mutations in the *rosa/ine* gene have on nervous functions. However, the substrate has not yet been identified for either transmitter.

In the following, we will present an overview of the *Drosophila* NTTs identified to date. We will concentrate our discussion on the genes identified by forward genetics and discuss, in particular, the *rosA/ine* gene in some detail.

3.2 EXCITATORY AMINO ACID TRANSPORTERS

Two different excitatory amino acid transporters have been reported for *Drosophila* to date: dEAAT1 and dEAAT2 (*Drosophila* excitatory amino acid transporters 1 and 2) (Seal et al., 1998; Besson et al., 1999, 2000; Kawano et al., 1999). The first of these was first reported by Seal et al. (1998). Subsequently, two other groups, Besson et al. (1999) and Kawano et al. (1999), independently reported the isolation and characterization of the same transporter, referring to it as dEAAT1 (Besson et al., 1999) and Dglt-1 (Kawano et al., 1999), respectively. All three groups used basically the same cloning strategy. Degenerate primers were designed from conserved regions of known mammalian glutamate transporters and were used to obtain partial *Drosophila* cDNA by reverse transcriptase polymerase chain reaction (RT-PCR). Partial cDNA clones were used as probes to screen a *Drosophila* cDNA library to isolate longer cDNA clones.

The open reading frames contained in the long cDNA clones isolated by the three groups predicted the same 479 amino acid protein having 35–45% sequence identity with previously identified glutamate transporters. The protein was most homologous to the lepidopteran *Trichoplusia* glutamate receptor (Donly et al., 1997) at 59% identity (Besson et al., 1999). The hydropathy profile of the protein was very similar to that reported for other glutamate transporters and revealed 8–10 hydrophobic stretches, although the exact number of TMDs was unclear (Seal et al., 1998; Besson et al., 1999; Kawano et al., 1999).

In situ hybridization to polytene chromosomes showed that the gene encoding the protein localized to 30A7-8 on the left arm of the second chromosome (Besson et al., 1999). Northern blot analysis revealed a single transcript of ~3.3 kb expressed abundantly in adult heads and at a much lower level in adult bodies (Seal et al., 1998; Besson et al., 1999). Weak expression was also detected in late embryos and larvae (Besson et al., 1999; Kawano et al., 1999).

The spatial pattern of dEAAT1 transcript expression was examined by in situ hybridization at three different developmental stages: stage 16 embryos (Seal et al., 1998; Besson et al., 1999; Kawano et al., 1999), the isolated central nervous system (CNS) of third instar larvae, and the adult brain (Besson et al., 1999). At stage 16, the dEAAT transcript was expressed exclusively in the brain and the ventral nerve cord. In the CNS of third instar larvae, strong expression of the transcript was observed in the optic lobe in characteristic half-ring structures. Also stained were numerous large cell bodies in the brain and ventral ganglia, which could be interneurons of the brain and motor neurons in the nerve cord, respectively. In the adult, an intense labeling was detected in the medulla of the optic lobe but not in the retina or lamina.

Functional assays were carried out by expressing dEAAT1 in COS-7 cells (Seal et al., 1998) or *Xenopus* oocytes (Seal et al., 1998; Kawano et al., 1999). COS-7 cells transient-

ly expressing dEAAT showed a three- to fourfold increase in the uptake of radiolabeled L-glutamate over control. The uptake was substrate concentration-dependent, saturable, and strongly Na^+-dependent. The transport activity also showed a high affinity for L- and D-aspartate but little affinity for D-glutamate. Expression of the transporter in *Xenopus* oocytes allowed measurement of substrate-induced steady-state currents in addition to assaying radiolabeled substrate transport. The currents are induced in part by the electrogenicity of the transport activity and by the activation of substrate-gated chloride conductances associated with the carrier (Seal et al., 1998). Functional assays in oocytes also showed that L-glutamate, L- and D-aspartate, and D,L-threo-B-hydroxyaspartate were all high-affinity substrates of the transporter.

The second excitatory amino acid transporter, dEAAT2, was isolated by BLAST (Basic Local Alignment Search Tool) searching the Berkeley Drosophila Genomic Project (BDGP) database (Besson et al., 1999) to identify a sequence with significant homology to known glutamate transporters. The sequence (mapping to 21D) thus identified was then used as probe to isolate cDNA clones, the largest of which contained an open reading frame encoding a predicted protein of 561 amino acids.

The dEAAT2 protein was 36% identical to dEAAT1 in amino acid sequence and had equally high sequence identity (35–45%) with previously identified excitatory amino acid transporters as dEAAT1, although, unlike dEAAT1, its homology to the lepteran glutamate transporter, TrnEAAT1 (Donly et al., 1997) was relatively low (31–33% identity). The hydropathy profile of dEAAT2 was similar to that of other excitatory amino acid transporters and showed 8–10 stretches of hydrophobic domains. As was characteristic of other neurotransmitter transporters (Shafqat et al., 1993), both dEAAT1 and dEAAT2 exhibited a long loop between presumptive TMD3 and TMD4.

The expression profiles of dEAAT2 mRNA were quite distinct from those of dEAAT1, although both were expressed almost exclusively in the nervous system. A developmental Northern analysis showed that dEAAT2 transcripts migrated as multiple bands with a major one at 3.2 kb (Besson et al., 1999) and were heavily expressed in the adult head. Unlike the dEAAT1 transcript, expression of dEAAT2 transcripts was either undetectable or barely detectable at other developmental stages or in adult bodies. In in situ hybridization studies of stages 15–16 embryos, dEAAT2 RNA probes stained a small number of nerve cells that were distinct from the ones stained with dEAAT1 probe in the ventral nerve cord. In addition, dEAAT2 RNA was expressed in small symmetrically arranged clusters of cells in the anterior of the embryo. These could be the Bolwig's organ, the larval photoreceptor organ (Besson et al., 1999). Unlike dEAAT1, no staining was found in the third instar larval CNS. In the adult head, the staining was largely confined to the retina, the lamina, and the ocelli.

Expression of dEAAT1 and dEAAT1 cDNAs, either transiently in *Drosophila* Schneider S2 cells or stably in a polyclonal S2 cell line, showed that dEAAT2 is a specific aspartate transporter (Besson et al., 2000). As was shown earlier (Seal et al., 1998), dEAAT1 cDNA transfected cells took up either L-glutamate or D-aspartate about equally well. By contrast, dEAAT2 was found to transport D-aspartate with high affinity (Km = 30 μM) in a sodium-dependent manner but L-glutamate with a much lower affinity (Km = 185 μM), the relative efficacy of transport (Vmax/Km) was 10- to 15-fold lower. All previously described glutamate transporters display substrate selectivity similar to that of dEAAT1, and dEAAT2 is the first known excitatory amino acid transporter to have the aspartate selectivity described by these authors.

3.3 SUMMARY

In summary, two members of this superfamily have been isolated and characterized. One of them, dEAAT1, has properties very similar to those described for other known glutamate transporters, whereas the other appears to be a high-affinity aspartate transporter. Their expression profiles suggest that both these transporters have important functions in the nervous system. The restricted expression of dEAAT2 in the adult retina and lamina is particularly noteworthy, although no known functions for aspartate have been described in the *Drosophila* retina to date. No mutants have been isolated in either of the genes encoding these proteins, and functions of the proteins in vivo are unknown.

3.4 NA^+/CL^--DEPENDENT TRANSPORTERS

Two *Drosophila* members of this superfamily have been isolated and characterized by cDNA cloning: a serotonin transporter (dSERT) (Corey et al., 1994; Demchyshyn et al., 1994) and a dopamine transporter (dDAT) (Porzgen et al., 2001). In addition, isolation of partial cDNA clones encoding a transporter with high-sequence homology to mammalian GABA transporters has been reported (Neckameyer and Cooper, 1998). Two other members of this superfamily were isolated by a forward genetic approach. The mutant phenotypes suggest that one of these functions primarily in the nervous system (*rosA/ine*: Burg et al., 1996; Soehnge et al., 1996), whereas the primary effect of the other occurs outside the nervous system (*blot*: Johnson et al., 1999). These are the only members of the neurotransmitter transporter superfamilies for which mutants have been isolated in the genes encoding the transporters.

Isolation of *Drosophila* members of this superfamily of transporters is of interest, in part because, in humans, the transporters for serotonin, dopamine, and norepinephrine are the sites of action of antidepressants and such psychostimulants as cocaine and amphetamines. Most of the reinforcing properties and abuse potential of psychostimulants are thought to arise from the blockade of the dopamine transporter (Ritz et al., 1987). Indeed, the two *Drosophila* members of this family isolated by cDNA cloning, discussed below, have been shown to be antidepressant- and cocaine-sensitive.

Drosophila Serotonin Transporter (dSERT). cDNA clones encoding a dSERT were isolated either by screening a *Drosophila* head cDNA library with a) a fragment of the human DA transporter cDNA (Demchyshyn et al., 1994) or b) a *Drosophila* cDNA fragment obtained by PCR amplification primed by degenerate oligonucleotides corresponding to conserved portions of the known Na^+/Cl^- transporters (Corey et al., 1994).

The predicted proteins reported by the two groups differed slightly in length: 581 (Corey et al., 1994) vs. 622 amino acids (Demchyshyn et al., 1994). However, except for the N-terminal 30–70 residues, the amino acid sequences were identical, which suggests that these represented products of the same gene. Hydropathy analysis showed that the proteins had 12 putative TMDs with a large extracellular loop between the third (TMD3) and the fourth (TMD4), which is consistent with the membrane topology proposed for all other known Na^+/Cl^--dependent transporters. The proteins showed highest overall amino acid homology with rat (Blakely et al., 1991; Hoffman et al., 1991) and human (Ramamoorthy et al., 1993; Lesch et al., 1993); 5-HT transporters; 52 and 53% identities, respectively, Corey et al., 1994; 51% identity, Demchyshyn et al., 1994) and slightly lower homology with human norepinephrine (Pacholczyk et al., 1991; 51% identities, Corey et

al., 1994; 47% identities, Demchyshyn et al. 1994), human dopamine (Giros et al., 1992; Vandenbergh et al., 1992; Pristupa, 1994; 47% identities, Demchyshyn et al., 1994), and rat/bovine dopamine transporters (Shimada et al., 1991; Kilty et al., 1991; Usdin et al., 1991; Giros et al., 1991; 48% identities, Corey et al., 1994).

The chromosomal in situ hybridization showed that the dSERT gene was located at 60C of the right arm of the second chromosome (Demchyshyn, 1994). Northern blot analysis revealed a strongly labeled ~3.3 kb transcript from adult heads but no detectable signals from adult bodies or embryos (Corey et al., 1994). In situ hybridization to embryos and larvae showed the accumulation of dSERT mRNA in a restricted number of cells in the ventral ganglia arranged in a stereotypic pattern (Demchyshyn et al., 1994) consistent with the pattern of distribution of 5-HT-containing neurons (Valles and White, 1988), which strongly suggests that dSERT functions as a SERT.

Xenopus oocytes injected with dSERT mRNA showed fivefold higher transport of 5-HT than that of GABA, glutamate, histamine, dopamine, or norepinephrine (Corey et al., 1994). The transport of 5-HT occurred with high affinity and in a concentration-dependent and saturable manner in both injected oocytes (Corey et al., 1994) and transfected HeLa cells (Demchyshyn, 1994). The reported Km of 490 nM ± 35 nM for HeLa cells and 637 ± 100 nM for oocytes compared favorably with the Km values determined for the cloned human (463 nM) (Ramamoorthy et al., 1993) and rat SERTs (320–529 nM) (Blakely et al., 1991; Hoffman et al., 1991). dSERT-mediated transport of 5-HT displayed an absolute requirement for Na^+ in both expression systems. However, unlike in mammalian SERTs, the requirement for Cl^- was not absolute. Substitution of Cl^- with nitrate, acetate, or gluconate inhibited 5-HT uptake by 85–91% in oocytes (Corey et al., 1994) and only by ~50% in HeLa cells (Demchyshyn et al., 1994).

The pharmacological profile of dSERT-mediated transport had some similarity, but was not identical to that of mammalian SERT-mediated transport (Corey et al., 1994; Demchyshyn et al., 1994). Corey et al. (1994) noted that, with respect to a certain group of antidepressants, dSERT had a pharmacological profile with closer similarity to the mammalian catecholamine transporters than to the mammalian 5-HT transporters. Thus, for example, fluoxetine and clomipramine are 6- to 71-fold lower in potency at dSERT than at the mammalian SERTs, whereas mazindol and nomifensine, strong inhibitors of the mammalian catecholamine transporters but not as effective inhibitors of the mammalian SERTs, were potent inhibitors of dSERT. Thus, the pharmacological profile of dSERT represents a mixture of those of the mammalian catecholamine and 5-HT transporters. dSERT is sensitive to cocaine, although the degree of sensitivity compared with human SERT reported by the two groups differs somewhat. Both groups agree that the specificity of dSERT for 5-HT is very high. For example, unlabeled 5-HT showed significant inhibition of [^{3}H]5-HT uptake by dilution, but the other potential substrates tested—epinephrine, norepinephrine, dopamine, tyramine, octopamine, and histamine—had little or no effect. These findings taken together established that dSERT indeed is a 5-HT transporter.

Drosophila Dopamine Transporter (dDAT). Because all monoamine transporters cloned contain a characteristic aspartate residue in the first TMD, Porzgen et al. (2001) utilized the sequence information of the first TMD of the human dopamine transporter (hDAT) to identify in the BDGP database a gene encoding a putative monoamine transporter. Primers were designed from the sequence in the database to amplify a DNA fragment encompassing the entire coding region from a *Drosophila* cDNA pool.

The isolated cDNA encoded a protein of 631 amino acids with highest homology to

the human norepinephrine, dopamine, and serotonin transporters and the *C. elegans* dopamine transporter (52, 49, 45, and 51% identity, respectively). Hydropathy analysis predicted 12 TMDs with intracellularly located N- and C-terminals and a large extracellular loop between TMD3 and TMD4 (EL2). Found in TMD2 and TMD5 of dDAT were leucine zipper motifs, observed in TMD2 of a number of neurotransmitter transporters (Amara and Kuhar, 1993), including dSERT (Demchyshyn et al., 1994).

The gene was localized to 53C7-14 on the right arm of the second chromosome. The developmental profile of mRNA expression, determined by semiquantitative RT-PCR (Porzgen et al., 2001), showed dDAT expression in late embryos and larval stages. Expression decreased during the pupal stage but increased again in adults, with the strongest expression in adult heads. In situ hybridization to whole-mount third instar larval CNS (Porzgen et al., 2001) showed that the dDAT expressing cells were distributed in a characteristic pattern consistent with the distribution pattern of dopamine-containing cells (Budnik and White, 1988).

The functional properties of dDAT were examined in a Madin–Darby canine kidney cell line stably expressing dDAT (Porzgen et al., 2001). The results showed that dopamine had the highest maximal uptake velocity (Vmax) and the highest apparent transport affinity of any substrate tested, and the rank order of Vmax for biogenic amines was dopamine > norepinephrine > tyramine > epinephrine. Dopamine uptake into dDAT-expressing cells showed an absolute dependence on extracellular Na^+ but a more relaxed dependence on Cl^-, as was the case of dSERT (Corey et al., 1994; Demchyshyn et al., 1994).

The pharmacological profile of dDAT, obtained with a series of high-affinity nonsubstrate inhibitors for the monoamine transporters, showed a pattern distinct from that of the hDAT but closer in similarity to profiles reported for mammalian norepinephrine transporters (NERT), reminiscent of the inhibitor pharmacological profile reported for dSERT (Corey et al., 1994). Thus, dDAT showed high affinity for the tricyclic antidepressants, desipramine, imipramine, amitriptyline, and nisoxetine, all of which are highly selective for inhibiting hNERT over hDAT. Thus, echoing the findings for dSERT, dDAT is a unique catecholamine transporter with the substrate specificity of human DAT but with inhibitor sensitivity most closely resembling mammalian NETs. dDAT was moderately sensitive to cocaine. It is one of two cocaine-sensitive targets identified in flies to date.

Electrophysiological properties of dDAT were also distinct from those of hDAT. Both dDAT and hDAT mediate transport-associated currents when expressed in *Xenopus* oocytes (Porzgen et al., 2001). The mammalian monoamine carriers characteristically exhibit a pronounced, substrate- and inhibitor-sensitive constitutive leak conductance (Mager et al., 1994; Galli et al., 1995; Sonders et al., 1997). dDAT seemed to lack this leak conductance.

GABA Transporter. Neckameyer and Cooper (1998) have reported on cDNA clones containing partial open reading frames that predict polypeptides with high sequence homology with mammalian GABA transporters over a stretch of 120 amino acids. The presumptive *Drosophila* GABA transporter gene was mapped to 102BC of the fourth chromosome. However, the full sequence of the transporter has not been obtained, and no other information has been reported on the transporter.

***Bloated tubules (Blot*).** The Blot protein is one of the two *Drosophila* members of the Na^+/Cl^--dependent transporter superfamily that were identified by a forward genetic approach; that is, isolation and genetic analysis of mutants preceded the identification of the protein. The *blot* gene was identified from enhancer trap lines that showed expres-

sion in the developing Malpighian tubules (Johnson et al., 1999). Initial search for such lines identified two, *l(3)1658* (Spradling et al., 1995) and *A434* (Bellen et al., 1989), with very similar patterns of reporter gene expression. Subsequently, two stronger alleles, $blot^{M51}$ and $blot^{M55}$, were generated by remobilization of the P-element insert in the *A434* line to induce imprecise excision of the P-insert (Johnson et al., 1999). $blot^{1658}$ was mapped to 74B on the left arm of the third chromosome (Spradling 1995; Johnson et al., 1999).

Johnson et al. (1999) were interested in the Malpighian tubules as a model system for analyzing the development of epithelial tissues. The Malpighian tubules are an insect equivalent of the renal system that excrete toxic waste and adjust and maintain ionic and osmotic balance (Wigglesworth, 1939). The Malpighian tubules originate from evagination of two pairs of primordia at the border between midgut and hindgut of the embryo. In larvae, they consist of two pairs of slender tubes with cells containing a large number of fluorescent inclusion materials. The lumen of the tubule is encircled by the brush border, which is covered with microvilli. Actin filaments are concentrated in a submembranous region beneath the apical (luminal) membrane, and they extend into the microvilli. In *blot* mutant larvae, the Malpighian tubules appear bloated (hence the name "*bloated tubules*") and show a dramatic reduction in the fluorescent inclusion material. The luminal side (apical side) of the epithelial cells has extensive folds protruding into the lumen, although actin-containing microvilli are still present. Animals homozygous for $blot^{1658}$ are late larval lethal (Spradling, 1995), whereas those homozygous for $blot^{M51}$ or $blot^{M55}$ are second-instar larval lethal.

The *blot* gene was cloned by obtaining a genomic fragment adjacent to the P-insert in the *A434* enhancer trap line by plasmid rescue and by using this fragment to carry out a chromosomal walk (Johnson et al., 1999). The open reading frame was identified from a composite cDNA generated from two partial cDNA clones isolated in cDNA library screening. The open reading frame predicted a protein of 1035 amino acids having 12 putative transmembrane domains and significant homology with members of the Na^+/Cl^--dependent transporter superfamily. The highest homology (28% identity in a stretch of 436 amino acids) was found with the rat orphan transporter Rb21A, for which no substrate has been identified (Smith et al., 1995). The membrane topology of Blot also more closely resembled the orphan transporters than other members of this transporter superfamily in that, although most members of this superfamily have only one large extracellular loop between TMD3 and TMD4, Blot has two others between TMD5 and TMD6 and TMD7 and TMD8, in addition to the one between TMD3 and TMD4.

Northern blot analysis detected two transcripts of 4.0 and 4.3 kb throughout the embryonic development, with the shorter one appearing to be primarily supplied maternally. In situ hybridization experiments showed that *blot* RNA was expressed primarily in epithelial tissues of ectodermal origin, in the nervous system of the embryo and larva, and also in the freshly laid egg and developing oocyte. Embryos lacking the maternally derived component of *blot* died in early stages of development. At the syncytial blastoderm stage, filamentous actin in the cortex was almost completely absent, the structure of the apical cortex was impaired severely, and cellularization failed completely. Thus, the feature common to both the early developmental phenotype of embryos lacking the maternal component of *blot* and the Malpighian phenotype of larvae appeared to be a dramatic alteration in the organization of the actin-containing cortical cytoskeleton. The substrate for the Blot transporter has not been identified, and it is not known how the observed phenotypes are produced by a loss or reduction in the Blot activity. This transporter appears to

be the only one of this superfamily identified in *Drosophila* to date that functions primarily outside the nervous system.

RosA/Ine Transporter. The receptor oscillation A (*rosA*) gene was first identified as an electroretinogram (ERG)-defective mutant in which an oscillation is superimposed on the light response of photoreceptors in both ERG and intracellular recordings (Wilcox and Pak, 1977; Wu and Wong, 1977). The oscillation occurs at frequencies ~50 Hz, and the cell undergoes hyperpolarization after the light stimulus (Burg et al., 1996). The *rosA* gene was genetically mapped to 24F-25A of the chromosome 2L by deficiency mapping (Burg et al., 1996). Once physically localized to a small region, P1 phage genomic DNA clones that covered this region were identified by using database resources of the *Drosophila* community (Flybase, 1999). The molecular identification of the *rosA* gene was accomplished through Northern analysis of wild-type and *rosA*-mutant mRNA by using genomic DNA fragments as probe. Several of the genomic fragments from the P1 clones identified a reduction in the transcript level in some, but not all, *rosA* mutant alleles. Northern analysis also indicated two transcripts detectable in adult tissue (a major transcript of 3.7 kb and a minor transcript of 5.7 kb), both of which were reduced in amount in some mutant alleles. A corresponding full-length cDNA was isolated from a *Drosophila* head cDNA library by using the same genomic fragment as probe. cDNA sequence analysis indicated that the transcript encoded a Na^+/Cl^--dependent NTT homologue, having 36–41% amino acid identity with other transporters of this class. However, there was not sufficient similarity with any one class of transporters to predict the substrate for this transporter. The predicted *RosA* transporter is unique in that it contains a much larger amino terminus (~300 amino acids) than any other Na^+/Cl^--dependent NTT reported to date. However, other structural similarities, such as 12 predicted transmembrane domains and a large extracellular loop #2 between TMD3 and TMD4, allowed this transporter to be classified as a Na^+/Cl^--dependent NTT.

To demonstrate that this cDNA was the *rosA* transcript, the P-element germline mediated transformation technique (Spradling, 1986) was used to rescue the mutant phenotype. The results clearly demonstrated that the isolated cDNA directly restored wild-type function in *rosA* mutants when introduced to the mutants (Burg et al., 1996). Tissue in situ hybridization experiments indicated that the *rosA* transcript was expressed in many tissue types in adults, including photoreceptors (Burg et al., 1996). The generalized expression pattern suggested that this particular transporter might serve a very basic function by transporting a molecule common to many cell types. Alternatively, the *rosA* gene might be generating splice variants to produce functionally distinct transporters. Some of these splice variants have been detected by Northern analysis of mRNA isolated from different developmental stages of *Drosophila*. For example, although adult head tissue yielded one major transcript of 3.7 kb, several transcripts were detected in the embryonic stage (12–24 h embryo), which ranged from 3.7 to 2.3 kb (Burg et al., 1996).

Another independently isolated mutant, *ine* (inebriated), was reported to enhance excitability of neural tissue, particularly when mutations in potassium channel genes were also present (Stern and Ganetzky, 1992). For example, when examined in a *Sh* mutant background (the Shaker gene encodes a K^+ channel), the *ine* mutation caused many motor defects in larvae and developmental abnormalities in adults (Stern and Ganetzky, 1992). Simultaneous with the molecular cloning of the *rosA* locus, the *ine* locus was identified by using RFLP (Restriction Fragment Length Polymorphism) recombination mapping. Once the *ine* gene was mapped to a small region (24F) of the *Drosophila* genome, a deletion mutant (ine^3) was generated to enable the physical identification of the *ine* locus in

the genomic DNA. From this analysis, genomic clones were obtained (via "chromosome hopping"), which then were used to isolate cDNA clones from an embryonic cDNA library (12–24 h library). Both the clones and the corresponding genomic regions were mapped, and one mutant allele (ine^3) was found to be a deletion of 2.4 kb in the central part of the coding region of the cDNA, whereas another mutant allele (ine^4), was found to be a nonsense mutation (Soehnge et al., 1996). Sequence analysis of the *ine* cDNA identified the *ine* gene product as a Na^+/Cl^--dependent neurotransmitter transporter, which was proposed initially to serve as a glutamate transporter. Tissue in situ hybridization experiments performed on *Drosophila* embryonic tissue demonstrated *ine* expression in the CNS and numerous other tissues in the developing embryo (Soehnge et al., 1996).

Because the *rosA* and *ine* genes encoded nearly identical proteins and were located in the same genomic region, it was possible that these two mutants, although derived through different mutagenesis screens, defined the same gene. To establish whether these two genes were identical, genetic complementation tests were done between mutant alleles from each gene. In this genetic test, a homozygous mutant of *rosA* was crossed to a homozygous mutant of *ine*. The *rosA/ine* heterozygotes, the F_1 progeny of this cross, were still mutant in the ERG phenotype (M. Burg, unpublished results), indicating that both *rosA* and *ine* mutations affected the same gene.

In addition to the genetic confirmation that *rosA* and *ine* were the same gene, all *ine* mutants exhibited the same *rosA* ERG mutant oscillation phenotype, and all *rosA* mutants showed both motor and developmental defects in a *Sh* mutant background, as is characteristic of *ine* (M. Burg, unpublished). The *rosA* cDNA isolated from an adult head cDNA library (Burg et al., 1996) and the *ine* cDNA isolated from an embryonic cDNA library (Soehnge et al., 1996) were very different in size; the former was 3.7 kb and the latter, only 2.4 kb. Sequence comparisons between the cDNAs showed that the open reading frames contained in the cDNAs were essentially identical, except that the sequence encoding the amino terminal 313 amino acids of the predicted *rosa* protein were replaced in the *ine* cDNA by a sequence encoding 27 different amino acids. This substitution occurred at an intron/exon boundary, with distinct exons encoding the different N-termini of the two proteins, which suggests that the two cDNAs represent splice variants. Indeed, Northern analysis and tissue localization of transcripts described above indicated that the *rosA/ine* transcript is very heterogeneous in expression pattern and that many splice variants are produced by this gene at different developmental stages (Burg et al., 1996).

One of the more useful methods for studying structure-function relationships in vivo is P-element mediated germline transformation by using promoters that express the gene of interest in a subset of cells. This method takes advantage of the availability of *Drosophila* mutants and the ease of making transgenic flies, which provides a unique advantage to *Drosophila* in the study of NTTs. The initial phenotypic rescue of the *rosA* photoreceptor mutant phenotype with this technique utilized the 3.7 kb "*rosA*" cDNA (Burg et al., 1996), subsequently named the *rosA/ine*-long transcript (Huang et al., 1999). This experiment was then repeated with the distinct 2.4 kb "*ine*" cDNA of embryonic origin (Soehnge et al., 1996), subsequently named the *rosA/ine*-short transcript (Huang et al., 1999; 2.3 kb), to determine whether the cDNA differences could represent functional divergence in transporter function in vivo. The results of this study indicated that, for all known phenotypes, the *rosA/ine*-long transcript was more effective in restoring *RosA/Ine* function than the *rosA/ine*-short transcript (Huang and Stern, 2000; Huang et al., 1999). The results suggested that the 313 aa N-terminus of this transporter (encoded only in the

rosA/ine-long transcript) has an important function in localization or expression of the RosA/Ine transporter.

In an attempt to identify substrate(s) for the RosA/Ine transporter, substrate uptake assays were performed on *Drosophila* S2 cell lines transformed with the *rosA/ine* 3.7 kb (long) or the *rosA/ine* 2.3 kb (short) cDNA. Transformation of S2 cell lines utilized the pRmHa-3 (Bieber, 1994) or the pMT/V5-His vector (Invitrogen Inc., Carlsbad, CA), both of which carried a metallothionine promoter to induce gene expression. Details of the procedure are presented in Appendix I. Unfortunately, none of the following compounds were taken up specifically by cells in which the expression of the RosA/Ine transporter was induced: GABA, dopamine, norepinephrine, glycine, serotonin, choline, taurine, proline, histamine, and creatine. Consequently, the transporter encoded by *rosA/ine* was classified as an "orphan" transporter.

Because the transport experiments failed to identify any candidate substrate for the RosA/Ine transporter, mutant phenotypes were examined further to obtain clues to the transporter function. An electrophysiological examination of the larval neuromuscular junction showed that *rosA/ine* mutants exhibited altered synaptic transmission (Burg at al., 1997). Another phenotype reported more recently is the sensitivity of *rosA/ine* mutants to high osmotic conditions. The *rosA/ine* mutants were found to be unable to tolerate a high-salt food, on which wild-type flies thrive (Huang et al, 1999). This phenotype indicated that there may be a component of osmotic regulation that involves the RosA/Ine transporter.

Recently, a *rosA/ine* homologue was cloned in *Manduca sexta* (Chiu et al., 2000). A cDNA fragment was generated by RT-PCR by using degenerate primers against conserved regions of mammalian NTTs to isolate a cDNA from an embryonic cDNA library. The cDNA encoded a Na^+/Cl^--dependent neurotransmitter transporter with 55% amino acid identity to RosA/Ine. Analysis of the transporter function by using the *Xenopus* heterologous expression system failed to identify the substrate for this transporter, which was reminiscent of results with RosA/Ine. Interestingly, this transporter had a long N terminus, a characteristic thought to be unique to the RosA/Ine transporter, along with the other characteristics common to all Na^+/Cl^--dependent neurotransmitter transporters. Oocytes injected with mRNA of this transporter were found to generate a chloride current on exposure to hyperosmotic conditions. This response appeared to be mediated via a phospholipase (PLC)-C-mediated signaling mechanism, because U73122 (a permeable PLC inhibitor) blocked this effect (Chiu et al., 2000). Thus far, this osmotic-sensing response, coupled with a PLC transduction cascade (presumably causing an intracellular Ca^{++} release), is the only glimpse into the molecular mechanism of this transporter type. Because the *Drosophila* mutant *rosA/ine* is sensitive to hyperosmotic conditions, it is possible that the RosA/Ine transporter might be functioning in vivo by responding to osmotic changes and transporting small osmolytes.

Identification of new genes in *Drosophila* has been facilitated greatly by the recent sequencing of the complete euchromatic genome of *Drosophila* (www.fruitfly.org). Mutants, once mapped, can now be screened efficiently from a host of candidate genes in the region to which the gene has been localized to identify the corresponding genes. Additionally, targeted mutagenesis can be performed on genes whose similarity to known proteins exists but precise function is unknown. Of the 26 predicted transporter genes in the *Drosophila* genome, only 12 have been identified through expression cloning or forward genetics approaches (Flybase, 1999). Analysis and mutagenesis of the remaining transporters will most likely provide new insights into the role transporters play in both neuro-

transmitter uptake and maintenance of basic physiological functions, such as osmolarity and resting membrane potential. It is also clear that the forward genetic method can yield surprises, as in the case of the *rosA/ine* gene, providing new insights into the role these proteins may serve in cells.

APPENDIX I. EXPRESSION OF THE ROSA/INE TRANSPORTER IN S2 CELLS AND NEUROTRANSMITTER UPTAKE ASSAY

Transformation and expression of *rosa/ine* in S2 cells. An attempt to identify molecules that might be transported by the RosA/Ine transporter consisted of inducing the expression of the RosA/Ine transporter in S2 cells transformed with the *pRMHa-3-rosA* or the *pMT/V5-His-ine* vectors (Bieber, 1994; Invitrogen, Inc.). S2 cells were co-transformed by using the *pRmHa-3-rosA/ine* or the *pMT/V5-His-ine* vector with another plasmid conferring selectable drug resistance, following previously established methods (Bieber, 1994). Transformed S2 cells expressing the transporter were then grown to a density of ~4×10^6 cells/ml at 25°C by using Schneider's media supplemented with 10% bovine serum albumin (Sigma, Inc., St. Louis, MO). The cells were then placed in media containing 0.7 mM $CuSO_4$ to induce RosA/Ine expression for 48 h (Bieber, 1994). Cells were then counted, and 1×10^6 cells were used for each assay. S2 cells that carried the *rosa/ine* vector and were grown under the same conditions, without the addition of $CuSO_4$, were used as negative controls.

Transmitter uptake assay. For each assay, cells were centrifuged at 500 x g (4 min.), resuspended in 1 ml of phospate buffered saline (2 mM NaH_2PO_4, 8 mM Na_2HPO_4, 170 mM NaCl, pH 7.4), centrifuged at 500 x g (4 min.), and resuspended in Na^+-free uptake buffer (150 mM KCl, 1 mM $CaCl_2$, 1 mM $MgCl_2$, 10 mM Tris-Cl, pH 7.5) for 15 min. Cells were then centrifuged at 500 x g for 4 min, and resuspended in uptake buffer (150 mM NaCl, 1 mM $CaCl_2$, 2 mM KC1 1mM $MgCl_2$, 10 mM Tris-Cl, pH 7.5) containing 1–10 μM radiolabeled substrate, and incubated for 30 min at room temperature. After incubation, the cell samples were centrifuged and washed with Na^+-free uptake buffer (3×), after which the cell pellet was dissolved in 10% sodium dodecyl sulfate, and an aliquot was then assayed with liquid scintillation counting. Comparisons of radioactive uptake were made between S2 cells that had the RosA/Ine transporter induced and those not induced.

ANNOTATED REFERENCES

Amara SG, Kuhar MJ (1993): Neurotransmitter transporters: Recent progress. Annu Rev Neurosci 16:73–93.

Bieber AJ (1994): Analysis of cellular adhesion in cultured cells. Methods Cell Biol 44:683–695.

Bellen HJ, O'Kane CJ, Wilson C, Grossniklaus U, Pearson RK, Gehring WJ (1989): P-element-mediated enhancer detection: A versatile method to study development in *Drosophila*. Genes Dev 3:1288–1300.

Besson M-T, Soustelle L, Birman S (1999): Identification and structural characterization of two genes encoding glutamate transporter homologues differently expressed in the nervous system of *Drosophila melanogaster*. FEBS Letters 443:97–104.

Besson M-T, Soustelle L, Birman S (2000): Selective high-affinity transport of aspartate by a *Drosophila* homologue of the excitatory amino-acid transporters. Curr Biol 10:207–210.

Blakely RD, Berson H, Fremeau R, Caron MG, Peek M, Prince H, Bradley C (1991): Cloning and expression of a functional serotonin transporter from rat brain. Nature (London) 354:66–70.

Budnik V, White K (1988): Catecholamine-containing neurons in *Drosophila melanogaster*: Distribution and development. J Comp Neurol 268:400-413.

Burg MG, Wang JW, Leung H-T, Pak WL, Wu C-F (1997): Physiological examination of *Drosophila rosA* mutants indicates possible function for a novel neurotransmitter transporter. Soc Neurosci Abstr 23:1133.

Burg MG, Geng C, Guan Y, Koliantz G, Pak WL (1996): *Drosophila rosA* gene, which when mutant causes aberrant photoreceptor oscillation, encodes a novel neurotransmitter transporter homologue. J Neurogenet 11:59–79.

Describes the molecular identification and functional rescue of the *rosA* mutant by using a cDNA in transgenic flies, under control of a heat-shock promoter. A ubiquitous tissue distribution of the transcript in the adult is revealed, with stronger expression in neural tissues and several regions of the digestive tract. Reports a larger predicted protein than Ine and demonstrates phenotypic rescue of the mutant by the *rosA* cDNA, providing evidence that the *rosA* cDNA does encode the protein altered in the *rosA* mutants.

Chiu C-S, Ross LS, Cohen BN, Lester HA, Gill SS (2000): The transporter-like protein inebriated mediates hyperosmotic stimuli through intracellular signaling. J Exp Biol 203:3531–3546.

A *Manduca* RosA/Ine homologue was used to demonstrate a putative role for the RosA/Ine-type transporter in regulation of osmotic concentration. A Xenopus oocyte system was used to show that the RosA/Ine homologue causes the oocyte to respond to osmotic change by releasing Ca^{++}. The antisera against the *Manduca* protein can detect the protein in the visual system of *Drosophila*, as well as in *Manduca*, which indicates that the localization, and presumably function, are similar to those of RosA in adult tissues.

Corey JL, Quick MW, Davidson N, Lester HA, Guastella J (1994): A cocaine-sensitive *Drosophila* serotonin transporter: Cloning, expression, and electrophysiological characterization. Proc Natl Acad Sci 91:1188–1192.

Demchyshyn LL, Pristupa ZB, Sugamori KS, Barker EL, Blakely RD, Wolfgang WJ, Forte MA, Niznik HB (1994): Cloning, expression, and localization of a chloride-facilitated, cocaine-sensitive serotonin transporter from *Drosophila melanogaster*. Proc Natl Acad Sci 91:5158–5162.

Donly BC, Richman A, Hawkins E, McLean H, Caveney S (1997): Molecular cloning and functional expression of an insect high-affinity Na^{+}-dependent glutamate transporter. Eur J Biochem 248:535–542.

FlyBase (1999): The FlyBase database of the *Drosophila* genome projects and community literature. Nucleic Acids Res 27:85–88.

Reference for the FLYBASE resource available at http://flybase.bio.indiana.edu:82/. Valuable resource for forward genetic and molecular approaches using *Drosophila* as a model system.

Galli A, DeFelice LJ, Duke BJ, Moore KR, Blakely RD (1995): Sodium-dependent norepinephrine-induced currents in norepinephrine-transporter-transfected HEK-293 cells blocked by cocaine and antidepressants. J Exp Biol 198:2197–2212.

Giros B, El Mestikawy S, Bertrand L, Caron MG (1991): Cloning and functional-characterization of a cocaine-sensitive dopamine transporter. FEBS Letters 295:149–154.

Giros B, El Mestikawy S, Godinot N, Zheng K, Han H, Yang-Feng T, Caron MG (1992): Cloning, pharmacological characterization, and chromosome assignment of the human dopamine transporter. Mol Pharmacol 42:383–390.

Hoffman BJ, Mezey E, Brownstein MJ (1991): Cloning of a serotonin transporter affected by antidepressants. Science 254:579–580.

Huang X, Huang Y, Huff L, Burg MG, Pak WL, Stern M (1999): The *Drosophila* inebriated/rosA transporter: Dual roles in the control of neuronal function and osmotic stress response. Soc Neurosci Abstr 25:1037.

Huang Y and Stern M (2000): Regulation of neuronal excitability by the inebriated encoded neurotransmitter transporter. Soc Neurosci Abstr 26:343.

Johnson K, Knust E, Skaer H (1999): Bloated tubules (*blot*) encodes a *Drosophila* member of the neurotransmitter transporter family required for organization of the apical cytocortex. Dev Biol 212:440–454.

Blot is a novel Na^+-Cl^--dependent neurotransmitter transporter in *Drosophila* with homology to many "orphan" transporters, including RosA/Ine; first report of a "non-neuronal" phenotype associated with *blot*, affecting cellular and embryonic organization of the cytoskeleton. Complete molecular and genetic characterization of *blot*, including transcript distribution analysis and detailed characterization of the mutant phenotype, is provided.

Kawano T, Takuwa K, Kuniyoshi H, Juni N, Nakajima T, Yamamoto D, Kimura Y (1999): Cloning and characterization of a *Drosophila melanogaster* cDNA encoding a glutamate transporter. Biosci Biotechnol Biochem 63:2042–2044.

Kilty JE, Lorang D, Amara SG (1991): Cloning and expression of a cocaine-sensitive rat dopamine transporter. Science 254:578–579.

Lesch K-P, Wolozin BL, Murphy DL, Riederer P (1993): Primary structure of the human platelet serotonin uptake site: Identity with the brain serotonin transporter. J Neurochem 60:2319–2322.

Mager S, Min C, Henry DJ, Chavkin C, Hoffman BJ, Davidson N, Lester HA (1994): Conducting states of a mammalian serotonin transporter. Neuron 12:845–859.

Neckameyer WS, Cooper RL (1998): GABA tranporters in *Drosophila melanogaster*: Molecular cloning, behavior, and physiology. Invert Neurosci 3:279–294.

Pacholczyk T, Blakely RD, Amara SG (1991): Expression cloning of a cocaine-sensitive and antidepressant-sensitive human noradrenaline transporter. Nature (London) 350:350–354.

Porzgen P, Park SK, Hirsh J, Sonders MS, Amara SG (2001): The antidepressant-sensitive dopamine transporter in *Drosophila melanogaster*: A primordial carrier for catecholamines. Mol Pharmacol 59:83–95.

Pristupa ZB, Wilson JM, Hoffman BJ, Kish SJ, Niznik HB (1994): Pharmacological heterogeneity of the cloned and native human dopamine transporter: Disassociation of [3H]WIN 35,428 and [3H]GBR 12,935 binding. Mol Pharmacol 45:125–135.

Ramamoorthy S, Bauman AL, Moore KR, Han H, Yang-Feng T, Chang AS, Ganapathy V, Blakely RD (1993): Anti-depressant-and cocaine-sensitive human serotonin transporter: molecular cloning, expression, and chromosomal localization. Proc Natl Acad Sci 90:2542–2546.

Ritz MC, Lamb RJ, Goldberg SR, Kuhar MJ (1987): Cocaine receptors on dopamine transporters are related to self-administration of cocaine. Science 237:1219–1223.

Seal RP, Daniels GM, Wolfgang WJ, Forte MA, Amara SG (1998): Identification and characterization of a cDNA encoding a neuronal glutamate transporter from *Drosophila melanogaster*. Receptors Channels 6:51–64.

Shafqat S, Velaz-Faircloth M, Guadano-Ferraz A, Fremeau RT Jr. (1993): Molecular characterization of neurotransmitter transporters. Mol Endocrinol 7:1517–1529.

Shimada S, Kitayama S, Lin C, Patel A, Nanthakumar E, Gregor P, Kuhar M, Uhl G (1991): Cloning and expression of a cocaine-sensitive dopamine transporter complementary cDNA. Science 254:576–578.

Smith KE, Fried SG, Durkin MM, Gustafson EL, Borden LA, Branchek TA, Weinshank RL (1995): Molecular cloning of an orphan transporter. A new member of the neurotransmitter transporter family. FEBS Letters 357:86–92.

Soehnge H, Huang X, Becker M, Whitley P, Conover D, Stern M (1996): A neurotransmitter transporter encoded by the *Drosophila* inebriated gene. Proc Natl Acad Sci 93:13262–13267.

Identification of the *ine* mutations by molecular mapping and sequence analysis, and localization of *ine* expression by tissue in situ localization of embryo whole mounts. Reports a shorter transcript variant than that identified by Burg et al. (1996); only the first intron differs in sequence, with the remainder of the putative Ine protein identical to the RosA protein.

Sonders MS, Zhu SJ, Zahniser NR, Kavanaugh MP, Amara SG (1997): Multiple ionic conductances of the human dopamine transporter: the actions of dopamine and psychostimulants. J Neurosci 17:960–974.

Spradling AC, Stern D, Kiss I, Roote J, Laverty T, Rubin GM (1995): Gene disruptions using P transposable elements: an integral component of the *Drosophila* genome project. Proc Natl Acad Sci 92:10824–10830.

Spradling AC (1986): P-element-mediated transformation. In DB Roberts (ed): *Drosophila*: A practical approach. Oxford: IRL Press, pp 175–195.

Stern M, Ganetzky B (1992): Identification and characterization in inebriated, a gene affecting neuronal excitability in *Drosophila*. J Neurogenet 8:157–172.

Usdin TB, Mezey E, Chen C, Brownstein MJ, Hoffman BJ (1991): Cloning of the cocaine-sensitive bovine dopamine transporter. Proc Natl Acad Sci 88:11168–11171.

Valles A, White K (1988): Serotonin-containing neurons in *Drosophila melanogaster*: Development and distribution. J Comp Neurol 268:414–428.

Vandenbergh DJ, Persico AM, Uhl GR (1992): A human dopamine transporter cDNA predicts reduced glycosylation, displays a novel repetitive element and provides radically-dimorphic Taq1 RFLPs. Mol Brain Res 15:161–166.

Wigglesworth VB (1939): The Principles of Insect Physiology. London: Menthuen.

Wilcox M, Pak WL (1977): Genetic alteration of the photoreceptor membrane resulting in light-induced oscillation superimposed on the receptor potential. Invest Ophthalmol Vis Sci Suppl:119.

Wu C-F, Wong F (1977): Frequency characteristics in the visual system of *Drosophila*: Genetic dissection of electroretinogram components. J Gen Physiol 69:705–724.

CHAPTER 4

TRANSGENIC MICE IN MONOAMINE TRANSPORTER RESEARCH

SARA R. JONES

4.1 INTRODUCTION

Experimentally designed mutant mice that lack a certain gene product are important research tools for studying transporters. Over the past six years, knockout mice that do not express neurotransmitter transporters have been used to unravel key issues regarding the selectivity, mode of action, physiology and behavioral role of amine neurotransmitters (Giros et al., 1996; Wang et al., 1997; Bengel et al., 1998; Rocha et al., 1998; Itokawa et al., 1999; Xu et al., 2000; Pan et al., 2001). This chapter is designed to introduce a few questions to which monoamine transporter knockout mice have provided insight and to describe some of the methods used to examine transporter function in transgenic mice in general. The dopamine transporter knockout (DAT KO) mouse will be the main example used throughout the chapter.

4.2 COCAINE EFFECTS IN DAT KO MICE

Because the DAT is thought to be the primary target of the rewarding actions of cocaine, it has been of interest as to why mice with no DAT still self-administer cocaine (Rocha et al., 1998). The other remaining targets of cocaine, the norepinephrine transporter (NET) and the serotonin transporter (SERT), seemed likely candidates as mediators of cocaine reward in mice without DAT. Two studies have attempted to answer the question, with differing results. One group focused on the SERT. First, DAT KO mice and SERT KO mice were shown separately to exhibit cocaine-induced reinforcement in a conditioned place preference paradigm (Sora et al., 1998). Then a double knockout of SERT and DAT was made that no longer showed place preference in response to cocaine administration (Sora et al., 2001). This result pointed toward SERT inhibition as an important event in cocaine action in DAT KO mice. Another group made measurements of extracellular dopamine (DA) in the nucleus accumbens of DAT KO mice using microdialysis and found that cocaine retained the ability to increase extracellular DA in this region (Carboni et al., 2001). Reboxetine, a NET inhibitor, also increased DA, and the conclusion was drawn that NET may be taking up DA in the nucleus accumbens of the DAT KO mouse, perhaps as an adaptation to the absence of the DAT. Our own results, however, do not support this finding. We have used fast-scan cyclic voltammetry in slices of the nucleus

Transmembrane Transporters. Edited by Michael Quick

ISBNs: 0-471-06517 (Hardcover); 0-471-43404-3 (Electronic)

accumbens, core and shell regions, to measure the impact of several uptake inhibitors, including cocaine, GBR 12909 (DAT inhibitor), desipramine (NET inhibitor), and fluoxetine (SERT inhibitor) on DA clearance. None of them altered the clearance of DA. Figure 4.1 shows the lack of effect of desipramine and fluoxetine on DA clearance. Figure 4.1A, upper panel, shows the averaged results on clearance rates, and the lower panel shows representative DA efflux curves before (filled circles) and after (open circles) application of desipramine (10 μM). Figure 4.1B follows an identical format for fluoxetine results. For methods see the section in this chapter on fast-scan cyclic voltammetry in brain slices. There were no effects of either transporter inhibitor on DA clearance in the nucleus accumbens of the DAT KO mouse. We have therefore concluded that the site of cocaine action in the DAT KO mouse that leads to elevated DA in the nucleus accumbens is not the accumbens itself but may lie in other brain regions, such as the ventral tegmental area where DA cell bodies are found.

4.3 TISSUE CONTENT OF MONOAMINES IN TRANSPORTER KNOCKOUT MICE

Monoamine transporter knockout mice all have marked reductions in the tissue content of the monoamine for which the transporter is deleted. For the DAT KO mouse, DA was decreased 85–95% in various brain regions (Jones et al., 1998). For the NET KO mouse, norepinephrine (NE) was decreased 55–70% (Xu et al., 2000); for the SERT KO mouse, serotonin (5-HT) was decreased 60–80% (Bengel et al., 1998). This decrease is primarily

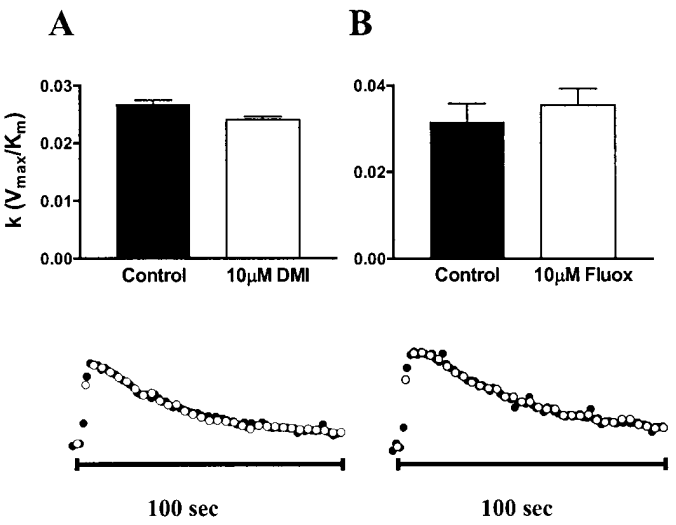

Figure 4.1. Efflux of DA (1 pulse stimulation) in slices of the shell of the nucleus accumbens in DAT KO mice. **A**) Desipramine (10 μM) does not alter the clearance rate of DA following release. **B**) Fluoxetine (10 μM) does not alter the clearance of DA. Upper panels, averaged data, lower panels, representative curves before (filled circles) and after (open circles) application of inhibitor.

due to a lack of recycling of released monoamine from the extracellular space back into presynaptic terminals. Typically, the vast majority of monoamine that is released is taken back up, repackaged into vesicles, and reused in later release. Monoamines use transporters to terminate neurotransmission, unlike other neurotransmitters. For example, released acetylcholine is degraded by an enzyme, acetylcholine esterase, to terminate its signal. The lack of retrieval of monoamines from the extracellular space in transporter knockout animals produces a unique situation. There is excess monoamine in the extracellular space, but inside the neurons that synthesize the monoamine, there is a deficit. Thus, there can by signaling hyperdopaminergia along with homeostatic hypodopaminergia (Gainetdinov et al., 1999).

Methods for Determining Tissue Content of Monoamines

Tissue homogenates of striatum or other brain regions are prepared by sacrificing mice and dissecting the brain regions of interest on a chilled aluminum block. The tissue is then placed in plastic microcentrifuge tubes and submerged in liquid nitrogen for rapid freezing. The tubes are then put in a –80ºC freezer until use. Tissue samples are homogenized in 0.1 M perchloric acid containing 0.1 mM sodium metabisulfite and 0.1 mM ethylenediamine tetraacetic acid (EDTA). For assay of monoamines and their metabolites, the chromatographic mobile phase consists of 0.05 M sodium phosphate monobasic, 0.05 mM EDTA, 0.4 mM octyl sodium sulfate, and 9% methanol, brought to pH 3.9 with phosphoric acid. A 10 cm C-18 reverse-phase column is used for separation of monoamines (Ultremex 3 C-18 IP, 100 × 4.6 mm, Phenomenex, Chicago, IL) on a high-performance liquid chromatography (HPLC) system with electrochemical detection (BAS, West Lafayette, IN). By this method 5-HT and its metabolite 5-hydroxyindole acetic acid (5-HIAA), DA and its metabolites homovanillic acid (HVA) and 3,4-dihdroxyphenylacetic acid (DOPAC), and NE are detected consistently. The concentration of the sample monoamines are determined by comparison of peak heights with those predetermined with freshly prepared standards that are run before each set of measurements (Del Bigio and Vriend, 1998; Jones et al., 1998).

4.4 MEASUREMENTS OF MONOAMINE UPTAKE IN TRANSPORTER KNOCKOUT MICE

Voltammetry

Fast-scan cyclic voltammetry is the electrochemical method of choice for studies of uptake in transporter knockout animals because it does not require disruption of the tissue or the addition of exogenous substrate. Typically, electrical stimulation is used to elicit the release of endogenous monoamine from the tissue slice or intact brain, and then uptake is measured following release (Davidson and Stamford, 1996; Bunin and Wightman, 1998; Callado et al., 2000; Wu et al., 2001). Alternatively, exogenous monoamine can be applied locally and electrochemical methods can be used to monitor the changes in levels of monoamine in brain tissue (Bickford-Wimer et al., 1991; Daws et al., 1998; Zahniser et al., 1999; Dickinson et al., 1999; Daws et al., 2000). Rotating disk electrode voltammetric measurements are another electrochemical technique used to measure the concentration

of monoamine in a dispersed-tissue suspension similar to a synaptosomal preparation (McElvain and Schenk, 1992; Earles and Schenk, 1998; Chen et al., 1998; Chen and Justice, 2000; Wayment et al., 2001).

Working with Exogenous Monoamines

It is important to understand that when one uses exogenously applied monoamines to probe the function of transporters, kinetic information to be gleaned is automatically limited. The use of exogenous DA to examine DA transport rates, for example, is widespread. Radioactively labeled or unlabeled DA is applied to measure uptake in vivo (Daws et al., 1998; Zahniser et al., 1999; Dickinson et al., 1999) and in brain slices (Adachi et al., 2001; Bailey et al., 2001), tissue homogenates (Reith and O'Reilly, 1990; Meiergard et al., 1997; Jones et al., 1998; Wayment et al., 2001), and cultured cells (Bennett et al., 1997; Pan et al., 2001). If low concentrations are used, reasonable estimates of DA uptake can generally be obtained. However, if high concentrations are used, the ability of the transporter to function normally is compromised. As an example, the effects of DAT substrates, including DA itself, on uptake of DA are similar to amphetamine, as shown in Figure 4.2. When there are high concentrations of extracellular substrate, the DAT takes up substrate into the presynaptic terminal, but vesicular uptake and storage of the substrate quickly becomes saturated, and the concentration of substrate on the inside of the terminal, near the internal portion of the DAT, increases dramatically. Under these conditions, the DAT transports DA (or any other substrate) in both the forward and reverse directions. Reversal of the DAT in essence means that DA is released from the cytoplasm through the DAT, as well as being taken up from the extracellular space. The kinetics of uptake during this dual process are complicated, to say the least. Figure 4.2 shows that exogenously applied DAT substrates act as competitive uptake inhibitors and releasers, or transporter reversers. The fact that the uptake portion of the curves does not

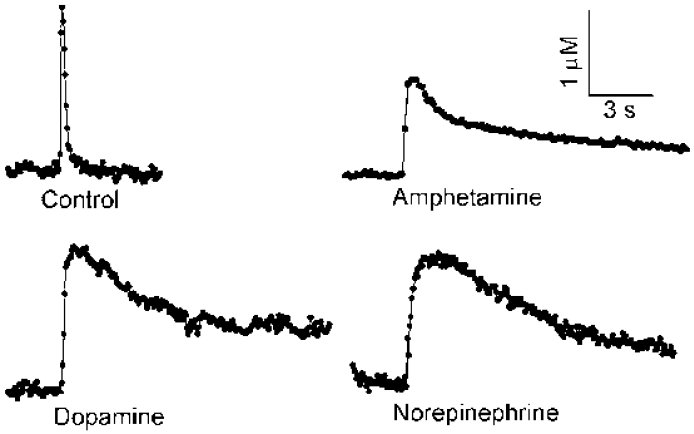

Figure 4.2. Effects of Amphetamine (10 μM), NE (100 μM) and DA (100 μM) on release and uptake of DA in caudate slices from wild-type mice. Measurements were made approximately 40 min after addition of drug. First-order rate constants for uptake are as follows: control 28 ± 6 s^{-1}, NE 0.10 ± 0.06 s^{-1}, DA 0.27 ± 0.11 s^{-1} (n=3 for each condition).

return to baseline demonstrates that the transporter is not at equilibrium with its substrate(s) and that a new baseline is being established. This situation is not optimal for measuring uptake rates. However, it is a common situation to measure uptake rates in the presence of high concentrations of exogenous substrate, as explained above. Care should always be taken in interpreting such data.

Fast-Scan Cyclic Voltammetry-Brain Slices

Slice Preparation. Mice are decapitated, and coronal brain slices (400 μm) containing the region of interest (caudate, nucleus accumbens, amygdala, etc.) are prepared using a vibrating tissue slicer (Leica VT 1000S; Leica Instruments, Solms, Germany). Slices are incubated for at least 1 h in artificial cerebrospinal fluid (aCSF) containing (in mM): NaCl 126, KCl 3, $MgCl_2$ 1.5, $CaCl_2$ 2.4, NaH_2PO_4 1.2, glucose 11, $NaHCO_3$ 25.9 (saturated with 95% O_2 – 5% CO_2), preheated to 34°C, before experiments. During experiments, slices are perfused with oxygenated aCSF at a flow rate of 1 ml/min. Electrode placements are made with the aid of a stereomicroscope.

Electrode Preparation. Carbon fiber (r=5 μm, Thornel T-650, Amoco, Greenville, SC) voltammetric microelectrodes are prepared from filamented borosilicate glass capillary tubes (inner diameter: 1.5 mm) using a micropipette puller (Narishige Instruments, Tokyo, Japan). Electrode tips are cut so that 50–200 μm of fiber is protruding.

Data Acquisition. The electrode potential is scanned linearly from –400 to 1000 mV and back to –400 mV at 300 V/s, repeated every 100 ms, using a potentiostat (EI400, Cypress Systems, Bloomington, IN) interfaced with a PC computer. A silver–silver chloride wire is used as a reference. Each electrode is calibrated with 10 μM DA at the end of the experiment to convert the magnitude of current at the oxidation potential of DA to concentration. DA release is evoked by single pulse stimulations (350 μA, 4 ms) from a bipolar stimulating electrode (MS 303/3, Plastics One, Roanoke, VA) placed 100–200 μm away from the carbon-fiber electrode. The stimuli are computer-generated and optically isolated (NL 800, Neurolog, Medical Systems Corp., Great Neck, NY) from the electrochemical system. The carbon-fiber microelectrodes are inserted 75 μm below the surface of the slice. Background-subtracted cyclic voltammograms are constructed by subtracting the background current obtained before release (15–50 nA) from the current measured following release. DA is identified as the substance detected by its characteristic cyclic voltammograms. Measured time courses of DA are analyzed by a Michaelis–Menten based set of kinetic equations (Wightman et al., 1988) to determine the concentration of DA detected and the rate of DA transport.

Measurements of Monoamine Clearance in Transporter Knockout Mice Using Fast-Scan Cyclic Voltammetry

The difference in clearance rate between the DAT KO and wild-type is ~300-fold (Figure 4.3), whereas the difference between the NET KO and wild-type is approximately 6-fold (Fig. 4.4), as measured by voltammetry in brain slices. This difference resides solely in the clearance rate in the wild type, as the NET KO and DAT KO mice have similar rates that are adequately described by diffusion. This comparison illustrates the relative dependence of the NE and DA systems on their transporters for normal function. The 5-HT system has clearance rates in the wild-type similar to the NE system, far slower than DA in the caudate nucleus (Bunin and Wightman, 1998).

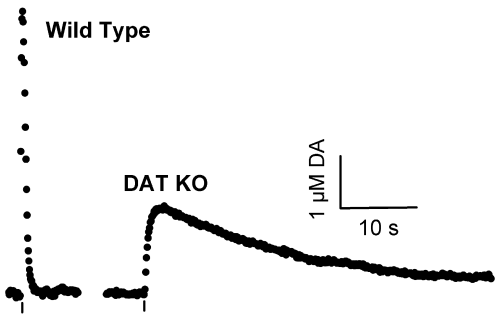

Figure 4.3. Efflux of DA (1 pulse stimulation, bars) in slices of the dorsal striatum of wild-type (WT) and DAT KO mice, measured every 100 ms (dots) by using cyclic voltammetry. Note the drastically reduced release and clearance of DA in the DAT KO compared with WT mice.

It appears the DA system in the basal ganglia is extremely dependent on high uptake rates for normal function. This point is also apparent in the effects of uptake inhibitors of the various monoamines on behavior. DA transport inhibitors have dramatic stimulatory and euphoric effects, whereas NE and 5-HT transport inhibitors have more subtle, though extremely important, effects on behavior (Plasnik and Kostowski, 1991; Detke and Lucki, 1996; Blier, 2001).

In Vivo Fast-Scan Cyclic Voltammetry Surgery

Rats are anesthetized with urethane (1.5 mg/kg, i.p.) and immobilized in a stereotaxic frame (David Kopf Instruments, Tajunga, CA). Body temperature is maintained at 37ºC with a Deltaphase Isothermal Pad (Braintree Scientific, Braintree, MA). The skull is exposed by making an incision along the midline followed by retraction of skin and muscle. Holes are drilled for reference, working, and stimulating electrodes. Flat skull coordinates are obtained from the brain atlas of Paxinos and Watson (1986) and are given in millimeters. Anteroposterior (AP) and mediolateral (ML) positions are referenced to bregma, and dorsoventral (DV) positions are referenced to dura. The stimulating electrodes are posi-

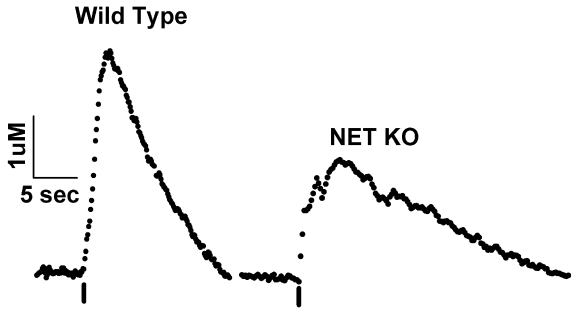

Figure 4.4. Electrically stimulated (30 pulses, 30 Hz, bars) DA release and uptake in the bed nucleus of the stria terminalis in wild-type (WT) and NET KO mice. Stimulations are denoted by bars beneath the curves. Extracellular NE levels were sampled every 100 ms (data points) by fast-scan cyclic voltammetry. Note the reduced release amount and clearance rate in the NET KO compared with WT mice.

tioned either in the medial forebrain bundle (–4.6 AP, 1.0 to 1.7 ML, –7.5 to –8.5 DV) to stimulate DA axons or ventral mesencephalon (–5.6 AP, 0.8 to 1.2 ML, –7.5 to –8.5 DV) to stimulate DA cell bodies. The working electrode is positioned in either the shell (1.4 AP, 1.2 ML, –7.0 DV) or the core (1.2 AP, 2.0 ML, –7.0 DV) of the nucleus accumbens or in the caudate putamen (1.2 AP, 1.75 to 3.75 ML, –4.5 to –5.5 DV). The reference electrode is implanted in superficial cortex contralateral to stimulating and working electrodes (Bergstrom and Garris, 1999).

Electrochemistry. Carbon-fiber microelectrodes are made by aspirating a single carbon fiber (r=2.5 μm; Thornel T-650, Amoco, Greenville, SC) into a glass capillary as described above in the brain slice voltammetry methods. Approximately 50 μm of the fiber extends beyond the glass capillary as the sensing probe. Electrochemistry is performed by an EI400 potentiostat as described above.

Microdialysis

Another possible method of estimating uptake rates in vivo in transporter knockout mice is by measuring the extraction fraction of monoamine using microdialysis. This technique has not been applied extensively to knockout mice as yet (Jones et al., 1998), and it is not a direct method. However it has the advantage of being a relatively simple experiment if an HPLC system is available. The theoretical basis for the estimation of uptake rate based on extraction fraction in microdialysis is outlined in a manuscript by J.B. Justice, Jr. (Smith and Justice, 1994). Briefly, if the extraction fraction is decreased, uptake may be increased (Smith and Justice, 1994).

4.5 SYNAPTOSOMES

Comment on the use of synaptosomes. It is tempting to use the synaptosomal preparation to define how transporters interact; that is, whether one monoamine transporter takes up another's normal substrate. This question has existed for a long time for the uptake of DA by NETs in the prefrontal cortex. A recent article discusses this possibility in light of results with synaptosomal preparations from NE and DAT KO mice (Moron et al., 2002). Care must be taken in interpreting these data, however. The conclusion of the article is that transporter-selective uptake inhibitors are not necessarily transmitter-selective uptake inhibitors because transporters can be promiscuous, taking up transmitters other than their own type. Although this is a true statement, using the uptake of tritiated monoamines into synaptosomes made from cortical and other brain regions provides no information at all on which transmitters are normally taken up by which transporters. For example, uptake of labeled DA into prefrontal cortical synaptosomes from DAT KO mice provides information only on the density of NETs, not on whether NETs actually take up DA in these mice. It is well known that the NET takes up DA very well, actually with a higher affinity than for NE (Giros et al., 1994; Syringas et al., 2000). So it is no surprise that exogenous, labeled DA is taken up by the NET. It would have been much more informative to perform voltammetry or microdialysis experiments that do not disrupt the tissue or utilize exogenous DA to ask such questions. In fact, an elegant article from the laboratory of Mark Wightman describes using electrically stimulated catecholamine release in slices of pre-

frontal cortex from wild-type, DAT and NET KO mice to address this question (Mundorf et al., 2001). Their conclusion was that heterologous uptake of catecholamines does normally occur in the prefrontal cortex (Mundorf et al., 2001).

Synaptosomal Preparation

Mice can be sacrificed by cervical dislocation, to avoid any interaction of anesthesia with the experimental results, or by asphyxiation with carbon dioxide, which leaves the tissue fairly rapidly. Striata or other brain regions of interest are dissected out on a chilled aluminum block and are placed in a ground-glass homogenizer containing 50 volumes (typically 2 ml for two mouse striata) of ice-cold 0.32 M sucrose buffer with 10 mM sodium phosphate, pH 7.4. Twelve up-and-down strokes in the homogenizer is a usual number. Debris and unbroken cells are then sedimented by centrifugation at 1000 to 2000 rpm for 10 min at 4ºC. The synaptosome-rich supernatant is retained and stored on ice until use.

[^{3}H]DA Uptake

A 25-μL aliquot of the synaptosomal suspension is added to assay tubes containing 5 nM [^{3}H]DA and a range of unlabeled DA concentrations (3 nM – 100 μM) in a total volume of 0.5 mL of Krebs-phosphate buffer (containing [in mM]: 136 NaCl, 4.8 KCl, 1.2 $MgCl_2$, 1.4 $CaCl_2$, 10 glucose, 1 ascorbate, 0.14 EDTA, and 0.12 pargyline, pH 7.4, oxygenated with 95%O_2/5%CO_2). Assay tubes are set up on ice, and all constituents are added (synaptosomes last!) to the tubes before the experiment begins by placement into an oscillating water bath set at 37ºC. The length of the uptake experiment is typically from 1 to 5 min, with 1 min desirable because it is on the linear portion of the uptake time-course. However, due to the difficulty of getting tubes into and out of baths in one min, 5 min is often the norm.

The incubation is terminated by the addition of 5 mL of ice-cold Kreb's buffer, followed by rapid passage through a GF/B filter that had previously been soaked in 1% polyethyleneimine (to reduce nonspecific binding) and then rinsed with buffer. Cell harvesters or other filter devices can be used. Filters are washed three times with 5 mL of ice-cold Kreb's to remove excess [^{3}H]DA, then placed into scintillation vials containing 5 mL of scintillation fluid. After a delay of more than 6 h for chemiluminescence decay, the filter is counted for tritium. The resulting uptake inhibition of cold saturation data can be analyzed with any nonlinear analysis computer program (Ligand or Graph Pad, for example) to estimate V_{max} (maximum uptake rate, equivalent to transporter density) and K_m (inverse of transmitter affinity for transporter). Nonspecific uptake can be measured by performing the experiment at 4ºC or by adding a maximal concentration of an uptake inhibitor such as nomifensine (10 μM) or mazindol (10 μM). The difference between nonspecific binding and total binding is defined as specific uptake. Specific uptake is then expressed as picomoles per milligram of protein per 5-min (or 1-min) incubation. V_{max} is expressed as picomoles/5-min/mg protein and K_m is expressed as molarity.

[^{3}H]5-HT Uptake

Brain stem and/or cortex samples are homogenized in 15 volumes of 0.32 M sucrose as described for DA uptake. The homogenates are centrifuged twice to purify the synaptosome-containing fraction. First, the homogenate is centrifuged for 10 min at 1000 x g to

remove debris, and then the supernatant is centrifuged for 10 min at 17,000 x g. The pellet is resuspended in sucrose at a final concentration of 1–2 mg/ml. 5-HT uptake is measured by using several concentrations of [^{3}H]5-HT (10–100 nM) (Reith and O'Reilly, 1990). Tubes containing 120 mM NaCl, 20 mM Tris-HCl, 5 mM KCl, 1.2 mM MgSO4, 2.5 mM CaCl2, 10 mM glucose, 1 mM ascorbate, and 0.1 mM pargyline plus [3H]5-HT are preincubated for 5 min at 37ºC. Brain synaptosomes are then added to each tube and uptake is allowed to occur for 5 min at 37ºC. The process is terminated by immersing the tubes in ice water, followed by rapid filtration through Whatman GF/B filters. Radioactivity is measured using liquid scintillation counting as described for DA uptake. Specific uptake is defined as occurring at 37ºC minus nonspecific uptake determined in tubes containing 0.1 mM fluoxetine incubated at 0ºC. Sodium dependence of uptake is often evaluated by substituting LiCl (120 mM) for NaCl in a separate set of experiments.

NET uptake assays are very similar to SERT uptake assays, simply by using [^{3}H]NE as the radioligand and nisoxetine or reboxetine as inhibitors to define nonspecific binding.

Monoamine Transporter Autoradiography

This is a general method that can be used for any monoamine transporter by changing the specific inhibitors. The following example is for SERT autoradiography. Slide-mounted cryostat tissue sections (20 μm) are thawed and equilibrated in sucrose buffer (320 mM sucrose, 10 mM sodium phosphate, 10 mM sodium iodide, pH 7.4) for 10 min at room temperature. Sections are then pre-incubated in the absence or presence of a mixture of GBR-12909 (1 μM) and nisoxetine (700 nM) to inhibit binding of [125I]RTI-55 to the DAT and NET, respectively. Pre-incubations last for 20 min before the addition of [125I]RTI-55 (50 pM) for 60 min at room temperature. Free and nonspecifically bound [125I]RTI-55 is removed by washing the sections in 2 × 20 min in ice-cold sucrose buffer, followed by 2 × 5s water and 1 × 10 s 20% ethanol. Sections are then dried under a cool stream of air and desiccated at 4ºC. Autoradiograms are prepared by exposing the slide-mounted tissue sections and [125I] Microscale standards to [3H] Hyperfilm (Amersham, Arlington Heights, IL) for 8–16 h at –20ºC. Autoradiograms are digitized using an AlphaImager 2000 image analysis system (Alpha Innotech, Inc., San Leandro, CA) and color scale assigned using NIH image (National Institutes of Health, Bethesda, MD). Tissue sections are then transferred to test tubes for gamma counting. Nonspecific binding is determined in the presence of 1 μM paroxetine (or 1 μM alaproclate) and should represent less than 10% of the total binding (Staley et al., 1994; Rocha et al., 1998).

Cell Culture Techniques to Measure Monoamine Uptake

Although to date there are no published reports of uptake measurements in transgenic mouse DA or NE neuron cultures, there are a few reports of mesencephalic cultures from transgenic mice for purposes other than measuring uptake (Mena et al., 1997; Sanchez-Ramos et al., 1997). We can easily adapt the methods for measuring uptake in fetal rat mesencephalic cultures to the mouse. Differences in uptake of tritiated 5-HT in primary cultures of SERT knockout and wild-type mice have been reported (Pan et al., 2001). In addition, the technology has been developed recently to create midbrain and hindbrain neurons from mouse embryonic stem cells (Lee et al., 2000).

Mesencephalic DA cell culture preparation. Fetal mice at embryonic day 15 are obtained from timed-pregnant mice. The mesencephalon is identified as extending from the

caudal border of the diencephalon to the caudal border of the mesencephalic flexure. This area has catecholamine-containing cells and includes the DA cells of the substantia nigra and the ventral tegmental area, but excludes the noradrenergic cells of the locus coeruleus and 5-HT cells of the raphe nucleus (Loren et al., 1976; Bennett et al., 1997). Tissues are dissected, rinsed, and mechanically dispersed by trituration through a medium-gauge needle. The single cell suspension is plated at 7.5×10^5 cells per 16-mm well. Culture surfaces are precoated overnight with poly-L-lysine (100 μg/ml). Culture media consists of Dulbecco's modified Eagle medium (4.5 g glucose/L, no pyruvate) supplemented with 10% fetal calf serum, 10% horse serum, 2 mM glutamine, 100 μg/ml streptomycin, and 100 units/ml penicillin. This medium is removed after 24 h, replaced with medium containing 2% serum for 24 h and then by medium without serum for the remainder of culture (usually 7–10 days).

[^{3}H] DA Uptake

Initial velocity uptake studies are conducted by using seven concentrations of unlabeled DA with the same concentration of radioactive DA ([^{3}H]DA, 50 nM) over a 2-min period. The concentrations of unlabeled DA can be 50, 100, 200, 400, 600, 800, and 1000 nM. Nonspecific uptake is determined by the addition of mazindol (10 μM), and specific uptake is determined by subtracting nonspecific counts from the total. The kinetic parameters of DA uptake, the affinity constant (K_m), and the maximal initial velocity of uptake (V_{max}) are estimated by the double-reciprocal plot method (Lineweaver–Burke plots) (Bennett et al., 1997).

Genetic Background

The importance of the genetic background on which mutations in specific genes are studied has been described extensively in reviews and commentaries (Banbury Conference, 1997; Crawley et al., 1997). Behavioral analyses of drug effects are notoriously sensitive to mouse strain differences. For example, C57BL/6J mice and related C57 strains willingly drink ethanol solutions, whereas DBA/2J and related DBA strains avoid any detectable concentrations of ethanol (Phillips et al., 1991; Crawley et al., 1997). The DBA/2 strain is more sensitive to the low-dose locomotor stimulant effects of ethanol than the C57BL/6 strain is (Crawley et al., 1997). The relative sensitivity of a mouse strain depends on the variable studied; sensitivity differences do not appear systematically across all response domains (Crawley et al., 1997).

It is extremely important to avoid the temptation to breed wild-type and homozygous mouse pairs separately. Although it requires fewer mice in a colony and curtails genotyping concerns, heterozygous breeding pairs should be maintained in order to provide littermates for testing of homozygous and wild-type mice. When using a mixed genetic background, it is possible that any one strain may be disproportionately represented if small numbers of mice are used for experiments. Therefore, larger-than-usual numbers of animals should be used for comparisons. However, it is preferable to create a back-crossed strain (at least 10 generations). If there is a question about background strain influences on experimental results, microsatellite marker genes can be examined to determine whether strain-specific alleles were inherited equally in the homozygous and wild-type mice (Mohn et al., 1999; Williams et al., 2001; Fortin et al., 2001).

REFERENCES

Adachi YU, Watanabe K, Higuchi H, Satoh T, Zsilla G (2001): Halothane decreases impulse-dependent but not cytoplasmic release of dopamine from rat striatal slices. Brain Res Bull 56:521–524.

Bailey CP, O'Callaghan MJ, Croft AP, Manley SJ, Little HJ (2001): Alterations in mesolimbic dopamine function during the abstinence period following chronic ethanol consumption. Neuropharmacol 41:989–999.

Banbury Conference (1997): Mutant mice and neuroscience: recommendations concerning genetic background. Banbury Conference on genetic background in mice. Neuron 19:755–759.

Bengel D, Murphy DL, Andrews AM, Wichems CH, Feltner D, Heils A, Mossner R, Westphal H, Lesch KP (1998): Altered brain serotonin homeostasis and locomotor insensitivity to 3,4-methylenedioxymethamphetamine ("Ecstasy") in serotonin transporter-deficient mice. Mol Pharmacol 53:649–655.

Bennett BA, Hollingsworth CK, Martin RS, Harp JJ (1997): Methamphetamine-induced alterations in dopamine transporter function. Brain Res 782:219–227.

Bergstrom BP, Garris PA (1999): Utility of a tripolar stimulating electrode for eliciting dopamine release in the rat striatum. J Neurosci Methods 87:201–208.

Bickford-Wimer P, Pang K, Rose GM, Gerhardt GA (1991): Electrically-evoked release of norepinephrine in the rat cerebellum: an in vivo electrochemical and electrophysiological study. Brain Res 558:305–311.

Blier P (2001): Crosstalk between the norepinephrine and serotonin systems and its role in the antidepressant response. J Psychiatry Neurosci 26 Suppl: S3–10.

Bunin MA, Wightman RM (1998): Quantitative evaluation of 5-hydroxytryptamine (serotonin) neuronal release and uptake: an investigation of extrasynaptic transmission. J Neurosci 18:4854–4860.

Callado LF, Hopwood SE, Hancock PJ, Stamford JA (2000): Effects of dizocilpine (MK801) on noradrenaline, serotonin and dopamine release and uptake. Neuroreport 11:173–176.

Carboni E, Spielewoy C, Vacca C, Nosten-Bertrand M, Giros B, Di Chiara G (2001): Cocaine and amphetamine increase extracellular dopamine in the nucleus accumbens of mice lacking the dopamine transporter gene. J Neurosci 21:RC141:1–4.

Chen N, Justice JB Jr (2000): Differential effect of structural modification of human dopamine transporter on the inward and outward transport of dopamine. Mol Brain Res 75:208–215.

Chen N, Trowbridge CG, Justice JB Jr (1998): Voltammetric studies on mechanisms of dopamine efflux in the presence of substrates and cocaine from cells expressing human norepinephrine transporter. J Neurochem 71:653–665.

Crawley JN, Belknap JK, Collins A, Crabbe, JC, Frankel W, Henderson N, Hitzemann RJ, Maxon SC, Miner LL, Silva AJ, Wehner JM, Wynshaw-Boris A and Paylor R (1997): Behavioral phenotypes of inbred mouse strains: implications and recommendations for molecular studies. Psychopharmacol (Berl) 132:107–124.

Davidson C, Stamford JA (1996): Serotonin efflux in the rat ventral lateral geniculate nucleus assessed by fast cyclic voltammetry is modulated by 5-HT1B and 5-HT1D autoreceptors. Neuropharmacology 35:1627–1634.

Daws LC, Toney GM, Gerhardt GA, Frazer A (1998): In vivo chronoamperometric measures of extracellular serotonin clearance in rat dorsal hippocampus: contribution of serotonin and norepinephrine transporters. J Pharmacol Exp Ther 286:967–976.

Daws LC, Gould GG, Teicher SD, Gerhardt GA, Frazer A (2000): 5-HT(1B) receptor-mediated regulation of serotonin clearance in rat hippocampus in vivo. J Neurochem 75:2113–2122.

Del Bigio MR, Vriend JP (1998): Monoamine neurotransmitters and amino acids in the cere-

brum and striatum of immature rats with kaolin-induced hydrocephalus. Brain Res 798:119–126.

Detke MJ, Lucki I (1996): Detection of seratonergic and noradrenergic antidepressants in the rat forced swimming test: the effects of water depth. Behav Brain Res 73:43–46.

Dickinson SD, Sabeti J, Larson GA, Giardina K, Rubenstein M, Kelly MA, Grandy DK, Low MJ, Gerhardt GA, Zahniser NR (1999): Dopamine D2 receptor-deficient mice exhibit decreased dopamine transporter function but no changes in dopamine release in dorsal striatum. J Neurochem 72:148–156.

Earles C, Schenk JO (1998): Rotating disk electrode voltammetric measurements of dopamine transporter activity: an analytical evaluation. Anal Biochem 264:191–198.

Fortin A, Diez E, Rochefort D, Laroche L, Malo D, Rouleau GA, Gros P, Skamene E (2001): Recombinant congenic strains derived from A/J and C57BL/6J: a tool for genetic dissection of complex traits. Genomics 74:21–35.

Gainetdinov RR, Jones SR, Caron MG (1999): Functional hyperdopaminergia in dopamine transporter knock-out mice. Biol Psychiatry 46:303–311.

Giros B, Jaber M, Jones SR, Wightman RM, Caron MG (1996): Hyperlocomotion and indifference to cocaine and amphetamine in mice lacking the dopamine transporter. Nature 379:606–612.

Giros B, Wang YM, Suter S, McLeskey SB, Pifl C, Caron MG (1994): Delineation of discrete domains for substrate, cocaine, and tricyclic antidepressant interactions using chimeric dopamine-norepinephrine transporters. J Biol Chem 269:15985–15988.

Itokawa K, Sora I, Schindler CW, Itokawa M, Takahashi N, Uhl GR (1999): Heterozygous VMAT2 knockout mice display prolonged QT intervals: possible contributions to sudden death. Mol Brain Res 71:354–357.

Jones SR, Gainetdinov RR, Jaber M, Giros B, Wightman RM, Caron MG (1998): Profound neuronal plasticity in response to inactivation of the dopamine transporter. Proc Natl Acad Sci 95:4029–4034.

Lee SH, Lumelsky N, Studer L, Auerbach JM, McKay RD (2000): Efficient generation of midbrain and hindbrain neurons from mouse embryonic stem cells. Nat Biotechnol 18:675–679.

Loren I, Bjorklund A, Falck B, Lindvall O (1976): An improved histofluorescence procedure for freeze-dried paraffin-embedded tissue based on combined formaldehyde-glyoxylic acid perfusion with high magnesium content and acid pH. Histochemistry 49:177–192.

McElvain JS, Schenk JO (1992): A multisubstrate mechanism of striatal dopamine uptake and its inhibition by cocaine. Biochem Pharmacol 43:2189–2199.

Meiergerd SM, Schenk JO, Sorg BA (1997): Repeated cocaine and stress increase dopamine clearance in rat medial prefrontal cortex. Brain Res 773:203–207.

Mena MA, Khan U, Togasaki DM, Sulzer D, Epstein CJ, Przedborski S (1997): Effects of wild-type and mutated copper/zinc superoxide dismutase on neuronal survival and L-DOPA-induced toxicity in postnasal midbrain culture. J. Neurochem 69:21–33.

Mohn AR, Gainetdinov RR, Caron MG and Kollee BH (1999): Mice with reduced NMDA receptor expression display behaviors related to schizophrenia. Cell 98:427–436.

Moron JA, Brockington A, Wise RA, Rocha BA, Hope BT (2002): Dopamine uptake through the norepinephrine transporter in brain regions with low levels of the dopamine transporter: Evidence from knock-out mouse lines. J Neurosci 22:389–395.

Mundorf ML, Joseph JD, Austin CM, Caron MG, Wightman RM (2001): Catecholamine release and uptake in the mouse prefrontal cortex. J Neurochem 79:130–142.

Pan Y, Gembom E, Peng W, Lesch KP, Mossner R, Simantov R (2001): Plasticity in serotonin uptake in primary neuronal cultures of serotonin transporter knockout mice. Developmental Brain Res 126:125–129.

Paxinos G and Watson C (1986): The rat brain in stereotaxic coordinates. Academic Press, San Diego.

Phillips TJ, Belknap JK, and Crabbe JC (1991): Use of recombinant inbred strains to assess vulnerability to drug abuse at the genetic level. J Addict Dis 10:73–87.

Plaznik A, Kostowski W (1991): The involvement of serotonin and noradrenaline in the psychopathological processes of stress and depression: animal models and the effect of antidepressant drugs. Pol J Pharmacol Pharm 43:301–322.

Reith ME, O'Reilly CA (1990): Inhibition of serotonin uptake into mouse brain synaptosomes by ionophores and ion-channel agents. Brain Res 521:347–351.

Rocha BA, Fumagalli F, Gainetdinov RR, Jones SR, Ator R, Giros B, Miller GW, Caron MG (1998): Cocaine self-administration in dopamine transporter knockout mice. Nature Neurosci 1:132–137.

Sanchez-Ramos JR, Song S, Facca A, Basit A, Epstein CJ (1997): Transgenic murine dopaminergic neurons expressing human Cu/Zn superoxide dismutes exhibit increased density in culture, but no resistance to methylphenylpyridinium-induced degeneration. J Neurochem 68:58–67.

Smith AD and Justice JB Jr (1994): The effect of inhibition of synthesis, release, metabolism and uptake on the microdialysis extraction fraction of dopamine. J Neurosci Methods 54:75–82.

Sora I, Hall FS, Andrews AM, Itokawa M, Li X-F, Wei H-B, Wichems C, Lesch K-P, Murphy DL, Uhl GR (2001): Molecular mechanisms of cocaine reward: Combined dopamine and serotonin transporter knockouts eliminate cocaine place preference. Proc Natl Acad Sci 98:5300–5305.

Sora I, Wichems C, Takahashi N, Li XF, Zeng Z, Revay R, Lesch KP, Murphy DL, Uhl GR (1998): Cocaine reward models: conditioned place preference can be established in dopamine- and in serotonin-transporter knockout mice. Proc Natl Acad Sci 95:7699–7704.

Staley JK, Basile M, Flynn DD, Mash DC (1994): Visualizing dopamine and serotonin transporters in the human brain with the potent cocaine analog [125I]RTI-55: in vitro binding and autoradiographic characterization. J Neurochem 62:549–556.

Syringas M, Janin F, Mezghanni S, Giros B, Constentin J, Bonnet JJ (2000): Structural domains of chimeric dopamine-noradrenaline human transporters involved in the Na(+)- and Cl(-)-dependence of dopamine transport. Mol Pharmacol 58:1404–1411.

Wang YM, Gainetdinov RR, Jones SR**,** Fumagalli F, Xu F, Miller G, Bock C, Caron MG (1997): Knockout of the vesicular monoamine transporter-2 gene results in neonatal death and postsynaptic sensitization to cocaine and amphetamine. Neuron 19:1285–1296.

Wayment HK, Schenk JO, Sorg BA (2001): Characterization of extracellular dopamine clearance in the medial prefrontal cortex: role of monoamine uptake and monoamine oxidase inhibition. J Neurosci 21:35–44.

Wightman RM, Amatore C, Engstrom RC, Hale PD, Kristensen EW, Kuhr WG, May LJ (1988): Real-time characterization of dopamine overflow and uptake in the rat striatum. Neurosci 25:513–523.

Williams RW, Gu J, Qi S, Lu L (2001): The genetic structure of recombinant inbred mice: high-resolution consensus maps for complex trait analysis. Genome Biol 2:Research0046.1-0046.18

Wu Q, Reith ME, Wightman RM, Kawagoe KT, Garris PA (2001): Determination of release and uptake parameters from electrically evoked dopamine dynamics measured by real-time voltammetry. J Neurosci Methods 112:119–133.

Xu F, Gainetdinov RR, Wetsel WC, Jones SR, Bohn LM, Miller GW, Wang YM, Caron MG (2000): Mice lacking the norepinephrine transporter are supersensitive to psychostimulants. Nat Neurosci 3:465–471.

Zahniser NR, Larson GA, Gerhardt GA (1999): In vivo dopamine clearance rate in rat striatum: regulation by extracellular dopamine concentration and dopamine transporter inhibitors. J Pharmacol Exp Ther 289:266–277.

CHAPTER 5

SEARCHING FOR NOVEL GENETIC VARIATION IN NEUROTRANSMITTER TRANSPORTERS

RANDY D. BLAKELY AND ALEXANDRA R. BELOUS

5.1 OVERVIEW

Neurotransmitter transporters are key components of synaptic transmission. Through the actions of vesicular neurotransmitter transporters, cytosolic neurotransmitters are packaged for release (Liu and Edwards, 1997; Reimer et al., 2001). Plasma membrane transporters limit synaptic transmission, efficiently removing neurotransmitter from the extracellular space on release in what we now understand to be a dynamically regulated process (Beckman and Quick, 1998; Blakely and Bauman, 2000). Over the past decade, multiple neurotransmitter transporter genes have been identified from *C. elegans* to man (Nelson, 1998), providing new opportunities to assess the degree by which transporter alterations contribute to synaptic function, behavioral variation, and clinical disorders. Because their activities impact signaling at multiple subtypes of receptors, plasma membrane transporter alterations induced by drugs are also complex. To help unravel the contributions of transporters to physiology and disease, investigators have disrupted several transporter genes in the mouse (Giros et al., 1996; Bengel et al., 1998; Xu et al., 2000), demonstrating the impact of transporter function on neurotransmitter clearance and homeostasis and providing models for the behavioral consequences that follow from full or partial loss of function. With the sequencing of human transporter genes, it has also become more straightforward to explore genetic variation that could contribute to clinical syndromes. In recent years, we have become interested in understanding human transporter genetic variation, and it is this goal that frames the current review.

The focus of the current review, the human serotonin (5-HT) transporter (SERT) is a particularly interesting molecule given the long association of disrupted serotonergic signaling in affective, anxiety, and obsessive/compulsive disorders (Murphy et al., 1989; Meltzer, 1990; Fuller, 1991; Horton, 1992) and the role of SERT in antidepressant response (Fuller and Wong, 1990) and the disease process (Owens and Nemeroff, 1994). But the physiologic importance of SERT in man is still an open question, as are what behavioral or physiologic alterations follow from structural changes in SERT genes and proteins. We have some clues for physiologic phenotypes from SERT knockout studies in the mouse (Bengel et al., 1998; Sora et al., 1998; Fabre et al., 2000; Li et al., 2000; Chen et al., 2001; Persico et al., 2001) and these are important leads. Now the task is to utilize this

Transmembrane Transporters. Edited by Michael Quick

ISBNs: 0-471-06517 (Hardcover); 0-471-43404-3 (Electronic)

information to identify human subjects with altered SERT genes. In this regard, polymorphisms in SERT promoter and intronic regions have been under intensive analysis for several years, and yet the data remain controversial. Subjects with changes in SERT protein structure, established through heritable changes in coding sequences, are likely to be rare but also may be highly informative. Some of us are now looking for such subjects, and, in the present review, we describe our general strategies for assessing functional polymorphisms in transporter genes, with a specific reference to SERT.

5.2 SEARCHING FOR RARE GENETIC VARIANTS IN CANDIDATE GENES

For complex disorders in general, as for the mental illnesses where disrupted serotonergic signaling is suspected in particular, two different strategies have dominated the attempt to understand genetic underpinnings. The first involves a genome-wide scan in affected subjects or pedigrees for the presence or segregation of polymorphic DNA markers. This top-down approach has the advantage of making no assumptions as to which gene contributes variation in a trait or the risk for occurrence of a disorder. This approach typically requires a large number of subjects (e.g., many hundreds) and benefits substantially from the careful acquisition of affected pedigrees or sibling pairs where preferential transmission of variant markers can be traced. Once association or linkage is found with a particular marker, the search is on for candidate genes and their variants that explain the linkage. The second common approach, which takes advantage of the biology suspected to underlie the disorder, involves the analysis of common polymorphisms for selected, candidate genes in affected subjects and unaffected controls. Candidate genes are chosen because they appear to lie in biochemical pathways supporting the affected behaviors, because they represent targets for drug response, or because of evidence that suggests that their expression or activity is altered in specific disorders. This approach also benefits from a large collection of affected subjects and controls but can, at least initially, be conducted without regard to whether the genetic variant used for analysis alters function. If the variant under study is found more often in affected subjects (or is transmitted more often in families to affected subjects), a new round of investigation can begin by looking for structural changes in the gene (or its neighbors) that supports association. The journals are full of these studies. They are relatively easy to conduct once subjects are collected, given the advances in polymorphism screening technology that exists today. This type of design can be biased by unknown reasons for shifts in allele frequency in test populations (stratification) that may have nothing to do with the expression or function of the gene. Another problem with this strategy is that it will miss highly informative changes in candidate genes if the variants are rare (say 1 or 2 families in several hundred under study) or their functional impact is small, except on rare genetic backgrounds.

Possibly, the DNA polymorphism being tracked is common and has a known functional impact on the protein. Unfortunately, this is often not the case. For example, in the SERT gene there is a common promoter polymorphism (5HTTLPR, see below) and intronic polymorphism [3rd intron, variable number tandem repeat (VNTR)] that may impact transporter mRNA expression. Since their initial description by Lesch and co-workers (1994; Heils et al., 1996; Lesch et al., 1996), more than 250 studies have appeared that examine their potential impact on anxiety, depression, and other psychiatric disturbances. Conflicting findings are expected in studies of complex disorders in human populations, and studies of the 5HTTLPR are no exception. A helpful orientation would be gained if

families existed where coding alterations, rather than transcriptional alterations, supported behavioral variation or identifiable disorders. But studies that have searched for heritable, coding changes in SERT exons have shown no evidence for common variants (Altemus et al., 1996; Cargill et al., 1999; Glatt et al. 2001). Also, even if enrichment can be achieved by targeting a defined clinical population, complex origins of diseases such as depression or anxiety may make it very difficult to detect contributions of SERT alleles in a general population study.

But perhaps we are expecting too much from such analyses. Major contributions have been made to the pathophysiology of brain disorders through the insightful examination of rare mutations whose presence in a general population would be missed due to their rarity or obscured in the overall complexity of the disorder. The trick is to find subjects for whom changes in gene structure lead as directly as possible to a phenotype. Consider Parkinson's disease (PD). The loss of dopamine neurons that supports PD has long been considered an environmentally triggered event (Calne and Langston, 1983). For the large majority of PD subjects, this may well be true. However, rare examples have been identified where PD "runs" in the family, and we now know the identity of the genetic variants supporting the illness in some of these families (Polymeropoulos et al., 1997; Kitada et al., 1998; Martin et al., 2001). It is clear that these specific variants do not support the larger number of idiopathic PD. However, the true value for medicine in the identification of rare, disease-associated mutations is the elucidation of a pathway. Scientists are now oriented toward other key determinants of α-synuclein and parkin function, and we now have a strong rationale for their therapeutic manipulation to support the health of DA neurons. Perhaps we can take some lessons from these efforts to understand the molecular foundations of mental illness. Given the significant investment currently being placed in population association studies of serotonin transporter and receptor genes, we argue that it is time to orient at least some of our energies toward a concerted effort to identify the rare families in whom SERT coding variants exist. Such an activity has the opportunity to redefine phenotypic categories and to clarify syndromes where serotonergic dysfunction plays a primary, rather than an indirect, role.

Our thoughts on searching for informative variants in the SERT gene arise from a specific context. Recently, we uncovered a polymorphism in the norepinephrine transporter (NET) in a single subject and her identical twin, who bore a diagnosis of orthostatic intolerance (OI) (Shannon et al., 2000; Robertson et al., 2001). OI is characterized by an excessively elevated heart rate on standing (>30 bpm elevation), little or no fall in blood pressure, and enhanced spillover of catecholamines to the circulation. Physiologic and biochemical studies with the proband's identical twin and family members supported the contention that the NET variant, A457P, supports the OI syndrome in our proband. OI is a common autonomic disorder (Robertson, 1999; Robertson et al., 2000), but our current investigations tell us that most OI is unlikely due to the A457P NET mutation. Is our discovery of a NET mutation in OI therefore of minor consequence? Certainly there may be other mutations in NET besides A457P that could support OI, and we are looking for these now. However, we suspect the situation is far more complex, owing to the many cellular and biochemical regulatory pathways that can destabilize heart rate or baroreflexes required for sustained, upright posture. Of greatest importance, the identification of individuals with a genetically encoded NET mutation solidifies the notion that hypernoradrenergic signaling, however derived, likely explains a significant fraction of OI-like disorders and thus focuses future efforts toward understanding mechanism and developing therapies. Moreover we are compelled to obtain a more intensive analysis of our ini-

tial family to understand the most penetrant characteristics that could define NET alterations in other contexts, including psychiatric disorders (Blakely, 2001).

Finally, we must be honest and admit that our focus on candidate gene studies arises primarily because we are also molecular biologists, fascinated with the structural organization and regulation of the transporters we research. Efforts we make to identify transporter contributions to specific behaviors or disorders also have the opportunity to shed light on how transporters are synthesized, localized, or fine-tuned to meet the needs of chemical signaling. It would do little for our immediate research programs to uncover variants in other genes, unless we could relate these directly to the molecules that establish our frame of reference. There are many open questions in transporter biology, and information gleaned from functional studies in vivo may be pivotal to providing new leads. There are more than 12,000 possible variations in the SERT protein that could be established through site-directed mutagenesis of cloned cDNAs. Although more than a hundred such mutations have been made in SERTs or its transporter homologues, these efforts are typically slow and expensive. Even more important, we must always remember our limitations to define relevant perturbations of function in vitro. Site-directed mutagenesis still has its place in SERT biology in the testing of functional hypotheses targeted to specific domains and residues (e.g., Barker et al., 1998; Chen et al., 2000; Adkins et al., 2001), but identification of physiologically relevant variants may not always be predictable from in vitro studies. We simply may not know enough to define the right models, set up the appropriate conditions, or ask the right questions to close the gap between in vitro and in vivo studies. One solution then is to let human physiology do some of the work for us, working from the assumption that critical sites in the transporter that dictate complex structure, function, or regulation can reveal themselves if we can define a reasonable *in vivo* phenotype. Just how we do the latter is critical and calls on all we know about serotonergic anatomy, pharmacology, and physiology. Below we trace our approaches in tackling this objective.

5.3 SEARCHING FOR TRANSPORTER GENE POLYMORPHISMS: DEFINING A GENERAL STRATEGY

In subsequent sections, we provide our current conception of the study populations and methods relevant to tackling the SERT gene as one example of uncovering variation in transporter genes. Here, we provide an overview to outline general issues that should be pertinent to the identification of variants in any candidate gene.

In Figure 5.1, we frame our considerations in terms of efforts necessary as one begins to look for genetic variation. First there is the selection of the candidate gene itself. A lab such as ours might work on several such genes, but a limited understanding of human gene structure or biological activities for some molecules could, in principle, limit opportunities to begin a directed search for human variants. Second, success in the effort will depend largely on critical partnerships between the basic scientist and clinical investigators who have a keen eye for human physiologic variation. In the absence of such partners, the human subjects targeted for the investigation are unlikely to be recruitable, and even more the fine-tuning of the candidate phenotypes will be far more limited. One is thus best off picking the candidate gene for which these partnerships are available. Discussions with clinicians as to how they encounter the functional or pharmacological aspects of this gene can help define candidate phenotypes.

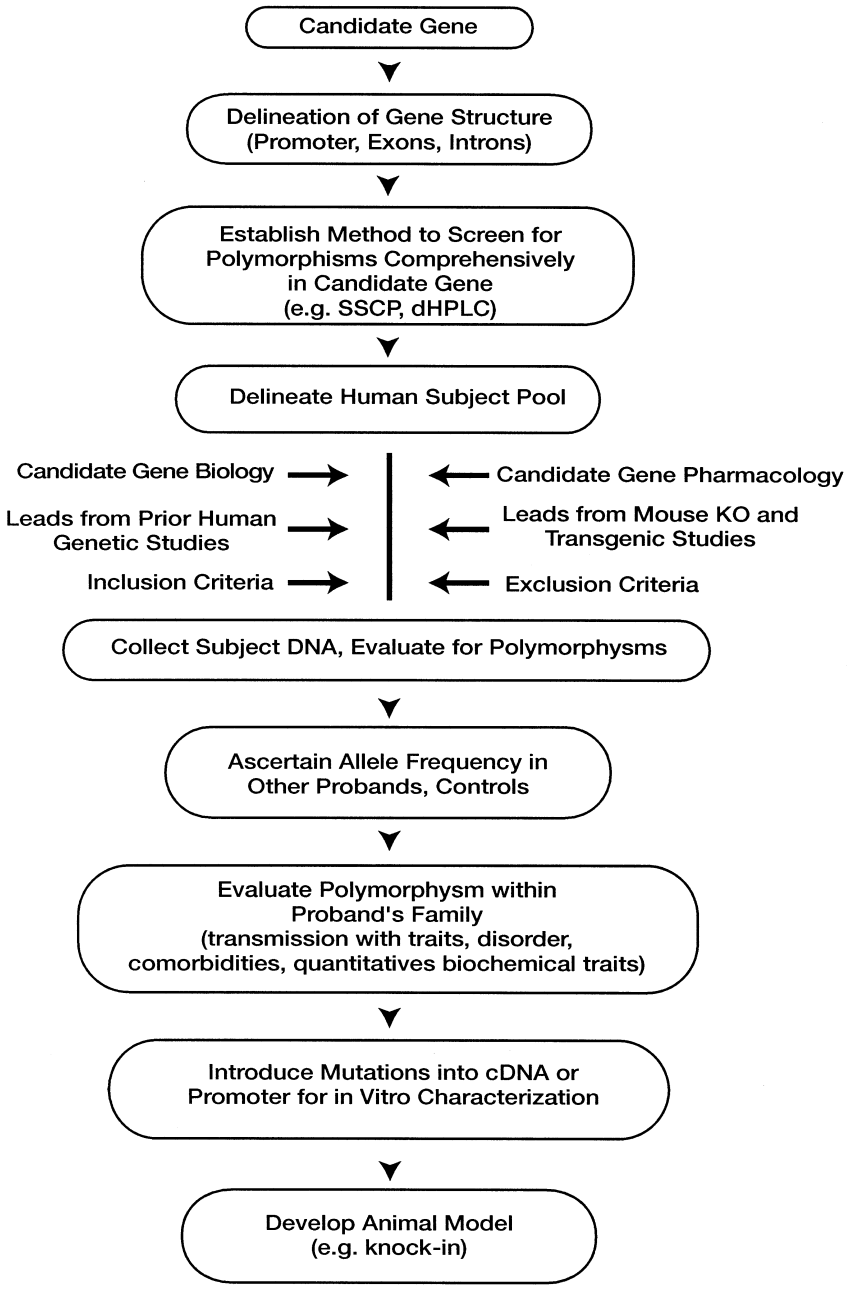

Figure 5.1. Flow diagram for the identification of genetic variants in candidate genes.

Once one is confident that the appropriate team is in place to tackle the chosen candidate on both basic and clinical dimensions, it is essential to define the organization of the gene and to determine what regions will be targeted for investigation. Exons tend to harbor fewer variants than intronic regions, owing to the conservation of amino acid sequences; introns, in many cases, may well lack functional impact. If the gene harbors multiple introns and the exons are spread out across a large expanse of genomic DNA, it may also be too costly to screen for variation in intronic sequences. In contrast, changes in the sequence of splice junctions are likely to disrupt mRNA splicing and result in an altered protein product. Changes in sequence in coding regions may not change the coding of the protein (so called "synonymous polymorpmisms"), owing to the degeneracy of the genetic code. "Nonsynonymous polymorphisms," or changes in sequence that do alter the structure of the protein, may or may not affect function of the protein, conclusions that can be reached only after additional in vitro and in vivo studies. Variations that lead to truncations, deletions, or expansions in the protein are, of course, most likely to yield a loss of function. Finally, enough may be known as to the structure of critical transcriptional regulatory regions in the promoter to include a limited segment of it in the analysis as well, although this is likely to greatly increase the extent of DNA coverage attempted. Moreover, enhancers for transcription may be located far from mRNA initiation sites, which would make complete coverage of regulatory regions impractical.

Next, one must establish a method that can provide for the analysis of a large number of subject DNAs with high accuracy and at reasonable costs. If multiple exons exist, and these are interrupted by large (>500 bp) introns, current strategies typically necessitate analyzing one or a few exons at a time. This will mean that for every individual analyzed, multiple DNA segments will be analyzed, increasing costs and labor. For small genes that are intronless or where exons are interrupted by small exons, only a few analyses can provide full coverage. For the SERT gene (see below), the situation is one of multiple exons separated by larger introns. Direct sequencing of DNA templates is expensive, and analysis is generally labor-intensive and can often pose challenges in interpretation of heterozygous alleles. As we note below, we have opted for denaturing high-performance liquid chromatography (dHPLC) methods that provide for semiautomated DNA analysis and allow for the detection of single nucleotide polymorphisms (SNPs), the most common type of sequence variation, based on pattern recognition rather than exact sequence reads.

With a method for detecting variation in hand, one can turn to the most challenging dimension of this effort, defining the human subject population. The analogy of finding a needle in a haystack is appropriate here and, if we are to have any chance at this effort, we certainly must be in the right haystack. Of course, no such restriction on populations to be screened would be necessary if we could sequence subject DNA with high fidelity, in large numbers of individuals, at little or no cost. But this is currently not the case for most of us, and, for cases involving single mutations in one or a few families, even the highest throughput analysis might not identify these variants. The effort therefore must begin with an enriched population, identified from what we know of the biology of our molecule, including the tissues and pathways of its expression, the functional role of these organs or circuits, and any known physiologic regulators of candidate gene activity.

In selecting our subjects, we may also not want to settle on just one phenotype, particularly if our molecule is expressed in multiple tissues. For example, we may choose to examine subjects with both a specific mental illness and a cardiovascular syndrome if our molecule is expressed in both the brain and the heart. We may limit our study population based on the gamut of physiological changes that occur when we pharmacologically ma-

nipulate our target. For example, if an antagonist of our candidate gene precipitates seizures, we might consider a population with epilepsy to be enriched for loss of function mutations. We must also consider what a "gain of function" might look like, as these mutations could also exist in our subjects. For example, we might find a mutation that fails to be negatively regulated normally, say by internalization from the plasma membrane. Considering excess function may be as useful strategically as loss of function, identifying such variants could help clarify regulatory mechanisms that normally constrain function for response to key modulators.

If we can recruit subjects who are actually challenged with a drug known to target our candidate protein, we have an added opportunity to limit our study population, for example, to nonresponders. Leads from clinical studies monitoring association with existing, common polymorphisms in our gene are also certainly worth considering, particularly if a consistent story has emerged. In the face of multiple, conflicting reports of linkage of extant polymorphisms, however, it may be prudent to weigh this information less heavily than others. If the gene has already been disrupted or overexpressed in the mouse, this information could be helpful in defining or limiting the subject population. Again, by example, if a knockout of the candidate gene leads to fatal seizures, we might consider an epileptic population to have greater rationale than others, always keeping in mind that a mouse phenotype will not always predict the human condition. Transgenic mouse lines can also be informative as to gain-of-function phenotypes. For example if our gene, when overexpressed in the mouse, precipitates a motor abnormality, we might reasonably consider human motor disorders as candidate syndromes enriched for gain-of-function alleles. Finally, we must develop inclusion and exclusion criteria for a genetic analysis. Even with very suspicious phenotypes, these could be environmentally triggered or representative of known pathologies that are unrelated to our candidate gene. Thus, we narrow our focus to cases where there is a family history of the disorder and where other known contributors to the phenotype (e.g., excessive drinking, trauma, overt pathology) have been ruled out. We will want to consider issues of ethnicity, gender, and age of onset, as there may be literature relating these issues either to our candidate directly or pointing more prominently to other causes. In the end, we must recognize that we are unlikely, either due to lack of information, technology, or patience, to be able to restrict the population just to those subjects having a variant in the gene in question, so we must gear our analytical approaches to allow for a significant fraction of negative findings.

Once the population has been defined, we move to the DNA collection stage. This often involves drawing blood on subjects to isolate lymphocyte DNA. One may also choose to immortalize lymphocytes for long-term banking of a renewable source of the subject's DNA. Alternatively, one may collect enough DNA from cheek swabs or mouthwash rinses to evaluate DNA polymorphisms, and this would certainly be a less traumatic experience if the population under study were children. Although not as much DNA will be recovered, we have found this approach adequate for sensitive screening methods. If our gene is expressed in peripheral blood cells, we may also be able to isolate RNA and then screen for sequence variation in the spliced transcripts that encode our protein. One problem with this approach is a false negative result arising from heterozygous subjects where the mutation destabilizes transcription of the mutant allele or impacts mRNA stability, thereby eliminating the mutant transcript from our samples. We might also choose to screen peripheral cells by using antibodies to gain insight into possible changes in protein structure arising from genetic changes. However, there is no reason a priori to expect that loss or gain of function will equate with altered gel mobility. Certainly, however, altered

electrophoretic mobility of mutant proteins obtained from tissue biopsies or circulating cells would help validate hypotheses as to how coding variants lead to a disruption of function.

Next, we move to polymorphism screening. Any identified sequence variants are registered and then categorized as coding or noncoding, synonymous or nonsynomymous, and, if nonsynonymous, whether they are conservative or nonconservative changes. Such classification can help prioritize in vitro experiments and give us a clue to whether there is likely to be a functional impact of the variant. In practice, of course, it is prudent to assay all variants as extensively as possible. To certify a link to behavior, physiology, or a disorder, we will need multiple individuals with the allele. Even if this is a rare variant, studies within the proband's family are possible and may be instrumental of linking gene to phenotype. We may not want to limit ourselves to a singular display of the phenotype but consider other ways in which the variant could express itself because different individuals may well harbor compensating genes that could mute an effect in one pathway but not another. In vitro studies with engineered mutant cDNAs or promoter constructs will allow us to define mechanistic features related to altered function, such as improper trafficking or substrate selectivity. Ultimately, conclusions reached in vitro must be validated in vivo. We can do this by direct assessments of biochemistry and physiology related directly to our protein (e.g., altered transport, binding, disrupted localization seen in biopsied samples), or we may gain from introducing the variant into an otherwise normal mouse gene, generating a "knocked-in" allele. The latter model has the added advantage of offering a system for the evaluation of pharmacologic or genetic therapies to improve the lives of subjects carrying specific mutations (assuming that the variant negatively impacts health or quality of life).

5.4 ANATOMICAL CONSIDERATIONS FOR ASSESSMENT OF SERT GENETIC VARIATION

In searching for phenotypes to consider in seeking variants in the SERT gene, we should first consider the anatomy of 5-HT systems and their relationship to SERT expression. 5-HT is a neurotransmitter synthesized by neurons of the midbrain and brainstem raphe complex, whose ascending projections course throughout virtually the entire forebrain and target circuits that regulate mood, arousal, aggression, and appetite, and whose descending projections reach the spinal cord and influence autonomic homeostasis and pain perception (Steinbusch, 1981; Tork, 1990; Jacobs and Azmitia, 1992; Mason, 2001). SERT proteins are found presynaptically on serotonergic axons and terminals throughout the adult rodent central nervous system (CNS) (Qian et al., 1995; Zhou et al., 1998). Interestingly, the thalamocortical system is transiently serotonergic in the early postnatal rat, with expression of SERT involved in capturing extracellular 5-HT for release (Lebrand et al., 1996; Lebrand et al., 1998). In addition, the gastrointestinal (GI) system is particularly rich in 5-HT (Gershon, 1999). Enterochromaffin cells lining the gut secrete large amounts of 5-HT in response to stretch and other stimuli and thereby modulate peristaltic reflexes and fluid secretion. In addition, many intrinsic enteric neurons are serotonergic. In the gut, SERTs are found on both enteric neurons and crypt epithelial cells (Wade et al., 1996; Gershon, 1999). Platelet secretory granules represent an important peripheral depot of 5-HT, released for modulation of vascular tone during platelet activation (Sneddon, 1973; Stolz, 1985; Houston and Vanhoutte, 1986). Lymphocytes also express

SERTs and have proven useful as an accessible source of SERT genomic DNA in association studies (Lesch et al, 1996), although the function of lymphocyte SERT is unclear (however, see Serafeim and Gordon, 2001; Serafeim et al., 2002). SERTs are also expressed in placenta (Balkovetz et al., 1989; Nguyen et al., 1999), where they may participate in restricting 5-HT access to the fetus, except under defined conditions. SERTs are also found on pulmonary endothelial cells and smooth muscle (Lee and Fanburg, 1986; Lee et al., 1989; Eddahibi et al., 2001), and SERT activity appears critical for hypoxia-induced smooth muscle cell proliferation, which suggests that SERT alleles could influence risk to pulmonary hypertension. Thus, although disrupted 5-HT signaling has long been considered relevant for psychiatric disorders, SERT dysfunction might also support more peripherally based phenotypes (Blakely, 2001), with phenotypes linked to GI, placenta and pulmonary dysfunction reasonable considerations. The transient expression of SERT in the forebrain thalamocortical system raises questions as to a possible perturbation by SERT variants of cortical development (Persico et al, 2001).

5.5 CLONING OF SERT AND THE ELUCIDATION OF SERT GENE STRUCTURE

Following the scheme we outline above for polymorphism identification and having chosen our candidate gene (SERT) for investigation, we now must understand the structure of the human gene and its reported patterns of genetic variation. Rodent cDNA cloning studies (Blakely et al., 1991; Hoffman et al., 1991) first revealed that SERTs exhibit a 12-transmembrane domain structure with intracellular amino and carboxy termini, as predicted for aminobutyric acid (GABA) (Guastella et al., 1990) and NETs transporters (Pacholczyk et al., 1991). Ramamoorthy and co-workers (1993) identified a human cDNA from a placental library and found this cDNA to induce antidepressant-sensitive 5-HT uptake on transfected, nonneuronal cells. A cDNA encoding an identical hSERT protein was amplified from human platelets and found to be identical to the sequence of a brain isolate (Lesch, et al., 1993). In situ hybridization localized SERT mRNA in neurons of human dorsal raphe (Austin et al., 1994), reinforcing the contention that the isolated placental, platelet, and brain SERT derive from a common gene. Using differential hybridization to somatic cell hybrid DNA panels and in situ hybridization of chromosome spreads, Ramamoorthy and co-workers (1993) established a single chromosomal localization for the SERT gene (SLC6A4) at 17q11.1–q11.2, a finding that has been confirmed independently (Gelernter et al., 1995). The identification of a single SERT gene locus is consistent with the identical sequence found for brain and peripheral SERTs. These studies have important consequences for attempts to identify human SERT polymorphisms as a) there is only a single gene to characterize; b) the same gene is expressed in brain and peripheral tissues, broadening possible phenotypes to consider; and c) there appears to be no other closely related 5-HT transporter that might compensate for altered SERT function arising from functional polymorphisms in coding sequences. No evidence has, as yet, been found in SERT mRNAs for coding variants generated by alternative RNA splicing. However, brain and peripheral SERTs do appear to differ in their extent of posttranslational, N-linked glycosylation. (Qian et al., 1995).

An initial delineation of the structure of the SLC6A4 gene was established by Lesch and co-workers (1995), who reported a 14-exon structure where each of the putative 12-transmembraine domains resides within a single exon. One 5′ noncoding exon was also

apparent. Further work has updated the structure of 3′ and 5′ regions of SLC6A4. 3′-RACE (Rapid Amplification of CDNA Ends) from JAR cells and human whole blood identified two commonly used polyadenylation sites (567 and 690 bp downstream of the stop codon) (Battersby et al., 1999). 5′-RACE suggested a single transcriptional start site localized 14 kb upstream of initiation of translation with proximally located TATA-like box and Ap-1 and CRE (Cyclic AMP Response) sites (Heils et al., 1995). The human SERT gene also contains an alternatively spliced, noncoding exon (now termed exon 1b), separated from exon 1 (now termed 1a) by a 736-bp intron (Fig. 5.2) (Bradley and Blakely, 1997). The alternatively spliced exon was found to be expressed in both brain and placental JAR cells. The function of this exon, with respect to SERT mRNA stability/translation or localization, has yet to be resolved.

A 1.5-kb genomic DNA segment upstream of hSERT exon 1a was initially characterized as the SERT promoter, demonstrating transcriptional activity in JAR cells (Heils et al., 1995). Within the 5′-end of this region Heils and co-workers further identified a repeat element bearing a 44-bp deletion polymorphism at position -1212 to -1255 (Heils et al., 1996). The polymorphism, termed the 5-HTTLPR (Fig. 5.2), generated polymerase chain reaction (PCR) products of 484 or 528 bp, representing the short (s) or long (l) allele, respectively. This polymorphism was suggested to be functionally significant as the s allele is less active than the l allele in reporter gene assays (Heils et al., 1996), findings supported by endogenous expression with lymphoblast cell lines, which express SERT (Lesch et al., 1996). Transfection of promoter constructs into lymphoblast cell lines demonstrated, for the l allele, two- to threefold greater basal transcriptional activity. Both alleles supported activation of reporter gene expression by activators of protein kinase C and adenylate cyclase pathways. The l and the s variants of the 5-HTTLPR have also been reported to direct transcription with different efficiencies in native cells, resulting in differential mRNA and protein expression in cultured raphe neurons, platelets, and postmortem brain tissue (Lesch et al., 1996; Heils et al., 1998;

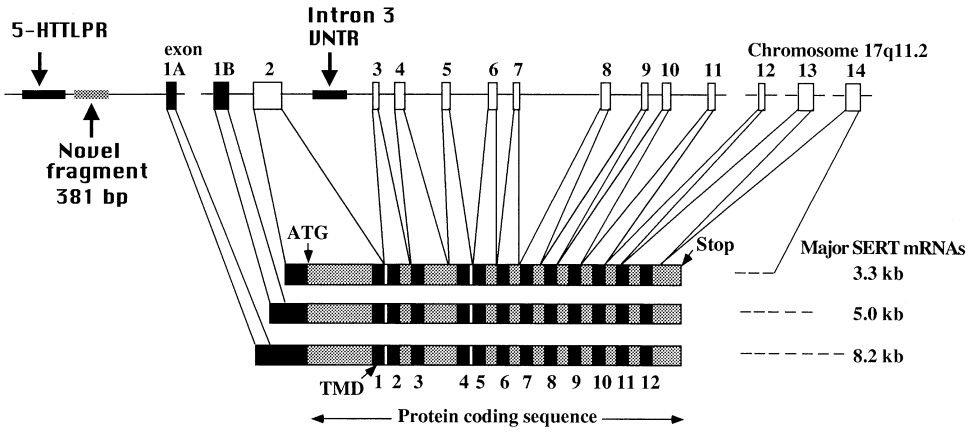

Figure 5.2. Schematic representation of the human SERT gene (SLC6A4). SLC6A4 is encoded by 15 exons, with two, alternatively spliced 5′ noncoding exons (1a and 1b). Alternative polyadenylation is also responsible for mRNA diversity. 5HTTLPR and VNTR designate a promoter repetitive sequence and a variable nucleotide tandem repeat sequence, respectively.

Little et al., 1998; Greenberg et al., 1999). In platelets as well as pulmonary smooth muscle cells, the l variant is associated with increased rates of 5-HT uptake (Greenberg et al., 1999; Eddahibi et al., 2001). Recently, three groups (Mortensen et al., 1999; Lesch et al., 1999; Flattem and Blakely, 2000) have reported a 381-bp insert between this polymorphic region and the transcription start site that lacks in the original description of the promoter (Fig. 5.2). This sequence appears to support transcriptional activity of the promoter region alleles (Mortensen et al., 1999) and may represent an unstable chromosomal element. Lesch's group has reported a reduction in instability of these sequences in subjects with major depression (Lesch et al., 1999), findings yet to be corroborated independently.

A VNTR polymorphism consisting of multiple copies of a 17-bp repeat in the 3rd intron (formerly designated as intron 2 polymorphisms before the identification of exon 1b) has also been reported (Lesch et al., 1994) (Fig 5.2). The VNTR is composed of 17 bp repeats, and the most prevalent alleles are the 10- and 12- repeat (Lesch et al., 1994). 9- and 11-repeat alleles have also been identified (Gelernter et al., 1999). Recent evidence suggests that the intron 3 VNTR polymorphism may act as a transcriptional enhancer (Fiskerstrand et al., 1999; Mackenzie and Quinn, 1999). There was also sequence difference between the 10- and 12-repeat that could result in ability of the 12-repeat to bind different factors than the 10-repeat. These findings support that intron 3 of the SLC6A4 plays an important role in transcriptional regulation, and this polymorphic region may help establish appropriate cell-specific expression of SERT in vivo. Together with the 5HTTLPR, the VNTR constitute known common genetic variations in the hSERT gene with which association studies have explored clinical phenotypes that might involve changes in SERT gene expression (Hahn and Blakely, 2002).

As noted, SNPs are the most common sequence variants in the human genome and are likely to provide the genetic variability inherent in most traits and common diseases. By convention, geneticists often note a site to be polymorphic if the frequency of the observed allele is >1%, whereas changes termed "mutations" are rare (Roses, 2000). Lesch and co-workers (1995) initially reported one synonymous change in a single bipolar patient. Four additional polymorphisms in the human SERT gene (two nonsynonymous, one synonymous, and one noncoding) were recently described through efforts to identify informative SNPs in the human genome (Cargill et al., 1999). Of the coding variants described by Cargill and co-workers (1999), one results in an alanine for glycine substitution at amino acid 56 in the N-terminus of the transporter, whereas the second is a nonconservative substitution of an aspartate for a lysine residue at amino acid 605 in the SERT C-terminus. Neither of these variants has yet to be explored for functional impact or association with a specific phenotype. Their location in cytoplasmic domains suggests that they could influence transporter regulation. Recently, several additional rare coding SNPs have been identified in the human SERT gene (Glatt et al., 2001) in a general population survey by using the National Human Genome Research Institutes (NHGRI) Polymorphism Discover Research Panel of 450 subjects of mixed ethnicity (Collins et al., 1998), but have not been characterized functionally. Even though these variants have been found in a small number of subjects, as we have argued, they may in fact alter SERT function in significant ways and could support behavioral or physiologic syndromes in the proband's or the proband's relatives. These studies attest to the rarity of SERT coding variants. This is an important finding with respect to future screening efforts, as one is unlikely to have to contend with re-isolation of common, uninformative coding variants; therefore, novel alleles should be more readily apparent.

5.6 ESTABLISHING METHODS FOR SCREENING OF NOVEL SERT GENE POLYMORPHISMS

With an understanding of the layout of the SERT gene and an initial appreciation for critical regulatory regions, it is now possible to develop methods to efficiently evaluate the gene in human subjects for polymorphisms. We choose to bypass analysis of introns as this additional 35 kb of genomic DNA is largely unstudied and of unknown importance. Evaluating the known promoter region approximately doubles the analytical task, adding ~2 kb to the 1890 bp of exonic material that encompasses the SERT coding sequence. Considering whether to include regulatory regions in a polymorphism discovery effort is, of course, largely determined by the budget and scale of the screening effort. Because our lab is focused on the biology of transporter proteins, we are naturally most interested in variants that would affect the coding potential of SERT and have thus confined our initial analysis to exons and splice junctions.

Given that existing coding variants are rare, we prefer not to sequence genomic DNA but rather to adopt a pattern recognition approach that would allow one to determine whether a segment of DNA harbors sequence variation, as compared with a reference template. Our current method is an approach based on temperature-modulated, dHPLC (Giordano et al., 1999; Spiegelman et al., 2000) and is performed with a WAVE system from Transgenomics, Inc. (Omaha, NE, USA) This system allows for the evaluation of elution profiles of partially denatured, double-stranded DNAs in an automated, gel-free system. The technique is sensitive to single-base changes in DNA sequence in up to ~600 bp of amplified DNA. First, we establish PCR amplicons containing DNA of relatively uniform melting profiles (as determined by WAVEMAKER software; Transgenomics) and cover each exon with 20–60 bp of surrounding sequence to ensure incorporation of splice junctions. As intronic sequences often contain uninformative SNPs, we try to limit the amount of intronic sequence analyzed. In some cases, however, the placement of oligonuclotide primers is limited by the existing melting profiles of the genomic DNA. In some cases, we split our DNA segment into two amplicons, which allows a more uniform melting profile for each respective amplicon. For SERT, our PCR amplicons thus range from 200 to 500 bp and are generated on genomic DNA purified from 8–10 ml of whole blood (Puregene DNA Extraction Kit, Gentra Systems, Minneapolis, MN, USA). All blood collections and DNA analyses are performed by following informed consent of subjects under approved Institutional Review Board protocols. PCR reactions are performed on a Gene Amp PCR System 2400 by using *AmpliTaq GoldTM* DNA polymerase (Perkin Elmer-Applied Biosystems, Inc., Foster City, CA) and *PfuTurbo* DNA polymerase (Stratagene, Inc., La Jolla, CA) mixed at a ratio of 9:1. As the system is sensitive to single base errors, the inclusion of a polymerase with high 5′–3′ exonuclease activity is essential. Other polymerase mixtures can be used, although the columns deteriorate or can clog if used with unapproved buffer components; one is advised to consult closely with the manufacturer before branching out to new polymerase cocktails.

Before chromatography, a proband's SERT gene, in the form of PCR products (50 ng) for each exon, is mixed with the equivalent amplified exon from a presequenced, unaffected subject. In this manner, both heterozygous and homozygous mutations can be identified because both will contribute a proportion of mutant strands for annealing with control templates. Samples are denaturated at 95°C for 4 min, followed by gradual reannealing from 95°C to 25°C over 30 min and then injected into a DNASepR column with the mobile phase consisting of a linear acetonitrile gradient in 0.1 M triethylamine

acetate buffer (TEAA), prepared by mixing of 0.1 M TEAA and 25% acetonitrile in 0.1 M TEAA. The calculated gradient, at a flow rate of 0.9 ml/min, is applied for all of the amplicons at column temperatures optimized for each amplicon. DNA is detected by UV absorbance, although one can implement a fluorescent detector if the oligonucleotides used for PCR amplification are end-labeled. Elution profiles for each amplicon are evaluated visually against chromatograms obtained from melted and re-annealed control samples to look for evidence of altered DNA elution, indicative of heteroduplex strand misalignment. All amplicons with suspicious elution profiles are sequenced on both strands by using amplicon or internal primers and fluorescent dideoxynucleotide terminators. This approach limits sequencing only to those templates suspected of harboring a sequence variant. Single-base mismatches are readily detected in this system. Figure 5.3 demonstrates the elution profile of an amplicon bearing a single base mutation compared with a control amplicon elution profile.

Next, the suspicious amplicon is sequenced by standard dideoxynucleotide approaches and, once the polymorphic base has been found, we perform a separate test to validate the presence of the polymorphism. If the sequence variation creates a unique restriction site, we digest amplicons from control and the proband and test for a restriction-fragment length polymorphism (RFLP). If an RFLP is not predicted, we utilize allele-specific

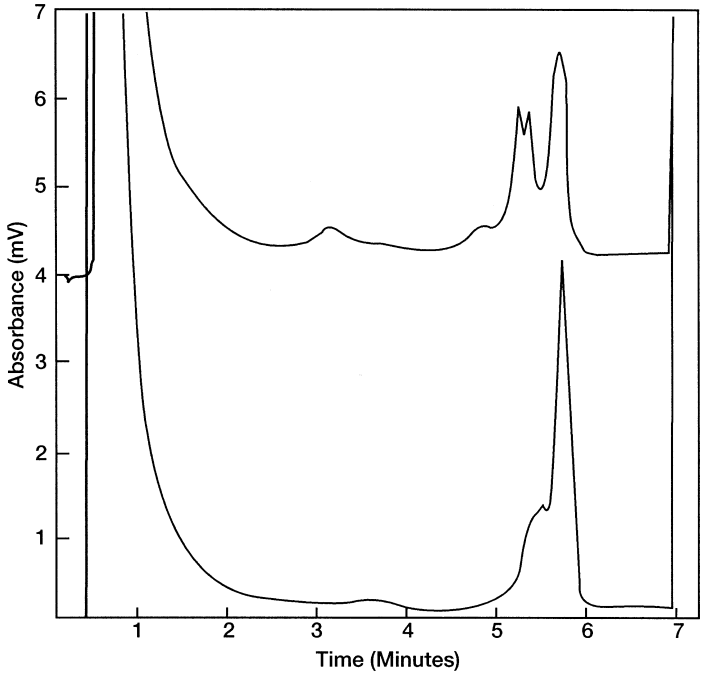

Figure 5.3. Identification of SERT polymorphisms using dHPLC. Shown are elution profiles for two amplicons of SLC6A4 following partial denaturation and chromatography on a WAVE dHPLC system. Note the readily distinguishable profiles of amplicons derived from a control SERT exon (bottom trace) and an amplicon bearing a heterozygous SNP (upper trace). Sequential processing of SERT amplicons on the WAVE system allows for efficient analysis of SERT sequence variations without recourse to DNA sequencing.

oligonucleotide (ASO) hybridization to validate the presence of the mutant allele (Shannon et al., 2000). In this latter strategy, subject and control amplicons are denatured onto nylon membranes and then hybridized to [32P]-labeled oligonucleotide probes carrying either the wild-type or the variant sequence. After the filters of excess probe have been washed, hybridization with the mutant oligonucleotide—but not the control oligonucleotide—is easily demonstrated on X-ray film.

As the dHPLC system is automated, samples can be loaded for unattended analysis. Our system has a 96-sample loader. Each run takes ~10 min, including time for column re-equilibration. If a gene has been divided into 15 amplicons, a single person's DNA can be evaluated in little more 2 h. Elution profiles are then evaluated for anomalous elution patterns and then either the amplicons are subjected to direct sequencing or another subject's DNA is analyzed. Our system allows for material for the analysis of approximately seven subjects to be loaded at a time. Once conditions for amplification have been set, this method provides a reasonably routine analysis of genomic structure with considerably lower sample costs than DNA sequencing. Pooling strategies, where multiple probands are combined for group analysis, can also be implemented to reduce costs further (Hoogendorn et al., 2000). The method is reasonably well suited to the sizes of samples available in clinical settings. For example, Glatt and co-workers (2001) reported SERT SNPs in 450 subjects drawn from the NHGRI Polymorphism Resource Panel (Collins et al., 1998). We have used this approach to evaluate juvenile obsessive-compulsive disorder (JOCD) subjects for novel SERT polymorphisms (Belous et al., 2000; Belous et al., manuscript in preparation) and are currently utilizing this method to explore SERT variation in major depressive disorder (MDD), irritable bowel syndrome (IBS), and IBS and MDD comorbid disorders (Belous et al., 2001). In our JOCD survey, we identified no novel coding variants but did detect a SNP (2631C) in exon 1b, the alternatively 5′ noncoding spliced exon (Bradley and Blakely, 1997). Subsequent genotyping of this SNP in our JOCD subjects and controls reveals an increase in its frequency in affected subjects, which suggests that it may itself make a functional contribution to SERT mRNA expression or be linked to another informative variant.

5.7 HINTS OF PHENOTYPES FOR VARIANT SERT ALLELES FROM GENETIC STUDIES IN MOUSE AND MAN

With an understanding of our candidate gene's structure and dHPLC methods in place to efficiently evaluate sequence variation, the task now turns to defining the subject pool. In this final section, we discuss the findings that have arisen from studies of SERT knockout mice, as well as provide a short review of leads apparent in studies of the hSERT 5HTTLPR and 3rd intron VNTR.

The cloning of the mouse SERT gene (Bengel et al., 1997) identified genomic sequences suitable for the creation of targeting vectors and the production of SERT knockout mice. Homozygous targeted mice were found to lack SERT mRNA and antidepressant-sensitive 5-HT transport and antagonist binding, as assessed in membranes and via autoradiography, and to have significantly lowered tissue stores of 5-HT (Bengel et al., 1998). Although heterozygous animals exhibit a reduction in mRNA and binding sites compared with wild-type controls, they retained full transport function. We speculate that retention of function may arise from altered trafficking to redistribute pools of transporters from intracellular pools to the cell surface. On the one hand, this may be a fortu-

itous demonstration of plasticity in the system and could indicate that CNS-based phenotypes may be hard to identify because the most common human variants are likely to be carried as heterozygous alleles. On the other hand, these changes arise from a null allele. Changes arising from an altered protein sequence that corrupts transporter maturation or function could have dominant-negative attributes, corrupting expression of the wild-type allele, as recent studies have suggested homomultimerism of SERT subunits (Kilic and Rudnick, 2000). Full loss of SERT function leads to significant changes in 5HT levels, receptor expression, and receptor signaling (Fabre et al., 2000; Li et al., 2000; Gobbi et al., 2001; Mossner et al., 2001). The density of 5-HT_{1A} receptors in the dorsal raphe was reduced in both male and female SERT knockout mice, but this reduction was more significant in females than in males (Li et al., 2000). Insensitivity to pharmacologic challenges or stressors that require intact autoreceptor function might represent useful phenotypes indicative of novel SERT polymorphisms. Further exploration of cognitive and somatosensory phenotypes are needed in these animals, given the disruptions of the barrel field formation evident in the homozygous knockouts (Salichon et al., 2001).

Two recent efforts to characterize the peripheral phenotypes of SERT knockout mice have revealed interesting facets of SERT biology that may translate to human conditions enriched for SERT sequence variants. Chen and co-workers (2001) have examined the impact of the SERT KO on GI function. As noted, SERT is richly expressed in the enteric nervous system, where it functions to terminate the actions of 5HT released by intrinsic myenteric and submucosal neurons (Wade et al., 1996; Gershon, 1999). Functional studies with SERT antagonists reveal a biphasic impact on colonic motility that is consistent with hyperactivation of 5HT receptors followed by their desensitization at higher concentrations of extracellular 5-HT (Wade et al., 1996). SERT is also found in the crypt epithelium, where it may limit effects on fluid secretion triggered by enterochromaffin cell-derived 5-HT. In the SERT knockouts, colonic motility, and stool water were altered, along with the increase in motility (diarrhea) that alternated irregularly with decreased motility (constipation), a phenotype often seen in human subjects suffering from IBS (Manning et al., 1978; Thompson, 1993). The knockout mouse studies also demonstrate that 5-HT levels in the gut are unaffected by SERT loss of function, unlike the CNS where a compensatory reduction is seen. This lack of compensation is in keeping with the physical separation of sites of primary production (enterochromaffin cells) and sites of clearance (crypt epithelium). Thus, loss of SERT function could establish a situation in the gut where exaggerated levels of extracellular 5-HT could occur, suggesting that a GI phenotype may be a penetrant phenotype for loss of function SERT polymorphisms. Also of note in the study on GI phenotypes in SERT knockout mice is the absence of 5HT from the blood. Presumably, with a lack of platelet transporters to sequester 5-HT from the blood, the 5HT that enters the blood cannot be protected from degradation or elimination. Screening subjects for hyposerotonemia may thus reveal novel loss of function alleles of hSERT.

In addition to the gut, pulmonary function has been explored recently in SERT knockout mice (Eddahibi et al., 2001). As expected from the notion that a single gene encodes SERT proteins in the brain and periphery, the homozygous SERT knockout eliminates SERT immunoreactivity in pulmonary smooth muscle cells and 5-HT uptake capacity. Interestingly, 5HT and SERT have been implicated in the proliferation of pulmonary smooth muscle cells arising from hypoxia (Lee et al., 1989; Eddahibi et al., 2001). Loss of SERT in the knockouts eliminates the 5-HT-triggered smooth muscle cell proliferation. Conceivably, elevated SERT expression, as provided by a gain-of-function variant, could increase risk for 5-HT dependent pulmonary hypertension (Eddahibi and Adnot, 2002).

Although functional coding variants have yet to be identified in hSERTs, functional variants in promoter and intronic regions have been investigated for their relationship to clinical syndromes. As noted above, the s alleles of the 5HTTLPR have been found to associate with reduced transcriptional activity of the SERT promoter and with neuroticism and anxiety traits (Lesch et al., 1996). However, the degree to which the 5-HTTLPR influences SERT expression is at present controversial, with both supportive (Little et al., 1998; Heinz et al., 2000) and contradictory (Willeit et al., 2001) evidence. Recently, Du and co-workers (Du et al., 2000) were able to replicate the finding of Lesch of an association between 5-HTTLPR s alleles and neuroticism, but only in a male population, the gender of the original Lesch studies. These findings suggest that gender-specific expression of phenotypes may need to be considered in evaluation of SERT variants and that neuroticism and anxiety continue to represent behavioral traits that may enrich for novel SERT alleles. Although an extensive review of the investigation of the 5HTTLPR in clinical studies is beyond the scope of the present study (for a recent comprehensive review, see Hahn et al., 2002), polymorphic status at the 5HTTLPR has been connected to autism (Cook et al., 1997; Klauck et al., 1997; Tordjman et al., 2001), affective disorders (Greenberg, 1998), drug abuse and alcoholism (Little et al., 1998; Twitchell et al., 2001), and OCD (McDougle et al., 1998; Bengel et al., 1999; Camarena et al., 2001). In a search focusing on loss-of-function SERT alleles, it may seem counterintuitive to utilize disorders that effectively respond to serotonin-selective reuptake inhibitors (SSRIs), such as anxiety, major depression, or OCD. Possibly, gain-of-function alleles may lurk in these syndromes. However, it should also be remembered that the mouse knockout studies show us that altered SERT expression is likely to trigger a series of compensatory changes leading to diminished serotonergic signaling. Diminished serotonergic tone might then be elevated by a pharmacologic reduction in residual 5-HT clearance, establishing 5HT levels high enough to desensitize somatic autoreceptors and thereby eliminate autoreceptor-based inhibition of raphe firing. Certainly this is a complex scenario that will only become clearer with clinical evaluation of subjects with bona fide transporter mutations. Until then, understanding whether SSRIs ameliorate or exacerbate changes in heterozygous knockout mice could be informative.

Given that SERTs are the major targets for SSRIs (Fuller and Wong, 1990; Barker and Blakely, 1995), phenotypes linked to SSRI responsiveness might be considered in the hunt for novel SERT alleles. In this regard, recent evidence suggests that the l allele of the 5-HTTLPR may be associated with a favorable response to SSRIs. Billett (1997) initially found no association between overall SSRI response and the 5-HTTLPR polymorphisms in 72 OCD patients. In contrast, Smeraldi and colleagues (1998) found an association between the 5HTTLPR l allele and response to fluvoxamine in 102 depressed patients with delusional depression (Smeraldi, 1998). Kim and co-workers (2000) evaluated 120 depressed patients and 252 controls and found that an s/s genotype in 5HTTLPR was associated with better response to fluoxetine or paroxetine. Zanardi (2000) found an association between the l allele of the 5-HTTLPR and response to paroxetine. An association between an l/l genotype and faster rate of paroxetine response was found by Pollock and collaborators (Pollock et al., 2000). Finally, Mundo and colleagues (2001) have reported that the 5-HTTLPR s allele predicts risk for mania in bipolar subjects treated with antidepressants, which suggests that drug-targeted phenotypes could be an important area for future analyses. The 3rd intron VNTR of SLC6A4 has also received attention in association and pharmacogenomic studies, although the number of studies is not as extensive as those involving the 5HTTLPR. Kim and colleagues (2000) found that a VNTR 12/12 genotype was associated with a better response to fluoxetine or paroxetine. The lack of a 12-bp repeat s

allele in the VNTR most powerfully predicted nonresponse. One possibility for incorporating these findings in the search for novel SERT alleles would be to target pharmacologically defined subjects bearing the "inappropriate" 5HTTLPR genotype. For example, one could target mania-exhibiting bipolar subjects expressing the l/l genotype as a population that can be enriched for novel alleles that could phenocopy the s/s genotype. By analogy with OI subjects who have a NET loss of function mutation and who have blunted responses to tyramine (Shannon et al., 2000), future studies might also account for blunted 5HT efflux triggered by a fenfluramine challenge as an indication of loss of function in SERT that could be determined genetically.

Overall, the existing studies with SERT promoter polymorphisms point to anxiety and affective disorders, alcoholism, autism, and OCD as important syndromes for which novel SERT polymorphisms might increase risk and thus be study populations for polymorphism discovery. We note that as SERT expression is not limited to the brain, comorbidities with peripheral syndromes, such as IBS or pulmonary hypertension, should also be considered (Blakely, 2001). Finally, inclusion of antidepressant responsiveness or fenfluramine challenges to query the functional status of SERTs in vivo could further narrow the study population to provide the best opportunity for success. We certainly have no reason to expect that SERT would be excluded from genetic variation. Although the SERT gene structure features distributed, small exons, which do not favor a high frequency of exonic mutations, such arguments could be made for other genes, including ion channels and other transporters where we have clear evidence of functional variants. More likely, we have only just begun to understand how to define the appropriate clinical populations. The leads provided by SERT transgenic studies and the existing association studies with common SERT variants establish initial syndromes to explore for SERT variants. High-throughput polymorphism discovery techniques that allow for the cost-effective analysis of DNA samples without recourse to sequencing are essential because the hunt is for rare variants and much "normal" DNA will need to be evaluated before informative variants are identified. Finding the first few variants may be anxiety-provoking and gut-wrenching, but hopefully the phenotypic lessons learned will translate into more effective diagnoses and therapies.

ACKNOWLEDGMENTS

The authors were supported by grants from the National Institutes of Health (Bethesda, MD; DA 07390; MH 58933; RDB) and the National Alliance for Research on Schizophrenia and Depression (ARB).

REFERENCES

Altemus M, Murphy DL, Greenberg B, Lesch KP (1996): Intact coding region of the serotonin transporter gene in obsessive-compulsive disorder. Am J Med Genet 67:409–411.

Adkins EM, Barker EL, Blakely RD (2001): Interactions of tryptamine derivatives with serotonin transporter species variants implicate transmembrane domain I in substrate recognition. Mol Pharmacol 59:514–523.

Austin MC, Bradley CC, Mann JJ, Blakely RD (1994): Expression of serotonin transporter messenger RNA in the human brain. J Neurochem 62:2362–2367.

Balkovetz DF, Tiruppathi C, Leibach FH, Mahesh VB, Ganapathy V (1989): Evidence for an

imipramine-sensitive serotonin transporter in human placental brush-border membranes. J Biol Chem 264:2195–2198.

Barker EL, Blakely RD (1995): Norepinephrine and serotonin transporters: molecular targets of antidepressant drugs. In Bloom FE, Kupfer DJ (eds): Psychopharmacology: The Fourth Generation of Progress. New York: Raven Press, pp 321–333.

Barker EL, Perlman MA, Adkins EM, Houlihan WJ, Pristupa ZB, Niznik HB, Blakely RD (1998): High affinity recognition of serotonin transporter antagonists defined by species-scanning mutagenesis: an aromatic residue in transmembrane domain I dictates species-selective recognition of citalopram and mazindol. J Biol Chem 273:19459–19468.

Battersby S, Ogilvie AD, Blackwood DH, Shen S, Muqit MM, Muir WJ, Teague P, Goodwin GM, Harmar AJ (1999): Presence of multiple functional polyadenylation signals and a single nucleotide polymorphism in the 3' untranslated region of the human serotonin transporter gene. J Neurochem 72:1384–1388.

Beckman ML, Quick MW (1998): Neurotransmitter transporters: regulators of function and functional regulation. J Membr Biol 164:1–10.

Belous AR, Hanna G, Blakely RD (2000): Evaluation of serotonin transporter gene polymorphisms in juvenile obsessive-compulsive disorder using temperature modulated heteroduplex chromatography. Soc Neurosci Abstr.

Belous AR, Brown L, Shelton R, Mertz H, Blakely RD (2001): Evaluation of serotonin transporter polymorphisms in mood disorders with comorbid gastrointestinal abnormalities using temperature modulated heteroduplex chromatography. Abstract # 2102 Amer Soc Human Genetics.

Bengel D, Heils A, Petri S, Seemann M, Glatz K, Andrews A, Murphy DL, Lesch KP (1997): Gene structure and 5'-flanking regulatory region of the murine serotonin transporter. Brain Res Mol Brain Res 44:286–292.

Bengel D, Murphy DL, Andrews AM, Wichems CH, Feltner D, Heils A, Mossner R, Westphal H, Lesch KP (1998): Altered brain serotonin homeostasis and locomotor insensitivity to 3, 4-methylenedioxymethamphetamine ("Ecstasy") in serotonin transporter-deficient mice. Mol Pharmacol 53:649–655.

Bengel D, Greenberg BD, Cora-Locatelli G, Altemus M, Heils A, Li Q, Murphy DL (1999): Association of the serotonin transporter promoter regulatory region polymorphism and obsessive-compulsive disorder. Mol Psychiatry 4:463–466.

Billett EA (1997): Obsessive compulsive disorder, response to serotonin reuptake inhibitors and the serotonin transporter gene. Mol Psychiatry 2:403–406.

Blakely RD, Berson HE, Fremeau RT Jr, Caron MG, Peek MM, Prince HK, Bradley CC (1991): Cloning and expression of a functional serotonin transporter from rat brain. Nature (London) 354:66–70.

Blakely RD (2001): Physiological genomics of antidepressant targets: Keeping the periphery in mind. J Neurosci 21:8319–8323.

Blakely RD, Berson HE, Fremeau RT, Caron MG, Peek MM, Prince HK, Bradley CC (1991): Cloning and expression of a functional serotonin transporter from rat brain. Nature (London) 354:3349–3354.

Blakely RD, Bauman AL (2000): Biogenic amine transporters: regulation in flux. Curr Opin Neurobiol 10:328–336.

Bradley CC, Blakely RD (1997): Alternative splicing of the human serotonin transporter gene. J Neurochem 69:1356–1367.

Calne DB, Langston JW (1983): Etiology of Parkinson's disease. Lancet 2:1457–1459.

Camarena B, Rinetti G, Cruz C, Hernandez S, de la Fuente JR, Nicolini H (2001): Association study of the serotonin transporter gene polymorphism in obsessive-compulsive disorder. Int J Neuropsychopharmacol 4:269–272.

Cargill M, Altshuler D, Ireland J, Sklar P, Ardlie K, Patil N, Shaw N, Lane CR, Lim EP, Kalyanaraman N, Nemesh J, Ziaugra L, Friedland L, Rolfe A, Warrington J, Lipshutz R, Daley GQ, Lander ES (1999): Characterization of single-nucleotide polymorphisms in coding regions of human genes. Nat Genet 22:231–238.

Chen JG, Rudnick G (2000): Permeation and gating residues in serotonin transporter. Proc Natl Acad Sci USA 97:1044–1049.

Chen JJ, Li Z, Pan H, Murphy DL, Tamir H, Koepsell H, Gershon MD (2001): Maintenance of serotonin in the intestinal mucosa and ganglia of mice that lack the high-affinity serotonin transporter: Abnormal intestinal motility and the expression of cation transporters. J Neurosci 21(16):6348–6361.

Collins F, Brooks LD, Chakravarti A (1998): A DNA polymorphism discovery resource for research on human genetic variation. Genome Res 8:1229–1231.

Cook EH Jr, Courchesne R, Lord C, Cox NJ, Yan S, Lincoln A, Haas R, Courchesne E, Leventhal BL (1997): Evidence of linkage between the serotonin transporter and autistic disorder. Mol Psychiatry 2:247–250.

Du L, Bakish D, Hrdina PD (2000): Gender differences in association between serotonin transporter gene polymorphism and personality traits. Psychiatr Genet 10:159–164.

Eddahibi S, Humbert M, Fadel E, Raffestin B, Darmon M, Capron F, Simonneau G, Dartevelle P, Hamon M, Adnot S (2001): Serotonin transporter overexpression is responsible for pulmonary artery smooth muscle hyperplasia in primary pulmonary hypertension. J Clin Invest 108:1141–1150.

Eddahibi S, Adnot S (2002): Anorexigen-induced pulmonary hypertension and the serotonin (5-HT) hypothesis: Lessons for the future in pathogenesis. Respir Res 3:9.

Fabre V, Beaufour C, Evrard A, Rioux A, Hanoun N, Lesch KP, Murphy DL, Lanfumey L, Hamon M, Martres MP (2000): Altered expression and functions of serotonin 5-HT1A and 5-HT1B receptors in knock-out mice lacking the 5-HT transporter. Eur J Neurosci 12:2299–2310.

Flattem NL and Blakely RD (2000): Modified structure of the human serotonin transporter promoter. Mol Psychiatry 5:110–115.

Fiskerstrand CE, Lovejoy EA, Quinn JP (1999): An intronic polymorphic domain has allele dependent differential enhancer activity in embryonic stem cells. FEBS Lett 458: 171–174.

Fuller RW (1991): Role of serotonin in therapy of depression and related disorders. J Clin Psychiatry Suppl:52–57.

Fuller RW, Wong DT (1990): Serotonin uptake and serotonin uptake inhibition. Ann NY Acad Sci 600:68–78.

Gelernter J, Pakstis AJ, Kidd KK (1995): Linkage mapping of serotonin transporter protein gene SLC6A4 on chromosome 17. Hum Genet 95:677–680.

Gelernter J, Cubells JF, Kidd JR, Pakstis AJ, Kidd KK (1999): Population studies of polymorphisms of the serotonin transporter protein gene. Am J Med Genet 88:61–66.

Gershon MD (1999): Review article: roles played by 5-hydroxytryptamine in the physiology of the bowel. Aliment Pharmacol Ther Suppl 2:15–30.

Giros B, Jaber M, Jones SR, Wightman RM, Caron MG (1996): Hyperlocomotion and indifference to cocaine and amphetamine in mice lacking the dopamine transporter. Nature (London) 379:606–612.

Giordano M, Oefner PJ, Underhill PA, Cavalli Sforza LL, Tosi R, Richiardi PM (1999): Identification by denaturing high-performance liquid chromatography of numerous polymorphisms in a candidate region for multiple sclerosis susceptibility. Genomics 15;56(3):247–253.

Glatt CE, DeYoung JA, Delgado S, Service SK, Giacomini KM, Edwards RH, Risch N, Freimer NB (2001): Screening a large reference sample to identify very low frequency sequence variants: comparisons between two genes. Nat Genet 27:435–438.

Gobbi G, Murphy DL, Lesch K, Blier P (2001): Modifications of the serotonergic system in mice lacking serotonin transporters: an in vivo electrophysiological study. J Pharmacol Exp Ther 296(3):987–995.

Greenberg BD, McMahon FJ, Murphy DL (1998): Serotonin transporter candidate gene studies in affective disorders and personality: promises and potential pitfalls. Mol Psychiatry 3:186–189.

Greenberg BD, Tolliver TJ, Huang SJ, Li Q, Bengel D, Murphy DL (1999): Genetic variation in the serotonin transporter promoter region affects serotonin uptake in human blood platelets. Am J Med Genet 88:83–87.

Guastella J, Nelson N, Nelson H, Czyzyk L, Keynan S, Miedel MC, Davidson N, Lester HA, Kanner BI (1990): Cloning and expression of a rat brain GABA transporter. Science 249:1303–1306.

Hahn M, Blakely RD (2002): Gene Organization and Polymorphisms of Monoamine Transporters: Relationship to Psychiatry and Other Complex Diseases. In Maarten E (ed): Neurotransmitter Transporters Structure, Function, and Regulation. Totowa, NJ: Humana Press (2nd Edition, pp. 111–169).

Heils A, Teufel A, Petri M, Seemann M, Bengel D, Balling U, Rieder P, Lesch KP (1995): Functional promoter and polyadenylation site mapping of the human serotonin (5-HTT) transporter gene. J Neural Transm Gen Sect 102:247–254.

Heils A, Teufel A, Petri S, Stober G, Rieder P, Bengel D, and Lesch KP (1996): Allelic variation of human serotonin transporter gene expression. J Neurochem 66: 2621–2624.

Heils A, Wichems C, Mossner R, Petri S, Glatz K, Bengel D, Murphy DL, Lesch KP (1998): Functional characterization of the murine serotonin transporter gene promoter in serotonergic raphe neurons. J Neurochem 70:932–939.

Heinz A, Jones DW, Mazzanti C, Goldman D, Ragan P, Hommer D, Linnoila M, Weinberger DR (2000): A relationship between serotonin transporter genotype and in vivo protein expression and alcohol neurotoxicity. Biol Psychiatry 47:643–649.

Hoffman BJ, Mezey E, Brownstein MJ (1991): Cloning of a serotonin transporter affected by antidepressants. Science 254:579–580.

Horton RW (1992): The neurochemistry of depression: evidence derived from studies of postmortem brain tissue. Mol Aspects Med 13:191–203.

Hoogendoorn B, Norton N, Kirov G, Williams N, Hamshere ML, Spurlock G, Austin J, Stephens MK, Buckland PR, Owen MJ, O'Donovan MC (2000): Cheap, accurate and rapid allele frequency estimation of single nucleotide polymorphisms by primer extension and DHPLC in DNA pools. Hum Genet 107(5):488–493.

Houston DS, Vanhoutte PM (1986): Serotonin and the vascular system: role in health and disease, and implications for therapy. Drugs 31:149–163.

Jacobs BL, Azmitia EC (1992): Structure and function of the brain serotonin system. Physiol Rev 72:165–229.

Kilic F, Rudnick G (2000): Oligomerization of serotonin transporter and its functional consequences. Proc Natl Acad Sci USA 28;97(7):3106–3111.

Kim DK, Lim SW, Lee S, Sohn SE, Kim S, Hahn CG, Carroll BJ (2000): Serotonin transporter gene polymorphism and antidepressant response. Neuroreport 11:215–219.

Kitada T, Asakawa S, Hattori N, Matsumine H, Yamamura Y, Minoshima S, Yokochi M, Mizuno Y, Shimizu N (1998): Mutations in the parkin gene cause autosomal recessive juvenile parkinsonism. Nature (London) 392:605–608.

Klauck SM, Poustka F, Benner A, Lesch KP, Poustka A (1997): Serotonin transporter (5-HTT) gene variants associated with autism? Human Mol Genet 6:2233–2238.

Lebrand C, Cases O, Adelbrecht C, Doye A, Alvarez C, El Mestikawy S, Seif I, Gaspar P (1996): Transient uptake and storage of serotonin in developing thalamic neurons. Neuron 17:823–835.

Lebrand C, Cases O, Wehrle R, Blakely RD, Edwards RH, Gaspar P (1998): Transient developmental expression of monoamine transporters in the rodent forebrain. J Comp Neurol 401:506–524.

Lee SL, Fanburg BL (1986): Serotonin uptake by bovine pulmonary artery endothelial cells in culture. I. Characterization. Am J Physiol 250:C761–765.

Lee SL, Dunn J, Yu FS, Fanburg BL (1989): Serotonin uptake and configurational change of bovine pulmonary artery smooth muscle cells in culture. J Cell Physiol 138:145–153.

Lesch KP, Wolozin B, Murphy DL, Rieder P (1993): Primary structure of the human platelet serotonin uptake site: identity with the brain serotonin transporter. J Neurochem 60: 3218–3226.

Lesch KP, Balling U, Gross J, Strauss K, Wolozin BL, Murphy DL, Rieder P (1994): Organization of the human serotonin transporter gene. J Neural Transm Gen Sect 95: 157–162.

Lesch KP, Balling U, Gross J, Strauss K, Wolozin BL, Murphy DL (1995): Organization of human serotonin transporter gene. J Neural Transm Gen Sect 102:247–254.

Lesch KP, Bengel D, Heils A, Sabol SZ, Greenberg BD, Petri S, Benjamin J, Muller CR, Hamer DH, Murphy DL (1996): Association of anxiety-related traits with a polymorphism in the serotonin transporter gene regulatory region. Science 274:1527–1531.

Lesch KP, Jatzke S, Meyer J, Stober G, Okladnova D, Mosner R, Reider P (1991): Mosaicism for a serotonin transporter gene promoter-associated deletion: decreased recombination in depression. J Neural Transm 106:1223–1230.

Li Q, Wichems C, Heils A, Lesch KP, Murphy DL (2000): Reduction in the density and expression, but not G-protein coupling, of serotonin receptors (5-HT1A) in 5-HT transporter knock-out mice: gender and brain region differences. J Neurosci 20:7888–7895.

Little KY, McLaughlin DP, Zhang L, Livermore CS, Dalack GW, McFinton PR, DelProposto ZS, Hill E, Cassin BJ, Watson SJ, Cook EH (1998): Cocaine, ethanol, and genotype effects on human midbrain serotonin transporter binding sites and mRNA levels. Am J Psych 155: 207–213.

Liu Y, Edwards RH (1997): The role of vesicular transport proteins in synaptic transmission and neural degeneration. Annu Rev Neurosci 20:125–156.

MacKenzie A, Quinn J (1999): A serotonin transporter gene intron 2 polymorphic region, correlated with affective disorders, has allele-dependent differential enhancer-like properties in the mouse embryo. Proc Natl Acad Sci USA 96:15251–15255.

Manning AP, Thompson WG, Heaton KW, Morris AF (1978): Towards a positive diagnosis of the irritable bowel. BMJ 2:653–654.

Martin ER, Scott WK, Nance MA, Watts RL, Hubble JP, Koller WC, Lyons K, Pahwa R, Stern MB, Colcher A, Hiner BC, Jankovic J, Ondo WG, Allen FH Jr, Goetz CG, Small GW, Masterman D, Mastaglia F, Laing NG, Stajich JM, Ribble RC, Booze MW, Rogala A, Hauser MA, Zhang F, Gibson RA, Middleton LT, Roses AD, Haines JL, Scott BL, Pericak-Vance MA, Vance JM (2001): Association of single-nucleotide polymorphisms of the tau gene with late-onset Parkinson disease. JAMA 286(18):2245–2250.

Mason P (2001): Contributions of the medullary raphe and ventromedial reticular region to pain modulation and other homeostatic functions. Annu Rev Neurosci 24:737–777.

McDougle CJ, Epperson CN, Price LH, Gelernter J (1998): Evidence for linkage disequilibrium between serotonin transporter protein gene (SLC6A4) and obsessive-compulsive disorder. Mol Psychiatry 3:577–585.

Meltzer HY (1990): Role of serotonin in depression. Ann NY Acad Sci 600:486–499.

Mortensen OV, Thomassen M, Larsen MB, Whittemore SR, Wiborg O (1999): Functional analysis of a novel human serotonin transporter gene promoter in immortalized raphe cells. Mol Brain Res 68:141–148.

Mossner R, Lesch KP, Hen R, Seif I (2001): Excessive activation of serotonin (5-HT) 1B receptors

disrupts the formation of sensory maps in monoamine oxidase a and 5-HT transporter knock-out mice. J Neurosci 21:884–896.

Mundo E, Walker M, Cate T, Macciardi F, Kennedy JL (2001): The role of serotonin transporter protein gene in antidepressant-induced mania in bipolar disorder: preliminary findings. Arch Gen Psychiatry 58:539–544.

Murphy DL, Zohar J, Benkelfat C, Pato MT, Pigott TA, Insel TR (1989): Obsessive-compulsive disorder as a 5-HT subsystem-related behavioral disorder. Br J Psychiatry Suppl 8:15–24.

Nelson N (1998): The family of Na+/Cl– neurotransmitter transporters. J Neurochem 5:1785–1803.

Nguyen TT, Tseng YT, McGonnigal B, Stabila JP, Worrell LA, Saha S, Padbury JF (1999): Placental biogenic amine transporters: in vivo function, regulation and pathobiological significance. Placenta 20(1):3–11.

Owens MJ, Nemeroff CB (1994): Role of serotonin in the pathophysiology of depression: Focus on serotonin transporter. Clin Chem 40:288–295.

Pacholczyk T, Blakely RD, Amara SG (1991): Expression cloning of a cocaine- and antidepressant-sensitive human noradrenaline transporter. Nature 350:350–354.

Persico AM, Mengual E, Moessner R, Hall FS, Revay RS, Sora I, Arellano J, DeFelipe J, Gimenez-Amaya JM, Conciatori M, Marino R, Baldi A, Cabib S, Pascucci T, Uhl GR, Murphy DL, Lesch KP, Keller F, Hall SF (2001): Barrel pattern formation requires serotonin uptake by thalamocortical afferents, and not vesicular monoamine release. J Neurosci 21:6862–6873.

Pollock BG, Ferrell RE, Mulsant BH, Mazumdar S, Miller M, Sweet RA, Davis S, Kirshner MA, Houck PR, Stack JA, Reynolds CF, Kupfer DJ (2000): Allelic variation in the serotonin transporter promoter affects onset of paroxetine treatment response in late-life depression. Neuropsychopharmacology 23:587–590.

Polymeropoulos MH, Lavedan C, Leroy E, Ide SE, Dehejia A, Dutra A, Pike B, Root H, Rubenstein J, Boyer R, Stenroos ES, Chandrasekharappa S, Athanassiadou A, Papapetropoulos T, Johnson WG, Lazzarini AM, Duvoisin RC, Di Iorio G, Golbe LI, Nussbaum RL (1997): Mutation in the alpha-synuclein gene identified in families with Parkinson's disease. Science 276:2045–2047.

Qian Y, Melikian HE, Rye DR, Levey AI, Blakely RD (1995): Identification and characterization of antidepressant-sensitive serotonin transporter proteins using site-specific antibodies. J Neurosci 15:1261–1274.

Ramamoorthy S, Bauman AL, Moore KR, Han H, Yang-Eeng T, Chang AS, Ganapathy V, Blakely RD (1993): Antidepressant- and cocaine-sensitive human serotonin transporter: Molecular cloning, expression and chromosomal localization. Proc Natl Acad Sci USA 90:2542-2546.

Reimer RJ, Fremeau RT Jr, Bellocchio EE, Edwards RH (2001): The essence of excitation. Curr Opin Cell Biol 13:417–421.

Robertson D (1999): The epidemic of orthostatic tachycardia and orthostatic intolerance. Am J Med Sci 317:75–77.

Robertson D, Shannon JR, Biaggioni I, Ertl AC, Diedrich A, Carson R, Furlan R, Jacob G, Jordan J (2000): Orthostatic intolerance and the postural tachycardia syndrome: Genetic and environment pathophysiologies. Pflugers Arch 441(2–3 Suppl):R48–51.

Robertson D, Flattem N, Tellioglu T, Carson R, Garland E, Shannon JR, Jordan J, Jacob G, Blakely RD, Biaggioni I (2001): Familial orthostatic tachycardia due to norepinephrine transporter deficiency. Ann NY Acad Sci 940:527–543.

Roses AD (2000): Pharmacogenetics and the practice of medicine. Nature (London) 405:857–865.

Salichon N, Gaspar P, Upton AL, Picaud S, Hanoun N, Hamon M, De Maeyer E, Murphy DL, Mossner R, Lesch KP, Hen R, Seif I (2001): Excessive activation of serotonin (5-HT) 1B receptors disrupts the formation of sensory maps in monoamine oxidase A and 5-HT transporter knock-out mice. J Neurosci 21:884–896.

Serafeim A, Gordon J (2001): The immune system gets nervous. Curr Opin Pharmacol 1:1398–1403.

Serafeim, A, Grafton G, Chamba A, Gregory CD, Blakely RD, Bowery NG, Barnes NM, Gordon J (2002): 5-hydroxytryptamine drives apoptosis in biopsy like Burkitt lymphoma cells: reversal by selective serotonin reuptake inhibitors. Blood 7:2545–2553.

Shannon JR, Flattem NL, Jordan J, Jacob G, Black BK, Biaggioni I, Blakely RD, Robertson D (2000): Orthostatic intolerance and tachycardia associated with norepinephrine-transporter deficiency. N Engl J Med 342(8):541–549.

Smeraldi E, Zanardi R, Benedetti F, Di Bella D, Perez J, Catalano M (1998): Polymorphism within the promoter of the serotonin transporter gene and antidepressant efficacy of fluvoxamine. Mol Psychiatry 3:508–511.

Sneddon JM (1973): Blood platelets as a model for monoamine-containing neurons. Prog Neurobiol 1:151–198.

Sora I, Wichems C, Takahashi N, Li XF, Zeng Z, Revay R, Lesch KP, Murphy DL, Uhl GR (1998): Cocaine reward models: conditioned place preference can be established in dopamine- and in serotonin-transporter knockout mice. Proc Natl Acad Sci USA 95:7699–7704.

Spiegelman JI, Mindrinos MN, Oefner PJ (2000): High-accuracy DNA sequence variation screening by DHPLC. Biotechniques 29(5):1084–1090, 1092.

Steinbusch HW (1981): Distribution of serotonin-immunoreactivity in the central nervous system of the rat-cell bodies and terminals. Neuroscience 6:557–618.

Stolz JF (1985): Uptake and storage of serotonin by platelets. In Vanhotte PM (ed): Serotonin and the Cardiovascular System. New York: Raven Press, pp 37–42.

Thompson WG (1993): Irritable bowel syndrome: pathogenesis and management. Lancet 341:1569–1572.

Tordjman S, Gutknecht L, Carlier M, Spitz E, Antoine C, Slama F, Carsalade V, Cohen DJ, Ferrari P, Roubertoux PL, Anderson GM (2001): Role of the serotonin transporter gene in the behavioral expression of autism. Mol Psychiatry 6(4):434–439.

Tork I (1990): Anatomy of the serotonergic system. Ann NY Acad Sci 600:9–34.

Twitchell GR, Hanna GL, Cook EH, Stoltenberg SF, Fitzgerald HE, Zucker RA (2001): Serotonin transporter promoter polymorphism genotype is associated with behavioral disinhibition and negative affect in children of alcoholics. Alcohol Clin Exp Res 25:953–959.

Willeit M, Stastny J, Pirker W, Praschak-Rieder N, Neumeister A, Asenbaum S, Tauscher J, Fuchs K, Sieghart W, Hornik K, Aschauer HN, Brücke T, Kasper S (2001): No evidence for in vivo regulation of midbrain serotonin transporter availability by serotonin transporter promoter gene polymorphism. Biol Psychiatry 50:8–12.

Wade PR, Chen J, Jaffe B, Kassem IS, Blakely RD, Gershon MD (1996): Localization and function of a 5-HT transporter in crypt epithelia of the gastrointestinal tract. J Neurosci 16:2352–2364.

Xu F, Gainetdinov RR, Wetsel WC, Jones SR, Bohn LM, Miller GW, Wang YM, Caron MG (2000): Mice lacking the norepinephrine transporter are supersensitive to psychostimulants. Nat Neurosci 3:465–471.

Zanardi R (2000): Efficacy of paroxetine in depression is influenced by a functional polymorphism within the promoter of the serotonin transporter gene. J Clin Psychopharmacol 20:105–107.

Zhou FC, Tao-Cheng JH, Segu L, Patel T, Wang Y (1998): Serotonin transporters are located on the axons beyond the synaptic junctions: anatomical and functional evidence. Brain Res 805:241–254.

CHAPTER 6

NONVIRAL GENE TRANSFER ALLOWS UP- AND DOWN-EXPRESSION OF THE BRAIN SEROTONIN TRANSPORTER WITH FUNCTIONAL CONSEQUENCES

MARIE-PASCALE MARTRES, VÉRONIQUE FABRE, MICHEL HAMON, AND BARBARA DEMENEIX

6.1 INTRODUCTION

Serotonin (5-HT) plays important roles in the central nervous system (CNS), participating in control of various motor, physiological, affective, and cognitive functions. Disturbances in serotonergic neurotransmission are involved in several neuronal and psychiatric diseases, including Alzheimer's disease, anxiety, and, in particular, major depression.

Among the proteins implicated in 5-HT neurotransmission, the serotonin transporter (SERT) is a key component, regulating both intensity and duration of the effects of 5-HT released into the synaptic cleft. Numerous psychoactive drugs target the SERT, including antidepressant drugs, such as selective serotonin reuptake inhibitors (SSRIs), which increase extracellular 5-HT (Thomas et al., 1987; Dechant and Clissold, 1991) and some drugs of abuse, such as cocaine (Lesch, 1997) and the amphetamine-derivative 3,4-methylenedioxymetamphetamine (MDMA or "Ecstasy") (Green et al., 1995). The contribution of SERT to 5-HT neurotransmission is limited by the lack of pharmacological approaches for modulating SERT levels in the CNS. In this context, the cloning of the SERT gene in different species (Blakely et al., 1991; Lesch et al., 1993; Chang et al., 1996) raised new opportunities for modifying SERT expression.

The most drastic approach was the creation of mice lacking the SERT (Bengel et al., 1998). However, the resulting profound alterations of the 5-HT systems (Bengel et al., 1998; Rioux et al., 1999; Fabre et al., 2000a; Mannoury La Cour et al., 2001), beginning probably from embryonic stages, are not relevant to antidepressant treatment in the adult and alternative approaches are needed.

Antisense oligodeoxynucleotide (ODN) administration can specifically inhibit expression of targeted proteins; for example, rat dopamine transporter (DAT; Silvia et al., 1997). However, major drawbacks include low stability, toxicity, and weak penetration of ODNs into cells. Their short action is particularly limiting when the target protein has a long half-life, as is the case for DAT (Silvia et al., 1997; Martres et al. 1998), or

Transmembrane Transporters. Edited by Michael Quick

ISBNs: 0-471-06517 (Hardcover); 0-471-43404-3 (Electronic)

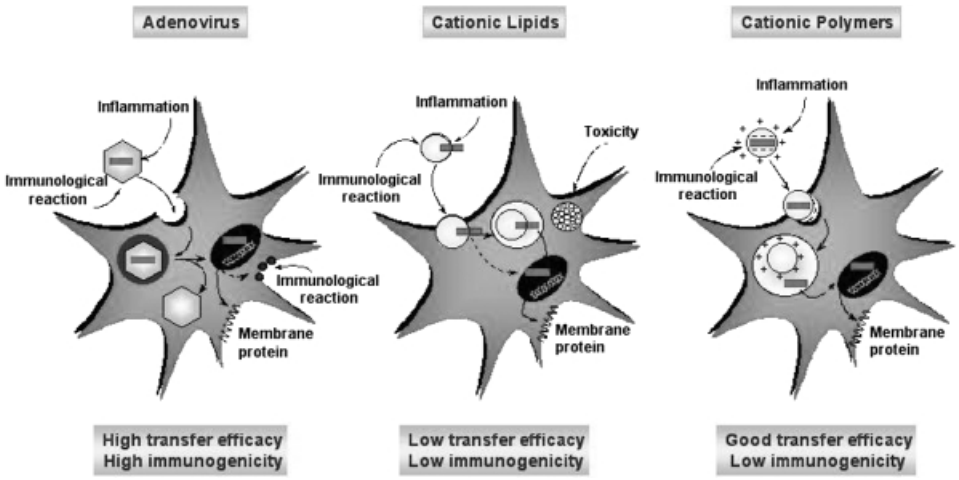

Figure 6.1. Schematic representation of various techniques of gene transfer into cells. Adapted from Crystal (1995). (See color insert.)

when long-lasting effects are necessary to study a phenomenon such as antidepressant effects.

An alternative method is direct gene transfer into the CNS (Fig. 6.1). Various strategies have been used: grafting of genetically modified cells (Jiao et al., 1993; Sabaté et al., 1995; Bachoud-Levi et al., 2000) or direct *in vivo* gene delivery by viral vectors, including adenoviruses (Akli et al., 1993; Horellou et al., 1994), herpes-virus derived vectors (During et al., 1994; Kesari et al., 1995; Antunes Bras et al., 1998), and adeno-associated viruses (Kaplitt et al., 1994). However, cell- and viral-mediated gene transfer procedures raise safety considerations as to the possible immunogenic and/or pathogenic effects of the vectors used (see Fisher and Ray, 1994; Crystal, 1995, 1996; Danos, 2000, for reviews).

In this respect, nonviral techniques offer numerous advantages. Chemical DNA carriers are of greater flexibility in use, and the risk of secondary complications is reduced (Crystal, 1995, 1996). Two main classes of molecules can be distinguished. Cationic lipids have been developed (Weiss et al., 1997; Byk et al., 1998), but amounts of DNA encapsulated are low and the efficacy of gene transfer is limited.

Cationic polymers display several advantages, including lesser toxicity and the possibility of transferring DNA of much larger size (see Lemkine and Demeneix, 2001, for review). Both the absence of toxicity of polyethylenimine (PEI) and its efficiency for transferring DNA in the adult rodent brain (Boussif et al., 1995; Abdallah et al., 1996; Goula et al., 1998; Martres et al., 1998) prompted us to use this approach to deliver sense or antisense SERT DNA coding sequences directly into the dorsal raphe nucleus (DRN) of adult rats (Fabre et al., 2000b). The resulting changes in SERT expression were assessed and possible functional alterations in 5-HT neurotransmission were followed by measuring 5-HT turnover and analyzing the binding and functional properties of the 5-HT_{1A}receptors and recording the sleep-wakefulness rhythm.

6.2 MATERIALS AND METHODS

Animals

All experiments were performed in conformity with institutional guidelines in compliance with national and international law and policies for use of animals in neuroscience research. Rats were housed under standard laboratory conditions: 12:12 h light–dark cycle (light on at 07:00), 22 ± 1°C ambient temperature, 60% relative humidity, food and water *ad libitum*.

Construction of Recombinant Plasmids and Preparation of DNA/PEI Complexes

For construction of the SERT sense plasmid, a cDNA comprising the entire coding sequence of the rat SERT (nucleotides 87 to 2400; Blakely et al., 1991) was subcloned into the pRc-CMV expression vector (Invitrogen, Cezgy Pontoise, France), containing the cytomegalovirus promoter and the bovine growth hormone (BGH) polyadenylation signal. For the antisense constructs, the complete coding sequence of SERT ("full antisense") or its last 468 nucleotides (nucleotides 1540–2007, "short antisense") were subcloned in reverse orientation into pRc-CMV (Fig. 6.2A). Plasmid DNAs were prepared by two centrifugations in CsCl gradient, resuspended in 10 mM Tris-HCl and 1 mM ethylene diamine tetraacetate (EDTA), pH 8, quantified (260 nm O.D.) and stored at –20°C.

The PEI concentration necessary to neutralize the DNA anionic charges was determined as follows: 0.5 μg of the various DNA preparations were mixed with PEI at different cationic charge equivalents (calculated by taking into account that 1 μg of DNA and 1 μl of 0.1 M PEI correspond, respectively, to 3 nmoles of phosphate and 100 nmoles of amine nitrogen). The DNA/PEI complexes were then electrophoresed in a 1% agarose gel and their migration profiles were compared.

Measurement of [^{3}H]5-HT Uptake in Transfected Cells

LLC-PK1 cells (pig kidney epithelial cells, ATCC n: CRL1392) were grown under a 7% O_2/93% air atmosphere at 37°C in Dulbecco's modified Eagle medium (DMEM) supplemented with 10% fetal bovine serum, 2 mM glutamine, 10 U/ml penicillin G, and 10 mg/ml streptomycin. DNA constructs were transfected into 60–80% confluent cells by electroporation (3–5 × 10^6 cells in 500 μl of DMEM without serum, 270 V, 1800 μF, relaxation time: 40 ms). Twenty-four hours after transfection, cells were transferred into 24-well plates and 24 h later expression of SERT measured by [^{3}H]5-HT uptake (Martres et al.; 1998). Cells were washed twice with 1 ml of uptake buffer (4 mM Tris, 6.25 mM N-(2-hydroxyethyl) piperazine-2'-(2-ethanesulphonic acid) (HEPES), 120 mM NaCl, 5 mM KCl, 1.2 mM $CaCl_2$, 1.2 mM $MgSO_4$, 5.6 mM glucose, and 0.5 mM ascorbic acid, final pH 7.4) and incubated in 500 μl of uptake buffer containing 3–6 nM [^{3}H]5-HT (15 Ci/mmol, Amersham, Buckinghamshire, UK), without or with 10 μM fluoxetine (Lilly, Indianapolis, IN, USA) to determine nonspecific uptake. After 7 min at 37°C, cells were washed quickly three times with 1 ml of uptake buffer at room temperature (RT), then solubilized in 500 μl of 0.1 N NaOH and the radioactivity counted by liquid scintillation spectrometry.

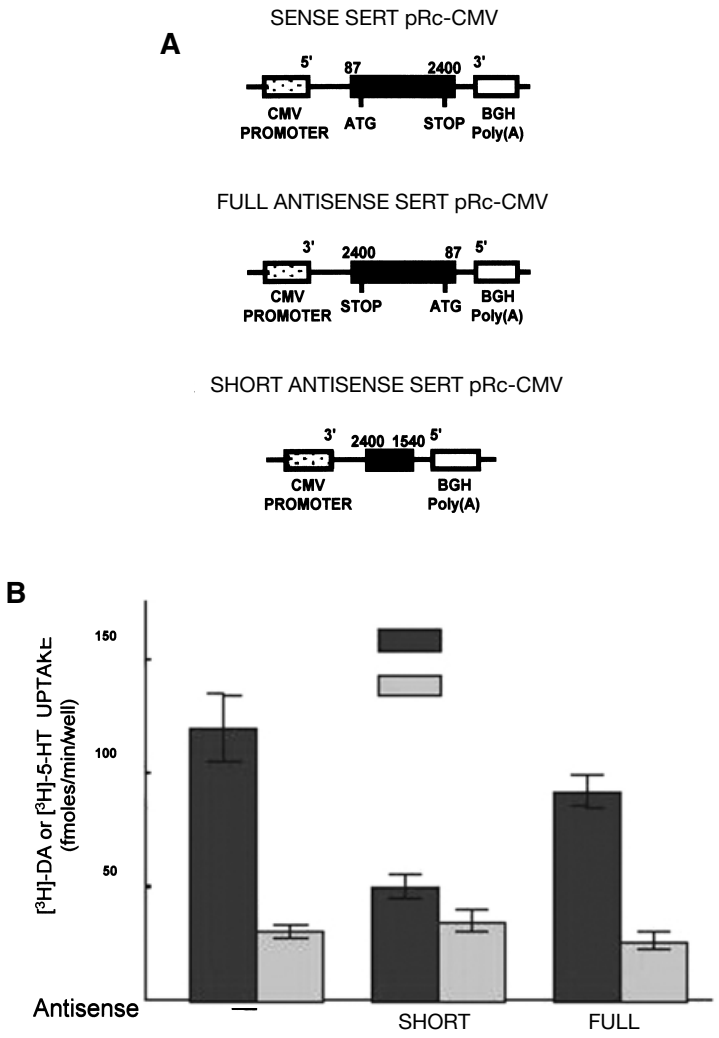

Figure 6.2. A) Expression vectors for sense and full and short antisense SERT. **B)** DNA construct expression in culture. Five µg of the sense SERT construct was transfected into LLC-PK1 cells ± 25 µg of each antisense construct. 2.5 µg of a pRc-CMV DAT was added in each transfection in order to assess its yield. [^{3}H]-5-HT and [^{3}H]-DA uptakes were measured 2 days posttransfection. Mean ± SEM of 8–15 determinations. **P*<0.001 compared with the value in the absence of antisense DNA (Student's *t*-test).

To correct for variations in transfection yields, 2.5 µg of pRc-CMV containing the entire coding sequence of the DAT gene (Martres et al., 1998) was cotransfected with the various SERT plasmids. The uptake of [^{3}H]DA (46 Ci/mmol, Amersham) was measured as already described with 3–6 nM [^{3}H]DA, in the absence or the presence of 10 µM nomifensine (RBI) (Research Biochemicals, Natick, MA, USA) to determine nonspecific uptake.

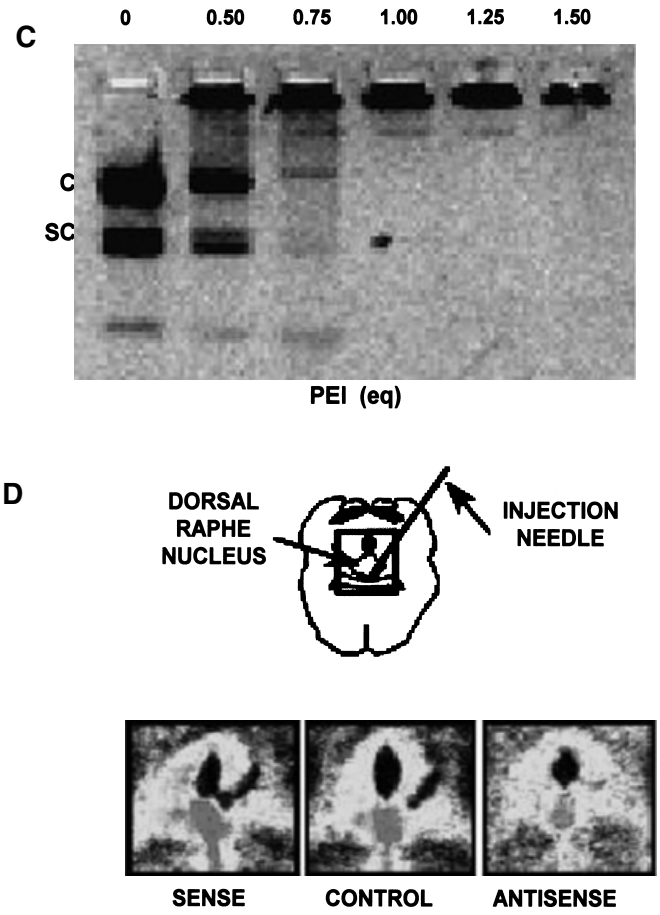

Figure 6.2. C) Complexation of DNA by PEI. SERT DNA construct (0.5 μg) was mixed with PEI at various charge ratios and complexes electrophoresed in 1% agarose gel stained with ethidium bromide. When the DNA is not entirely neutralized by PEI, the plasmid migrates under coiled (C) and supercoiled (SC) forms. **D)** Autoradiographic labeling of SERT in the dorsal raphe nucleus 3 days post-injection of sense (sense) or nonrecombinant plasmid (control) or 7 days after administration of the short antisense plasmid (antisense). Increasing OD values corresponded from blue, green, yellow to red. From Fabre, et al., 2000b, copyright 2000, Society for Neuroscience. (See color insert.)

Intra-Cerebral Gene Transfer and Dissection

Adult male Sprague Dawley rats (250–300 g weight) were anaesthetized with chloral hydrate (400 mg/kg, i.p.) and positioned in a stereotaxic apparatus (David Kopf Instruments, Phymap, Paris, France). The needle (outer diameter: 0.46 mm) of a 10 μl Hamilton syringe was lowered into the DRN (angle 32°C, A = 0.12 cm, L = 0.40 cm, H = 0.28 cm from the interaural zero, according to the atlas of Paxinos and Watson, 1986). Just before injection, plasmid DNA was diluted in 5% glucose at 0.25 μg/μl. Linearized PEI of 22 kDa (a gift of J.P. Behr) was diluted to 0.01 M in 5% glucose and added to the DNA solu-

tion at 6 charge equivalents. The mixture was vortexed (30 s) and equilibrated for 10 min at RT before injection. Two min after the needled was lowered, 2 µl of the DNA/PEI complex was injected manually over 5 min. The needle was left in place for another 5 min to allow a good diffusion before its removal. Paired control rats received the nonrecombinant pRc-CMV under the same conditions of complexation with PEI.

At various times after injection, rats were decapitated and their brains were removed. The hypothalamus was dissected out, and a coronal cut was made at an interaural anteriority ~0.50 cm. The posterior part of the brain was frozen in isopentane at –30°C, and the hippocampus, the striata, and the anterior cortex were dissected out for binding experiments. For immunoautoradiographic experiments, rats were anaesthetized with pentobarbital (60 mg/kg, i.p.) and perfused transcardially with 300 ml of 0.9% NaCl and 0.1% $NaNO_2$. After decapitation, the brain was removed and frozen as described above.

Quantitative Autoradiography

[^{3}H]Citalopram binding: Coronal sections (20 µm) at the level of the DRN were cut at –20°C, thaw-mounted onto gelatin-coated slides, and stored at –20°C until use. For the labeling procedure, slides were brought to RT and preincubated for 15 min in 50 mM Tris-HCl buffer containing 120 mM NaCl and 5 mM KCl, pH 7.4, at 25°C. Incubations proceeded for 1 h at 25°C in fresh buffer with 0.7 nM [^{3}H]citalopram (85 Ci/mmol, Dupont-NEN, Boston, MA, USA). Nonspecific binding was estimated from adjacent sections with 10 µM fluoxetine. Sections were washed twice (5 min) in ice-cold Tris buffer, dried in air, and apposed to ^{3}H-Hyperfilm (Amersham: 4 days, 4°C). Optical density was measured by using a computerized image analysis system (Biocom, les Ulis, France) and converted to femto-moles [^{3}H]citalopram specifically bound per milligram tissue according to a ^{3}H-standard scale.

Immunoautoradiography with anti-SERT, anti-DAT, or anti-5-HT_{1A} receptor antibodies: Polyclonal antibodies specific to the rat 5-HT_{1A}receptor were used according to Gérard et al. (1994), as well as polyclonal antibodies specific to the rat DAT (Martres et al., 1998) or to the rat SERT (gift of Zhou et al., 1996). Coronal sections (20 µm) were fixed for 3 min with 4% paraformaldehyde in phosphate buffered saline (PBS) (50 mM NaH_2PO_4\Na_2HPO_4, 154 mM NaCl, pH 7.4) at 4°C and washed. They were preincubated for 1 h in PBS with 3% bovine serum albumin (BSA) and 1% donkey serum and incubated overnight at 4°C with affinity-purified anti-5-HT_{1A} receptor, nonpurified anti-DAT or anti-SERT antibodies at 1/5000, 1/20,000 or 1/5000 dilution, respectively. After extensive washes, sections were incubated (2 h at RT) in the same solution supplemented with donkey anti-rabbit [^{125}I]IgG (750-3000 Ci/mmol, Amersham) and 1 mM NaI, washed, dried, and apposed to ßmax films (Amersham) for 2–5 days. Optical density on the immunoradiograms was measured as already described.

[^{35}S]GTP-γ-S binding: Autoradiography of agonist-stimulated [^{35}S]GTP-γ-S binding was performed as described (Waeber and Moskowitz, 1997). Brain sections (20 µm) were preincubated at 25°C for 15 min in 50 mM HEPES, pH 7.5, containing 100 mM NaCl, 3 mM $MgCl_2$, 0.2 mM ethyleneglycol-bis(β-aminoethyl ether)-N,N,N',N'-tetraacetic acid (EGTA), and 0.2 mM dithiothreitol and incubated for 15 min in the same buffer supplemented with 2 mM iguanosine diphosphate GDP (Boehringer Mannheim, Mannheim, Germany) and 10 µM of 8-cyclopentyl-1,3-dipropylxanthine (CPDPX; Research Biochemicals), an adenosine receptor antagonist, to reduce nonspecific binding (Laitinen and Jokinen, 1998). Sections were incubated (1 h, 30°C) in the same buffer with 0.05 nM

[^{35}S]GTP-γ-S (1000 Ci/mmol, Amersham) supplemented (stimulated conditions) or not (basal conditions) with 10 μM 5-carboxamido-tryptamine (5-CT; Research Biochemicals). Nonspecific binding was determined on adjacent sections with 10 μM WAY 100635 (Wyeth-Ayerst, Princeton, NJ, USA). Optical density was measured as above.

[^{3}H]5-HT Synaptosomal Uptake

Brain tissues were homogenized in 15–20 volumes (v/w) of 0.32 M sucrose with a glass-Teflon potter (Heidolf Bioblock, Illkizch, France). Homogenates were diluted to 40 vol with 0.32 M sucrose, centrifuged (1000 g, 10 min), and the supernatants were re-centrifuged (10,000 g, 30 min). Pellets were gently resuspended in 50 vol of 0.32 M sucrose, and 25 μl aliquots were incubated in 500 μl of uptake buffer (see above) containing 3–6 nM [^{3}H]5-HT, with or without 10 μM fluoxetine to determine nonspecific uptake. After 7 min at 37°C, samples were diluted with 3 ml of ice-cold buffer and rapidly filtered through Whatman GF/B glass-fiber filters (Ihymep) presoaked with 0.05% PEI. After three washes with ice-cold buffer, filters were dried and radioactivity counted by scintillation spectrometry.

[^{3}H]Citalopram Membrane Binding

Tissues were homogenized in 40 volumes (v/w) of ice-cold 50 mM Tris-HCl containing 120 mM NaCl and 5 mM KCl, pH 7.4, by using a Polytron (Touzart-Matignon, Vitzy-sur-Seine, France). Homogenates were centrifuged (40,000 g, 20 min), and pellets were resuspended in 40 vol of buffer and incubated (37°C, 10 min) to remove endogenous 5-HT. Membranes were spun down (40,000 g, 20 min) and washed threefold by resuspension/centrifugation. The final pellet was suspended in 10 vol of the same buffer, and aliquots (25 μl) were incubated in 500 μl with 0.7 nM or various concentrations (0.2–6 nM) of [^{3}H]citalopram. Nonspecific binding was determined in the presence of 10 μM fluoxetine. After 1 h at 25°C, samples were diluted and rapidly filtered as already described. Kinetic parameters of [^{3}H]citalopram-specific binding were calculated by using the program Ligand.

Measurements of Tissue Levels of 5-HT and its Metabolite

Aliquots (200 μl) of homogenates in 0.32 M sucrose (prepared for the uptake measurement) were mixed with $HClO_4$ (0.1 M final), 0.05% $Na_2S_2O_5$, and 0.05% disodium EDTA and were centrifuged (30,000 g, 15 min, 4°C). Supernatants were neutralized with 2 M KH_2PO_4/K_2HPO_4, pH 7.4, supplemented with 0.01 mg/ml ascorbate oxidase, and $KClO_4$ precipitate was removed by centrifugation (30,000 g, 10 min, 4°C). Aliquots (10 μl) of supernatants were injected directly into a high-performance liquid chromatography (HPLC) column (Ultrasphere IP, Beckman, Gagny, France; 25 cm × 4.6 cm, C18 reverse-phase, particle size 5 μm) protected with a Brownlee precolumn. The mobile phase (at a 1 ml/min flow rate) consisted of 70 mM KH_2PO_4, 2.1 mM triethylamine, 0.1 mM disodium EDTA, 1.25 mM octane sulfonate, and 16% methanol, adjusted to pH 3.02 with solid citric acid. The electrochemical detection system (ESA 5011, Collaborative Research, Bedford, MA, USA) comprises an analytical cell with dual coulometric monitoring electrodes (+50 mV and +350 mV). The generated signal was integrated by a computing integrator

(System-Gold, Beckman), and quantitative determinations of 5-HT and its metabolite 5-hydroxyindoleacetic acid (5-HIAA) were performed with reference to pure standards.

Protein Concentrations

Proteins were quantified according to Lowry et al. (1951) with BSA as standard.

Electrophysiological Studies

Young male rats (~100 g weight) were used because brain tissues from such young animals were more resistant to hypoxia occurring for the preparation of brain slices. Rats were decapitated 8 days after intra-DRN injection. Brains were removed rapidly and placed in an ice-cold Krebs solution continuously bubbled with carbogen (95% O_2/5% CO_2). Vibratome slices (400 μm) containing the DRN were cut (4°C) and maintained at RT in an artificial cerebrospinal fluid for 1 h and transferred to a recording chamber. Extracellular recordings were made with glass microelectrodes (filled with 2 M NaCl, impedance: 10–15 MΩ) introduced into the DRN area, as described (Haj-Dahmane et al., 1991). After identification of the cells as serotonergic neurons, basal activity was recorded before application of the 5-HT_{1A} receptor agonist, ipsapirone, at 10–1000 nM. This drug was added to the superfusing fluid for 3 min, and the resulting changes in firing rate of the recorded neurons were computed and registered graphically.

Recording of Sleep/Wakefulness Cycles

Immediately after injection into the DRN of adult male rats with DNA/PEI complexes, animals were implanted with three sets of electrodes (made of enameled nichrome wire, 150 μm in diameter) for polygraphic sleep monitoring (Maudhuit et al., 1994). Two electrodes were inserted through the skull onto the dura over the right frontal and occipital cortex to record the electroencephalogram (EEG), two electrodes were positioned subcutaneously on each side of the orbit for the electrooculogram (EOG), and two electrodes were inserted into the neck muscles for the electromyogram (EMG). All electrodes were anchored to the skull and soldered to a mini-connector and both were embedded with acrylic cement. Animals were housed in individual recording cages and allowed to recover for 6 days. They were connected to the recording cables for a 2-day habituation. On the eighth day after injection of the plasmids, polygraphic recordings were scored manually every 30 s epoch and, for each animal, the amounts of wakefulness (W), slow wave sleep (SWS), and paradoxal or rapid eye movement sleep (PS or REMS) were computed and calculated over 3-h periods throughout 24 consecutive hours.

Rats were then decapitated and their brains were removed. The hypothalamus was dissected out for the measurement of [^{3}H]5-HT synaptosomal uptake, and the rest of the brain was frozen in isopentane at –30°C for binding and autoradiography.

Statistical Calculations

ANOVA was applied and Student's *t*-test was used to compare values for rats injected with recombinant constructs with those for paired control rats, injected with the nonrecombinant pRc-CMV.

6.3 RESULTS

Plasmid Efficiency In LLC-PK1 Cells

To test the efficiency of different plasmid constructs, the epithelial cell line LLC-PK1, which does not express SERT, was transiently transfected with sense plasmid (5 μg) alone or together with each antisense plasmid (25 μg). Measurement of [^{3}H]5-HT uptake showed that the sense construct allowed expression of a functional SERT (Fig. 6.2B), the activity of which was inhibited by cotransfection with either antisense construct. The short antisense construct exhibited the greatest efficacy (58% inhibition vs. 23% for the full antisense) and was used in subsequent *in vivo* experiments. As expected from their selectivity, neither short nor long antisense plasmids significantly affected [^{3}H]DA uptake induced by cotransfection with a plasmid encoding DAT (Fig. 6.2B).

DNA Complexation by PEI

We tested neutralization of the anionic charges of the DNA constructs by the cationic polymer PEI. We assumed that when DNA-PEI complexes are submitted to an electrophoretic field, they should not migrate if all the negative charges (PO_4^-) of DNA are neutralized by the positive charges (NH_4^+) of PEI. In the example depicted in Figure 6.2C, it was necessary to use PEI at 0.75–1.0 charge equivalents to completely neutralize the charges of DNA. We worked with a net-positive charge of DNA-PEI complexes above neutralization in order to bind and compact all the DNA and to provide a good penetration of complexes into brain cells. Accordingly, for *in vivo* experiments, we used this batch of PEI at a charge ratio of six equivalents of PEI amines for each DNA phosphate.

SERT Protein Expression in the DRN after Plasmid Injections

Previous studies showed that DAT was overexpressed as early as 3 days post-injection of a sense plasmid in the rat brain, whereas under-expression required 7 days post-injection of an antisense plasmid (Martres et al., 1998). So for the first SERT expression studies, the same time intervals were selected.

As illustrated in Figure 6.2D, a significant increase (+23±7%, n=6, P<0.01) in specific labeling of the DRN by [^{3}H]citalopram was observed 3 days after administration of the sense construct. In contrast, a clear-cut decrease in [^{3}H]citalopram binding in the DRN (–28±3%, n=6, P<0.01) was noted 7 days after injection of the short antisense construct. In contrast, the specific labeling of the DRN by [^{3}H]citalopram did not differ between nonrecombinant pRc-CMV-injected rats and intact control animals (not shown).

SERT Expression and Activity after Plasmid Injections

Significant increases (+10–29%) in [^{3}H]5-HT synaptosomal uptake were observed in all forebrain areas studied 3 days after intra-DRN administration of sense plasmid (Fig. 6.3, Top). In contrast, significant decreases (–24% to 31%) in [^{3}H]5-HT uptake were found in the same areas 7 days after antisense injection (Fig. 6.3, Bottom). In rats injected with the pRc-CMV nonrecombinant plasmid complexed with PEI, [^{3}H]5-HT uptake was similar to that measured by using synaptosomes from noninjected animals (not shown).

Quantification of the SERT protein with [^{3}H]citalopram showed significant increases

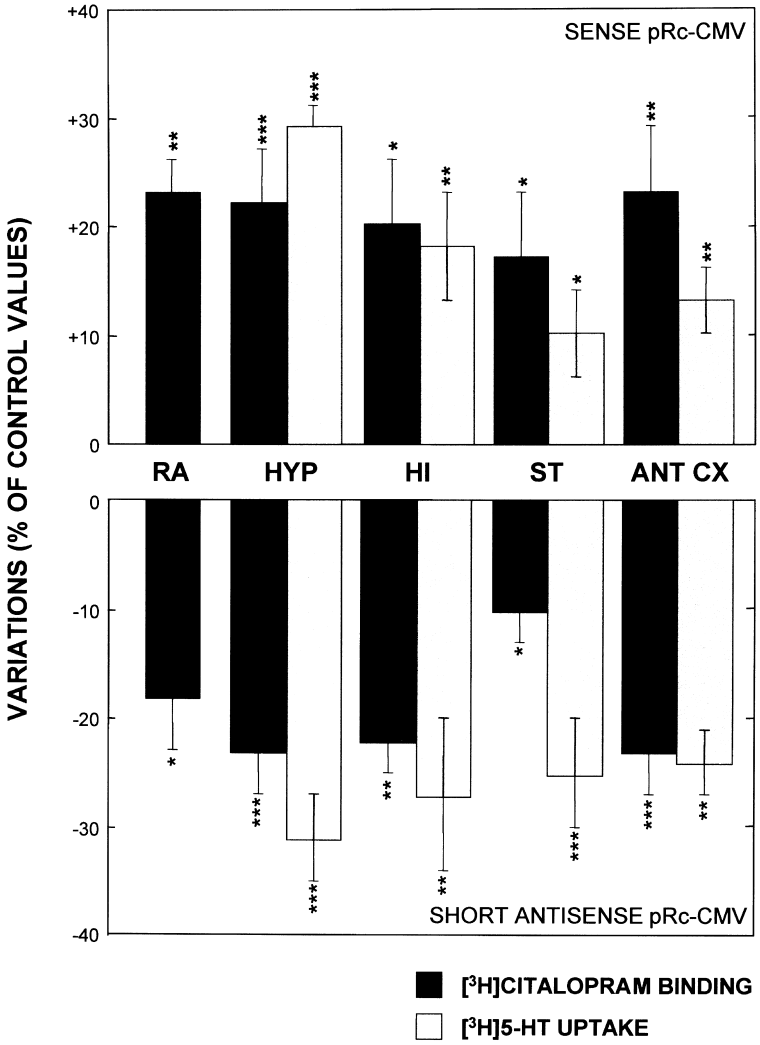

Figure 6.3. Effects of sense or antisense DNA/PEI complex administration on SERT activity and levels. [^{3}H]5-HT synaptosomal uptake was measured in the hypothalamus (HYP), hippocampus (HI), striatum (ST), and anterior cortex (ANT CX), 3 days (top) or 7 days (bottom) after intra-DRN injection of sense or antisense constructs. Membrane binding assays were performed with 0.7 nM [^{3}H]citalopram in the same brain regions and in the anterior raphe area (RA). Both parameters are expressed as percentage of control values of rats injected with the nonrecombinant pRc-CMV and sacrificed 3 or 7 days later. Mean ± SEM of values in three experiments, each performed with five rats. Control values for [^{3}H]5-HT uptake, in fmol/min/mg prot., are 255±11 (HYP), 136±9 (HI), 210±7 (ST) and 227±8 (ANT CX); and for [^{3}H]citalopram-specific binding, in fmol/mg prot., 228±21 (RA), 365±20 (HYP), 155± 9(HI), 264±14 (ST), and 226±21 (ANT CX). *P<0.05; **P<0.01; ***P<0.005 compared with paired control rats (Student's t-test). From Fabre et al., 2000b, copyright 2000, Society for Neuroscience.

(+15–25%) in the five brain areas in rats injected with the sense plasmid (Fig. 6.3, Top) and, conversely, a significant decrease (–10% to 30%) 3 (not shown) and 7 days (Fig. 6.3, Bottom) after injection of the short antisense construct. Saturation studies performed with membranes from the anterior cortex showed that the Bmax of [^{3}H]citalopram binding was decreased by 40%, 3 and 7 days after administration of the short antisense plasmid, compared with paired control rats, without modification of the Kd (not shown).

Specifity of the Intra-DRN Administration of Constructs

Seven days after intra-DRN administration of the SERT sense or antisense constructs, relative DAT levels were quantified by immunoautoradiography with selective polyclonal antibodies. In both cases, no modification in immunolabeling of DAT was observed, neither in the DRN, nor in the substantia nigra (a region rich in DA cell bodies) or the striatum (containing a high density of DA terminals) (Fig. 6.4). In the same animals, the immunolabeling of the SERT in the DRN showed a 26% increase and a 23% decrease, respectively, after sense and antisense injection.

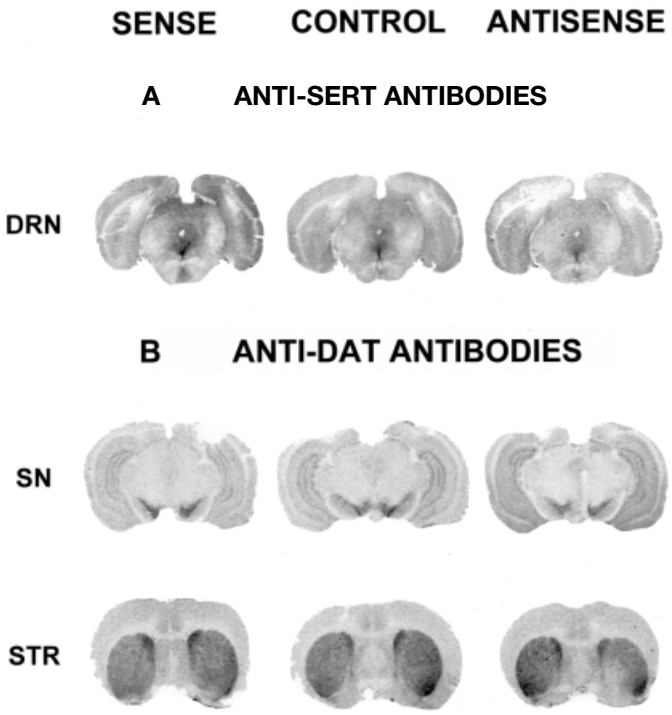

Figure 6.4. Immunoautoradiographic labeling of the SERT and DAT after intra-DRN injection of sense, antisense, or nonrecombinant (control) constructs. Immunoautoradiographs of coronal sections with anti-SERT antibody (**A**) at the level of the dorsal raphe nucleus (DRN) or with anti-DAT antibody (**B**) at the level of the substantia nigra (SN) or the striatum (STR), performed 7 days after intra-DRN plasmid administration. From Fabre et al., 2000b, copyright 2000, Society for Neuroscience.

Time-Course of RST Over-Expression

We performed this study by using synaptosomes from the hypothalamus, a region where the effects are the most marked. An elevated [^{3}H]5-HT uptake capacity, similar to that previously noted on day 3, was observed from day 7 after sense plasmid injection up to 2 weeks (not shown). Four weeks later, [^{3}H]5-HT uptake did not differ significantly between rats injected with the sense plasmid or the nonrecombinant pRc-CMV. Indeed, uptake capacity in rats injected with the control vector did not differ from levels in untreated rats over the whole experimental period.

Levels of 5-HT and its Metabolite after Intra-DRN Injections

Three days after injection of the sense construct, 5-HT levels were increased significantly in the hippocampus (+16%), whereas they remained unaffected in the hypothalamus (Table 6.1). In contrast, 5-HIAA levels were increased significantly (+33%) in the latter but not the former area. As a result, a significant elevation of the 5-HIAA/5-HT ratio was noted in the hypothalamus of sense plasmid-injected rats. No significant effects of the treatments on both 5-HT and 5-HIAA levels were found in the striatum and anterior cortex.

Three days (not shown) as well as 7 days (Table 6.1) after intra-DRN injection of the short antisense plasmid, a significant decrease in 5-HT levels was observed in the hypothalamus and hippocampus, but not in the striatum and anterior cortex (not shown). In contrast, 5-HIAA levels in the four brain areas studied were not affected significantly. Accordingly, the 5-HIAA/5-HT ratio in both the hypothalamus and hippocampus was higher in antisense plasmid-injected rats than in paired controls.

5-HT$_{1A}$ Receptors after Plasmid Injections

Autoradiographic Experiments

5-HT$_{1A}$ receptor density measured by quantitative immunoautoradiography by using selective polyclonal antibodies showed no significant change in the DRN and the hippocampus 8 days after intra-DRN injection of the sense or antisense plasmids (Fig. 6.5 and Table 6.2). However, the increase of [^{35}S]GTP-γ-S binding induced by the 5-HT$_{1A}$ receptor agonist, 5-CT, was higher (+38%) in the DRN of rats injected with the sense plasmid and lower (–17%) in those injected with the short antisense plasmid, compared with that measured in paired controls (Fig. 6.5 and Table 6.2). No difference was observed in the hippocampus. In both areas, the stimulatory effect of 10 μM 5-CT on [^{35}S]GTP-γ-S binding was completely inhibited by 10 μM WAY 100,635 in the three groups of rats and did not differ with the nonstimulated binding (not shown).

Electrophysiological Experiments

No significant differences between control rats and rats injected with either the sense or antisense plasmids were observed concerning the spontaneous firing rate of 5-HT neurons in the DRN. However, the potency of the 5-HT$_{1A}$ receptor agonist ipsapirone to inhibit, in a concentration-dependent manner, the discharge of these neurons was decreased signifi-

Table 6.1. Effects of intra-DRN injection of sense or antisense constructs on 5-HT and 5-HIAA levels

	5-HT (ng/mg prot)		5-HIAA (ng/mg prot)		5-HIAA/5-HT	
	Control	Sense	Control	Sense	Control	Sense
Hypothalamus	5.10 ± 0.15	5.36 ± 0.20^{NS} (+ 5%)	2.91 ± 0.09	3.86 ± 0.17*** (+33%)	0.57 ± 0.02	0.72 ± 0.02** (+26%)
Hippocampus	1.91 ± 0.10	2.22 ± 0.11* (+16%)	2.42 ± 0.12	2.69 ± 0.17^{NS} (+11%)	1.26 ± 0.09	1.25 ± 0.06^{NS} (–1%)
	Control	Antisense	Control	Antisense	Control	Sense
Hypothalamus	5.50 ± 0.28	3.36 ± 0.36*** (–39%)	2.81 ± 0.17	2.38 ± 0.14^{NS} (–15%)	0.51 ± 0.05	0.91 ± 0.12** (+79%)
Hippocampus	2.22 ± 0.26	1.58 ± 0.11* (–29%)	2.35 ± 0.09	2.23 ± 0.16^{NS} (–5%)	1.05 ± 0.08	1.47 ± 0.13** (+40%)

5-HT and 5-HIAA levels and 5-HIAA/5-HT ratios were measured 3 or 7 days after intra-DRN injection of sense or antisense constructs. Paired controls were injected with the nonrecombinant vector. Means ± SEM for 8–10 rats. NS: not significant, *$P < 0.05$, **$P < 0.01$, ***$P < 0.005$ compared with paired control values (Student's *t*-test). From Fabre et al., 2000b, copyright 2000, Society for Neuroscience.

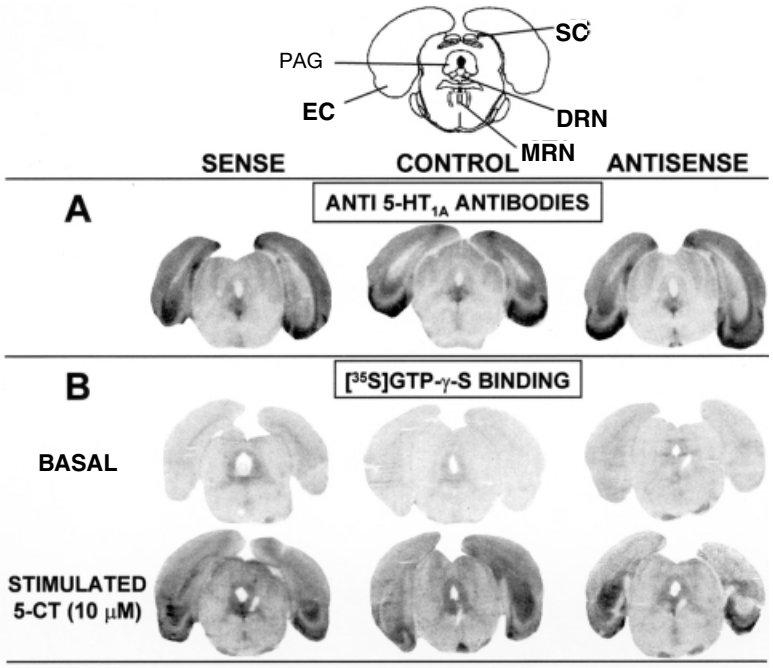

Figure 6.5 Autoradiographic analysis of 5-HT_{1A} receptors 8 days after intra-DRN injection of sense, antisense, or nonrecombinant (control) constructs. Coronal sections at the level of the DRN. **A)** Representative immunoautoradiograms of sections labeled with anti-5–HT_{1A} receptor antibodies. **B)** Autoradiograms of sections labeled by [^{35}S]GTP-γ-S without (basal) or with (stimulated) 10 μM 5-CT. DRN: dorsal raphe nucleus; EC: entorhinal cortex; MRN: median raphe nucleus; PAG: periaqueductal gray; SC: superior colliculi. From Fabre et al., 2000b, copyright 2000, Society for Neuroscience.

cantly 8 days after injection of the antisense plasmid (Fig. 6.6). This finding contrasts with the absence of modification in rats injected with the sense plasmid.

Sleep/Wakefulness Rhythms after Injections

The 24-h periods of wakefulness (W), slow wave sleep (SWS), and paradoxal sleep (PS or REMS) were similar in rats injected on the eighth day before the recording session with either the sense, antisense, or nonrecombinant plasmids. However, marked differences were noted in the sleep/wakefulness circadian rhythm between rats injected with the antisense or nonrecombinant plasmids. During the light period, an increase in the amounts of wakefulness (W: +32±4%, $P<0.005$) and a decrease in those of slow wave sleep (SWS: –11±3%, $P<0.05$) and paradoxal sleep (PS or REMS: –28±15%, ns) were found in rats injected with the antisense plasmid compared with paired controls (Fig. 6.7). In contrast, during the dark period, wakefulness was decreased (–12±3%, $P<0.05$) and sleep was increased (SWS: +19±8%, ns; PS: +85±15%, $P<0.05$) in the antisense plasmid-injected animals.

These changes resulted in an overall decrease of the amplitude of the sleep/wakefulness circadian rhythm (Fig. 6.7). This phenomenon was particularly prominent for PS,

Table 6.2. Effects of intra-DRN injection of sense or antisense constructs on 5-HT_{1A} receptors

	Antibodies (OD)		[^{35}S]GTP-γ-S (% of stimulation)	
	DRN	Hippocampus	DRN	Hippocampus
Control	11.3 ± 0.4	14.1 ± 0.3	+169 ± 7	+338 ± 20
Sense	10.6 ± 0.4^{NS}	13.9 ± 1.3 ^{NS}	+234 ± 28* (+38%)	+371 ± 52 ^{NS}
Antisense	10.2 ± 0.5 ^{NS}	14.2 ± 0.3 ^{NS}	+140 ± 5* (–17%)	+321 ± 20 ^{NS}

Immunoautoradiographic labeling with anti-5-HT_{1A} antibodies and [^{35}S]GTP-γ-S binding were measured in the DRN and hippocampus 8 days after intra-DRN injection of sense, antisense, or nonrecombinant (control) plasmids. Results expressed as optical density values (OD) or percentage of stimulation by 10 μM 5-CT over basal [^{35}S]GTP-γ-S binding. Mean ± SEM of seven determinations (each determination is the mean of data from six sections per rat). NS: nonsignificant, *$P < 0.05$ compared with paired control values (Student's *t*-test). From Fabre et al., 2000b, copyright 2000, Society for Neuroscience.

which was equivalent during the light and the dark periods, contrasting with the normal rhythm; that is, larger amounts of PS expressed during the light versus the dark period. No modifications in the sleep/wakefulness circadian rhythm were noted in rats injected with the sense plasmid compared with paired controls.

6.4 DISCUSSION

Our data demonstrate, for the first time to our knowledge, modulation of SERT expression in the rat brain by nonviral gene transfer. The resulting variations in SERT density produce marked alterations in 5-HT turnover, 5-HT_{1A} autoreceptor functional status and sleep/wakefulness circadian rhythm, as expected given the key role of SERT in controlling 5-HT neurotransmission.

An advantage of PEI as gene carrier is its apparent lack of cytotoxic effects, in agreement with previous observations (Boussif et al., 1995; Abdallah et al., 1996; Martres et al., 1998) and with our data: a) no modification in the synaptosomal [^{3}H]5-HT uptake in the hypothalamus was observed between rats injected with nonrecombinant plasmid complexed with PEI and noninjected rats; b) throughout the time-course study, no difference was seen in the effect of injection of nonrecombinant plasmid; and c) electrophysiological activity in 5-HT cells of the DRN was normal after administration of the different DNA/PEI complexes. Moreover, the basal activity of these cells was the same whatever the construct administered.

This transfer strategy, previously used for modifying DAT expression in the rat brain (Martres et al., 1998), produced long-term changes in SERT expression. Indeed, administration of complexes formed with sense or antisense SERT plasmid and PEI at 6 charge equivalents induced, respectively, significant increases or decreases in SERT labeling, both in the DRN and in various forebrain areas. In all cases, these variations were associated with parallel modifications in SERT immunolabeling at the level of the DRN and in [^{3}H]5-HT synaptosomal uptake, which suggests that these functional changes concerned 5-HT neurons in projection areas.

Time-course studies showed that SERT over-expression persisted for at least 14 days after a single injection of the sense construct-PEI complex. Down-expression of SERT

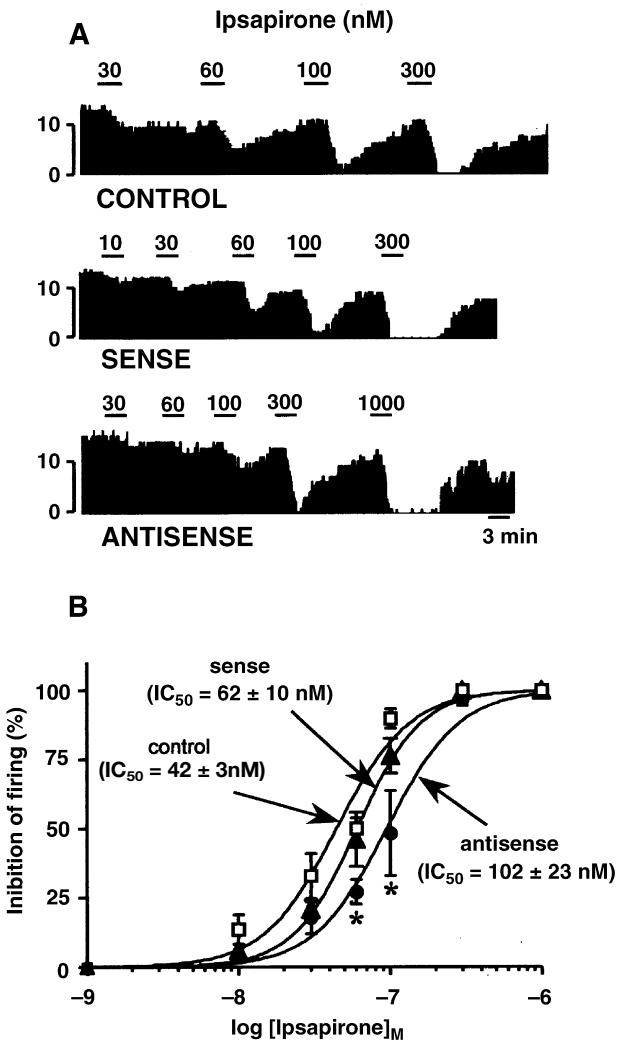

Figure 6.6 Effects of sense/antisense administration on ipsapirone inhibition of DRN 5-HT neuron firing. **A)**: Integrated firing rate (spikes/10 s) histograms of 5-HT neurons of the DRN in brain stem slices exposed to ipsapirone (10–1000 nM). Recordings were made 8 days after injection of sense, antisense, or nonrecombinant (control) plasmid. Each horizontal bar represents bath application of ipsapirone for 3 min at concentration indicated. **B)** Concentration-response curves of ipsapirone-induced inhibition of firing rates of 5-HT neurons. Percentage of the baseline firing rate in paired control rats (open squares), in rats injected with the sense (dark triangles) or the antisense plasmid (dark circles). Mean ± SEM of three to five independent determinations. IC_{50} (± SEM) values were calculated by nonlinear regression analysis, by using Inplot 4. *P<0.05 compared with paired control rats (Student's t-test). From Fabre et al., 2000b, copyright 2000, Society for Neuroscience.

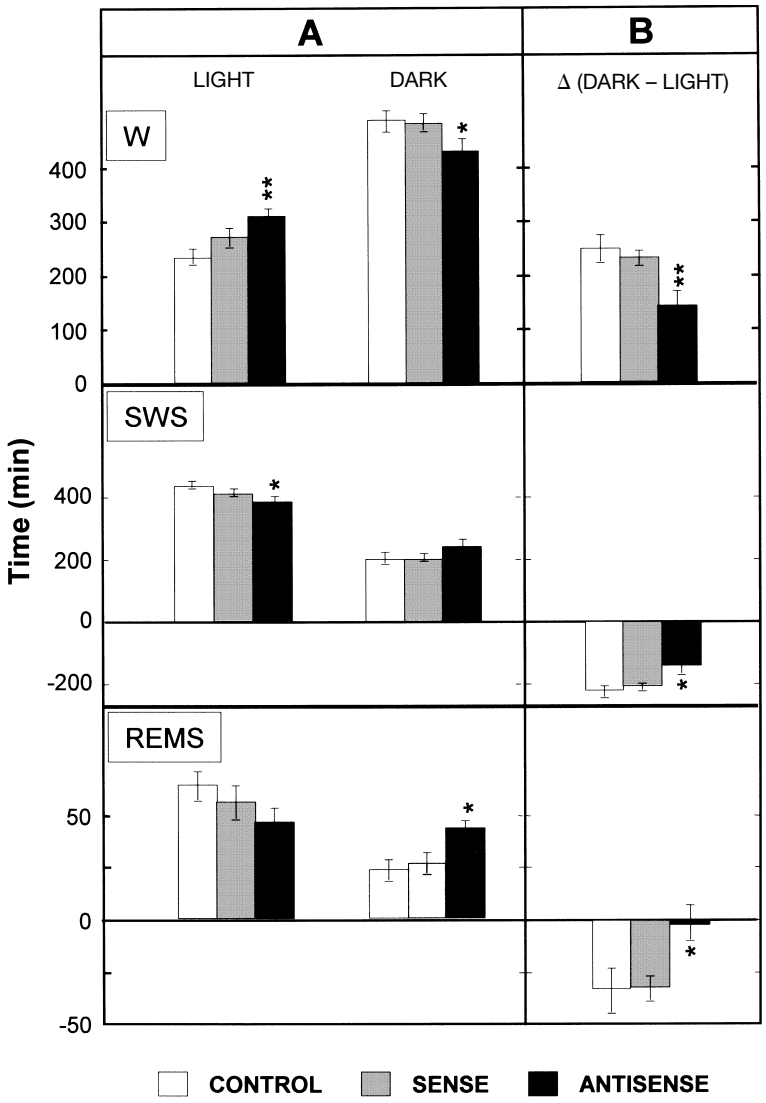

Figure 6.7 Effects of various plasmids on circadian sleep/wakefulness rhythms. **A)** Quantitative analysis of W (wakefulness), SWS (slow wave sleep), or REMS (rapid eye movement sleep) during light and dark periods made 8 days post-injection of sense, antisense or nonrecombinant (control) constructs into the DRN. Mean ± SEM in min per 12 h of the light or dark periods obtained in 7 rats. **B)** Difference in the amounts of each vigilance state between the dark and light periods (min of 12 h-dark period minus min of 12 h-light period). Mean ± SEM of seven independent determinations. **P*<0.05 and ***P*<0.005 versus paired control rats (Student's *t*-test). From Fabre et al., 2000b, copyright 2000, Society for Neuroscience.

was maximum as soon as on the third day after injection of the antisense construct. By comparison, a significant down-expression of DAT was detected only on day 7 post-injection of antisense plasmid (Martres et al., 1998). This difference suggests that SERT has a shorter half-life than DAT (Silvia et al., 1997; Martres et al., 1998), although these two membrane transporters are members of the same protein family.

As expected, administration of the sense construct induced, three days later, significant increases in 5-HIAA levels and 5-HIAA/5-HT ratio in the hypothalamus and in 5-HT levels in the hippocampus. Such changes are reminiscent of those reported after tianeptine administration, an atypical tricyclic antidepressant that stimulates *in vivo* 5-HT uptake (Fattaccini et al., 1990; Marinesco et al., 1996), suggesting a common mechanism of action (increased 5-HT reuptake, which, in turn, decreases extracellular 5-HT levels). Interestingly, 5-HT levels were decreased and the 5-HIAA/5-HT ratios increased in the hypothalamus and hippocampus of rats injected with antisense plasmid. Similar changes have been reported in rats injected with D-fenfluramine, which releases 5-HT by reversing SERT activity (Fattaccini et al., 1991; Sabol et al., 1992), and decreased 5-HT tissue levels were observed in mice lacking the SERT (Bengel et al., 1998).

In the DRN, 5-HT neurons are controlled negatively by 5-HT_{1A}autoreceptors on soma and dendrites (Sotelo et al., 1990; Haj-Dahmane et al., 1991). Chronic increases in extracellular 5-HT levels by long-term treatment with SSRIs produce 5-HT_{1A} autoreceptor desensitization (Chaput et al., 1986; Le Poul et al., 2000). Therefore, we analyzed the functional status of 5-HT_{1A} autoreceptors to assess long-term changes in extracellular 5-HT levels in transfected rats. At a time when SERT expression was significantly modified, no change in 5-HT_{1A} receptor level was noted in the DRN and hippocampus. However, the 5-HT_{1A} receptor-mediated increase in [^{35}S]GTP-γ-S binding by 5-CT was significantly enhanced or reduced in the DRN after injection of the sense or antisense plasmid, respectively. Interestingly, such changes were not observed in the hippocampus, in agreement with previous observations after chronic treatment with SSRIs (Le Poul et al., 2000) and in SERT –/– mice (Fabre et al, 2000a; Mannoury La Cour et al., 2001).

Further functional assessment of 5-HT_{1A} autoreceptors by electrical recording of DRN 5-HT neurons showed a reduced potency of ipsapirone, a well-characterized 5-HT_{1A} receptor agonist (Haj-Dahmane et al., 1991), in inhibiting neuronal firing in antisense injected rats. This finding confirmed association of SERT down-regulation with desensitization of 5-HT_{1A} autoreceptors, as observed after chronic SERT blockade by SSRIs (Chaput et al., 1986; Le Poul et al., 2000) or SERT gene knockout (Fabre et al., 2000a; Mannoury La Cour et al., 2001). Such similarities emphasize the capacity of 5-HT_{1A} autoreceptors to adapt to long-term enhancement in extracellular 5-HT levels that (probably) occurs under these experimental conditions. Interestingly, over-expression of the SERT, which presumably decreases extracellular 5-HT concentration, did not affect sensitivity of DRN 5-HT_{1A} autoreceptors, although this state probably stimulates binding of G protein to 5-HT_{1A} autoreceptors as assessed by GTP-γ-S assays. The lack of adaptive supersensitivity after such treatments supports the idea that 5-$HT_{\mathbf{1A}}$ autoreceptors are not tonically activated under normal physiological conditions.

In line with the well-established involvement of serotonergic systems in sleep regulation (Jouvet, 1969), our data indicate that SERT down-expression in the rat brain induced a significant decrease in the amplitude of circadian sleep/wakefulness rhythm. However, in agreement with the lack of effect of tianeptine on sleep in rats (Lejeune et al., 1988), no changes in sleep/wakefulness circadian rhythm were noted after increased SERT expression. The SERT is highly expressed in the hypothalamic suprachiasmatic nucleus, where

the circadian oscillator is localized (Amir et al., 1997). Lesion of this nucleus abolishes circadian rhythms in rats (Mouret et al., 1978). One hypothesis is that antisense-induced changes in 5-HT neurotransmission, particularly in the hypothalamus, might affect the circadian oscillator activity, thereby altering sleep/wakefulness rhythms. Interestingly, 5-HT uptake blockade by SSRIs increases W and decreases SWS and PS during the light period (Maudhuit et al., 1994).

In conclusion, our data show nonviral gene transfer to modulate efficiently SERT expression in the rat brain. The fact that 20–30% variations in SERT density are enough to induce significant alterations in 5-HT neurotransmission underlines the pivotal role of the SERT in the 5-HT system regulation.

Our data also show that the use of the cationic polymer PEI as a carrier represents a promising way to transfer DNA in the adult (nonmitotic) brain. In addition to its safety, the great advantage of this technique compared with viral gene transfer methods is its high flexibility, accommodating large constructs; that is, sense or antisense, partial or entire sequences, associated with universal or tissue-specific promotors. This technique should be particularly useful to test plasmid DNA constructs or cell-specific promoters, short-circuiting the need to create transgenic lines.

In comparison with the antisense ODN strategy, this novel approach has two main advantages: first, in addition to inactivating mRNA, it also allows over-expression of specific proteins, as presently illustrated; second, probably due to a continuous transcription of RNA from the cDNA, a single administration of DNA is sufficient to produce significant alteration of an expressed protein, 14–21 days after administration in rats or up to 90 days in the mouse brain (Abdallah et al., 1996).

Concerning use of nonviral carriers, such as cationic lipids, a previous *in vitro* comparative study has shown that PEI compares very favorably with the lipopolyamine transfectam and is 10^4-fold more efficient than polylysine for introducing DNA into cell lines (Boussif et al., 1995). Moreover, *in vivo* studies (Abdallah et al., 1996, and B. Demeneix, unpublished) also showed that gene transfer with PEI provides high levels of transgene expression in the mouse mature CNS, with numbers of transfected cells in the same range as those reported for adenoviral gene transfer and one-order-of-magnitude greater than with all other nonviral vectors described so far.

ACKNOWLEDGMENTS

We are grateful to Dr. L. Lanfumey and C. Mannoury La Cour for electrophysiological studies, to Dr. J. Adrien and B. Boutrel for recording sleep/wakefulness rhythms, to N. Hanoun and C-M. Fattaccini for measuring serotonin turnover, and to C. Sais for the drawing of figures.

ANNOTATED REFERENCES

Abdallah B, Hassan A, Benoist C, Goula D, Behr JP, Demeneix BA (1996): A powerful nonviral vector for in vivo gene transfer into the adult mammalian brain: Polyethylenimine. Hum Gene Ther 7:1947–1954.

Akli S, Caillaud C, Vigne E, Stradford-Perricaudet LD, Poenaru L, Perricaudet M, Kahn A, Peschanski MR (1993): Transfer of a foreign gene into brain using adenovirus vectors. Nature Gene 3:224–228.

Amir S, Robinson B, Ratovitski T, Rea MA, Steward J, Simantov R (1997): A role for serotonin in the circadian system revealed by the distribution of serotonin transporter and light-induced fos immunoreactivity in the suprachiasmatic nucleus and intergeniculate leaflet. Neuroscience 84:1059–1073.

Antunes Bras JM, Epstein AL, Bourgoin S, Hamon M, Cesselin F, Pohl M (1998): Herpes simplex virus 1-mediated transfer of preproenkephalin A in the rat dorsal root ganglia. J Neurosci 70:1299-1303.

Bachoud-Levi AC, Remy P, Nguyen JP, Brugieres P, Lefaucheur JP, Bourdet C, Baudic S, Gaura V, Maison P, Haddad B, Boisse MF, Grandmougin T, Jeny R, Bartolomeo P, Della Barba G, Degos JD, Lisovoski F, Ergis AM, Pailhous E, Cesaro P, Hantraye P, Peschanski M (2000): Motor and cognitive improvements in patients with Huntington's disease after neural transplantation. Lancet 356:1975–1979.

First and nice demonstration of improvements of symptoms in Huntington's patients after transplantation of fetal striatal neuroblasts.

Bengel D, Murphy DL, Andrews AM, Witchems CH, Feltner D, Heils A, Mössmer R, Wetsphal H, Lesch KP (1998): Altered brain serotonin homeostasis and locomotor insensitivity to 3,4-methylenedioxymetamphetamine ("ecstasy") in serotonin transporter deficient mice. Mol Pharmacol 53:649–655.

Blakely RD, Berson HE, Fremeau RT, Caron MG, Peck MM, Prince HK, Bradley CC (1991): Cloning and expression of a functional serotonin transporter from rat brain. Nature (London) 354:66–70.

Boussif O, Lezoualc'h F, Zanta MA, Mezgny, M, Scherman D, Demeneix BA, Behr JP (1995): A novel, versatile vector for gene oligonucleotide transfer into cells in culture and in vivo: polyethylenimine. Proc Natl Acad Sci USA 92:7297–7303.

First demonstration of PEI efficiency in vivo.

Byk G, Soto J, Mattler C, Frederic M, Scherman D (1998): Novel non-viral vectors for gene delivery: synthesis of a second-generation library of mono-functionalized poly-(guanidinium)amines and their introduction into cationic lipids. Biotechnol Bioeng 61:81–87.

Chang AS, Chang SM, Starnes DM, Schroeter S, Bauman AL, Blakely RD (1996): Cloning and expression of the mouse serotonin transporter. Mol Brain Res 43:185–192.

Chaput Y, De Montigny C, Blier P (1986): Effects of selective 5-HT reuptake blocker, citalopram, on the sensitivity of 5-HT autoreceptors: Electrophysiological studies in the rat brain. Naunyn Schmiedeberg's Arch Pharmacol 333:342–348.

Crystal RG (1995): The gene as a drug. Nature Med 1:15–17.

Crystal RG (1996): Transfer of genes to humans: Early lessons and obstacles to success. Science 270:404–410.

Danos O (2000): Gene transfer. Bull Acad Natl Med 184:1177–1179.

Dechant KL, Clissold SP (1991): Paroxetine: A review of its pharmaco-dynamic and pharmacokinetic properties, and therapeutic potential in depressive illness. Drugs 41:225–253.

During MJ, Naegele JR, O'Malley KL, Geller AI (1994): Long-term behavioral recovery in Parkinsonian rats by an HSV vector expressing tyrosine hydroxylase. Science 266:1399–1403.

Fabre V, Beaufour C, Evrard A, Rioux A, Hanoun N, Lesch KP, Murphy DL, Lanfumey L, Hamon M, Martres MP (2000a): Altered expression and functions of serotonin 5-HT1A and 5-HT1B receptors in knock-out mice lacking the 5-HT transporter. Eur J Neurosci 12:2299–2310.

Fabre V, Boutrel B, Hanoun N, Lanfumey L, Fattaccini CM, Demeneix B, Adrien J, Hamon M, Martres MP (2000b): Homeostatic regulation of serotonergic functions by the serotonin transporter as revealed by nonviral gene transfer. J Neurosci 20:5065–5075.

Interesting demonstration of transfection of postmitotic neurons correlated with functional modifications.

Fattaccini CM, Bolanos-Gimenez F, Gozlan H, Hamon M (1990): Tianeptine stimulates uptake of 5-hydroxytryptamine in vivo in the rat brain. Neuropharmacology 29:1–8.

Fattaccini CM, Gozlan H, Hamon M (1991): Differential effects of D-fenfluramine and p-chloroamphetamine on H75/12-induced depletion of 5-hydroxytryptamine and dopamine in rat brain. Neuropharmacology 30:15–23.

Fisher LJ, Ray J (1994): In vivo and ex vivo gene transfer to the brain. Curr Opin Neurobiol 4:735–741.

Gérard C, Langlois X, Gingrich J, Doucet E, Vergé D, Kia IK, Raisman R, Gozlan H, El Mestikawy S, Hamon H (1994): Production and characterization of polyclonal antibodies recognizing the intracytoplasmic third loop of the 5-hydroxytryptamine$_{1A}$ receptor. Neuroscience 62:721–739.

Goula D, Remy JS, Erbacher P, Wasowicz M, Levi G, Abdallah B, Demeneix BA (1998): Size, diffusibility and transfection performance of linear PEI/DNA complexes in the mouse central nervous system. Gene Ther 5:712–717.

Green AR, Cross AJ, Goodwin GM (1995): Review of the pharmacology and clinical pharmacology of 3,4-methylenedioxymetamphetamine (MDMA or "Ecstasy"). Psychopharmacology 119:247–260.

Haj-Dahmane S, Hamon M, Lanfumey L (1991): K^+ channel and 5-hydroxytryptamine$_{1A}$ autoreceptor interactions in the rat dorsal raphe nucleus: An in vitro electrophysiological study. Neuroscience 41:495–505.

Horellou P, Vigne E, Castel MN, Barnéoud P, Colin P, Perricaudet M, Delaère P, Mallet J (1994): Direct intracerebral gene transfer of an adenoviral vector expressing tyrosine hydroxylase in a rat model of Parkinson's disease. Neuroreport 6:49–53.

Jiao S, Gurevich V, Wolff J (1993): Long-term correction of rat model of Parkinson's disease by gene therapy. Nature (London) 362:450–453.

Jouvet M (1969): Biogenic amines and the states of sleep. Science 163:32–41.

Kaplitt MG, Leone P, Salmuski R, Xiao X, Pfaff DW, O'Malley KL, During MJ (1994): Long-term gene expression and phenotypic correction using adeno-associated virus vectors in the mammalian brain. Nature Genet 8:148–153.

Interesting data on behavioral recovery after intra-striatal injection of an adenovirus expressing tyrosine-hydroxylase in unilateral 6-hydroxydopamine-lesioned rats.

Kesari S, Randazzo BP, Valyi-Nagi T, Huang QS, Brown SM, Maclean AR, Lee VM, Trojanowski JQ, Fraser NW (1995): Therapy of experimental human brain tumors using a neuro attenuated herpes simplex virus mutant. Lab Invest 73:636–648.

Laitinen JT, Jokinen M (1998): Guanosine 5'-(gamma-[^{35}S]thio)triphosphate auto-radiography allows selective detection of histamine H3 receptor-dependent G protein activation in rat brain tissue sections. J Neurochem 71:808–816.

Lejeune F, Poignant J, Reure H (1988): Electrophysiological studies of tianeptine, a new enhancer of serotonin uptake with antidepressant activity. Neurophysiol Clin 18:369–381.

Lemkine GF, Demeneix BA (2001): Polyethylenimines for in vivo gene delivery. Curr Opin Mol Ther 3:178–182.

Le Poul E, Boni C, Hanoun N, Laporte AM, Laaris N, Chauveau T, Hamon M, Lanfumey L (2000): Differential adaptation of brain 5-HT$_{1A}$and 5-HT$_{1B}$ receptors and 5-HT transporter in rats treated chronically with fluoxetine. Neuropharmacology 39:110–122.

Detailed studies on the marked regional differences of changes in 5-HT neurotransmission induced by chronic inhibition of the 5-HT transporter.

Lesch KP (1997): Molecular biology, pharmacology, and genetics of the serotonin transporter: Psychobiological and clinical implications. In Baumgarten HG, Göthert M. (eds): Serotonin Neurons and 5-HT Receptors in the CNS. Berlin: Springer 129:671–705.

Lesch KP, Wolozin BL, Estler HC, Murphy DL, Riederer P (1993): Isolation of a cDNA encoding the human brain serotonin transporter. J Neural Trans Gen Sect 95:157–162.

Lowry OH, Rosebrough NJ, Farr A, Randall RJ (1951): Protein measurement with the Folin phenol reagent. J Biol Chem 193:265–275.

Mannoury La Cour C, Boni C, Hanoun N, Lesch KP, Hamon M, Lanfumey L (2001): Functional consequences of 5-HT transporter gene disruption on 5-HT1A receptor-mediated regulation of dorphal raphe and hippocampal cell activity. J Neurosci 15:2178–2185.

Marinesco S, Poncet L, Debilly G, Jouvet M, Cespuglio R (1996): Effects of tianeptine, sertraline and clomipramine on brain serotonin metabolism: a voltametric approach in the rat. Brain Res 736:82–90.

Martres MP, Demeneix B, Hanoun N, Hamon M, Giros B (1998): Up- and down-expression of the dopamine transporter by plasmid DNA transfer in the rat brain. Eur J Neurosci 10:3607–3616.

Maudhuit C, Jolas T, Hamon H, Adrien J (1994): Effects of acute and chronic treatment with amoxapine and cericlamine on the sleep/wakefulness cycle in the rat. Neuropharmacology 33:1017–1025.

Mouret J, Coindet J, Debilly G, Chouvet G (1978): Suprachiasmatic nuclei lesions in the rat: alterations in sleep circadian rhythms. Electroencephalogr Clin Neurophysiol 15:102–108.

Paxinos P, Watson C (1986): The rat brain in stereotaxic coordinates. London, UK: Academic Press.

Rioux A, Fabre V, Lesch KP, Möessner R, Murphy DL, Lanfumey L, Hamon M, Martres MP (1999): Adaptive changes in serotonin 5-HT2A receptors in mice lacking the serotonin transporter. Neurosci Lett 262:113–116.

Sabaté O, Horellou P, Vigne E, Colin P, Perricaudet M, Buc-Caron M-H, Mallet J (1995): Transplantation to the rat brain of human neural progenitors that were genetically modified using adenovirus. Nature (London) 9:256–260.

Sabol KE, Richards JB, Seiden LS (1992): Fluoxetine attenuates the D,L-fenfluramine-induced increase in extracellular serotonin as measured by in vivo dialysis. Brain Res 585:421–424.

Silvia CP, Jaber M, King GR, Ellinwood EH, Caron MG (1997): Cocaine and amphetamine elicit differential effects in rats with unilateral injection of dopamine transporter antisense oligodeoxynucleotides. Neuroscience 76:737–747.

Sotelo C, Cholley B, El Mestikawy S, Gozlan H, Hamon H (1990): Direct immuno-histochemical evidence of the existence of 5-HT_{1A} autoreceptors on serotonergic neurons in the midbrain raphe nuclei. Eur J Neurosci 2:1144–1154.

Thomas DR, Nelson DR, Johnson AM (1987): Biochemical effects of the antidepressant paroxetine, a specific 5-hydroxytryptamine uptake inhibitor. Psychopharmacology 93:193–200.

Waeber C, Moskowitz MA (1997): 5-Hydroxytryptamine$_{\mathbf{1A}}$ and 5-hydroxy-tryptamine$_{\mathbf{1B}}$ receptors stimulate [^{35}S]guanosine-5'-O-(3-thio)triphosphate binding to rodent brain sections as visualized by in vitro autoradiography. Mol Pharmacol 52:623–631.

Weiss B, Davidkova G, Zhou LW, Zhang SP, Morabito M (1997): Expression of a D2 dopamine receptor antisense RNA in brain inhibits D2-mediated behaviors. Neurochem Int 31:571–580.

Zhou FC, Xu Y, Bledsoe S, Lin R, Kelley MR (1996): Serotonin transporter antibodies: production, characterization, and localization in the brain. Brain Res Mol Brain Res 43:267–278.

CHAPTER 7

METHODS IN STUDYING THE REGULATION AND TRAFFICKING OF TRANSMEMBRANE TRANSPORTERS

SCOTT L. DEKEN, DAN WANG, AND MICHAEL W. QUICK

7.1 WHY STUDY REGULATION AND TRAFFICKING OF TRANSPORTERS?

The movement of ionic and polar substances through the nonpolar core of plasma membranes requires transmembrane transporters. Transport proteins move molecules such as pyruvate, amino acids, sugars, nucleotides, and neurotransmitters across membranes, along with ions such as Na^+, K^+, Ca^{2+}, and Cl^- (Stein, 1986). Significant attention has been given to the trafficking of transporters that remove neurotransmitter from the synaptic cleft at neuronal contacts (Liu et al., 1999). The expression and regulation of these neurotransmitter transporters have profound influences on postsynaptic responses to presynaptic activity (Beckman and Quick, 1998). This chapter focuses on the different approaches used to study the regulation and trafficking of Na^+/Cl^--coupled neurotransmitter transporters.

Normal behavior and general health depend on the proper functioning of neurotransmitter transporters (Jaber et al., 1997; Beckman and Quick, 2000). Studies show that neurotransmitter transporters play a role in regulating the time course of neurotransmitter levels in the synaptic cleft (Isaacson et al., 1993; Giros et al., 1996; Diamond and Jahr, 1997). Distinct behavioral effects caused by altered transporter function are demonstrated by the actions of cocaine, amphetamine, and alcohol (Amara and Sonders, 1998); by diseases such as depression, obsessive-compulsive disorder, schizophrenia, and epilepsy (Beckman and Quick, 2000); and by the binding of therapeutic drugs to transporters for the treatment of drug abuse and psychiatric disease (Iverson, 2000). These behavioral effects are probably caused by the ineffective regulation of transporters in vivo.

Na^+/Cl^--coupled neurotransmitter transporters are regulated by second-messenger cascades, protein–protein interactions, and extracellular transporter ligands (Beckman and Quick, 1998). Transporter regulation occurs by pathways involving nitric oxide, calmodulin, neurotrophic factors, protein kinase A, protein kinase B, and, most notably, protein kinase C (PKC; Beckman and Quick, 2000). Transport rates and cell surface expression levels of transporters are regulated by protein–protein interactions (Deken et al., 2000; Geerlings et al., 2000; Torres et al., 2001). Modulation of neuronal trans-

Transmembrane Transporters. Edited by Michael Quick

ISBNs: 0-471-06517 (Hardcover); 0-471-43404-3 (Electronic)

porters also occurs by exposure to transporter agonists and antagonists. This regulation occurs by redistribution of the transporter from sites on the plasma membrane to intracellular storage sites, or vice versa (Bernstein and Quick, 1999). The trafficking events and protein interactions that are responsible for transporter redistribution are poorly understood.

The general processes of endocytosis, intracellular sorting, and exocytosis within mammalian cells, more specifically neurons, are becoming increasingly clear (Buckley et al., 2000). The specificity of proteins to their destinations stems from numerous protein–protein interactions. Some neuronal plasma membrane transporters have been shown to target endosomes after clathrin-mediated endocytosis (Daniels and Amara, 1999; Melikian and Buckley, 1999). Knowing how neurons regulate transporter function and expression will help clarify the physiological roles of transporters and possibly lead to the development of therapeutic drugs for numerous neurological diseases involving transporters (Iversen, 2000).

7.2 BACKGROUND AND HISTORY

GABA (γ aminobutyric acid) transporter 1 (GAT1) was first cloned in 1990 and was the first member of the Na^+/Cl^--coupled neurotransmitter transporters to be cloned (Guastella et al., 1990). Other members of this family include dopamine, serotonin, and norepinephrine transporters (Rudnick, 1998). The nerve terminals of GABAergic neurons contain GAT1 proteins localized in intracellular storage compartments and on the cell surface (Minelli et al., 1995). This simple statement poses many questions about trafficking and regulation: How is GAT1 targeted to nerve terminals? Where is the intracellular storage compartment of GAT1 in nerve terminals? What signals induce GAT1 endocytosis and exocytosis? What are the mechanisms by which GAT1 is internalized and put on the plasma membrane? Is GAT1 function regulated on the plasma membrane? Is GAT1 recycled back to the plasma membrane after internalization, or is it destined to be degraded? These are just some of the questions our lab and others have tried to answer (and are still trying to answer) since the cloning of GAT1.

Neurons synthesize proteins in the cell body, far from the nerve terminal where GAT1 will eventually reside; therefore, GAT1 must travel down GABAergic axons from the cell body (Ahn et al., 1996). This polarized expression of GAT1 is also seen when GAT1 is transfected into polarized epithelial cells, which suggests similar sorting mechanisms in each of the cell types (Pietrini et al., 1994). In GABA transporters 2 and 3 and the betaine transporter, all close relatives to GAT1, sorting from the endoplasmic reticulum to their final destinations requires signaling sequences in the C-terminal tail (Perego et al., 1997 and Muth et al., 1998). However, if the C-terminal tail of GAT1 is truncated, it still localizes to the apical membranes of polarized epithelial cells, homologous to the axonal end of neurons (Perego et al., 1997). These data suggest that the correct sorting of GAT1 after ER exit is not contained strictly in GAT1's C-terminal tail and that other regions or interacting proteins must help to map GAT1 to nerve terminals after synthesis. GAT1 appears to be distributed in intracellular compartments, as well as on the plasma membrane, but where GAT1 is stored intracellularly is still undetermined.

The redistribution of GAT1 from intracellular compartments to the cell surface or vice versa can be seen by multiple mechanisms (Quick et al., 1997). GAT1 moves on and off

the plasma membrane in response to substrates and transport inhibitors (Bernstein and Quick, 1999). Internalization of GAT1 on the plasma membrane can be achieved by phorbol 12-myristate 13-acetate (PMA)-induced PKC activation or by the activation of PKC by G-protein coupled receptors (Corey et al., 1994 and Beckman et al., 1999). Direct tyrosine phosphorylation also appears to regulate transporter activity on the plasma membrane (Law et al., 2000). The endocytic and exocytic mechanisms for GAT1 internalization and externalization have yet to be determined. Syntaxin 1A, a protein involved in synaptic vesicle fusion to the plasma membrane (Bennett et al., 1992), increases GAT1 cell surface expression by redistribution of intracellular GAT1 to the plasma membrane (Horton and Quick, 2001). Interestingly, syntaxin 1A not only increases GAT1 cell surface expression but it also regulates its function by decreasing GAT1 translocation rates (Deken et al., 2000).

Studies involving the transporters of dopamine (DAT), serotonin (SERT), and norepinephrine (NET) (monoamine transporters) also provide insight into the trafficking behaviors of neurotransmitter transporters (Blakely and Bauman, 2000). As seen with GAT1, significant amounts of monoamine transporters can be found intracellularly. The DAT colocalizes with the endosomal marker transferrin, but it is unclear whether it is recycled back to the plasma membrane or is degraded (Daniels and Amara, 1999; Melikian and Buckley, 1999). DAT is internalized via a dynamin-dependent mechanism, which suggests a clathrin-mediated endocytosis event for DAT removal from the plasma membrane (Daniels and Amara, 1999; Saunders et al., 2000). Activation of PKC causes the internalization of DAT, SERT, and NET from the plasma membrane (Vaughn et al., 1997; Qian et al., 1997). Similar regulatory responses with GAT1 are also seen by the SERT's ability to regulate its cell surface expression in response to substrates, such as cocaine and amphetamines (Ramamoorthy and Blakely, 1999). Monoamine transporters also interact with proteins on the plasma membrane to increase transporter surface expression. DAT surface expression is increased by its PDZ-mediated protein–protein interaction with PICK1, a PKC-binding protein (Staudinger et al., 1995 and Torres et al., 2001). Whether or not there are generalized regulating factors and trafficking routes for neurotransmitter transporters is still in question.

Numerous strategies have been used to study the regulation and trafficking of transporters. Probably the oldest and most widely used experimental approach is radiolabeled substrate uptake. Uptake assays are useful for determining changes in affinity and maximum transport capacity. In this way, one can determine the functional significance of different drug treatments to cells expressing transporters. A change in affinity suggests a functional change in individual transporters, whereas a change in maximum transport capacity reveals a change in the total surface expression of the transporters. Biotinylation assays, described below, are a more accepted means to determine changes in cell surface expression. Colocalization studies with marker proteins can be used to determine the intracellular localization of transporters. Green fluorescent protein (GFP) tagging, antibody staining, and cellular fractionation techniques can be used to visualize the intracellular location of transporters and marker proteins. Co-immunoprecipitation studies can help determine whether transporters physically interact with other proteins. Immunoisolation experiments provide a powerful tool not only to determine in which cellular organelles transporters reside but also to determine what other proteins are found on these transporter-composed organelles. Each of these methods will be described in detail below.

7.3 BIOTINYLATION, FRACTIONATION, GFP TAGGING, IMMUNOPRECIPITATION, AND IMMUNOISOLATION

A biotinylation assay is an easy and direct method to determine levels of cell surface proteins. Plasma membrane levels of transporters before and after treatments that move transporter on and off the cell surface can be analyzed directly. The incubation of biotin to nonpermeabilized cells allows biotin to bind exclusively to cell surface proteins because biotin binds strongly to proteins and cannot cross the plasma membrane. The cell surface proteins are then pulled down by the addition of an avidin complex, which is heavy and also binds very tightly to biotin molecules. The cell surface proteins that are bound to the "heavy" biotin-avidin complex are then separated from intracellular proteins by centrifugation (Altin and Pagler, 1995). The isolated proteins are then run on a sodium dodecyl sulfate polyacrylamide gel electrophoresis (SDS-PAGE) gel, and protein levels are quantified by Western blot. Qian et al. used biotinylation to determine cell surface expression levels of human SERT proteins before and after PMA (a PKC activator) treatment. They found that PKC activation causes a reduction in the amount of SERT on the cell surface (Qian et al., 1997; see Fig. 7). Davis et al. used biotinylation to show that the glutamate transporter protein levels on the plasma membrane are enhanced by PKC activation in C6 glioma cells (Davis et al., 1998; see Fig. 4). Our lab has also used biotinylation studies to show that GAT1 levels on the plasma membrane are affected by syntaxin 1A expression (Horton and Quick, 2001; see Fig. 1), agonists and antagonists of GAT1 (Berstein and Quick, 1999; see Fig. 4), tyrosine kinase inhibitors (Law et al., 2000; see Fig. 3), and PKC activation (Beckman et al., 1999; see Fig. 3). A schematic of biotinylation is shown in Figure 7.1.

Cell fractionation is a useful way to study trafficking and subcellular distribution of proteins. The fractionation experiment consists of two main steps: the disruption of the cell membrane and the isolation of specific cellular organelles. The gentler the disruption of the cell membrane, the more functional the purified organelles are (Dealtry and Rickwood, 1992). This method has provided scientists with a powerful tool to study transporter biology. The method for cell fractionation is shown in Figure 7.2. Neurobiologists have been able to purify synaptic vesicles and study vesicular transporter function (Floor and Feist, 1989; Krantz et al., 2000). Presynaptic plasma membrane transporters have long been studied by fractionating purified synaptosomes. Melikian and Buckley used fractionation studies to determine the intracellular localization of the dopamine transporter. They isolated large, dense-core vesicles; synaptic vesicles; and endosomes by knowing the size and sedimentation properties of these different organelles. With each of these cellular fractions, they used Western blot analysis to determine where the dopamine transporter resides intracellularly. The dopamine transporter was not found on fractions containing large, dense-core vesicles or synaptic vesicles but was located on endosomes. The DAT found on endosomes cofractionated with the transferrin receptor, EEA1, and rab5A; which are all endosomal markers (Melikian and Buckley, 1999; see Fig. 6). We are currently trying to determine the intracellular locations of GAT1. We have preliminary evidence from subcellular fractionation techniques that GAT1 can be found in endosomal and synaptic vesicle populations. We have also used immunoisolation techniques to separate GAT1-containing vesicles from synaptophysin containing synaptic vesicles.

The gene encoding GFP was isolated from the jellyfish *Aequoria victoria* in 1992 and has become a popular tool for scientists studying protein localization and trafficking

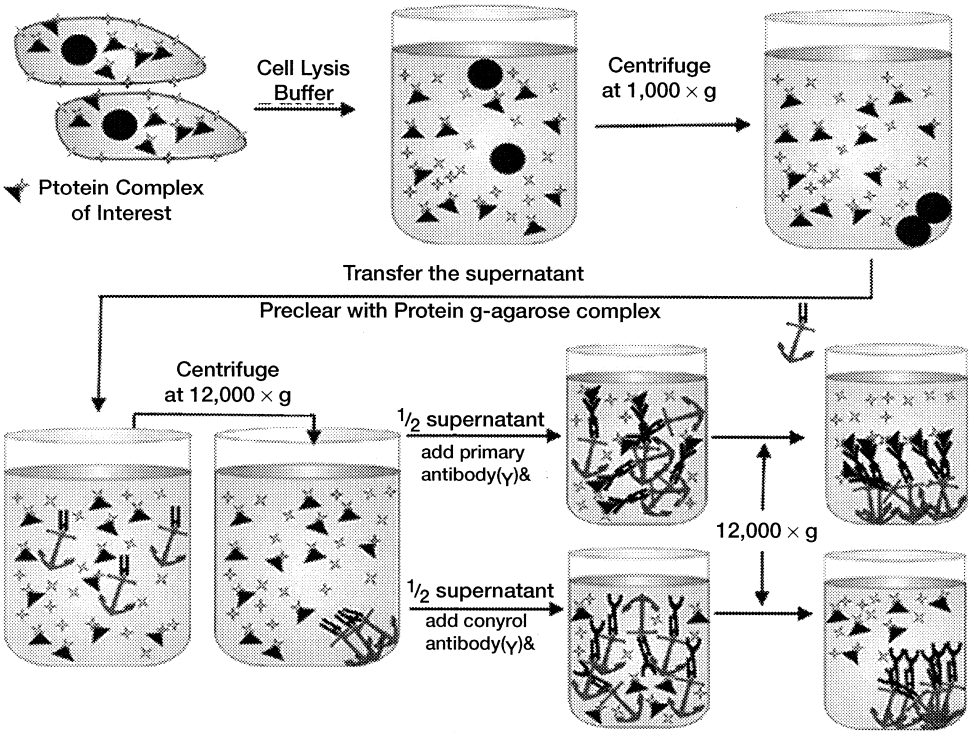

Figure 7.1 Schematic of biotinylation experiment.

(Prasher et al., 1992). As its name implies, GFP proteins are flourescent in the green wavelength, so they can be visualized by using standard FITC (fluoresceinisothiocyanate) excitation and emission filters. The tagging of GFP to proteins of interest is useful because one may visualize the movement of the protein of interest in real-time (Tarasova et al., 1997). GFP tagging offers many advantages over antibody staining: no substrates normally needed for fluorescence, no cumbersome protocols, no potential artifacts, and no need for expensive primary and secondary antibodies. One must be aware, however, that the addition of the GFP protein to the protein of interest may affect normal protein trafficking and localizations, so one must be sure to perform appropriate control experiments. The use of GFP chimeras to study transporter trafficking is still in its infancy. Daniels and Amara used a GFP-tagged DAT to study DAT trafficking. They used real-time imaging to show that significant DAT quantities are internalized within 30 min of PMA treatment (Daniels and Amara, 1999; Figs. 4D and 5). They also used this construct to show that PMA-induced internalization can be blocked by the expression of a dominant-negative dynamin construct and to show that DAT colocalizes with the transferrin receptor and AC17 (a lysosomal marker). We have recently obtained a chimera of a GAT1 construct containing GFP on its C-terminal tail (generous gift from Henry Lester, Caltech, Pasadena, CA). We are currently investigating the trafficking and localization of this construct in much the same way as the Daniels and Amara study.

The trafficking of proteins around a cell's interior results from numerous protein–pro-

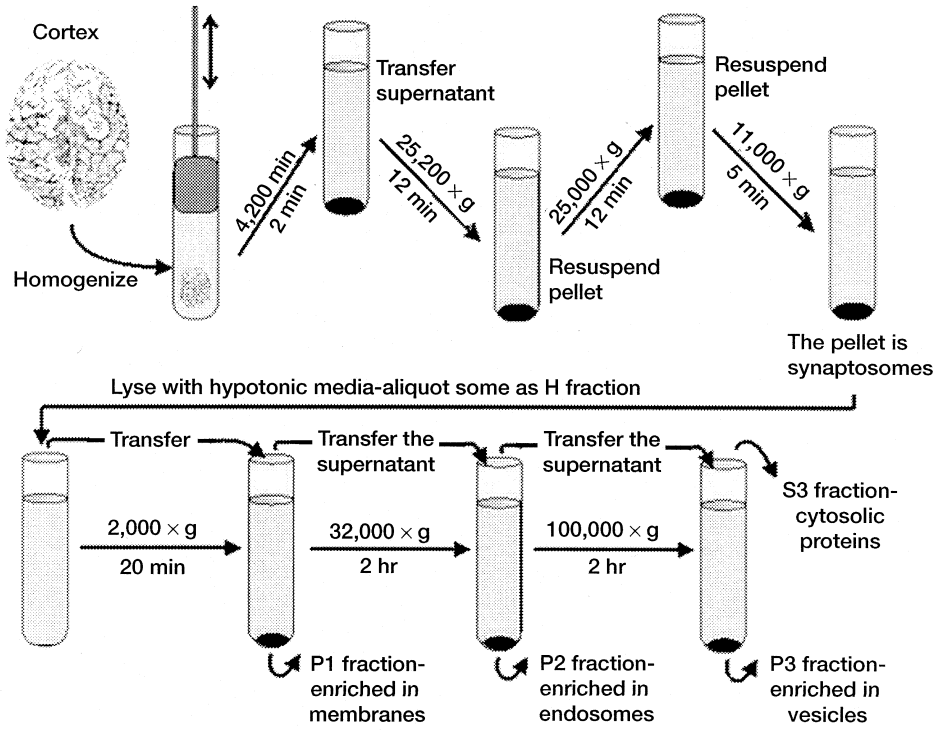

Figure 7.2 Schematic of fractionation experiment.

tein interactions. The most common way to study whether proteins interact is by performing an immunoprecipitation experiment. Immunoprecipitation is a simple process that consists of cell lysis, antibody–antigen complex formation, and collection and analysis of the immune complex. The procedure for immunoprecipitation is shown in Figure 7.3. Our lab has used immunoprecipitation studies to show an interaction between GAT1 and syntaxin 1A (Beckman et al., 1998; see Fig. 4). Since then numerous studies involving transporters have taken advantage of the ease of immunoprecipitation to show GLYT1 and GLYT2's interaction with syntaxin 1A (Greerling et al., 2000 and Greerling et al., 2001), SERT's interaction with the catalytic subunit of protein phosphatase 2 (Bauman et al., 2000), DAT and NET's interaction with PICK1 (Torres et al., 2001), EAAC1's (Excitatory Amino Acid Carrier) interaction with GTRAP3-18 (Lin et al., 2001), and EAAT4's (Excitatory Amino Acid Transporter) interaction with both GTRAP41 and GTRAP48 (Jackson et al., 2001). Each of these interactions results in a functional modulation of the transporter.

In addition to pulling down proteins by using immunoprecipitation, one can also pull down entire cellular organelles. This is a method by which one can characterize the protein components of specific cellular organelles. Melikian and Buckley used this technique to show that DAT is localized to the same organelle as the transferrin receptor (Melikian and Buckley, 1999). Our lab is currently using this technique to immunoisolate synaptic vesicles in nerve terminals. Preliminary data suggest GAT1 is on a vesicle population distinct from neurotransmitter-filled synaptic vesicles. The GAT1-containing vesicle population is devoid of synaptophysin but contains rab3a and synaptobrevin.

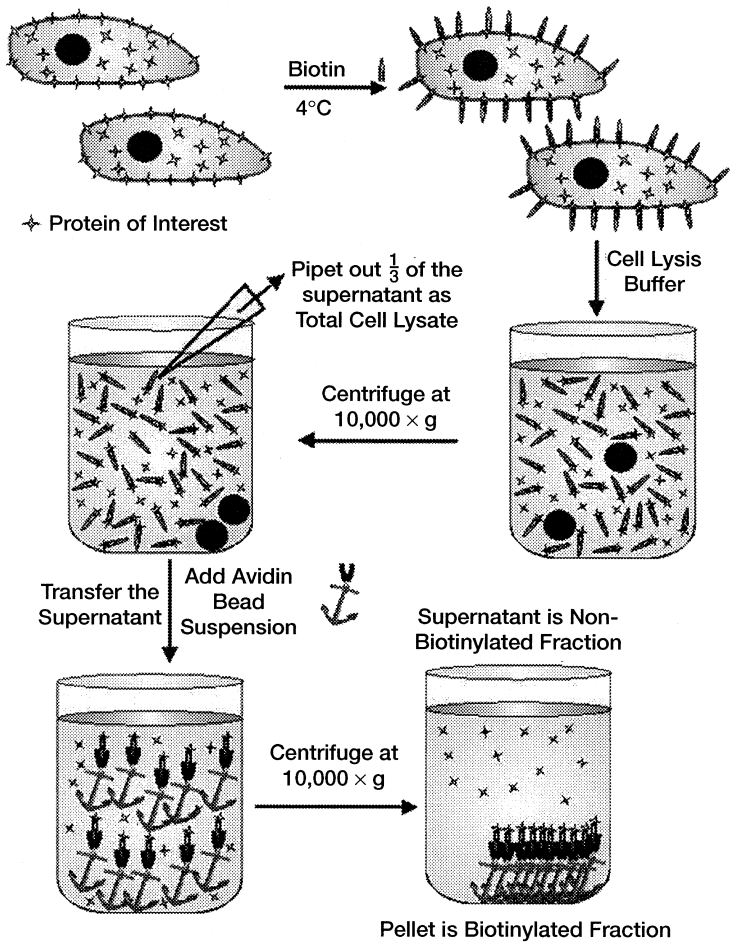

Figure 7.3 Schematic of immunoprecipitation experiment.

7.4 PROTOCOLS FOR BIOTINYLATION, FRACTIONATION, IMMUNOPRECIPITATION, AND IMMUNOISOLATION

Biotinylation Experiment

1. Grow cells of interest to 90% confluency in a six-well plate.
2. Wash twice with 37°C Krebs-Ringer's-HEPES (KRH) medium containing (in mM): 130 NaCl, 1.3 KCl, 2.2 $CaCl_2$, 1.2 $MgSO_4$, 1.2 KH_2PO_4, 10 HEPES (N-(2-hydroxyethyl) piperazine-2'-(2-ethanesulphonic acid)), pH 7.4.
3. Incubate with desired drug.
4. Wash twice with 37°C KRH medium.
5. Treat with sulfosuccinimido-NHS-biotin (2 mg/ml; Pierce Chemical, Rockford, IL) at 4°C for 1 h in phosphate buffered saline (PBS)/Ca^{2+}-Mg^{2+} containing (in mM): 138 NaCl, 2.7 KCl, 1.5 KH_2PO_4, 9.6 Na_2HPO_4, 1 $MgCl_2$, and 0.1 $CaCl_2$, pH 7.4.

6. Wash three times, 10 min each with 100 mM glycine in PBS/Ca^{2+}-Mg^{2+} solution to remove nonbound biotin molecules.
7. Wash three times quickly with PBS/Ca^{2+}-Mg^{2+} solution.
8. Lyse the cells with 250 μl/well radioimmunoprecipitation assy (RIPA) buffer containing (in mM): 10 Tris, pH 7.4; 150 NaCl; and 1 EDTA with 0.1% SDS, 1% Triton X-100, 1% sodium deoxycholate, supplemented with protease inhibitors (1 μg/ml apotinin, 1 μg/ml leupeptin, 250 μM PMSF (phenylmethylsulfonyl fluoride) for 1 h at 4°C with vigorous shaking.
9. Centrifuge the lysates at 1,000 x g for 20 min at 4°C to remove nuclear contaminants.
10. Take 125 ul of supernatant, spike with protease inhibitors, and store at –80°C. This is the total cell lysate fraction.
11. Take the rest of the supernatant and add avidin bead suspension (175 μl of beads/1250 μl of supernatant; Pierce) for 1 h at room temperature with constant shaking.
12. Centrifuge the suspension at 10,000 x g for 10 min at 4°C.
13. Take the supernatant, spike with protease inhibitors, and store at –80°C. This is the nonbiotinylated or intracellular fraction.
14. Wash the remaining bead suspension three times with RIPA buffer.
15. Elute the absorbed proteins with SDS sample buffer containing (in mM): 62.5 Tris-Cl, pH 6.8; 2% SDS; 100 β-mecaptoethanol for 30 min at room temperature.
16. Spike the bead eluate with protease inhibitors, and store at –80°C. This is the biotinylated or cell surface fraction.

Fractionation of Synaptic Vesicles and Endosomes from Nerve Terminals

Synaptosome Preparation

1. Remove cortex from three rats and place into 15 mL sucrose solution containing (in mM): 320 sucrose, 1 EDTA, .25 DTT, ph 7.4; separate into smaller pieces; pour cortex, and sucrose into Dounce homogenizer glass tube (on ice).
2. Homogenize cortex (10 strokes—nice and slow).
3. Transfer contents into plastic centrifuge tube; add 10 mL sucrose solution to glass tube and pour it into a conical centrifuge tube.
4. First spin (2 min) at 4200 x g.
5. Transfer supernatant carefully (do not get any pellet here—be conservative) and place it into another plastic conical tube (dispose of the pellet).
6. Second spin (12 min) at 25,200 x g. Setup can be done during these spins and during the water bath incubation.
7. Dispose of supernatant; resuspend pellet into 25 mL sucrose solution (slowly disperse tissue in 1–2 mL at first, then add remaining).
8. Third spin (12 min) at 25,200 x g.
9. Dispose of supernatant; resuspend in 25 mL HBS (slowly disperse in 1–2 mL as before). Spin for (5 min) at 11,000 x g.
10. Resuspend the synaptosomes in 2 mL HEPES buffered saline containing (in mM):

142 NaCl, 2.4 KCl, .5 ascorbic acid, 10 D-glucose, 10 HEPES, 1 $MgCl_2$, 1.2 $CaCl_2$, 1.2 K_2HPO_4, ph 7.4, mixing slowly and thoroughly.

11. Determine protein concentration. Can store at –80°C or continue.

Fractionation and Synaptic Vesicle Purification

1. Lyse synaptosomes with lysis buffer (hypotonic media: 2 mM HEPES and 0.5 mM EGTA in water, pH 7.4). Add in a 1:9 ratiometric solution with synaptosomes [1 mL (1 mg) synaptosomes: 9 mL lysis buffer].
2. Lyse on ice for 45 min with gentle shaking.
3. Centrifuge lysed synaptosomes at 500 x g (2900 rpm for Sw 41 Ti) for 20 min.
4. Pellet is P1—determine protein concentration and store in 20 μg aliquots.
5. Take the supernatant from step 14 and centrifuge at 27,000 x g (12,600 rpm for Sw 41 Ti) for 45 min. Pellet is P2—determine protein concentration and store in 20 μg aliquots.
6. Collect supernatant from step 16 and centrifuge at 100,000 x g (24,200 rpm for Sw 41 Ti) for 1 h. Pellet is P3, supernatant is S3—determine protein concentration and store in 20 μg aliquots.
7. Load 20 μg of each of the following into an SDS-PAGE gel containing the synaptosome fraction, P1 fraction (enriched in plasma membrane), P2 fraction (enriched in endosomes), P3 fraction (enriched in vesicles), and S3 fraction (synaptosome cytosol).

Immunoprecipitation

1. Lyse cells with lysis buffer containing (in mM): 9.1 dibasic sodium phosphate; 1.7 monobasic sodium phosphate, pH 7.4; 150 NaCl; 0.5% sodium deoxycholate; 0.1% SDS; 0.25 phenylmethylsulfonyl fluoride; 1 μg/ml aprotinin; 1.0 activated sodium orthovanadate; 5.0 sodium pyrophosphate for 1 h at 4°C.
2. Centrifuge the lysate at 12,000 x g for 2 min at 4°C.
3. Transfer the supernatant into a fresh microtube and hold on ice.
4. Preclear the lysate using 10 μl of protein G-agarose conjugate (Sigma, St. Louis, MO) and incubate for 1 h at 4°C.
5. Centrifuge the mixture at 12,000 x g for 5 min at 4°C. Transfer the supernatant to a fresh microfuge tube.
6. Divide the supernatant into two aliquots and add sufficient NET gel buffer containing (in mM): 50 Tris-HCl, pH 7.5; 150 NaCl; 0.1% NP-40; 1.0 EDTA, pH 8.0; 0.25% gelatin; 0.02% sodium azide to obtain a volume of 0.5 ml for each aliquot.
7. To one aliquot of supernatant, add 1 μg of affinity-purified antibody against the target protein. To the second supernatant, add 1 μg of control antibody or pre-immune serum. Incubate for 1 h at 4°C.
8. Centrifuge the mixture at 12,000 x g for 5 min at 4°C.
9. Discard the supernatant and add one volume of RIPA buffer to resuspend the protein G-agarose beads. Incubate for 30 min at 4°C. Centrifuge the mixture at 12,000 x g for 5 min at 4°C. Repeat two more times.

10. Add 20 μl of SDS sample buffer. Run on SDS-PAGE gel to analyze immunoprecipitated complex.

Immunoisolation of Synaptic Vesicles from Nerve Terminals

1. Purify synaptic vesicles as described by the fractionation of synaptic vesicles above.
2. Take the P100 pellet and add 500 μl of 2 M sucrose.
3. Load the synaptic vesicles to the bottom of a 0.3, 0.8, and 1.2 M sucrose gradient. Centrifuge the gradient for 3 h at 350,000 x g. The light membrane fractions (0.3 and 0.8 M sucrose fractions) contain purified synaptic vesicles.

Preparation of antibody-protein A conjugated to dynabeads complex

4. Make a homogenous suspension of protein A conjugated to dynabeads (pA-DB) (Dynal Biotech, Oslo, Norway) by vortexing 1–2 min.
5. Transfer 200 μl of pA-DB to a centrifuge tube.
6. Place the tube on magnetic isolation device (MID) for 1 min and pipette off the fluid.
7. Add 200 μl of PBS and resuspend.
8. Repeat Step 3.
9. After final wash, remove washing buffer and resuspend in 200 μl coating buffer (0.1 M borate buffer, pH 9.5).
10. Add chosen linker IgG to DB and mix thoroughly for 1–2 min. The ratio of pA-DB to IgG should be 200 μl pA-DB: 60 μg IgG.
11. Incubate at 37°C for 16–24 h (or longer at lower temperatures) with bidirectional mixing.
12. After incubation collect pA-DB with MID. Wash pA-DB twice for 5 min at 4°C with PBS/0.1% BSA, pH 7.4.
13. Resuspend pA-DB in 200 μl incubation buffer containing (2 mM): EDTA; 5% FBS; PBS, pH 7.4. Add affinity-purified antibody against the target protein at the ratio of 200 μl pA-DB: 30 μg IgG.
14. Incubate the mixture for 30 min at 4°C with bidirectional mixing.
15. Collect pA-DB with MID and wash 4 times, 5 min each, at 4°C with PBS/0.1% BSA.
16. Resuspend pA-DB in 500 μl incubation buffer.

Isolationof synaptic vesicle populations

17. Add 500 μl of purified synaptic vesicles to the pA-DB complex. Incubate for 1–12 h at 4°C with continuous mixing.
18. Collect pA-DB with MID, save the supernatant (nonbound fraction), and wash three times, 15 min each, in 1 mL incubation buffer.
19. Collect synaptic vesicle PA-DB complex bound fraction and add SDS sample buffer. Run on SDS-PAGE gel to analyze vesicle contents (bound fraction).

ANNOTATED REFERENCES

Ahn I, Mundigl O, Muth TR, Rudnick G, Caplan MJ (1996): Polarized expression of GABA transporters in Madin-Darby canine kidney cells and cultured hippocampal neurons. J Biol Chem 271: 6917–6924.

Altin JG, Pagler EB (1995): A one-step procedure for biotinylation and chemical cross-linking of lymphocyte surface and intracellular membrane-associated molecules. Anal Biochem 224(1):382–389.

Amara SG and Sonders MS (1998): Neurotransmitter transporters as molecular targets for addictive drugs. Drug Alcohol Dep 51: 87–96.

Bauman AL, Apparsundaram S, Ramamoorthy S, Wadzinski BE, Vaughan RA, Blakely RD (2000): Cocaine and antidepressant-sensitive biogenic amine transporters exist in regulated complexes with protein phosphatase 2A. J Neurosci 20(20): 7571–7578.

Beckman ML, Bernstein EM, Quick MW (1998): Protein kinase C regulates the interaction between a GABA transporter and syntaxin 1A. J Neurosci 18: 6103–6112.

This paper demonstrates the syntaxin 1A inhibition of GABA uptake through GAT1. PC12 cells expressing GAT1 were used to immunoprecipate GAT1 with anti-syntaxin 1A antibody, thus demonstrating an interaction between the two proteins.

Beckman ML, Bernstein EM, Quick MW (1999): Multiple G protein-coupled receptors initiate protein kinase C redistribution of GABA transporters in hippocampal neurons. J Neurosci 19: RC1–6.

Beckman ML and Quick MW (1998): Neurotransmitter transporters: regulators of function and functional regulation. J Membrane Biol 164: 1–10.

Beckman ML and Quick MW (2000): The ups and downs of neurotransmitter transporters. Neuroscientist 6: 199–207.

Bennett MK, Calakos N, Scheller RH (1992): Syntaxin: a synaptic protein implicated in docking synaptic vesicles at presynaptic active zones. Science 257: 255–259.

Berstein EM, Quick MW (1999): Regulation of gamma-aminobutyric acid (GABA) transporters by extracellular GABA. J Biol Chem 274: 889–895.

Blakely RD, Bauman AL (2000): Biogenic amine transporters: regulation in flux. Curr Opin Neurobiol 10(3): 328–336.

Buckley KM, Melikian HE, Provoda CJ, Waring MT (2000) Regulation of neuronal function by protein trafficking: a role for the endosomal pathway. J Physiol 525 Pt 1:11–19.

Corey JL, Davidson N, Lester HA, Brecha N, Quick MW (1994): Protein kinase C modulates the activity of a cloned γ-aminobutyric acid transporter expressed in Xenopus oocytes via regulated subcellular redistribution of the transporter. J Biol Chem 269: 14759–14767.

Davis KE, Straff DJ, Weinstein EA, Bannerman PG, Correale DM, Rothstein JD, Robinson MB (1998): Multiple signaling pathways regulate cell surface expression and activity of the excitatory amino acid carrier 1 subtype of Glu transporter in C6 glioma. J Neurosci 18(7): 2475–2485.

Daniels GM, Amara SG (1999): Regulated trafficking of the human dopamine transporter. Clathrin-mediated internalization and lysosomal degradation in response to phorbol esters. J Biol Chem 274(50): 35794–35801.

The authors study the regulation of the DAT by protein kinase C (PKC) by using a GFP-tagged DAT construct. Activation of PKC causes the surface fluorescence from GFP tagged DAT to redistribute to intracellular locations.

Dealtry GB, Rickwood D (1992): Cell Biology Labfax (Labfax Series). Oxford, UK: Academic Press, Inc.

Deken SL, Beckman ML, Boos L, Quick MW (2000): Transport rates of GABA transporters: regulation by the N-terminal domain and syntaxin 1A. Nature Neurosci 3: 998–1003.

Diamond JS, Jahr CE (1997): Transporters buffer synaptically released glutamate on a submillisecond time scale. J Neurosci 17(12): 4672–4687.

Floor E, Feist BE (1989): Most synaptic vesicles isolated from rat brain carry three membrane proteins, SV2, synaptophysin, and p65. J Neurochem 52(5): 1433–1437.

Geerlings A, Lopez-Corcuera B, Aragon C (2000): Characterization of the interactions between the glycine transporters GLYT1 and GLYT2 and the SNARE protein syntaxin 1A. FEBS Lett 470(1): 52–54.

Geerlings A, Nunez E, Lopez-Corcuera B, Aragon C (2001): Calcium- and syntaxin1-mediated trafficking of the neuronal glycine transporter GLYT2. J Biol Chem 276(20): 17584–17590.

Giros B, Jaber M, Jones SR, Wightman RM, Caron MG (1996): Hyperlocomotion and indifference to cocaine and amphetamine in mice lacking the dopamine transporter. Nature (London) 379: 606–612.

Guastella J, Nelson N, Nelson H, Czyzyk L, Keyman S, Miedel MC, Davidson N, Lester HA, Kanner BI (1990): Cloning and expression of a rat brain GABA transporter. Science 249: 1303–1306.

Horton N, Quick MW (2001): Syntaxin 1A up-regulates GABA transporter expression by subcellular redistribution. Mol Membr Biol 18(1): 39–44.

Isaacson, JS, Solis, JM, Nicoll RA (1993): Local and diffuse synaptic actions of GABA in the hippocampus. Neuron 10:165–175.

Iversen L (2000): Neurotransmitter transporters: fruitful targets for CNS drug discovery. Mol Psychiatry 5:357–362.

Jaber, M, Jones, S, Giros, B, Caron, MG (1997): The dopamine transporter: a crucial component regulating dopamine transmission. Move Disord 12(5): 629–633.

Jackson M, Song W, Liu MY, Jin L, Dykes-Hoberg M, Lin CI, Bowers WJ, Federoff HJ, Sternweis PC, Rothstein JD (2001): Modulation of the neuronal glutamate transporter EAAT4 by two interacting proteins. Nature (London) 410(6824): 89–93.

Krantz DE, Waites C, Oorschot V, Liu Y, Wilson RL, Tan PK, Klumperman J, Edwards RH (2000): A phosphorylation site regulates sorting of the vesicular acetylcholine transporters to dense core vesicles. J Cell Biol 149(2): 379–396.

Law R, Stafford A, Quick MW (2000): Functional regulation of GABA transporters by direct tyrosine phosphorylation. J Biol Chem 275: 23986–23991.

Lin CI, Orlov I, Ruggiero AM, Dykes-Hoberg M, Lee A, Jackson M, Rothstein JD (2001): Modulation of the neuronal glutamate transporter EAAC1 by the interacting protein GTRAP3-18. Nature (London) 410(6824): 84–88.

Liu Y, Krantz DE, Waites C, Edwards RH (1999): Membrane trafficking of neurotransmitter transporters in the regulation of synaptic transmission. Trends Cell Biol 9: 356–363.

Melikian HE, Buckley KM (1999): Membrane trafficking regulates the activity of the human dopamine transporter. J Neurosci 19(18): 7699–7710.

In the study presented here, DAT stably transfected PC12 cells were used to study the intracellular locations of DAT after internalization. Through organelle immunoisolation DAT was shown to localize to the recycling endosome.

Minelli A, Brecha NC, Karschin C, DeBiasi S, Conti F (1995): GAT1, a high-affinity GABA plasma membrane transporter, is localized to neurons and astroglia in the cerebral cortex. J Neurosci 15(11): 7734–7746.

Muth TR, Ahn J, Caplan MJ (1998): Identification of sorting determinants in the C-terminal cytoplasm tails of the γ-aminobutyric acid transporter GAT-2 and GAT-3. J Biol Chem 273: 25616–25627.

Perego C, Bulbarelli A, Longhi R, Caimi M, Villa A, Caplan MJ, Pietrini G (1997): Sorting of two polytopic proteins, the γ-aminobutyric acid and betaine transporters, in polarized epithelial cells. J Biol Chem 272: 6584–6592.

Pietrini G, Suh YJ, Edelmann L, Rudnick G, Caplan MJ (1994): The axonal γ-aminobutyric acid transporter GAT4 is sorted to the apical membrane of polarized epithelial cells. J Biol Chem 269: 4668–4674.

Prasher DC, Eckenrode VK, Ward WW, Prendergast FG, Cormier MJ (1992): Primary structure of the *Aequorea Victoria* green-fluorescent protein. 111(2): 229–233.

Qian Y, Galli A, Ramamoorthy S, Risso S, DeFelice LJ, Blakely RD (1997): Protein kinase C activation regulates human serotonin transporters in HEK-293 cells via altered cell surface expression. J Neurosci 17(1): 45–57.

Qian et al. demonstrate by cell surface biotinylation that activation of PKC down-regulates serotonin transporter expression on the plasma membrane.

Quick MW, Corey JL, Davidson N, Lester HA (1997): Second messengers, trafficking-related proteins, and amino acid residues that contribute to the functional regulation of the rat brain GABA transporter GAT1. J Neurosci 17: 2967–2979.

Ramamoorthy S, Blakely RD (1999): Phosphorylation and sequestration of serotonin transporters differentially modulated by psychostimulants. Science 285(5428): 763–766.

Rudnick G. (1998): Bioenergetics of neurotransmitter transport. J Bioenerg Biomembr 30(2):173–185.

Saunders C, Ferrer JV, Shi L, Chen J, Merrill G, Lamb ME, Leeb-Lundberg LM, Carvelli L, Javitch JA, Galli A (2000): Amphetamine-induced loss of human dopamine transporter activity: an internalization-dependent and cocaine-sensitive mechanism. Proc Natl Acad Sci USA 97(12): 6850–6855.

Staudinger J, Zhou J, Burgess R, Elledge SJ, Olson EN (1995): PICK1: a perinuclear binding protein and substrate for protein kinase C isolated by the yeast two-hybrid system. J Cell Biol 128(3): 263–271.

Stein WD (1986): Transport and diffusion across cell membranes. Orlando, FL: Academic Press, Inc.

Tarasova NI, Stauber RH, Choi JK, Hudson EA, Czerwinski G, Miller JL, Pavlakis GN, Michejda CJ, Wank SA (1997): Visualization of G protein-coupled receptor trafficking with the aid of the green fluorescent protein and recycling of cholecystokinin receptor type A. J Biol Chem 272(23): 14817–14824.

Torres GE, Yao WD, Mohn AR, Quan H, Kim KM, Levey AI, Straudinger J, Caron MG (2001): Functional interaction between monoamine plasma membrane transporters and the synaptic PDZ domain-containing protein PICK1. Neuron 30(1): 121–134.

Vaughan RA, Huff RA, Uhl GR, Kuhar MJ (1997): Protein kinase C-mediated phosphorylation and functional regulation of dopamine transporters in striatal synaptosomes. J Biol Chem 272: 15541–15546.

CHAPTER 8

CHEMICAL MODIFICATION STRATEGIES FOR STRUCTURE-FUNCTION STUDIES

GARY RUDNICK

8.1 WHAT CAN CHEMICAL MODIFICATION TELL US ABOUT TRANSPORTERS?

In this chapter we discuss the approach of chemical modification to obtain information about the structure and function of transmembrane transporters. This technique, when combined with mutagenesis, provides a powerful tool for examining transporters and understanding their mechanism. The value of this approach comes from the ability to focus on the properties of individual amino acid residues, to measure their accessibility, and also to examine their involvement in various functional properties of the protein. In the case of transporters, this information is especially valuable, because it can provide important structural information about the disposition of the polypeptide chain within the membrane. Moreover, the reactions catalyzed by transporters are characterized predominantly by conformational transitions that are best revealed by measuring changes in residue accessibility and reactivity in a functional setting.

Much of the material in this review is related to the substituted cysteine accessibility method (SCAM), which has been described in detail in two recent and excellent reviews by Javitch (1998) and Karlin and Akabas (1998). These reviews focused primarily on the techniques and how they are applied. In this chapter, we discuss more the application to transport proteins and how SCAM and similar techniques can be used to obtain information about transporter structure and function. Almost all of these methods and approaches are based on the seminal studies of Kaback and collaborators who introduced the idea of cysteine scanning for analysis of membrane transport proteins in the early 1990s (van Iwaarden et al., 1991).

General Structure of Transport Proteins

Most transporters of interest, especially those with the ability to couple ion fluxes to solute transport, are polytopic membrane proteins. This designation indicates that the polypeptide chain crosses the membrane many times, resulting in a structure with multiple transmembrane (TM) segments. Each of these TM domains usually contains a preponderance of hydrophobic amino acid residues. Connecting the TM domains are internal and external loop (EL and IL, respectively) segments, containing predominantly hydrophilic residues, located on either side of the membrane. High-resolution structures,

Transmembrane Transporters. Edited by Michael Quick

ISBNs: 0-471-06517 (Hardcover); 0-471-43404-3 (Electronic)

such as those obtained by X-ray crystallography, are rare for transporters because of their poor ability to form crystals suitable for diffraction. In the absence of high-resolution structures, the determination of important structural features such as transmembrane topology have been addressed best by chemical modification with labeling reagents. As an example, the topology of the multidrug resistance (MDR) protein was determined by using permeant and impermeant biotinylating reagents (Loo and Clarke, 1995; Kimura et al., 1997; Tang et al., 1998; Wakabayashi et al., 2000). In many cases, the targeted residues were single cysteines, although lysine residues have also been used for topology studies (Gallivan et al., 1997; Chen et al., 1998; Fu and Maloney, 1998; Grunewald et al., 1998; Olsowski et al., 1998; Seal et al., 2000; Slotboom et al., 2001; Ye et al., 2001).

Mechanism of Transport

Most workers in the area of membrane transport interpret transporter function within the framework of an alternating access mechanism (Fig. 8.1). In this mechanism, a binding site for the transported substrate is formed by transmembrane domains. Access to this site

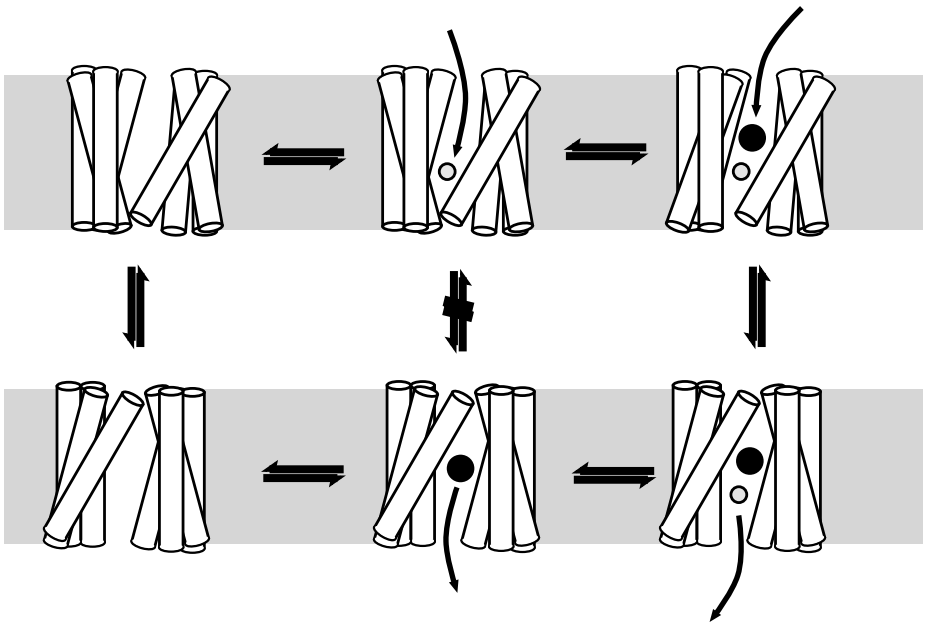

Figure 8.1. Mechanism for coupling transport of two solutes (symport or cotransport). The illustration depicts a transporter composed of multiple transmembrane helices (white rods) embedded in a lipid bilayer membrane (gray bar). The transporter can couple the vectorial translocation of two solutes, shown as the small gray and large black circles. Only when both solutes are bound (upper right) is the transporter able to undergo the conformational change that opens access to the internal aqueous phase (below the membrane) and closes access from the external aqueous phase (lower right). From this conformation, solutes dissociate to the inside, and when the binding site is empty (lower left), a second conformational change regenerates the original form of the transporter (upper left) ready to bind external solutes. For optimal coupling between the two solute fluxes, the transporter with only one solute bound (upper and lower middle) should not interconvert between internal and external conformations.

can be occluded by gates that block access to either the external or internal aqueous medium. In Figure 8.1, these gates are depicted as parts of transmembrane helices that tilt within the membrane to block or permit access to the binding site. When the external gate is open, the internal gate is closed, and similarly, the external gate is closed when the internal gate is open. In this mechanism, the binding site is alternately exposed to the external or internal medium, but not to both simultaneously. Substrate influx is accomplished by substrate binding when the external gate is open, followed by closing of the external gate and opening of the internal gate, and finally dissociation of the substrate on the inside. To regenerate the original form of the transporter, the internal gate must close and the external gate must open.

For substrate transport to be coupled to ion flux, this mechanism needs to be modified only slightly. If an ion such as Na^+ is cotransported with substrate, then it also must be bound before closing the external gate. The conformational changes that open and close gates to the binding sites must occur only when both substrate and Na^+ are bound, or when the site is empty. This will ensure that movement of Na^+ and substrate through the transporter will be strictly coupled. For this mechanism to accommodate countertransport also, for example exchange of substrate for K^+, then the countertransported ion must bind to the form of the transporter with its internal gate open, and interconversion to the external-open state would occur only when K^+ was bound. Thus, for cotransport, or symport, we expect that both solutes must bind to the transporter together before interconversion from the external-facing to the internal-facing form. For countertransport, or antiport, we expect that interconversion between forms occurs only if one of the solutes, but not both, is bound at the binding site.

What constitutes a gate opening or closing? Because the opening of one gate should occur only when the other one is closed, there must be conformational changes that involve both routes of access to the substrate-binding site. Therefore, it is unlikely that gate opening or closing involves only a few residues on one side of the binding site. It is more likely to represent a concerted conformational change involving hydrophilic loop domains on both surfaces and the transmembrane domains that connect them.

Predicted Behavior of Residues Involved in Transport

Before undertaking chemical modification studies, it is useful to consider the possible effects of perturbing residues important for the transport mechanism. For a residue in or near the substrate-binding site, there is a clear prediction (Fig. 8.2). Modification of the residue should block or severely decrease substrate binding, particularly if the bulk of the modified residue is greater than that of the endogenous residue at that position. Conversely, if the site is occupied with substrate, the modifying reagent may be unable to approach the residue to react with it. This protection by substrate is frequently cited as evidence that a given residue is in the binding site, although other interpretations are possible. Binding sites are likely to exist also for co- and countertransported ions coupled to substrate transport. We would expect that their modification would inhibit ion binding and that ion binding should protect residues that are part of an ion-binding site.

Another expectation for binding site residues is that they should spend part of the reaction cycle exposed to the external medium and part exposed to the internal medium. Depending on the relative amount of time actually exposed to either side, it may be possible to demonstrate that a given residue is accessible from both sides of the membrane by using chemical modification to measure the accessibility.

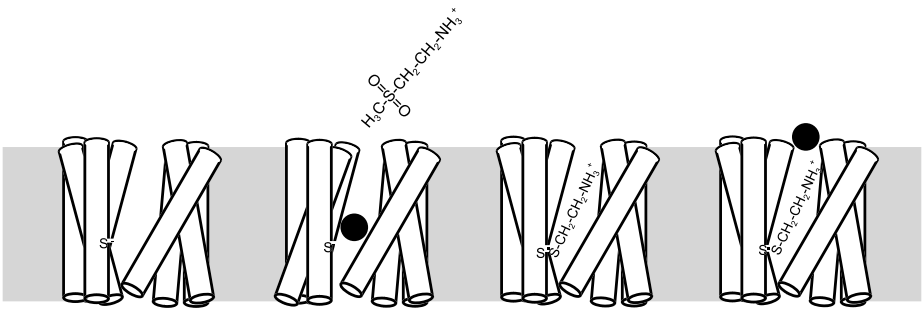

Figure 8.2. Modification of a cysteine residue near a binding site by 2-aminoethylmethanethiosulfonate (MTSEA). A thiolate anion (S^-) from a cysteine residue near the solute-binding site (left) is occluded by bound solute (left center), preventing its reaction with MTSEA. In the absence of the solute ligand, MTSEA reacts with the ionized cysteine residue, modifying it to a disulfide containing the 2-thioethylamine group from MTSEA (center right). Once the binding site is modified, the solute is sterically prevented from binding (right).

Conformational Changes

The reactions that actually lead to transport involve conformational changes that alternately expose the substrate site to the internal and external medium. The events that trigger or permit the conformational changes are the binding and dissociation of substrates and ions. It is likely that these binding events themselves cause conformational changes that precede the transport steps. One can imagine that small conformational changes occur as each cotransported ligand binds to the transporter and that, when all ligands are bound, these culminate in the translocation event, a larger conformational change that changes the accessibility of the binding sites. During these conformational changes, the exposure of individual residues is likely to change, increasing or decreasing their accessibility to reagents in the medium. If a reactive amino acid is present at one of these positions, its rate of modification by reagents in the medium should change during the binding and transport steps of the catalytic cycle. Therefore, measuring the rates of modification at many positions on the protein surface may identify those residues that participate in the conformational transitions of the transporter.

General Strategy for Chemical Modification

In practical terms, the largest barrier to identifying interesting residues is that it is not clear where to start looking. Transport proteins are composed of multiple transmembrane domains; some form the substrate binding site and permeation pathway and others play supporting roles in the mechanism. There are no signature sequences or consensus sites that have been identified as characteristic of transporter binding sites, so most approaches are based on guessing, sometimes on the basis of other evidence, but frequently not. A particular region is typically targeted for scanning [or SCAMing (Karlin and Akabas, 1998)] by systematic mutagenesis of all the residues in that region.

Each residue in the sequence is replaced, one at a time, with another amino acid. For scanning mutagenesis, any residue could be used as a replacement. For chemical modifi-

cation, however, the choice is typically a reactive residue such as cysteine. This process will generate a series of single replacement mutants, each containing a selected amino acid such as cysteine in place of a different endogenous amino acid. Cysteine seems to be well tolerated as a replacement for amino acid residues in most proteins. The lactose permease and the tetracycline resistance transporter of *E. coli* have been studied extensively by this method (Frillingos et al., 1998; Tamura et al., 2001). In the lactose permease, there were only 6 positions out of 417 where replacement with cysteine was incompatible with transport activity (Frillingos et al., 1998). Apparently, the polarizability of cysteine and its ability to dissociate to the thiolate anion allow it to replace polar residues as well as nonpolar ones.

Choice of Replacement Amino Acid

One approach is to replace the endogenous residues with an amino acid that disrupts transport function at positions where it is inserted. For example, the large bulk of a tryptophan residue is likely to disrupt function where there are close contacts between the endogenous residue and other parts of the protein that are important for function. However, at positions in contact with solvent or lipid, the added bulk may have little effect on function. This property has been utilized to identify domains within transmembrane helices that contact the lipid bilayer (Sharp et al., 1995; Hasler et al., 2001). However, if the goal is to identify residues that have particular importance for the transport mechanism, it is advisable to use an amino acid with less tendency to disrupt protein structure.

A small amino acid such as alanine is frequently used for scanning mutagenesis. The advantage of alanine is that, like cysteine, it is relatively inert and is expected to disrupt function only when it replaces an amino acid essential to function. When alanine or cysteine is used, most mutants will have significant activity, possibly equivalent to that of the wild-type transporter. In critical parts of the protein, however, replacement will produce a mutant with little or no activity, and some key regions of the sequence may have clusters of these critical residues.

Effect of Substitution

When replacement leads to loss in activity, it is sometimes possible to learn about the function of that residue by identifying which amino acids restore function at that position. For example, if an endogenous lysine residue can be replaced only with arginine, the protein is likely to require a positive charge at that position. Alternatively, a phenylalanine might be replaced by tyrosine at a position with a requirement for an aromatic residue.

Some charged residues in transmembrane domains are found in salt bridges with charged residues of the opposite polarity. Replacement of either residue with a small, neutral amino acid will result in an unpaired charge in the membrane interior, disrupting the transmembrane structure and thereby its function. However, simultaneously replacing both charged residues frequently restores activity (King et al., 1991). In some examples, swapping the positions of the positively and negatively charged residues leads to restoration of function (Sahin-Toth et al., 1992), demonstrating that the absolute position of the charge is less important than the proximity of two oppositely charged residues.

Partial Reactions

In many cases, loss of activity on replacement of an endogenous amino acid is not due to disruption of a charged pair. Understanding more about the role of an essential residue may be facilitated by assays of partial reactions. For example, if a high-affinity ligand still binds to the protein, it may be possible to assess the effect of mutation on binding. If substrate binds competitively with the ligand, then substrate binding could also be assessed by its ability to displace the high-affinity ligand. In serotonin transporter (SERT), replacement of Tyr-176 with cysteine resulted in an inactive transporter, but some binding activities were retained (Chen et al., 1997b). A radiolabeled cocaine analog (β-CIT) bound to the Y176C mutant, but its affinity was ~10-fold weaker than for wild-type. Likewise, the potency of serotonin (5-HT) to displace β-CIT was also decreased in the Y176C mutant, indicating that at least one role of Tyr-176 was to increase the affinity for substrate (Chen et al., 1997b).

Because transport is a multistep reaction, inactivation of transport will occur if any of the steps in the cycle are blocked by amino acid replacement. However, even in the absence of net transport, partial reactions can indicate which of the steps in the cycle continue to operate normally. In some cases, only net transport is blocked, but exchange reactions in which substrate is transported back and forth across the membrane are still active. Examples of this behavior include E325A in lactose permease (Carrasco et al., 1986), which is postulated to be defective in H^+ dissociation on the cytoplasmic face of the transporter. Another example is the glutamate transporter GLT-1, where a Glu to Asp mutation at position 404 apparently blocks the ability of K^+ to exchange with glutamate and forces the transporter into an exchange-only mode (Kavanaugh et al., 1997).

Replacement with a Reactive Amino Acid

When an unreactive amino acid such as alanine is used to replace the endogenous residue, we learn only about the effect of the mutation itself. No further modification at that position is possible without making a different mutation. However, when a reactive amino acid such as cysteine is used, the position can be derivatized after the protein has been synthesized and delivered to its site of activity in the membrane. Mutations that have no effect on activity by themselves may render the transporter sensitive to reagents that react selectively with that amino acid.

Because of its reactivity, cysteine is most often used for these studies. However, other reactive residues have been used for this purpose. For surface labeling studies, lysine residues are frequently derivatized with impermeant *N*-hydroxysuccinamide derivatives of biotin. By generating a series of mutants with single lysine residues in the predicted extracellular domains of SERT, it was possible to use lysine-directed biotinylation to localize each of these domains to the external face of the membrane, thereby verifying the predicted transmembrane topology (Chen et al., 1998). Similarly, reagents that selectively target other residues, such as glutamate, aspartate, histidine, and arginine, could potentially be used for scanning. However, the ability to selectively derivatize cysteine with high efficiency under relatively mild conditions has made it the amino acid of choice for most of these investigations.

When planning to insert reactive amino acids to study their potential role in transport function, it is essential first to evaluate the reactivity of the native transporter. In most cases, the native protein will contain some reactive residues that must be identified and

replaced before testing the reactivity of other positions. This process requires mutagenesis to replace endogenous reactive residues until the background reactivity of the transporter is low enough that insertion of a reactive residue at a single position will be sufficient to increase measurably the overall reactivity. In SERT, only three cysteines were predicted to lie within the external domain of the protein, and systematic mutagenesis of these three residues suggested that two of the three formed a disulfide in the second extracellular loop (EL2) (Chen et al., 1997a). The third reacts with extracellular cysteine reagents, but only when lithium replaced sodium in the medium (Chen et al., 1997a; Ni et al., 2001). Of the seven cysteine residues predicted to lie on the internal face of the protein, only four react with cysteine reagents (Androutsellis-Theotokis and Rudnick, 2002). Creating a form of the transporter that is resistant to modification by cysteine reagents required replacement of five endogenous cysteine residues. Likewise, in dopamine transporter, five endogenous cysteines were removed to generate a form resistant to the effect of cysteine reagents on activity (Ferrer and Javitch, 1998).

In this phase of the project, it is helpful to remove not only cysteine residues whose modification changes activity, but also those cysteines that react without altering activity. If possible, all cysteines should be replaced (van Iwaarden et al., 1991; Loo and Clarke, 1995; Fu and Maloney, 1998; Seal and Amara, 1998; Zarbiv et al., 1998; Hall et al., 1999; Tamura et al., 2001), although this may be prohibited if it causes unacceptable losses in activity or expression. It is conceivable that some cysteine residues may be both reactive and also essential for activity, making it impossible to generate a form of the transporter resistant to cysteine reagents. However, even in this case it may be possible to study a closely related protein, possibly from another species, lacking that essential cysteine.

General Strategy

Once a suitable background is established, the active mutants, each with a single reactive residue inserted, are tested for sensitivity to a specific reagent. First, the effect of that reagent on transport activity is tested. If no alteration in activity is observed, reagents that attach a label at the reactive position can indicate whether the residue is accessible to the medium. However, if modification leads to inactivation, there are many aspects of the process that can be explored. In particular, the rate of reaction, the extent of inactivation, and the sensitivity to the presence of substrates, ions, or inhibitors can all be used to gain information about structure and function.

8.2 REACTIVITY

If the mutant has any activity, even for binding or exchange, we can hazard the assumption that it is folded properly, and we can address issues of structure and function. To test whether the inserted residue is reactive, we use selective-modifying reagents and look for evidence of modification. Ideally, a change in activity is an easily determined endpoint for modification. If there is no effect of the modifying reagent on activity, it may still react with the residue, but not in a way that affects activity. This can be detected by using a labeling approach, such as biotinylation, which can detect the modification even if activity is not changed.

Detecting the Modification Reaction

If there is no effect on activity, it is still possible to determine accessibility by labeling the protein. In principle, it is possible to identify the reactive cysteine by derivatizing it with a reagent containing a radioactive, fluorescent, or other label. In the case of transporters, which may be of low abundance on the cell surface, it is likely that reactive residues on other proteins will overwhelm the signal from a single introduced cysteine on the transporter. When combined with immunoprecipitation or immunodetection, however, these labeling techniques have the sensitivity to detect labeling of low-abundance proteins. This approach is usually less quantitative than inactivation, which is a disadvantage, but it is frequently the only way to detect the reactivity of a residue that is not crucial for activity.

The techniques used to detect the surface exposure of a noncritical residue are usually based on labeling with biotin. Residues exposed on the cell surface should react with the appropriate labeling reagent. For lysine residues, reagents such as Sulfo-NHS-biotin are quite membrane-impermeant and form a stable covalent bond that is resistant to reducing agents used in preparation of samples for gel electrophoresis. These reagents are frequently used to locate proteins to the plasma membrane, with the assumption that there will be exposed lysine residues to react with the biotinylating reagent. However, the technique has been combined with mutagenesis to measure the exposure of predicted external loops in SERT (Chen et al., 1998). Methanethiosulfonate (MTS) reagents containing a biotin moiety also have been used to label cysteine residues on SERT (Chen et al., 1998).

Once proteins on the surface of the cell are labeled, the task is to identify the protein of interest in the pool of labeled proteins. Two procedures have generally proven useful. Both involve an antibody that reacts with the protein and an avidin-based reagent to detect the biotin label. In both methods, intact cells are biotinylated with the reagent, leading to labeling of all proteins with accessible lysine or cysteine residues. After detergent solubilization, the labeled proteins are separated by one of two methods. In the first, labeled proteins are precipitated with immobilized avidin or streptavidin, and this biotinylated pool is separated by gel electrophoresis and analyzed by Western blotting to evaluate the level of the antigen of interest. In the second method, the protein is immunoprecipitated from the detergent lysate, separated by gel electrophoresis, and blotted with avidin or streptavidin. This second method presents a minor problem for MTS reagents, which modify cysteines to mixed disulfides. Typical gel sample buffers contain reducing agents that will cleave the disulfide. Therefore, nonreducing gels are required when working with biotinylating MTS reagents.

Accessibility

Depending on the reagent used, the accessibility of a residue may provide information about its topological location. Reagents that permeate the membrane slowly or not at all can be used to detect residues exposed on the cell surface. Using labeling as a criterion, the external loop structure of polytopic membrane transport proteins have been determined (Loo and Clarke, 1995; Chen et al., 1998; Grunewald et al., 1998; Seal et al., 2000). Strategies exist to determine the internal loop structure of these proteins as well. With membrane-impermeant reagents, residues that react only when the plasma membrane is disrupted by homogenization or detergent are likely to face the cytoplasm (Ferrer and Javitch, 1998; Androutsellis-Theotokis et al., 2001). Alternatively, residues labeled by membrane-permeant reagents but not by impermeant reagents are likely to

reside on internal or transmembrane domains (Loo and Clarke, 1995; Kimura et al., 1996).

In topology studies, when cysteine or lysine residues in predicted loop regions do not react with external reagents, it is premature to conclude that those residues are internal. They could be external, but folded into a solvent-inaccessible domain, and therefore unreactive. Demonstrating that the residues are internal requires positive evidence that the residues will react when the interior surface of the membrane is exposed to modifying reagents. This is usually achieved by disrupting the membrane either mechanically or with detergent. Both methods can be quite mild, but it is essential to demonstrate that the structure of the protein is not compromised. In the case of bacterial proteins, it is possible to prepare sealed, inside-out vesicles that retain transport activity, but this is usually not possible with eukaryotic cells. Short of measuring transport, the retention of other catalytic or binding properties can provide some assurance that the method used to disrupt the membrane structure does not damage the protein.

As with studying the reactivity of proteins in intact cells, it is important to start with an unreactive background. Lysine residues are quite abundant on internal loops, and removing all of them in any given protein might prove to be tedious. In this case, cysteine residues provide the most likely alternative. Replacement of cysteines on predicted internal domains may be required to eliminate background inactivation or reactivity toward cysteine reagents in disrupted cells. However, not all predicted internal cysteine residues are reactive. For example, in DAT, cysteines at internal loop positions 135 and 342 react with MTS reagents, leading to inactivation (Ferrer and Javitch, 1998). However, of the corresponding cysteine residues in SERT, Cys-357 modification leads to inactivation but Cys-155 is unreactive (Androutsellis-Theotokis et al., 2001).

The accessibility of reactive residues on the inner or outer surface of a transporter can also provide information about the points at which transmembrane domains begin and end. Patterns of reactivity are expected to be quite different in transmembrane domains and loops. Transmembrane residues might be totally inaccessible to modifying reagents or, if they do react, might show a pattern where one side of an α-helix is exposed through a pore or binding site. In extramembranous loops, we would expect other patterns, including instances where many consecutive residues react. Even though parts of some loops may adopt a compact conformation in which some residues are sequestered from the medium, careful analysis of the reactivity patterns might allow identification of the transition point between transmembrane and loop domains.

8.3 MODIFICATION OF ACTIVITY

Residues whose modification leads to a change in transport activity can be extremely informative in understanding the relationship between structure and function. In evaluating the nature of this modification, it is important to be able to compare different positions with respect to the rate and extent of the change. For the purposes of this discussion, we will consider inactivation that accompanies modification, although other changes in function, such as changes in rate constants or affinities, or ionic requirements could be analyzed by a similar strategy.

Inactivation could be complete or incomplete. When incomplete, we assume that maximal treatment with the modifying reagent reduces but does not eliminate activity. Incom-

plete inactivation results when the fully modified transporter continues to function, but with a lower V_{max} or with a higher K_M for substrate. In turn, either of these phenomena could result from a change in an individual rate constant for one or more steps in the transport cycle. If the number of binding sites can be determined by using a high-affinity ligand, we would expect it to be unchanged after modification that leads to incomplete inactivation, although affinity for the ligand might decrease. Aside from binding, other partial reactions, such as substrate exchange, could also be used to determine whether the modification affects the steps required for that partial activity. A change in K_M could also reflect a simple change in affinity at the substrate-binding site. If high-affinity ligand binding is competitively displaced by substrate, then this assay can be used to determine any change in substrate affinity.

Measurement of Reaction Rates

The rate at which a chemical modification occurs depends on both the reactivity of the amino acid residue and its accessibility to the modifying reagent. The chemical reactivity can vary for a variety of reasons. For a cysteine residue, the degree of dissociation to the thiolate anion is an important determinant of reactivity with MTS reagents, which react preferentially with the ionized form. Anything that affects the pKa of a cysteine residue, such as the local environment, will affect its reactivity. Other factors affect the reagent. For example, the reactivity of charged MTS reagents is influenced by electrostatic interactions near the site of reaction. Even with model systems, positively charged reagents react somewhat faster than negatively charged reagents because of the electrostatic attraction of positively charged reagents and repulsion of negatively charged reagents by the negative thiolate anion (Stauffer and Karlin, 1994). However, in both SERT and β-receptor, the positively charged reagents 2-aminoethylmethanethiosulfonate (MTSEA) and MTSET react much faster than MTSES, even taking into account their different reactivity towards simple thiols (Javitch et al., 1994; Chen et al., 1997b). In both cases this was attributed to the influence of the ligand binding sites, which normally bind positively charged compounds. A possible mechanism for this influence is a negative charge or aromatic rings near the binding site that could facilitate the approach of positively charged compounds and repel negative compounds.

The accessibility of an amino acid to the medium is a major determinant in its rate of reaction. For a polytopic membrane protein such as a transporter, the most accessible residues are those on extracellular loops. Next are those residues in transmembrane segments that face the permeability pathway or another aqueous pore within the transmembrane domain. Residues exposed on the intracellular face of the protein, as on internal loops, will not be accessible in intact cells, but might be very accessible in permeabilized cells or in membranes. Least accessible are residues packed into the core of the protein, either by tight folding of hydrophilic loops or by tight packing of transmembrane domains.

Determining Rates and Extents of Inactivation

A general strategy is helpful in determining the rate and extent of inactivation. We have found it useful to measure the amount of remaining activity after treatment with varying concentrations of modifying reagents for a given time period. As the concentration of the modifying reagent increases, the activity usually decreases to a minimum, which could be

zero activity, although often the level of activity decreases to a plateau value below which it does not drop with increasing reagent. From this plateau value, we can calculate the extent of inactivation. The rate is then calculated from the midpoint on the inactivation curve, or the concentration of reagent that results in 50% of maximal inactivation. At this concentration, the preset time of inactivation represents the half-time for the process, assuming first-order kinetics. This time, divided by the natural log of 2 (0.693), gives the first-order rate constant (in reciprocal time units) at that concentration of reagent. Dividing the rate constant by the concentration gives the second-order rate constant in units of reciprocal time × reciprocal concentration (see Fig. 8.3).

Another reason to determine the reagent concentration giving 50% of maximal inactivation is that the process is most sensitive to modulation at that point. For example, if the maximal inactivation was 50%, and 1 mM reagent gave 25% inactivation (lower right

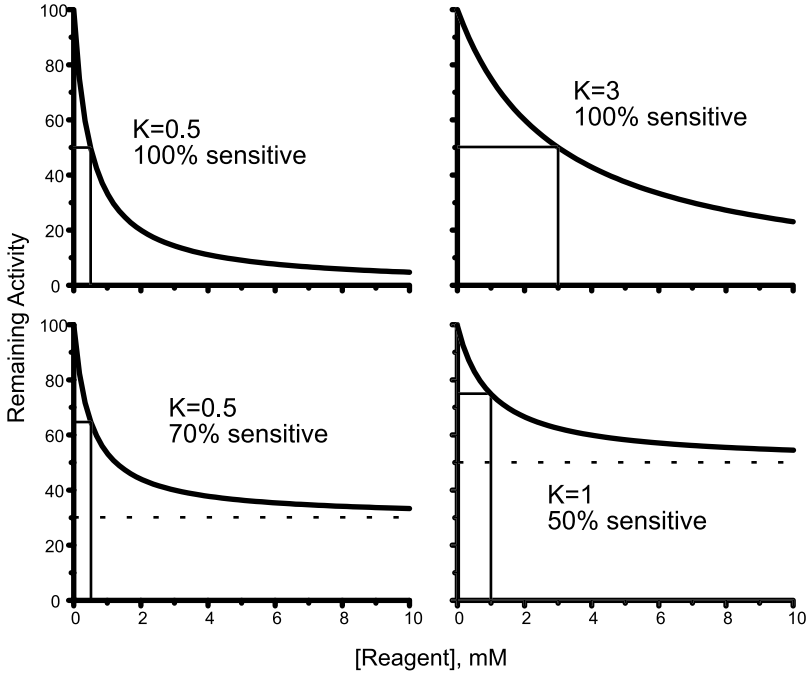

At reagent concentration (R) giving 1/2 maximal inactivation,
Reaction time (t) is the half time ($T_{1/2}$) for inactivation.

$$\text{First order rate constant } (v) = \frac{ln(2)}{T_{1/2}} \quad \text{time}^{-1}$$

$$\text{Second order rate constant} = \frac{v}{R} \quad M^{-1} \cdot \text{time}^{-1}$$

Figure 8.3. Analysis of inactivation data and determination of rate constants. Measuring the influence of ligand binding or other factors on inactivation rate is best done under conditions where inactivation is half-maximal. This requires determining the maximum extent of inactivation and the dependence of inactivation rate on the inactivating reagent. The four panels show examples of chemical modification of four hypothetical residues with different maximal sensitivities to inactivation and different reactivities. The calculation of second-order inactivation rate constants is shown below the plots.

panel, Fig. 8.3), then the reaction would be most sensitive to modification of the process at that concentration. If a concentration of 10 mM had been chosen arbitrarily, giving 46% inactivation, then the effect of an agent that increased or decreased the rate of inactivation might not be as easily determined as it would be at 1 mM. It would certainly be difficult to detect the effect of any agent that increased the rate of inactivation. Without knowledge of the maximal extent of inactivation, it would be impossible to know what concentration corresponds to the midpoint of the inactivation curve.

Binding Site Residues

If the rate of inactivation or other modification of transporter activity is decreased in the presence of substrate, there is the possibility that the residue being modified is part of the substrate-binding site. In this scenario, binding of substrate physically occludes the residue and prevents approach of the modifying reagent (Fig. 8.2). If there are high-affinity ligands that bind at the same site as substrate, their binding should also be blocked by modification of a binding site residue, although inhibitors or other ligands that bind to allosteric sites might continue to bind normally after modification. However, just observing protection by substrate is not proof that a residue is at or near the binding site. In fact, it should be stated at the outset that it is extremely difficult to prove that a residue is in the substrate-binding site without a high-resolution structure, such as determined by X-ray diffraction of protein crystals. Short of this kind of evidence, it is possible to show that a residue is not at the binding site, and, if all attempts fail to disprove the hypothesis that the residue is in the binding site, we can continue to entertain the possibility—but with the caution that there may be other explanations for the data.

One alternative is that the transporter undergoes a conformational change when substrate binds or that a conformational change must precede substrate binding (Fig. 8.4). The conformational change could occlude from the medium residues that are distant from the binding site. When substrate is bound, the residues will be occluded; when the binding site is empty, they will be more accessible. However it would be incorrect to conclude that they are present at the binding site. Another, similar situation occurs for residues that become occluded when substrate is transported. The conformational changes that close off the substrate-binding site from extracellular access and open it to cytoplasmic access could also occlude residues on the transporter surface. In particular, we would expect that residues forming the gate that closes off access to the external medium would be occluded when the gate closes. If transport is required for occlusion, it may be possible to distinguish the direct protection by substrate binding from indirect protection by substrate transport. In the latter case, nontransported inhibitors may hold the transporter in the outward-facing configuration and fail to protect. In fact, they can stimulate inactivation. This is the case for norepinephrine transporter (NET), where a cysteine at position 155 reacts with MTSET, leading to inactivation (Chen and Rudnick, 2000). When the substrate dopamine was transported, the resulting conformational change occluded Cys-155, the putative gate residue, and protected against inactivation. Cocaine is not transported, but it increased the accessibility of Cys-155, presumably by holding the protein in an outward-facing conformation (Chen and Rudnick, 2000). A similar situation occurred with the GLT-1 glutamate transporter where the nontransported inhibitor dihydrokainate stimulated, and D-aspartate inhibited, inactivation by MTSET reaction with a cysteine at position 403 (Zarbiv et al., 1998).

Two methods have been used to exclude direct occlusion by substrate as a mechanism

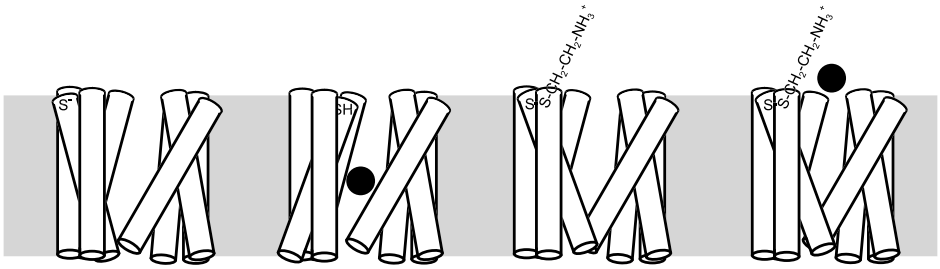

Figure 8.4. Protection by induced conformational change. A reactive thiolate anion (S^-) belonging to a cysteine residue is conformationally coupled to ligand binding. The reactive cysteine residue (left) is protected when a substrate ligand (black circle) binds to the transporter. As shown, the residue is protonated and buried within the protein interior in response to substrate binding (left center). In the absence of substrate, the anionic form reacts with MTSEA (right center) and, in some cases, this may lock the transporter in a form that cannot bind substrate (right).

of protection. In many transporters, accessory ions such as Na^+, Cl^-, or K^+ are involved in the transport process. The presence of these ions may be required for substrate binding, or they may participate only in steps that follow binding. If it is found that a particular ion, or other cofactor, is required for protection—but not substrate binding—then we can conclude that the inhibition is not likely to result directly from occlusion by substrate but rather from conformational changes that follow substrate binding.

These conformational changes are frequently temperature-dependent, a property that may not be shared by substrate binding. Therefore, protection may show a temperature dependence quite different from substrate binding. In SERT, substrate protection of inactivation that results from modifying a cysteine at the putative binding site position 172 was not Na^+- or temperature-dependent, but protection from inactivation at the endogenous Cys-357 required Na^+ and did not occur at low temperature (Chen and Rudnick, 2000; Androutsellis-Theotokis et al., 2001).

8.4 REVERSAL OF MODIFICATION

In some cases, modification of a reactive residue is a reversible process. In particular, the modification of cysteine residues by MTS reagents produces a disulfide between the cysteine sulfur atom and the thio-alkyl group $–S(CH_2)_2$-X where X is an ammonium group for MTSEA, a trimethylammonium group for MTSET, and a sulfonate group for MTSES, for example. If the disulfide is reduced by free thiols, it will release the modifying group and regenerate a free cysteine. This would be expected to restore the activity of the unmodified transporter, and, in most cases, this is precisely what happens, but the conditions that render the disulfide reactive towards reducing agents can give unique insight into the structure and function of the transporter that might not be obtainable otherwise.

One difference between inactivation and reactivation is that the inactivated transporter does not transport. The effect of substrate on an inactivated transporter might be quite different from its effect on the active form. In SERT I179C, inactivation with MTSET blocked transport but not binding (Chen et al., 1997b). Inactivation was not sensitive to

the presence of 5-HT, but reactivation was enhanced by 5-HT in the presence of Na^+. The different response of these two reactions is likely to be due to the consequences of 5-HT binding in the active and modified proteins. 5-HT bound to active SERT is rapidly transported followed by recycling of the transporter to its initial state. However, the inactivated form could not progress through the cycle to deliver 5-HT to the cytoplasm, and therefore 5-HT remained bound and affected the rate of reactivation (Chen and Rudnick, 2000). In the presence of Na^+, 5-HT increased the rate of reactivation, presumably by inducing a conformational change that increased the accessibility to Cys-179. In the functional transporter, that accessible conformation was not stable, presumably because 5-HT binding led to other conformational changes involved in transport.

Some modified cysteine residues cannot be reactivated. This could result from severe denaturation that might follow modification of a residue that played a key role in the structural integrity of the protein. A more likely possibility is that the cysteine is located in a crevice with limited accessibility to the medium. Modification produces a further steric impediment to accessibility, preventing approach of the reducing agent to the disulfide. Thus, residues in external loops would be expected to reactivate faster than those in the permeation pathway. Indeed, in SERT there is a progressive decrease in the rate of reactivation from Cys-109 to Cys-179 to Cys-172. SERT I172C was totally unresponsive to reduction by free cysteine or dithiothreitol added from the outside of intact cells. However, it reactivated spontaneously, presumably due to reduction by internal thiols, which suggests its location in a part of the transporter that was exposed alternately to the external and cytoplasmic media (Chen and Rudnick, 2000).

8.5 CONCLUSIONS

This overview of strategies and procedures certainly does not cover all the applications of chemical modification in the study of transporters. We have not described methods involving fluorescence, cross-linking, or spin-labeling to elucidate transporter structure and function (Kaback et al., 2001). In addition to these methods, we can expect to see a continuing development of tools based on these approaches in the future. The focus of these studies would be significantly sharpened if we had high-resolution structures available for transporters of interest. However, until we do, chemical modification combined with mutagenesis provides one of the best approaches to understanding transporter structure and relating it to function.

ANNOTATED REFERENCES

Androutsellis-Theotokis A, Ghassemi F and Rudnick G (2001): A conformationally sensitive residue on the cytoplasmic surface of serotonin transporter. J Biol Chem M107462200.

Androutsellis-Theotokis A and Rudnick G (2002): Accessibility and Topology of Predicted Intracellular Residues in Serotonin Transporter. Submitted

Carrasco N, Antes LM, Poonian MS and Kaback HR (1986): Lac permease of *Escherichia coli*: Histidine -322 and glutamic acid-325 may be components of a charge-relay system. Biochem 25:4486-4488.

Chen JG, Liu-Chen S and Rudnick G (1997a): External cysteine residues in the serotonin transporter. Biochem 36:1479-1486.

Chen JG, Liu-Chen S and Rudnick G (1998): Determination of external loop topology in the serotonin transporter by site-directed chemical labeling. J Biol Chem 273:12675-12681.

Chen JG and Rudnick G (2000): Permeation and gating residues in serotonin transporter. Proc Natl Acad Sci USA 97:1044-1049.

Chen JG, Sachpatzidis A and Rudnick G (1997b): The third transmembrane domain of the serotonin transporter contains residues associated with substrate and cocaine binding. J Biol Chem 272:28321-28327.

The authors used cysteine scanning to define part of a transporter binding site by measuring transport and binding in response to cysteine modification. In addition to two residues near the substrate binding site, a third residue required for transport but not binding was identified as a potential gate residue.

Ferrer JV and Javitch JA (1998): Cocaine alters the accessibility of endogenous cysteines in putative extracellular and intracellular loops of the human dopamine transporter. Proc Nat Acad Sci USA 95:9238-9243.

Frillingos S, Sahintoth M, Wu JH and Kaback HR (1998): Cys-scanning mutagenesis: A novel approach to structure-function relationships in polytopic membrane proteins. FASEB Journal 12:1281-1299.

The authors describe the development of cysteine scanning as an approach to understanding how transporters work. The description covers their discovery of the element sulfur, and how its reactivity in amino acid residues provides a tool for addition of a wide variety of probes at specific locations within a transport protein.

Fu D and Maloney PC (1998): Structure-function relationships in OxlT, the oxalate/formate transporter of oxalobacter formigenes. Topological features of transmembrane helix 11 as visualized by site-directed fluorescent labeling. J Biol Chem 273:17962-17967.

Gallivan JP, Lester HA and Dougherty DA (1997): Site-specific incorporation of biotinylated amino acids to identify surface-exposed residues in integral membrane proteins. Chem Biol 4:739-749.

Grunewald M, Bendahan A and Kanner BI (1998): Biotinylation of single cysteine mutants of the glutamate transporter GLT-1 from rat brain reveals its unusual topology. Neuron 21:623-632.

Hall JA, Fann MC and Maloney PC (1999): Altered substrate selectivity in a mutant of an intrahelical salt bridge in UhpT, the sugar phosphate carrier of *Escherichia coli*. J Biol Chem 274:6148-6153.

Hasler U, Crambert G, Horisberger JD and Geering K (2001): Structural and functional features of the transmembrane domain of the Na,K-ATPase beta subunit revealed by tryptophan scanning. J Biol Chem 276:16356-16364.

Javitch J, Li X, Kaback J and Karlin A (1994): A cysteine residue in the third membrane-spanning segment of the human D2 dopamine receptor is exposed in the binding-site crevice. Proc Nat Acad Sci USA 91:10355-10359.

Javitch JA (1998): Probing structure of neurotransmitter transporters by substituted-cysteine accessibility method. Methods Enzymol 296:331-346.

Kaback HR, Sahin-Toth M and Weinglass AB (2001): The kamikaze approach to membrane transport. Nat Rev Mol Cell Biol 2:610-620.

Karlin A and Akabas MH (1998): Substituted-cysteine accessibility method. Methods Enzymol 293:123-145.

This review describes the authors' discovery of the amino acid cysteine and how its reactivity with methanethiosulfonate reagents has given insight into the pore residues in ion channels. Although these proteins are less sophisticated than transporters, they provide a good model system for understanding accessibility of a solute transmembrane permeation pathway to the extracellular medium.

Kavanaugh MP, Bendahan A, Zerangue N, Zhang Y and Kanner BI (1997): Mutation of an amino acid residue influencing potassium coupling in the glutamate transporter GLT-1 induces obligate exchange. J Biol Chem 272:1703-1708.

Kimura T, Ohnuma M, Sawai T and Yamaguchi A (1997): Membrane topology of the transposon 10-encoded metal-tetracycline/H^+ antiporter as studied by site-directed chemical labeling. J Biol Chem 272:580-585.

Kimura T, Suzuki M, Sawai T and Yamaguchi A (1996): Determination of a transmembrane segment using cysteine-scanning mutants of transposon Tn10-encoded metal: tetracycline/H^+ antiporter. Biochem 35:15896-15899.

King SC, Hansen CL and Wilson TH (1991): The interaction between aspartic acid 237 and lysine 358 in the lactose carrier of *Escherichia coli*. Biochim Biophys Acta 1062:177-186.

Loo T and Clarke D (1995): Membrane topology of a cysteine-less mutant of human P-glycoprotein. J Biol Chem 270:843-848.

This paper describes one of the first uses of chemical modification to determine the transmembrane topology of a transporter. The authors used permeant and non-permeant cysteine reagents to specifically react with cysteine residues engineered into the cytoplasmic and extracellular domains of an ATP driven transporter.

Ni YG, Chen JG, Androutsellis-Theotokis A, Huang CJ, Moczydlowski E and Rudnick G (2001): A lithium-induced conformational change in serotonin transporter alters cocaine binding, ion conductance, and reactivity of cys-109. J Biol Chem 276:30942-30947.

Olsowski A, Monden I and Keller K (1998): Cysteine-scanning mutagenesis of flanking regions at the boundary between external loop I or IV and transmembrane segment II or VII in the GLUT1 Glucose Transporter. Biochem 37:10738-10745.

Sahin-Toth M, Dunten RL, Gonzalez A and Kaback HR (1992): Functional interactions between putative intramembrane charged residues in the lactose permease of Escherichia coli. Proc Natl Acad Sci USA 89:10547-51.

Seal RP and Amara SG (1998): A reentrant loop domain in the glutamate carrier EAAT1 participates in substrate binding and translocation. Neuron 21:1487-98.

Seal RP, Leighton BH and Amara SG (2000): A model for the topology of excitatory amino acid transporters determined by the extracellular accessibility of substituted cysteines. Neuron 25:695–706.

Sharp LL, Zhou J and Blair DF (1995): Features of MotA proton channel structure revealed by tryptophan-scanning mutagenesis. Proc Natl Acad Sci USA 92:7946-50.

Slotboom DJ, Konings WN and Lolkema JS (2001): Cysteine-scanning mutagenesis reveals a highly amphipathic, pore-lining membrane-spanning helix in the glutamate transporter GltT. J Biol Chem 276:10775-10781.

Stauffer DA and Karlin A (1994): Electrostatic potential of the acetylcholine binding sites in the nicotinic receptor probed by reactions of binding-site cysteines with charged methanethiosulfonates. Biochem 33:6840-6849.

Tamura N, Konishi S, Iwaki S, Kimura-Someya T, Nada S and Yamaguchi A (2001): Complete cysteine-scanning mutagenesis and site-directed chemical modification of the Tn10-encoded metal-tetracycline/H^+ antiporter. J Biol Chem 276:20330-20339.

The authors describe the complete cysteine scanning of a transporter. The results allow inferences about the helical nature and length of each transmembrane domain, and also about the helix packing within the membrane.

Tang XB, Fujinaga J, Kopito R and Casey JR (1998): Topology of the region surrounding Glu681 of human AE1 protein, the erythrocyte anion exchanger. J Biol Chem 273:22545-53.

van Iwaarden P, Pastore J, Konings W and Kaback H (1991): Construction of a functional lactose permease devoid of cysteine residues. Biochem 30:9595-9600.

Wakabayashi S, Pang T, Su X and Shigekawa M (2000): A novel topology model of the human Na^+/H^+ exchanger isoform 1. J Biol Chem 275:7942-7949.

Ye LW, Jia ZZ, Jung T and Maloney PC (2001): Topology of OxlT, the oxalate transporter of Oxalobacter formigenes, determined by site-directed fluorescence labeling. J Bacteriol 183:2490-2496.

Zarbiv R, Grunewald M, Kavanaugh MP and Kanner BI (1998): Cysteine scanning of the surroundings of an alkali-ion binding site of the glutamate transporter GLT-1 reveals a conformationally sensitive residue. J Biol Chem 273:14231-14237.

CHAPTER 9

METHANETHIOSULFONATE REAGENT ACCESSIBILITY STUDIES, CYSTEINE-SCANNING MUTAGENESIS, PROTEIN OVEREXPRESSION, AND FUNCTIONAL RECONSTITUTION: A STRATEGY FOR STUDYING THE STRUCTURE/FUNCTION RELATIONSHIPS WITHIN THE MITOCHONDRIAL CITRATE TRANSPORT PROTEIN

RONALD S. KAPLAN

9.1 OVERVIEW

The mitochondrial anion transporters, situated within the inner mitochondrial membrane, catalyze a high-magnitude flux of specific metabolites across this otherwise impermeable membrane. These inner membrane carrier proteins provide substrates to and remove products from numerous metabolic pathways involving reactions catalyzed by enzymes located in the cytoplasm, as well as in the mitochondrial inner membrane plus matrix compartments. Since these metabolic pathways are of central importance to the bioenergetics of eukaryotic cells, it follows that the associated transport proteins occupy a prominent position within intermediary metabolism.

To date, at least 14 anion transporter functions have been extensively characterized, and an additional 5–10 functions have been characterized to a lesser extent (for reviews see Kramer and Palmieri, 1992; Kaplan, 1996; Palmieri and van Ommen, 1999; Palmieri et al., 2000; Kaplan, 2001). At the level of their primary structure, all known mitochondrial carriers display a set of common characteristics: a basic isoelectric point, a mature size of ~300 amino acids, the presence of three homologous 100 amino acid domains as identified by dot-matrix analysis, and a signature sequence motif. In terms of topology, the transporters are thought to contain six putative transmembrane domains per monomer. Moreover, the homodimer is believed to be the functional unit (e.g., see Kotaria et al., 1999).

During the past decade, the author's laboratory has focused primarily on the elucidation of the structure/function relationships within the mitochondrial citrate transport pro-

Transmembrane Transporters. Edited by Michael Quick

ISBNs: 0-471-06517 (Hardcover); 0-471-43404-3 (Electronic)

tein (CTP) utilizing a battery of approaches (Kaplan et al., 1990; Kaplan and Mayor, 1993; Kaplan et al., 1993; Gremse et al., 1995; Kaplan et al., 1995; Kotaria et al., 1999; Kaplan et al., 2000a; Kaplan et al., 2000b; Walters and Kaplan, 2000; Xu et al., 2000). In this chapter, we discuss one of the most efficacious of these approaches, namely the use of cysteine-scanning mutagenesis in concert with overexpression and functional reconstitution of the isolated transporter mutants, followed by determination of the accessibility of engineered transmembrane Cys residues to methanethiosulfonate (MTS) reagents. This strategy enables one to identify engineered cysteines that reside in water-accessible versus water-inaccessible environments within the membrane. The resulting information then permits a deduction of those residues, which comprise an aqueous pathway through the protein, as well as those residues that face the lipid bilayer. Importantly, if the substrate resembles a given MTS reagent in size and hydrophilicity, it is likely that the identified aqueous pathway is tantamount to the substrate translocation pathway through the protein. Additionally, based on the size of the MTS reagents, a minimal estimate of the diameter of the translocation pathway can be obtained. Finally, by observing the periodic changes in residue accessibility to MTS reagents, information can be gleaned regarding the secondary structure of a given transmembrane domain.

9.2 CRITICAL REVIEW OF VARIOUS EXPERIMENTAL APPROACHES

Due to the inherent difficulties in obtaining well-ordered crystals of membrane transport proteins that diffract to high resolution, a number of noncrystallographic strategies have been developed to probe transporter secondary and tertiary structure (Note: See Kaback and Wu, 1997 and Kaback et al., 2001, for reviews of the application of many of these approaches to the lactose permease.) Two such recent approaches have been used to study helix-packing arrangements in the tertiary structure. They involve the engineering of cysteine residues in two transmembrane helices and measuring the distances between these cysteines via either site-directed spin-labeling combined with electron paramagnetic resonance or via dithiol crosslinking (Wu et al., 1996; Wang and Kaback, 1999). These strategies provide information that complements the functional data (and bolsters the resulting implications regarding transporter structure) that are obtained by the MTS approach. However, in terms of identifying water-accessible and water-inaccessible residue locations within a transmembrane domain, as well as providing inferential information regarding the secondary structure of transmembrane domains and the likely translocation pathway through a given transport protein, it is the opinion of this author that the MTS approach is unsurpassed.

9.3 GENERAL EXPERIMENTAL STRATEGY

Our overall strategy consists of the following steps. First, the amino acid residues in a given transmembrane domain are mutated one by one to cysteine by using the Cys-less transporter open reading frame as the starting template. Second, each single Cys mutant is overexpressed in *E. coli*, the inclusion body fraction (in which the transporter accumulates) is isolated, and the mutated transporter is extracted from isolated inclusion bodies with the detergent sarkosyl. Third, the solubilized transporter is incorporated into phospholipid vesicles. Fourth, the effect of the MTS reagents on reconstituted transporter

function is determined. This consists of an initial series of range finding experiments, conducted with each single Cys mutant, in which the concentration of a given MTS reagent [i.e., [2-(Trimethylammonium)ethyl]methanethiosulfonate bromide (MTSET); (2-aminoethyl)-methanethiosulfonate hydrobromide (MTSEA); and sodium (2-sulfonatoethyl)-methanethiosulfonate (MTSES)] is varied by three orders of magnitude, in order to determine the MTS concentration range over which transport inhibition is obtained. Once the inhibitory concentration range is identified, activity versus time profiles are generated at 4–5 different concentrations of a given MTS reagent with each mutant, in order to determine the rate constant for inhibition.

9.4 SUPPOSITIONS IMPLICIT TO THE MTS APPROACH

Several suppositions are implicit to this approach. Since these assumptions have been previously described in detail (Akabas et al., 1992; Akabas et al., 1994; Javitch et al., 1995; Cheung and Akabas, 1996; Karlin and Akabas, 1998), they will be discussed here only briefly. First, it is postulated that if, following mutation of a given wild-type residue to Cys, significant citrate transport is retained, then the structure of the mutated transporter is similar to the wild-type carrier structure. Accordingly, it is further inferred that the side chain of the introduced Cys occupies a position in the three-dimensional structure that is similar to that of the original wild-type side chain. Second, it is postulated that within a transmembrane domain, only those amino acids that reside on a water-accessible surface of the transporter will react rapidly with MTSET and MTSES. This idea is based on the following: a) the observation that these two polar reagents are impermeable to a lipid bilayer in the absence of either a channel or a transport protein (Holmgren et al., 1996; Kaplan et al., 2000a) and thus will not readily access residues facing the hydrophobic milieu, and b) the finding that MTS reagents react 5×10^9 more rapidly with the thiolate anion (formed only on exposure of the sulfhydryl group to water) compared with the unionized thiol group. Third, it is posited that addition of XCH_2CH_2X to an accessible cysteine will be sufficiently disruptive (via steric blockage, eletrostatic effects, and/or indirect propagation of conformational change) to inhibit transport. Thus, rapid inhibition of transport is interpreted as evidence that the modified Cys side-chain resides within the aqueous transport pathway in a domain, which is sufficiently narrow such that its modification blocks substrate transport. Fourth, because citrate is hydrophilic and of similar size and occupies a volume similar to the MTS reagents (Table 9.1), it is inferred that both will access similar domains, and therefore the MTS-accessible surface of a transmembrane domain constitutes a portion of the substrate translocation pathway through the protein.

9.5 PROPERTIES OF THE MTS REAGENTS

A word about the properties of the MTS reagents is in order. (Note: For an excellent recent review on the properties of these reagents and their use in the study of channel proteins see Karlin and Akabas, 1998). These reagents are charged, water-soluble, and cysteine-specific. They react with protein cysteine residues to form a mixed disulfide via the covalent addition of $-SCH_2CH_2X$ to a reduced sulfhydryl group, where X represents $N(CH_3)_3^+$, NH_3^+, or SO_3^- for MTSET, MTSEA, and MTSES, respectively. As depicted in Table 9.1, the fully extended conformations of each of these reagents fit into a 6.0×12.0

Table 9.1. Calculated Molecular Dimensions of Citrate and the MTS Reagents*

Structure	Long Axis (Å)	Short Axis (Å)	Volume $(Å)^3$
Citrate	10.0	6.0	134
MTSES	12.0	6.0	140
MTSET	11.5	6.0	173
MTSEA	10.0	5.5	113

*Lengths were measured to the nearest 0.5 Å and volumes to the nearest cubic angstrom, based on optimized extended structures with standard Van der Waals radii using the Quanta program (Molecular Simulations, Inc.). Reproduced from Kaplan et al. (2000a) with permission from J. Biol. Chem.

Å cylinder (diameter × length). It is noteworthy that the volume occupied by the three reagents varies considerably, such that MTSET > MTSES > MTSEA due to the differing size of the headgroups of the three reagents. Interestingly, a Cys-MTSET complex displays a considerably more delocalized charge than do the comparable MTSEA or MTSES complexes (Xu et al., 2000). Karlin and Akabas (1998) have reported extensive data on the half-life and reactivity of these reagents in aqueous solutions. In terms of half-life, MTSEA and MTSET have relatively short half-lives of 12 and 11 min, respectively (pH 7.0, 20°C). Reducing either the pH or the temperature substantially increases the half-life values. In contrast, the half-life for MTSES is considerably longer (i.e., 370 min). In terms of relative rate constants for reaction with simple thiols, it was observed that MTSET > MTSEA > MTSES (12.5, 4.5, 1, respectively; calculated from Table II in Karlin and Akabas, 1998). Thus, the reduced half-life values of MTSET and MTSEA are mitigated to some extent by their increased reactivities.

Regarding the relative permeability of MTSEA compared with MTSET and MTSES, both Holmgren et al. (1996) and the author's group (Kaplan et al., 2000a) have observed that MTSEA quite readily penetrates a lipid bilayer. Utilizing liposomes loaded with 5,5'-dithio-bis-(2-nitrobenzoic acid) and dithiothreitol (in the absence of incorporated protein), we observed that MTSET and MTSES do not significantly permeate the lipid bilayer, whereas MTSEA is quite permeable. A consequence of this is that MTSEA can approach a residue, both from the site of addition as well as from the opposite side of the membrane, which results in somewhat higher inhibition rate constants for residues that are located near the opposite side of the membrane. Therefore, MTSEA cannot be used to probe membrane sidedness.

9.6 DETAILED EXPERIMENTAL PROTOCOLS

I will now proceed with detailed protocols for each step described in the "General Experimental Strategy" section.

Construction of Single Cys CTP Gene Mutants via Site-Directed Mutagenesis

Single Cys CTP gene mutants are routinely prepared by using the QuikChange Site-Directed Mutagenesis Kit (Stratagene, La Jolla, CA). Mutagenic primers are designed by following the manufacturer's guidelines and are analyzed with the Oligo 5.0 software

(National Biosciences, Inc., Plymouth, MN, USA). All primers are synthesized and purified via sodium dodecyl sulfate polyacrylamide gel electrophoresis (SDS-PAGE) commercially. Polymerase chain reaction (PCR) amplifications and the subsequent cloning steps (Novagen, Madison, WI, USA) are carried out according to the manufacturer's specifications. The Cys-less CTP gene in pET-21a(+) is utilized as the starting template in amplification reactions at amounts ranging from approximately 6–20 ng per reaction. The Cys-less CTP construct (i.e., C28S/C73V/C192S/C256S) has been shown to display functional properties that are quite similar to the wild-type protein (Kaplan et al., 2000a; Xu et al., 2000).

Following transformation of XL1-Blue competent cells, plasmid DNA is purified with the Wizard Plus SV Minipreps DNA Purification System (Promega, Madison, WI) and is screened for the presence of the gene insert via restriction digestion with *Nde*I and *Bam*HI (i.e., the original cloning sites). The DNA from three to four positive clones is partially sequenced to ensure the presence of the desired mutation. The efficiency of the site-specific mutagenesis in the absence of unintended mutations is ~75%. Plasmids scoring positive for the desired mutation are sequentially subcloned into the storage (NovaBlue) and expression (BL21(DE3)) hosts (Novagen, Madison, WI, USA) as previously described (Kaplan et al., 1995). The presence of the intended mutation is confirmed by sequencing both strands of the entire CTP open reading frame by using plasmid that is purified from the expression strain as template. Sequencing is performed routinely by the fee-for-service Iowa State University DNA Sequencing and Synthesis Facility.

Overexpression of Single Cys Citrate Transport Protein Mutants

A single, isolated bacterial colony of BL21(DE3) cells containing plasmid with the desired mutation in the CTP gene open reading frame is used to inoculate 700 ml of LBC medium (1% bactotryptone, 0.5% yeast extract, 1% NaCl, pH 7.5, 50 μg of carbenicillin/ml). Cultures are grown with shaking (350 rpm) at 37°C to an absorbance at 600 nm of ~0.8 (6–7 h). CTP expression is then induced via the addition of IPTG (1 mM). Two hours later, 200 ml aliquots of cells (three aliquots per incubation flask) are harvested by cooling on ice for 5 min followed by centrifugation at 5,000 x g for 5 min. Note the following: a) all centrifugations are conducted at 4°C; and b) unless indicated otherwise, all subsequent steps are performed on ice. The supernatants are discarded and the bacterial pellets are stored on ice until all cultures are harvested. The cell pellets are resuspended in 20 ml of Buffer A [50 mM Tris-HCl, 2 mM ethylene diamine tetraacetate (EDTA), pH 8.0] and suspensions originating from the same incubation flask are combined (i.e., total volume ~60 ml). Cell lysis is accomplished via the addition of lysozyme (92 μg/ml, prepared immediately before use in Buffer A) and Triton X-100 (0.1%), followed by incubation at 30°C for 15 min with gentle mixing every 5 min. Each lysate is then sonicated (Branson Sonifier 250 [Branson Ultrasonics Corp., Danbury, CT, USA] with a standard flat tip, output control = 1.7; duty cycle = 70%; output meter reading = 35–45) for 30 s on ice, followed by cooling for at least 30 s. Care is taken to ensure that the temperature of the sonicate does not increase significantly. Typically, 4–8 cycles of sonication are required until sample viscosity decreases sufficiently. Each sonicate is divided into two aliquots and is centrifuged at 12,000 x g for 20 min. The resulting pellets are resuspended in 3 ml of Buffer B (10 mM Tris-HCl, 0.1 mM EDTA, pH 7.0; 1.0 mM dithioerythritol), the corresponding samples combined, and centrifuged at 12,000 x g for 30 min. Each combined, washed pellet is resuspended in 2 ml of Buffer B and fractionated via centrifu-

gation through a step gradient consisting of 12.4 ml of 40% (w/v) sucrose and 18.6 ml of 53% sucrose at 131,000 x g for 4.5 h. (Note that the sucrose solutions are prepared in Buffer B.) The resulting pellet (which consists of inclusion bodies) is resuspended in 30 ml of Buffer B and centrifuged at 12,000 x g for 20 min. The washed pellet is then slowly solubilized via the addition of 6.0 ml of 1.2% (w/v) sarkosyl (Fluka, Buchs, Switzerland; dissolved in Buffer B) followed by the combined action of careful, repetitive pipetting and scraping, until clarity is achieved, typically 60-120 min. The solubilized transporter is then centrifuged at 314,000 x g for 45 min. A portion of the resulting supernatant containing a given single Cys CTP mutant is incorporated directly into liposomes, whereas the remainder is quickly frozen in liquid nitrogen and stored at –80°C in small aliquots. The above procedure results in 25–70 mg of single Cys CTP mutant per liter of *E. coli* culture at a purity of ~70%.

Incorporation of Single Cys CTP Variants into Phospholipid Vesicles and Determination of the Quantity of Incorporated Protein

In the first step, phospholipid vesicles are prepared as follows. Asolectin (soybean L-α-phosphatidylcholine, 233 mg; stored in chloroform at –20°C; Sigma, St. Louis, MO) is aliquoted into a 30-ml Corex tube (Corning, Corning, NY, USA) and dried under a stream of gaseous nitrogen. The dried lipid is then washed with diethyl ether by redissolving the lipid and evaporating as above. The resulting dried lipid is placed under vacuum for at least 30 min in order to remove any residual solvent. Vesicles are then prepared by bath sonication (Branson Model 2510) of the solvent-free lipid in 2.1 ml of Buffer C [120 mM N-(2-hydroxyethyl) piperazine-2'-(2-ethanesulphonic acid) (HEPES), 50 mM NaCl, 1 mM EDTA, pH 7.4]. Sonication is continued until the suspension clarifies.

In the second step, sarkosyl-solubilized mutant transporter is incorporated into the asolectin vesicles via the freeze-thaw-sonication technique as follows. Solubilized CTP mutants (typically 5 μl, but values have ranged from 3 μl to 250 μl) is added to a mixture consisting of 525 μl of asolectin vesicles, 60 μl of Buffer C, 200 μl of Buffer B, 120 μl of 400 mM citrate, 40 μl of 10% (v/v) Triton X-114, and 45 μl of 1.2% sarkosyl in Buffer B. The final volume of ~995 μl is kept constant by maintaining a protein + 1.2% sarkosyl volume of 50 μl. With higher volumes of protein, the volume of Buffer B is reduced. This mixture is gently vortexed and rapidly frozen in liquid nitrogen. The proteoliposomes are quite stable once they are frozen. Immediately before assay, a proteoliposomal sample is thawed for 10 min in a beaker of water at room temperature and then sonicated with a probe sonicator (Branson Sonifier 250 with a microtip; output control = 1.7; output meter reading = 8–10; 70% duty cycle; 30 bursts; total sonication time is 21 s) on ice. The freeze-thaw-sonication protocol yields a heterogeneous population of large, mainly unilamellar, citrate-loaded proteoliposomes, which are well suited for transport studies. This procedure has been applied successfully to reconstitute a wide variety of transport proteins (see Kaplan et al., 1990 for a list of the salient references). Extraliposomal citrate is then removed via addition of the proteoliposomes onto a Dowex-1 (Sigma, St. Louis, MO, USA) column (i.e., ~2 ml of resin in a Pasteur pipette with a glass wool plug), which is pre-equilibrated with 12 ml of Buffer C. The proteoliposomes are eluted with Buffer C and the opalescent fraction (1.25 ml) is collected and assayed for transport. Note: The removal of external citrate allows the triggering of the subsequent transport reactions via addition of a precise concentration of external citrate with the desired specific radioactivity.

When needed, the quantity of CTP that actually incorporates into the liposomes is de-

termined via centrifugation of the Dowex eluate for 1.5 h at 314,000 x g (maximum). The resulting supernatant and pellet fractions are then assayed for protein by a modified Amido Black method, which was developed by Kaplan and Pedersen (1989) in order to permit the accurate quantification of protein in the presence of a vast excess of lipid and/or detergent.

Measurement of the Effect of MTS Reagents on Reconstituted Citrate Transport

General Strategy for Determining Transport Kinetics Applicable to Any Transporter. A general sequence of reagent addition is illustrated in Figure 9.1, which can be applied to any transporter as long as a known inhibitor exists that can efficiently stop the transport reaction. (Note: The designations indicated below correspond to a given time interval depicted in Fig. 9.1.) The basic idea is that three types of incubations are conducted for any given proteoliposomal sample. The Experimental Incubation begins with proteoliposomes (or other types of vesicles containing the transporter of interest) that are sequentially incubated with buffer (instead of transport inhibitor dissolved in buffer; A1), water (instead of MTS reagent; B1), radiolabeled transport substrate (to trigger the transport reaction; C1), and finally transport inhibitor (which serves to quench the transport reaction). The Control Incubation begins with proteoliposomes that receive transport inhibitor (to block the transporter of interest before the addition of substrate; A2), water (instead of MTS reagent; B2), radiolabeled transport substrate (to trigger uptake by all processes other than the transporter of interest; C2), and finally buffer (instead of transport inhibitor). Thus, the difference in radioactivity taken up in the Experimental versus the Control Incubations represents the inhibitor-sensitive transport rate (or the total transport activity) observed in the absence of MTS reagent. Finally, the MTS Reagent Incubation begins with proteoliposomes, which sequentially receive buffer (instead of transport inhibitor; A3); MTS reagent (to covalently modify a given Cys residue; B3; purchased from Toronto Research Chemicals, Toronto, Canada); radiolabeled transport substrate (to trigger the transport reaction; C3); and finally, transport inhibitor (to stop the transport reaction). The proportion of activity remaining after incubation with a given MTS reagent is calculated by: 1) subtracting the Control Incubation transport rate from the MTS Reagent Incubation transport rate; and 2) determining the ratio of this difference to the inhibitor-sensitive transport rate determined in the absence of MTS reagent as described above.

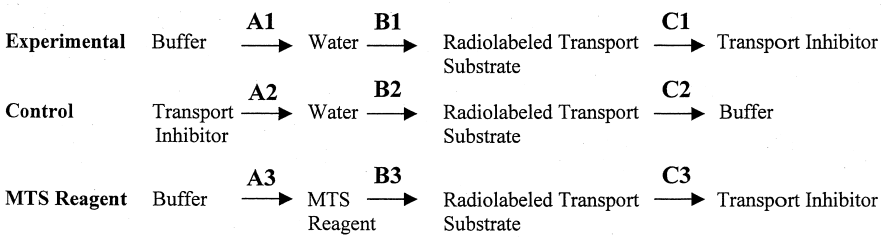

Figure 9.1. General transport kinetics protocol for ascertaining inhibition due to an MTS reagent. A, B, and C denote time intervals between sequential reagent additions. Buffer refers to the solution in which the transport inhibitor is dissolved and will vary depending on the solubility properties of a given inhibitor. Importantly, MTS reagents are dissolved in distilled water immediately before use.

An important point with respect to the above strategy concerns the methodology used to separate radiolabeled substrate that is transported into proteoliposomes (or other membrane vesicles) from residual untransported, external label. Two common approaches involve the use of either posttransport ion exchange columns, when a transport substrate has substantial charge, or with transport substrate that is uncharged, the use of small prespun Sephadex columns where the separation of intraliposomal label from external label is based on molecular size (Penefsky, 1979; Kaplan and Pedersen, 1985).

Specific Transport Kinetics Protocol Applied to the Reconstituted Mitochondrial Citrate Transporter. Proteoliposomes (45 μl) are incubated with 3.5 μl of buffer (i.e., the buffer in which 1,2,3-benzenetricarboxylate (BTC) is dissolved) for 30 s followed by the addition of 3.5 μl of freshly dissolved MTS reagent. The MTS reagent concentration is varied from 10 μM to 40 mM, depending on the specific single Cys mutant-reagent combination being tested. These values are determined from an initial series of range-finding experiments, which are described below. Transport is subsequently triggered by the addition of 21.5 μl of [1,5-^{14}C]citrate (Amersham Biosciences, Uppsala, Sweden; specific radioactivity ~2.4×10^4 dpm/nmol; transport reaction mix concentration 1.04 mM). Reactions are carried out for a time interval defined by the intrinsic activity of a given single Cys mutant. These time intervals (i.e., interval C in Fig. 9.1) are determined empirically such that, in the absence of MTS reagent, ~2,000-2,500 cpm are taken up into liposomes in an inhibitor (BTC)-sensitive manner. It should be noted that with the Cys-less CTP this level of uptake corresponds to initial rate conditions (Xu et al., 2000). Transport incubations are subsequently quenched by the addition of 3.5 μl of BTC (final concentration = 9.0 mM; BTC is the specific, defining inhibitor of the CTP). Utilizing the above protocol, multiple reactions are performed in which the preincubation time interval with the MTS reagent before the [^{14}C]citrate addition (i.e., interval B3 in Fig. 9.1) is varied, thereby enabling the generation of an extent of inactivation versus time plot. Experimental and Control Incubations are performed both at the beginning and the end of each time course experiment (thus permitting an assessment of the functional stability of each mutant during the time course). In these Experimental and Control Incubations, water is added in place of the MTS reagent. Otherwise, the Experimental Incubation is conducted exactly as described, except only a single time interval is used between the addition of water and the subsequent addition of radiolabeled citrate (i.e., interval B1 in Fig. 9.1). In the Control Incubation the order of addition of buffer and BTC is reversed using the same time intervals as in the Experimental Incubation. Accordingly, the Control Incubation receives 3.5 μl of BTC at the beginning of the reaction sequence and buffer in place of BTC at the end of the incubation. Thus, at the end of the reaction sequence the Experimental and Control tubes contain identical concentrations of each constituent with only the order of reagent addition being altered. For additional detail see Kaplan et al. (1990) and Kaplan et al. (2000a).

Following all transport incubations, intraliposomal radiolabeled citrate is separated from extraliposomal label by chromatography on Dowex columns. These columns consist of 1.2 ml of resin in a Pasteur pipette, which contains a glass wool plug and has been equilibrated with 10 ml of Buffer C. At the end of each transport incubation, 60 μl of the reaction mix is placed onto the resin, eluted with Buffer C, and the first 4 ml of the flow-through is collected. Then, 2 ml of the flow-through are mixed with 10 ml of Ready Safe Scintillation Cocktail (Beckman Instruments, Fullerton, CA, USA) and the intraliposomal radioactivity is quantified via liquid scintillation counting.

Control Studies. An important set of initial experiments to perform involves control studies in which the Cys-less transporter is incorporated into liposomes and the effect of a broad range of MTS reagent concentrations on transport activity is determined. We find that in the concentration ranges of 25 μM–30 mM MTSET, 30 μM–100 mM MTSES, and 10 μM–10 mM MTSEA, these reagents do not significantly alter Cys-less CTP function (i.e., <20% change observed) and thus do not have a nonspecific effect on either the liposomal bilayer or on the CTP. It is essential that such studies be performed before MTS range finding and rate constant studies so that one can ascertain the range of reagent concentrations over which any observed effects will be directly attributable to binding to the specifically engineered Cys.

Initial Assessment of the MTS Reagent Concentration Required for Inhibition. With each single Cys mutant–MTS reagent combination, an initial range finding experiment is conducted consisting of a series of incubations (i.e., typically seven) in which the concentration of a given MTS reagent is varied by 3 orders of magnitude. Thus, with MTSET the typical range is 25 μM–30 mM; with MTSES, 30 μM–40 mM; and with MTSEA, 10 μM–10 mM. The incubation time (i.e., interval B3 in Fig. 9.1) is usually on the order of 30 s–2 min. The purpose of these experiments is to determine the approximate reagent concentration needed to obtain: *i*) maximum inhibition; and *ii*) varying levels of inhibition at times that can be accurately measured (i.e., >5 s).

Determination of Rate Constants for MTS Inhibition of Single Cys Mutants. Following an initial assessment of the MTS reagent concentration required to obtain inhibition at a measurable rate, we then determine the time course for inhibition by varying the time interval between the MTS reagent addition and the addition of the [^{14}C]citrate (i.e., interval B3 in Fig. 9.1). These time courses are typically conducted at 4–5 different reagent concentrations, which vary at least several-fold. The resulting rate constants are then calculated as described in the legend to Figure 9.3 (see Kaplan et al. 2000a for further detail). It is noteworthy that by varying the length of the incubation time interval with a given MTS reagent from 5 s up to several hours and the reagent concentration from 7.5 μM to 40 mM, one can determine rate constants that vary by more than 7 orders of magnitude.

9.7 EXPERIMENTAL RESULTS OBTAINED WITH THIS STRATEGY

My laboratory has utilized the above strategy to explore the functional role of transmembrane domain IV (TMDIV) within the yeast mitochondrial CTP (Kaplan et al., 2000a). Accordingly, residues 173–194 were mutated one by one to cysteine. Following overexpression in *E. coli*, each CTP mutant was extracted from the isolated inclusion body fraction with sarkosyl, and functionally reconstituted in liposomes. Figure 9.2 shows the reconstituted citrate transport specific activity values measured with each of the 22 single Cys CTP mutants, as well as the starting Cys-less CTP. All mutants displayed significant BTC-sensitive citrate transport activity (i.e., the defining inhibitor-sensitive function of the mitochondrial CTP), with the exception of the R181C and R189C mutations. Therefore, we concluded that, with the exception of the two nonfunctional mutants, the overall structural and functional integrity of the CTP has been maintained with this panel of single Cys mutants.

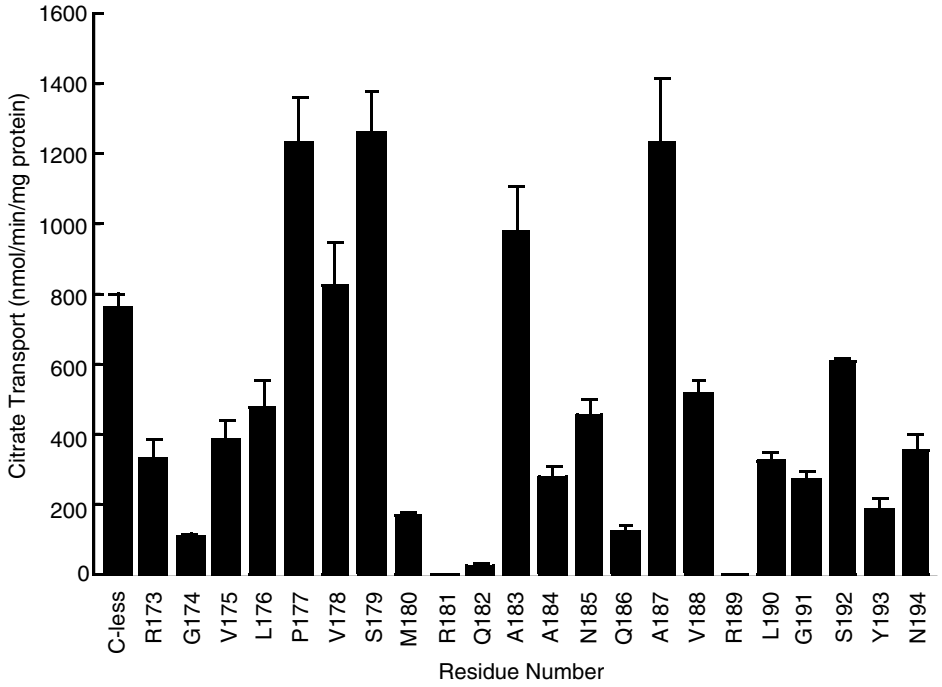

Figure 9.2. Specific citrate transport activities of single cysteine CTP variants. Overexpressed, solubilized Cys-less and single Cys CTP variants were incorporated into phospholipid vesicles. Transport incubations were carried out at room temperature and BTC-sensitive [^{14}C]citrate/citrate exchange was measured. Data represent means ± SE from at least four separate incubations. Reproduced from Kaplan et al. (2000a) with permission from *Journal of Biological Chemistry*.

We then measured the accessibility of each single Cys mutant to MTSES, MTSET, and MTSEA. The data obtained are depicted in Figure 9.3. Several points merit comment. First, depending on residue position, the calculated rate constants vary by as much as 7 orders of magnitude. In certain positions, adjacent residues display rate constants that vary by 4 to 5 orders of magnitude. Second, from residues 177–193, the rate constant data displays a periodicity of ~4, a value which is strongly suggestive of an α-helical secondary structure in this region. Moreover, with three separate reagents an identical periodicity is observed. Thus, with the three independently fitted data sets, the peaks and troughs are located at identical residue positions, thereby clearly defining the highly accessible and inaccessible faces of this helix. The water-accessible face of the TMDIV helix consists of Pro-177, Val-178, Arg-181, Gln-182, Asn-185, Gln-186, Arg-189, Leu-190, and Tyr-193. The water-inaccessible face consists of Ser-179, Met-180, Ala-183, Ala-184, Ala-187, Val-188, Gly-191, and Ser-192. We infer that the water-accessible face constitutes a portion of the citrate translocation pathway, whereas the water-inaccessible surface faces the lipid bilayer. Figure 9.4 depicts the results of computer modeling of residues 177–193 based on the MTS reagent reactivity data.

Importantly, superimposed on the periodic change in the rate constant values, there exists a gradient of decreasing accessibility from the near side of the membrane (i.e., residue 193; the residue nearest to the site of reagent addition) to the far side (i.e., residue 174). This gradient is denoted by the dashed line in Figure 9.3. Thus, externally added MTS

reagent in general has greater accessibility to residues that reside closest to its site of addition. It is noteworthy that the slope of this line is similar with MTSES and MTSET but is markedly reduced with MTSEA. This finding reflects the fact that since MTSEA readily permeates the lipid bilayer by passive diffusion, it can likely approach a given TMDIV residue from either side of the membrane. This permeation results in an increased accessibility to residues located at the far side of the membrane compared with the accessibility observed with MTSES and MTSET (which cannot permeate the bilayer by passive diffusion). In panel 9.3D, the mean deviation from the straight lines from panels 9.3A–C is plotted. This permits an elimination of the slope of the line, with only the wave function remaining. This panel therefore emphasizes the regularity of the observed periodicity.

9.8 ISSUES REGARDING DATA INTERPRETATION

It is noteworthy that with certain single Cys mutants, we have observed an MTS reagent induced stimulation rather than inhibition of function. Stimulation is observed under two circumstances. The first circumstance occurs when modification with a given MTS reagent restores the charge present in the original wild-type residue. For example, when either Arg181 or Arg189 in TMDIV are mutated to Cys, all measurable function is lost. However, chemical modification of the Cys with MTSEA, which serves to restore positive charge at these sites, results in a partial restoration of function (Xu et al., 2000). The second circumstance of activation arises following the modification of Cys residues that are near the membrane/aqueous phase interface. Although the basis for this stimulation is less clear, we have speculated that modification of a residue near the entrance to the translocation pathway may deform either the pathway and/or its gating in a manner that results in increased function. Importantly, since in both scenarios the rate constants for stimulation in essence measure side-chain accessibility, as do the rate constants for inhibition, which are seen with most residues, they may therefore be interpreted in the same manner as the inhibition rate constants.

Another matter for discussion involves the interpretation of a negative result. One can envision that such a finding (i.e., the lack of an effect on transport) can arise from: *i*) the inability to label a given residue, thereby reflecting a combination of the residue's accessibility to the MTS reagent, as well as its reactivity (Note: a reduced reactivity could arise from the lack of formation of the reactive thiolate anion and/or steric constraints to the formation of the addition product.); and/or *ii*) a labeling reaction that has no functional consequence. The latter could arise if, for example, labeling of a given residue did not sterically block or deform the transport pathway by either direct or indirect means. Consequently, negative results should be interpreted with caution and when possible corroborated with direct measurement of labeling.

Finally, it is important to note that even residues facing the hydrophobic bilayer will typically react with the MTS reagents, although at a markedly reduced rate. This reaction likely reflects fluctuations in a residue's accessibility during the transport cycle, as well as the contention that even buried residues are likely to react at significant rates (Karlin and Akabas, 1998). In this instance, the observed inhibition of transport may arise due to either: *i*) a direct steric block of the transport pathway made possible by a combination of the flexibility of the MTS reagent and a rigid body motion (e.g., translation or twisting) of the helix; and/or *ii*) a destabilization of the helical structure as a consequence of the disruption caused by the attempted placement of a charged moiety into the lipid bilayer (Kaplan et al., 2000a).

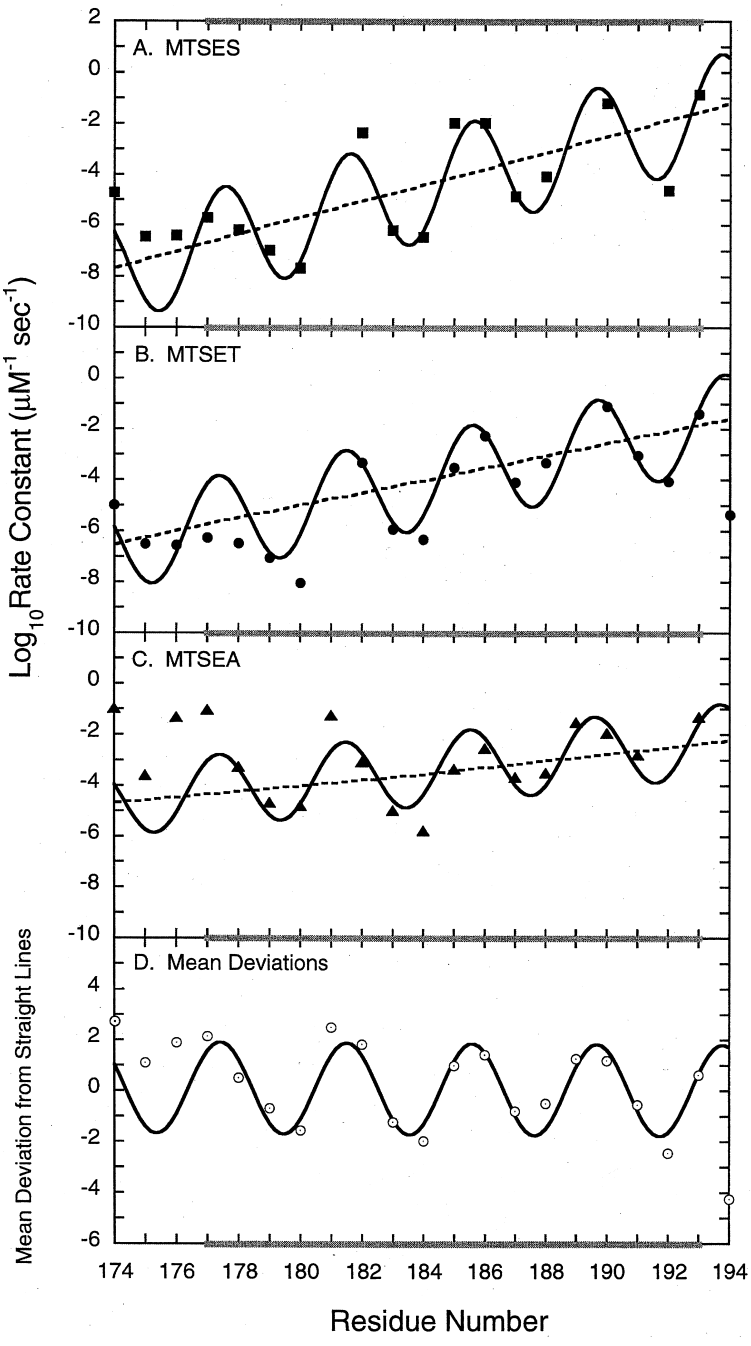

Figure 9.3. Rate constants for inactivation of citrate transport by MTS reagents versus location of engineered cysteine. Time course data for inactivation (activation) of a given single-Cys CTP variant by the MTS reagents were fitted to a simple exponential function by unweighted Marquardt nonlinear least squares: $r_t = (r_0 - r_\infty) \bullet e^{-m \bullet c \bullet t} + r_\infty$ where r_t is the observed activity remaining at time t (seconds), r_0 is the initial activity, r_∞ is the asymptotic activity at $t = \infty$, c is reagent concentration (μM^{-1}), and m is the rate constant for inactivation ($\mu M^{-1} sec^{-1}$). Estimates of m (which range over 7

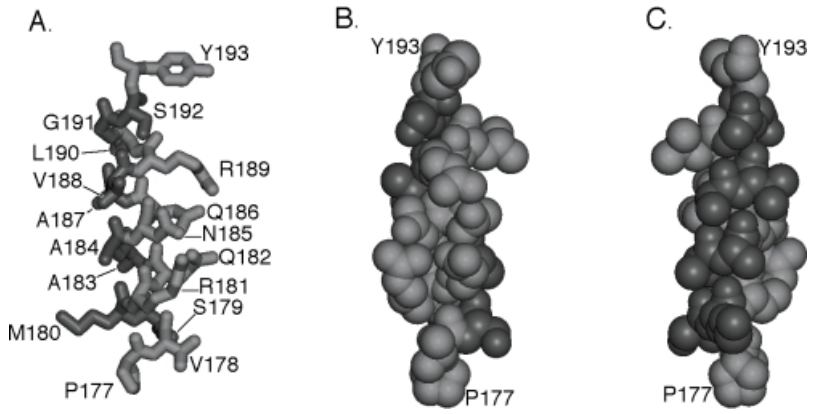

Figure 9.4. Graphical representation of residues 177–193 within TMDIV colored on the basis of reactivity toward the MTS reagents. Residues were colored based on the mean of the deviations from the straight lines as depicted in Figure 9.3D. Residues with values less than zero are colored blue, whereas those with values greater than zero (i.e., more reactive and therefore more accessible) are red. The sequence was modeled initially as a standard α-helix, with amino- and carboxyl-terminal residues capped as amides. The structure was lightly minimized by using the CHARMm force field (Brooks et al., 1983) to allow adjustment of the backbone around Pro177. A) Stick figure representation of the modeled helix, side view, with less reactive residues on the left and more reactive residues on the right. B) Space-filling representation, showing the face of the helix containing the more reactive residues (i.e., water-accessible). C) Space-filling representation, showing the face of the helix containing the less reactive residues (i.e., water-inaccessible). Reproduced from Kaplan et al. (2000a) with permission from *Journal of Biological Chemistry*. (See color insert.)

---

orders of magnitude) are reliable as judged from replicate experiments producing standard errors less than 20% of each estimate. The rate constant for inactivation, m, can be interpreted as a measure of a residue's accessibility to the MTS reagent. The broad range of estimates of m dictated that further analyses be confined to $\log_{10}$ transformed values. For each data set (MTSES, MTSET, and MTSEA) a Fourier analysis, as implemented in Mathematica (Wolfram Research, Champaign, IL, USA), revealed a regular periodicity of 4 between residues 177 and 193 with a noticeable loss of signal when flanking sites were included. Therefore, further analyses were restricted to residues 177 through 193. For each MTS reagent, estimates of $\log_{10} m$ were fitted to the periodic function $\log_{10} m = sn - i + a\bullet\mathrm{Sin}((n - x)\bullet 2\pi/p)$ by using unweighted Marquardt nonlinear least squares. The magnitude of the rate constant for inactivation ($\log_{10} m$) is a function of position (residue number, n) with the straight line ($sn - i$) describing the slope (s) and intercept (i) of the overall trend in a data set and the trigonometric function ($a\bullet\mathrm{Sin}((n - x)\bullet 2\pi/p)$) describing the periodicity on either side of the line (p is the number of residues/2π radians, a is amplitude, and x is a constant setting the register with respect to position, n). Reproduced from Kaplan et al. (2000a) with permission from *Journal Biological Chemistry*.

9.9 ADDITIONAL METHODOLOGICAL NOTES

The use of the anionic detergent sarkosyl to solubilize the overexpressed CTP from the inclusion body fraction is particularly critical. We have tested many nonanionic detergents that proved ineffective at solubilizing the CTP. Fiermonte et al. (1993) first demonstrated the effectiveness of sarkosyl in solubilizing mitochondrial transporters. We subsequently showed that 20 different mitochondrial transporters, which differ substantially in amino acid sequence, are effectively solubilized by this detergent (Kaplan et al., 1995; Mayor et al., 1997). It should be pointed out that, during the solubilization step, patience is required, as the complete extraction of transporter from inclusion bodies can take >1 h of careful, repetitive pipetting and scraping. In addition, we have shown based on CD analysis that the detergent solubilized Cys-less CTP contains a substantial amount of α-helical content, which approaches that observed with transporter that has been reconstituted into liposomes (unpublished). This leads to the conclusion that either the CTP exists in the inclusion bodies in a partially folded state, and/or following solubilization with sarkosyl the transporter folds to a near-native structure. Interestingly, the solubilized transporter is extremely stable and retains most of its reconstitutable activity even after storage in sarkosyl for several weeks at 4°C.

The selection of which reagent(s) to initially screen warrants discussion. We routinely conduct an initial range-finding experiment with MTSET and MTSES. Because these reagents are membrane-impermeant and thus will only approach a water-accessible Cys through an aqueous pathway originating from the site of addition (i.e., the cis side of the bilayer), they are effective sidedness reagents. Moreover, since they are oppositely charged, they provide information regarding the electrostatics of the residues lining the aqueous pathway. If we see no effect on transport by either reagent, experiments are then conducted with MTSEA in order to ascertain whether this more widely permeable reagent can inhibit transport. This provides inferential information as to whether a lack of inhibition with MTSETs or MTSETS reflects a residue that is inaccessible, or alternatively a residue that reacts, but for which there is no functional consequence.

9.10 FINAL THOUGHTS

In conclusion, it is the opinion of this author that the combination of overexpression of a panel of single Cys transporter mutants spanning a transmembrane domain, functional reconstitution of the overexpressed mutants in a liposomal system, and probing of the relative accessibilities of the mutants to MTS reagents, which vary in properties, represents a powerful armamentarium that provides information unattainable by other noncrystallographic methods. While we are currently applying these strategies to mitochondrial transporters, and related strategies have already proven useful in the study of channel (Akabas et al., 1992; Akabas et al., 1994; Kurz et al., 1995; Cheung and Akabas, 1996; Karlin and Akabas, 1998), receptor (Javitch et al., 1995), and other transport proteins (Hall and Maloney, 2001; Fu et al., 2001; Kamdar et al., 2001), I believe that the combination of approaches described above will prove broadly applicable in the future to the study of diverse transporter types from a wide variety of membranes and organisms.

ACKNOWLEDGMENTS

I would like to thank Ms. June A. Mayor for critically reading this manuscript. The author was supported by National Institutes of Health (Bethesda, MD) Grant GM-54642 and National Aeronautics and Space Administration (Marshall Space Flight Center, AL, USA) Grant NAG8-1827 during the writing of this chapter.

ANNOTATED REFERENCES

Akabas MH, Kaufmann C, Archdeacon P, Karlin A (1994): Identification of acetylcholine receptor channel-lining residues in the entire M2 segment of the alpha subunit. Neuron 13:919–927.

Akabas MH, Stauffer DA, Xu M, Karlin A (1992): Acetylcholine receptor channel structure probed in cysteine-substitution mutants. Science 258:307–310.

First studies describing the substituted-cysteine accessibility method (SCAM). Methanethiosulfonate derivatives were used in combination with cysteine-scanning mutagenesis to study ion conduction in the nicotinic acetylcholine receptor channel.

Brooks BR, Bruccoleri RE, Olafson BC, States DJ, Swaminathan S, Karplus M (1983): CHARMM: a program for macromolecular energy, minimization, and dynamics calculations. J Comp Chem 4:187–217.

Cheung M, Akabas MH (1996): Identification of cystic fibrosis transmembrane conductance regulator channel-lining residues in and flanking the M6 membrane-spanning segment. Biophys J 70:2688–2695.

Fiermonte G, Walker JE, Palmieri F (1993): Abundant bacterial expression and reconstitution of an intrinsic membrane-transport protein from bovine mitochondria. Biochem J 294:293–299.

First demonstration of the ability to overexpress a mitochondrial carrier in *E. coli* and to solubilize functionally reconstitutable transporter from isolated inclusion bodies with the detergent sarkosyl.

Fu D, Sarker RI, Abe K, Bolton E, Maloney PC (2001): Structure/function relationships in OxlT, the oxalate-formate transporter of oxalobacter formigenes: Assignment of transmembrane helix 11 to the translocation pathway. J Biol Chem 276:8753–8760.

Gremse DA, Dean B, Kaplan RS (1995): Effect of pyridoxal 5'-phosphate on the function of the purified mitochondrial tricarboxylate transport protein. Arch Biochem Biophys 316:215–219.

Hall JA, Maloney PC (2001): Transmembrane segment 11 of UhpT, the sugar phosphate carrier of *Escherichia coli*, is an alpha-helix that carries determinants of substrate selectivity. J Biol Chem 276:25107–25113.

Holmgren M, Liu Y, Xu Y, Yellen G (1996): On the use of thiol-modifying agents to determine channel topology. Neuropharmacology 35:797–804.

Javitch JA, Fu D, Chen J, Karlin A (1995): Mapping the binding-site crevice of the dopamine D2 receptor by the substituted-cysteine accessibility method. Neuron 14:825–831.

*Kaback HR, Sahin-Toth M, Weinglass AB (2001): The kamikaze approach to membrane transport. Nat Rev Mol Cell Biol 2:610–620.

*Kaback HR, Wu J (1997): From membrane to molecule to the third amino acid from the left with a membrane transport protein. Q Rev Biophys 30:333–364.

*Excellent reviews summarizing the use of a battery of noncrystallographic approaches to study the structure/function relationships of a membrane transport protein (i.e., the lactose permease).

Kamdar G, Penado KMY, Rudnick G, Stephan MM (2001): Functional role of critical stripe residues in transmembrane span 7 of the serotonin transporter: Effects of Na+, Li+, and methanethiosulfonate reagents. J Biol Chem 276:4038–4045.

Kaplan RS (2001): Structure and function of mitochondrial anion transport proteins. J Membr Biol 179:165–183.

Kaplan RS (1996): Mitochondrial transport processes. In Schultz SG, Andreoli TE, Brown AM, Fambrough DM, Hoffman JF, Welsh MJ (eds): Molecular Biology of Membrane Transport Disorders. New York: Plenum Press, pp 277–302.

Kaplan RS, Mayor JA (1993): Structure, function and regulation of the tricarboxylate transport protein from rat liver mitochondria. J Bioenerg Biomembr 25:503–514.

Kaplan RS, Mayor JA, Brauer D, Kotaria R, Walters DE, Dean AM (2000a): The yeast mitochondrial citrate transport protein: Probing the secondary structure of transmembrane domain iv and identification of residues that likely comprise a portion of the citrate translocation pathway. J Biol Chem 275:12009–12016.

Kaplan RS, Mayor JA, Gremse DA, Wood DO (1995): High-level expression and characterization of the mitochondrial citrate transport protein from the yeast *Saccharomyces cerevisiae*. J Biol Chem 270: 4108–4114.

First use of the overexpression/functional reconstitution approach to identify the transport function encoded by a specific yeast gene. Thus, the gene encoding the yeast mitochondrial CTP was identified via overexpression of its functional protein product, thereby demonstrating the utility of this approach.

Kaplan RS, Mayor JA, Johnston N, Oliveira DL (1990): Purification and characterization of the reconstitutively active tricarboxylate transporter from rat liver mitochondria. J Biol Chem 265:13379–13385.

Kaplan RS, Mayor JA, Kotaria R, Walters DE, Mchaourab HS (2000b): The yeast mitochondrial citrate transport protein: determination of secondary structure and solvent accessibility of transmembrane domain IV using site-directed spin labeling. Biochemistry 39:9157–9163.

Kaplan RS, Mayor JA, Wood DO (1993): The mitochondrial tricarboxylate transport protein: cDNA cloning, primary structure, and comparison with other mitochondrial transport proteins. J Biol Chem 268:13682–13690.

Kaplan RS, Pedersen PL (1989): Sensitive protein assay in presence of high levels of lipid. Methods Enzymol 172:393–399.

This paper describes a modified Amido Black protein assay, which enables the accurate quantification of small amounts of protein in the presence of very high levels of lipid (e.g., proteoliposomes).

Kaplan RS, Pedersen PL (1985): Isolation and reconstitution of the *n*-butylmalonate-sensitive dicarboxylate transporter from rat liver mitochondria. J Biol Chem 260:10293–10298.

Karlin A, Akabas MH (1998): Substituted-cysteine accessibility method. Methods Enzymol 293:123–145.

An excellent review summarizing the underlying premises and uses of the substituted-cysteine accessibility method (SCAM), as well as the properties of the MTS reagents.

Kotaria R, Mayor JA, Walters DE, Kaplan RS (1999): Oligomeric state of wild-type and cysteineless yeast mitochondrial citrate transport proteins. J Bioenerg Biomembr 31:543–549.

Kramer R, Palmieri F (1992): Metabolite carriers in mitochondria. In Ernster L (ed): Molecular Mechanisms in Bioenergetics. Amsterdam: Elsevier, pp 359–384.

Kurz LL, Zuhlke RD, Zhang H-J, Joho RH (1995): Side chain accessibilities in the pore of a K^+ channel probed by sulfhydryl-specific reagents after cysteine-scanning mutagenesis. Biophys J 68:900–905.

Mayor JA, Kakhniashvili D, Gremse DA, Campbell C, Kramer R, Schroers A, Kaplan RS (1997):

Bacterial overexpression of putative yeast mitochondrial transport proteins. J Bioenerg Biomembr 29:541–547.

This paper identified a set of 32 genes within the yeast genome that putatively encode mitochondrial transport proteins. Overexpression was attempted with a subset of these genes, namely those that encode mitochondrial transporters of unknown function, and was achieved with 19 of the 26 gene products.

Palmieri L, Runswick MJ, Fiermonte G, Walker JE, Palmieri F (2000): Yeast mitochondrial carriers: bacterial expression, biochemical identification and metabolic significance. J Bioenerg Biomembr 32:67–77.

Palmieri F, van Ommen B (1999): The mitochondrial carrier protein family. In Papa et al. (eds): Frontiers of Cellular Bioenergetics. New York: Kluwer Academic/Plenum Publishers, pp 489–519.

Penefsky HS (1979): A centrifuged-column procedure for the measurement of ligand binding by beef heart F1. Methods Enzymol 56:527–530.

Walters DE, Kaplan RS (2000): Models of the transmembrane domains of the yeast mitochondrial citrate transport protein. J Mol Model 6:587–594.

Wang Q, Kaback HR (1999): Proximity relationships between helices I and XI or XII in the lactose permease of *Escherichia coli* determined by site-directed thiol cross-linking. J Mol Biol 291:683–692.

Wu J, Voss J, Hubbell WL, Kaback HR (1996): Site-directed spin labeling and chemical crosslinking demonstrate that helix V is close to helices VII and VIII in the lactose permease of *Escherichia coli*. Proc Natl Acad Sci USA 93:10123–10127.

Xu Y, Kakhniashvili DA, Gremse DA, Wood DO, Mayor JA, Walters DE, Kaplan RS (2000): The yeast mitochondrial citrate transport protein: probing the roles of cysteines, Arg(181), and Arg(189) in transporter function. J Biol Chem 275:7117–7124.

CHAPTER 10

PEPTIDE MAPPING OF DOPAMINE TRANSPORTER LIGAND AND SUBSTRATE INTERACTION SITES

MARGARET J. LOWE, JON D. GAFFANEY, AND ROXANNE A. VAUGHAN

10.1 INTRODUCTION

The dopamine transporter (DAT) is a neuronal membrane protein that controls synaptic transmission by actively transporting dopamine (DA) from the extracellular space into the cell. This is the primary mechanism of clearance of synaptic DA, and DAT is a major regulator of DA tone (Giros et al., 1996). DAT belongs to a family of Na^+ and Cl^--driven neurotransmitter transporters that share most structural and functional similarity with the norepinephrine (NET) and serotonin transporters (SERT) (Masson et al., 1999; Chen and Reith, 2000). The monoamine transporters are targets for psychostimulant drugs, such as cocaine and amphetamine, and are fundamental to the etiology of a wide range of psychological and neurodegenerative disorders, such as depression, attention deficit disorder, schizophrenia, and Parkinson's Disease. Cocaine and many other structurally dissimilar abused and therapeutic drugs, such as GBR 12909, mazindol, methylphenidate (Ritalin), and bupropion (Wellbutrin), bind to DAT with high affinity and inhibit its transport activity. This results in increased synaptic DA levels that are believed to mediate the reinforcing or therapeutic actions of the compounds (Ritz et al., 1987; Kuhar et al., 1991). In contrast to these nontransported uptake blockers, amphetamine-related drugs and neurotoxins such as 1-methyl-4-phenylpyridinium (MPP^+) are substrates for DAT and exert their effects by being transported into the neuron (Pifl et al., 1993).

Single-copy cDNAs of DAT have been cloned from human, rat, mouse, bovine, *C. elegans*, and *D. melangaster* libraries (Vandenbergh et al., 1992; Shimada et al., 1991; Bruss et al., 1999; Usdin et al., 1991; Jayanthi et al., 1998; Porzgen et al., 2001). Hydropathy and sequence analysis predict 12 transmembrane-spanning domains (TMs) with intracellularly oriented N- and C- and termini and a large glycosylated extracellular loop between TMs 3 and 4 (Povlock and Amara, 1997). Some aspects of this predicted structure and topology have been verified, but we currently have little understanding of the three-dimensional structure of the protein or arrangement of TM helices. It is presumed that the TMs create a path for DA and ions through the lipid bilayer, but which TMs are involved and the molecular mechanisms responsible for translocation are not known. Many other aspects of DAT structure and function are also unknown, including the sites

Transmembrane Transporters. Edited by Michael Quick

ISBNs: 0-471-06517 (Hardcover); 0-471-43404-3 (Electronic)

of binding for substrates and inhibitors, whether various classes of DAT inhibitors bind to the same or different sites, or how antagonist binding results in inhibition of transport.

These questions have been addressed by a large number of studies using various approaches such as classical pharmacology, protein modification, and mutagenesis (reviewed in Chen and Reith, 2000). Most studies are compatible with an interpretation that uptake and inhibitor sites are integrally linked at some mechanistic level, although it is also clear that uptake and binding functions do not respond identically to all mutations or treatments (Schweri, 1990; Johnson et al., 1992; Kitayama et al., 1992; Giros et al., 1994; Buck and Amara, 1994, 1995; Ferrer and Javitch, 1998; Lin et al., 1999, 2000; Chen et al., 2001). Conceptually these findings may best be interpreted as the active sites on the protein for substrates and inhibitors consisting of overlapping but not identical domains.

Structural analysis of DA analogs shows that optimum transport activity occurs when molecules possess a phenyl ring with a primary ethylamine side chain (Meirgerd and Schenk, 1994), although compounds without phenolic hydroxyl groups, such as MPP^+, phenethylamine, and amphetamines, are also transported (Chen and Justice, 2000). Recent evidence shows that the cationic, and possibly zwitterionic, forms of DA are the chief substrate for transport (Berfield et al., 1999). DA transport inhibitors also contain ring structures, and most contain nitrogen atoms (Carroll et al., 1997), which suggests the potential for similarities in the mechanism of antagonist and substrate binding. Together these results implicate involvement of amino acids that are negatively charged, polar, and aromatic as the most likely to interact with substrates and inhibitors. Mutagenesis of these types of amino acids in many regions of DAT result in diminution or loss of transport activity and/or cocaine binding (Kitayama et al., 1992; Danek-Burgess and Justice, 1999; Lin et al., 1999; Loland et al., 1999; Chen et al., 2001). However, in the absence of information on the three-dimensional structure of DAT, it is difficult to ascertain whether the effects of mutations are due to specific disruptions of ligand or substrate interaction sites or to alterations of protein structure that impact the sites nonspecifically.

Our group has used peptide-mapping techniques to address the issues of DAT protein structure and active sites for antagonist and substrates. One approach is to covalently label the protein with radioactive analogs of uptake blockers, digest it with proteases, and determine the region of ligand–protein interaction by epitope-specific immunoprecipitation of the labeled fragments. With this strategy, we have identified two regions in the N-terminal half of DAT that interact with four different uptake blockers. One of the inhibitors becomes incorporated in both sites, implicating their three-dimensional proximity and suggesting that they contribute to a binding pocket for transport antagonists. These regions may also participate in substrate binding or translocation if active sites for substrates and inhibitors consist of overlapping domains as suggested by pharmacological and molecular studies.

In addition to defining ligand interaction sites, we have identified extracellular loop 2 (EL2) as one of the most protease-sensitive sites on DAT and found that it displays differential sensitivity to proteolysis depending on which photoaffinity ligand is bound. This finding suggests that DAT exhibits distinct ligand-induced protein conformations that may be related to transport inhibition. We are pursuing this observation by monitoring ligand and substrate-induced conformations of EL2 by using Western blotting, which allows us to examine the effects of a wider variety of antagonists and substrates than is reasonable with photoaffinity labeling. These strategies represent a positive-function approach to examination of several aspects of DAT active sites, structure, and mechanisms of transport and transport inhibition that can be integrated with molecular and pharmaco-

logical results. The methods described here should be adaptable to analysis of other transporters or systems.

10.2 PHOTOAFFINITY LABELING OF DAT

We have used four photoaffinity ligands based on two different classes of uptake blockers to irreversibly label DAT (Figure 10.1A). These compounds are [^{125}I]RTI 82 and [^{125}I]GAII34, tropane ring-containing compounds related to cocaine, and [^{125}I]DEEP and [^{125}I]AD 96, which are structurally related to GBR piperidine/piperazine compounds (Grigoriadis et al., 1989; Agosten et al., 1999; Dutta et al., 2001). The compounds contain an azido (N_3) group that, on activation by ultraviolet (UV) light, covalently attaches to the protein and allows analysis of the labeled protein and ligand-binding site by sodium dodecyl sulfate polyacrylamide gel electrophoresis (SDS-PAGE). Unfortunately, the high reactivity of the azido moiety precludes prediction as to the type of amino acid modified (Guillory, 1989). [^{125}I]DEEP and [^{125}I]RTI 82 have affinities near 10 nM, whereas those of [^{125}I]AD 96 and [^{125}I]GAII34 are ~150 nM. All of these compounds label DAT to levels sufficient for easy analysis, although more incorporation into nonspecific proteins occurs with the lower-affinity ligands. The specific activities range from 1600 to 2000 Ci/mmol, and the compounds are stored at –20°C, where they maintain sufficient chemical and radioactive integrity to be useful for several months. Presumably other classes of DAT blockers, such as methylphenidate, mazindol, or nomifensine, could be developed

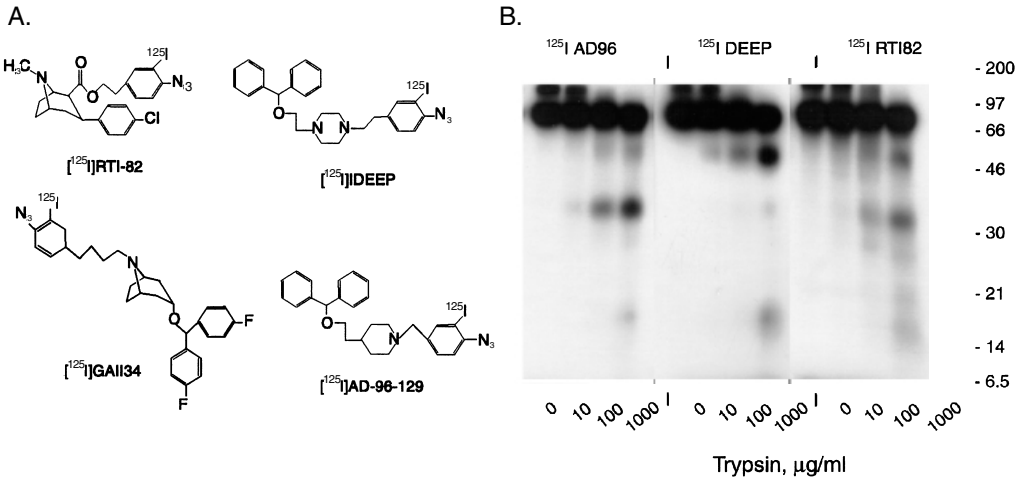

Figure 10.1. Peptide mapping of DAT ligand binding sites. **A**). DAT photoaffinity labels used for mapping studies. [^{125}I]RTI 82 and [^{125}I]GAII34 are tropane ring-containing compounds related to cocaine; [^{125}I]DEEP and [^{125}I]AD96 are piperidine/piperazine analogs derived from the GBR series. **B**). Spectrum of DAT photoaffinity-labeled fragments. DATs labeled with [^{125}I]AD96, [^{125}I]DEEP, or [^{125}I]RTI 82 were gel-purified and treated with the indicated concentrations of trypsin. DATs labeled with [^{125}I]DEEP primarily produce 45 and 14 kDa fragments, whereas DATs labeled with [^{125}I]RTI 82 primarily produce 32 and 16 kDa fragments. A hybrid pattern consisting of both the 45 and 32 kDa fragments is produced from DATs labeled with [^{125}I]AD 96 (From Vaughan et al., 2001, by permission).

as irreversible ligands and adapted for use in these protocols. However, it may not be possible to use these methods for analyzing substrate interaction sites because the addition of both iodine and azido moieties to DAT substrates would adversely affect their affinity and ability to be transported.

For most experiments, we photolabel DAT from rat striatum, although we have also successfully photolabeled DAT from other brain regions of the rat, including nucleus accumbens and frontal cortex; from caudate putamen of other species, including human, dog, and mouse; and from rat and human DAT expressed heterologously in cell lines (Vaughan et al., 1996; Huff et al., 1997). Photolabeling can be performed on fresh or frozen tissue or cell membranes. The ligands that we have used are not activated by ambient light, and all procedures can be carried out under normal room illumination. Photolabeling is performed by homogenizing the tissue or cells in a suitable buffer, preparing membranes by centrifugation, and allowing the ligand to bind reversibly to the protein. Pharmacological characterization of labeling can be performed by including cocaine or other DAT blockers during the reversible binding step, which will displace the radioactive label and prevent its subsequent covalent incorporation. After completion of reversible binding, the sample is irradiated with UV light to covalently attach the ligand to the protein, and unbound ligand is removed by washing the membranes.

Once DAT is covalently labeled, it can be subjected to various treatments depending on the experimental purpose. These include a) direct electrophoresis of the solubilized membranes to analyze or gel-purify the sample, b) immunoprecipitation of the intact protein, c) proteolytic digestion and analysis of the gel-purified protein, and d) proteolytic digestion of the protein followed by epitope-specific immunoprecipitation of the fragments. Procedural variations for each of these purposes are described below, and specific recipes and protocols are presented at the end of the chapter. All procedures involving radioiodinated ligands should be performed using appropriate radiation shielding, precautions, personnel monitoring, and waste handling as established by the investigator's institutional radiation safety office.

10.3 IMMUNOPRECIPITATION

We have generated several rabbit polyclonal antibodies directed against specific epitopes of the rat DAT primary sequence (Vaughan et al., 1993). The antibodies that have been useful for peptide mapping are antibodies 15 and 16 directed against residues 6–30 and 42–59 in the N-terminal tail; antibody 5 directed against residues 225–236 in EL2; antibody 12 directed against residues 541–554 in EL6; and antibody 18 directed against residues 580–608 in the C-terminal tail. These antibodies also recognize DATs from human, mouse, and dog to various extents (Vaughan et al., 1996). Antibodies to other DAT epitopes have been described (Miller et al., 1998), and many are available commercially.

For immunoprecipitation, the photolabeled membranes are solubilized in detergent followed by addition of immunoprecipitation (IP) buffer containing antiserum. If SDS is used for solubilization, it must be diluted to 0.1% so as not to denature the antibodies; we solubilize with 0.5% SDS to minimize sample dilution. DATs from striatal membranes can also be solubilized with 1% Triton X-100, and 0.1% Triton can substitute for SDS in IP buffer. The diluted sample and antibodies are incubated for 1–2 h, followed by collection of immune complexes using protein A Sepharose beads. The sample is eluted from the beads and analyzed by electrophoresis and autoradiography. Because nonspecific

bands can appear in immunoprecipitated samples, it is essential to perform control experiments to verify immunoprecipitation specificity. These include comparison of signals from immune and preimmune serum, and by inclusion of the immunizing peptide during immunoprecipitation to prevent precipitation of DAT. To rule out nonspecific effects of peptides, we also include a control containing an irrelevant peptide, which should not inhibit immunoprecipitation.

10.4 PROTEOLYSIS OF GEL-PURIFIED DAT

After completion of photoaffinity labeling, striatal or cell membranes can be solubilized and analyzed by SDS-PAGE and autoradiography. DAT migrates on 8% SDS-PAGE gels at ~80 kDa, consistent with its amino acid composition and extent of glycosylation. When striatal membranes are analyzed directly by SDS-PAGE, several other radiolabeled proteins of various molecular weights are usually seen (Agoston et al., 1997; Vaughan et al., 2001). Those proteins are not DAT aggregates or proteolytic products, as their labeling is not displaced by DA-uptake blockers, and they are not precipitated by DAT antibodies. However, because they interfere with peptide mapping analyses, it can be useful to separate them from DAT by using a gel-purification procedure that consists of electrophoresis of crude membranes followed by excision and electroelution of the 80-kDa region of the gel. Because DAT is the only radiolabeled protein in this region of the gel, proteolytic digestion and re-electrophoresis of these samples permits unequivocal visualization of DAT peptide fragments.

For preparative studies, we photolabel at least 25–50 mg tissue to provide enough sample for several analyses, and load 175–200 μl of the solubilized membranes into each of several lanes of a prep gel. Large gels (15 × 17 cm) are used for these procedures in order to load large amounts of protein and obtain good separation of peptide fragments. We use high- and low-range Rainbow Molecular Weight Markers from Amersham (Uppsala, Sweden) to minimize misinterpretation of mass standards, and phosphorescent orientation markers (Identikit; Sigma, St. Louis, MO) placed on the gel backing paper for gel-film alignment. Because of the large amount of sample loaded, these prep gels require only short autoradiographic exposures (1–2 h). After drying and autoradiography, the gel is taped to a light box and the film is aligned with it by using the orientation markers. The 80-kDa region of the gel containing DAT is excised with a razor blade, and the gel pieces are pooled and hydrated in gel running buffer. After the paper backing is removed, the gel pieces are placed into the chamber of a BioRad Electroelutor (Hercules, CA) fitted with 3500 or 15,000 Da molecular-weight cut-off caps, and samples are electrophoresed at 10 mamp/chamber for 4–5 h. This extracts 50–70% of the sample in a volume of ~500 μl per chamber. If more than one chamber is used, the samples are pooled and, if desired, can be concentrated by using a Centricon 30 concentration device (Amicon, Danvers, MA). The electroeluted samples can then be digested with trypsin or V8 protease and re-electrophoresed on 15 to 17% single-concentration or 9–16% gradient SDS-PAGE gels.

An example of results obtained with this kind of protocol is shown in Figure 10.1B, which shows a parallel analysis of DATs labeled with [^{125}I]DEEP, [^{125}I]RTI 82, and [^{125}I]AD 96. Digestion of [^{125}I]DEEP-labeled DATs produces major fragments of 45 and 14 kDa, whereas digestion of [^{125}I]RTI 82-labeled DATs produces major fragments of 32 and 16 kDa. These different mapping patterns indicate that the two ligands are incorporated into different regions of the protein, an interpretation confirmed by epitope-specific

immunoprecipitation (Vaughan, 1995; Vaughan and Kuhar, 1996). The spectrum of fragments from DATs labeled with [^{125}I]AD 96 is a hybrid of the [^{125}I]DEEP and [^{125}I]RTI 82 patterns, with fragments visible at both 45 and 32 kDa. This result is consistent with the possibility that [^{125}I]AD 96 is incorporated into both of the domains labeled by [^{125}I]DEEP and [^{125}I]RTI 82.

Proteolysis of gel-purified samples provides an easy way to detect radiolabeled fragments and to compare the labeling patterns of different ligands, with the important advantage that fragments can be visualized regardless of their ability to be immunoprecipitated. Although it is possible to analyze these samples by epitope-specific immunoprecipitation, the protease remaining can digest the antibodies. Adding SDS after proteolysis does not completely inhibit protease activity, and boiling is not an option as it produces in transporter aggregation. We use protease inhibitors and add carrier protein to serve as a competitor substrate for the protease, which are the most satisfactory methods of dealing with this issue.

10.5 IN SITU PROTEOLYSIS OF DAT

An alternative to analysis of gel-purified DAT is to subject photolabeled membrane suspensions to proteolysis, followed by epitope-specific immunoprecipitation of the fragments. For this procedure, rat striatal membranes are photoaffinity-labeled and suspended in buffer. The membranes are treated with protease for a short period of time, pelleted to remove the protease, and subjected to immunoprecipitation. The advantages of this strategy are that proteolysis is performed on native protein, information can be obtained pertaining to the proximity of the binding sites to membrane structure, and the topological sensitivity of protease sites can be examined. The major disadvantage is that because of the nonspecifically photolabeled proteins present in the membranes, DAT fragments must be immunoprecipitated to be visualized, and labeled fragments that have lost antibody epitopes due to proteolysis will not be detected.

Figure 10.2A shows the immunoprecipitation profile of the major [^{125}I]DEEP- and [^{125}I]RTI 82-labeled fragments generated by in situ proteolysis and their origin in the primary sequence. The 45-kDa fragment labeled with [^{125}I]DEEP immunoprecipitates with antisera 15 and 16 and represents the N-terminal half of the protein, whereas the 32-kDa fragment labeled with [^{125}I]RTI 82 immunoprecipitates with antisera 5, 12, and 18 and represents the C-terminal half of the protein. The smaller fragments precipitate only with antisera 16 or 5, localizing the incorporation of [^{125}I]DEEP to TMs 1–2 and [^{125}I]RTI 82 to TMs 4–7. These fragments are retained in membranes after proteolysis, demonstrating that they contain integral membrane structure and indicating that ligand binding occurs close to or within transmembrane spanning domains (Vaughan and Kuhar, 1996).

Comparable analysis of the benzotropine analog [^{125}I]GAII34 demonstrated its incorporation in TMs 1–2, similar to [^{125}I]DEEP (Vaughan et al., 1999). No interaction was seen in TMs 4–7, showing that, although the tropane ring is an essential component of the cocaine pharmacophore (Carroll et al., 1992), it is insufficient to produce identical incorporation of [^{125}I]GAII34 and [^{125}I]RTI 82. Whether this is due to differences in the position of the azido moieties or to other structural differences between the compounds is currently under investigation. In contrast to these three ligands that primarily label a single site, epitope-specific immunoprecipitation has shown that [^{125}I]AD 96 undergoes incor-

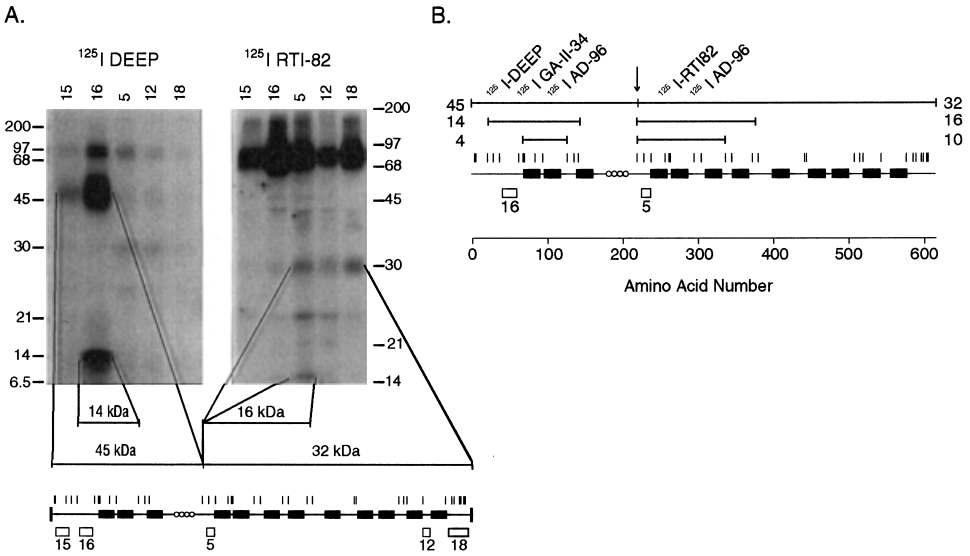

Figure 10.2. In situ proteolysis and epitope-specific immunoprecipitation of DAT fragments. **A**) Rat striatal membranes photoaffinity labeled with [^{125}I]DEEP or [^{125}I]RTI 82 were treated with trypsin and were immunoprecipitated with the antisera indicated at the tops of the gels. The 45-kDa [^{125}I]DEEP-labeled fragment immunoprecipitates with antisera 15 and 16, while the 14-kDa fragment precipitates only with serum 16. The 32-kDa [^{125}I]RTI 82-labeled fragment immunoprecipitates with antisera 5, 12, and 18, while the 16-kDa fragment precipitates only with serum 5. The schematic diagram of DAT below the autoradiograph shows the positions of the 12 transmembrane domains (filled rectangles), antibody epitopes (numbered rectangles), and potential trypsin cut sites (tick marks). The lines connecting the photolabeled fragments to the diagram indicate their origin in the primary sequence. (From Vaughan and Kuhar 1996, by permission). **B**) Summary of photoaffinity-label incorporation sites. Schematic representation of DAT sequence and photoaffinity-labeled peptide fragments, with numbered bars above the sequence indicating the masses of the major fragments and their origin in the primary sequence. [^{125}I]DEEP and [^{125}I]GAII34 become incorporated primarily into TMs 1-2, [^{125}I]RTI 82 becomes incorporated into TMs 4-7, and [^{125}I]AD 96 becomes incorporated into both TMs 1–2 and TMs 4–7. (From Vaughan et al., 2001, by permission).

poration in both the TM 1–2 and TM 4–7 domains (Vaughan et al., 2001). This finding suggests that the labeled domains are close together three-dimensionally and, in conjunction with the finding that all four ligands bind to these sites, also suggests that these domains contribute to a binding pocket for multiple antagonists. A summary of the binding sites for the four photoaffinity labels is shown in Figure 10.2B.

These studies have also shown that EL2 is one of the most protease-sensitive sites on the protein, being cut by trypsin at or near R218, between the consensus glycosylation sites and epitope 5 (arrow, Fig. 10.2B). Proteolysis here generates the 45 kDa N-terminal fragment that is glycosylated but does not immunoprecipitate with serum 5, and the 32 kDa C-terminal fragment that immunoprecipitates with serum 5 but is not glycosylated (Vaughan and Kuhar, 1996). The sensitivity of this site to proteolysis depends on which ligand is bound. Sensitivity is greater when DAT is labeled with ligands that are incorporated in TMs 1–2 than that labeled with ligands that are incorporated in TMs 4–7 (Vaughan et al., 2001). This finding suggests that different uptake blockers may induce

different DAT conformations in which R218 is more or less accessible to protease, and that stabilization of EL2 may be related to transport inhibition.

10.6 MONITORING DAT PROTEOLYSIS BY WESTERN BLOTTING

We have recently begun to examine the effects of uptake inhibitors and substrates on DAT conformation by using Western blotting to identify proteolytic fragments. Proteolysis of R218 can be monitored by immunoblotting with monoclonal antibody 16 (MAb 16) generated against amino acids 42–59 to detect the 45 kDa N-terminal fragment previously identified by photolabeling. By using immunoblotting rather than photolabeling to detect this fragment, the protease sensitivity of EL2 can be assessed in the presence of a variety of antagonists and substrates.

For these experiments nonphotolabeled striatal membranes are incubated with DAT inhibitors or substrates, treated with trypsin, and analyzed by Western blotting. In the absence of exogenous compounds, DAT is very sensitive to proteolysis, and trypsin produces easily detectable levels of the 45 kDa N-terminal fragment (Figure 10.3). However, in the presence of DA uptake blockers such as (–) cocaine, mazindol, GBR 12909, or β–CFT, fragment production is reduced substantially. This effect correlates with the affinity of the compounds at DAT, and is not observed in the presence of the inactive stereoisomer (+) cocaine, or the NET and SERT blockers desipramine and imipramine. These results indicate that binding of uptake blockers at DAT results in inhibition of fragment production, possibly by inducing a conformational change in EL2 that reduces the accessibility of R218 to trypsin. In contrast, fragment production was not affected by

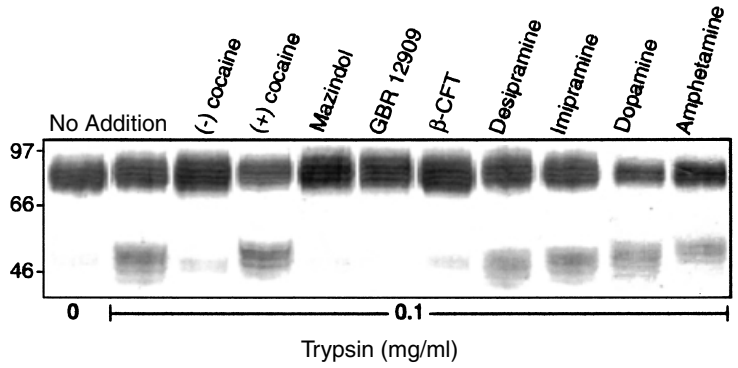

Figure 10.3. Antagonist-induced inhibition of DAT proteolysis. Rat striatal membranes incubated in the presence or absence of DA uptake inhibitors or substrates were treated with or without trypsin as indicated, followed by electrophoresis and Western blotting with MAb16. The blot shows the full-length protein at 80 kDa and the 45 kDa N-terminal fragment produced by proteolysis of R218 in EL2. Little to no proteolysis is observed in the absence of protease and, in the absence of ligand, trypsin generates an easily detectable band at 45 kDa. The production of this fragment by trypsin is essentially abolished when the membranes are incubated with the uptake inhibitors (–) cocaine, mazindol, GBR 12909, and β-CFT, but not by inclusion of (+) cocaine, desipramine, imipramine, DA, or amphetamine. These data indicate that binding of uptake inhibitors, but not substrates at DAT, induces protease resistance of EL2, possibly by producing a conformational change that results in R218 becoming inaccessible to the protease.

binding of the substrates DA or amphetamine. These results suggest that substrates and inhibitors induce different conformations of DAT, and that inhibitors may exert their effects by inducing or stabilizing a particular conformation of EL2. In addition, the similarity of effect induced by multiple structurally dissimilar uptake inhibitors suggests that they act by the same or a shared mechanism, which supports the concept of common or overlapping binding sites for antagonists. It may be possible to examine conformational changes occurring in regions of the protein other than EL2 by using proteases that will cut at other sites or antibodies to other epitopes. It may also be possible to use these procedures to examine additional aspects of DAT structure and function, such as influx or efflux-specific conformations or the role of ions in transport and binding.

10.7 SUMMARY

Our studies have shown that four structurally dissimilar DAT ligands bind to two distinct sites in TMs 1–2 and 4–7. These results are compatible with several mutagenesis, chimera, and substituted cysteine accessibility studies that implicate the involvement of residues or domains in these regions in DAT function (Kitayama et al., 1992; Giros et al., 1994; Buck and Amara, 1994, 1995; Danek-Burgess and Justice, 1999; Ferrer and Javitch, 1998; Loland et al., 1999; Lin et al., 1999, 2000; Lee et al., 1998, 2000; Chen et al., 1999, 2001). Similar results have been found for SERT (Barker et al., 1998, 1999; Chen et al., 1997; Chen and Rudnick, 2000), suggesting a conservation of function in these domains. Our findings also suggest that parts of these two domains are close together three-dimensionally and contribute to a shared antagonist binding pocket, some of the first evidence pertaining to the three-dimensional proximity of TM helices. It is not clear how these results might relate to potential oligomerization of neurotransmitter transporters (Kiliac and Rudnick, 2000; Hastrup et al., 2001). Protease sensitivity studies suggest that uptake blockers stabilize the structure of EL2, a mechanism of transport inhibition also implicated in zinc binding-site studies (Loland et al., 1999). Our future work will be directed toward examining additional irreversible ligands and identifying more precisely their sites of incorporation. Together these studies will continue to define the active sites, structure, and molecular basis of action of DAT and other neurotransmitter transporters.

10.8 DETAILED PROTOCOLS

Photoaffinity labeling DAT from rat striatum

1. Sacrifice rat by decapitation, and dissect and weigh the striatum. Place the tissue in ice-cold sucrose phosphate (SP) buffer (10 mM sodium phosphate, 0.32 M sucrose, pH 7.4).
2. Homogenize the tissue using a Brinkman Polytron PT 2100 Homogenizer (Brinkman Instruments, Westbury, NY) at setting 6 for 10 s. For 25 to 30 mg striatum use 10 ml of buffer in a 15-ml centrifuge tube.
3. Centrifuge the homogenate at 12,000 x g for 12 min at 4°C. For this and all other procedures membranes should be pelleted at forces that pack them gently and permit easy resuspension or solubilization, as undesirable effects occur in tightly packed membranes.

4. Discard the supernatant and gently suspend the pellet in SP at 20 mg/ml original wet weight (o.w.w.).
5. During the centrifugation steps, dilute the source photoaffinity label into SP to a concentration of 6–10 nM. Combine the suspended membrane sample with an equal volume of diluted radiolabel for a final ligand concentration of 3–5 nM (this can be done in the centrifugation tube). Incubate on ice for 1 h. Cocaine or other uptake blockers can be included during this step for pharmacological displacement analyses.
6. Transfer the membrane suspension to a shallow vessel, such as a petri plate, and irradiate with UV light at a distance of about 1 cm for 45 s. Observe eye safety precautions during this step (wear plastic goggles and do not look directly at light).
7. Transfer the membrane suspension back to the centrifuge tube and centrifuge at 12,000 x g at 4 °C for 12 min. Discard supernatant.
8. Wash the pellet with 10 ml of 50 mM Tris-HCl, pH 8.0; centrifuge; and discard supernatant. At this point the radioligand is attached covalently to DAT, and the sample can be processed in one of the following ways:
   A) For immediate electrophoresis: Add 1× SDS-PAGE sample buffer (60 mM Tris-HCl, pH 6.8; 2% SDS; 10% glycerol; and 5 mM dithiothreitol) to obtain a final tissue concentration of 20 mg/ml o.w.w., and vortex until membranes dissolve. Do not heat the sample, as this will cause DAT to aggregate.
   B) For immunoprecipitation: Add 1× SDS-PAGE sample buffer containing reduced SDS (0.5%) at 20 mg/ml o.w.w., and vortex until membranes dissolve.
   C) For in situ proteolysis: Suspend membranes in 50 mM Tris-HCl, pH 8.0, at 50 mg/ml o.w.w.
9. Samples may be processed immediately or stored at –20°C.

Immunoprecipitation of DAT or DAT fragments

1. Prepare protein A Sepharose beads by washing lyophilized beads twice in 10 volumes of immunoprecipitation buffer (IPB) consisting of 50 mM Tris HCl, pH 8.0, plus 0.1% SDS, then add enough IPB to make 50% beads by volume. Beads may be prepared in advance and stored refrigerated for up to one week.
2. Dilute immune or preimmune antiserum to appropriate concentration (1:30–1:400) with IPB.
3. Add one-part solubilized DAT sample to four-parts dilute antiserum. We typically use 25–50 µl sample and 100-200 µl dilute antiserum. For peptide blocking experiments add 50 µg/ml of the immunizing or irrelevant peptide to parallel samples. Incubate on rotator at 4°C for 1–2 h.
4. Add 50 µl of a 50% slurry of protein A beads to each tube and incubate 1 h at 4°C.
5. Centrifuge briefly at low speed, remove and discard supernatant.
6. Wash beads twice with 1 ml ice-cold IPB.
7. Add 100 µl sample buffer to the protein A beads; vortex, then centrifuge at low speed. Remove the supernatant, which contains DAT; then electrophorese nonproteolyzed samples on 8% gels and proteolyzed samples on 15 to 17% single-concentration or 9–16% gradient gels.

Electrophoresis and Gel Purification of DAT

1. Electrophorese solubilized photolabeled membranes on an 8% SDS-PAGE polyacrylamide gel. For preparative procedures, we use 1.5-mm-thick 15 × 17 cm BRL gels with a 15-well comb and load 175–200 µl sample/lane. For analytical purposes, we load 25-µl sample either on a large gel or a BioRad mini-gel. Electrophorese large gels overnight at 7 mA and mini-gels for 2 h at 100 mA.
2. Dry the gel and place at least two orientation markers or radioactive dye spots on the gel backing paper. Expose gel to film at –70°C for 1–2 h for preparative gels or overnight for analytical gels.
3. Develop film and identify DAT. On an 8% gel, rat striatal DAT will migrate between the 66 and 97 kDa markers, whereas DATs expressed in cultured cells migrate with a slightly higher M_r, closer to the 97-kDa marker. Use of acrylamide concentrations >10% will result in significantly reduced electrophoretic mobility of DAT. Unequivocal identification of DAT migration can be accomplished by using a parallel sample for immunoprecipitation or pharmacological displacement of labeling.
4. Tape the gel to a light box and align the film on top of the gel by using the phosphorescent orientation marks. Excise the gel pieces containing DAT by using a sharp razor blade.
5. Hydrate the gel pieces in electrophoresis running buffer (25 mM Tris, 192 mM glycine, pH 8.8) and remove paper backing. Store at –20°C, if desired.
6. Place up to six gel pieces in the bottom of a BioRad electroelution chamber fitted with 3500 or 15,000 molecular weight cut-off membrane cap.
7. Fill upper and lower chamber with electrophoresis running buffer and electroelute with a current of 10 mA per chamber for 4–6 h.
8. Disassemble the electrophoresis chamber and collect the sample. Store at –20°C. Sample recovery can be monitored by using a Geiger counter to check input and output radioactivity.

Proteolysis of gel-purified DAT

1. Prepare electroeluted DAT by using protocol outlined in 10.8.3.
2. Prepare protease at twice the intended final concentration in 50 mM Tris-HCl, pH 8.0, (trypsin 0.4–3mg/ml; V8 protease 0.02–1 mg/ml). Combine 25 µl of protease with 25 µl of DAT sample and incubate 1 h at 22°C.
3. Add trypsin inhibitor equal to the highest trypsin concentration and 100 µl sample buffer. If proteolyzed samples will be subjected to immunoprecipitation, use reduced SDS sample buffer (0.5% SDS) and add 1 mg/ml carrier protein.
4. Electrophorese on 15 to 17% single-concentration or 9–16% gradient polyacrylamide gels.

In situ proteolysis

1. Prepare photolabeled membrane suspensions as described in protocol outlined in 10.8.1.

2. Prepare trypsin solution at twice the intended final concentration in 50 mM Tris-HCl, pH 8.0 (1–200 μg/ml trypsin).
3. Combine 25 μl of trypsin with 25 μl of membrane suspension, vortex gently, and incubate at 22°C for 10 min.
4. Add 50 μl trypsin inhibitor in 50 mM Tris-HCl, pH 8.0, equal to highest trypsin concentration and vortex.
5. Centrifuge samples at 11,000 x g for 10 min at 4°C. Remove supernatant and, if desired, save for electrophoresis or immunoprecipitation. Solubilize membrane pellet with 25 μl 0.5% SDS sample buffer for immunoprecipitation.

Western blotting of DAT or DAT fragments

1. Prepare striatal membrane suspensions as described in protocol outlined in 10.8.1, with inclusion of 0.1 μl/mg protease inhibitor cocktail (Sigma) in initial homogenization step.
2. After first centrifugation, resuspend the membranes in 10 ml SP with no protease inhibitor**.** Centrifuge at 12,000 x g for 12 min at 4°C. Suspend membranes in 50 mM Tris, pH 8, at 50 mg/ml o.w.w.
3. Prepare trypsin and DAT ligands or substrates at concentrations three times that of the desired final concentration and hold them on ice.
4. Combine 25 μl membranes and 25 μl of inhibitor or substrate in microcentrifuge tubes, vortex, and incubate for 25–30 min at 22°C to allow binding to equilibrate. Add 25 μl of trypsin, vortex, and incubate for 10 min at 22°C.
5. Add trypsin inhibitor equal to highest trypsin concentration, and place the tubes on ice. Centrifuge samples at 12,000 x g for 10 min at 4°C. Discard the supernatant, solubilize the pellet with 25 μl of sample buffer, and load onto 10% polyacrylamide mini-gels (Bio-Rad MiniProtean III). Electrophorese at 150 volts at room temperature until the dye front approaches the bottom of the gel (~1.5 h).
6. Remove the gel from the plates and place in transfer buffer (10% methanol, 0.01% SDS, 100 mM glycine, 10 mM Tris-HCl) for 2–3 min. Hydrate 0.2 μm PVDF (polyvinylidene difloride) membrane with 100% methanol, wash twice with deionized water, and equilibrate for 1–2 min in transfer buffer.
7. Assemble the transfer cassette, place the transfer unit in an ice-water bath to minimize heat buildup, and transfer for 2 h at 250 mA. Remove the PVDF membrane, rinse with water, and allow to air dry completely (overnight) before proceeding.
8. Rewet the membrane with 100% methanol, rinse with water, and block with 3% bovine serum albumin (BSA) in phosphate buffered saline (PBS, 10 mM sodium phosphate; 150 mM NaCl, pH 7.4) for 1.5 h, followed by 5% nonfat dry milk for 0.5 h.
9. Wash the membrane two times for 5 min with wash buffer (PBS plus 0.1% Igepal CA-630) and once with PBS.
10. Probe the membrane with rDAT monoclonal antibody 16 diluted 1:1000 in 3% BSA/PBS for 1 h at 22°C on a shaker. Wash the membrane four times with wash buffer and once with PBS for 5 min each.

11. Add goat anti-mouse IgG conjugated to alkaline phosphatase diluted 1:5000 in 3% BSA/PBS and incubate on a shaker for 1 h at room temperature. Wash the membrane four times with wash buffer and once with PBS for 5 min each.
12. Develop the membrane with the alkaline phosphatase substrate 5-bromo-4-cholro-3-indolyl phosphate/nitro blue for ~10 min until DAT bands appear and background is at a minimum.
13. Wash the membrane twice with wash buffer and once with PBS for 5 min, and allow to dry. The blot can be scanned for image quantitation and storage.

FOOTNOTES

The chemical abbreviations are as follows: [^{125}I]DEEP ([^{125}I]-1-[2-(diphenylmethoxy)-ethyl]-4-[2-azido-3-iodophenyl)ethyl]piperazine); [^{125}I]AD-96, (4-[2-(diphenylmethoxy)ethyl]-1-[(4-azidophenyl)-methyl]-piperidine; [^{125}I]RTI-82 ([^{125}I]-3-β-(p-chlorophenyl)tropane-2β-carboxylic acid, 4'-azido-3-iodophenylethyl ester); [^{125}I]GAII34, ([^{125}I]N-n-butyl-4-(4"-azido-3"-iodopheny)]-4',4"-difluoro-3α-diphenylmethoxy)-tropane).

ACKNOWLEDGMENTS

We thank Heather Holden for assistance with manuscript preparation and Vickie Swift for artwork.

ANNOTATED REFERENCES

Agoston GE, Vaughan R, Lever JR, Izenwasser S, Terry PD, Newman AH: (1997) A novel photoaffinity label for the dopamine transporter based on N-substituted-4',4''-difluoro-3α-(diphenylmethoxy)tropane. Bioorg Med Chem Lett 7: 3027–3032.

Barker EL, Perlman MA, Adkins EM, Houliha WJ, Pristupa ZB, Niznik HB, Blakely RD (1998) High affinity recognition of serotonin transporter antagonists defined by species-scanning mutagenesis. J Biol Chem 273: 19459–19468.

This paper describes the use of human-drosophila serotonin transporter chimeras to identify domains contributing to antagonist binding, followed by mutagenesis of individual residues to identify specific contact points. This identified Y95 in TM1 of SERT as contributing both positive and negative determinants to binding of mazindol and citalopram.

Barker EL, Moore KR, Rakhshan F, Blakely RD (1999) Transmembrane domain I contributes to the permeation pathway for serotonin and ions in the serotonin transporter. J Neurosci 19:4705–4717.

This study examines the functional role of D98 in TM1 of SERT. This residue, like its homologue D79 in DAT, was found to be essential for transport and binding of cocaine and other antagonists. Substrate analogs designed to compensate for the structural changes in amino acid mutations were used as an additional check for the specificity of mutagenesis effects in substrate recognition.

Berfield JL, Wang LC, Reith MEA (1999) Which form of dopamine is the substrate for the human dopamine transporter: the cationic or the uncharged species? J Biol Chem 274:4876–4882.

Bruss M, Wieland A, Bonisch H (1999) Molecular cloning and functional expression of the mouse dopamine transporter. J Neural Transm 106:657–662.

Buck K, Amara SG (1994) Chimeric dopamine-norepinephrine transporters delineate structural domains influencing selectivity for catecholamines and 1-methyl-4-phenylpyridinium. Proc Natl Acad Sci USA 91:12584–12588.

Studies used DAT-NET chimeras to identify functional domains for substrate action. Substrate affinity was attributed to TMs 1–3, and translocation mechanisms were attributed to TMs 5–8.

Buck K, Amara SG (1995) Structural domains of catecholamine transporter chimeras involved in selective inhibition by antidepressants and psychomotor stimulants. Mol Pharmacol 48:1030–1037.

Studies used DAT-NET chimeras to identify functional domains for binding of antidepressants and psychomotor stimulants. Contributions to cocaine binding were found in TM1, and primary and secondary affinity sites of binding of GBR analogs at DAT were attributed to TMs 4–8 and 1–3, respectively.

Carroll FI, Lewin AH, Boja JW, Kuhar MJ (1992) Cocaine receptor: biochemical characterization and structure-activity relationship of cocaine analogues at the dopamine transporter. J Med Chem 35:969–981.

Classic studies defining structure-activity relationships of cocaine analog binding at DAT.

Carroll FI, Lewin AH, Kuhar MJ (1997). Dopamine transporter uptake blockers: structure-activity relationships. In MEA Reith (ed): Neurotransmitter Transporters: Structure, Function, and Regulation.. Totowa, NJ: Humana Press, 263–296.

Chen J-G, Sachpatzidis A, Rudnick, G (1997) The third transmembrane domain of the serotonin transporter contains residues associated with substrate and cocaine binding. J Biol Chem 272:28321–28327.

Cysteine scanning mutagenesis study showing contributions of residues in TM3 of SERT for transport and cocaine binding. One of the sites is conserved in DAT and NET, suggesting the likelihood for functional similarities of these residues in all three monoamine transporters.

Chen J-G, Rudnick G (2000) Permeation and gating residues in serotonin transporter. Proc Natl Acad Sci USA 97:1044–1049.

Cysteine scanning mutagenesis of TM3 in SERT and NET implicating isoleucine residues at positions 172 and 179 of SERT and 155 of NET in substrate permeation and gating.

Chen N, Ferrer J, Javitch JA, Justice JB Jr (1999) Transport-dependent accessibility of cytoplasmic loop cysteine in the human dopamine transporter. J Biol Chem 275:1608–1614.

Cysteine scanning mutagenesis study of DAT showing increases in sulfhydryl reactivity of Cys 342 during DA transport. Because this residue is believed to be on the internal face of the protein, this is evidence for intracellularly located substrate-induced conformational changes and gating.

Chen N, Justice JB (1998) Cocaine acts as an apparent competitive inhibitor at the outward-facing conformation of the human norepinephrine transporter: kinetic analysis of inward and outward transport. J Neurosci 18:10257–10268.

Use of rotating-disk electrode voltammetry examines influx and tyramine-induced efflux of DA. In combination with pharmocological analysis of cocaine inhibition, the study defines an outward-facing protein conformation as the site of cocaine action.

Chen N, Justice JB (2000) Differential effect of structural modification of human dopamine transporter on the inward and outward transport of dopamine. Brain Res Mol Brain Res 75: 208–15.

Chen N, Reith MEA (2000) Structure and function of the dopamine transporter. Eur J Pharmacol 405:329–339.

An outstanding review summarizing the current status of knowledge on DAT structure–func-

tion properties.

Chen N, Vaughan RA, Reith MEA (2001) The role of conserved tryptophan and acidic residues in the human dopamine transporter as characterized by site-directed mutagenesis. J Neurochem 77:1116–1127.

Danek-Burgess KS, Justice JB (1999) Effect of serine mutations in transmembrane domain 7 of the human norepinephrine transporter on substrate binding and transport. J Neurochem 73:656–664.

Study involves the use of rotating-disk electrode voltametry and site-directed mutagenesis to assess the effects of TM7 serines 354 and 357 on DA transport in NET. The results suggest that these residues are involved in substrate transport but not by a mechanism of direct hydrogen bonding with DA hydroxyls.

Dutta AK, Xiang-Shu F, Vaughan RA, Gaffaney JD, Wang N, Lever JR, Reith MEA (2001) Design, synthesis, and characterization of a novel, 4-[2-(diphenylmethoxy)ethyl]-1-benzyl piperidine-based, dopamine transport photoaffinity label. Life Sci 68:1839–1849.

Ferrer JV, Javitch JA (1998) Cocaine alters the accessibility of endogenous cysteines in putative extracellular and intracellular loops for the human dopamine transporter. Proc Natl Acad Sci USA 95:9238–9243.

Cysteine-scanning mutagenesis studies show that cocaine and DA affected the accessibility of several intra- and extracellular cysteines at positions 90, 135, 306, and 342 in DAT. This finding suggests that antagonists and substrates induce conformational changes that affect the three-dimensional orientation of these residues.

Giros B, Wang Y-M, Suter S, McLeskey SB, Pifl C, Caron MG (1994) Delineation of discrete domains for substrate, cocaine, and tricyclic antidepressant interactions using chimeric dopamine-norepinephrine transporters. J Biol Chem 269:15985–15988.

Studies use DAT-NET chimeras to identify potential functional domains for substrate and inhibitor binding. Uptake mechanisms are attributed to TMs 1–5 and cocaine interactions, to TMs 6–8.

Giros B, Jaber M, Jones S, Wightman RM, Caron MG (1996) Hyperlocomotion and indifference to cocaine and amphetamine in mice lacking the dopamine transporter. Nature (London) 379:606–612.

Grigoriadis DE, Wilson AA, Lew R, Sharkey S, Kuhar MJ (1989) Dopamine transport sites selectively labeled by a novel photoaffinity probe: [^{125}I]DEEP. J Neurosci 9:2664–2670.

Guillory RJ (1989) Design, implementation and pitfalls of photoaffinity labeling experiments. General Principles Pharmac Ther 41:1–25.

Hastrup H, Karlin A, Javitch JA (2001) Symmetrical dimer of the human dopamine transporter revealed by cross-linking Cys-306 at the extracellular end of the sixth transmembrane segment. Proc Natl Acad Sci USA 98:10055–10060.

This study uses chemical cross-linking and mutagenesis to identify dimeric interactions between dopamine transporters mediated by Cys 306 at the extracellular end of TM6.

Huff RA, Vaughan RA, Kuhar MJ, Uhl GR (1997) Phorbol ester increase dopamine transporter phosphorylation and decrease transport V_{max}. J Neurochem 68: 225–232.

Jayanthi LD, Appasundaram S, Malone MD, Ward E, Miller DM, Eppler M, Blakely RD (1998) The *Caenorhabditis elegans* gene T23G5.5 encodes an antidepressant- and cocaine-sensitive dopamine transporter. Mol Pharm 54:601–609.

Johnson KM, Bergmann JS, Kozikowski AP (1992) Cocaine and dopamine differentially protect [^{3}H]mazindol binding sites from alkylation by N-ethylmaleimide. Eur J Pharmacol 227:411–415.

Kiliac F, Rudnick G (2000) Oligomerization of serotonin transporter and its functional consequences. Proc Natl Acad Sci USA 97:3106–3111.

Analysis of serotonin transport by using wild-type sulfhydryl-insensitive and engineered

sulfhydryl-sensitive SERT isoforms, suggesting requirement for oligomerization for transport activity.

Kitayama S, Shimada S, Xu H, Markham L, Donovan D, Uhl GR (1992) Dopamine transporter site-directed mutations differentially alter substrate transport and cocaine binding. Proc Natl Acad Sci USA 89:7782–7785.

Site-directed mutagenesis study of charged and polar residues in TMs 1 and 7 of DAT. Results implicate requirement of D79 in TM1 for DA transport and cocaine analog binding, and involvement of TM7 serines 356 and 359 for DA transport.

Kuhar MJ, Ritz MC, Boja JW (1991) The dopamine hypothesis of the reinforcing properties of cocaine. Trends in Neuroscience 14:299–302.

Lee S-H, Kang S-S, Son H, Lee Y-S (1998) The region of the dopamine transporter encompassing the 3rd transmembrane domain is crucial for function. Biochem Biophys Res Comm 246:347–352.

Species chimera study of bovine and human DAT implicating TM3 for cocaine binding.

Lee S-H, Chang M-Y, Lee K-H, Park BS, Chin HR, Lee Y-S (2000) Importance of valine at position 152 for the substrate transport and 2β-carbomethoxy-3β–(4-fluorophenyl) tropane binding of dopamine transporter. Mol Pharmacol 57:883–889.

Site-directed mutagenesis of TM3 of DAT substituting bovine residues into human DAT. Defines V152 as a critical residue for high-affinity cocaine binding.

Lin Z, Wang W, Kopajtic T, Revay RS, Uhl GR (1999) Dopamine transporter transmembrane phenylalanine mutations can selectively influence dopamine uptake and cocaine analog recognition. Mol Pharmacol 56:434–447.

Lin Z, Itokawa M, Uhl GR (2000) Dopamine transporter proline mutations influence dopamine uptake, cocaine analog recognition and expression. FASEB J 14:715–728.

Loland CJ, Norregaard L, Gether U (1999) Defining proximity relationships in the tertiary structure of the dopamine transporter. J Biol Chem 274:36928–36934.

Identification of residues in EL2, TM7, and TM8 in DAT that create a zinc binding site involved in inhibition of transport but not antagonist binding. This binding site establishes the three-dimensional spatial proximity of these residues when zinc is present.

Masson J, Sagne D, Hanon M, El Mestikaway S (1999) Neurotransmitter transporters in the central nervous system. Pharmacol Rev 51:439–464.

This outstanding comprehensive review covers various aspects of the major neurotransmitter transporters.

Meirgerd SM, Schenk JO (1994) Striatal transporter for dopamine: catechol structure-activity studies and susceptibility to chemical modification. J Neurochem 62:998–1008.

Use of rotating-disk electrode voltametry to examine structural requirements for transport and SAR of DA analog transport.

Miller GW, Gilmor ML, Levey AI (1998) Generation of transporter-specific antibodies. Methods in Enzymology 296:407–422.

Pifl C, Giros B, Caron MG (1993) Dopamine transporter expression confers cytotoxicity to low doses of the parkinsonism-inducing neurotoxin 1-methyl-4-phenylpyridinium. J Neurosci 13:4246–53.

Porzgen P, Park SK, Hirsch J, Sanders MS, Amara SG (2001) The antidepressant-sensitive dopamine transporter in *Drosophila melanogaster*: a primordial carrier for catecholamines. Mol Pharmacol 59: 83–95.

Povlock S, Amara S (1997) The structure and function of norepinephrine, dopamine, and serotonin transporters. In MEA Reith (ed): Neurotransmitter Transporters, Structure, function, and Regulation Totowa, NJ: Humana Press, pp 1–28.

Ritz MC, Lamb RJ, Goldberg SR, Kuhar MJ (1987) Cocaine receptors on dopamine transporters are related to self-administration of cocaine. Science 237:1219–1223.

Schweri M (1990) N-Ethylmaleimide irreversibly inhibits the binding recognition site of ^{3}H threo-(±) methylphenidate to the stimulant binding site. Neuropharmacol 29:901–908.

Shimada S, Kitayama S, Lin C-L, Patel A, Nanthakumar E, Gregor P, Kuhar MJ, Uhl G (1991) Cloning and expression of a cocaine-sensitive dopamine transporter complementary DNA. Science 25:576–578.

Usdin TB, Mezery E, Chen C, Brownstein MJ, Hoffman BJ (1991) Cloning of the cocaine-sensitive bovine dopamine transporter. Proc Natl Acad Sci USA 88:11168–11171.

Vandenbergh DJ, Persico AM, Uhl GR (1992) A human dopamine transporter cDNA predicts reduced glycosylation, displays a novel repetitive element and provides racially-dimorphic TaqI RFLPs. Brain Res Mol Brain Res 15:161–166.

Vaughan R, Uhl G, Kuhar M J(1993) Recognition of dopamine transporters by anti-peptide antibodies. Mol Cell Neurosci 4:209–215.

Vaughan RA, Brown VL, McCoy MT, Kuhar MJ (1996) Species- and brain-region specific dopamine transporters: immunological and glycosylation characteristics. J Neurochem 66:2146–2152.

Vaughan RA (1995) Photoaffinity-labeled ligand binding domains on dopamine transporters identified by peptide mapping. Mol Pharmacol 47:956–964.

Vaughan RA, Kuhar MJ (1996) Dopamine transporter ligand binding domains: Structural and functional properties revealed by limited proteolysis. J Biol Chem 271:21672–21680.

Vaughan RA, Agoston GE, Lever JR, Newman AH (1999) Differential binding of tropane-based photoaffinity ligands on the dopamine transporter. J Neurosci 19:630–636.

Vaughan RA, Gaffaney JD, Lever JR, Reith MEA, Dutta AK (2001) Dual Incorporation of photoaffinity ligands on dopamine transporters implicates proximity of labeled domains. Mol Pharmacol 59: 1157–1164.

CHAPTER 11

MASS SPECTROMETRY OF MEMBRANE TRANSPORT PROTEINS

JULIAN P. WHITELEGGE, H. RONALD KABACK, AND JOHANNES LE COUTRE

11.1 INTRODUCTION

Membrane proteins comprise about one-third of a typical proteome, which represents the full complement of proteins translated in cells. Many critical functions, including cell surface recognition, transport of molecules into and out of cells, transmembrane signaling, as well as electron transport and oxidative phosphorylation, are accomplished by this important class of proteins. Therefore, the study of membrane protein structure and dynamics is a major focus of biochemistry and biophysics today.

Although high-resolution X-ray crystallography and nuclear magnetic resonance have provided structures of some important intrinsic membrane proteins, including those with both α-helical bundles and β-barrel porin motifs, the physicochemical properties of these amphiphilic molecules preclude routine structure determination. Consequently, lower resolution methods that provide structural information as well as techniques that offer insights into membrane protein dynamics provide alternative approaches (Kaback et al., 2001). The emerging discipline of proteomics; that is, assessing the entire protein complement of a cell as an interactive network, places further pressure to provide routine and comprehensive measurements of membrane proteins. This chapter focuses on recent experiments using mass spectrometry to provide structural insights on membrane proteins.

Two of the most significant classes of integral membrane proteins are transport proteins and channels (le Coutre and Kaback, 2001). Transporters use the free energy stored in an electrochemical ion gradient or generated via hydrolysis of adenosine triphosphate (ATP) into a substrate concentration gradient across the membrane. Another family, ion channels, do not transduce energy but function as selective ion-conducting pores, many modulated by gating events, to move ions down an electrochemical gradient. A third class of solute translocating membrane proteins consists of β-barrel-type porins.

Malfunction of certain channels and transporters is significant with respect to human disease, implicated in cystic fibrosis, diabetes, stroke, and antibiotic resistance, to cite but a few examples. Furthermore, at least two of the most widely prescribed drugs in the world, fluoxetine (Prozac®) and omeprazole (Prilosec®), target membrane transporters, whereas others such as Verapamil or Lidocaine are specific Ca^{2+}- or Na^{+}-channel blockers used in the treatment of hypertension or as a local anesthetic, respectively.

Transmembrane Transporters. Edited by Michael Quick

ISBNs: 0-471-06517 (Hardcover); 0-471-43404-3 (Electronic)

11.2 THE LACTOSE PERMEASE OF *ESCHERICHIA COLI*

Lactose permease (lac permease) of *Escherichia coli* is a paradigm for membrane transport proteins. Encoded by the *lacY* gene, the permease is a polytopic membrane protein that catalyzes the cellular accumulation of β-galactosides against a concentration gradient at the expense of a H^+ electrochemical gradient (interior negative and/or alkaline) (reviewed in Kaback et al., 2001; le Coutre and Kaback, 2001). The protein catalyzes the coupled stoichiometric translocation of galactosides and protons. With 417 amino acid residues, the permease spans the cytoplasmic membrane in 12 α-helical segments connected by relatively hydrophilic loops, and both the N- and C-termini are on the cytoplasmic side. *LacY* was the first gene encoding a membrane protein to be cloned and sequenced, which led to its overexpression and purification in a fully functional state, as well as the demonstration that the protein is structurally and functionally a monomer. Thus, all properties of the β-galactoside transport system in *E. coli* can be assigned to a single gene product.

Functional lac permease devoid of eight native Cys residues has been constructed and used for Cys-scanning and site-directed mutagenesis (reviewed in Kaback et al., 2001). Thus, each residue in lac permease has been replaced with a Cys residue or other residues, allowing delineation of the functional groups that play an irreplaceable role in the transport mechanism, as well as creating a library of mutants with a single Cys residue at each position encoded by a cassette *lacY* gene with a unique restriction site about every 100 bp for structure/function studies.

11.3 PRIMARY STRUCTURE, HOMOGENEITY AND PURITY

A well-resolved mass spectrum of an intact protein defines its native covalent state, a profile that summarizes the primary structure and heterogeneity (Whitelegge et al., 1998). Fragmentation of the protein by chemical or proteolytic means and further mass spectrometry provides sequence-dependent information, and tandem mass spectrometry yields true amino acid sequence data and definition of post-translational modifications, thereby solving the primary structure. Mass spectrometry of intrinsic membrane proteins and derived peptides has been difficult because they are often extremely amphipathic in nature. However, various analytical procedures are helping to make such studies routine. Mass spectrometry requires transfer of the protein to the gas phase, and two major ionization techniques are available (Fig. 11.1). Matrix-assisted laser desorption ionization, time-of-flight mass spectrometry (MALDI-TOF) uses laser excitation to desorb dry samples co-crystallized with a suitable small molecule matrix such as cinnamic acid which usually also donates charges to the analyte. Electrospray ionization (ESI) involves nebulization of liquid sample at high voltage to produce multiply charged protein ions. The superior accuracy and resolution, as well as the ability to couple HPLC separation directly to the nebulizer, make ESI the preferred technique, although the sensitivity and tolerance of complex mixtures afforded by MALDI-TOF provides certain advantages.

Because both ionization techniques are generally intolerant of salt, detergent, and lipid, it is necessary to remove such contaminants before mass spectrometry. This process often involves precipitation of the protein with organic solvents and solubilization with high concentrations of organic acids, although chromatography is sometimes suitable for purification without prior precipitation (Whitelegge et al., 1998). Lac permease is precip-

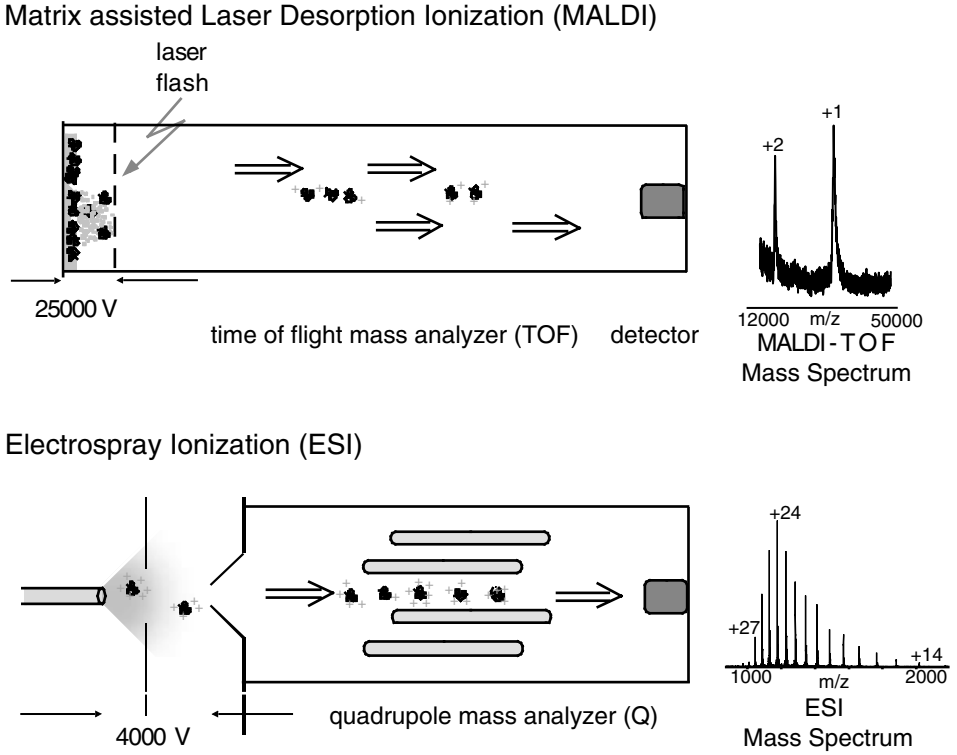

Figure 11.1. Protein and Peptide Mass Spectrometry. Two ionization techniques allow application of mass spectrometry to biological macromolecules. MALDI uses laser excitation, usually UV, to rapidly excite matrix crystals containing the analyte. Some analyte is transferred to the gas phase during desorption, and molecules carrying charge (ions) are accelerated toward the mass analyzer via application of a large potential difference. A time-of-flight mass analyzer is most commonly used because of its ability to detect the very high m/z that typically results as a consequence of MALDI's characteristic single charging. A spectrum of a 31,500 Da membrane protein shows some doubly charged ions as well. ESI involves spraying a solution of analyte from a charged nebulizer, generating multiply charged ions at atmospheric pressure. The ions are then taken into the mass analyzer for measurement of mass to charge ratio. A traditional quadrupole mass analyzer is shown, although ion-trap, ion cyclotron resonance, and time-of-flight analyzers are available with ESI sources. A typical protein mass spectrum shows a family of signals derived from molecular ions carrying from 14 to 27 charges (protons).

itated at the interface of a chloroform/methanol/water phase separation (Wessel and Flugge, 1984) and solubilized with 90% formic acid, which provides a relatively pure form of the protein compatible with positive-ion mass spectrometry.

MALDI-TOF

Permease prepared as described can be mixed with matrix solution or applied to a thin layer of dried matrix (Cadene and Chair, 2000) for successful MALDI-TOF analysis. The spectrum is dominated by the singly charged ion ($M+H^+$), while smaller amounts of doubly and triply charged ions are present. Because the mass spectrometer measures the mass

to charge ratio (m/z), multiple charging has the effect of moving the signal to much lower m/z values ($M+2H^+/2$ and $M+3H^+/3$). Mass accuracy is in the range 0.1–0.3%, and resolution is insufficient to detect subtle modifications, such as oxidation (+16 Da) or formylation (+28 Da). Nevertheless, the sensitive readout of mass and purity is useful.

Liquid-chromatography (LC) ESI-MS

Permease solubilized in formic acid can be analyzed by ESI. Although most membrane proteins can be retained and eluted with a gradient of 5–100% isopropanol in the presence of 60% formic acid (Whitelegge et al., 1998), the permease requires 90% formic acid and the complete absence of isopropanol for retention by the column (PLRP/S, Polymer Labs, Amherst, MA, USA). These conditions shorten column life, and the prolonged exposure of the protein to 90% formic acid leads to the appearance of covalent formylation adducts that increase the measured mass by 100–150 Da and appearance of excessive heterogeneity (not shown).

Consequently, a protocol for size-exclusion chromatography (SEC) has been developed, which requires initial solubilization of permease in 90% formic acid, followed by immediate transfer to a less-reactive solvent, chloroform/methanol/1% aqueous formic acid (4/4/1; v/v), used initially by Fearnley and Walker (1996) for analysis of mitochondrial inner membrane proteins by ESI. Chromatography under these conditions quickly separates the permease from the high concentration of formic acid in the loading sample while providing continued solubility. The spectrum is practically devoid of formylation adducts while the initiating *N*-formylmethionine is retained (Whitelegge et al., 1999; le Coutre et al., 2000). The SEC-MS technique has proved effective for many different membrane (and other) proteins (le Coutre et al., 2000; Zhang et al., 2001). The main disadvantage is the lack of chromatographic resolution in SEC, such that samples must be quite highly purified before injection. Analysis of the oligomeric spinach thylakoid cytochrome b_6f complex exhibits co-elution of five larger subunits between 17–35 kDa, which have to be distinguished in the mass spectrum, close to the limit of complexity that may be resolved where ion series overlap (Zhang et al., 2001).

ESI is the preferred ionization technique because of superior mass accuracy (typically better than 0.01% error) and resolution. Ligand-sensitive Cys modifications in lac permease with *N*-ethylmaleimide and 2-(4'-maleimidylanilino)naphthalene-6-sulfonic acid have been monitored by ESI-MS (Whitelegge et al., 1999; le Coutre et al., 2000). Of course, modifications that change mass less dramatically (disulfide formation, –2 Da; isoaspartate formation, +1 Da) must be identified with smaller peptides derived from the parent protein. In cases of excessive heterogeneity, such as multiple, variable glycosylation, multiply charged molecular ions from different charge states may overlap and lead to an ESI spectrum that cannot always be interpreted. Under these circumstances, MALDI-TOF is used because the singly charged ions are nearly always resolved from the doubly charged species.

11.4 SECONDARY/TERTIARY STRUCTURAL INFORMATION USING MASS SPECTROMETRY

As mentioned previously, structural analysis of intrinsic membrane proteins is problematic; even where structures have been solved by X-ray crystallography, further insight into

protein dynamics unavailable from a static crystalline form is needed. Mass spectrometry is now being used to provide such insights. Site-specific cleavage (protease, chemical) has been used to probe membrane protein structure in different states. A good example is the mammalian Na^+/K^+ ATPase, where site-specific chemical cleavage is providing otherwise unattainable structural insights (Shimon et al., 1998; Goldshleger and Karlish, 1999; Patchornik et al., 2000; Shin et al., 2001; Goldshleger et al., 2001a). Crosslinking, either with native thiols, engineered thiols, or specific crosslinking reagents or combinations of these, is being applied successfully to rhodopsin (Cai et al., 2001; Hwa et al., 2001), and these studies have been extended to investigate functional binding partners (Cai et al., 2001b; Itoh et al., 2001).

11.5 STRUCTURAL DYNAMICS USING MASS SPECTROMETRY

The approaches discussed so far typically rely on separation of protein from lipids/detergents in aqueous acidic organic solvent mixtures. However, as reported in a recent study, membrane-spanning peptides in defined lipid vesicle suspensions were delivered to the ESI source, yielding discrete peptide ions that were resolved from the lipids by virtue of their m/z differences (Demmers et al., 2000; Demmers et al., 2001). Thus, it has been possible to perform hydrogen/deuterium (H/D) exchange experiments on membrane bound peptides in situ by using mass spectrometry, thereby raising the prospect of using ESI-MS for H/D exchange experiments of larger native membrane proteins. Unfortunately, attempts to perform such experiments with intact transmembrane proteins have so far yielded spectra only by addition of 50% trifluoroethanol to the sample immediately before measurement (Demmers and Heck, unpublished observations). The organic solvent is presumably necessary to disrupt the bilayer, dissociate lipids from the proteins, and monomerize the protein. Such disruption may potentially denature the protein and lead to H/D exchange, which limits the value of the approach. Konnerman and colleagues have developed stopped-flow ESI-MS for studying rapid kinetics, so it may be possible to use this technique to rapidly add organic solvent prior to MS so that minimal backbone H/D exchange occurs (Kolakowski et al., 2000).

11.6 OXIDATION OF SPECIFIC RESIDUES IN THE PERMEASE: A CASE STUDY

The high degree of accuracy of the LC-MS technology with membrane proteins provides unparalleled possibilities in the determination of reaction mechanisms and structural features on the molecular and atomic level (Kaback et al., 2001; Whitelegge et al., 1999; le Coutre et al., 2000).

The structural model of the permease, as derived from a variety of biophysical and biochemical techniques, makes detailed predictions for every charged residue within the membrane (Kaback et al., 2001). Although four of these residues—Asp240 (helix VII), Lys 319 (helix X), Asp237 (helix VII), and Lys358—are not essential for active transport; neutral replacement of any one inactivates the permease. Remarkably, however, double neutral replacements for Asp240 and Lys319 or Asp237 and Lys358 yield permease with significant activity. Single neutral replacements inactivate because an unpaired charge is left in the low dielectric of the membrane. However, activity is recovered when the

charge-pair partner is also neutralized. Furthermore, Asp237 and Lys358 can be reversed with no effect on activity. Interestingly, although double neutral replacement for Asp237 and Lys358 yields highly active permease, only ~10% of the normal complement of permease is found in the membrane. Thus, the Asp237-Lys358 charge pair is important for insertion of the protein into the membrane. In contrast, double neutral replacement of Asp240 and Lys319 yields permease with ~30% wild-type activity, but reversal of the residues leads to complete inactivation, and double neutral replacement has no effect on insertion of the mutant permease into the membrane. Finally, recent experiments show that the distance between positions 240 and 319 increases by ~4 Å on binding of ligand, and crosslinking Cys residues at the two positions blocks transport (Zhang et al., 2002).

Replacement of Asp240 with a Cys residue in the Cys-less permease (single-Cys D240C) abolishes ability to catalyze active transport (Sahin-Toth and Kaback, 1993). Oxidation of the mutant with peroxide leads to recovery of transport activity. However, prolonged exposure to the oxidant renders the permease inactive again (Voss et al., 1998). It has been proposed that during the course of oxidation Cys 240 is progressively oxidized from the sulphenic via a sulphinic to a sulphonic acid, with the sulphinic acid being isosteric with Asp. Because mutant D240C has only one Cys residue, the molecular weight of the protein should increase by 16 a.m.u. with each oxidation step (Fig. 11.3).

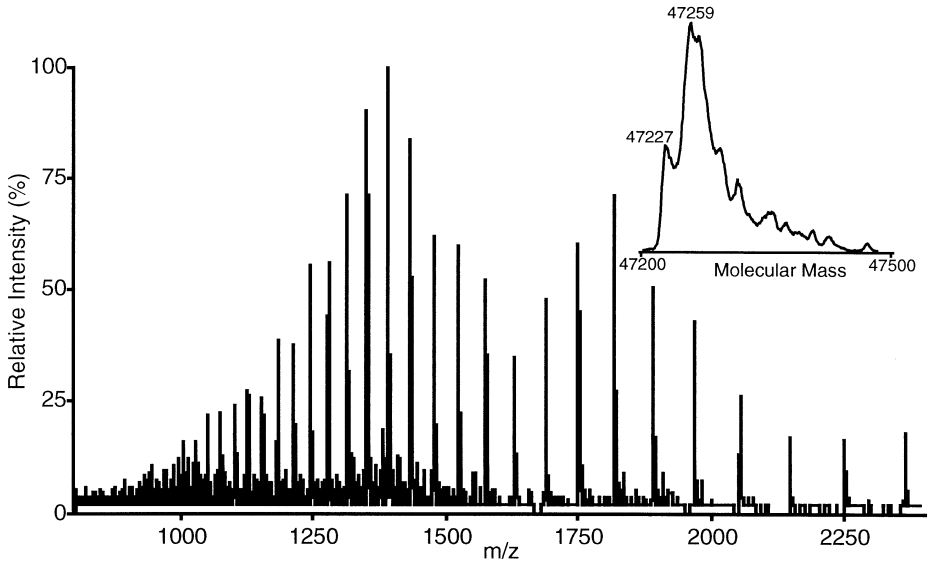

Figure 11.2. Electrospray-ionization mass spectrum of E. coli lac permease. Samples of permease (mutant D240C) were precipitated in an aqueous chloroform/methanol phase separation and dissolved in 90% formic acid before immediate size-exclusion chromatography and ESI mass spectrometry. The charge state distribution reveals ions carrying from 20 to 50 protons with each having a distinct m/z. Deconvolution (Mac Spec 3.3, Applied Biosystems, Foster City, CA) reveals the molecular mass profile of the "zero-charged" species. This sample was treated with 40 mM H_2O_2 for 15 min, before precipitation, which resulted in oxidation of most of the protein from 47,227 Da to 47,259 Da. The ability to partially resolve covalent modifications of this nature make ESI mass spectrometry preferable to MALDI for larger proteins.

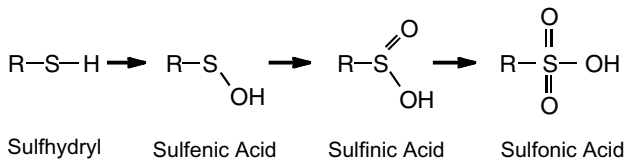

Figure 11.3. Progressive oxidation of a Cys residue. Starting from the cysteinyl thiol group, three oxidation steps lead to sulphonic acid with the addition of one oxygen atom each per reaction step.

As shown, gradual oxidation can be followed on the atomic level, and the different oxidation states can be correlated with activity. Purified D240C permease is oxidized with 40 mM H_2O_2, followed by quenching with 0.8 M thiodiglycol, and the sample is subjected to LC-MS as described. In Figure 11.2, a typical ion spectrum for the D240C mutant is shown after mild oxidation in the presence of H_2O_2. Deconvoluted mass peaks for several time points after initiation of oxidation are shown in Figure 11.4. Clearly the mass peaks shift from a molecular weight of 47,227 without oxidation to a molecular weight of 47,275 after 1 h of oxidation. Moreover, comparing individual mass peaks with each other (e.g., 30 s with 5 min) demonstrates that the increase in molecular weight occurs in discrete steps of 16 a.m.u., thus reflecting the covalent addition of oxygen to the permease. The deduced degree of oxidation (i.e., number of oxygen added) is shown in Figure 11.4 for mutant D240C and Cys-less permease by using 40 and 400 mM H_2O_2. To ensure that oxidation indeed occurs at Cys240 and to rule out nonspecific oxidation of the protein, control measurements with Cys-less permease protein were performed. Importantly, incubation of the Cys-less mutant with 40 mM H_2O_2 does not alter the molecular weight of the protein, which indicates that no oxidation of other residues occurs. This is not the case when a higher concentration of H_2O_2 (400 mM) is used where it is apparent that five covalent oxygen atoms are added to the protein. Therefore, on oxidizing single-Cys D240C permease with 40 mM H_2O_2 only the Cys at position 240 is oxidized. Oxidation of Cys240 occurs instantaneously to a mass equal to 2 oxygen atoms, which corresponds to a sulfinic acid. The addition of one oxygen atom to form the sulfenic acid is in reversible equilibrium with the sulfhydryl group and therefore not detected after quenching with thiodiglycol. Finally, within the course of 1 h, the sulfinic acid is oxidized to the final state, a sulfonic acid with three covalently added oxygen atoms.

To correlate the oxidation states of D240 with the activity of the permease, active transport measurements were performed on right-side-out vesicles after oxidation for given time intervals (Fig. 11.5). Only after 5-min or 60-min exposure to H_2O_2 is transport activity observed. Clearly, the activity of the protein diminishes between 5-min and 60-min exposure to H_2O_2, which indicates that the active species is a sulfinic acid and not the sulphonic acid. Based on the decay in activity, it was suggested previously that the species that rescues activity might be the sulfinic acid (Voss et al., 1998). Strikingly, transport activity in single-Cys D240C permease can also be rescued by negatively charged thiol reagents (Sahin-Toth and Kaback, 1993; Dunten et al., 1993) or alkylsulfonates (Frillingos and Kaback, 1996), indicating that at position 240 both a negative charge and a specific steric configuration are required for active transport. Figure 11.6 shows the D240-K319 salt bridge and its pivotal position between the residues involved in proton translocation and sugar binding.

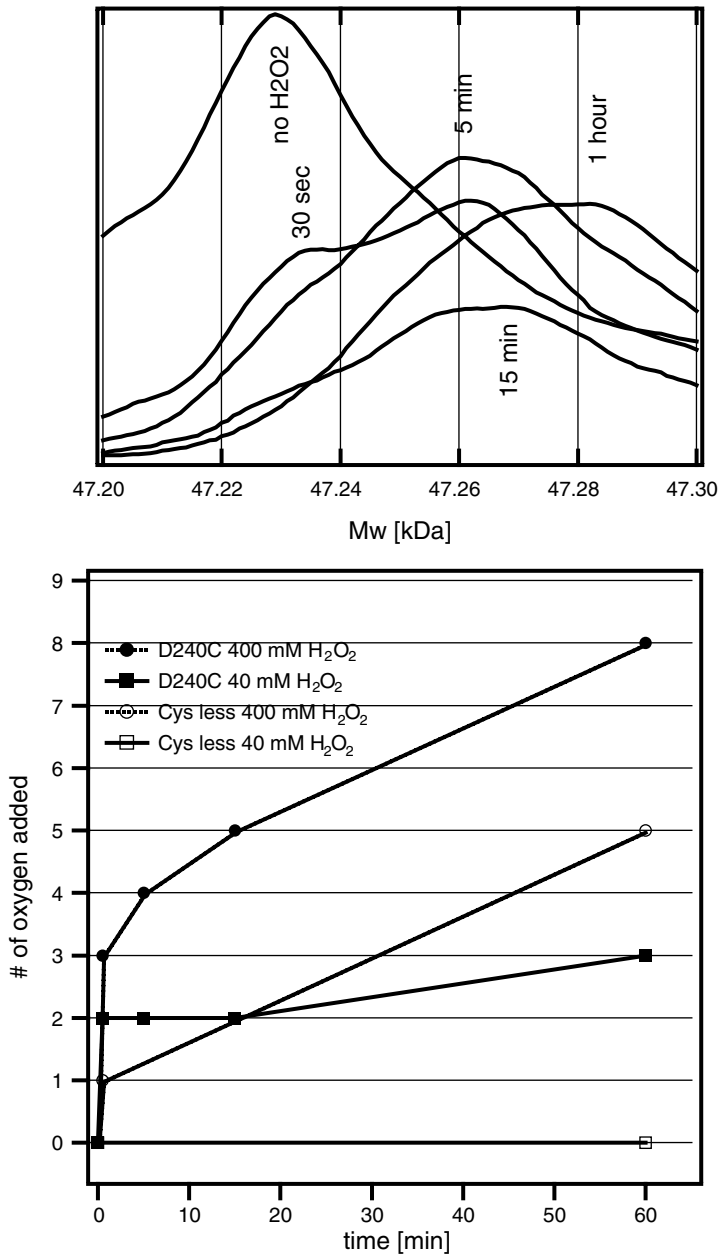

Figure 11.4. Time course of oxidation of mutant D240C. Top: Deconvoluted mass peaks of mutant D240C shift towards higher molecular weight with prolonged exposure to 40 mM H_2O_2. Importantly, increase of the molecular weight under the conditions described occurs in discrete steps of 16 a.m.u., reflecting oxidation of C240. Bottom: Time course of the increase in molecular weight of D240C permease after exposure to 40 mM H_2O_2 indicates formation of a sulphonic acid at position 240. Under the same conditions, Cys-less permease exhibits no increase in mass, indicating no oxidation. At higher concentrations of H_2O_2 (400 mM), nonspecific oxidation of Cys-less permease clearly occurs.

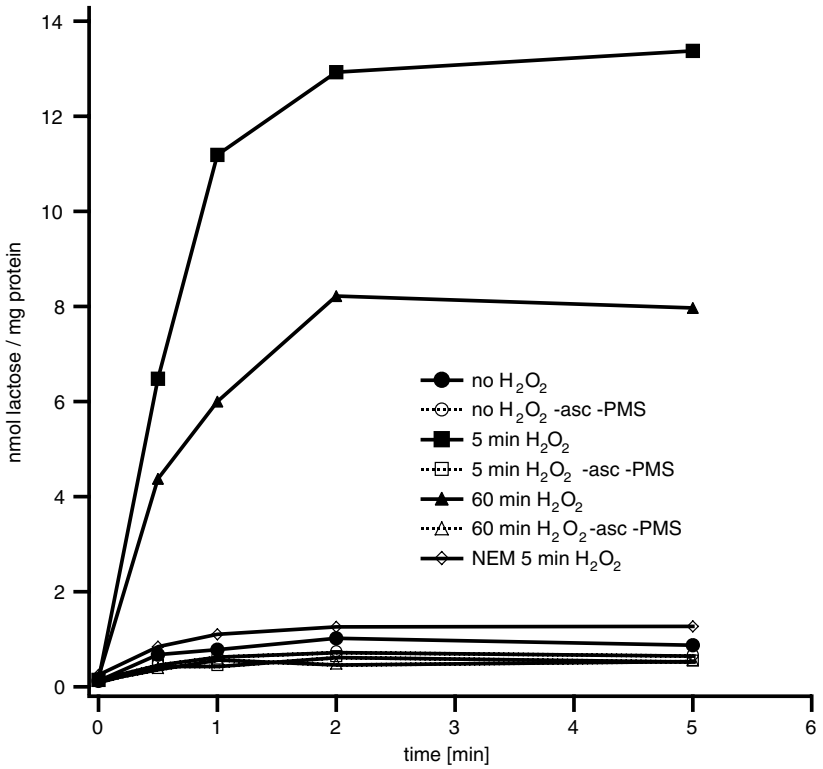

Figure 11.5. Active transport by mutant D240C in different oxidation states. Right-side-out vesicles were oxidized with 40 mM H_2O_2, and the reaction was quenched with 0.8 M thiodiglycol at the time indicated (Voss et al., 1998). Samples were washed and resuspended in 100 mM KP_i, (pH 7.5)/10 mM $MgSO_4$, at a protein concentration of 4 mg/ml. For each time point, 50 µl vesicles were incubated at room temperature with 20 mM ascorbate and 0.1 mM phenazine methosulfate under oxygen for 5 min. [1-^{14}C]Lactose was added to a final concentration of 0.4 mM at t = 0 and incubated was continued under oxygen for 0, 0.5, 1, 3, and 5 min. Reactions were quenched, filtered, and washed with 3 ml quenching buffer [100 mM KP_I (pH 5.5)/100 mM $LiCl_2$]. Activity after 5 min is comparable with wild-type levels and decreases with increasing oxidation time, indicating that the active species is a sulfinic acid at position 240.

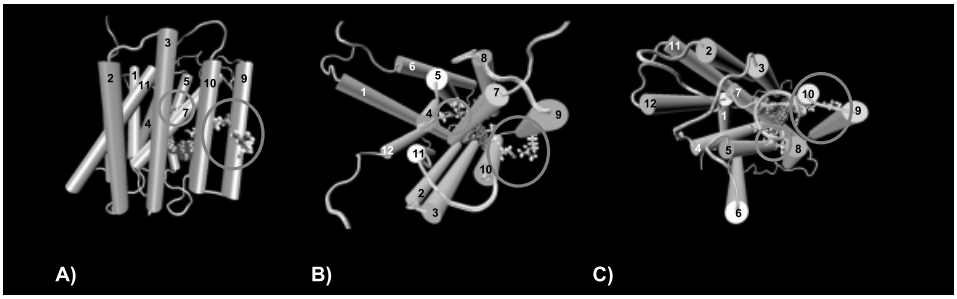

Figure 11.6. Helix packing model of lac permease (**A**) sideview with cytoplasmic side on top, (**B**) cytoplasmic view, and (**C**) periplasmic view. The D240/K319 salt bridge, shown in red and green, is located between the residues involved in proton translocation (E325 and R302 encircled in red) and the residues involved in substrate binding (E126 and R144 encircled in green). The additional irreplaceable residues E269 and H322 are obstructed by the helices. (See color insert.)

REFERENCES

Cadene M, Chait BT (2000): A robust, detergent-friendly method for mass spectrometric analysis of integral membrane proteins. Anal Chem 72:5655–5658.

Cai K, Itoh Y, Khorana HG (2001a): Mapping of contact sites in complex formation between transducin and light-activated rhodopsin by covalent crosslinking: use of a photoactivatable reagent. Proc Natl Acad Sci USA 98:4877–4882.

Cai K, Klein-Seetharaman J, Altenbach C, Hubbell WL, Khorana HG (2001b): Probing the dark state tertiary structure in the cytoplasmic domain of rhodopsin: proximities between amino acids deduced from spontaneous disulfide bond formation between cysteine pairs engineered in cytoplasmic loops 1, 3, and 4. Biochemistry 40:12479–12485.

Demmers JA, Haverkamp J, Heck AJ, Koeppe RE, Killian JA (2000): Electrospray ionization mass spectrometry as a tool to analyze hydrogen/deuterium exchange kinetics of transmembrane peptides in lipid bilayers. Proc Natl Acad Sci USA 97:3189–3194.

Demmers JA, van Duijn E, Haverkamp J, Greathouse DV, Koeppe RE, Heck AJ, et al. (2001): Interfacial positioning and stability of transmembrane peptides in lipid bilayers studied by combining hydrogen/deuterium exchange and mass spectrometry. J Biol Chem 276:34501–34508.

Dunten RL, Sahin-Toth M, Kaback HR (1993): Role of the charge pair aspartic acid-237-lysine-358 in the lactose permease of *Escherichia coli*. Biochemistry 32:3139–3145.

Fearnley IM, Walker JE (1996): Analysis of hydrophobic proteins and peptides by electrospray ionization MS. Biochem Soc Trans 24:912–917.

Frillingos S, Kaback HR (1996): Chemical rescue of Asp237—>Ala and Lys358—>Ala mutants in the lactose permease of *Escherichia coli*. Biochemistry 35:13363–13367.

Goldshleger R, Karlish SJ (1999): The energy transduction mechanism of Na,K-ATPase studied with iron-catalyzed oxidative cleavage. J Biol Chem 274:16213–16221.

Goldshleger R, Patchornik G, Shimon MB, Tal DM, Post RL, Karlish SJ (2001): Structural organization and energy transduction mechanism of Na+,K+-ATPase studied with transition metal-catalyzed oxidative cleavage. J Bioenerg Biomembr 33:387–399.

Hwa J, Klein-Seetharaman J, Khorana HG (2001): Structure and function in rhodopsin: mass spectrometric identification of the abnormal intradiscal disulfide bond in misfolded retinitis pigmentosa mutants. Proc Natl Acad Sci USA 98:4872–4876.

Itoh Y, Cai K, Khorana HG (2001): Mapping of contact sites in complex formation between light-activated rhodopsin and transducin by covalent crosslinking: use of a chemically preactivated reagent. Proc Natl Acad Sci USA 98:4883–4887.

Kaback HR, Sahin-Toth M, Weinglass AB (2001): The kamikaze approach to membrane transport. Nat Rev Mol Cell Biol 2:610–620.

Kolakowski BM, Simmons DA, Konermann L (2000): Stopped-flow electrospray ionization mass spectrometry: a new method for studying chemical reaction kinetics in solution. Rapid Commun Mass Spectrom 14:772–776.

Konings WN, Barnes EM, Jr., Kaback HR (1971): Mechanisms of active transport in isolated membrane vesicles. 2. The coupling of reduced phenazine methosulfate to the concentrative uptake of beta-galactosides and amino acids. J Biol Chem 246:5857–5861.

le Coutre J, Kaback HR (2001): Structure function relationships of integral membrane proteins: membrane transporters vs channels. Biopolymers–Pept Sci 55:297–307.

le Coutre J, Whitelegge JP, Gross A, Turk E, Wright EM, Kaback HR et al. (2000): Proteomics on full-length membrane proteins using mass spectrometry. Biochemistry 39:4237–4242.

Patchornik G, Goldshleger R, Karlish SJ (2000): The complex ATP-Fe(2+) serves as a specific affinity cleavage reagent in ATP-Mg(2+) sites of Na,K-ATPase: Altered ligation of Fe(2+) (Mg(2+)) ions accompanies the E(1)—>E(2) conformational change. Proc Natl Acad Sci USA 97:11954–11959.

Sahin-Toth M, Kaback HR (1993): Properties of interacting aspartic acid and lysine residues in the lactose permease of *Escherichia coli*. Biochemistry 32:10027–10035.

Shimon MB, Goldshleger R, Karlish SJ (1998): Specific Cu2+-catalyzed oxidative cleavage of Na,K-ATPase at the extracellular surface. J Biol Chem 273:34190–34195.

Shin JM, Goldshleger R, Munson KB, Sachs G, Karlish SJ (2001): Selective Fe2+-catalyzed oxidative cleavage of gastric H+,K+-ATPase: implications for the energy transduction mechanism of P-type cation pumps. J Biol Chem 276:48440–48450.

Voss J, Sun J, Venkatesan P, Kaback HR (1998): Sulfhydryl oxidation of mutants with cysteine in place of acidic residues in the lactose permease. Biochemistry 37:8191–8196.

Wessel D, Flugge UI (1984): A method for the quantitative recovery of protein in dilute solution in the presence of detergents and lipids. Anal Biochem 138:141–143.

Whitelegge JP, Gundersen CB, Faull KF (1998): Electrospray-ionization mass spectrometry of intact intrinsic membrane proteins. Protein Sci 7:1423–1430.

Whitelegge JP, le Coutre J, Lee JC, Engel CK, Prive GG, Faull KF et al. (1999): Toward the bilayer proteome, electrospray ionization-mass spectrometry of large, intact transmembrane proteins. Proc Natl Acad Sci USA 96:10695–10698.

Zhang W, Guan L, Kaback HR (2002): Helices VII and X in the lactose permease of *Escherichia coli*: Proximity and ligand-induced distance changes. J Mol Biol 315:53–62.

Zhang H, Whitelegge JP, Cramer WA (2001): Ferredoxin: NADP+ oxidoreductase is a subunit of the chloroplast cytochrome b6f complex. J Biol Chem 276:38159–38165.

CHAPTER 12

AMPEROMETRIC RECORDING OF AMPHETAMINE-INDUCED DOPAMINE EFFLUX

DAVID SULZER, KRISTOPHER M. KAHLIG, YVONNE SCHMITZ, CHRISTINE SAUNDERS, AND AURELIO GALLI

12.1 INTRODUCTION

Amphetamine (AMPH) and its derivatives are the only widely used class of drugs known to elicit transmitter release by a non-exocytic mechanism. AMPH was first synthesized by Edeleau in 1887 (Ellinwood et al., 2000), and the name of the drug was derived as an acronym for alpha-methyl-phenethyl-amine. The mechanisms by which AMPH acts to induce monoamine release include actions at plasmalemmal uptake transporters and synaptic vesicles. In addition, AMPH inhibits monoamine oxidase and stimulates catecholamine synthesis.

Although some of the initial steps of AMPH's action have been clarified, the mechanism driving AMPH-induced reverse transport of dopamine (DA) at the plasma membrane and synaptic vesicle membranes remains controversial. The purpose of this chapter is to highlight some of the data contributed by electrochemical recording on the effects of AMPH on synaptic vesicles, and on AMPH-induced DA release, with particular emphasis on the role of the DA transporter (DAT).

12.2 EFFECTS OF AMPH ON QUANTAL TRANSMITTER RELEASE

It has long been observed that AMPH, tyramine, and other psychostimulants release monoamines from isolated chromaffin vesicles (Carlsson et al., 1963). AMPH crosses the plasma membrane by diffusion (Zaczek et al., 1991a; Zaczek et al., 1991b; Jones et al., 1998), and as a substrate for the DAT (Zaczek et al., 1991a; Zaczek et al., 1991b; Wall et al., 1995; Sitte et al., 1998). Then, AMPH redistributes catecholamines from intracellular stores (e.g., vesicles) to the cytosol (Sulzer and Rayport, 1990; Rudnick and Wall, 1992a). However, only in the past decade have efforts more clearly demonstrated the role of these cytoplasmic compartments in the action of this drug.

There are at least three hypotheses proposed to explain the mechanism by which AMPH redistributes vesicular monoamines to the cytosol. According to the *weak base hypothesis*, AMPH redistributes monoamines to the cytosol by collapsing the proton gradi-

Transmembrane Transporters. Edited by Michael Quick

ISBNs: 0-471-06517 (Hardcover); 0-471-43404-3 (Electronic)

ent responsible for accumulation of transmitter into the vesicle (Sulzer and Rayport, 1990; Rudnick and Wall, 1992a). Alternatively, as a substrate for the vesicular monoamine transporters, VMAT1 and VMAT2 (Gonzalez et al., 1994; Peter et al., 1994; Erickson et al., 1996), AMPH competitively inhibits monoamine uptake. Because of the leak of vesicular transmitter from the vesicles (Floor et al., 1995; Pothos et al., 2000), this inhibition of monoamine uptake would result in net reduction of vesicular monoamine pools. Finally, binding of nontransported AMPH to the cytosolic face of the VMAT apparently induces release of transmitter from vesicles (Floor and Meng, 1996), although the mechanism of this phenomenon remains obscure.

Both VMAT2 and the predominantly peripheral transporter VMAT1 bind AMPH and its derivatives (Gonzalez et al., 1994). In membranes derived from cell lines expressing VMAT1 or VMAT2, the uptake of labeled monoamine was inhibited by methAMPH (Peter et al., 1994). Similarly, when the transporters were expressed in a fibroblast cell line, the accumulation of labeled serotonin was inhibited by AMPH, phenethylamine, methylenedioxymethamphetamine (MDMA, "Ecstasy"), and fenfluramine (Erickson et al., 1996). In both studies, with the exception of fenfluramine, VMAT2-expressing cells were more sensitive to AMPH and its derivatives than VMAT1-expressing cells. *d*-AMPH was several-fold more effective than its *l*-stereoisomer.

If AMPH redistributes DA from synaptic vesicles, an important prediction is that the drug should decrease the amount of transmitter released per vesicle fusion event; that is, the "quantal size." This prediction became testable with the development of carbon fiber electrodes (see Techniques) capable of measuring monoamine release (Gonon et al., 1981), followed by rapid amperometric methods capable of recording quantal exocytosis, first from chromaffin cells (Wightman et al., 1991), and later from axon terminals of cultured neurons (Pothos et al., 1998) or from neuronal somata (Bruns and Jahn, 1995; Chen et al., 1995; Hochstetler et al., 2000). In these experiments, AMPH provided the first instance of a manipulation that affected the quantal size of catecholamine release, as amperometric recordings demonstrated that 10 μM of AMPH for 10 min decreased quantal size by 50% in PC12 cells (Sulzer et al., 1995). In addition, quantal release from the giant DA neuron of *Planorbis corneus* demonstrated the existence of two classes of DA vesicles that were depleted differentially by AMPH (Anderson et al., 1998): At low concentrations, AMPH preferentially depleted the large vesicles, whereas at higher concentrations, AMPH depleted small vesicles more than large vesicles.

As a side note, rapid perfusion of AMPH as well as nonpsychostimulant weak bases induced quantal exocytosis from chromaffin cells (Mundorf et al., 1999). It was suggested that exocytosis was due to a weak base mechanism, as the accumulation of intravesicular calcium by chromaffin vesicles is also dependent on H^+ gradients (Bulenda and Gratzl, 1985). The level of calcium redistributed from the vesicles by AMPH may be sufficient to induce vesicular exocytosis. However, AMPH has not been observed to induce exocytosis from central neurons (Jones et al., 1998; Schmitz et al., 2001).

12.3 EFFECTS OF AMPH ON DAT: PRESENT CONTROVERSIES

AMPH-induced release of DA from presynaptic nerve terminals occurs by carrier-mediated release, which is not dependent on action potential depolarization, is only slightly calcium-dependent (Pierce and Kalivas, 1997), and has been labeled "reverse transport". One of the models used to explain the effect of AMPH is the facilitated exchange diffu-

sion model (Fischer and Cho, 1979; Burnette et al., 1996). This model assumes that AMPH-induced DA release is mediated by the DAT and that it results from translocation of AMPH into the cell followed by a counter movement of DA out to the extracellular compartment. By acting as a substrate, AMPH increases the number of inward-facing transporter binding sites and thus increases the rate of reverse transport. In contrast, the weak base or vesicle depletion model (Sulzer and Rayport, 1990; Sulzer et al., 1992) proposes that the elevated cytoplasmic DA concentration and its altered gradient across the plasma membrane caused by AMPH induce a reversed transport of DA. This process is independent of AMPH interacting with the DAT (Sulzer et al., 1995). It should also be noted that apart from its ability to elicit reverse transport as a competitive substrate, AMPH increases the apparent Km of DAT (Schmitz et al., 2001).

In 1998, Jones et al. suggested that, although vesicular depletion is rate-limiting, the facilitated exchange diffusion mechanism is critical for producing DA release by AMPH (Jones et al., 1998). This conclusion was based mainly on the observation that DA displacement from the vesicle by Ro4-1248 and reserpine-like compounds do not cause evident DA efflux. Therefore, simply increasing the intracellular DA concentration was not enough to cause DA bulk overflow. AMPH has to interact with the DAT.

Although some of the initial steps of the AMPH action have been clarified, the mechanism driving the AMPH-induced reverse transport of DA at the plasma membrane is still controversial. Direct measurements of DA outside single cells can provide unique information about such dynamic processes, including DAT-mediated DA efflux and AMPH-induced reverse transport of DA. Electrochemical methods can be used to monitor extracellular DA levels. The following sections deal with electrophysiological recordings of DAT activity and amperometric measurements of DAT-mediated DA release.

Structure of the DAT. DAT is a member of a gene family that includes transporters for norepinephrine (NE), DA, gamma-aminobutyric acid (GABA), serotonin (5-HT), glycine, proline, and taurine. All members share structural features and mechanisms suggestive of a common ancestor. The cDNA for the human DAT encodes a primary sequence of 620 amino acids. Hydrophobicity analysis of the sequence predicted the presence of 12 membrane-spanning segments, which are presumed to be α-helices (Giros et al., 1992; Ferrer and Javitch, 1998). In the predicted topology, the amino and the carboxy terminals are both cytoplasmic. The most highly conserved sequences are thought to encompass the 12 hydrophobic (membrane-spanning) domains and flanking amino acids. The presence of three or four potential glycosylation sites in the large second extracellular loop is consistent with the identification of a photoaffinity-labeled DAT glycoprotein (Bannon et al., 1995). Putative consensus sequences for various protein kinases are present on the DAT. These sites have been shown to be involved in its trafficking and regulation (Vaughan et al., 1997; Zhu et al., 1997; Daniels and Amara, 1999; Melikian and Buckley, 1999; Pristupa et al., 1998).

Mechanism of DAT Function

Dopamine transporters operate by coupling the transmembrane translocation of substrate to the movement of driving ions down pre-established electrochemical gradients. Substrates of the DAT include DA, AMPH, and tyramine. The most widely held concept of how co-transporters function is founded on the alternating access model (Jardetzky, 1966), in which the binding sites for substrates and co-substrates are alternately exposed to extracellular or cytoplasmic environments via conformational changes in the trans-

porter protein. The thermodynamic work of the transporter is accomplished by coupling the flux of substrate to the movement of co-transported ions down their electrochemical gradients. The stoichiometry inferred from transporter studies on DAT-expressing cells and membrane vesicles is $2Na^+ : 1Cl^- : 1DA^+$ (Gu et al., 1994). Because DA is a monovalent cation at physiological pH, no ions are counter-transported; the transport cycle moves two net positive charges, which it does at slow rates (~1 cycle/s).

In HEK-293 cells stably transfected with the human DAT cDNA (hDAT cells) (Ferrer and Javitch, 1998), it is possible to record currents generated by DAT activity by using the patch-clamp technique in the whole-cell configuration (Saunders et al., 2000). At a fixed voltage, neurotransmitter transporter currents increase with increasing substrate concentrations. These currents have been used in the past to evaluate Michaelis–Menten kinetics (Galli et al., 1995; Sonders et al., 1997; Petersen and DeFelice, 1999). At saturating substrate concentrations, the DA-induced hDAT-mediated current increases exponentially at negative membrane potentials without reaching saturation (Sonders et al., 1997; Saunders et al., 2000). The hDAT-mediated currents are sensitive to common blockers of [^{3}H]DA uptake such as mazindol (MZ) and cocaine (Sonders et al., 1997; Sitte et al., 1998; Saunders et al., 2000). Most interestingly, AMPH can stimulate an hDAT-mediated current (Sonders et al., 1997; Sitte et al., 1998; Saunders et al., 2000). Similar to the DA-induced current, the AMPH-mediated current is blocked by MZ (Saunders et al., 2000) and cocaine, as well as by replacing extracellular Na^+ with Li^+ (Sonders et al., 1997).

Recent electrophysiological studies of native as well as cloned neurotransmitter transporters revealed that they could produce brief and rare channel-like openings comparable with those generated by ligand-gated ion channels (Sonders and Amara, 1996). Models for this anomalous mode of neurotransmitter transporters have been established (Galli et al., 1996; Lin et al., 1996; DeFelice and Blakely, 1996), in which substrate, Na^+ and Cl^- induce the carrier to transport in the alternating access mode (Fig. 12.1A, B), and rarely switching to a channel-like mode (Fig. 12.1C). The alternating access model assumes that a state transition for the substrate permeation (A↔B) results in the transport of a single neurotransmitter molecule (Fig. 12.1A, B). The channel-like mode (Fig. 12.1C) is a low-probability event that consists of hundreds of ions crossing the membrane (by using the transporter aqueous pore), down their electrochemical gradients (DeFelice and Blakely, 1996; Beckman and Quick, 1998).

Over the past few years, researchers have tried to understand whether the aqueous pore of a transporter could represent a permeation pathway for its own substrates. Electrophysiological techniques such as patch-clamp were used to monitor channel-like activity of the neurotransmitter transporters (DeFelice and Blakely, 1996; DeFelice and Galli, 1998).

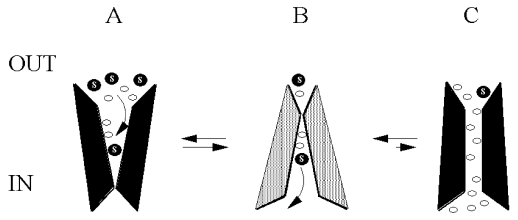

Figure 12.1. Model for neurotransmitter transporters function.

These strategies, however, did not reveal information about the substrate movement *per se*. To test whether the channel-like activity is an active state in the transport process, experiments were performed by using the patch-clamp technique combined with amperometric measurements. The amperometric technique measures the concentration of catecholamine by oxidation/reduction reactions. In Galli et al. (1998), this technique was adopted to provide the first nonradioactive measurement of transport flux across isolated membrane patches. This study demonstrated that the channel-like activity of the norepinephrine transporter (NERT)is a low-probability event and an active state of the transporter, meaning that it mediates reuptake of transmitter. Therefore, occasionally, transmitter can cross the cell membrane through the NERT aqueous pore (Galli et al., 1998), at least in this expression system.

In addition to mediating the uptake of transmitter into nerve terminals, transporters can also cause non-Ca^{++}-mediated efflux of the transmitter from the nerve terminal (Attwell et al., 1993). There are essentially two mechanisms that elicit to reverse transport from neurons: first, by changing the transmembrane ion gradients and voltage; and, second, *via* the actions of pharmacological compounds, such as AMPH. Lately, we have been studying the reverse transport mechanism of DAT in real-time at the single-cell level. For this purpose, we used the patch-clamp technique to monitor outward currents generated by the reverse transport mechanism of the hDAT combined with amperometry to record DAT-mediated DA efflux.

DAT-mediated DA Efflux

To simultaneously record DA efflux and hDAT-mediated outward currents from a single cell, hDAT cells were voltage-clamped with a whole-cell patch pipette, while an amperometric electrode was placed onto the cell membrane (Fig. 12.2A). In order to stimulate DA efflux, the whole-cell electrode was filled with a solution containing (in mM): 90 NaCl, 40 KCl, 0.1 $CaCl_2$, 2 $MgCl_2$, 1.1 EGTA [ethyleneglycol-bis(β-aminoethyl ether)-N,N,N',N'-tetraacetic acid], 10 HEPES [*N*-(2-hydroxyethyl) piperazine-2'-(2-ethanesulphonic acid)], and 30 dextrose, adjusted to pH 7.35 and 270 mOsm with 2 mM DA. The bath solution contained (in mM): 130 NaCl, 1.3 KCl, 1.3 KH_2PO_4, 0.5 $MgSO_2$, 1.5 $CaCl_2$, 10 HEPES, and 34 dextrose, adjusted to pH 7.35 and 300 mOsm. The amperometric electrode, touching the cell membrane, measures the concentration of catecholamine by oxidation/reduction reactions. The electrode was held at +700 mV, a potential greater than the redox potential of DA. Stepping the membrane voltage between –40 and + 100 mV with the whole-cell pipette from a holding potential of –20 mV, we recorded hDAT-mediated currents blocked by bath application of 5 μM MZ. To isolate the hDAT current, we subtracted the current recorded in the presence of external MZ from the current recorded in the control condition (high intracellular Na^+ and DA). At membrane potentials more positive than –25 mV (data not shown), the hDAT current becomes outward. Panel B shows an example of the transporter current at –40 (inward current) and +80 mV (outward current). At the same time, we monitored DA efflux with the amperometric electrode (panel C). We isolated the hDAT-mediated DA efflux by subtracting background currents (traces recorded in the presence of 5 μM MZ) from amperometric traces recorded in control conditions (high intracellular Na^+ and DA), for each potential tested. By convention, oxidation current is plotted positive and reduction current is plotted negative. Therefore, an upward deflection in the amperometric currents corresponds to an outward flux of DA.

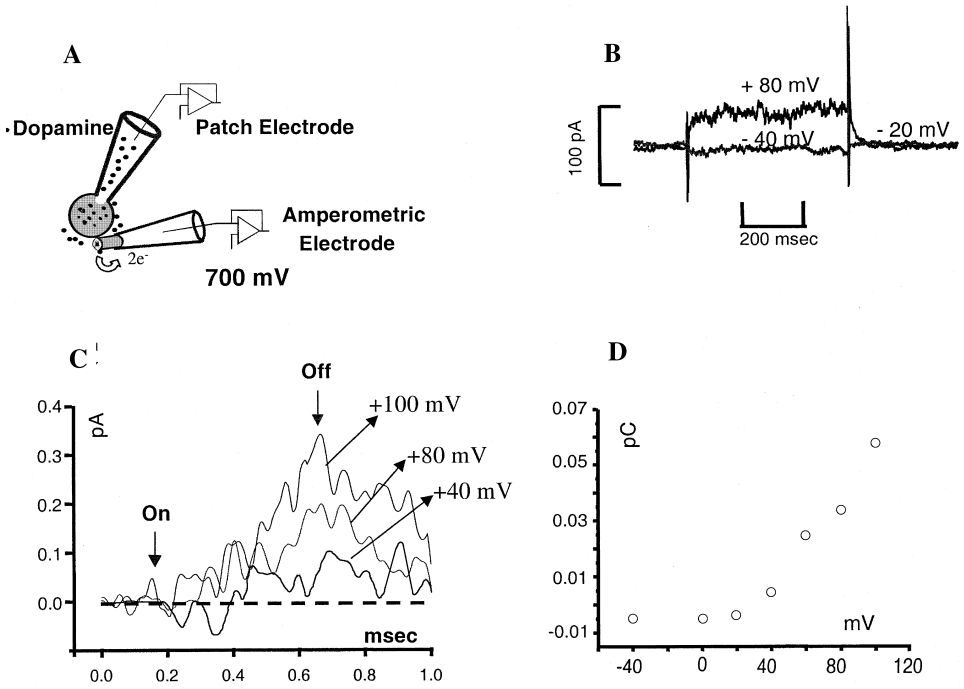

Figure 12.2. DAT-mediated DA efflux is voltage-dependent.

Panel C shows oxidation currents obtained by voltage clamping the hDAT cell at different voltages (+40, +80, and +100 mV) with the whole-cell pipette (the same cell, as in panel B). At the "on" of the voltage step, for voltages more positive than +20 mV, the amperometric electrode recorded an oxidation current (positive) that increased during the entire duration of the voltage step. This positive current is indicative of DA efflux. At the "off" of the voltage step, the amperometric current relaxed to baseline. The "on" and "off" of the voltage step are defined by the vertical arrows in panel C. Moving the carbon fiber away from the patch caused the oxidative response to become smaller and slower. As expected for DA oxidation, the oxidative response diminished when we reduced the carbon fiber voltage to +300 mV, and disappeared completely on further reduction.

In panel D, we plot the integral of the oxidation current (Q) during the voltage step (500 ms) against the test voltage applied to the cell. The relationship between Q and the number of the DA molecules reacted is given by Faraday's law: $Q = zeM$. In this equation, Q is the total charge involved in the redox reaction (Coulombs), M is the number of molecules reacted, and z is the number of electronic charges (e) transferred per reacted molecule. For DA, under these experimental conditions, z is equal to 2 (Ciolkowski et al., 1994; Sulzer and Pothos, 2000). Therefore, DA efflux increased at positive voltages without reaching saturation in the range of voltages studied. In contrast, DA efflux saturates at negative voltages. Previous studies had indicated that DA uptake (influx) is voltage-dependent (Sonders et al., 1997). However, whether catecholamine efflux is voltage-dependent is still under debate (Chen et al., 1998).

12.4 MECHANISM OF AMPH-INDUCED DA EFFLUX

To induce DA efflux, AMPH has to interact with the DAT (Jones et al., 1998). The interaction of AMPH with DAT has been viewed by several groups as the ability of AMPH to stimulate inward ion fluxes through the DAT (Sitte et al., 1998; Pifl and Singer, 1999). In these models, substrates of the DAT such as AMPH would induce an inward current, most likely produced by a flow of Na^+ into the cell, sufficient to stimulate efflux of intracellular substrate. In agreement with this, multiple studies have suggested a strong relationship between intracellular Na^+ and the mechanism of substrate-induced monoamine efflux (Rudnick and Wall, 1992a; Rudnick and Wall, 1992b; Chen et al., 1998; Sitte et al., 1998; Pifl and Singer, 1999). Moreover, Chen et al. have shown for the human norepinephrine transporter (hNET), that DA efflux mediated by hNET is stimulated by raising the intracellular Na^+ concentration with ouabain (Chen et al., 1998). Under their experimental conditions, DA efflux is not affected by depolarized membrane potentials obtained with high extracellular K^+. These results are consistent with a model involving facilitated exchange between external substrates and internal DA and do not involve net movement of charges in each transport cycle of the carrier, and is therefore likely to be voltage-independent (Chen et al., 1998).

Recently, intriguing new experiments have challenged a simple model of facilitated exchange diffusion (Sitte et al., 1998; Pifl and Singer, 1999; Chen and Justice, 2000; Cowell et al., 2000). In particular, results from Sitte et al. (1998) support the hypothesis that the releasing properties of DAT substrates are not proportionally related to their ability to be taken up by the DAT, but instead, to their ability to elicit DAT-mediated inward currents (see above).

Once more, it is conceivable that the substrate-induced influx of Na^+ ions could enhance the probability of reverse transport (Sitte et al., 1998; Sitte et al., 2001). This would agree with the channel theory of neurotransmitter transporters in which the aqueous pore of the transporter gated by the substrate allows for a large number of ions to cross the plasma membrane (DeFelice and Blakely, 1996; Sonders and Amara, 1996; Beckman and Quick, 1998). These novel hypotheses require experiments in which the intracellular ionic composition and cell membrane potential are carefully controlled while DA efflux is monitored. Combining the patch-clamp technique with amperometry promises an approach to define whether AMPH-induced DA-efflux through the DAT is an electrogenic process, and whether it is dependent on the intracellular Na^+ concentration and cell membrane voltage.

12.5 TECHNIQUES

Construction of Carbon Fiber Electrodes

Materials

Borosilicate capillaries (A-M Systems, Carlsborg, WA, USA, #6270), 1.2 mm × 0.68 mm, stored in 70% ethanol

5-μm carbon fiber (Amoco Polymers, BP Solvay, Houston, TX, USA)

Epoxy resin (Epoxy Technology, Billerica, MA, #301)

Electrode puller (Sutter Instrument, model P-97)
Vacuum line, vacuum flask, and fine gauge plastic tubing
Fine dissection scissors, scalpel
Acetone, beaker, hot plate
Oven
Electrode beveler (Sutter Instrument, Novato, CA; BV-10)

Manufacturing Steps

1. Cut a strand of fiber ~5 inches in length, and separate a single carbon fiber from the strand. Use magnifying glass and bright light for better visibility.
2. Connect a glass capillary to the vacuum line, and suck a single carbon fiber into the capillary while pressing one end of the fiber down. Remove the capillary containing the fiber from the vacuum line. Cut the ends of the fiber with a scalpel.
3. Pull the capillary containing a fiber into two electrodes by using a puller. After pulling, but before removing the electrodes from the puller, cut the fiber between the two halves with fine dissection scissors. Then remove the pulled electrodes and cut the fibers with the dissection scissors to about 1/2 inch from the tip.
4. To insulate the electrode, use an epoxy resin prepared in a glass test tube according to the manufacturer's instructions. We store the resin in desiccant; however, we find that the epoxy is adequate for only five months once opened. Dip the electrode tips into the epoxy for 20 or 30 s so that epoxy enters the tip by capillary action. Heat acetone in a beaker until it begins to boil, and clean off excess epoxy by dipping the electrode two or three times into the hot acetone.
5. Place the electrodes upright and heat overnight in a 100°C oven.
6. Examine the electrodes under a dissection microscope and cut off the excess fiber extending from the glass capillary tip with a scalpel.
7. The electrode is beveled before use at 30–45°. Some electrodes can be cut and beveled several times.

ACKNOWLEDGMENTS

We thank Drs. Lynette C. Dawns, Alan Frazer, William Clarke, Charles France, and Louis J. DeFelice for helpful editorial comments. This work was supported by National Alliance for Research on Schizophrenia and Depression Young Investigator (A.G.) and Independent Investigator (D.S.) Awards, and by grants from the National Institute of Drug Abuse (DA13975; A.G.)(07418; D.S.).

REFERENCES

Anderson BB, Chen G, Gutman DA, Ewing AG (1998): Dopamine levels of two classes of vesicles are differentially depleted by amphetamine. Brain Research 788:294–301.

Attwell D, Barbour B, Szatkowski M (1993): Nonvesicular release of neurotransmitter. Neuron 11:401–407.

Bannon MJ, Granneman JG, Kapatos G (1995): The dopamine transporter: potential involvement in neuropsychiatric disorders. *In* Bloom FE, Kupfer, DJ (eds): Psychopharmacology: The Fourth Generation of Progress. New York: Raven Press, Ltd. pp 179–188.

Beckman ML, Quick MW (1998): Neurotransmitter transporters: regulators of function and functional regulation. J Membr Biol 164:1–10.

Bruns D, Jahn R (1995): Real-time measurement of transmitter release from single synaptic vesicles. Nature (London) 377:62–65.

Bulenda D, Gratzl M (1985): Matrix free Ca2+ in isolated chromaffin vesicles. Biochemistry 24:7760–7765.

Burnette WB, Bailey MD, Kukoyi S, Blakely RD, Trowbridge CG, Justice JB Jr (1996): Human norepinephrine transporter kinetics using rotating disk electrode voltammetry. Anal Chem 68:2932–2938.

Carlsson A, Hillarp N, Waldeck B (1963): Analysis of the Mg++-ATP dependent storage mechanism in the amine granules of the adrenal medulla. Acta Physiol Scand 59: Suppl 215.

Chen G, Gavin PF, Luo G, Ewing AG (1995): Observation and quantitation of exocytosis from the cell body of a fully developed neuron in Planorbis corneus. J Neurosci 15:7747–7755.

Chen N, Justice JB Jr. (2000): Differential effect of structural modification of human dopamine transporter on the inward and outward transport of dopamine. Mol Brain Res 75:208–215.

Chen N, Trowbridge CG, Justice JB Jr (1998): Voltammetric studies on mechanisms of dopamine efflux in the presence of substrates and cocaine from cells expressing human norepinephrine transporter. J Neurochem 71:653–665.

Ciolkowski EL, Maness KM, Cahill PS, Wightman RM (1994): Disproportionation during electrooxidation of catecholamines at carbon-fiber microelectrodes. Anal Chem 66:3611–3617.

Cowell RM, Kantor L, Hewlett GH, Frey KA, Gnegy ME (2000): Dopamine transporter antagonists block phorbol ester-induced dopamine release and dopamine transporter phosphorylation in striatal synaptosomes. Eur J Pharmacol 389:59–65.

Daniels GM, Amara SG (1999): Regulated trafficking of the human dopamine transporter: clathrin-mediated internalization and lysosomal degradation in response to phorbol esters. J Biol Chem 274:35794–35801.

DeFelice LJ, Blakely RD (1996): Pore models for transporters? Biophys J 70:579–580.

DeFelice LJ, Galli A (1998): Electrophysiological analysis of transporter function. Adv Pharmacol 42:186–90.

Ellinwood E, King G, Lee T (2000): Chronic amphetamine use and abuse. In Bloom F and Kupfer D (eds): Psychopharmacology. New York: Raven Press.

Erickson JD, Schafer MK, Bonner TI, Eiden LE, Weihe E (1996): Distinct pharmacological properties and distribution in neurons and endocrine cells of two isoforms of the human vesicular monoamine transporter. Proc Natl Acad Sci USA 93:5166–5171.

Ferrer JV, Javitch JA (1998): Cocaine alters the accessibility of endogenous cysteines in putative extracellular and intracellular loops of the human dopamine transporter. Proc Natl Acad Sci USA 95:9238–9243.

Fischer JF, Cho AK (1979): Chemical release of dopamine from striatal homogenates: evidence for an exchange diffusion model. J Pharm & Exper Therap 208:203–209.

Floor E, Leventhal PS, Wang Y, Meng L, Chen W (1995): Dynamic storage of dopamine in rat brain synaptic vesicles in vitro. J Neurochem 64:689–699.

Floor E, Meng L (1996): Amphetamine releases dopamine from synaptic vesicles by dual mechanisms. Neuroscience Letters 215:53–56.

Galli A, Blakely RD, DeFelice LJ (1996): Norepinephrine transporters have channel modes of conduction. Proc Natl Acad Sci USA 93:8671–8676.

Galli A, Blakely RD, DeFelice LJ (1998): Patch-clamp and amperometric recordings from norepinephrine transporters: channel activity and voltage-dependent uptake [see comments]. Proc Natl Acad Sci USA 95:13260–13265.

Galli A, DeFelice LJ, Duke BJ, Moore KR, Blakely RD (1995): Sodium-dependent norepinephrine-induced currents in norepinephrine-transporter-transfected HEK-293 cells blocked by cocaine and antidepressants. J Exp Biol 198:2197–2212.

Giros B, el Mestikawy S, Godinot N, Zheng K, Han H, Yang-Feng T, Caron MG (1992): Cloning, pharmacological characterization, and chromosome assignment of the human dopamine transporter. Mol Pharm 42:383–390.

Gonon F, Buda M, Cespuglio R, Jouvet M, Pujol JF (1981): Voltammetry in the striatum of chronic freely moving rats: detection of catechols and ascorbic acid. Brain Res 223:69–80.

Gonzalez, AM, Walther D, Pazos A, Uhl GR (1994): Synaptic vesicular monoamine transporter expression: distribution and pharmacologic profile. Brain Res Mol Brain Res 22:219–226.

Gu H, Wall SC, Rudnick G (1994): Stable expression of biogenic amine transporters reveals differences in inhibitor sensitivity, kinetics, and ion dependence. J Biol Chem 269:7124–7130.

Hochstetler SE, Puopolo M, Gustincich S, Raviola S, Wightman RM (2000): Real-time amperometric measurements of zeptomole quantities of dopamine released from neurons. Anal Chem 72:489–496.

Jardetzky O (1966): Simple allosteric model for membrane pumps. Nature (London) 211:969–970.

Jones SR, Gainetdinov RR, Wightman RM, Caron MG (1998): Mechanisms of amphetamine action revealed in mice lacking the dopamine transporter. J Neurosci 18:1979–1986.

Lin F, Lester HA, Mager S (1996): Single-channel currents produced by the serotonin transporter and analysis of a mutation affecting ion permeation. Biophys J 71:3126–3135.

Melikian HE, Buckley KM (1999): Membrane trafficking regulates the activity of the human dopamine transporter. J Neurosci 19:7699–7710.

Mundorf ML, Hochstetler SE, Wightman RM (1999): Amine weak bases disrupt vesicular storage and promote exocytosis in chromaffin cells. J Neurochem 73:2397–2405.

Peter D, Jimenez J, Liu Y, Kim J, Edwards RH (1994): The chromaffin granule and synaptic vesicle amine transporters differ in substrate recognition and sensitivity to inhibitors. J Biol Chem 269:7231–7237.

Petersen CI, DeFelice LJ (1999): Ionic interactions in the *Drosophila* serotonin transporter identify it as a serotonin channel. Nat Neurosci 2:605–610.

Pierce RC, Kalivas PW (1997): Repeated cocaine modifies the mechanism by which amphetamine releases dopamine. J Neurosci 17:3254–3261.

Pifl C, Singer EA (1999): Ion dependence of carrier-mediated release in dopamine or norepinephrine transporter-transfected cells questions the hypothesis of facilitated exchange diffusion. Mol Pharm 56:1047–1054.

Pothos EN, Davila V, Sulzer D (1998): Presynaptic recording of quanta from midbrain dopamine neurons and modulation of the quantal size. J Neurosci 18:4106–4118.

Pothos EN, Larsen KE, Krantz DE, Liu Y, Haycock JW, Setlik W, Gershon MD, Edwards RH, Sulzer D (2000): Synaptic vesicle transporter expression regulates vesicle phenotype and quantal size. J Neurosci 20:7297–7306.

Pristupa ZB, McConkey F, Liu F, Man HY, Lee FJ, Wang YT, Niznik HB (1998): Protein kinase-mediated bidirectional trafficking and functional regulation of the human dopamine transporter. Synapse 30:79–87.

Rudnick G, Wall SC (1992a): The molecular mechanism of "ecstasy" [3,4-methylenedioxymethamphetamine (MDMA)]: serotonin transporters are targets for MDMA-induced serotonin release. Proc Natl Acad Sci USA 89:1817–1821.

Rudnick G, Wall SC (1992b): p-Chloroamphetamine induces serotonin release through serotonin transporters. Biochemistry 31:6710–6718.

Saunders C, Ferrer JV, Shi L, Chen J, Merrill G, Lamb ME, Leeb-Lundberg LMF, Carvelli L, Javitch JA, Galli A (2000): Amphetamine-induced loss of human dopamine transporter activity: An internalization-dependent and cocaine-sensitive mechanism. Proc Natl Acad Sci USA 97: 6850–6855.

Schmitz Y, Lee CJ, Schmauss C, Gonon F, Sulzer D (2001): Amphetamine distorts stimulation-dependent dopamine overflow: effects on D2 autoreceptors, transporters, and synaptic vesicle stores. J Neurosci 21:5916–5924.

Sitte HH, Hiptmair B, Zwach J, Pifl C, Singer EA, Scholze P (2001): Quantitative analysis of inward and outward transport rates in cells stably expressing the cloned human serotonin transporter: inconsistencies with the hypothesis of facilitated exchange diffusion. Mol Pharm 59:1129–1137.

Sitte HH, Huck S, Reither H, Boehm S, Singer EA, Pifl C (1998): Carrier-mediated release, transport rates, and charge transfer induced by amphetamine, tyramine, and dopamine in mammalian cells transfected with the human dopamine transporter. J Neurochem 71:1289–1297.

Sonders MS, Amara SG (1996): Channels in transporters. Cur Opin Neurobio 6:294–302.

Sonders MS, Zhu SJ, Zahniser NR, Kavanaugh MP, Amara SG (1997): Multiple ionic conductances of the human dopamine transporter: the actions of dopamine and psychostimulants. J Neurosci 17:960–974.

Sulzer D, Chen TK, Lau YY, Kristensen H, Rayport S, Ewing A (1995): Amphetamine redistributes dopamine from synaptic vesicles to the cytosol and promotes reverse transport. J Neurosci 15:4102–4108.

Sulzer D, Pothos E, Sung HM, Maidment NT, Hoebel BG, Rayport S (1992): Weak base model of amphetamine action. Ann NY Aca Sci 654:525–528.

Sulzer D, Pothos EN (2000): Regulation of quantal size by presynaptic mechanisms. Rev Neurosci 11:159–212.

Sulzer D, Rayport S (1990): Amphetamine and other psychostimulants reduce pH gradients in midbrain dopaminergic neurons and chromaffin granules: a mechanism of action. Neuron. 5:797–808.

Vaughan RA, Huff RA, Uhl GR, Kuhar MJ (1997): Protein kinase C-mediated phosphorylation and functional regulation of dopamine transporters in striatal synaptosomes. J Biol Chem 272:15541–15546.

Wall SC, Gu H, Rudnick G (1995): Biogenic amine flux mediated by cloned transporters stably expressed in cultured cell lines: amphetamine specificity for inhibition and efflux. Mol Pharm 47:544–550.

Wightman RM, Jankowski JA, Kennedy RT, Kawagoe KT, Schroeder TJ, Leszczyszyn DJ, Near JA, Diliberto EJ Jr, Viveros OH (1991): Temporally resolved catecholamine spikes correspond to single vesicle release from individual chromaffin cells. Proc Natl Acad Sci USA 88:10754–10758.

Zaczek R, Culp S, De Souza EB (1991a): Interactions of [3H]amphetamine with rat brain synaptosomes. II. Active transport. J Pharm & Exp Ther 257:830–835.

Zaczek R, Culp S, Goldberg H, McCann DJ, De Souza EB (1991b): Interactions of [3H]amphetamine with rat brain synaptosomes. I. Saturable sequestration. J Pharm & Exp Ther 257:820–829.

Zhu SJ, Kavanaugh MP, Sonders MS, Amara SG, Zahniser NR (1997): Activation of protein kinase C inhibits uptake, currents and binding associated with the human dopamine transporter expressed in Xenopus oocytes. J Pharm & Exp Ther 282:1358–1365.

CHAPTER 13

VOLTAGE CLAMP AND FLUOROMETRIC TECHNIQUES FOR STUDYING GLUTAMATE TRANSPORTER FUNCTION

ANASTASSIOS V. TZINGOUNIS, H. PETER LARSSON,
AND MICHAEL P. KAVANAUGH

13.1 INTRODUCTION

Despite the important roles of glutamate transporters in synaptic transmission and neuropathophysiology, many fundamental structure-function questions about these molecules remain. Early radiolabel uptake measurements in brain tissue demonstrated a specific glutamate and aspartate uptake activity that was sodium-dependent and involved potassium counter-transport (Balcar and Johnston, 1972; Kanner and Sharon, 1978). A gene family encoding five glutamate transporters has been cloned, and electrophysiological recording from native tissues and transfected cell lines has shown that glutamate is co-transported with three sodium ions and one proton, whereas one potassium ion is counter-transported (for review, see Danbolt, 2001). Despite progress in characterizing the pharmacology and equilibrium thermodynamics, many important physiological and biophysical questions remain about the detailed nature of the transport process. For example, uncertainty exists about the substrate binding order, the transporter cycling rate, the identity of the rate-limiting step of the cycle, and the probability that a molecule of bound transmitter is transported compared with unbinding to the outside. Fundamental questions also exist about the protein gating, such as which region of the glutamate transporters undergoes conformational changes during glutamate transport? Developing a model to accommodate the transporters' complex behavior requires the use of multiple techniques. In this chapter we will review some current approaches useful in elucidating these structural and functional properties. We will focus on: i) the use of site-specific fluorescent labeling to detect conformational changes in the transport cycle and to identify structural domains involved in alternating access gating during the transport cycle, ii) the use of concentration jumps to gain kinetic information, and iii) the use of computer modeling to integrate experimental data into self-consistent structure-function models.

13.2 VOLTAGE CLAMP FLUOROMETRY (VCF) METHOD

Voltage clamp fluorometry (VCF) is a method used to detect and identify conformational changes in a membrane transport protein. VCF takes advantage of the intrinsic environ-

Transmembrane Transporters. Edited by Michael Quick

ISBNs: 0-471-06517 (Hardcover); 0-471-43404-3 (Electronic)

mental sensitivity of a fluorescent probe. To conduct VCF, glutamate transporters are covalently labeled with a probe and changes in fluorescence are measured during manipulations that specifically influence the glutamate transport cycle. If the residue that the fluorescent probe is attached to (or protein structures in the area around that residue) undergoes a conformational change, this often leads to a detectable change in fluorescence as a consequence of the change in the environment of the probe. For example, before the conformational change the probe could be exposed to the extracellular solution and after the conformational change buried in the protein. The fluorescent probe, generally attached to a site-specifically introduced cysteine residue, can thus report conformational changes that influence the environment around that residue during some phase of the glutamate transport cycle.

The labeled transporters are voltage-clamped, and the electrogenic transport current is measured in response to voltage steps and substrate applications. The fluorescence is measured simultaneously in order to correlate the kinetics and voltage dependence of the fluorescence to the kinetics and voltage dependence of the electrogenic current. These measurements can thus provide information correlating conformational changes in the transporters with charge-moving steps in the transport cycle. An example of such data reflecting conformational changes in the C-terminal region of the EAAT3 (Excitatory Amino Acid Transporter 3) transporter is shown below. VCF can also be used to monitor specific changes in accessibility as described below.

Fluorescence labeling protocol

Cysteines are introduced by site-directed mutagenesis into putative extracellular loops or pore regions of glutamate transporters, one at a time, and are analyzed after reaction with cysteine-specific fluorescent probes. The cysteines can be introduced into a wild-type (rather than Cys-less) EAAT3 background, because EAAT3 does not react with any of the fluorescence probes tested to date. This is verified by comparing fluorescence in oocytes expressing transporters before and after labeling and must of course be determined for each transporter to be studied. The mutant transporters are labeled with cysteine-specific fluorescent probes, such as tetra-methyl rhodamine maleimide (TMRM) (Mannuzzu et al, 1996; Cha and Bezanilla, 1997; Loo et al., 1998; Baker et al., 1998; Li and Lester, 2000), Oregon Green maleimide, or different Alexa maleimide probes (Molecular Probes; see www.probes.com/handbook/toc.html for a list of probes and a description of their uses).

The following labeling protocol (modified from Mannuzzu et al., 1996) is used to minimize labeling of cysteine residues in endogenous proteins (which are relatively abundant in Xenopus oocyte membranes) in order to maximize the signal-to-noise ratio for the fluorescence signal (i.e., TMRM labeling of the introduced cysteine versus TMRM labeling of endogenous membrane proteins): i) The mRNA encoding the cysteine-substituted transporters are injected into Xenopus oocytes. ii) The oocytes are incubated at 8°C for 4–5 days to allow synthesis of the channel protein. The low temperature keeps the transporters from reaching the plasma membrane, presumably by trapping in the endoplasmic reticulum (ER). The oocytes are kept at 8°C, instead of at 12°C as in earlier fluorescence studies, because the lower temperature more efficiently keeps the transporters from reaching the plasma membrane for longer periods of time (Larsson and Kavanaugh, unpublished observations). iii) The oocytes are prelabeled with the nonfluorescent membrane-impermeable tetra-glycine maleimide (TGM) at 10 mM for 1 h at 18°C to block en-

dogenous cysteines and prevent them from being labeled during the TMRM treatment. Alternatively, the 10 mM 3-maleimidopropionic acid (Li and Lester, 2000) can also be used to block the endogenous reactive sulfhydryl groups. iv) The oocytes are incubated at room temperature (21°C) for 14–18 h to allow the transporters to reach the plasma membrane. The density of transporters is tested by two-electrode voltage clamp recordings, to ensure that large enough numbers of transporters have reached the surface (>0.3 μA at –80mV, in 1 mM glutamate). v) When the transporter density in the plasma membrane is large enough, the oocytes are then labeled with 5 mM fluorescent maleimide probe at room temperature for 30 min to 1 h followed by extensive washing.

Recording Techniques

The fluorescent probes, now covalently attached to the introduced cysteine, report on the environmental changes that the cysteine is undergoing during transport. The labeled oocytes are placed animal-side down in a recording chamber on an inverted epifluorescence microscope (Cha et al., 1998). A photomultiplier tube (PMT) measures the fluorescence from the oocytes, and at the same time the current is recorded with a two-electrode voltage clamp amplifier. The analog output of the PMT and voltage clamp amplifiers are converted digitally by using a Digidata A/D converter (Axon Instruments, Foster City, CA) interfaced to a Macintosh or PC. Figure 13.1 shows an example of simultaneous flu-

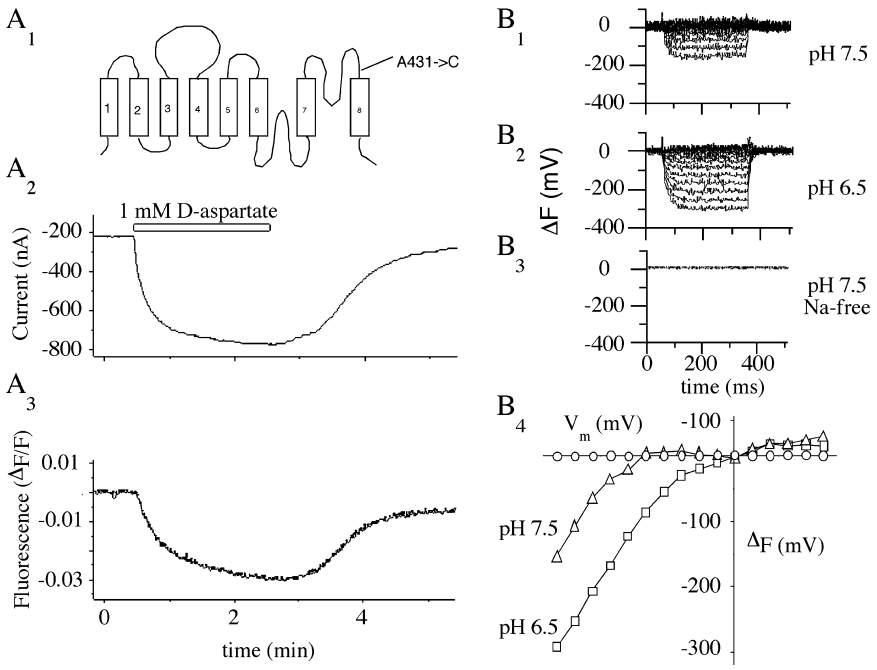

Figure 13.1. Fluorescence measurement in oocytes under two-microelectrode voltage clamp. **A)** Representative oocyte modified with Oregon Green maleimide during bath application of D-aspartate for duration indicated by bar. Holding potential = –60 mV **(B)** Measurement of voltage and time-dependent fluorescence changes in the absence of amino acid substrate.

orescence and current recording from an oocyte expressing the neuronal glutamate transporter EAAT3 labeled at Cys-431. The technique shows that in this functional labeled transporter, glutamate or aspartate induces a dramatic change in fluorescence with a time course that matches the transport current as the amino acid enters and is washed out of the chamber. Application of amino acids not recognized by the transporter to not induce fluorescence changes. Moreover, rapid voltage-dependent changes in fluorescence are also observed in the absence of amino acid. These latter changes are pH and sodium-dependent and are kinetically similar to sodium-dependent charge movements that occur before glutamate binds (Wadiche et al., 1995b). This example shows the utility of the fluorescence technique for detecting state changes that are not otherwise readily detectible in order to gain information about questions such as binding order of substrates (see modeling section below). Whereas the time-dependence of the fast fluorescent signals obtained in whole oocytes matches reasonably well with presteady state currents, higher resolution kinetic measurements of the fluorescence and the current can be also be made by using the cut-open oocytes technique in combination with fluorescence measurements on an upright microscope (Cha et al., 1998; Cha and Bezanilla, 1997). This technique allows measurement of current and fluorescence from the same population of transporters and minimizes errors due to space-clamp inhomogeneity and series resistance of the oocyte cytosol. The cut-open oocyte technique also allows perfusion of the interior of the oocyte to change the ionic composition of the cytosol. This could be used, for example, to test the effect of intracellular substrates on the conformational changes during transport.

Accessibility Methods to Study Gating

A common model for glutamate transport is based on an alternating-access model (Kanner and Bendahan, 1982). In this model, the substrate binding sites are alternatively exposed to the extracellular and the intracellular solutions. The uptake of glutamate involves the binding of sodium and glutamate and a proton to extracellularly exposed binding sites, followed by a conformational change that causes these binding sites to now be exposed to the intracellular solution, which contains a high concentration of potassium. The exposure of the binding sites to the intracellular solution allows for the release of the glutamate and sodium and a proton to the intracellular solution followed by potassium binding.

If glutamate is transported by such an alternating access mechanism, then some of the residues of glutamate transporter should be exposed alternately to the intracellular and the extracellular solution during the transport cycle. One could test the alternative access model by measuring the intracellular and extracellular accessibility of cysteine introduced in glutamate transporters. The accessibility of the introduced cysteines could be tested during conditions that favor either extracellular or intracellular exposure of the substrate binding sites. One approach to measure the accessibility of cysteine residues in glutamate transporters would be to apply the cysteine accessibility method strategy used to study the movement of the S4 transmembrane domain in Shaker K channels (Larsson et al., 1996; Baker et al., 1998) and in Na channels (Yang and Horn 1995, Yang et al., 1996) in order to determine whether specific residues in the glutamate transporter are alternatively intracellularly and extracellularly exposed during glutamate transport.

To measure the accessibility of a given cysteine one can measure its susceptibility to modification by a methanethiosulfonate (MTS) reagent (Wilson and Karlin 1998). If the cysteine is in a region that undergoes a conformational change during the glutamate transport cycle, then the modification of this cysteine by a charged MTS reagents may alter

some of the properties of the transporter (Borre et al., 2002). Modification by MTS reagents of pore residues in ion channels renders the channels nonconducting or reduces the ionic current through the channel, and modification by MTS reagents of residues in the voltage sensor of voltage-gated ion channels alters the voltage sensitivity and the kinetics of the channels (Larsson et al., 1996; Yang et al., 1996). Because we are trying to identify residues that are involved in the conformational changes that lead to glutamate transport, we expect that modification by MTS reagents of these residues will result in changes in some of the properties of the transporters. Indeed, modification by MTSEA 2-(aminoethyl)methanethiosulfonate of certain residues eliminates the Na-dependent capacitance transients and earlier studies have shown, for example, that modification of engineered cysteines by MTSET 2(trimethylammonium)methanethiosulfonate can eliminate the chloride currents associated with glutamate transport. To detect the modification of the cysteine, several approaches can be used: changes in the transient sodium currents, changes in the ligand-activated current, and changes in the fluorescence from a fluorescently labeled reporter cysteine (a cysteine different from the cysteine under investigation) using VCF.

Detecting Accessibility with VCF

To detect cysteine modification by using VCF, two cysteines are introduced in the transporter. One of these cysteines is labeled with a fluorescent probe, and the other is the cysteine for which the accessibility will be tested. The change in the fluorescence from the fluorescent probe is the reporter for the modification by MTS reagents of the other cysteine. This method is designed to work for two cysteines that can be labeled differentially; that is they must be differntially sensitive to labeling conditions or selective in the chemistry and/or size of the label to be introduced. Practically, this is seen in a number of cysteine mutations that have been introduced into glutamate transporters (Kanner BI, Borre L, and Kavanaugh MP, unpublished observations). For this technique, ideally the first cysteine should be easily labeled with the large fluorescent probes, whereas the second cysteine should be readily labeled only by small MTS reagents.

Recording Conditions

The rate of modification is measured for 0, 1, 10, 100, and 1000 μM extracellular glutamate in a Na-Ringer solution. A majority of the glutamate transporters appear to have their binding sites facing the extracellular solution when a sodium-based solution with 0 glutamate is applied extracellularly (Wadiche et al., 1995a, and see model below). The probability of finding the binding sites exposed to the extracellular solution should decrease with increasing glutamate concentration. At 1000 μM glutamate, more of the binding sites should be facing the intracellular solution due to the relatively slow return step of the glutamate transporter to the outside during a transport cycle. If there is a substantial change in the rate of modification between the 0 and 1000 μM glutamate solution for a specific residue, this change is interpreted as a change in accessibility for that residue (e.g., a residue that is facing the intracellular solution, or is buried in the protein, at 1000 μM glutamate versus that exposed to the external solution at 0 μM glutamate). Predictions from kinetic models (described below) suggest that we should expect to find residues that are exposed mainly to the intracellular or the extracellular solution depending on the concentration of extracellular glutamate, sodium, pH, and membrane potential. Residues that

are alternatively exposed to the intracellular and the extracellular solution have been identified with this method in earlier investigation of voltage-gated ion channels, leading to the elucidation of the molecular mechanism of voltage gating in K and Na channels (Baker et al., 1998; Larsson et al., 1996; Yang et al., 1996).

13.3 SUBSTRATE CONCENTRATION JUMPS

Within the past several years, the application of piezo-switched glutamate jumps to excised outside-out patches has been introduced to study glutamate transporter kinetics with high time resolution. This technique is a powerful approach to study transporters as one can easily and completely control the ion concentrations in both the intracellular and extracellular environment of the transporters. L-glutamate (and/or alkali cations) can be applied rapidly (<1 ms) by using a piezo electric switch (Maconochie and Knight, 1989). The fast application and removal of glutamate for varying lengths of time, using single or paired pulses, can generate a significant amount of kinetic information (Auger and Attwell, 2000; Bergles et al., 1997; Bergles and Jahr, 1998; Bergles and Jahr, 1997; Mennerick et al., 1999; Otis and Jahr, 1998; Otis and Kavanaugh, 2000; Otis et al., 1997; Wadiche and Kavanaugh, 1998). Alternatively, photolysis uncaging techniques coupled with whole-cell recording can be applied to gain similar information (Grewer et al., 2001; Grewer et al., 2000; Watzke et al., 2001; Watzke and Grewer, 2001; Watzke et al., 2000), although with this technique transmitter concentrations are difficult to control and rapidly remove. For optimal results using piezo-switched applications, outside-out patches should be used because they are smaller and their surface is readily accessible, such that rapid exchange times (50-300 μs) can be achieved. Inside-out patches tend to give less reproducible results, presumably because of omega-shaped deformations of membrane inside the pipette tip, leading to significant diffusional barriers and slower concentration changes. To avoid errors in kinetic estimates, the solution exchange time must be faster than the relaxation kinetics of the system under study.

Glutamate transport is associated with a thermodynamically uncoupled chloride conductance that exhibits a higher conductance with chaotropic anions, such as NO_3^- and SCN^- (Eliasof and Jahr, 1996; Wadiche et al., 1995b; Wadiche and Kavanaugh, 1998). In contrast, the stoichiometrically coupled current is associated with movement of the thermodynamically coupled ions. The kinetics of both currents give distinct information, and the currents can be studied separately and compared by recording with or without the impermeant anion gluconate. Although the overall dynamics of the stoichiometric current are similar to the anion current, the former current has somewhat faster kinetics (Auger and Attwell, 2000; Bergles et al., 1997; Grewer et al., 2000; Otis and Kavanaugh, 2000). The related but nonidentical kinetics suggest that the anion current activation reflects the occupancy of a subset of states in the cycle (see model below).

Solutions and Patch Excision

Standard patch recording techniques are used for oocytes expressing glutamate transporters (Wadiche and Kavanaugh, 1998). Before patches are excised, the expression level is assessed through the use of a two-electrode voltage clamp. For optimal results, we use stage V oocytes in which application of 1 mM glutamate (–70 mV) elicits ~1 μA of current. Oocytes are placed in cultures dishes, and the vitelline membrane is removed by us-

ing fine-tipped surgical forceps. For outside-out patches, patch pipettes are pulled from thick-walled borosilicate glass (O.D 1.5 mm; I.D 1.1 mm; Warner Instrument Corp.). Then, the pipettes are polished to a tip diameter of ~0.5–1 μm and filled with internal solution depending on the experimental protocol. For studying forward transport, the pipettes contain 110 mM $KSCN^-$, 10 mM KCl, 3 mM $MgCl_2$, 5 mM N-(2-hydroxyethyl) piperazine-2'-(2-ethanesulphonic acid) (HEPES), and 10 mM ethyleneglycol-bis(β-aminoethyl ether)-N,N,N',N'-tetraacetic acid (EGTA). For exchange experiments, the pipette contains 110 $NaSCN^-$, 10 mM NaCl, 5 mM HEPES, 10 mM EGTA, and variable glutamate. The use of EGTA is important in order to chelate Ca^{2+}, which otherwise leads to the activation of chloride channels. The solutions are titrated to pH 7.5 by using Tris base. With these intracellular solutions, the pipette tip resistance should be between 1–5 MΩ. The extracellular recording solutions contains 110 NaCl, 3 mM $MgCl_2$, and 5 mM HEPES. For studying stoichiometric currents, anions are replaced by gluconate. Following formation of a cell-attached seal, it is our experience that patch excision from oocytes should be done slowly over a 30–60 s period, particularly for pipettes that have higher resistances.

Exchange Apparatus

To rapidly apply a glutamate concentration jump, we use drawn borosilicate theta-shaped glass tubing that is continuously perfused with control and test solution (Maconochie and Knight, 1989; Wadiche and Kavanaugh, 1998). The glass is obtained from Warner Instruments (Borosilicate Theta; O.D 1.5 mM). Polyethylene (P10) tubing is inserted into the back end of the glass and connected to a 2-, 4-, or 6-barrel manifold (Warner Instruments). The theta tube is mounted on a holder attached to a piezo-activated switch (Burleigh Instruments, New York, NY, USA), allowing for a rapid change between control and test solutions. The piezo unit is computer-controlled by using the same pCLAMP software and A/D converter that controls acquisition of data from the amplifier, providing flexibility and accuracy in the protocol design. The pipette containing the excised outside-out patch is placed in front of the theta tube in the control stream, as close to the interface with the glutamate stream as possible, such that only control solution bathes the patch. Trial and error is necessary to identify optimal placement and obtain a reproducible response when the switch is activated. At the end of the experiment, the solution exchange time is checked by rupturing the patch. A hypotonic solution is perfused through one channel of the theta tube; the resulting junction potential results in a current that follows the time course of the solution exchange.

Figure 13.2 illustrates the use of the glutamate jump technique. Following application of saturating glutamate, the anion current activates rapidly. In the continuous presence of glutamate, the peak current decays to a steady-state level and returns to baseline following the removal of glutamate. The peak response is believed to reflect nearly synchronous entrance of the glutamate-bound transporters to conducting states, whereas the sustained component reflects the desynchronized transporters cycling at steady state (Wadiche and Kavanaugh, 1998). The rapid activation of the anion current indicates it is gated early on in the cycle. The glutamate binding rate can be estimated by measuring the activation rate of the anion current at different glutamate concentrations, ranging from 1 μM to 10 mM (Grewer et al., 2000; Mennerick et al., 1999; Otis and Jahr, 1998; Wadiche and Kavanaugh, 1998). With limiting glutamate concentrations and under ionic conditions favoring forward transport ($[Na^+]_o$ and $[K^+]_i$), the rise of the anion current should be dependent

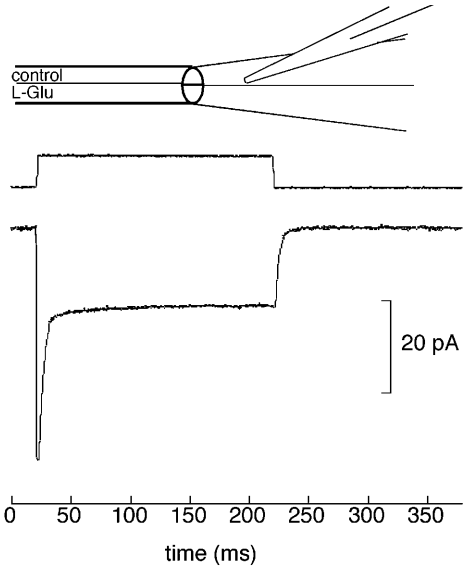

Figure 13.2. Concentration jump set up. **A)** Cartoon of the theta tube application and recording pipette. **B)** Glutamate concentration jump (10 mM L-Glu; 200 ms) applied to an excised outside-out patch expressing EAAT3 held at –70 mV. The intracellular solution contains KSCN. The open-tip solution exchange time is shown above the trace.

on the increasing extracellular glutamate concentration until the binding is no longer the rate-limiting step. The limiting slope of the current activation rate versus the glutamate concentration allows an estimate of the binding rate constant.

As mentioned earlier, glutamate transport is coupled to the downstream movement of three sodium ions and one proton and counter-transport of one potassium ion (Zerangue and Kavanaugh, 1996; Levy et al., 1998). This is the basis of the stoichiometric current, reflecting a net movement of two charges across the membrane electrical field. As a consequence, at least some of the steps in the glutamate cycle are predicted to be voltage-dependent. To determine the effect membrane potential has on transport kinetics, varying concentrations of glutamate and alkali cations can be applied while holding the patch at various potentials. As shown in Figure 13.3, the decay of the peak anion current to steady state is strongly dependent on voltage. In contrast, the return of the steady state current to baseline following the removal of glutamate is less voltage-dependent. To interpret these data and assign voltage dependencies to different steps, a constrained kinetic model is developed as described below.

An important question is how quickly glutamate transporters cycle. Wadiche et al. (1995a) estimated that the time it takes for a transporter to complete one full cycle is ~70 ms. This measurement was based on transporter density estimates in oocytes. One can also gain information about the transporter cycling time in patches by applying a paired-pulse protocol (Bergles and Jahr, 1997; Otis and Kavanaugh, 1998; Auger and Attwell, 2000). A conditioning glutamate pulse is applied to reach steady state and is followed by a second pulse administered at varying interpulse time intervals. Then the time constant for the recovery of the peak current is determined. Figure 13.3 illustrates an example of such an experiment. However, because the transporters can return to the initial unbound

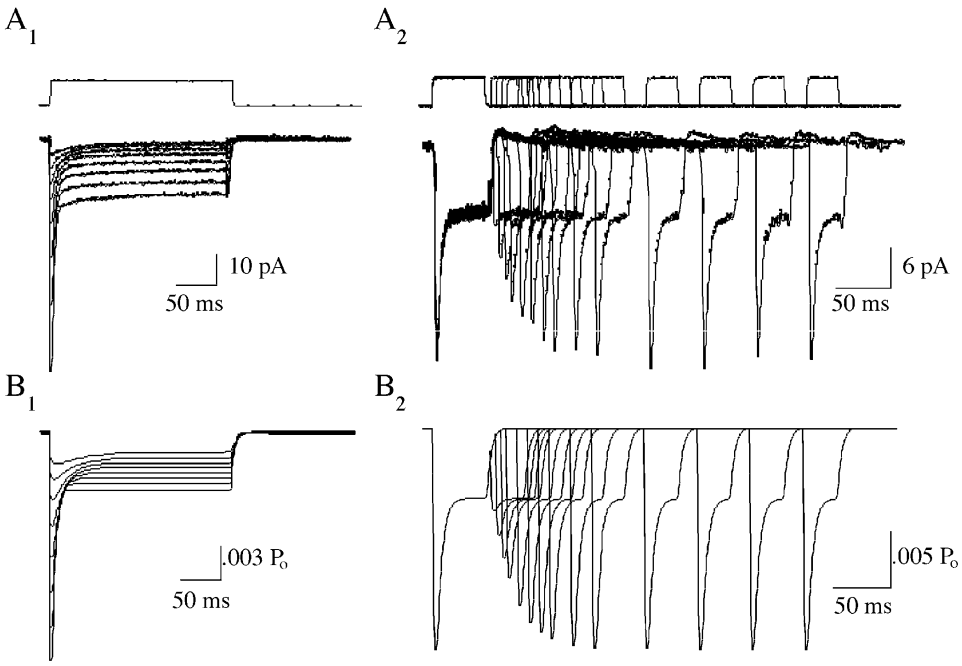

Figure 13.3. A_1) Rapid application of 10 mM glutamate to outside-out patches (200 ms, –90 to +50 mV). **A_2)** Recovery from steady state (–80 mV) following a 50 ms conditioning pulse (10 mM glutamate), followed by a test pulse of 30 ms (10 mM glutamate) applied at various intervals after the conditioning pulse. **B_1–B_2)** Computer simulation of the patch current-voltage relationship and recovery rate by using the model described.

state by either unbinding glutamate to the outside or by completing the cycle, the recovery rate should be regarded as the maximum attainable transporter cycling rate. Again, as described below, the use of a constrained kinetic simulation that can fit the recovery kinetics together with a large number of independent data sets is required to arrive at meaningful estimates of the microscopic rates and the net cycling rate.

13.4 SIMULATION OF TRANSPORT BEHAVIOR WITH KINETIC MODELING

Computer modeling is an invaluable technique for studying transporter kinetics due to the complexity of even the minimal kinetic schemes required to describe the data. Such models provide a conceptual framework for how transport might occur. They also allow us to test hypotheses and to predict behavior under conditions that might not be easily tested experimentally. Several commercial programs exist that make the development of kinetic models quite easy. We have found that the program Madonna, versions of which are available for both PC and Macintosh, is a particularly flexible and user-friendly modeling program (http://www.berkeleymadonna.com).

A primary goal in model building is to keep the model as simple as possible while accurately describing all the available data. In this section we describe the use of data from the neuronal glutamate transporter EAAT3 to provide an example of building a kinetic

model. The scheme is a Markov model in which the transporters move through a series of distinct kinetic steps with voltage-dependent rate constants for the transitions between the different states that do not change over time. To formulate a well-constrained model one first needs to accumulate a large set of steady-state and presteady-state data. Our approach is to use data obtained from both concentration and voltage jumps to constrain the rates governing the transitions between states, as well as additional steady-state data (Wadiche et al., 1995a).

There is compelling evidence from steady-state voltage clamp recordings that glutamate transport is coupled to the cotransport of three sodium ions and one proton and the counter-transport of one potassium ion (Levy et al., 1998; Zerangue and Kavanaugh, 1996). As this coupled glutamate transport cannot be explained by a single file mechanism, an alternating access cyclical model is used as a starting point to explain the coupling (Kanner and Bendahan, 1982). Once a general kinetic scheme is selected, a model with the minimum number of kinetically distinguishable states consistent with the stoichiometry can be determined. However, defining the substrate binding order requires extensive testing of each model. For example, with EAAT3, the precise binding order of protons in regards to glutamate is controversial. Protons may bind to EAAT3 either before glutamate (Auger and Attwell, 2000; Seal et al., 2001; Watzke et al., 2000), after glutamate (Otis and Jahr, 1998), or in a random order. One can distinguish among the different possibilities by determining the influence glutamate and protons and sodium have on the steady-state kinetic parameters K_m and I_{max}. For instance, if the glutamate I_{max} is independent of the external proton concentration, while the glutamate K_m is not, then, a proton binds before glutamate (Stein, 1990). However, if the glutamate I_{max} and K_m are reliant on extracellular proton concentration and a similar dependence is observed for the proton I_{max} and K_m with respect to extracellular glutamate concentration, then, the order of binding is more consistent with a random order (Stein, 1990). Our steady-state data (Tzingounis and Kavanaugh, unpublished observation) can be described by a model in which two sodium ions bind, followed by binding of glutamate and a proton in a random order, and then a third sodium ion, as represented in the model shown in Figure 13.4.

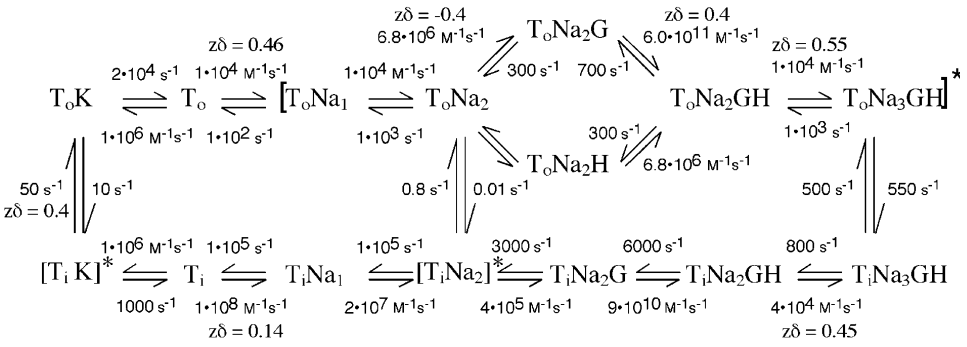

Figure 13.4. Alternating access model. Asterisk denotes states from which the anion conductance is gated and α denotes opening rate, while β denotes closing rate. For the T_oNa_1*, T_oNa_2*, T_oNa_2H*, T_oNa_2GH* states $\alpha = 8094\ s^{-1}$ and $\beta = 5\ s^{-1}$. For the T_oNa_3GH* state $\alpha = 12{,}600\ s^{-1}$ and $\beta = 700\ s^{-1}$. For the T_iNa_2* $\alpha = 4700\ s^{-1}$ and $\beta = 10\ s^{-1}$, whereas for the T_iK* state $\alpha = 4700\ s^{-1}$ and $\beta = 0.001\ s^{-1}$. The valence of the voltage-dependent rate constants is shown above; the displayed rates are for –70 mV.

By applying glutamate concentration jumps to excised patches at different membrane potentials and with different intracellular solutions, we can functionally isolate a subset of the rates constants to better constrain the form of the overall model and the individual rates. For example, replacement of intracellular K^+ ions with Na^+ and glutamate shifts the transporter to an exchange mode, eliminating the contribution of the K^+-dependent rate constants. As a result, the relaxation time constants to baseline following glutamate removal are dominated primarily by the backward rate constants of the Na-hemicycle, which thus leads to the isolation of an even smaller number of rate constants (Otis and Kavanaugh, 1998). In addition, paired pulse data help constrain the cycling rate of the transporters under these different ionic conditions.

The transport cycle moves net charge across the membrane, which leads to a voltage-dependent transport rate (Brew and Attwell, 1987; Wadiche et al., 1995a; Wadiche and Kavanaugh, 1998). An important question for the understanding of the transport cycle is the identity of the steps in the transport cycle that involve movement of charge through the electrical field across the membrane. A major constraint for the model is that, at steady state, two net charges are transported inside for every cycle. Qualitative information regarding the voltage-dependent steps in the cycle can be obtained by analyzing the steady-state current-voltage relationship (I-V). For instance, I-Vs induced by different glutamate concentrations provide significant information regarding the glutamate cycle. At large hyperpolarized potentials and saturating glutamate concentrations (1 mM) the I-V has a positive slope. This finding indicated that either the rate-limiting step in the glutamate cycle or the step preceding it is voltage-dependent. Also, at low glutamate concentrations, the steady-state current-voltage relationship becomes saturated at negative membrane potentials (Kanai et al., 1994), suggesting that glutamate binding becomes rate-limiting at these potentials. Either lowering the proton concentration or the sodium concentration prevents this current saturation at negative potentials, indicating that voltage-dependent proton and sodium binding are now rate-limiting (Tzingounis et al., in preparation). These data suggest, then, that either the proton and sodium binding or a conformational change associated with their binding is voltage-dependent.

More quantitative information regarding the voltage-dependent steps comes from performing voltage jumps and measuring presteady-state and steady-state currents. Following a voltage change, the transporters will approach the new equilibrium with an exponential time course whose time constant is equal to the sum of the forward and the backward rates (Lauger, 1991). Once all the data have been accumulated, one can build the model and attempt to fit the data. Figure 13.3 shows a comparison of predictions of our provisional model, which fits the experimental data reasonably well. To further validate the model, new experimental data are consistently compared with the predicted data, and adjustments are made. The model should be able to fit all the experimental data with one set of rate constants. Because of the difficulty in arriving at a unique set of parameters in such a complex model, it is up to the investigator to repeatedly test and judge its validity. The model is complete only when the investigator has exhausted every kinetic measurement possible; that is, it is never finished.

REFERENCES

Auger C, Attwell D (2000): Fast removal of synaptic glutamate by postsynaptic transporters. Neuron 28: 547–558.

Baker OS, Larsson HP, Mannuzzu LM, Isacoff EY (1998): Three transmembrane conformations and sequence-dependent displacement of the S4 domain in shaker K+ channel gating. Neuron 20:1283–1294.

Balcar VJ, Johnston GARJ (1972): The structural specificity of the high affinity uptake of L-glutamate and L -aspartate by rat brain slices. Neurochem 19:2657–2666.

Bergles DE, Dzubay JA, Jahr CE (1997): Glutamate transporter currents in bergmann glial cells follow the time course of extrasynaptic glutamate. Proc Natl Acad Sci USA 94:14821–14825.

Bergles DE, Jahr CE (1997): Synaptic activation of glutamate transporters in hippocampal astrocytes. Neuron 19:1297–1308.

Bergles DE, Jahr CE (1998): Glial contribution to glutamate uptake at Schaffer collateral-commissural synapses in the hippocampus. J Neurosci 18:7709–7716.

Borre L, Kavanaugh MP, Kanner BI (2002): Equilibrium between coupled and uncoupled modes of a neuronal glutamate transporter. J Biol Chem 277:13501–13507.

Brew H, Attwell D (1987): Electrogenic glutamate uptake is a major current carrier in the membrane of axolotl retinal glial cells. Nature (London) 327:707–709.

Cha A, Bezanilla F (1997): Characterizing voltage-dependent conformational changes in the Shaker K+ channel with fluorescence. Neuron 19:1127–1140.

Cha A, Bezanilla F (1998): Structural implications of fluorescence quenching in the Shaker K+ channel. J Gen Physiol 112:391–408.

Cha A, Zerangue N, Kavanaugh M, Bezanilla F (1998): Fluorescence techniques for studying cloned channels and transporters expressed in Xenopus oocytes. Meth Enzymol 296:566–578.

Danbolt N (2001): Glutamate uptake. Prog Neurobiol 65:1–105.

Eliasof S, Jahr CE (1996): Retinal glial cell glutamate transporter is coupled to an anionic conductance. Proc Natl Acad Sci USA 93:4153–4158.

Grewer C, Madani-Mobarekeh SA, Watzke N, Rauen T, Schaper K (2001): Substrate translocation kinetics of excitatory amino acid carrier 1 probed with laser-pulse photolysis of a new photolabile precursor of D-aspartic acid. Biochemistry 40:232–240.

Grewer C, Watzke N, Wiessner M, Rauen T (2000): Glutamate translocation of the neuronal glutamate transporter EAAC1 occurs within milliseconds. Proc Natl Acad Sci USA 97:9706–9711.

Kanai Y, Stelzner M, Nussberger S, Khawaja S, Hebert SC, Smith CP, Hediger MA (1994): The neuronal and epithelial human high affinity glutamate transporter: insights into structure and mechanism of transport. J Biol Chem 269:20599–20606.

Kanner BI, Bendahan A (1982): Binding order of substrates to the sodium and potassium ion coupled L-glutamic acid transporter from rat brain. Biochemistry 21:6327–6330.

Kanner BI, Sharon I (1978): Active transport of L -glutamate by membrane vesicles isolated from rat brain. Biochemistry 17:3949–3953.

Larsson HP, Baker OS, Dhillon DS, Isacoff EY (1996): Transmembrane movement of the shaker K+ channel S4. Neuron 16:387–397.

Lauger P (1991): Electrogenic ion pumps. Sunderland, MA: Sinauer.

Levy LM, Warr O, Attwell D (1998): Stoichiometry of the glial glutamate transporter GLT-1 expressed inducibly in a Chinese hamster ovary cell line selected for low endogenous Na+-dependent glutamate uptake. J Neurosci 18:9620–9628.

Li M, Farley RA, Lester HA (2000): An intermediate state of the gamma-aminobutyric acid transporter GAT1 revealed by simultaneous voltage clamp and fluorescence. J Gen Physiol 115:491–508.

Loo DD, Hirayama BA, Gallardo EM, Lam JT, Turk E, Wright EM (1998): Conformational changes couple Na+ and glucose transport. Proc Natl Acad Sci USA 23:7789–7794.

Maconochie DJ, Knight DE (1989): A method for making solution changes in the sub-millisecond range at the tip of a patch pipette. Pflugers Arch 414:589–596.

Mannuzzu LM, Moronne MM, Isacoff EY (1996): Direct physical measure of conformational rearrangement underlying potassium channel gating. Science 271:213–216.

Mennerick S, Shen W, Xu W, Benz A, Tanaka K, Shimamoto K, Isenberg KE, Krause JE, Zorumski CF (1999): Substrate turnover by transporters curtails synaptic glutamate transients. J Neurosci 19:9242–9251.

Otis TS, Jahr CE (1998): Anion currents and predicted glutamate flux through a neuronal glutamate transporter. J Neurosci 18:7099–7110.

Otis TS, Kavanaugh MP (2000): Isolation of current components and partial reaction cycles in the glial glutamate transporter EAAT2. J Neurosci 20:2749–2757.

Otis TS, Kavanaugh MP, Jahr CE (1997): Postsynaptic glutamate transport at the climbing fiber-Purkinje cell synapse. Science 277:1515–1518.

Seal RP, Shigeri Y, Eliasof S, Leighton BH, Amara SG (2001): Sulfhydryl modification of V449C in the glutamate transporter EAAT1 abolishes substrate transport but not the substrate-gated anion conductance. Proc Natl Acad Sci USA 98:15324–15329.

Stein WD (1990): Channels, Carriers, and Pumps: An introduction to membrane transport. New York, NY:Academic Press.

Wadiche JI, Arriza JL, Amara SG, Kavanaugh MP (1995a): Kinetics of a human glutamate transporter. Neuron 14:1019–1027.

Wadiche JI, Amara SG, Kavanaugh MP (1995b): Ion fluxes associated with excitatory amino acid transport. Neuron 15:721–728.

Wadiche JI, Kavanaugh MP (1998): Macroscopic and microscopic properties of a cloned glutamate transporter/chloride channel. J Neurosci 18:7650–7661.

Watzke N, Bamberg E, Grewer C (2001): Early intermediates in the transport cycle of the neuronal excitatory amino acid carrier EAAC1. J Gen Physiol 117:547–562.

Watzke N, Grewer C (2001): The anion conductance of the glutamate transporter EAAC1 depends on the direction of glutamate transport. FEBS Lett 503:121–125.

Watzke N, Rauen T, Bamberg E, Grewer C (2000): On the mechanism of proton transport by the neuronal excitatory amino acid carrier 1. J Gen Physiol 116:609–622.

Wilson GG, Karlin A (1998): The location of the gate in the acetylcholine receptor channel. Neuron 6:1269–1281.

Yang N, George AL, Horn R (1996): Molecular basis of charge movement in voltage-gated sodium channels. Neuron 16:113–122.

Yang N, Horn R (1995): Evidence for voltage-dependent S4 movement in sodium channels. Neuron 15:213–218.

Zerangue N, Kavanaugh MP (1996): Flux coupling in a neuronal glutamate transporter. Nature (London) 383:634–637.

CHAPTER 14

STUDIES OF GLIAL GLUTAMATE TRANSPORTERS IN HIPPOCAMPAL MICROCULTURES

STEVEN MENNERICK, ROBERT J. CORMIER, AND CHARLES F. ZORUMSKI

14.1 INTRODUCTION

Plasma membrane transporters play major roles in clearing neurotransmitters from the synaptic cleft following release at synapses in the mammalian central nervous system (CNS), and in regulating the ambient extracellular levels of neurotransmitters. This is in contrast to the mammalian neuromuscular junction, where enzymatic hydrolysis is responsible for rapid clearance of acetylcholine. Additionally, there are significant differences among CNS transmitter systems in the relative contributions of neuronal versus glial transporters, with some transmitter systems predominantly, if not exclusively, using neuronal transporters (e.g., monoamines) and others (e.g., glutamate) using both neuronal and glial transport (Gadea and Lopez-Colome, 2001a, b).

Our research group is interested in the role of glial glutamate transporters at fast synapses in the hippocampus. Despite strong suggestions from biochemical studies, direct evidence demonstrating a major role for glutamate transporters in synaptic function was slow to develop. The delay resulted, in part, from the difficulty of studying transporter function during synaptic transmission. Over the past decade, several preparations have been developed in which simultaneous monitoring of neuronal responses and glial and neuronal transporter function has been possible. Additionally, the ability to manipulate gene expression in experimental preparations and to express transporter genes in heterologous systems has greatly enhanced understanding of the function of neuronal and glial transporters. In our laboratory, we have examined the role of glial glutamate transporters by using a preparation of hippocampal cells grown in a microculture environment. In this review, we will briefly discuss the role of transporters in glutamate-mediated synaptic transmission and describe methods for monitoring transporter and glial function in hippocampal microcultures.

14.2 GLUTAMATE NEUROTRANSMISSION AND GLUTAMATE TRANSPORTERS

Before addressing the primary focus of this chapter, which covers our own studies in culture, this section provides an overview of the role of transporters in glutamate neurotrans-

Transmembrane Transporters. Edited by Michael Quick

ISBNs: 0-471-06517 (Hardcover); 0-471-43404-3 (Electronic)

mission. For a more extensive review of the topic of glutamate uptake and glutamate neurotransmission, readers are referred to a recent comprehensive review (Danbolt, 2001).

Glutamate is present in intracellular fluid at a concentration of ~10 mM and in synaptic vesicles at 60–150 mM (Burger et al., 1989). Following Ca^{2+} influx into nerve terminals, glutamate is released into the synaptic cleft where it achieves peak levels of 1–2 mM that decay in a few milliseconds (Clements et al., 1992). Under these conditions, postsynaptic responses mediated by neuronal α-amino-3-hydroxy-5-isoxazole-4-propionic acid receptors (AMPARs) rapidly activate and deactivate. The decay of AMPAR excitatory postsynaptic currents (EPSCs) is governed by the channel-closing rate (Hestrin, 1992), although desensitization may contribute under conditions of high transmitter release (Thio et al., 1992; Trussell et al., 1993; Kinney et al., 1997). N-methyl-D-aspartate receptor-mediated (NMDAR) EPSCs activate more slowly and decay over tens of milliseconds. This slow time course results largely from the intrinsic kinetics of NMDAR ion channels (Lester et al., 1990). These observations strongly suggest that the time course of EPSCs results from ion channel kinetics following brief exposure to high glutamate concentrations.

Following release, the concentration of glutamate in the synaptic cleft rises and falls rapidly (Clements et al., 1992). The decay of the synaptic glutamate concentration results largely from diffusion from the synaptic cleft, although glutamate transporters are required to remove transmitter from the extracellular space (Mennerick and Zorumski, 1994; Tong and Jahr, 1994; Bergles and Jahr, 1997; Bergles and Jahr, 1998) and to lower the ambient extracellular glutamate concentration to about 1 μM (Bouvier et al., 1992). The duration of significant glutamate levels at synapses and the distance over which a significant concentration diffuses remain uncertain. Present evidence indicates that glutamate transporters buffer synaptic glutamate on a submillisecond time scale, limiting peak postsynaptic activation (Diamond and Jahr, 1997). Studies of transport kinetics are limited, but both rapid binding to transporters (Tong and Jahr, 1994) and translocation of glutamate (Mennerick et al., 1999; Auger and Attwell, 2001) appear to participate in limiting the duration that glutamate persists at synapses and to diminishing the spread of glutamate to extrasynaptic sites. The ability of transporters to limit glutamate spillover may have a major impact on the activation of metabotropic glutamate receptors (mGluRs) (Scanziani et al., 1997) and desensitization of ionotropic receptors in local synaptic circuits.

To date, five glutamate transporters have been cloned (GLAST, GLT-1, EAAC1, EAAT4, and EAAT5) (Danbolt, 1994, 2001). EAAC1 (also called EAAT3) is a neuronal transporter present in both excitatory and inhibitory neurons (Kanai and Hediger, 1992). GLAST (EAAT1) (Storck et al., 1992) and GLT-1 (EAAT2) (Pines et al., 1992) are primarily glial transporters, although GLT-1 mRNA exists in neurons (Schmitt et al., 1996) and recent studies indicate neuronal expression of GLT-1 as well (Grunert et al., 1994; Furuta et al., 1997; Mennerick et al., 1998; Beckstrom et al., 1999). EAAT4 is expressed predominantly in cerebellum, whereas EAAT5 is primarily localized to retina (Fairman et al., 1995; Arriza et al., 1997; Eliasof et al., 1998). These transporters have relatively high apparent affinities for glutamate with EC50s in the range of 10–50 μM. Glutamate transport is Na^+-dependent and uses ion gradients to drive glutamate into cells. Present evidence suggests that each transport cycle involves the influx of three Na^+ and one glutamate anion, and the efflux of one K^+. Each cycle also involves the movement of one pH-changing ion, resulting in intracellular acidification (probably reflecting the influx of one H^+) (Wadiche et al., 1995a; Wadiche et al., 1995b; Zerangue and Kavanaugh, 1996). Importantly, glutamate transport involves a net charge translocation and can thus be stud-

ied by using electrophysiological methods. Although most glutamate transport is not Cl^--dependent, glutamate transporters have an associated Cl^- conductance that has channel-like properties (Fairman et al., 1995). This Cl^- conductance is most prominent in EAAT4 but also has been described with EAAC1, GLAST, and EAAT5 (Wadiche et al., 1995a). GLT-1 appears to have the smallest anion conductance of the recombinant transporters. The function of the Cl^- conductance is unclear because it is not linked thermodynamically to glutamate transport (Wadiche et al., 1995a; Bergles et al., 1997). The presence of the Cl^- conductance provides a useful means for monitoring the activity of glutamate transporters, particularly on short time scales. However, the anion current has recently been suggested not to be as closely associated with glutamate removal steps as previously thought (Auger and Attwell, 2001).

Several studies, including those from our laboratory, strongly suggest that glial glutamate transport contributes to regulating glutamate levels following release at synapses in the hippocampus (Mennerick and Zorumski, 1994; Bergles and Jahr, 1997; Bergles and Jahr, 1998). Under conditions of high transmitter release, inhibition of glial glutamate transport prolongs both AMPAR- and NMDAR-mediated EPSCs, which suggests a role in controlling the time course of synaptic events (Mennerick and Zorumski, 1995b). Effects on AMPAR EPSCs are most apparent when AMPAR desensitization is inhibited but can also be observed when desensitization is intact, particularly under conditions of high probability of transmitter release (Mennerick and Zorumski, 1995b; Otis et al., 1996; Higgs and Lukasiewicz, 1999). When the probability of release is low, transport inhibition does not alter EPSC time course. This suggests that diffusion is the primary means of clearing glutamate for small quantal-content synaptic events. Similar observations about the role of transmitter release probability have been described in cerebellar slices by using pharmacological transporter inhibition (Takahashi et al., 1995). Other studies indicate that neuronal transporters are activated by glutamate released at synapses in cerebellum (Takahashi et al., 1996; Otis et al., 1997; Auger and Attwell, 2001).

14.3 USE OF ELECTROPHYSIOLOGY TO STUDY TRANSPORTER KINETICS: VOLTAGE AND SUBSTRATE PULSES

Our own work has focused on the use of voltage-clamp techniques to probe the role of glutamate transporters during glutamatergic synaptic transmission, which is described in subsequent sections. Our studies highlight some advantages of electrophysiological techniques for the study of transporter behavior. The current section briefly reviews the use of electrophysiology, largely by other groups, to study the kinetics of native and recombinant transporters. A complete understanding of transporters must include an analysis of the speed with which transporters remove extracellular neurotransmitter substrate. Several studies have exploited the high temporal resolution of electrophysiology to isolate charge movements of transporters. From these measurements the rates of various steps in the transport cycle can be calculated. These studies commonly involve the perturbation of the baseline equilibrium of transporters with either a step-like change in membrane voltage or substrate concentration. Our review focuses on glutamate transporters, but similar techniques have been applied to virtually all sodium-dependent transporters, including glucose (Parent et al., 1992), monoamine (Galli et al., 1995; Galli et al., 1998), and γ aminobutyric acid (GABA) (Lester et al., 1994; Mager et al., 1996) transporters.

Kinetics of transporter turnover have been estimated by using an analysis of presteady-

state currents generated by glutamate transporters expressed in *Xenopus* oocytes, which have the advantage of expressing large amounts of transporter protein and generating large electrophysiological signals. Presteady-state currents are thought to represent the voltage-dependent loading and unloading of Na^+ ions from the transporter in absence of substrate (Parent et al., 1992; Lester et al., 1994). Transient outward currents are recorded with depolarizing voltage pulses; inward currents are recorded with hyperpolarizing voltage pulses. The transient nature of these currents (in the sustained presence of the voltage stimulus) and the symmetry of charge with voltage pulses of equal and opposite polarity suggest that the currents are capacitive and do not result from the actual permeation of ions through a channel. Examples of presteady-state currents obtained from an oocyte expressing the mouse GLAST glutamate transporter are shown in Figure 14.1.

Often, a nontransported substrate analog, such as the GLT-1 specific antagonist dihydrokainate (Wadiche et al., 1995b) or the broad-spectrum antagonist DL-threo-beta-benzyloxyaspartate (TBOA) (Shimamoto et al., 1998; Mennerick et al., 1999) is used to isolate presteady-state currents. Charge movements do not occur in the presence of these antagonists; therefore, presteady-state currents can be isolated from other capacitive and ionic currents unrelated to transporters by digitally subtracting currents in the presence of antagonist from currents in the absence of antagonist.

The major information gained from an analysis of presteady-state currents is an estimate of the number of transporters in a cell (Wadiche et al., 1995b). This information is obtained by plotting the integral of the antagonist-sensitive current (charge transfer) as a function of membrane potential. This relationship is voltage-dependent, and a fit with a Boltzmann distribution provides estimates of $V_{1/2}$, the half voltage of activation and of k, the slope factor. The parameters of the Boltzmann fit also provide an estimate of $z\delta$, the equivalent charge movement (where z is the ion's valence and δ is the fraction of the electrical field sensed). Given that the total charge movement (Q_{max}) is known from the integral of the presteady-state currents, the number of transporters (N) in the oocyte can be estimated by $N=Q_{max}/e_o z\delta$, where e_o is the elementary charge.

In a complementary steady-state analysis (performed on the same oocyte as the

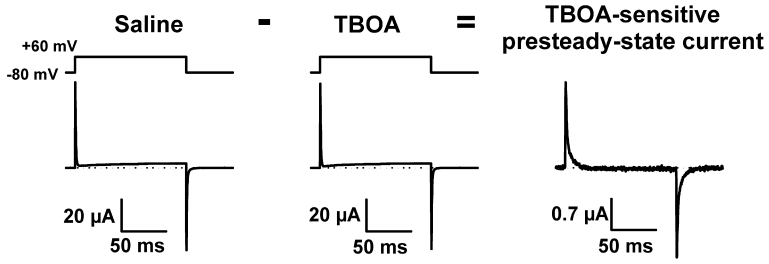

Figure 14.1. Presteady-state currents isolated from *Xenopus* oocytes expressing the mouse GLAST transporter. Left panel: In normal saline, a voltage pulse from –80 mV to + 60 mV (top trace) generates large capacitive and small ionic leak and voltage-gated currents. The dotted line indicates the zero current level. Middle panel: Shows the response to the same voltage protocol (in the same cell) but in the presence of 100 µM TBOA. Note that the cell's endogenous capacitive currents greatly exceed the TBOA-sensitive currents, so no difference between the currents in the absence and presence of TBOA is apparent at this gain and sweep speed. However, the right panel shows that on digital subtraction, TBOA-sensitive transient currents are apparent. Note the change in the *y*-axis calibration bar for this panel. Currents were filtered at 2 kHz and sampled at 10 kHz.

presteady-state analysis), a saturating concentration of radiolabeled glutamate is perfused onto the oocyte and the steady-state current amplitude is measured at –70 mV. The amplitude of the current in combination with the estimate of transporter number from presteady-state analysis can be used to estimate the number of elementary charges per second (ϕ) translocated by a transporter operating at steady state. ($\phi = I_{ss}/Ne_o$). After the experiment the amount of glutamate taken up by the oocyte is measured, yielding a measure (v) of the number of elementary charges transported per substrate molecule. This was estimated to be 2 for glutamate transporters (Wadiche et al., 1995b). The turnover rate is subsequently calculated as ϕ/v. From this analysis, the turnover time of glutamate transporters was estimated to be ~70 ms. Note that these studies make use of a unique advantage of *Xenopus* oocytes: These cells are sufficiently large to study radiotracer uptake into the same cell from which electrophysiological recordings are made.

A second major use of electrophysiology has been the rapid application of substrate onto excised membrane patches. These studies are typically performed in the presence of a chaotropic anion (e.g., nitrate or thiocyanate), which readily permeates the transporter anion conductance (see above) because currents in excised patches bathed in physiological saline are too small to resolve reliably. These studies can be performed either with recombinant transporters or with transporters expressed in native cells. The anion-conducting states of the transporter are thought to represent early stages of the transport cycle (Otis and Jahr, 1998) and therefore have been used to measure rates of entry and exit from these early states. Probably the most straightforward method for studying turnover rate of transporters is paired-pulse application of substrate to excised membrane patches. A brief (~10 ms) application of substrate elicits a transient anion current. With brief wash intervals, responses to subsequent identical substrate pulses are depressed, likely reflecting the desychronization of transporters and their population of various nonconducting, late stages of the transport cycle. With longer wash periods between paired pulses, the response gradually recovers with a time course that can be used to estimate the transporter cycling time. These estimates have suggested cycling times of 11–60 ms, depending on experimental conditions such as ambient temperature, membrane potential, and transporter isoform (Bergles and Jahr, 1997; Bergles and Jahr, 1998; Otis and Jahr, 1998; Otis and Kavanaugh, 2000; Auger and Attwell, 2001). These results are in general agreement with results from the presteady-state analyses, although on balance they suggest a slightly faster cycling time than presteady-state estimates. These slow cycling times suggest that, although glutamate removal may initially be fast (Auger and Attwell, 2001), apparently there is not time for individual transporters to "recycle" and remove multiple glutamate molecules during fast synaptic events, where the glutamate concentration is thought to rise and fall quite quickly (Bergles et al., 1999).

Rapid substrate applications have also been used to study other facets of transporter behavior. For instance, studies of currents in response to rapid substrate applications were used to estimate the rate of substrate association with transporter. From plots of the slope of the relationship between substrate concentration and time constant of activation (Wadiche and Kavanaugh, 1998), estimates of 6.8×10^6 M^{-1} s^{-1} were obtained. These techniques have also been used to "calibrate" the kinetics of synaptically evoked transporter currents to the intrinsic kinetics of the transporters (Bergles et al., 1997; Bergles and Jahr, 1997). Because synaptically generated currents were always slower than responses to step application and removal of glutamate to patches, it was suggested that significant synaptic and extrasynaptic glutamate persists for tens of milliseconds following release (Bergles et al., 1997; Bergles and Jahr, 1997; Dzubay and Jahr, 1999).

14.4 HIPPOCAMPAL MICROCULTURES AS A MODEL TO STUDY GLUTAMATE TRANSMISSION AND TRANSPORTERS

Our major interest in the study of glutamate transporters has been their action during synaptic transmission. To study glutamate-mediated transmission and modulation, it is important to use a preparation in which single-axon synapses, ambient glutamate levels, glutamate receptors, and glutamate transporters can be manipulated with precision. Because of the low frequency of encountering monosynaptically connected neurons, single axon transmission between pairs of neurons is difficult to study in brain slices or conventional neuronal cultures. In typical hippocampal mass cultures only ~30% of neuronal pairs are connected (Mennerick et al., 1995). Although this is an improvement over hippocampal slices, the frequency is sufficiently low to make systematic study difficult. This difficulty can be overcome by growing cells in a microculture environment (Segal and Furshpan, 1990; Segal, 1991). Microcultures are prepared by plating cells on dots of collagen that are dispersed on a nonadhesive substrate (agarose). The microcultures consist of glial islands (20–1000 μm in diameter) that are colonized by neurons (Fig. 14.2). The glial cells are primarily type I astrocytes that stain with antibodies against glial fibrillary acidic protein (GFAP; Fig. 14.2B2). On microislands containing two neurons, the frequency of encountering monosynaptically connected neurons is >80% (Mennerick et al., 1995). Additionally, neurons on islands containing only a single neuron form self-synapses (autapses) that have properties similar to synapses in conventional cultures or brain slices. On single neuron islands, single axon transmission can be studied in its simplest form by using a brief voltage step to depolarize the neuron and evoke transmitter release. Spontaneous EPSCs on single neuron islands have properties of miniature EPSCs (mEPSCs, thought to represent the response to a single vesicle of transmitter) and arise from the same axon involved in evoked synaptic transmission. Considering the average miniature EPSC amplitudes of ~10 pA and typical evoked EPSCs of 1–20 nA, we estimate that autaptic evoked responses represent release of ~100–2000 quanta of transmitter.

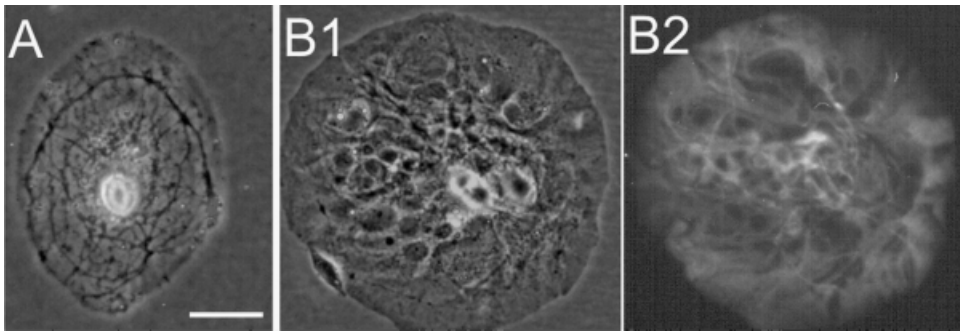

Figure 14.2. Single-neuron microculture and astrocyte immunostain. **A)** Phase-contrast photomicrograph of a single-neuron microculture such as that used for electrophysiology studies. Note that astrocytes are not readily apparent because of their flat morphology and phase-dark appearance. Neurites are visible extending from the soma of the neuron to surrounding glial areas. **B)** Another microculture stained with an antibody against GFAP. Phase-contrast image is shown in (**B1)** and a fluorescence image in (**B2)**. Note that two bright neuronal somas near the center of the microculture do not stain for GFAP. Scale bar indicates 26 μm for (**A**)and 43μM for (**B**).

Autapses are also observed on two-neuron islands, which makes it possible to study two synaptic targets of a single neuron - the autaptic response and the postsynaptic response in the second neuron (Mennerick and Zorumski, 1995a). This provides a useful tool in certain experiments and has been exploited in studies of network plasticity (Fitzsimonds et al., 1997). Two types of synapses are encountered on microislands-glutamatergic using synapses in which AMPARs and NMDARs mediate transmission and GABAergic synapses by using $GABA_A$ receptors (Bekkers and Stevens, 1991; Mennerick et al., 1995). The neuronal transmitter phenotype can be determined easily because glutamate and GABA responses differ pharmacologically and physiologically. In our cultures of postnatal rat hippocampus, about half of the single-neuron microislands have a glutamatergic neuron and half have a GABAergic neuron. By using the hippocampus of embryonic rats, it is possible to enrich the single-neuron islands for glutamatergic cells (Banker and Goslin, 1998).

A major advantage of the microcultures is that astrocytes can be studied directly during synaptic transmission (Mennerick and Zorumski, 1994). It is also possible to record glial transporter currents in situ (Bergles and Jahr, 1997; Clark and Barbour, 1997), but a disadvantage of in situ studies is that the extent of gap junction coupling of glia is likely large. Therefore, the number and extent of activated synapses being monitored is unclear. Although most microislands have more than one glial cell, the entire glial island usually can be adequately voltage-clamped (through the gap junctions between the glia). The experimenter knows from the size of the autaptic current of the neuron approximately how many synapses are activated and contribute to the glial current. Using dual recordings from neurons and astrocytes, we routinely observe glutamate-evoked currents in glial cells following glutamate release at synapses. An example of a dual recording from a single neuron and an underlying astrocyte is shown in Figure 14.3A. The neuron was stimulated at a 400 ms interval with 1.5 ms depolarizations to 0 mV but was otherwise clamped at –70 mV. The astrocytes (lower traces) were clamped at –70 mV throughout. Based on current-voltage curves of glial responses, inhibition of glial responses by sodium replacement with lithium, and the use of pharmacological antagonists, the glial currents largely (>80%) reflect electrogenic glutamate uptake. Thus, glial glutamate transporters are activated by synaptically released glutamate.

Glutamate transport is voltage-dependent. Therefore, glial glutamate transport can be selectively inhibited over neuronal transport by glial depolarization. Because of the ability to monitor an EPSC from a physically confined set of synapses all arising from one cell and the ability to alter the membrane potential of the glia associated with this set of synapses, one can study reciprocal interactions between the glia and the neuron. Again, because of the distributed nature of synapses in situ, this is a unique advantage of microcultures. Using this approach, we found that glial uptake contributes little to the decay of AMPAR-mediated synaptic responses when the probability of transmitter release is low. However, when the probability of release increases and desensitization of AMPARs is inhibited with cyclothiazide (CYZ), EPSCs are prolonged by glial depolarization or by pharmacological inhibition of glutamate transport (Mennerick and Zorumski, 1994). In some neurons, AMPAR EPSCs are prolonged by glutamate transport inhibition in the absence of CYZ, which suggests that the probability of glutamate release affects the time course of EPSCs (Mennerick and Zorumski, 1995b). This could occur if there is crosstalk between adjacent synapses, spillover of synaptic glutamate onto extrasynaptic receptors “shared” by several synapses, or if there is multivesicular release of transmitter from a single release site, causing glutamate within the cleft to persist longer when transmitter

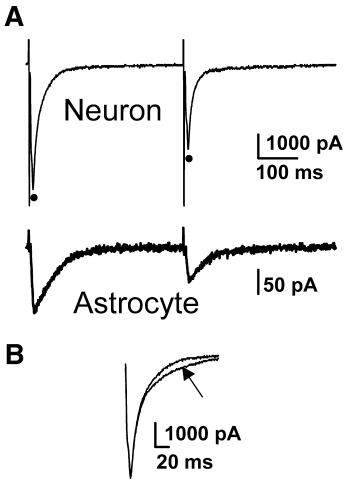

Figure 14.3. Dual recording of neurons and astrocytes during synaptic transmission. **A)** Top traces represent the membrane current in a solitary microculture neuron. The neuron was stimulated with twin depolarizing pulses from –70 mV to 0 mV for 1.5 ms, separated by 400 ms. The very fast transient currents (truncated) represent the fast capacitive and ionic currents that flow during the depolarization. The secondary, slower inward current (peak indicated by dots) represents the autaptic EPSC. The bottom traces represents a voltage-clamp recording from the underlying astroycte bed, clamped to –70 mV throughout the trace. **B)** Two EPSCs are superimposed. One is a re-plot of the first EPSC from (**A**). The second EPSC (arrow) represents a trace obtained while underlying astrocytes were clamped to +60 mV, beginning 2 s before the neuronal stimulation. Reversal of the astrocytes' membrane potential had no effect on the peak autaptic current or early phases of the EPSC decay but slightly slowed the late phase of the EPSC decay.

release probability is high. A presynaptic influence on EPSC decay has been observed also at cerebellar synapses (Takahashi et al., 1995; Kinney et al., 1997) and brain stem synapses (Trussell et al., 1993).

Glial transporter currents activated by synaptic glutamate release on hippocampal microcultures appear to reflect directly the degree of glutamate output at synapses. In a series of studies, we found that manipulations that alter presynaptic glutamate release, including changes in the extracellular calcium/magnesium ratio and presynaptic inhibitors (baclofen or adenosine), increase or decrease glial responses during synaptic transmission in the expected direction based on changes in the amplitude of autaptic neuronal currents. Furthermore, nonpharmacological manipulation of glutamate release (e.g., paired-pulse synaptic plasticity) causes changes in the amplitude of glial currents (Mennerick and Zorumski, 1994; Mennerick and Zorumski, 1995a). Similar results have been obtained in recordings from glia in hippocampal slice preparations and have been used to support the argument of a postsynaptic localization of change with long-term potentiation (Diamond et al., 1998; Luscher et al., 1998).

In another use of glial transporter currents, the percentage of synaptic released glutamate captured by transporters compared with that lost by diffusion can be calculated. If one makes estimates of the number of charges moved per glutamate molecule on each transporter cycle (Wadiche et al., 1995b), the number of transmitter molecules in a vesicle of glutamate, and the size of a miniature EPSC (Mennerick and Zorumski, 1995b), one

can calculate the number of glutamate molecules released by an evoked synaptic event and the corresponding number of molecules taken up by transporters (Mennerick et al., 1996). Both in culture (Mennerick et al., 1996) and in situ (Otis et al., 1997; Auger and Attwell, 2001), it appears that glial and neuronal transporters are capable of capturing a high percentage of released glutamate (20–80%). Thus, despite their slow cycle time, high numbers of transporters are capable of efficient transmitter removal.

Synaptic glutamate release on hippocampal microcultures also activates glial AMPARs. Interestingly, when glutamate is applied exogenously to hippocampal astrocytes, most of the evoked current is mediated by rapidly desensitizing AMPARs (Mennerick et al., 1996). This finding suggests that glial AMPARs may be distributed further from synapses than glial glutamate transporters and neuronal AMPARs. However, the function of glial AMPARs remains uncertain. Hippocampal glia do not exhibit NMDAR-mediated responses and to date we have not observed currents in glial cells in response to mGluR agonists, although robust mGluR signals in microculture glia can be observed by using calcium imaging (Cormier et al., 2001). Other groups, however, have observed mGluR-mediated changes in calcium levels in astrocytes in response to synaptic activation (Nedergaard, 1994; Parpura et al., 1994), providing another means for neuronal-glial signaling. Although robust in culture, the relevance of ionotropic receptors to glial function in situ is unclear. Hippocampal astrocytes in situ also appear to have AMPA receptors (Steinhauser et al., 1994; Verkhratsky and Steinhauser, 2000), and Ca^{2+}-permeable AMPA receptors on Bergmann glia in cerebellum appear critical for proper morphological ensheathment of glutamate synapses and thus indirectly influence glutamate clearance (Iino et al., 2001).

The ability of glial transporters to remove synaptically released glutamate supports the idea that glia are important participants in synaptic transmission. In addition to clearing glutamate after release and maintaining low ambient glutamate levels, glia are capable of releasing glutamate under certain conditions via reverse transport. This glial glutamate release can activate neuronal glutamate receptors and thus modulate synaptic transmission as well (Maki et al., 1994). Reverse transport is favored when glia are depolarized (increased $[K^+]_o$) or when cellular energy is low (hypoxia, low glucose) (Attwell et al., 1993; Rossi et al., 2000). Again, the confined physical environment of microcultures offers the possibility of studying the kinetics and amplitude of glutamate release via reverse transport by directly voltage-clamping the glial island and using the neuron's glutamate-gated receptors as a bioassay of the degree of glial glutamate release.

Although glutamate transport is not strictly energy-dependent (i.e., does not directly require hydrolysis of adenosine triphosphate, ATP), changes in energy metabolism alter the function of Na^+/K^+-ATPases and cause changes in ionic gradients that result in diminished glutamate transport. This suggests that glutamate transport reflects cellular energy status, and evidence indicates a close coupling between CNS glucose utilization and glutamate transmission (Pellerin and Magistretti, 1994).

14.5 ADVANTAGES AND LIMITATIONS OF MICROCULTURES

Microcultures consist of one or a few neurons residing on an underlying complement of astrocytes in a physically restricted and isolated space. Typical microislands used for physiological studies are 50–500 μm in diameter. Importantly, each microisland has no physical or synaptic contact with any other microisland in a culture dish. The physical boundaries provide major advantages for studying the electrophysiological properties of

both neurons and glial cells, allowing studies that are difficult in slice preparations or mass cultures. Some specific examples are given in the previous section. Polysynaptic or network contributions to synaptic responses can be eliminated by restricting experiments to microcultures containing only a single excitatory neuron and its associated astrocytes.

On single-neuron microislands, autaptic responses are typically very large (>1000 pA peak response). Because the charge transfer observed during glutamate transport is low (only a few net charges per cycle), the large amount of glutamate released by a single neuron at its autapses may be important in providing sufficient transmitter to produce reliable signals in the astrocytes. It is also relatively easy to manipulate either pre- or postsynaptic neuronal function to observe effects on glial cells.

The physical restrictions of microcultures also have advantages specific to the study of GFAP-positive astrocytes. These glial cells form extensive gap junctions (Stephens et al., 1993) that can make it impossible to voltage-clamp responses effectively in either slice preparations or mass cultures. Based on the dual recordings from glial cells on a single microisland, we have found that if studies are restricted to microislands of 300 μm or less in diameter, the entire glial bed of the microculture can be reasonably well voltage-clamped (Mennerick and Zorumski, 1994). This allows experimental control over glial membrane potential, an important variable in the operation of transporters driven by electrochemical gradients. Furthermore, the restricted space of the microcultures enhances the ability to achieve rapid, but gentle solution exchanges over the entire island.

There are also significant limitations of microculture methods. Most disadvantages can be viewed as sacrifices that must be weighed against the advantages of added experimental control noted above. Most notably, these cultures are prepared from early postnatal animals, and thus may reflect a relatively early phase of synaptic development. It is also possible that culture environments alter cell phenotype in unanticipated ways that may limit generalization of results. For example, microculture (and mass culture) neurons express GLT-1 transporter protein (Mennerick et al., 1998; Plachez et al., 2000), a primarily glial transporter that is expressed transiently during development by neurons in situ (Furuta et al., 1997) and after ischemic insults (Martin et al., 1997). In culture, expression of GLT-1 appears to be dendritic (Mennerick et al., 1998), whereas it is reported in white matter during development (Furuta et al., 1997). Also, in hippocampus, the glial transporter GLAST is the dominant transporter in astrocytes early in development and is supplanted in prominence by GLT-1 over the first two weeks of postnatal life (Ullensvang et al., 1997). Over the time course of our studies (2–3 weeks in vitro), we observe robust GLAST expression in astrocytes, but GLT-1 does not increase notably. It is not known whether significant functional differences exist between GLAST and GLT-1, but it is important to keep in mind that studies in microculture astrocytes primarily represent studies of the GLAST transporter.

14.6 MICROCULTURE PREPARATION

Dish Preparation

Careful preparation of tissue culture dishes is a major step in the plating of microcultures. The microcultures consists of islands of glia and neurons on an otherwise nonpermissive background. For our studies, we prepare culture dishes the day before plating. A 0.15% agarose solution serves as the nonpermissive substrate. The agarose solution is prepared

in tissue-culture water, and the solution is sterilized in an autoclave for 20 min. While still warm, a small drop of agarose is spread uniformly across the bottom of a 35 mm plastic culture dish by using a bent sterile Pasteur pipette and is allowed to dry overnight. We typically use 35 mm plastic tissue culture dishes for platings, although microcultures can also be grown on glass coverslips (Segal and Furshpan, 1990), and we have successfully used glass coverslips for our imaging studies (Cormier et al., 2001). Special care needs to be taken to ensure that the agarose does not bead up, especially if glass is used (Segal et al., 1998).

The day after agarose application, a solution of rat-tail collagen dissolved in acetic acid is sprayed on the bottom of the dishes using either a microatomizer (Thomas Scientific, Inc., Swedesboro, NJ) or a homemade atomizer that uses bottled air to atomize a droplet of collagen suspended from a capillary tube. We have found that the latter is preferable, as commercial atomizers can exhibit considerable variability in the size of droplets produced. This step is critical for preparing microcultures of appropriate size for physiological studies. Based on trial and error, we now hold dishes in the air at arm's length from the atomizer to coat with collagen droplets. This procedure usually results in small collagen dots (50–500 μm diameter), which work best for synaptic studies. Following collagen application, the dishes are sterilized for 30 min by ultraviolet irradiation in a tissue culture hood. Several adhesive substrates other than rat-tail collagen have been used successfully for hippocampal microcultures. We have found that human placental collagen (Sigma, St. Louis, MO) gives similar results to rat-tail collagen, and we have had some success using Matrigel (Collaborative Research, Bedford, MA).

Cell Preparation

The culture medium consists of supplemented Dulbecco's Eagle's minimal essential medium (DMEM). The day of plating, supplements are added to MEM at the following final concentrations: horse serum (5% v/v), fetal calf serum (5% v/v), D-glucose (17 mM), glutamine (400 μM), penicillin (50 U ml^{-1}), and streptomycin (50 μg ml^{-1}).

Prior to hippocampal dissection, a solution of 0.02% (weight/volume) bovine serum albumin (BSA) is prepared in L-15 medium. A 9-ml quantity of this solution is filter-sterilized (via a 0.2 μm syringe filter), warmed to 37°C, and gently bubbled through a cotton-plugged, sterile Pasteur pipette with 95% O_2/5% CO_2 for later use as a dissection solution. Papain is dissolved (1 mg/ ml) in a separate 3 ml aliquot of the BSA/L-15 solution. The papain solution is also filter-sterilized and warmed to 37°C and oxygenated.

Hippocampal cells are prepared from neonatal (1–3 day old) rat pups. Although older animals can be used, we have found cell viability to decrease with increasing age. We have also successfully grown postnatal mouse hippocampal cultures, although in our hands inclusion of insulin/transferrin/selenium mixture (Sigma) to the plating media is essential to survival of the mouse cultures. All instruments used for dissection are sterilized by immersion in 70% ethanol for at least 30 min before use. At the time of dissection, rat pups are anesthetized and decapitated rapidly by using sharp scissors. The skull is removed gently by cutting along the midline with small surgical scissors and by using forceps to pull the skull away laterally. The brain is removed gently with a spatula into a culture dish containing warmed, oxygenated BSA/L-15 solution. The brain is hemisected along the midline, the cerebellum and midbrain are removed, and hippocampi are dissected from surrounding cortex by using a blunt spatula. Transverse hippocampal slices ~500-μm thick are cut by using a small surgical scalpel, and the slices are transferred to

the papain solution. Hippocampal slices are gently agitated intermittently during a 25-minute incubation in papain. Following enzymatic digestion, papain is removed and slices are placed in supplemented MEM. Pasteur pipettes of decreasing diameter are used to triturate the slices until a single-cell suspension is obtained. Six hippocampi (three rat pups) yield ~5 ml of the cell suspension, which we subsequently dilute 15-fold in supplemented MEM. This yields a cell density of ~20,000 cells/ml, and 1.5 ml of this final suspension is added to each culture dish. We do not routinely feed the cultures with fresh media following plating; however, 72 h after plating, cultures are treated with 10 μM cytosine arabinoside (ARA-C) to inhibit glial proliferation.

For synaptic physiology, we typically use cultures 8–15 days following plating. For unknown reasons, our microcultures do not survive as long as conventional high-density mass cultures. Whereas, conventional cultures can survive for several months, our microcultures typically survive 3–4 weeks. Others have reported longer survival of microcultures by using a somewhat different culturing protocol (Segal and Furshpan, 1990).

Following plating, glial cells adhere to the collagen droplet and expand over several days, often filling the entire collagen droplet. The glia exhibit a flattened morphology and large, prominent nuclei when viewed with phase-contrast optics. Both by electrophysiological and by dye-coupling criteria, we have observed extensive gap-junction coupling of microculture glia. Additionally the cells express GFAP immunoreactivity. These features are all typical of Type I astrocytes in other primary culture systems (Stephens et al., 1993).

In the dissection process, neurons usually lose their dendrites and axons and have a spherical, bright appearance under phase-contrast optics. Neurons adhere to the glial cells on microislands following plating, and, over time in culture, re-grow their processes. Some of these processes remain on top of the glial bed, whereas others are embedded between the layers of glial appendages (Mennerick et al., 1996), thus simulating the situation in vivo, where glia surround neuronal processes and synapses (Peters et al., 1991). By physiological, pharmacological, and immunohistochemical criteria, about half the neurons in microcultures are GABAergic, and half are glutamatergic. Cells with larger somata and thicker, more elaborate processes tend to be excitatory (Segal and Furshpan, 1990; Mennerick et al., 1995); these visual characteristics allow us to select excitatory cells for study *a priori* with a high degree of success. In most cases, we find five or more single-neuron microcultures suitable for recording in a single culture plate. For dual recordings from glia and neurons, we exercise bias toward choosing smaller microcultures with neurites that appear to be buried between glia.

14.7 PHYSIOLOGY METHODS

Electrophysiological Recordings

Microculture recordings use conventional whole-cell patch clamp methods. An inverted microscope (Nikon, Melville, NY, USA) equipped with phase-contrast optics and a 40× phase-contrast objective is used to visualize cells. Two recording headstages are necessary for dual neuron/glia recordings. These are mounted onto remotely operated hydraulic micromanipulators (Narishige, Eastmeadow, NY, USA) for positioning. For our recordings, we typically use two patch-clamp amplifiers. However, we have also used a patch amplifier to record the small-amplitude glial currents and a discontinuous voltage-clamp

amplifier for autaptic currents, which can be quite large. The outputs of the amplifiers are interfaced with a computer through an analog-to-digital converter (Axon Instruments, Union City, CA). For dual neuron/glia recordings, the interface and acquisition software must be capable of multichannel data acquisition. Both Axon Instruments and HEKA (HEKA Elektronik, Lambrecht/Pfalz, Germany) now sell dual headstage amplifiers (Multiclamp 700A and EPC9/2, respectively) capable of dual patch-clamp recording and multichannel data acquisition. Our data acquisition and analysis software is a combination of commercially available programs (pClamp, Axon Instruments) and custom applications. Data processing is achieved with spreadsheet programs (Microsoft Excel, Seattle, WA, USA, or Wavemetrics IgorPro, Lake Oswego, OR, USA) and scientific graphing programs (SPSS SigmaPlot; Chicago, IL, USA).

Patch Pipettes and Intracellular Recording Solutions

Patch pipettes are pulled from thick-walled borosillicate glass (1.2 mm outer diameter, World Precision Instruments, Sarasota, FL) to a tip diameter of ~1.0 μm by using a Brown-Flaming electrode puller (Sutter Instruments, Novato, CA, USA). Tips are lightly fire-polished by using a microforge (Narishige), and the pipettes are filled with a solution consisting of (in mM): potassium gluconate (140), sodium chloride (4), ethyleneglycol-bis(β-aminoethyl ether)-N,N,N',N'-tetraacetic acid (EGTA) (5), calcium chloride (0.5), N-(2-hydroxyethyl) piperazine-2'-(2-ethanesulphonic acid) (HEPES) (10), magnesium ATP (2), and guanosine triphosphate (0.5). The pH of the solution is adjusted to 7.25 by using potassium hydroxide. When filled with this pipette solution, pipettes have an open-tip resistance of 3–6 MΩ, measured with small voltage-command pulses applied to the patch pipette with the pipette tip submerged in the bath solution.

When the whole-cell recording configuration is achieved, the contents of the patch pipette diffuse quickly into the cell and replace the cytoplasmic contents. Therefore, selection of the patch-pipette solution is important. For instance, potassium is used as the main monovalent cation in the neuronal pipette solution in order to preserve normal action potential propagation down the axon during neuronal stimulation (see below). Potassium is typically used in the glial patch pipette because of the dependence of glutamate transport on intracellular potassium (Barbour et al., 1991), although Cs^+ has been used in successful recordings of glial transport currents as well.

Extracellular Recording Solutions

At the time of experiment, cells are switched from growth medium to an extracellular recording solution that contains (in mM): sodium chloride (140), potassium chloride (4), calcium chloride (2), magnesium chloride (1), glucose (10), and HEPES (10). The pH is adjusted to 7.25 with NaOH. Experiments are performed at room temperature (22–24°C). Conventional methods can be used to heat cultures and perform experiments at physiological temperatures.

During synaptic studies, the extracellular recording solution in which a microculture is bathed is continuously exchanged by using a local microperfusion system that allows reliable and gentle solution flow. The perfusion system consists of a mutibarrel pipette constructed from seven teflon tubes tightly enveloped with heat-shrink tubing (Small Parts, Miami Lakes, FL) and glued inside the hub of a blunted 21-gauge hypodermic needle.

Silicone sealant is used to make a water-tight seal between the collar of heat-shrink and the needle hub. The teflon tubes are attached to solution reservoirs (10 ml glass syringes), which are positioned 6–12 inches above the microscope stage. Outflow from the reservoirs can be either manually controlled (XPERTEK miniature flow-through valve, P.J. Cobert Associates, St. Louis, MO), or electronically controlled by miniature solenoid flow-through valves (Lee Valve Co., Essex, CT) and a commercially available valve controller (Automate Scientific, San Francisco, CA). Solution flow rate is adjusted by changing the height of the solution reservoirs or by altering flow resistance by changing the tubing diameter in a section of the flow lines.

We find that this multibarrel pipette is sufficiently gentle that it does not interfere with recordings, yet is fast enough that multiple solutions can be tested on an individual microculture. The pipette is mounted on an electrode holder positioned by micromanipulator ~500 μm from the microculture under study. During an experiment, outflow from one reservoir is always on while outflow from the others is off, which allows constant perfusion of the microculture with either control bath solution or with one of up to six experimental solutions. The solution flow rate is usually ~100 μl/min. Changes in junction currents at the tip of an open patch pipette suggest that local solution switches are achieved in 200–500 ms.

For study of glial responses to exogenous glutamate applications, faster solution exchanges are necessary. For fast drug applications, we use an array of 1.2 mm (outer diameter) glass capillaries tapered at their output to an outer diameter of ~400 μm. Gravity-driven solution flow from a given tube is controlled electronically with a miniature solenoid flow-through valve (Lee Valve Co.). Solution exchanges ~10 ms can be achieved on intact cells with this system. A disadvantage is that the linear array of tubes requires repositioning to align the relevant tube with the recorded cell before each drug application. Also, rapid solution flow (~1 ml/min) tends to result in disruption of the gigaseal and loss of the recording.

Recording Method

We use phase-contrast optics and a 40× "dry" objective for visualizing the target cell. The recording pipette is filled with the chosen potassium or cesium-based intracellular solution and mounted in the headstage pipette holder. Slight positive pressure is applied to the pipette tip through the side port to prevent contamination of the pipette tip by bath debris. The pipette is then submerged in the bath and lowered until the tip just touches the target astrocyte. With relief of the positive and subsequent application of slight negative pressure, a high resistance (1–100 gigaohms) seal between the pipette tip and cell membrane usually forms. For glial cells, which flatten considerably in culture, there is a limited margin for error in manipulating the patch pipette. Contact between the recording pipette and the glial cell can be monitored either visually or electrically, by observing a slight increase in pipette resistance indicative of membrane contact. Following seal formation, the whole-cell recording mode is achieved by rupturing the membrane beneath the patch pipette with slight suction. For reasons that are unclear, increases in access resistance during recordings are more common with glial recordings than with neuronal recordings. Negative pressure applied constantly during recordings helps to prevent increases in access resistance during recordings (neurons do not tolerate a sustained negative pressure). Also, we typically use lower resistance pipettes for astrocyte recordings than neuron recordings because the lower resistance pipettes decrease the probability of access resistance increases.

For most experiments, both the neuron and glial cells are voltage-clamped at –70 mV. A brief (1.5 ms) voltage pulse to 0 mV is sufficient to trigger an action potential in the axon of the neuron that escapes clamp. The resulting neuronal currents include very fast transient currents, reflecting the capacitive charging of the membrane and the partially clamped sodium and potassium action currents. Stimulation will not elicit an evoked autaptic response when the sodium-channel blocker tetrodotoxin is present in the extracellular bath (Bekkers and Stevens, 1991). This suggests that a breakaway action potential is necessary for synaptic stimulation and that the electronic depolarization caused by the pulse to 0 mV imposed at the soma is not sufficient to trigger release.

With single-neuron excitatory microcultures, these transient currents are followed by an inward excitatory autaptic current. By pharmacological and kinetic criteria, these currents are mediated by AMPA receptors, and, under appropriate conditions (ambient glycine and no extracellular Mg^{2+}), NMDA receptors also contribute to the response.

We typically stimulate neurons at a frequency <0.1 Hz to avoid frequency-dependent facilitation and depression of synaptic responses. Most synapses in the cultures exhibit paired-pulse and frequency-dependent depression. However, by lowering the probability of initial transmitter release depression is relieved and facilitation often emerges (Mennerick and Zorumski, 1995a). Thus, like many synapses, both negative and positive short-term plasticity can be elicited from autapses.

Transporter-associated Chloride Conductance

A significant problem in studying glial glutamate transporter currents is that these responses, either when elicited by synaptic transmission or by exogenous glutamate applications, are relatively small (10–250 pA peak current). This makes systematic studies of these currents difficult, particularly when examining currents in outside-out patches by using rapid solution exchanges. Glutamate transporters also have an associated chloride conductance that is not linked stoichiometrically to the transport process (Wadiche et al., 1995a). However, this chloride conductance is relatively large and is activated by glutamate with an apparent affinity similar to the transport currents (Mennerick et al., 1999). This makes it advantageous to study the chloride currents for drawing inferences about the function of the transporters. Additionally, the relatively large size of the chloride conductance makes it possible to record these currents in outside-out membrane patches by using rapid applications of glutamate or transport substrates.

The transporter-associated chloride conductance is highly permeable to the chaotropic anion, thiocyanate (SCN). Thus to record these currents, NaCl in the extracellular solution is usually replaced by NaSCN and potassium gluconate in the patch pipette solution is replaced by potassium thiocyanate.

14.8 IMAGING STUDIES IN MICROCULTURES

Glutamate transporter activity can also be monitored by imaging the levels of intracellular ions. The use of fluorescence methods is discussed in detail by Kavanaugh (Chapter 13), and imaging is discussed by Kung (Chapter 15). We briefly describe the application of imaging to the study of glutamate transporters in our laboratory as an adjunct to electrophysiology. Because the co-transport of three Na^+ ions and the movement of one pH-changing ion (most likely H^+ influx) accompany the transport of one glutamate molecule, either $[Na^+]$ or $[H^+]$ may be imaged as a measure of glutamate transport. Also, analogous

to use of the anion current to monitor transport function electrophysiologically, recently developed anion indicators such as 6-methoxyquinolinium derivatives (Molecular Probes, Eugene, OR) could, in principle, be used to monitor transporter function. The chloride indicators, however, suffer from the limitation of not being ratio-able. Imaging provides the advantage of high spatial resolution but typically suffers from temporal resolutions and sensitivities that are less than those obtained with electrophysiology.

The indicators used to image $[Na^+]$ (SBFI) and $[H^+]$ (BCECF) are both ratio-able and thus provide stable measurements under various conditions, such as indicator concentration and cell thickness. The absorption and emission spectra of SBFI are similar to fura-2, which allows the same filter set to be used to image either $[Ca^{2+}]$ or $[Na^+]$. Although the absorption spectra of BCECF are different from fura-2 and SBFI, the emission spectra are similar. Therefore, a standard imaging rig with a 10-position filter wheel can measure $[Na^+]$, $[H^+]$, and $[Ca^{2+}]$ with four excitation filters and single-emission filter/dichroic mirror combination. Thus, any Ca^{2+} imaging rig is ready to study glutamate transport.

For imaging studies, we use microcultures grown on glass coverslips (Cormier et al., 2001). Isolated hippocampal cells are plated onto 12-mm-diameter #0 glass cover slips (Carolina Biological Supply Co., Burlington, NC, USA) at a density of 75 cells/mm^2. Before plating, four coverslips are placed in a 35 mm plastic tissue culture dish and are coated with 0.15% agarose as described previously. These dishes are dried overnight and sprayed with small droplets of collagen by using a microatomizer. As with our routine microcultures, astrocyte proliferation is halted by treatment with 10 μM cytosine arabinoside after 3 days in vitro. Experiments are performed on cells that have been in culture for 7–14 days.

At the time of study, a single glass coverslip containing microislands is placed in a chamber suitable for imaging. The chambers are made by drilling 18-mm holes into the bottom of plastic 35 mm tissue culture dishes and covering the holes with 25-mm-diameter #1 glass coverslips. Cells are loaded with the cell-permeant forms of dyes for the species to be imaged (e.g., SBFI AM for sodium imaging studies) in standard extracellular recording solution. Before loading with SBFI AM (Molecular Probes), the extracellular solution is equilibrated in an incubator for 1 h. The extracellular solution is then replaced with the same solution containing 5 μM SBFI AM, and the cells are returned to the incubator for 45 min. The cells are then rinsed twice in extracellular solution and returned to the incubator for an additional 45 min.

Imaging is typically done at room temperature (22°C) on the stage of a Nikon Eclipse inverted microscope equipped with phase-contrast and fluorescence optics, 40× objective, intensified CCD (PTI), and frame grabber (Scion Corporation, Frederick, MD, USA). Light from a 75 W Xenon arc lamp is directed sequentially through 340 and 380 nm band-pass filters (Chroma, Brattleboro, VT, USA) for 100 ms each by using a filter wheel (Sutter Instruments). We use custom software for imaging and analysis, but commercial packages are available (Metafluor, Universal Imaging, Downington, PA). Dark image values are subtracted electronically on the camera controller. Ratio values (340/380) are converted to sodium concentrations by using standard methods (Grynkiewicz et al., 1985). R_{min} and R_{max} values are determined by imaging sodium standards in a microcuvette.

For our studies, an imaging chamber is fixed to the microscope stage. This chamber has a laminar flow superfusion system to keep the chamber continuously replenished with fresh extracellular solution. Test solutions are delivered to selected microislands by using a gravity-driven multibarrel system with a common port (50–60 μM tip opening). The tip

of this local perfusion system is placed ~50 μM from the microisland being observed, and solution flows at a rate of 0.15 ml/min (Cormier et al., 2001).

14.9 ANTIBODY STAINING METHODS

For immunocytochemistry, cultures are rinsed in phosphate-buffered saline (PBS) and fixed with 4% paraformaldehyde and 0.2% glutaraldehyde for 5 min. Following fixation, cultures are treated with 1.5% hydrogen peroxide, blocked with serum from the animal in which the secondary antibody is raised and permeabilized with 0.1% Triton X-100. Primary antibodies against glutamate transporters are diluted in blocking solution and administered at concentrations determined empirically. In control experiments designed to block the primary antibody, the primary antibody is incubated overnight in 10-to 100-fold molar excess of free oligopeptide.

Antibody binding to permeabilized cells is determined by using a horseradish peroxidase/diaminobenzidine tetrahydrochloride reaction with nickel intensification (Vector ABC Elite Kit, Vector Laboratories, Burlingame, CA). In some experiments, the primary antibody is visualized by using a Cy3- or FITC-conjugated secondary antibody obtained from Chemicon (Temecula, CA, USA).

14.10 SUMMARY

Microcultures of neurons and astrocytes provide a useful experimental preparation for studying the role of glia and glutamate transporters in synaptic physiology. The preparation offers good experimental control over a number of important variables and provides a convenient system for recording directly and simultaneously from neurons and glia during synaptic transmission. Although derived from immature animals and subject to potential alterations in phenotype as a result of the culture environment, synaptic transmission in the microcultures mimics many fundamental features of synapses in situ.

ACKNOWLEDGMENTS

The authors thank A. Benz for help in the development and maintenance of the microcultures. Work in the authors' laboratories is supported by grants MH45493 and GM47969, the Bantly Foundation, The National Alliance for Research in Schizophrenia and Depression, and the Klingenstein Fund, NS40488, and AA12952.

ANNOTATED REFERENCES

Arriza JL, Eliasof S, Kavanaugh MP, Amara SG (1997): Excitatory amino acid transporter 5, a retinal glutamate transporter coupled to a chloride conductance. Proc Natl Acad Sci USA 94:4155–4160.

Attwell D, Barbour B, Szatkowski M (1993): Nonvesicular release of neurotransmitter. Neuron 11:401–407.

Auger C, Attwell D (2001): Fast removal of synaptic glutamate by postsynaptic transporters. Neuron 28:547–558.

The authors suggest that a component of glutamate removal is very fast and suggest that anions may influence the kinetics of transport.

Banker G, Goslin K (eds) (1998): Culturing nerve cells, Second Edition. Cambridge, MA: The MIT Press.

This text is a must-have for those interested in primary cultures of CNS tissue. The text includes protocols for purified astrocyte cultures and preparation of microcultures.

Barbour B, Brew H, Attwell D (1991): Electrogenic uptake of glutamate and aspartate into glial cells isolated from the salamander (Ambystoma) retina. J Physiol (London) 436:169–193.

Beckstrom H, Julsrud L, Haugeto O, Dewar D, Graham DI, Lehre KF, Storm-Mathisen J, Danbolt NC (1999): Interindividual differences in the levels of the glutamate transporters GLAST and GLT, but no clear correlation with Alzheimer's disease. J Neurosci Res 55:218–229.

Bekkers JM, Stevens CF (1991): Excitatory and inhibitory autaptic currents in isolated hippocampal neurons maintained in cell culture. Proc Natl Acad Sci USA 88:7834–7838.

Bergles DE, Jahr CE (1997): Synaptic activation of glutamate transporters in hippocampal astrocytes. Neuron 19:1297–1308.

Bergles DE, Jahr CE (1998): Glial contribution to glutamate uptake at schaffer collateral-commissural synapses in the hippocampus. J Neurosci 18:7709–7716.

Bergles DE, Dzubay JA, Jahr CE (1997): Glutamate transporter currents in Bergmann glial cells follow the time course of extrasynaptic glutamate. Proc Natl Acad Sci USA 94:14821–14825.

Bergles DE, Diamond JS, Jahr CE (1999): Clearance of glutamate inside the synapse and beyond. Curr Opin Neurobiol 9:293–298.

Bouvier M, Szatkowski M, Amato A, Attwell D (1992): The glial cell glutamate uptake carrier countertransports pH-changing anions. Nature (London) 360:471–474.

Burger PM, Mehl E, Cameron PL, Maycox PR, Maumert M, Lottspeich F, De Camilli P, Jahn R (1989): Synaptic vesicles immunoisolated from rat cerebral cortex contain high levels of glutamate. Neuron 3:715–720.

Clark BA, Barbour B (1997): Currents evoked in Bergmann glial cells by parallel fibre stimulation in rat cerebellar slices. J Physiol (London) 502:335–350.

Clements JD, Lester RA, Tong G, Jahr CE, Westbrook GL (1992): The time course of glutamate in the synaptic cleft. Science 258:1498–1501.

Cormier RJ, Mennerick S, Melbostad H, Zorumski CF (2001): Basal levels of adenosine modulate mGluR5 on rat hippocampal astrocytes. Glia 33:24–35.

Danbolt NC (1994): The high affinity uptake system for excitatory amino acids in the brain. Prog Neurobiol 44:377–396.

Danbolt NC (2001): Glutamate uptake. Prog Neurobiol 65:1–105.

This is the most comprehensive review published to date on all facets of glutamate transporters.

Diamond JS, Jahr CE (1997): Transporters buffer synaptically released glutamate on a submillisecond time scale. J Neurosci 17:4672–4687.

Diamond JS, Bergles DE, Jahr CE (1998): Glutamate release monitored with astrocyte transporter currents during LTP. Neuron 21:425–433.

Dzubay JA, Jahr CE (1999): The concentration of synaptically released glutamate outside of the climbing fiber-Purkinje cell synaptic cleft. J Neurosci 19:5265–5274.

Eliasof S, Arriza JL, Leighton BH, Amara SG, Kavanaugh MP (1998): Localization and function of five glutamate transporters cloned from the salamander retina. Vision Res 38:1443–1454.

Fairman WA, Vandenberg RJ, Arriza JL, Kavanaugh MP, Amara SG (1995): An excitatory amino-

acid transporter with properties of a ligand-gated chloride channel. Nature (London) 375:599–603.

Fitzsimonds RM, Song HJ, Poo MM (1997): Propagation of activity-dependent synaptic depression in simple neural networks. Nature (London) 388:439–448.

Furuta A, Rothstein JD, Martin LJ (1997): Glutamate transporter protein subtypes are expressed differentially during rat CNS development. J Neurosci 17:8363–8375.

Gadea A, Lopez-Colome AM (2001a): Glial transporters for glutamate, glycine, and GABA: II. GABA transporters. J Neurosci Res 63:461–468.

Gadea A, Lopez-Colome AM (2001b): Glial transporters for glutamate, glycine and GABA I. Glutamate transporters. J Neurosci Res 63:453–460.

Galli A, Blakely RD, Defelice LJ (1998): Patch-clamp and amperometric recordings from norepinephrine transporters—channel activity and voltage-dependent uptake. Proc Natl Acad Sci U S A 95:13260–13265.

Galli A, DeFelice LJ, Duke BJ, Moore KR, Blakely RD (1995): Sodium-dependent norepinephrine-induced currents in norepinephrine-transporter-transfected HEK-293 cells blocked by cocaine and antidepressants. J Exp Biol 198:2197–2212.

Grunert U, Martin PR, Wassle H (1994): Immunocytochemical analysis of bipolar cells in the macaque monkey retina. J Comp Neurol 348:607–627.

Grynkiewicz G, Poenie M, Tsien RY (1985): A new generation of Ca^{2+} indicators with greatly improved fluorescence properties. J Biol Chem 260:3440–3450.

Hestrin S (1992): Activation and desensitization of glutamate-activated channels mediating fast excitatory synaptic currents in the visual cortex. Neuron 9:991–999.

Higgs MH, Lukasiewicz PD (1999): Glutamate uptake limits synaptic excitation of retinal ganglion cells. J Neurosci 19:3691–3700.

Iino M, Goto K, Kakegawa W, Okado H, Sudo M, Ishiuchi S, Miwa A, Takayasu Y, Saito I, Tsuzuki K, Ozawa S (2001): Glia-synapse interaction through Ca^{2+}-permeable AMPA receptors in Bergmann glia. Science 292:926–929.

Kanai Y, Hediger MA (1992): Primary structure and functional characterization of a high-affinity glutamate transporter. Nature (London) 360:467–471.

Kinney GA, Overstreet LS, Slater NT (1997): Prolonged physiological entrapment of glutamate in the synaptic cleft of cerebellar unipolar brush cells. J Neurophysiol 78:1320–1333.

Lester HA, Mager S, Quick MW, Corey JL (1994): Permeation properties of neurotransmitter transporters. Annu Rev Pharmocol Toxicol 34:219–249.

Lester RA, Clements JD, Westbrook GL, Jahr CE (1990): Channel kinetics determine the time course of NMDA receptor- mediated synaptic currents. Nature (London) 346:565–567.

Luscher C, Malenka RC, Nicoll RA (1998): Monitoring glutamate release during LTP with glial transporter currents. Neuron 21:435–441.

Mager S, Kleinberger-Doron N, Keshet GI, Davidson N, Kanner BI, Lester HA (1996): Ion binding and permeation at the GABA transporter GAT1. J Neurosci 16:5405–5414.

Maki R, Robinson MB, Dichter MA (1994): The glutamate uptake inhibitor L-trans-pyrrolidine-2,4- dicarboxylate depresses excitatory synaptic transmission via a presynaptic mechanism in cultured hippocampal neurons. J Neurosci 14:6754–6762.

Martin LJ, Brambrink A, Lehmann C, Porteracailliau C, Koehler R, Rothstein J, Traystman RJ (1997): Hypoxia-ischemia causes abnormalities in glutamate transporters and death of astroglia and neurons in newborn striatum. Ann Neurol 42:335–348.

Mennerick S, Zorumski CF (1994): Glial contributions to excitatory neurotransmission in cultured hippocampal cells. Nature (London) 368:59–62.

This paper demonstrates a role for astrocytes in clearing glutamate following the action-

potential mediated (multiquantal) release of glutamate at synapses in culture. Subsequent work confirmed a similar function in situ (Clark and Barbour 1997; Bergles and Jahr, 1998).

Mennerick S, Zorumski CF (1995a): Paired-pulse modulation of fast excitatory synaptic currents in microcultures of rat hippocampal neurons. J Physiol (London) 488:85–101.

Mennerick S, Zorumski CF (1995b): Presynaptic influence on the time course of fast excitatory synaptic currents in cultured hippocampal cells. J Neurosci 15:3178–3192.

Mennerick S, Benz A, Zorumski CF (1996): Components of glial responses to exogenous and synaptic glutamate in rat hippocampal microcultures. J Neurosci 16:55–64.

Mennerick S, Que J, Benz A, Zorumski CF (1995): Passive and synaptic properties of neurons grown in microcultures and in mass cultures. J Neurophysiol 73:320–332.

This paper documents a protocol for preparing microcultures and compares electrophysiological and synaptic profiles of hippocampal neurons grown in microcultures and in more conventional mass cultures.

Mennerick S, Dhond RP, Benz A, Xu W, Rothstein JD, Danbolt NC, Isenberg KE, Zorumski CF (1998): Neuronal expression of the glutamate transporter GLT-1 in hippocampal microcultures. J Neurosci 18:4490–4499.

Mennerick S, Shen W, Xu W, Benz A, Tanaka K, Shimamoto K, Isenberg KE, Krause JE, Zorumski CF (1999): Substrate turnover by transporters curtails synaptic glutamate transients. J Neurosci 19:9242–9251.

Nedergaard M (1994): Direct signaling from astrocytes to neurons in cultures of mammalian brain cells. Science 263:1768–1771.

Otis TS, Jahr CE (1998): Anion currents and predicted glutamate flux through a neuronal glutamate transporter. J Neurosci 18:7099–7110.

Otis TS, Kavanaugh MP (2000): Isolation of current components and partial reaction cycles in the glial glutamate transporter EAAT2. J Neurosci 20:2749–2757.

Otis TS, Wu Y-C, Trussell LO (1996): Delayed clearance of transmitter and the role of glutamate transporters at synapses with multiple release sites. J Neurosci 16:1634–1644.

Otis TS, Kavanaugh MP, Jahr CE (1997): Postsynaptic glutamate transport at the climbing fiber-Purkinje cell synapse. Science 277:1515–1518.

Parent L, Supplisson S, Loo DDF, Wright EM (1992): Electrogenic properties of the cloned Na^+/glucose cotransporter. I. Voltage-clamp studies. J Membr Biol 125:49–62.

Parpura V, Basarsky TA, Liu F, Jeftinija K, Jeftinija S, Haydon PG (1994): Glutamate-mediated astrocyte-neuron signalling. Nature (London) 369:744–747.

Pellerin L, Magistretti PJ (1994): Glutamate uptake into astrocytes stimulates aerobic glycolysis: a mechanism coupling neuronal activity to glucose utilization. Proc Natl Acad Sci USA 91:10625–10629.

Peters A, Palay SL, Webster HD (1991): Synapses. In: The Fine Structure of the Nervous System, 3rd Edition, pp 138–211. New York: Oxford University Press.

Pines G, Danbolt NC, Bjørås M, Zhang Y, Bendahan A, Eide L, Koepsell H, Storm-Mathisen J, Seeberg E, Kanner BI (1992): Cloning and expression of a rat brain L-glutamate transporter. Nature (London) 360:464–467.

Plachez C, Danbolt NC, Recasens M (2000): Transient expression of the glial glutamate transporters GLAST and GLT in hippocampal neurons in primary culture. J Neurosci Res 59:587–593.

Rossi DJ, Oshima T, Attwell D (2000): Glutamate release in severe brain ischaemia is mainly by reversed uptake. Nature (London) 403:316–321.

Scanziani M, Salin PA, Vogt KE, Malenka RC, Nicoll RA (1997): Use-dependent increases in glutamate concentration activate presynaptic metabotropic glutamate receptors. Nature (London) 385:630–634.

Schmitt A, Asan E, Puschel B, Jons T, Kugler P (1996): Expression of the glutamate transporter GLT1 in neural cells of the rat central nervous system: non-radioactive in situ hybridization and comparative immunocytochemistry. Neuroscience 71:989–1004.

Segal MM (1991): Epileptiform activity in microcultures containing one excitatory hippocampal neuron. J Neurophysiol 65:761–770.

Segal MM, Furshpan EJ (1990): Epileptiform activity in microcultures containing small numbers of hippocampal neurons. J Neurophysiol 64:1390–1399.

Original description of the microculture method applied to hippocampal neurons. Details of the culture protocol are given.

Segal MM, Baughman RW, Jones KA, Huettner JE (1998): Mass cultures and microislands of neurons from postnatal rat brain. In: Culturing Nerve Cells, Second Edition (Banker G, Goslin K, eds), pp 309–338. Cambridge, MA: The MIT Press.

Shimamoto K, Lebrun B, Yasuda-Kamatani Y, Sakaitani M, Shigeri Y, Yumoto N, Nakajima T (1998): DL-threo-beta-benzyloxyaspartate, a potent blocker of excitatory amino acid transporters. Mol Pharmacol 53:195–201.

This is an important paper in the pharmacology of glutamate transporters because it reports the synthesis of the first broad-spectrum nonsubstrate transport blocker. As a nonsubstrate inhibitor, this drug does not promote the phenomenon of heteroexchange; elease of a small amount of intracellular glutamate as the transporter takes up substrate inhibitor.

Steinhauser C, Jabs R, Kettenmann H (1994): Properties of GABA and glutamate responses in identified glial cells of the mouse hippocampal slice. Hippocampus 4:19–35.

Stephens GJ, Djamgoz MBA, Wilkin GP (1993): A patch clamp study of excitatory amino acid effects on cortical astrocyte subtypes in culture. Receptors Channels 1:39–52.

Storck T, Schulte S, Hofmann K, Stoffel W (1992): Structure, expression, and functional analysis of a Na(+)-dependent glutamate/aspartate transporter from rat brain. Proc Natl Acad Sci USA 89:10955–10959.

Takahashi M, Kovalchuk Y, Attwell D (1995): Pre- and postsynaptic determinants of EPSC waveform at cerebellar climbing fiber and parallel fiber to Purkinje cell synapses. J Neurosci 15:5693–5702.

Takahashi M, Sarantis M, Attwell D (1996): Postsynaptic glutamate uptake in rat cerebellar Purkinje cells. J Physiol (London) 497:523–530.

Thio LL, Clark GD, Clifford DB, Zorumski CF (1992): Wheat germ agglutinin enhances EPSCs in cultured postnatal rat hippocampal neurons by blocking ionotropic quisqualate receptor desensitization. J Neurophysiol 68:1930–1938.

Tong G, Jahr CE (1994): Block of glutamate transporters potentiates postsynaptic excitation. Neuron 13:1195–1203.

This paper suggests a very fast role of transporters in binding extracellular glutamate following release at the synapse. Block of transporters increased mEPSC peak amplitudes but had no effect mEPSC decay time course, suggesting that block of transporters effectively raises the synaptic concentration of glutamate without altering the time course of removal from the cleft, which is primarily determined by diffusion. See also Diamond and Jahr (1997).

Trussell LO, Zhang S, Raman IM (1993): Desensitization of AMPA receptors upon multiquantal neurotransmitter release. Neuron 10:1185–1196.

Ullensvang K, Lehre KP, Storm-Mathisen J, Danbolt NC (1997): Differential developmental expression of the two rat brain glutamate transporter proteins GLAST and GLT. Eur J Neurosci 9:1646–1655.

Verkhratsky A, Steinhauser C (2000): Ion channels in glial cells. Brain Res Brain Res Rev 32:380–412.

Wadiche JI, Kavanaugh MP (1998): Macroscopic and microscopic properties of a cloned glutamate transporter chloride channel. J Neurosci 18:7650–7661.

Wadiche JI, Amara SG, Kavanaugh MP (1995a): Ion fluxes associated with excitatory amino acid transport. Neuron 15:721–728.

Wadiche JI, Arriza JL, Amara SG, Kavanaugh MP (1995b): Kinetics of a human glutamate transporter. Neuron 14:1019–1027.

This paper combines clever analysis of steady-state and presteady-steady state currents with measurement of uptake into single oocytes to quantify the rate of transporter turnover. Results suggest turnover of a few tens of cycles per second and suggest that transporter numbers must be very high near the synapse to significantly influence the glutamate transient.

Zerangue N, Kavanaugh MP (1996): Flux coupling in a neuronal glutamate transporter. Nature (London) 383:634–637.

CHAPTER 15

IMAGING MONOAMINE TRANSPORTERS IN THE BRAIN

HANK F. KUNG AND MEI-PING KUNG

15.1 INTRODUCTION

Neurotransmitters are chemical messengers that are normally released in the synaptic cleft after a presynaptic signaling event. The chemical messengers bind to the postsynaptic receptors, through which neuronal signals are propagated. The processes play an important role on maintaining and regulating normal brain activity. Abnormalities in central nervous system (CNS) functions usually are associated with changes in the neuroreceptors and the presynaptic binding sites (transporters), and they are often targets for drug treatment of various neurological diseases (Cooper, 1996). In vivo imaging of the receptors and the transporters in the brain using positron emission tomography (PET) or single photon emission computed tomography (SPECT) provides powerful tools for studying CNS function in normal or disease states (Kegeles and Mann, 1997; Volkow et al., 1996). Imaging agents may be based on two types of isotopes. ^{99m}Tc ($T_{1/2}$, 6 h; 140 KeV) and ^{123}I ($T_{1/2}$, 13 h; 159 KeV) are routinely used for SPECT, whereas ^{11}C ($T_{1/2}$, 20 min; 511 KeV) and ^{18}F ($T_{1/2}$, 110 min; 511 KeV) are commonly used for PET. It is well recognized that PET has higher resolution, higher sensitivity, and better quantitative capability than SPECT. However, more hospitals are equipped with SPECT scanners; therefore, SPECT is more practical as a routine procedure (Cherry 2001; Garcia et al., 2000; Phelps 2000). Recent advances in physics and instrumentation on nuclear medicine imaging have extended the potential for imaging the receptors or binding sites in the brains of small animals (i.e., rats or mice) (Cherry 2001; Fahey 2001; Green et al., 2001; Kornblum et al., 2000; Phelps 2000). The small animal imaging devices are suitable for evaluating binding sites in the brains of transgenic animals noninvasively.

An on-site cyclotron is required to use PET tracers for imaging studies, especially for ^{11}C ($T_{1/2}$, 20 min). Most of the ^{11}C-labeled PET imaging agents are based on a labeling process with ^{11}C-methyliodide, which reacts with precursors rapidly to provide the desired tracer by an alkylation reaction. Because ^{11}C has a half-life of 20 min, the production and imaging by using the ^{11}C tracers pose extreme logistic and technical challenges. It is not readily available for routine clinical use yet. Tracers labeled with ^{18}F ($T_{1/2}$, 110 min) could be prepared by an off-site facility and shipped to the clinical facilities where the PET scanning devices are located. Recently, 2-[^{18}F]-fluoro-2-deoxy-glucose (FDG) has been approved by the U.S. Food and Drug Administration (FDA) for diagnosis of

Transmembrane Transporters, Edited by Michael Quick
ISBN 0-471-06513-7

epilepsy and detection of cancer. PET imaging as a clinical diagnostic tool is rapidly expanding to many hospitals. It is possible that additional tracers labeled with ^{18}F, including tracers specific for monoamine transporters, will be available in the future for routine clinical diagnosis.

Currently, SPECT neuroimaging studies of the brain are mostly performed by using ^{123}I ($T_{1/2}$ = 13 h, and emitting a gamma ray of 159 KeV). Radioiodination is readily achieved by either oxidative iodination or by iododestannylation reaction. For binding site-specific compounds, the iodine provides a suitable method to introduce a radioactive iodine, ^{123}I, into the tracer molecules for SPECT imaging (Wilbur, 1992). A large number of ^{123}I-labeled compounds have been prepared as CNS receptor-specific imaging agents and are routinely used for SPECT imaging studies. One of the major drawbacks of using ^{123}I-labeled compounds for routine imaging is the availability of the isotope. It is produced by cyclotrons or by accelerators; therefore, it is not readily available in the nuclear medicine clinics and requires overnight shipment from production sites. As a consequence it is relatively expensive and less accessible. On the contrary, ^{99m}Tc is the most suitable radionuclide commonly used in nuclear medicine clinics. This radionuclide has several advantages: i) favorable physical characteristics, $T_{1/2}$ = 6 h, and emitting a gamma ray of 140 KeV; ii) wide availability through the use of $^{99}Mo/^{99m}Tc$ generators; and iii) kit formulation (containing all of the ingredients and reaction vials in one package) providing simple preparation procedures for various ^{99m}Tc-based radiopharmaceuticals. The basic technetium chemistry of small molecules as radiopharmaceuticals has been reviewed previously (Hom and Katzenellenbogen, 1997; Jurisson and Lydon, 1999; Steigman and Eckelman, 1992). From a chemist's point of view, Tc chemistry is very challenging because of the nature of the metallic property, which is not readily amenable for incorporation into small molecule-based ligands for receptors or specific binding sites of biological importance. Technetium is a transition metal and requires chelating agents to stabilize it at different valence states. Due to the hazards and complications often associated with handling radioactive ^{99}Tc ($T_{1/2} = 2.1 \times 10^5$ yr, a β-emitter) in micromolar chemical quantity for common synthetic and analytical chemical procedures, a close surrogate, nonradioactive rhenium (Re), is often used instead for the complex confirmation and characterization. Perrhenate (+7 oxidation state) is the most common starting material. After reduction and complexation, the molecular sizes are usually large and bulky, which limit the flexibility in targeting a specific receptor or biological process(es) (Hom and Katzenellenbogen, 1997; Jurisson et al., 1993; Jurisson and Lydon, 1999). The ^{99m}Tc brain-imaging agents developed so far are mainly aimed at measuring regional perfusion or its changes due to a particular disease state. The brain uptake of [^{99m}Tc]HMPAO and [^{99m}Tc]ECD is based on simple diffusion due to high lipophilicity. However, the trapping mechanism(s) for brain retention of [^{99m}Tc]HMPAO and [^{99m}Tc]ECD are quite different: in vivo instability for HMPAO versus enzymatic degradation of ester groups in vivo for ECD (Walovitch et al., 1994; Jurisson et al., 1993).

When using in vivo imaging of CNS receptors or binding sites to evaluate the functional status of the receptors, the radiopharmaceutical, which is normally administered via an i.v. injection, is in a tracer level (in nano- or picogram quantity). Thus, the imaging agents used for diagnostic purposes are generally free of any pharmacological side effects. However, the tracers have other very stringent requirements before they can be applied successfully (Eckelman, 1998). The basic requirements for a useful receptor or site-specific imaging agent of the brain are the following:

1. Display high affinity to receptors or site-specific binding sites (K_i < 10 nM). The binding affinity required usually is inversely related to the density of the receptors or the specific binding sites to be imaged (Eckelman, 1998).
2. Exhibit high selectivity to the receptors or specific binding sites (affinity to other receptors >100-fold lower).
3. Can be labeled with ^{18}F, ^{11}C, ^{123}I or ^{99m}Tc in a short time with high labeling yield (>50%), high radiochemical purity (>95%), and high in vitro stability.
4. Can penetrate the intact blood-brain barrier and display high selective uptake and retention in regions known to have high density of receptors or specific binding sites.
5. Show relative high in vivo stability and low toxicity.
6. Show kinetic properties that can be readily modeled to obtain quantitative information.
7. Display a biodistribution pattern, which leads to an acceptable radiation exposure to humans.

Because of the stringent requirements and difficulties listed above, many ligands for CNS receptors and specific binding sites have been developed, but only a few are commercially available for routine clinical use.

15.2 DOPAMINE TRANSPORTER (DAT) IMAGING AGENTS

Development of DAT Imaging Agents

Ligands for dopamine transporters (DAT) are useful in evaluating changes in presynaptic DAT sites in vivo and in vitro, especially for patients with movement disorders such as Parkinson's disease (PD), which is characterized by a selective loss of DA neurons in the basal ganglia and substantia nigra. The first successful DAT imaging agent for PET, [^{11}C]CFT (WIN35,428), was reported in 1993 for evaluation of patients with PD (Frost et al., 1993). Numerous other [^{11}C]phenyltropanes have been reported (Schonbachler et al., 2002; Verhoeff, 1999). A similar SPECT imaging agent [^{123}I]β-CIT was reported in the early 1990s, which suggested a strong correlation between the decrease in localization in the putamen area and PD symptoms (Innis, 1994; Innis et al., 1993; Seibyl, 1999). The results of using ^{123}I agents for imaging patients with PD provided an impetus for further development of these agents for diagnosing and monitoring treatment. Currently, [^{123}I]β-CIT (Carroll et al., 1995; Seibyl et al., 1997; Seibyl et al., 1995), [^{123}I]FP-β-CIT (Abi-Dargham et al., 1996; Booij et al., 1997), [^{123}I]IPT (Goodman, et al., 1994; Mozley et al., 1996; Tatsch et al., 1997) and [^{123}I]altropane (Fischman et al., 1998; Madras et al., 1998) are being developed for this purpose. In Europe [^{123}I]FP-β-CIT (DatScan®, Amersham PLC, Buckinghampshire, UK) is commercially available for routine clinical use.

All of the successful agents for imaging DAT belong to a group of tropane derivatives, which share a similar backbone structure of cocaine. Many other potentially useful tropane derivatives have been reported. However, due to difficulty in the logistics of supply and distribution, ^{123}I-labeled compounds other than sodium iodide, commonly used for thyroid functional study, are difficult to use in the United States. Because ^{123}I is a cyclotron-produced isotope, which costs 100 times more than a similar ^{99m}Tc-labeled agent,

^{99m}Tc will be highly desirable for routine clinical study. In addition, the advantage of ready availability and ease of use with ^{99m}Tc agents (essentially 24 h a day) provides a strong incentive for their development.

Development of ^{99m}Tc-based small molecules as receptor imaging agents has been reviewed recently (Hom et al., 1997). The effort in developing [^{99m}Tc]TRODAT-1 was based on using a small and neutral $[Tc^{v}O]^{+3}N_2S_2$ core to maximize the possibility of initial delivery of radioactive tracers into the brain following an intravenous injection. Without the suitable properties (small size and optimal lipophilicity) to penetrate intact blood-brain barrier (BBB), no ^{99m}Tc-labeled agents can be used as imaging agents for specific binding sites in the brain. It is well established that when [^{99m}Tc]pertechnetate (TcO_4^-) is reduced in the presence of a reducing agent, such as stannous chloride, and a "soft" chelating ligand, such as N_2S_2, a neutral and lipophilic $[Tc^{v}O]^{+3}N_2S_2$ center core (generally referred to as BAT or DADT) is formed (Davison et al., 1981; Lever et al., 1985; Mahmood et al., 1991; Steigman, 1992). Only the "bared" $[Tc^{v}O]^{+3}N_2S_2$ core (with no methyl or amide substitutions on the ring system) was used for [^{99m}Tc]TRODAT-1, which has led to the first successful ^{99m}Tc DAT imaging agent for human study (Fig. 15.1) . In developing ^{99m}Tc-labeled DAT imaging agents, several research groups have also reported potential ^{99m}Tc-labeled tropanes (Aronson et al., 1996; Hoepping et al., 1998; Madras et al., 1996; Meltzer et al., 1997; Tamagnan et al., 1996; Zoghbi et al., 1997). Only [^{99m}Tc] TRODAT-1 has been tested successfully in normal subjects and parkinsonian patients.

The initial binding study of [Re]TRODAT-1, a nonradioactive surrogate of [^{99m}Tc]TRODAT-1, showed an inhibition constant of about 14 nM by using rat striatal

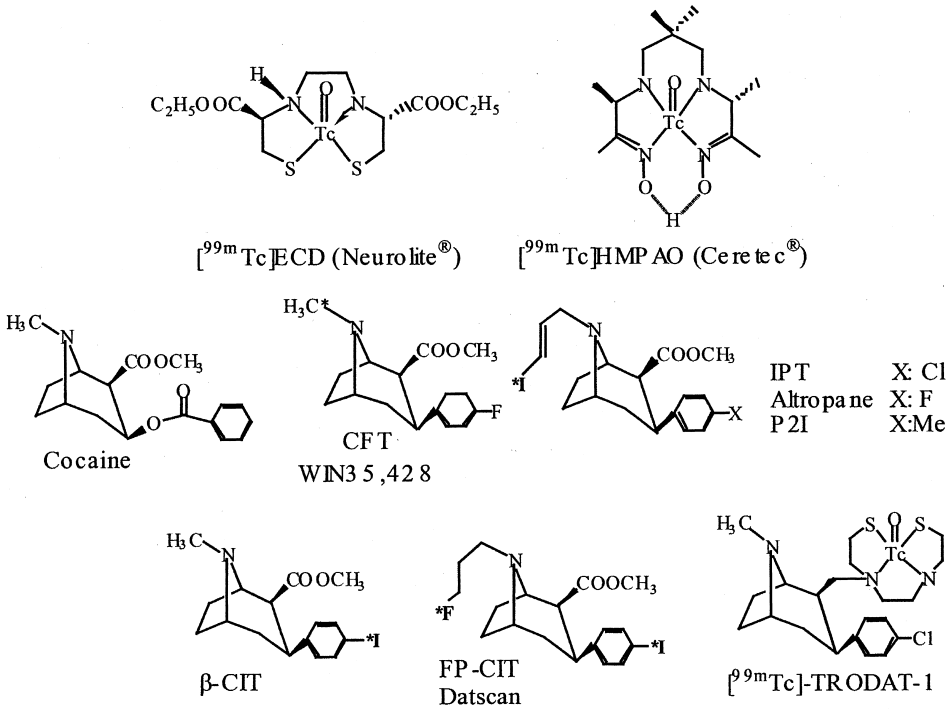

Figure 15.1. Chemical structures of ^{11}C, ^{123}I and ^{99m}Tc labeled tropanes as DAT imaging agents.

membrane homogenates. The in vitro binding affinity was about 50–100 times lower than that of IPT (Meegalla et al., 1997; Meegalla et al., 1998). They are diastereomers as indicated by the corresponding Re-diastereomers A and B. However, both isomers displayed selective uptake in the striatal area, suggesting that the localization is consistent with the dopamine transporter distribution. To identify and characterize the diastereomers, the corresponding Re complexes were prepared and the structures were determined. It appears that both isomers are in the syn conformation (Fig. 15.2). Both of these isomers surprisingly displayed about equal binding affinity to DAT, but the pharmacokinetics of DAT

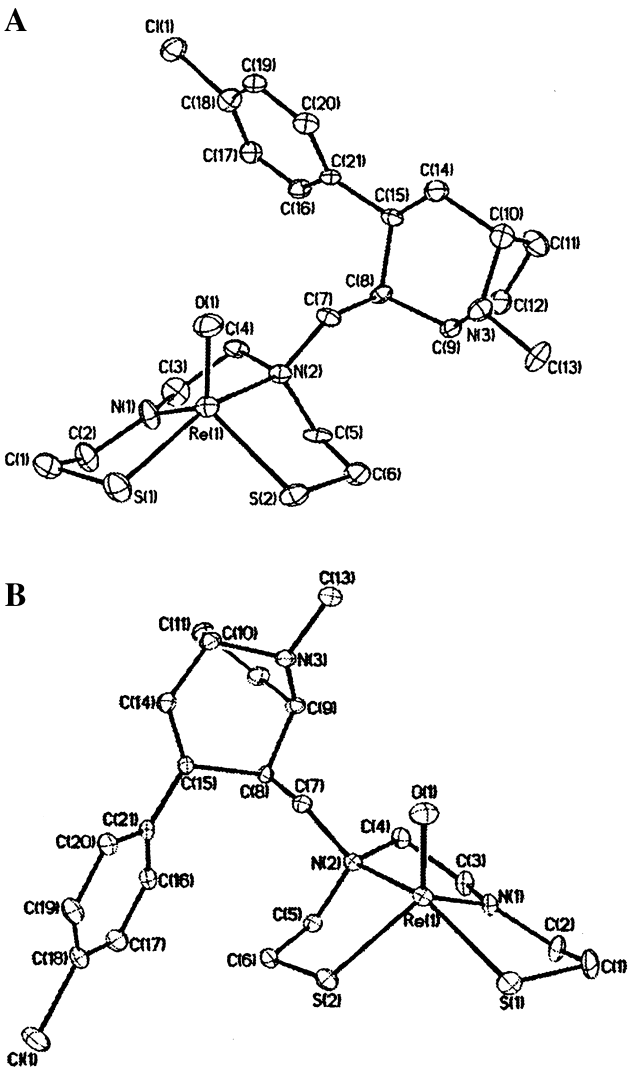

Figure 15.2. The N-alkyl substituted $[Tc^{v}O]^{+3}N_2S_2$ complexes formed diastereomers. X-ray structure analyses on the two Re-TRODAT-1 isomers, nonradioactive surrogates of the corresponding Tc-99m compounds, showed that both complexes have a syn configuration and they displayed similar binding affinity towards DAT (Meegalla et al., 1998).

binding in vivo favors isomer A at the equilibrium state (Meegalla et al., 1998). For practical reasons all of the clinical studies of [^{99m}Tc]TRODAT-1 have been carried out with a mixture of diastereomers.

The brain uptake of a racemic mixture of [^{99m}Tc]TRODAT-1 is ~25% of that reported for [^{123}I]IPT or [^{123}I]β-CIT. Comparing IPT versus TRODAT-1 in rats, the brain uptake (percentage of dose per organ) was 1.62 and 0.28 for IPT and 0.43 and 0.12 for TRODAT-1 at 2 and 60 min, respectively; target to nontarget ST/CB ratio at 60 min was 15.9 versus 2.7. The specific rat striatal uptake can be blocked by pretreating animals with a dose of competing DAT ligand, β-CIT. Rats that had prior 6-hydroxydopamine lesions in the substantia nigra showed a dramatic reduction of [^{99m}Tc]TRODAT-1 uptake in striatal region (Kung et al., 1997). Initial phase I clinical study of [^{99m}Tc]TRODAT-1 showed that the compound is safe and radiation dosimetry is well within the acceptable limits (Mozley et al., 1998). More importantly, [^{99m}Tc]TRODAT-1 binding to the caudate-putamen region in Parkinson's patients was found to be reduced dramatically (Mozley et al., 1999; Mozley et al., 2000). Kinetic modeling of [^{99m}Tc]TRODAT-1 in baboons demonstrated that the uptake in the striatum region can be evaluated by a three-compartment model. The quantitation can be achieved by transforming the data into a simple ratio method based on a reference-region approach (Acton et al., 1999b; Acton et al., 2000). The reference region method will greatly improve the ease of data analysis and provide a semi-quantitative approach readily applicable for routine clinical use.

Application of DAT Imaging

Imaging DAT in normal humans and effects of aging on DAT

It has been noticed since the first DAT imaging study was reported by using [^{11}C]CFT that DAT binding appears to decrease with age in normal human controls (Frost et al., 1993; Poyot et al., 2001; Wong et al., 1993). The effect of aging (reduction of binding sites 5–8% per decade) has been reproduced by using several other tracers: [^{99m}Tc]TRODAT-1 (Mozley et al., 1999), [^{123}I]β-CIT (Van Dick et al., 1995), [^{123}I]FP-β-CIT (Abi-Dargham et al., 1996; Booij et al., 2001; Booij et al., 1997; Tissingh et al., 1997), [^{123}I]IPT (Mozley et al., 1996; Tatsch et al., 1997) and [^{123}I]altropane (Fischman et al., 2001; Fischman et al., 1998).

Parkinson's Disease and parkinsonism

Most of the reported clinical studies of DAT imaging in humans are related to movement disorders, for differentiation between idiopathic and nonidiopathic parkinsonism. The effectiveness has been demonstrated by using either [^{99m}Tc]TRODAT-1 (Fig. 15.3) (Huang et al., 2001; Mozley et al., 2000; Tzen et al., 2001), [^{123}I]β-CIT (Seibyl 1999; Seibyl et al., 1996; Seibyl et al., 1995), [^{123}I]FP-β-CIT (Abi-Dargham et al., 1996; Booij et al., 2001; Booij et al., 1997; Tissingh, 1997), [^{123}I]IPT (Mozley et al., 1996; Tatsch et al., 1997) and [^{123}I]altropane (Fischman et al., 2001; Fischman et al., 1998). The imaging for the defects of dopamine system by using PET or SPECT imaging agents based on phenyltropanes appears to be more sensitive and easier to perform than using [^{18}F]fluoro-DOPA. The latter is based on in situ synthesis of the dopamine precursors in the presynaptic neurons (Brooks 2000; Tissingh et al., 1997). Deficiency in DAT concentration in movement disorders, such as Machado–Joseph's disease, has been reported, suggesting that the in vivo imaging technique is very useful in differential diagnosis and monitoring

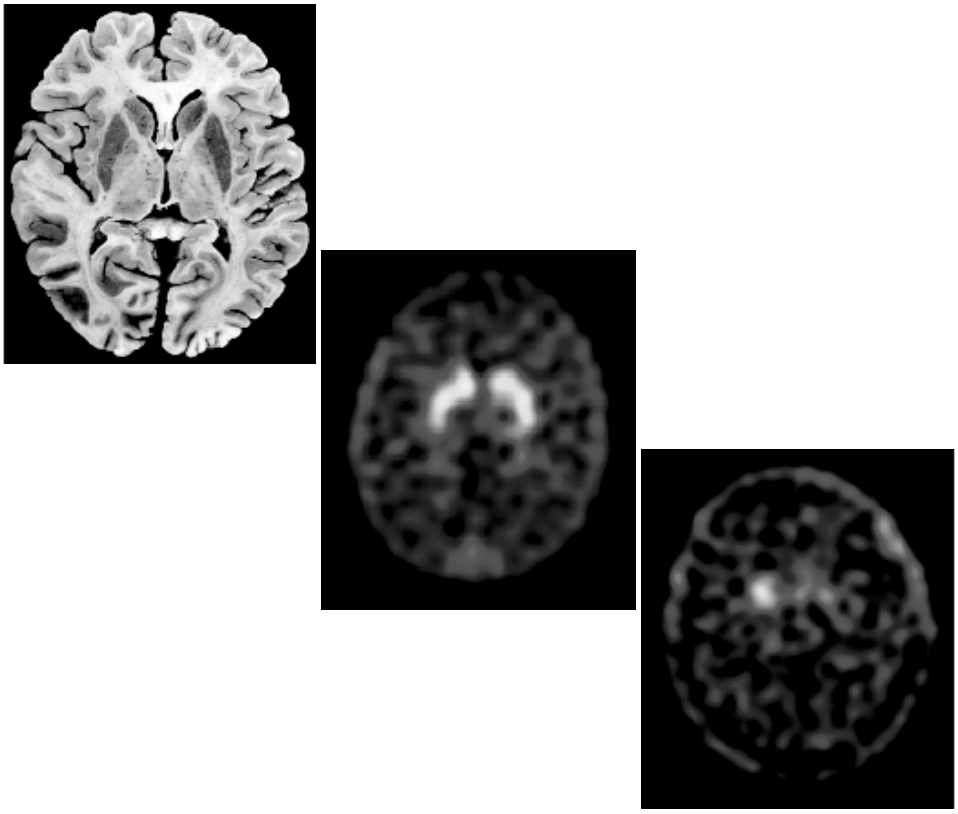

Figure 15.3. Transaxial, SPECT images of human brain at 3 h post-i.v. injection of 20 mCi of [^{99m}Tc]TRODAT-1 for normal and parkinsonian subject, respectively. In the normal subject, a high accumulation of [^{99m}Tc]TRODAT-1 was observed in caudate and putamen, where dopamine transporters are concentrated, whereas the parkinsonian patient (right) displayed a dramatic decreased uptake in this region of the brain. A comparable post-mortem brain section of a normal human is displayed on the left. (See color insert.)

the progression of this genetic disease, which caused an over-expression of CGA repeats (coded for glutamine) in the neurons. (Yen et al., 2000). This is an example of direct link between genetic defects and movement disorder detected by DAT imaging.

Attention Deficit Hyperactivity Disorder (ADHD)

Another area of application with the DAT imaging agents is in detection of attention deficit hyperactivity disorder (ADHD) (Dresel et al., 2000; Krause et al., 2000). It was found that compared with age-matched normal controls, ADHD patients showed a 30% higher density of DAT in the brain. The density of DAT was reduced significantly after treatment of methylphenidate (Ritalin®), demonstrating the mechanism of drug action in vivo. It also points out the possibility that the in vivo imaging method could be used to differentiate the young patients with genuine ADHD before subjection to an indiscriminate drug treatment.

Drug abuse

There are other nontropane-based DAT imaging agents, including GBR-13119 (Kilbourn, 1988), nomifensine (Tedroff et al., 1988) and methylphenidate as well as cocaine. Methylphenidate (Ritalin®) (Ding et al., 1995; Volkow et al., 1995a; Volkow et al., 1996) and cocaine (Volkow et al., 1995b; Volkow et al., 1999) labeled with ^{11}C were first developed in the Brookhaven National Laboratory (Upton, NY, USA). They serve an important role as probes for pharmacokinetic study of two widely used and abused drugs; that is, cocaine and methylphenidate. Both DAT imaging agents are useful in demonstrating in living human brain that the blockage of DAT is the essential factor in increasing the dopamine concentration in the synaptic cleft. Occupancy of the specific binding site in the brain is the prominent mechanism of action of the drugs; as a consequence, the pharmacological actions induced by increasing dopamine concentration in the synapse are propagated (Volkow et al., 2001; Fowler et al., 2001; Volkow et al., 2000). Changes in DAT concentration, measured by imaging with [^{123}I]β-CIT in patients who abused cocaine, have been reported (Malison et al., 1995). The dynamics of DAT, as well as DA concentration and re-enforcement effects in the synaptic cleft of the normal and drug abuse patients, remains to be investigated.

15.3 SEROTONIN TRANSPORTER (SERT) IMAGING AGENTS

It is generally accepted now that alterations in serotonergic neuronal function in the CNS occur in patients with major depression (Harvey 1997; Owens and Nemeroff, 1994). Recent reviews have summarized the important associations between the serotonergic functions and depression (Frazer 1997; Hyttel 1994; Owens and Nemeroff, 1994; Staley et al., 1998). Several lines of evidence support the involvement of serotonin in the brain, as reported by Owens and Nemeroff (1994), include: i) reduced cerebrospinal fluid (CSF) concentrations of 5-hydroxyindoleacetic acid (5-HIAA), the major metabolite of serotonin (5-HT) in drug-free depressed patients; ii) reduced concentrations of 5-HT and 5-HIAA in postmortem brain tissues of depressed and (or) suicidal patients (Mann 1998); iii) decreased plasma tryptophan concentrations in depressed patients and a profound relapse in remitted depressed patients who have responded to a serotonergic antidepressant when brain tryptophan availability is reduced (Heninger et al., 1996); iv) in general, all clinically efficacious antidepressants modulate 5-HT neurotransmission following chronic treatment; v) clinically efficacious antidepressant action by inhibitors of 5-HT uptake; vi) increases in the density of 5-HT_2 binding sites in postmortem brain tissue of depressed patients and suicide victims, as well as in platelets of drug-free depressed patients; and vii) decreased number of SERT binding sites in postmortem brain tissues of suicide victims and depressed patients.

A series of newer antidepressants preferentially increase 5-HT transmission by inhibiting 5-HT uptake. Selective serotonin reuptake inhibitors (SSRIs) are those drugs that preferably inhibit 5-HT uptake compared with dopamine or norepinephrine uptakes. They have no or only slight effect on other uptake mechanisms, neurotransmitter receptors, and enzymes. At least five SSRIs, that is, citalopram, fluoxetine, fluvoxamine, paroxetine, and sertraline, are approved by the FDA (Hyttel 1994). These SSRIs have revolutionized the management of depression for millions of patients, and they are prescribed widely for treating various other mental disorders.

Imaging of SERT in humans would provide a useful tool to understand how alterations

of this system are related to depressive illness and other psychiatric disorders and therefore potentially can benefit millions of patients who are being treated with SSRIs. Development of selective tracers for PET or SPECT imaging has made it possible to study in vivo neuroreceptors or specific binding sites noninvasively in the human brain (Eckelman 1998; Hom and Katzenellenbogen, 1997; Meltzer et al., 1998). The first successful radioligand was [^{11}C]R(+)McN5652 for PET imaging (Fig. 15.4) (Szabo et al., 1995 #14047; Suehiro et al., 1994 #15748). It showed excellent inhibition of 5-HT reuptake in rat brain synaptosomes (K_i = 0.40 nM for inhibition of 5-HT reuptake) and moderate selectivity toward other monoamine transporters (dopamine and norepinephrine transporters (DAT and NET, respectively); K_i = 23.5 and 1.82 nM, respectively) (Maryanoff et al., 1990). Specific binding of [^{11}C]R(+)McN5652 correlates well with the known density of SERT sites in the human brain (Parsey et al., 2000; Szabo et al., 1995; Szabo et al., 1996; Szabo et al., 1999). Recent reports in which [^{11}C]R(+)McN5652 for imaging SERT as an indicator of serotonin neuron was used have suggested that 3,4-methylenedioxymetamphetamine (MDMA or "Ecstasy") may cause an irreversible decrease of SERT binding sites (McCann et al., 1998; Ricaurte et al., 2000). Despite successful demonstration in imaging SERT in humans, there are some disadvantages to using [^{11}C]R(+)McN5652: This compound has active in vivo metabolites of this compound, which appear to penetrate the brain, and the background activity of this tracer is relatively high. Therefore, the kinetic modeling of this compound is complicated and makes it difficult to perform quantitative measurement.

In search for an improved SPECT ligand for SERT, several radioiodinated compounds were evaluated, including 4-iodo-R-tomoxetine reported previously (Fig. 15.4). (Chumpradit et al., 1992; Kung et al., 1992; Soudijn and Wijngaarden, 1997; Suehiro et al., 1994). Among these tracers, only [^{123}I]5-iodo-6-nitroquipazine (INQP, Fig. 15.4) (Biegon et al., 1993; Mathis et al., 1992; Mathis et al., 1993) showed promising properties for mapping SERT sites in monkey brain (Jagust et al., 1996). No human study of [^{123}I]INQP has been reported. Previously, it has been suggested that [^{123}I]β-CIT (Fig. 15.1), a SPECT imaging agent, binding to both DAT and SERT, will be able to clarify

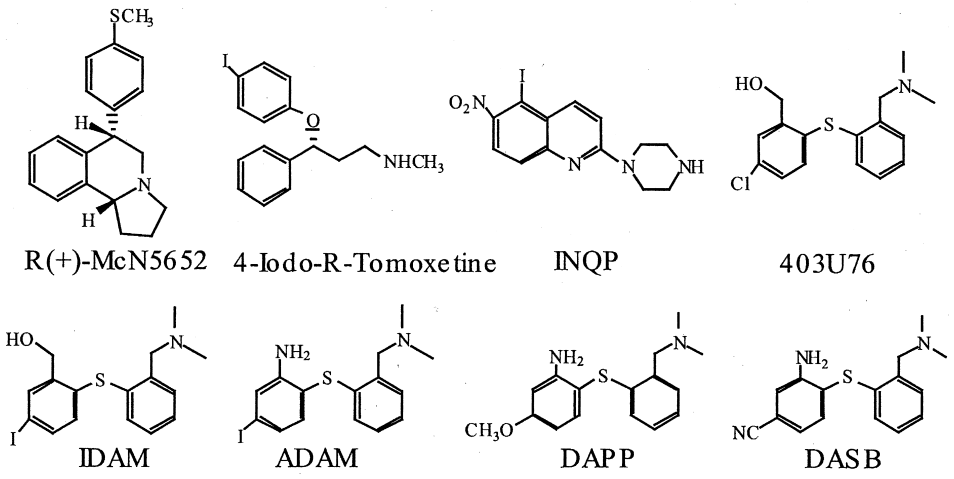

Figure 15.4. Chemical structures of SERT imaging agents

pathological changes in both dopaminergic and serotonergic systems. However, overlapping uptake regions and differential kinetics of [^{123}I]β-CIT binding to DAT and SERT were observed (Fujita et al., 1996; Kuikka et al., 1995; Laruelle et al., 1993; Tiihonen et al., 1997). Nonetheless, the effect of a selective SSRI in human brain in vivo has been measured directly by [^{123}I]β-CIT/SPECT imaging of SERT sites in depressed patients undergoing treatment with citalopram (Pirker et al., 1995; Tauscher et al., 1999). Recently, [^{123}I]β-CIT/SPECT imaging showed a significant reduction (30%) of SERT binding in the midbrain area in the depressed subjects compared with the controls (Malison et al., 1998; Meltzer et al., 1998; Staley et al., 1998; Willeit et al., 2000). A recent report on [^{123}I]β-CIT/SPECT imaging of a group of patients suggests that schizophrenia is generally not associated with alterations of DAT in the striatum or SERT in the brainstem (Laruelle et al., 2000). A more selective series of compounds, nor-β-CIT (N-demethylated analog of β-CIT) (Bergstrom et al., 1997) and its related derivatives (Blough et al., 1997), have been reported recently as improved SPECT imaging agents for SERT. It is suggested that [^{123}I]nor-β-CIT might be a suitable alternative tracer for visualization of SERT sites in the human brain with SPECT (Bergstrom et al., 1997; Hiltunen et al., 1998). However, [^{123}I]nor-β-CIT still binds to both DAT and SERT, and the selectivity is improved only marginally, which is not sufficient to distinguish between these two monoamine transporter sites in vivo.

A phenylthiophenyl derivative, 403U76 (Fig. 15.4), was reported as an inhibitor of serotonin uptake and norepinephrine uptake in rat brain synaptosomes (K_i = 2.1 and 55 nM, respectively). No inhibition of dopamine uptake was observed. (Ferris et al., 1995) It appears that 403U76 was one of the candidates of antidepressants developed by Glaxo-Wellcome (Brieaddy 1993; Mehta et al., 1990). Surprisingly, no other reports on 403U76 have appeared after 1996. To develop a new SERT selective imaging agent, a series of derivatives based on the substituted phenylthiophenyl core structure were prepared (Oya et al., 1999). Methods for synthesis of phenylthiophenyl or the phenoxyphenyl derivatives resulted in different types of coupling reactions to form the desired ring system for developing specific SERT imaging agents (Zhuang et al., 2000). Among the compounds prepared, radioiodinated analogs IDAM and ADAM (Fig. 15.4) are the most promising candidates with several attractive properties: high binding affinity and selectivity (Acton et al., 1999a; Kung et al., 1999; Oya et al., 1999). In vitro binding study showed that IDAM displayed an excellent affinity to SERT sites (K_i = 0.097 nM, using membrane preparations of LLC-PK_1 cells expressing the specific transporter) and showed >1,000-fold selectivity for SERT over NET and DAT (expressed in the same LLC-PK_1 cells). Biodistribution of [^{125}I]IDAM (partition coefficient = 473; 1-octanol/buffer) in the rat brain showed a high initial uptake (2.44% dose at 2 min after i.v. injection) with the specific binding peak at 60 min post-injection (hypothalamus-cerebellum/cerebellum = 1.75). Preliminary SPECT imaging with [^{123}I]IDAM in baboons demonstrated an excellent localization of regions in the midbrain area known to have a high concentration of SERT binding sites. Despite the fact that [^{123}I]IDAM showed promise as a new SERT radioligand for in vivo imaging, a small modification of the substitution group on the benzene rings has produced significant improvements on the imaging properties of the ligand. Synthesis and characterization of an improved SERT imaging agent, [^{123}I]ADAM (Fig. 15.4), was achieved. The new compound, ADAM, displayed an extremely potent binding affinity toward SERT (K_i = 0.013 nM, in membrane preparations of LLC-PK_1 cloned cell lines expressing the specific monoamine transporter). It also showed >1,000-fold selectivity for SERT over NET and DAT (K_i = 699 and 840 nM, for NET and DAT, respectively). The radiola-

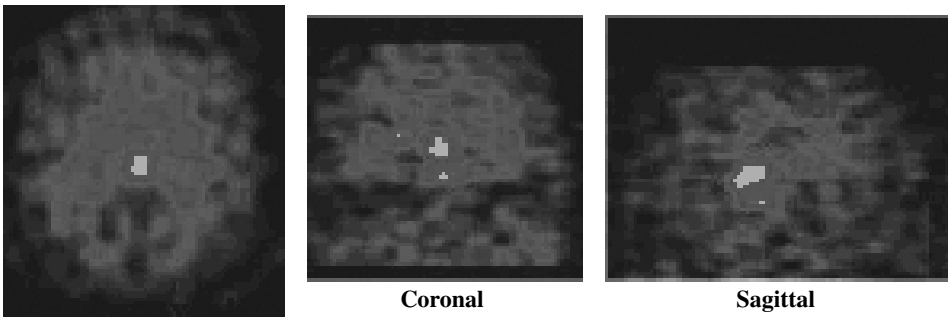

Figure 15.5. SPECT images of a normal subject's brain at 5 h after injection of [^{123}I]ADAM. (See color insert.)

beled compound [^{125}I]ADAM showed an excellent brain uptake in rats (1.41% dose at 2 min post-i.v. injection), and consistently displayed the highest uptake (between 60–240 min post-i.v. injection) in hypothalamus, a region with the highest density of SERT. The specific uptake of [^{125}I]ADAM in the hypothalamus exhibited the highest target to nontarget ratio ([hypothalamus-cerebellum]/cerebellum) of 3.97 at 120 min post-i.v. injection). The preliminary imaging study of [^{123}I]ADAM in the brain of a baboon by SPECT at 180–240 min post-i.v. injection indicated a specific uptake in midbrain region rich in SERT. It is apparent that [^{123}I]ADAM showed a significant improvement over [^{123}I]IDAM as a SPECT imaging agent for SERT in the brain. Initial imaging study in humans suggests that the agent clearly localized in the region of hypothalamus region of the brain where the concentration of SERT is the highest (Fig. 15.5). It is expected that this agent will provide the expected biological properties suitable for imaging SERT in the human brain. Currently, [^{123}I]ADAM is being developed for human study.

Recently, a group of ^{11}C labeled compounds, based on a similar phenylthiophenyl ring system, was reported; among which, DASB, DAPP, and MADAM showed the most promising properties (Houle et al., 2000; Wilson et al., 2000). Similar to that of IDAM or ADAM, DASB displayed an excellent binding affinity towards SERT (K_i = 1.10 nM), whereas the binding affinity to the other monoamine transporters was a few thousand-fold lower. After an i.v. injection in rats, [^{11}C]DASB showed good brain uptake and selective localization in the hypothalamus regions of the brain, suggesting selective binding to the SERT. Initial human studies showed that [^{11}C]DASB had good brain penetration and that it was localized in the hypothalamus region rich in SERT binding sites (Fig. 15.6). The specific binding in the striatum and hypothalamus regions can be blocked by pretreatment of SSRI, such as paroxetine or citalopram (Houle et al., 2000). Subsequently, by using the same ligand it was reported that a significant decrease in striatal SERT binding potential was found after either treatment, compared with changes found over a four-week period in healthy subjects. For patients treated with 20 mg/day of paroxetine, the mean proportion of SERT sites occupied was 83%. For patients treated with 20 mg/day of citalopram, the mean SERT occupancy was 77% (Ginovart et al., 2001; Meyer et al., 2001a; Meyer et al., 2001b). A direct measurement of drug occupancy for SSRI on SERT binding sites, an important factor in drug efficacy, is clearly demonstrated by the in vivo imaging technique (Frazer, 2001).

The potential applications of in vivo imaging agents for SERT include evaluation of

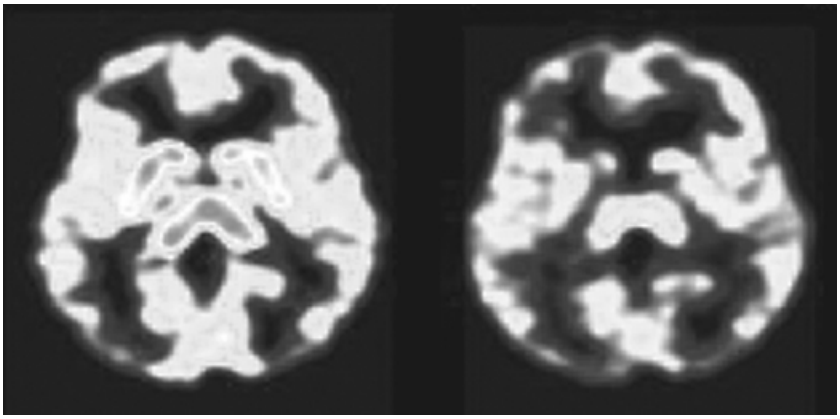

Figure 15.6. PET imaging of SERT in the normal human brain. Effects of citalopram on [^{11}C]DASB PET scan with a treatment of 20 mg citalopram/day for four weeks. Images represent summated frames normalized to mean summated cerebellum values (PET images kindly provided by the courtesy of Dr. Sylan Houle, University of Toronto). (See color insert.)

the mechanism of drug action, identification and validation of drug target, investigation of the effectiveness of drug treatment (or the lack thereof), and involvement of SERT in drug abuse (alcohol, cocaine, methamphetamine, MDMA).

15.4 NOREPINEPHRINE TRANSPORTER (NET) IMAGING AGENTS

There is no successful NET imaging agent currently available for human study. It was reported that [^{11}C]nomifensine might display a brain localization related to NET distribution (Salmon et al., 1990; Tedroff et al., 1988). However, nomifensine also shows high binding affinity to DAT; the density of DAT binding sites in the brain is higher than that of NET, therefore images of nomifensine distribution showed prominently the DAT binding. A more selective ligand for NET will be needed. A highly selective NET ligand, nisoxetine, was reported, but the in vivo kinetics did not favor mapping of the NET in the brain; the nonspecific binding in vivo was too high (Haka and Kilbourn, 1989; Tejani-Butt, 1992). Recently, reboxetine, a selective NET inhibitor, has been introduced as an antidepressant (Burrows et al., 1998; Dekeyne et al, 2001; Gorman and Sullivan, 2000). It is the first selective and specific norepinephrine reuptake inhibitor available for clinical use. It was demonstrated that reboxetine dose-dependently and potently inhibits presynaptic norepinephrine reuptake (K_i = 8 nM); it has more than 1000 and 130 times greater selectivity for blocking NET compared with DAT and SERT, respectively (Wong et al., 2000). In the future, reboxetine may be a candidate for developing NET-specific imaging agent.

15.5 CONCLUSION

Recent advances have demonstrated that it is possible to use tracers for imaging the monoamine transporters DAT and SERT in conjunction with PET and SPECT. The ease of use and the availability of these tracers will ultimately determine the widespread clini-

cal usefulness of these agents. It is likely that the tracers for monoamine transporters will be used to evaluate the drug saturation experiments in humans to facilitate the development of treatments targeting specific monoamine transporters.

ACKNOWLEDGMENTS

This work was supported by grants awarded by the National Institutes of Health (NS-18509 and NS-24538). The authors thank Drs. Alan Wilson, Sylvan Houle, and Aapo Ahonen for their helpful discussions and Ms. Jennifer Rodabaugh for her assistance in preparation of this manuscript.

REFERENCES

Abi-Dargham A, Gandelman MS, DeErausquin GA, et al. (1996): SPECT imaging of dopamine transporters in human brain with iodine-123-fluoroalkyl analogs of beta-CIT. J Nucl Med 37:1129–1133.

Acton PD, Kung MP, Mu M, et al. (1999a): Single-photon emission tomography imaging of serotonin transporters in the non-human primate brain with the selective radioligand [^{123}I]IDAM. Eur J Nucl Med 26:854–861.

Acton PD, Kushner SA, Kung MP, et al. (1999b): Simplified reference region model for the kinetic analysis of [^{99m}Tc]TRODAT-1 binding to dopamine transporters in nonhuman primates using single-photon emission tomography. Eur J Nucl Med 26:518–526.

Acton PD, Meyer PT, Mozley PD, et al. (2000): Simplified quantifications of dopamine transporters in humans using [^{99m}Tc]TRODAT-1 and single photon emission tomography. Eur J Nucl Med 27:1714–1718.

Aronson B, Enmon JL, Izenwasser S, et al. (1996): Synthesis and ligand binding of h^6-(2*b*-carbomethoxy-3*b*-phenyltropane) transition metal complexes. J Med Chem 39:1560–1563.

Bergstrom KA, Halldin C, Hall H, et al. (1997): In vitro and in vivo characterization of nor-beta-CIT: a potential radioligand for visualization of the serotonin transporter in the brain. Eur J Nucl Med 24:596–601.

Biegon A, Mathis CA, Hanrahan SM, et al. (1993): [^{125}I]5-Iodo-6-nitroquipazine: A potent and selective ligand for the 5-hydroxytryptamine uptake complex II in vivo studies in rats. Brain Res 619:236–246.

Blough BE, Abraham P, Mills AC, et al. (1997): 3 Beta-(4-ethyl-3-iodophenyl)nortropane-2 beta-carboxylic acid methyl ester as a high-affinity selective ligand for the serotonin transporter. J Med Chem 40:3861–3864.

Booij J, Bergmans P, Winogrodzka A, et al. (2001): Imaging of dopamine transporters with [^{123}I]FP-CIT SPECT does not suggest a significant effect of age on the symptomatic threshold of disease in Parkinson's disease. Synapse 39:101–108.

Booij J, Tissingh G, Winogrodzka A, et al. (1997): Practical benefit of [^{123}I]FP-CIT SPET in the demonstration of the dopaminergic deficit in Parkinson's disease. Eur J Nucl Med 24:68–71.

Brieaddy LE, Substituted diphenylsulfides as serotonin uptake inhibitors. USA Patent WO 93/12080, June 24, 1993.

Brooks DJ (2000): Morphological and functional imaging studies on the diagnosis and progression of Parkinson's disease. [Review] [67 refs]. J Neurol 247 Suppl 2:II11–18.

Burrows GD, Maguire KP, Norman TR (1998): Antidepressant efficacy and tolerability of the selective norepinephrine reuptake inhibitor reboxetine: a review. J Clin Psychiatry 14:4–7.

Carroll FI, Scheffel U, Dannals RF, et al. (1995): Development of imaging agents for the dopamine transporter. Med Res Rev 15:419–444.

Cherry SR (2001): Fundamentals of positron emission tomography and applications in preclinical drug development. J Clin Phar 41:482–491.

Chumpradit S, Kung MP, Panyachotipun C, et al. (1992): Iodinated tomoxetine derivatives as selective ligands for serotonin and norepinephrine uptake sites. J Med Chem 35:4492–4497.

Cooper JR (1996): The biochemical basis of neuropharmacology: Oxford, UK: Oxford University Press.

Davison A, Jones AG, Orvig C, et al. (1981): A new class of oxotechnetium(+5) chelate complexes containing a $TcON_2S_2$ core. Inorg Chem 20:1629–1632.

Dekeyne A, Gobert A, Iob L, et al. (2001): Discriminative stimulus properties of the selective norepinephrine reuptake inhibitor, reboxetine, in rats. Psychopharmacology 158:213–218.

Ding YS, Fowler JS, Volkow ND, et al. (1995): Carbon-11-d-threo-methylphenidate binding to dopamine transporter in baboon brain. J Nucl Med 36:2298–2305.

Dresel S, Krause J, Krause K-H, et al. (2000): Attention deficit hyperactivity disorder: binding of [^{99m}Tc]TRODAT-1 to the dopamine transporter before and after methylphenidate treatment. Eur J Nucl Med 27:1518–1524.

Eckelman WC (1998): Sensitivity of new radiopharmaceuticals. Nucl Med Biol 25:169–173.

Fahey FH (2001): Positron emission tomography instrumentation. Radiologic Clin North Amer 39:919–929.

Ferris RM, Brieaddy L, Mehta N, et al. (1995): Pharmacological properties of 403U76, a new chemical class of 5-hydroxytryptamine- and noradrenaline-reuptake inhibitor. J Pharm Pharmacol 47:775–781.

Fischman AJ, Bonab AA, Babich JW, et al. (2001): [^{11}C, ^{127}I] Altropane: A highly selective ligand for PET imaging of dopamine transporter sites. Synapse 39:332–342.

Fischman AJ, Bonab AA, Babich JW, et al. (1998): Rapid detection of Parkinson's disease by SPECT with altropane: a selective ligand for dopamine transporters. Synapse 29:128–141.

Fowler JS, Volkow ND, Wang JG, et al. (2001): [(11)]Cocaine: PET studies of cocaine pharmacokinetics, dopamine transporter availability and dopamine transporter occupancy. Nucl Med Biol 28:561–572.

Frazer A (1997): Antidepressants. J Clin Psychiatry 6:9–25.

Frazer A (2001): Serotonergic and noradrenergic reuptake inhibitors: prediction of clinical effects from in vitro potencies. J Clin Psychiatry 62:16–23.

Frost JJ, Rosier AJ, Reich SG, et al. (1993): Positron emission tomographic imaging of the dopamine transporter with [^{11}C]-WIN 35,428 reveals marked declines in mild Parkinson's disease [see comments]. Ann Neurol 34:423–431.

Fujita M, Takatoku K, Matoba Y, et al. (1996): Differential kinetics of [^{123}I]beta-CIT binding to dopamine and serotonin transporters. Eur J Nucl Med 23:431–436.

Garcia EV, Faber TL, Galt JR, et al. (2000): Advances in nuclear emission PET and SPECT imaging. IEEE Engineering Med & Biol 19:21–33.

Ginovart N, Wilson AA, Meyer JH, et al. (2001): Positron emission tomography quantification of [(11)C]-DASB binding to the human serotonin transporter: modeling strategies. J Cereb Blood Flow Metab 21:1342–1353.

Goodman MM, Kung M-P, Kabalka GW, et al. (1994): Synthesis and characterization of radioiodinated N-(3-iodopropen-1-yl)-2b-carbomethoxy-3b-(4-chlorophenyl)tropanes: potential dopamine reuptake site imaging agents. J Med Chem 37:1535–1542.

Gorman JM, Sullivan G (2000): Noradrenergic approaches to antidepressant therapy. J Clin Psychiatry 1:13–16.

Green MV, Seidel J, Vaquero JJ, et al. (2001): High resolution PET, SPECT and projection imaging in small animals. Comput Med Imaging Graph 25:79–86.

Haka M, Kilbourn M (1989): Synthesis and regional mouse brain distribution of [^{11}C]-nisoxetine, a norepinephrine uptake inhibitor. Nucl Med Biol 16:771–774.

Harvey BH (1997): The neurobiology and pharmacology of depression: a comparative overview of serotonin selective antidepressants. S Afr Med J 87:540–550.

Heninger GR, Delgado PL, Charney DS (1996): The revised monoamine theory of depression: a modulatory role for monoamines, based on new findings from monoamine depletion experiments in humans. Pharmacopsychiatry 29:2–11.

Hiltunen J, Akerman KK, Kuikka JT, et al. (1998): Iodine-123 labeled nor-beta-CIT as a potential tracer for serotonin transporter imaging in the human brain with single-photon emission tomography. Eur J Nucl Med 25:19–23.

Hoepping A, Reisgys M, Brust P, et al. (1998): TROTEC-1: a new high-affinity ligand for labeling of the dopamine transporter. J Med Chem 41:4429–4432.

Hom RK, Katzenellenbogen JA (1997): Technetium-99m-labeled receptor-specific small-molecule radiopharmaceuticals: recent developments and encouraging results. Nucl Med Biol 24:485–498.

Houle S, Ginovart N, Hussey D, et al. (2000): Imaging the serotonin transporter with positron emission tomography: Initial human studies with [^{11}C]DAPP and [^{11}C]DASB. Eur J Nucl Med 27:1719–1722.

Huang WS, Lin SZ, Lin JC, et al. (2001): Evaluation of early-stage Parkinson's disease with ^{99m}Tc-TRODAT-1 imaging. J Nucl Med 42:1303–1308.

Hyttel J (1994): Pharmacological characterization of selective serotonin reuptake inhibitors (SSRIs). Int Clin Psychopharmacol 1:19–26.

Innis RB (1994): Single photon emission tomography imaging of dopamine terminal innervation: a potential clinical tool in Parkinson's disease. Eur J Nucl Med 21:1–5.

Innis RB, Seibyl JP, Scanley BE, et al. (1993): Single photon emission computed tomographic imaging demonstrates loss of striatal dopamine transporters in Parkinson's disease. Proc Natl Acad Sci USA 90:11965–11969.

Jagust WJ, Eberling JL, Biegon A, et al. (1996): Iodine-123-5-iodo-6-nitroquipazine: SPECT radiotracer to image the serotonin transporter. J Nucl Med 37:1207–1214.

Jurisson SS, Berning D, Jia W, et al. (1993): Coordination compounds in nuclear medicine. Chem Rev 93:1137–1156.

Jurisson SS, Lydon JD (1999): Potential technetium small molecule radiopharmaceuticals. Chem Rev 99:2205–2218.

Kegeles LS, Mann JJ (1997): In vivo imaging of neurotransmitter systems using radiolabeled receptor ligands. Neuropsychopharmacology 17:293–307.

Kilbourn MR (1988): In vivo binding of [^{18}F]GBR 13119 to the brain dopamine uptake system. Life Sci 42:1347–1353.

Kornblum HI, Araujo DM, Annala AJ, et al. (2000): In vivo imaging of neuronal activation and plasticity in the rat brain by high resolution positron emission tomography (microPET). Nat Biotech 18:655–660.

Krause K-H, Dresel SH, Krause J, et al. (2000): Increased striatal dopamine transporter in adult patients with attention deficit hyperactivity disorder: effects of methylphenidateb as measured by single photon emission computed tomography. Neurosci Lett 285:107–110.

Kuikka JT, Bergstrom KA, Ahonen A, et al. (1995): Comparison of iodine-123 labelled 2 beta-carbomethoxy-3 beta-(4-iodophenyl)tropane and 2 beta-carbomethoxy-3 beta-(4-iodophenyl)-N-(3-fluoropropyl)nortropane for imaging of the dopamine transporter in the living human brain. Eur J Nucl Med 22:356–360.

Kung M-P, Chumpradit S, Billings JJ, et al. (1992): 4-Iodotomoxetine: A novel ligand for serotonin uptake sites. Life Sci 51:95–106.

Kung M-P, Stevenson DA, Plössl K, et al. (1997): [^{99m}Tc]TRODAT-1: a novel technetium-99m complex as a dopamine transporter imaging agent. Eur J Nucl Med 24:372–380.

Kung MP, Hou C, Oya S, et al. (1999): Characterization of [^{123}I]IDAM as a novel single-photon emission tomography tracer for serotonin transporters. Eur J Nucl Med 26:844–853.

Laruelle M, Abi-Dargham A, van Dyck C, et al. (2000): Dopamine and serotonin transporters in patients with schizophrenia: an imaging study with [^{123}I]beta-CIT. Biol Psychiatry 47:371–379.

Laruelle M, Baldwin RM, Malison RT, et al. (1993): SPECT imaging of dopamine and serotonin transporters with [^{123}I]beta-CIT: pharmacological characterization of brain uptake in nonhuman primates. Synapse 13:295–309.

Lever SZ, Burns HD, Kervitsky TM, et al. (1985): Design, preparation and biodistribution of a technetium-99m triaminodiathol complex to access regional cerebral blood flow. J Nucl Med 26:1287–1294.

Madras BK, Jones AG, Mahmood A, et al. (1996): Technepine: a high affinity technetium-99m probe to label the dopamine transporter in brain by SPECT imaging. Synapse 22:239–246.

Madras BK, Meltzer PC, Liang AY, et al. (1998): Altropane, a SPECT or PET imaging probe for dopamine neurons: I. dopamine transporter binding in primate brain. Synapse 29:93–104.

Mahmood A, Halpin WA, Baidoo KE, et al. (1991): Structure of a neutral N-alkylated diaminedithiol (DADT) ^{99}Tc^{V} complex: syn[^{99}TcO(NET-TMDADT)]. Acta Crystallogr, Sect C: Cryst Struct Commun 47:254–257.

Malison RT, Best SE, Wallace EA, et al. (1995): Euphorigenic doses of cocaine reduce [^{123}I]beta-CIT SPECT measures of dopamine transporter availability in human cocaine addicts. Psychopharmacology 122:358–362.

Malison RT, Price LH, Berman R, et al. (1998): Reduced brain serotonin transporter availability in major depression as measured by [^{123}I]-2 beta-carbomethoxy-3 beta-(4-iodophenyl)tropane and single photon emission computed tomography. Biol Psychiatry 44:1090–1098.

Mann JJ (1998): The neurobiology of suicide. Nat Med 4:25–30.

Maryanoff EM, Vaught JL, Shank RP, et al. (1990): Pyrroloisoquinoleines antidepressants. 3. A focus on serotonin. J Med Chem 33:2793–2797.

Mathis CA, Biegon A, Taylor SE, et al. (1992): [I-125]5-Iodo-6-nitro-2-piperazinylquinoline: a potent and selective ligand for the serotonin uptake complex. Eur J Pharmacol 210:103–104.

Mathis CA, Taylor SE, Biegon A, et al. (1993): [^{125}I]5-Iodo-6-nitroquipazine: a potent and selective ligand for the 5-hydroxytryptamine uptake complex I in vitro studies. Brain Res 619:229–235.

McCann UD, Szabo Z, Scheffel U, et al. (1998): Positron emission tomographic evidence of toxic effect of MDMA ("Ecstasy") on brain serotonin neurons in human beings. Lancet 352:1433–1437.

Meegalla SK, Plössl K, Kung M-P, et al. (1997): Synthesis and characterization of Tc-99m labeled tropanes as dopamine transporter imaging agents. J Med Chem 40:9–17.

Meegalla SK, Plössl K, Kung M-P, et al. (1998): Specificity of diastereomers of [^{99m}Tc]TRODAT-1 as dopamine transporter imaging agents. J Med Chem 41:428–436.

Mehta NB, Hollingsworth CE, Brieaddy LE, et al. Halogen substituted diphenylsulfides. Europe Patent EP 0 402 097 A1, May 6, 1990.

Meltzer CC, Smith G, DeKosky ST, et al. (1998): Serotonin in aging, late-life depression, and Alzheimer's disease: the emerging role of functional imaging. Neuropsychopharmacology 18:407–430.

Meltzer PC, Blundell P, Jones AG, et al. (1997): A technetium-99m SPECT imaging agent which targets the dopamine transporter in primate brain. J Med Chem 40:1835–1844.

Meyer JH, Kruger S, Wilson AA, et al. (2001a): Lower dopamine transporter binding potential in striatum during depression. Neuroreport 12:4121–4125.

Meyer JH, Wilson AA, Ginovart N, et al. (2001b): Occupancy of serotonin transporters by paroxetine and citalopram during treatment of depression: A [(11)C]DASB PET imaging study. Am J Psychiatry 158:1843–1849.

Mozley P, Stubbs J, Plössl K, et al. (1998): Biodistribution and dosimetry of TRODAT-1: A technetium-99m tropane for imaging dopamine transporters. J Nucl Med 39:2069–2076.

Mozley PD, Acton PD, Barraclough ED, et al. (1999): Effects of age on dopamine transporters in healthy humans. J Nucl Med 40:1812–1817.

Mozley PD, Schneider JS, Acton PD, et al. (2000): Binding of [^{99m}Tc]TRODAT-1 to dopamine transporters in patients with Parkinson's disease and in healthy volunteers. J Nucl Med 41:584–589.

Mozley PD, Stubbs JB, Kim H-J, et al. (1996): Dosimetry of an iodine-123-labeled tropane to image dopamine transporters. J Nucl Med 37:151–159.

Owens MJ, Nemeroff CB (1994): Role of serotonin in the pathophysiology of depression: focus on the serotonin transporter. Clin Chem 40:288–295.

Oya S, Kung M-P, Acton PD, et al. (1999): A new single-photon emission computed tomography imaging agent for serotonin transporters: [^{123}I] IDAM, 5-Iodo-2-((2-((dimethylamino)methyl)phenyl)thio)benzyl alcohol. J Med Chem 42:333–335.

Parsey RV, Kegeles LS, Hwang DR, et al. (2000): *In vivo* quantification of brain serotonin transporters in humans using [^{11}C]McN 5652. J Nucl Med 41:1465–1477.

Phelps ME (2000): PET: The merging of biology and imaging into molecular imaging. J Nucl Med 41:661–681.

Pirker W, Asenbaum S, Kasper S, et al. (1995): beta-CIT SPECT demonstrates blockade of 5HT-uptake sites by citalopram in the human brain in vivo. J Neural Transm Gen Sect 100:247–256.

Poyot T, Conde F, Gregoire MC, et al. (2001): Anatomic and biochemical correlates of the dopamine transporter ligand ^{11}C-PE2I in normal and parkinsonian primates: Comparison with 6-[^{18}F]fluoro-L-dopa. J Cereb Blood Flow Metab 21:782–792.

Ricaurte GA, McCann UD, Szabo Z, et al. (2000): Toxicodynamics and long-term toxicity of the recreational drug, 3, 4-methylenedioxymethamphetamine (MDMA, "Ecstasy"). Toxicol Lett 112–113:143-146.

Salmon E, Brooks DJ, Leenders KL, et al. (1990): A two-compartment description and kinetic procedure for measuring regional cerebral [^{11}C]nomifensine uptake using positron emission tomography. J Cereb Blood Flow Metab 10:307–316.

Schonbachler RD, Gucker PM, Arigoni M, et al. (2002): PET imaging of dopamine transporters in the human brain using [^{11}C]-beta-CPPIT, a cocaine derivative lacking the 2beta-ester function. Nucl Med Biol 29:19–27.

Seibyl JP (1999): Single-photon emission computed tomography of the dopamine transporter in Parkinsonism. J Neuroimaging 9:223–228.

Seibyl JP, Laruelle M, van Dyck CH, et al. (1996): Reproducibility of iodine-123-beta-CIT SPECT brain measurement of dopamine transporters. J Nucl Med 37:222–228.

Seibyl JP, Marek K, Sheff K, et al. (1997): Test/retest reproducibility of iodine-123-betaCIT SPECT brain measurement of dopamine transporters in Parkinson's patients. J Nucl Med 38:1453–1459.

Seibyl JP, Marek KL, Quinlan D, et al. (1995): Decreased single-photon emission computed tomographic [^{123}I]beta-CIT striatal uptake correlates with symptom severity in Parkinson's disease. Ann Neurol 38:589–598.

Soudijn W, van Wijngaarden I (1997): 5-HT Transporter. In: Olivier B, I. van Wijngaarden, W. Soudijn (eds): Serotonin receptors and their ligands. New York: Elsevier Science. 27:327–361.

Staley JK, Malison RT, Innis RB (1998): Imaging of the serotonergic system: Interactions of neuroanatomical and functional abnormalities of depression. Biol Psychiatry 44:534–549.

Steigman J, Eckelman WC (1992): The Chemistry of Technetium In Medicine. Washington, DC: National Academy of Sciences.

Suehiro M, Scheffel UA, Ravert HT, et al. (1994): Highly potent indanamine serotonin uptake blockers as radiotracers for imaging serotonin uptake sites. Nucl Med Biol 21:1083–1091.

Szabo Z, Kao PF, Scheffel U, et al. (1995): Positron emission tomography imaging of serotonin transporters in the human brain using [^{11}C](+)MCN5652. Synapse 20:37–43.

Szabo Z, Mohamadiyeh M, Scheffel U, et al. (1996): Impulse-response function and kinetic-model of C-11-labeled (+)MCN5652. J Nucl Med 37:125.

Szabo Z, Scheffel U, Mathews WB, et al. (1999): Kinetic analysis of [^{11}C]McN5652: A serotonin transporter radioligand. J Cereb Blood Flow Metab 19:967–981.

Tamagnan G, Gao YG, Baldwin RM, et al. (1996): Synthesis of beta-CIT-BAT, a potential Tc-99m imaging ligand for dopamine transporter. Tetrahedron Lett 37:4353–4356.

Tatsch K, Schwarz J, Mozley PD, et al. (1997): Relationship between clinical features of Parkinson's disease and presynaptic dopamine transporter binding assessed with [^{123}I]IPT and single-photon emission tomography. Eur J Nucl Med 24:415–421.

Tauscher J, Pirker W, de Zwaan M, et al. (1999): In vivo visualization of serotonin transporters in the human brain during fluoxetine treatment. Eur Neuropsychopharmacol 9:177–179.

Tedroff J, Aquilonius SM, Hartvig P, et al. (1988): Monoamine re-uptake sites in the human brain evaluated in vivo by means of ^{11}C-nomifensine and positron emission tomography: The effects of age and Parkinson's disease. Acta Neurol Scand 77:192–201.

Tejani-Butt S (1992): [^{3}H]-Nisoxetine: a radioligand for quantification of norepinephrine uptake sites by autoradiography or by homogenate binding. J Pharmacol Exp Ther 260:427–436.

Tiihonen J, Kuikka JT, Bergstrom KA, et al. (1997): Single-photon emission tomography imaging of monoamine transporters in impulsive violent behavior. Eur J Nucl Med 24:1253–1260.

Tissingh G, Bergmans P, Winogrodzka A, et al. (1997): Nigrostriatal dopaminergic imaging with iodine-123-beta CIT-FP/SPECT and fluorine-18-FDOPA/PET [letter] [see comments]. J Nucl Med 38:1271–1272.

Tzen KY, Lu CS, Yen TC, et al. (2001): Differential diagnosis of Parkinson's disease and vascular parkinsonism by ^{99m}Tc-TRODAT-1. J Nucl Med 42:408–413.

Van Dick CH, Seibyl JP, Malison RT, et al. (1995): Age-related decline in dopamine transporter binding in human striatum with [^{123}I]β-CIT SPECT. J Nucl Med 36:1175–1181.

Verhoeff NP (1999): Radiotracer imaging of dopaminergic transmission in neuropsychiatric disorders. Psychopharmacology 147:217–249.

Volkow ND, Ding YS, Fowler JS, et al. (1995a): A new PET ligand for the dopamine transporter: studies in the human brain. J Nucl Med 36:2162–2168.

Volkow ND, Fowler JS, Gatley SJ, et al. (1996): PET evaluation of the dopamine system of the human brain. J Nucl Med 37:1242–1253.

Volkow ND, Fowler JS, Logan J, et al. (1995b): Carbon-11-cocaine binding compared at subpharmacological and pharmacological doses: a PET study. J Nucl Med 36:1289–1297.

Volkow ND, Fowler JS, Wang GJ (1999): Imaging studies on the role of dopamine in cocaine reinforcement and addiction in humans. J Psychopharmacol 13:337–345.

Volkow ND, Wang G-J, Fowler JS, et al. (2001): Therapeutic doses of oral methylphenidate significantly increase extracellular dopamine in the human brain. J Neurosci 21: RC 121: 1–5.

Volkow ND, Wang GJ, Fischman MW, et al. (2000): Effects of route of administration on cocaine induced dopamine transporter blockade in the human brain. Life Sci 67:1507–1515.

Walovitch RC, Cheesman EH, Maheu LJ, et al. (1994): Studies of the retention mechanism of the

brain perfusion imaging agent [^{99m}Tc]-bicisate ([^{99m}Tc]-ECD). J Cereb Blood Flow Metab 1:S4–S11.

Wilbur DS (1992): Radiohalogenation of proteins: An overview of radionuclides, labeling methods, and reagents for conjugate labeling. Bioconj Chem 3:433–470.

Willeit M, Praschak-Rieder N, Neumeister A, et al. (2000): [^{123}I]-beta-CIT SPECT imaging shows reduced brain serotonin transporter availability in drug-free depressed patients with seasonal affective disorder. Biol Psychiatry 47:482–489.

Wilson AA, Ginovart N, Schmidt M, et al. (2000): Novel radiotracers for imaging the serotonin transporter by positron emission tomography: synthesis, radiosynthesis, and in vitro and ex vivo evaluation of (11)C-labeled 2-(phenylthio)araalkylamines. J Med Chem 43:3103–3110.

Wong DF, Yung B, Dannals RF, et al. (1993): In vivo imaging of baboon and human dopamine transporters by positron emission tomography using [^{11}C]WIN35,428. Synapse 15:130–142.

Wong EH, Sonders MS, Amara SG, et al. (2000): Reboxetine: a pharmacologically potent, selective, and specific norepinephrine reuptake inhibitor. Biol Psychiatry 47:818–829.

Yen T-C, Lu C-S, Tzen K-Y, et al. (2000): Decreased dopamine transporter binding in Machado–Joseph disease. J Nucl Med 41:994–998.

Zhuang ZP, Choi SR, Hou C, et al. (2000): A novel serotonin transporter ligand: (5-iodo-2-(2-dimethylaminomethylphenoxy)-benzyl alcohol (ODAM). Nucl Med Biol 27:169–175.

Zoghbi SS, Tamagnan G, Baldwin RM, et al. (1997): Synthesis of a dopamine transporter binding cyclopentadiene phenyltropane conjugate complexed with Re and Tc-99m. J Nucl Med 38:100P.

CHAPTER 16

MEASURING AND MODELING THE SPATIOTEMPORAL PROFILE OF GABA AT THE SYNAPSE

LINDA S. OVERSTREET, GARY L. WESTBROOK, AND MATHEW V. JONES

16.1 INTRODUCTION

By clearing neurotransmitter from the synaptic cleft, transmembrane transporters may influence the properties of synaptic signaling. For example, because neurotransmitter receptors desensitize in the prolonged presence of transmitter, one predicted role of transport is to ensure that the synaptic cleft concentration of transmitter is held at a low resting value between signaling events. Another prediction is that transporters may shorten the duration of the postsynaptic response by rapidly clearing transmitter from the cleft after the contents of each synaptic vesicle have been released. A third prediction is that transporters may ensure point-to-point transmission by preventing neurotransmitter molecules from spilling out of the synapse where they were released, so that they cannot mediate crosstalk between synapses.

Each of these predictions suggests avenues by which transporter function could be modulated pharmacologically to yield a clinical benefit. However, these avenues are not as uncluttered as one might hope. As an example, consider the antiepileptic drug tiagabine (Treiman, 2001), which is a competitive inhibitor of the synaptic gamma aminobutyric acid (GABA) transporter GAT1. Block of GAT1 by tiagabine could in theory reduce seizure occurrence by prolonging the exposure of postsynaptic receptors to GABA, thus prolonging inhibitory postsynaptic currents (IPSCs). In addition, blockade of GAT1 could increase the number of inhibitory synapses activated by promoting crosstalk between GABAergic synapses. In contrast to these beneficial effects are some predicted side effects. An elevation of ambient GABA concentration could desensitize postsynaptic $GABA_A$ receptors and activate presynaptic $GABA_B$ receptors, both of which would reduce synaptic inhibition and therefore increase seizure susceptibility. Without knowing the precise contribution of transport to each of the aforementioned processes, it is difficult to forecast whether the clinical action of transporter blockade will be dominated by the beneficial effects or the harmful side effects. In addition to transport, simple diffusion of neurotransmitter out of the cleft could also maintain a low resting concentration and curtail the postsynaptic response. Dilution of the cleft transmitter concentration into the much larger extrasynaptic volume may also be sufficient to prevent transmitter released at one synapse from reaching high enough concentrations at neighboring synapses to allow

Transmembrane Transporters. Edited by Michael Quick

ISBNs: 0-471-06517 (Hardcover); 0-471-43404-3 (Electronic)

crosstalk. Thus, to understand the forces governing the concentration, time course, and spread of transmitter, it is necessary to evaluate the relative contributions of transport and diffusion, rather than considering either process in isolation.

The first step in evaluating the relative contributions of diffusion and transport to regulation of the cleft transmitter concentration must of course be some set of assays for *measuring* the cleft concentration. Such assays must collectively be sensitive to very low and very high transmitter concentrations, and have a high temporal resolution. Standard tools for assaying neurotransmitter concentrations, such as microdialysis or amperometry are generally not suitable for measuring concentrations *within the synapse* because they rely on inserting probes into the tissue that are much larger than the synapse itself. Optical methods, for example to detect fluorescence changes in transmitter-sensitive dyes, could be extremely useful for these purposes but are not yet available with appropriate sensitivity for most applications. Fortunately, the synapses themselves are endowed with built-in detectors of cleft transmitter concentration and duration: the postsynaptic neurotransmitter receptor/ion channels.

This chapter provides an overview of electrophysiological methods for the measurement of transmitter concentration and time course in the synaptic cleft, and the use of such measurements to generate quantitative predictions about the role of transport in synaptic function. The chapter is divided into two halves. In the first half, we describe our own experimental strategies for measuring the ambient synaptic GABA concentration, and the size and duration of the concentration transient after release of single vesicles at inhibitory hippocampal synapses. The second half of the chapter is devoted to building a quantitative picture of events during synaptic transmission by integrating our measurements with other kinds of information, such as the diffusional parameters of GABA, the ultrastructure of the synapse and surroundings, the density of synapses within the tissue, and the kinetics of $GABA_A$ receptors and GABA transporters. This picture takes the form of a simple Monte Carlo simulation of synaptic transmission, constrained as much as possible by the experimental data of ourselves and others, which allows for predictions of the relative contributions of transport and diffusion to shaping synaptic responses and the possible nature of crosstalk between synapses.

16.2 EXPERIMENTAL MEASUREMENTS

Regulation of the Ambient Synaptic GABA Concentration

Probably, the simplest functional assay for the contribution of transport at inhibitory synapses is to observe the changes in transmission that occur when GABA transporters are blocked pharmacologically. Experiments such as this one have been conducted many times, most often by using synchronous stimulation of a large number of inhibitory fibers (Dingledine and Korn, 1985; Hablitz and Lebeda, 1985; Roepstorff and Lambert, 1992; Thompson and Gahwiler, 1992; Roepstorff and Lambert, 1994; Draguhn and Heinemann, 1996). Under these conditions, blocking GABA transporters dramatically prolongs the IPSC duration, and sometimes increases IPSC amplitude. The degree of prolongation depends on the number of fibers activated, hence on the amount of GABA released. However, although synchronous activation of many fibers is a hallmark of epileptiform activity, it may be rare under normal conditions. To assess the effects of GABA transporter blockade under more subtle stimulation, we evoked single-axon "autaptic" IPSCs in hippocam-

pal cultured neurons (Fig. 16.1A; see Overstreet et al., 2000, for details). In contrast to previous experiments using more intense stimuli, the GABA transporter inhibitors tiagabine or NO711 produced only occasional and modest prolongation of single-axon IPSCs. Instead, we observed a robust *reduction* in IPSC amplitude of up to 50% on transport blockade. This reduction was mimicked by application of low concentrations (0.5–5 μM) of GABA, suggesting that uptake blockade may have increased the ambient synaptic GABA concentration. However, neither the effects of uptake blockers nor of GABA itself were prevented by $GABA_B$ receptor antagonists, and therefore did not reduce synaptic release of GABA via activation of presynaptic $GABA_B$ autoreceptors (Fig. 16.1B). Further tests for a presynaptic effect, for example, changes in the paired-pulse ratio (Fig. 16.1C) or coefficient of variance, were also negative. Finally, miniature IPSCs (mIPSCs) arising from the release of individual synaptic vesicles were also reduced in amplitude by blockade of uptake in hippocampal slices (Fig. 16.1D). This latter experiment confirms a postsynaptic site of action and also suggests that the microenvironment of the synapse, including the role of GABA uptake, is similar between the slice and culture preparations. The uptake blockers had very little direct blocking effect on $GABA_A$ channel function (Overstreet et al., 2000), suggesting that the reduced IPSC amplitude occurred as a consequence of the intended blockade of GABA transport.

These observations can be explained if uptake blockade elevates extracellular GABA, which then desensitizes postsynaptic $GABA_A$ receptors. If this were the case, uptake blockade should mimic desensitization caused by directly applying GABA to $GABA_A$ receptors. Figure 16.2 illustrates the desensitization of $GABA_A$ receptors in response to low concentrations of GABA in excised outside-out patches. Even low GABA concentrations caused substantial desensitization (Fig. 16.2A, EC_{50} = ~2 μM), which recovered slowly after GABA was removed (Fig. 16.2B, time constant = ~10 s). The time course of recovery of IPSC amplitude after removal of the uptake blocker (Fig. 16.3A) closely paralleled the time course of recovery from desensitization after removal of GABA (Fig. 16.2B). These results strongly support the argument that the amplitude of the IPSC is regulated by $GABA_A$ receptor desensitization, which itself is a sensitive indicator of the ambient con-

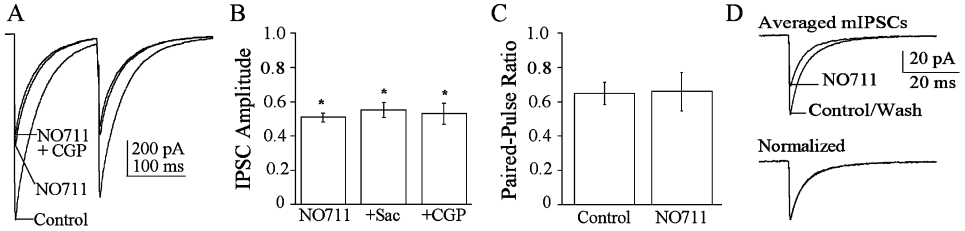

Figure 16.1. Reductions in IPSC and mIPSC amplitude caused by blocking GABA uptake. **A)** Autaptic IPSCs were evoked in cultured hippocampal neurons grown on glial microislands. Perfusion of the GABA transport inhibitor NO711 (100 μM) reduced IPSC amplitude, with minimal effects on IPSC duration, whether or not the $GABA_B$ receptor antagonist CGP55845 (1 μM) was present. **B)** The $GABA_B$ receptor antagonists CGP55845 (1 μM) and 2-hydroxysaclofen (200 μM) had no effect on IPSC amplitude reduction caused by NO711. **C)** NO711 did not alter the IPSC paired-pule ratio, a standard test for presynaptic effects. **D)** NO711 reduced miniature IPSC amplitude at synapses on granule cells in hippocampal slices, confirming a postsynaptic locus of action. mIPSC duration was not altered by blocking uptake. Adapted from Overstreet et al. (2000).

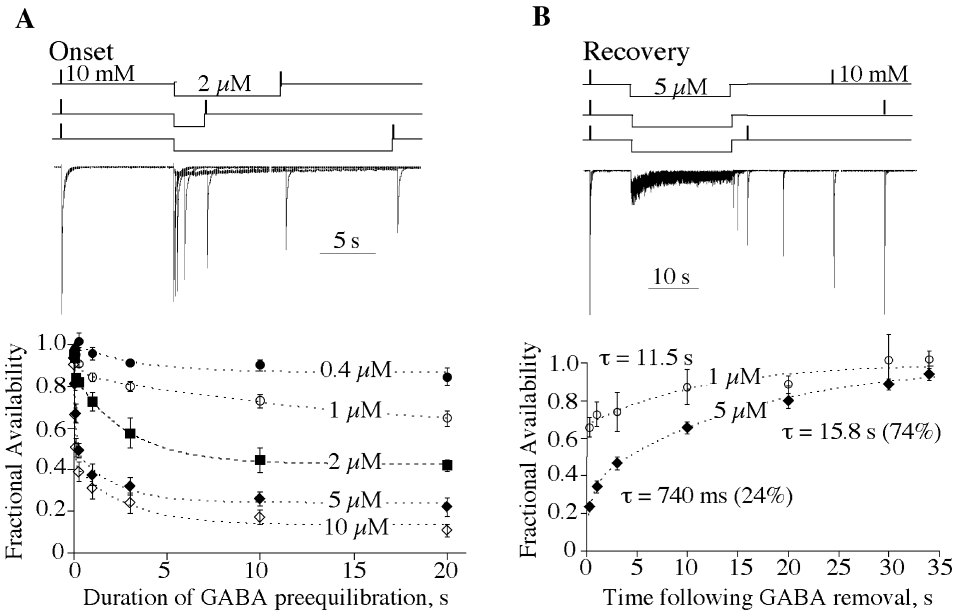

Figure 16.2. Dose-dependence and kinetics of $GABA_A$ channel desensitization. Channels were isolated by excising outside-out patches from cultured hippocampal neurons and were activated by rapidly exchanging the solutions bathing the patch pipette. **A)** *Top:* To examine the onset of desensitization, a brief test pulse of saturating GABA (10 mM) was followed by a conditioning pulse of low GABA concentration and variable duration. Immediately after the conditioning pulse, a second test pulse was used to assay the fraction of available receptors. *Bottom:* Concentrations as low as 0.4 μM induced desensitization, the rate and extent of which increased with increasing concentrations, with an EC_{50} of ~2 μM. **B)** *Top:* The recovery from desensitization was assessed by applying a test pulse of saturating GABA, followed by a low concentration conditioning pulse of fixed duration (20 s). After a varying wash interval, a second test pulse was given to assay the fraction of recovered receptors. *Bottom:* Recovery from desensitization was dominated by a slow component of ~10–15 s. See Overstreet et al. (2000) for details of the rapid solution exchange methods.

centration of GABA in the synapse. We estimated the maximum resting concentration of GABA in the synapse by comparing the reduction in IPSC amplitude caused by uptake blockers with the concentration dependence of desensitization (Fig. 16.3B). In the presence of uptake blockers, the synaptic cleft concentration rises to ~1 μM (Note that this is an upper limit; when uptake is intact, the resting cleft concentration must be much less than 1 μM, but an exact value cannot be assigned by using this method). This low concentration is near the EC_{50} for inducing desensitization of $GABA_A$ receptors, but is about ten times less than the EC_{50} for activating $GABA_A$ receptors (Fig. 16.3B). Thus, uptake blockade elevates ambient GABA but preferentially desensitizes synaptic $GABA_A$ receptors, resulting in a net reduction of charge carried by single-axon IPSCs rather than an increase. From the therapeutic point of view, this would appear to be an undesirable effect. During epileptiform activity, however, GABAergic interneurons fire synchronously at high rates (Velazquez and Carlen, 1999), and this synchrony may in fact perpetuate network oscillations (Cobb et al., 1995) and seizures (Schwartzkroin and Haglund, 1986). In

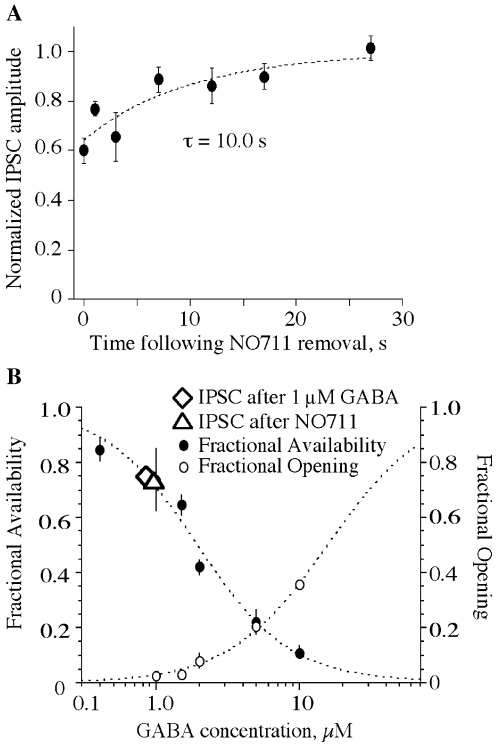

Figure 16.3. Uptake blockade reduces IPSC amplitude by elevating ambient GABA. **A)** Autaptic IPSCs were evoked before and at varying intervals after rapid perfusion of NO711 (100 μM). The NO711-induced reduction of IPSC amplitude recovers with a time course that matches the recovery of $GABA_A$ receptors from desensitization induced by GABA itself (see Fig. 16.2B), suggesting that uptake blockade induced desensitization of postsynaptic receptors by elevating the ambient synaptic GABA levels. **B)** A plot of steady-state desensitization versus GABA concentration (filled circles, data from Fig. 16.2A) allows interpolation of the ambient synaptic GABA concentration caused by NO711. The amplitude reduction in NO711 is similar to that caused by direct application of 1 μM GABA, a concentration that causes very little channel opening (open circles, data from Fig. 16.2A). Adapted from Overstreet et al. (2000).

such a situation, the effects of uptake blockade will be complex and may include a reduction in IPSC amplitude, such as we observed, coupled with the IPSC prolongations observed by others previously during high-intensity stimulation, as well as spillover of GABA that could increase the activation of $GABA_B$ receptors (Isaacson et al., 1993; Scanziani, 2000) and either activate or desensitize $GABA_A$ receptors. We explore the issue of spillover further in the section on modeling.

The Concentration Transient Following Vesicular Release

We now turn to the question of measuring the size and time course of changes in cleft concentration that activate $GABA_A$ receptors during IPSCs. This problem involves a rapidly changing concentration and therefore inherently requires kinetic reasoning and

methods. A strategy that has been used successfully at excitatory synapses in culture is to assay the ability of synaptically released glutamate to replace a rapidly unbinding competitive antagonist of the postsynaptic receptors (Clements et al., 1992). This method, and the related one that we will illustrate below, exploits the fact that receptors bathed in an antagonist solution are constantly undergoing rounds of antagonist binding, unbinding, and rebinding. When transmitter is released during this situation it may be able to compete with the antagonist for receptor binding sites. The degree of competition depends on a) the relative concentrations of transmitter and antagonist, and b) whether the duration of transmitter in the cleft is comparable with the antagonist unbinding time constant. By constructing dose-response curves for antagonism of synaptic current amplitude, and for equilibrium antagonism of the receptor, Clements et al. (1992) showed that NMDA receptor-mediated synaptic currents were blocked less than would be predicted if the antagonist were in equilibrium with the receptor. This result suggested that some antagonist unbinding had occurred before glutamate was cleared from the cleft, thus allowing additional channels to be activated. The cleft concentration and duration of glutamate were estimated from the observed mismatch between the two dose-response curves combined with quantitative knowledge of the rapid antagonist unbinding kinetics. The authors concluded that glutamate reached a peak cleft concentration of about 1 mM and decayed to low levels within about a millisecond. A second study, also in culture, obtained roughly similar estimates by using AMPA receptor-mediated EPSCs (Diamond and Jahr, 1997).

Although ingenious, this method of comparing equilibrium antagonism with that observed at the synapse requires complete antagonism curves to be constructed for both the isolated receptor response and for the synaptic response. Thus, it is suitable for experiments on cultured neurons where the concentration of antagonist can be changed rapidly many times during a recording, but is difficult to implement in brain slices because of the time required for full exchange of the bathing medium. In order to measure the synaptic concentration and time course of GABA in the hippocampal slice, we therefore used a slightly different strategy that focused on changes in both amplitude and shape of the IPSC caused by competitive antagonists, rather than solely in amplitude. Diamond and Jahr (1997) also used shape changes caused by antagonist to constrain their estimates of the synaptic glutamate transient in culture. The reasoning behind the modified method is as follows: If an antagonist unbinds rapidly, then some receptors will become free to bind GABA while it is still present in the cleft after the release of a vesicle. These receptors will open slightly later in time than they would have if the antagonist were not present, because their binding and activation has been delayed by the time required for the antagonist to unbind. The result will be a new, delayed component of the mIPSC rising phase. The size and shape of this component will depend on the concentration and kinetics of the antagonist and, importantly, also on the concentration and duration of GABA in the cleft. In order for the experiments to yield quantitative estimates of the cleft transmitter profile, the kinetics of antagonist binding and unbinding must be known. Additional precision can be obtained if a kinetic model of the postsynaptic receptor is available. The methods we used to obtain these prerequisite measurements of antagonist and $GABA_A$ receptor kinetics are beyond the scope of this chapter, but these methods have been described thoroughly (Jones and Westbrook, 1995; Jones et al., 1998; Jones et al., 2001).

Figure 16.4 shows the basic experimental results that allow for an estimate of the synaptic GABA transient in hippocampal slices. Miniature IPSCs were recorded in the absence and presence of two structurally similar competitive antagonists: SR95531 has a high affinity and a slow unbinding time constant (τ_u = ~100 ms; labeled “Slow-off” in the

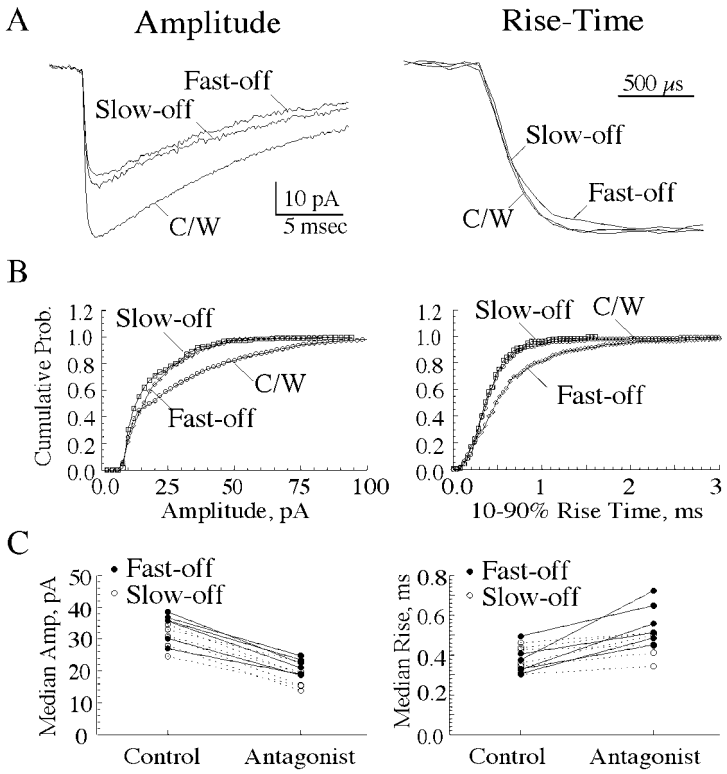

Figure 16.4. A rapidly unbinding competitive antagonist slows the mIPSC rising phase. Miniature IPSCs were recorded in the presence and absence of slowly unbinding (slow-off 130 nm) and rapidly unbinding (fast-off 3μm) antagonists. Concentrations of the two antagonists were matched to give similar reductions in mIPSC amplitude (left panels). Control mIPSCs and mIPSCs after antagonist washout were averaged (C/W) and their measured parameters were pooled to compensate for any drifts during the long recordings. **A)** Only the fast-off antagonist slowed the mIPSC rising phase (right panel, traces normalized for comparison), suggesting that it was partially replaced at the receptors by GABA still present in the cleft for a portion of the mIPSC rising phase. **B)** Cumulative amplitude (left) and rise-time (right) distributions for the mIPSCs used to create the averages in (**A**). The slowing of mIPSC rising phase by the fast-off antagonist was highly significant (Mann–Whitney U test). **C)** Aggregate data for five recordings in which both the slow-off and fast-off antagonists were applied to the same neuron with intervening washes. No significant slowing of mIPSC rise time was observed for the slow-off antagonist, whereas the fast-off significantly slowed the rise time in every recording.

figure); SR-95103 has a low affinity and fast unbinding constant (τ_u = ~2 ms; labeled "Fast-off"). Concentrations of the two antagonists were chosen to give a similar block of mIPSC amplitude (Fig. 16.4, left panels). This is an important control to ensure that any shape changes caused by the fast-off antagonist were not merely detection or measurement artifacts caused by reducing mIPSC amplitude. In contrast to the similar amplitude reductions, only the fast-off antagonist slowed the rising phase of mIPSCs (Fig. 16.4, right panels). This effect is barely detectable when viewed in the average mIPSC waveforms (Fig. 16.4A, right) but is obvious in the cumulative rise-time distribution (Fig.

16.4B, right) and was highly significant over the population of neurons examined (Fig. 16.4C, right). Therefore, release of individual vesicles results in a GABA pulse in the cleft that lasts long enough to compete slightly with the fast-off antagonist during the rising phase of the mIPSC but not with the slow-off antagonist. The fact that the slowing of the median mIPSC rise time (from ~400 to 500 μs) is much less than the fast-off antagonist unbinding time constant suggests that cleft GABA declines to low levels in much less than 2 ms.

To obtain precise estimates of the concentration and duration of GABA in the cleft, we compared our measured mIPSCs with simulated mIPSCs generated with a kinetic model of $GABA_A$ receptors (Fig. 16.5 and Table 16.1; Jones and Westbrook, 1995; Jones et al., 1998; Jones et al., 2001) driven by a variety of hypothetical synaptic GABA concentration transients. Figure 16.6A illustrates fits of model simulations to the recorded mIPSC traces, in the absence and presence of the fast-off antagonist. All kinetic rates in the model were held fixed, and only the peak concentration and decay time constant of the simulated synaptic GABA concentration pulse were allowed to vary. An immediate conclusion from these comparisons is that peak concentrations of GABA at the synapse would need to be in the millimolar range in order to produce mIPSC rising phases as fast as those we observed in experiments. However, if the peak GABA concentration is high and lasts for longer than a millisecond, then the simulated mIPSC decay phase becomes pro-

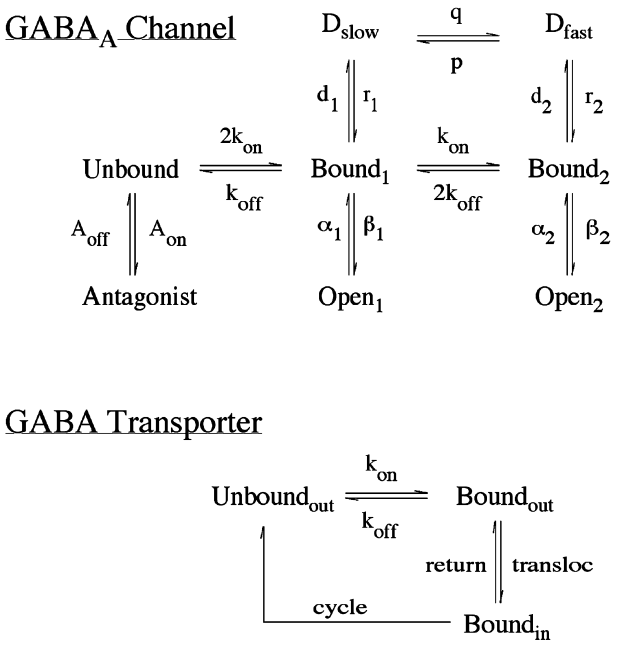

Figure 16.5. Kinetic Models of $GABA_A$ receptor and GABA transporter. The $GABA_A$ channel model was developed from a number of different kinetic experiments by using rapid solution exchange methods in outside-out patches from neurons in culture and slice (Jones and Westbrook, 1995; Jones et al., 1998; Jones et al., 2001). The transporter model is a highly simplified "best guess" that approximates the published macroscopic affinity and turnover rate of GAT1 expressed in *Xenopus* oocytes (Mager et al., 1993). Rate constants for both models are given in Table 16.1.

Table 16.1. Rate constants for $GABA_A$ receptor and GABA transporter models shown in Figure 16.5

$GABA_A$ Receptor					
k_{on}	5×10^6	$M^{-1}s^{-1}$	d_2	1250	s^{-1}
k_{off}	160	s^{-1}	r_2	25	s^{-1}
α_1	1100	s^{-1}	p	2	s^{-1}
β_1	200	s^{-1}	q	10^{-2}	$M^{-1}s^{-1}$
α_2	142	s^{-1}	A_{on}	3.8×10^7	$M^{-1}s^{-1}$
β_2	2500	s^{-1}	A_{off}	370	s^{-1}
d_1	13	s^{-1}			
r_1	0.2	s^{-1}			
GABA Transporter					
$k_{on} = 5 \times 10^6$ $M^{-1}s^{-1}$					
$k_{off} = 20$ s^{-1}					
transloc = 20 s^{-1}					
return = 0 s^{-1}					
cycle = 10^6 s^{-1}					

longed in the presence of the fast-off antagonist. This occurs because of the prolonged opportunity for rebinding of GABA after antagonist unbinding. Because this effect is not observed in the experimental data, a second conclusion is that the synaptic GABA concentration pulse must be briefer than a millisecond. The most likely parameters of the synaptic GABA transient can be visualized by plotting the error between the experimentally recorded and simulated mIPSCs versus the peak concentrations and durations used to drive the simulations (Fig. 16.6B). This error surface displays a distinct and deep global minimum (i.e., best fit) when the synaptic GABA pulse peaks at 3–5 mM but decays within 300–600 μs.

The estimate obtained here is directly at odds with a previous conclusion that the synaptic GABA transient remains near the foot of the $GABA_A$ receptor concentration-response curve (i.e., below about 10 μM), based on analysis of the covariation of mIPSC amplitudes generated by the release of single vesicles but sensed simultaneously by two cells (Frerking et al., 1995). The observations of that study, however, might be explained by covariation in the number of receptors present at the two postsynaptic sites, rather than the variations in cleft concentrations that the authors concluded. Our peak concentration estimate is also ten times higher than the estimate of ~300 μM obtained by comparison of the potentiation by zolpidem of mIPSCs and currents in outside-out patches activated by 1 ms GABA pulses (Perrais and Ropert, 1999). However, these two estimates are compatible if one considers that the total exposure to GABA is the same for a 1 ms pulse of 300 μM and a 300 μs pulse of 1 mM. Our estimates are essentially identical to those for the glutamate transient at cultured synapses obtained by using related methods (Clements et al., 1992; Diamond and Jahr, 1997) and to an estimate of the GABA transient at cultured synapses based on modeling the changes in mIPSC amplitude and rise time caused by chlorpromazine (Mozrzymas et al., 1999). From these agreements it is reasonable to conclude that the factors controlling clearance of transmitter in culture are quite similar to those in the more intact slice. Unfortunately, we were prevented from directly measuring the effects of GABA uptake on the peak and duration of the synaptic GABA transient be-

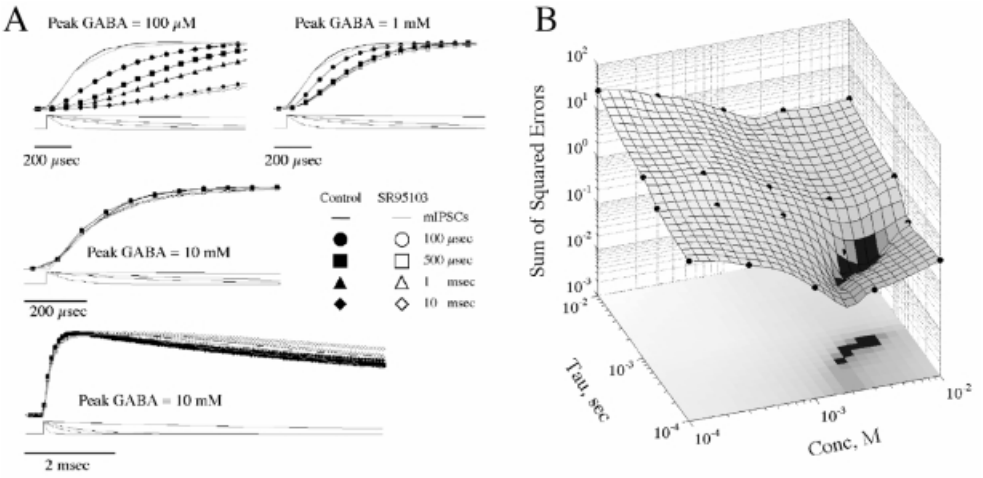

Figure 16.6. Quantitative estimation of the concentration profile of GABA at the synapse. **A)** Experimentally recorded mIPSCs (thick lines) in control (black) and in the presence of the rapidly unbinding antagonist SR-95103 (grey) were compared with simulations from a model of $GABA_A$ receptor kinetics (symbols, see Fig. 16.5). Traces have been normalized to their peak values for comparison of their shapes. All model parameters were fixed to the values in Table 16.1, except for the peak concentration and decay time constant of the synaptic GABA pulse (thin lines below each set of data and simulated traces), which were systematically varied. A peak concentration of GABA above 1 mM was necessary to reproduce the rise time of the mIPSC. However, such a concentration prolongs the simulated mIPSC decay in the presence of antagonist (open triangles and diamonds) unless the pulse decays in less than 1 ms (open circles and squares). **B)** A plot of the sum of squared errors between the simulations and the data versus the peak concentration and decay time constant of the GABA pulse reveals a deep minimum (i.e., best fit) at a peak concentration of 3–5 mM with a decay of 300–600 μs (dark areas). These are thus the most probable parameters of the synaptic GABA pulse that gave rise to the experimentally observed mIPSC properties.

cause the uptake blockers NO711 and tiagabine both have small direct actions at $GABA_A$ receptors (Overstreet et al., 2000), which resemble the action of a weak competitive antagonist and slow the rise times of mIPSCs so that further slowing by the fast-off antagonist becomes uninterpretable. We therefore attempted to predict the relative contributions of uptake and diffusion by using numerous experimental observations by ourselves and others to frame a quantitative model of the movement of GABA molecules in the vicinity of the synapse, as described below.

16.3 MONTE CARLO MODELING OF DIFFUSION AND UPTAKE

Quantitative modeling can provide insight into those behaviors of a system that are not easily accessible to direct experimental measurement. Modeling is also fraught with hazards that can be minimized only by using as much experimental data as possible to constrain model parameters to realistic values. The most common models of chemical processes, including ion channel and transporter function, rely on solving differential equations that describe how the system changes with time or space. Such solutions can be

obtained either by deriving an exact analytical equation for the solution or by numerical approximation (Gershenfeld, 1999). In both cases, the differential equations governing the system must be written down before anything else can be done, which means that absolutely everything included in the model simulation must be describable by relatively simple equations. There are two situations in which modeling with differential equations may not be the best choice. First, the requirement that everything be expressed in equations forces simplifying assumptions that might limit the complexity of the systems that can be modeled. For example, complex geometries are difficult to express with equations. Second, differential equations are smooth, continuous, and deterministic, whereas many processes of interest are inherently discrete and random. For example, the entry and exit of a *single* molecule in the cleft cannot be described by differential equations. Differential equations represent the *average* behavior over an infinitely large ensemble of trials.

An alternative approach is to explicitly simulate the random motions of individual molecules and the random state changes of individual receptors and transporters. This method of simulating randomness is referred to as Monte Carlo modeling (after the city famous for gambling). Monte Carlo modeling does not require that the system be describable in simple equations. Complex geometries can easily be simulated by simply listing the locations of all the surfaces. Similarly, reaction mechanisms are defined as lists of reaction states (e.g., unbound, bound, open, desensitized) along with the probabilities of making transitions between them. The motion of each transmitter molecule is tracked by listing its spatial coordinates, then iteratively moving it by a randomly chosen distance in a randomly chosen direction. At each step of the iteration, the new location is checked against the locations of spatial barriers (e.g., membrane surfaces) and effector molecules (e.g., receptors and transporters). If the transmitter encounters an effector, then a sequence of random state changes proceeds according to the listed reaction steps and transition probabilities. Therefore, the discrete motions and state changes of all the individual molecules and effectors are obtained directly, including the natural fluctuations that would actually exist in the system being modeled. We used the Monte Carlo simulation program MCell to model the diffusion and uptake of GABA in the vicinity of synapses in dentate gyrus. A thorough description of MCell, including a theoretical discussion of Monte Carlo methods, practical issues, and examples, is provided in Stiles and Bartol (2001).

A number of parameters must be included in such a model, including: 1) tissue geometry; 2) the spatial distributions and kinetics of $GABA_A$ receptors and transporters; and 3) the diffusion coefficient of GABA molecules in the extracellular space. We used a simplified tissue geometry based on published anatomical studies of inhibitory synapses in dentate gyrus. Halasy and Somogyi (1993) measured the mean length of inhibitory synapses as 200–300 nm, which yields a diameter of ~320 nm when corrected by assuming that the orientation and depth of synapses relative to the plane of tissue section were distributed uniformly and that synapses are circular disks. For simplicity, we modeled the tissue as $320 \times 320 \times 320$ nm cubes representing cell membranes that are impermeable to GABA and separated by 15 nm spaces. Simplifying the tissue in this way could potentially introduce a systematic bias. In differential equation modeling, the extracellular space is often treated as a porous medium characterized by two parameters: volume fraction (α, the fraction of tissue volume occupied by the extracellular space) and tortuosity (γ, the square root of the ratio of the diffusion coefficient in the tissue, D*, to that in free solution, D, also equal to the ratio of the increased path length caused by obstacles to that of the free path length) (Barbour and Hausser, 1997; Nicholson and Sykova, 1998). Our cubic space

yields a volume fraction of 0.12, very similar to the estimate of 0.117 from analysis of electron micrographs of excitatory synapses by Rusakov and Kullmann (1998). Further, it yields a tortuosity of ~1.6, within the range measured in brain tissue (Nicholson and Sykova, 1998) and close to the value of 1.34 estimated from electron micrographs (Rusakov and Kullmann, 1998). Thus, our simplification introduces little more bias than the classical assumption of a porous medium. A few intercube spaces were designated as synaptic clefts and were populated postsynaptically with ~50 $GABA_A$ receptors, with kinetics as shown in Figure 16.5 and Table 16.1. Every face of every cube in the simulation contained ~50 GABA transporters that operated as shown in Figure 16.5 and Table 16.1. These parameters yield equilibrium kinetics of EC_{50} = 5 μM and V_{max} = 20 s^{-1}, near the values reported for the GAT1 transporter by Mager et al. (1993). In the model, half of the GABA molecules that bind are transported and half unbind without being transported. We released 1000–5000 molecules of GABA from an instantaneous point source at the center of one synaptic cleft. The diffusion coefficient of GABA (D) determines how far molecules move on each iteration, which would have a value of about 7×10^{-6} cm^2s^{-1} in a free solution (Jones et al., 2001). However, the *effective* diffusion coefficient (D^*) in the extracellular space depends on a variety of factors, including the viscosity of extracellular fluid and microscopic obstacles such as extracellular matrix proteins. The value of D* in the synapse has not been measured. We therefore used a range of plausible D* values ranging from 0.03 to 1.0×10^{-6} cm^2s^{-1}. Neighboring synapses were located 400–1500 nm from the release site, a range that includes the likely nearest neighbor distances between synapses. Halasy & Somogyi (1993) measured the density of GABA positive symmetric synapses in the granule cell layer as 120×10^6 mm^{-3}, yielding 1 synapse per 0.73 μm^3 and a mean spacing of 1.2 μm, assuming spherically symmetric and uniform spacing. More realistic estimates, based on Poisson spacing for example, would yield even closer nearest neighbor distances (Rusakov and Kullmann, 1998).

Figure 16.7A illustrates the simulated release of a single vesicle containing 5000 molecules of GABA at a synapse surrounded by tissue containing GABA transporters. Two neighboring synapses are also shown, at distances of about 0.5 and 1 μm from the release site. The diffusion coefficient of GABA was 0.3×10^{-6} cm^2s^{-1}, which is the value that best reproduced our experimental measurements of the synaptic GABA transient. Under these conditions, GABA molecules began to leave the cleft within 100 μs and, by 1 ms, were mostly distributed extrasynaptically. Indeed, within 1 ms some GABA molecules had already reached a neighboring synapse and had bound to receptors there, despite the presence of GABA transporters in the intervening space. After 25 ms, GABA was widely distributed at low concentrations (100 nM – 30 μM) over a volume of a few μm^3 that is likely to contain neighboring inhibitory synapses. Removing the transporters from the tissue entirely had essentially no effect on the speed of clearance of GABA from the releasing synapse (Fig. 16.7B) or on the simulated mIPSC, consistent with the data shown in Figure 16.1D. This is because there are 50 times more GABA molecules than transporters within the cleft itself. In contrast, it has been proposed that the time course of glutamate clearance from the cleft is sensitive to transport blockade (Diamond and Jahr, 1997), which would require an extremely high density of transporters immediately surrounding glutamatergic synapses, many times more than there are glutamate receptors in the cleft. The GABA transporter GAT1 is closely associated with GABAergic synapses (Minelli et al., 1995; Conti et al., 1998), with a surface density recently estimated at 1000–5000 μm^{-2} in the molecular layer of cerebellum (Chiu et al., 2001a and b). The surface density in dentate gyrus has not yet been measured. Our model makes the conservative assumption

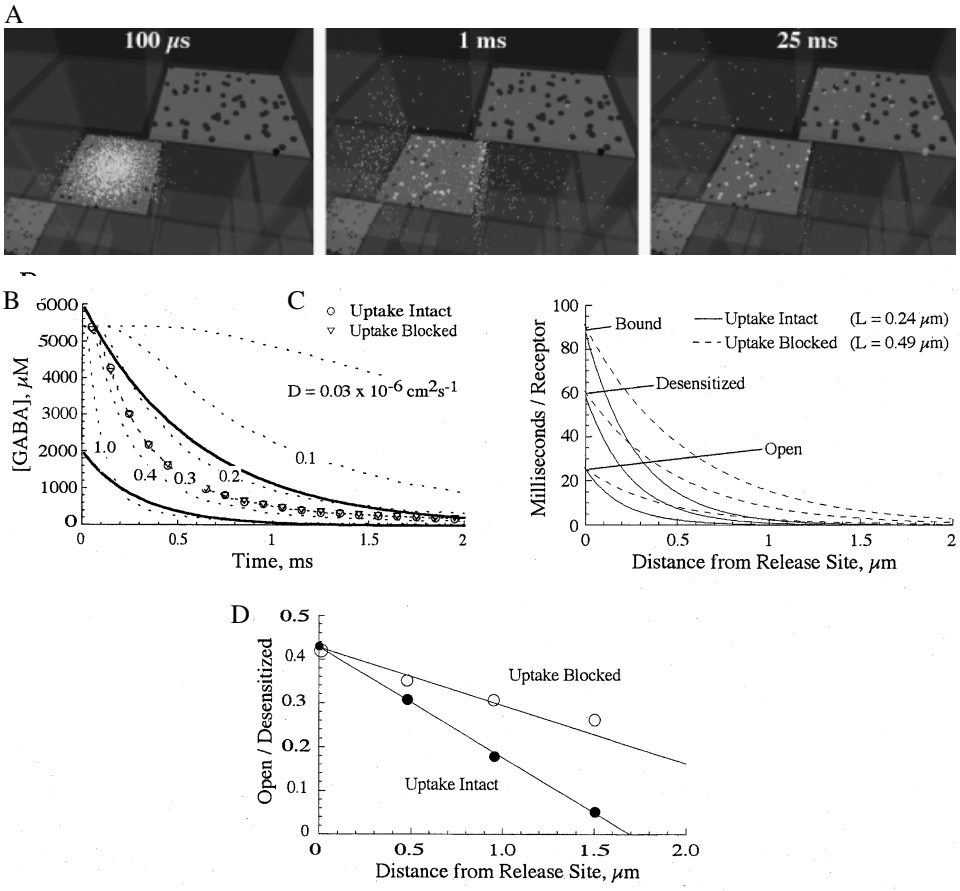

Figure 16.7. Monte Carlo simulations of GABA diffusion and uptake in dentate gyrus. **A)** The simulated tissue consisted of GABA-impermeable cubes 320 nm in length, representing cell membranes (gray). The extracellular space exists *between* the cubes and was 15 nm wide. A few intercube spaces were designated as "synapses" (postsynaptic faces in red) and were populated with $GABA_A$ receptors (black and colored objects on the red background) at a density of ~50 per face, whereas all faces of all cubes contained GABA transporters at the same density (not shown for clarity). Receptors and transporters operated according to Figure 16.5 and Table 16.1. Channel states are color-coded as follows: black = Unbound, grey = $Bound_1$, white = $Bound_2$, orange = $Open_1$, yellow = $Open_2$, blue = D_{fast}, purple = D_{slow}. A mass of 5000 GABA molecules (green) were released instantaneously at the center of the middle synapse and moved randomly with $D^* = 0.3 \times 10^{-6}$ cm^2s^{-1}. The iteration time step was 10 μs. The time after GABA release is shown at the top of each panel. GABA has started to leave the releasing synapse within 100 μs and has been largely cleared by 1 ms. In addition, starting at about 1 ms, GABA molecules have reached the neighboring synapse 0.5 μm away (upper synapse) and have begun to bind to the receptors there. (See color insert.) **B)** Simulations with different values for D* (dashed lines) give a cleft transmitter time course that falls within the experimentally measured limits (thick solid lines) only when D* is near 0.3×10^{-6} cm^2s^{-1}. With this value, the cleft GABA time course is not altered by blocking uptake. **C)** The average time that receptors spend in bound, desensitized, or open states declines with distance, defining the space constant (L) for crosstalk. Blocking uptake doubles this space constant. **D)** The ratio of time that receptors spend open to time spent desensitized also declines with distance. Receptors distant to the release site are thus increasingly likely to desensitize than to open. Blocking uptake reduces the steepness of this relation and allows a larger fraction of distant receptors to open.

that there are enough transporters in the tissue surrounding the synapse to adequately clear GABA, but it assigns them the simplest (i.e., uniform) spatial distribution.

Figure 16.7B also shows the time course of cleft clearance in simulations by using a range of different values of D*. Superimposed for comparison are the outer boundaries of our experimentally measured synaptic GABA concentration time course. Only certain values of D* produce a simulated time course that falls within the experimentally determined range, suggesting that D* is approximately 0.3×10^{-6} cm^2s^{-1}. This value is about 20 times slower than in free solution, which suggests that the extracellular space is highly viscous or highly tortuous. Either of these possibilities is quite plausible given the abundance of extracellular matrix proteins and glycosylated side chains of membrane proteins, which probably occupy a significant fraction of extracellular volume.

Although we modeled an instantaneous delivery of GABA, passive emptying of the vesicle through a fusion pore is relatively fast (Stiles et al., 1996) and is unlikely to account for the slow effective diffusion coefficient. The value of D* has important implications because it controls not only the duration of transmitter in the cleft but also the likelihood of crosstalk between synapses. Rusakov and Kullmann (1998) simulated crosstalk under a range of D* values (all of which were faster than our present estimate) and concluded that crosstalk at NMDA receptor-mediated synapses would only be effective if D* were quite slow. Our model reveals a similar prediction, but with some interesting twists related to the specific kinetics of $GABA_A$ receptors and GABA transporters. Figure 16.7C shows the effects of GABA spillover on the $GABA_A$ receptors at various distances from the releasing synapse, with uptake intact and blocked. The average time spent by receptors in the bound, open, and desensitized states falls off with a space constant (L) of 0.24 μm when uptake is active, yielding a low and slowly rising wavefront of GABA at distant receptors. When uptake is blocked, this space constant doubles to 0.49 μm, which allows GABA to reach distant receptors more easily. Note that channels at all distances spend more time desensitized than open because desensitized states are longer and partially absorbing (Jones and Westbrook, 1995; Overstreet et al., 2000). Figure 16.7D shows that the ratio of time spent in open versus desensitized states also falls off with distance. This is because a low and slowly rising GABA exposure is a better stimulus for desensitization than it is for channel opening (see Fig. 16.3B). Therefore, in these simulations, GABA crosstalk is more likely to desensitize the neighboring receptors than to open them. Blocking uptake alleviates this bias by allowing GABA to spread more rapidly and widely in a shorter time, resulting in a higher and faster wavefront at the nearby receptors, and in less cross-desensitization

16.4 CONCLUSION

We have illustrated one experimental program for understanding some of the factors that control the fate of GABA molecules released into the synaptic cleft. Our measurements indicate that ambient GABA levels are well below 1 μM, whereas release of a GABA-containing vesicle causes a spike of GABA concentration into the millimolar range that decays to low levels in a few hundred microseconds. Comparisons of experimental data with Monte Carlo simulations of the perisynaptic space suggest that diffusion is the rate-limiting step in clearing GABA from the cleft, but nonetheless occurs much slower than in free solution. Uptake does not shorten the synaptic GABA transient, but contributes significantly to limiting the spread of GABA away from its release site. Despite this con-

tribution, GABA molecules may still reach neighboring synapses within a micron or so of their release site. At neighboring synapses, few receptors will bind GABA, but those that do will be more likely to desensitize than to open. A surprising prediction therefore is that crosstalk between GABAergic synapses may occur even in the presence of uptake, but will reduce rather than increase signaling at neighboring sites. Therefore, GABA uptake blockers may increase net inhibition not by prolonging the duration of GABA in the cleft after a vesicle is released, but by allowing GABA to spread itself more readily through the tissue.

As always, model-dependent results must be interpreted with cautious consideration of the assumptions that were made. In particular, the channel kinetics we used were based on those observed in outside-out patches, whereas mIPSCs have faster deactivation (Banks and Pearce, 2000) and may differ with respect to desensitization (Mellor and Randall, 2001), although it is clear that synaptic $GABA_A$ receptors do undergo profound desensitization (Overstreet et al., 2000; Mellor and Randall, 2001), including visits to closed states that resemble D_{fast} in our models (Brickley et al., 1999). A better model for the kinetics of the postsynaptic receptors would probably alter our predictions somewhat, although whether the general picture would be changed is not clear. Unfortunately, little experimental data is available that directly reveals the microscopic kinetics of receptors at the synapse. Estimates of microscopic transporter kinetics, especially for the GABA binding/unbinding steps, are also subject to considerable refinement. Nonetheless, models such as those we have illustrated make definite testable predictions and are valuable aids to developing intuition about the complex interactions of geometry, diffusion, and the kinetics of receptors and transporters that shape synaptic transmission.

ANNOTATED REFERENCES

Banks MI, Pearce RA (2000): Kinetic differences between synaptic and extrasynaptic $GABA_A$ receptors in CA1 pyramidal cells. J Neurosci 20:937–948.

Barbour B, Hausser M (1997): Intersynaptic diffusion of neurotransmitter. Trends Neurosci 20:377–384.

Brickley SG, Cull-Candy SG, Farrant M (1999): Single-channel properties of synaptic and extrasynaptic $GABA_A$ receptors suggest differential targeting of receptor subtypes. J Neurosci 19:2960–2973.

Chiu C-S, Kartalov E, Unger M, Quake S, Lester HA (2001a): Single-molecule measurements calibrate green fluorescent protein surface densities on transparent beads for use with 'knock-in' animals and other expression systems. J Neurosci Methods 105:55–63.

Chiu C-S, Labarca C, Deshpande P, Barghshoon S, Davidson N, Quake S, Lester HA (2001b): Knock-in mice carrying GABA transporter (MGAT1)-GFP fusion protein: Method for absolute MGAT1 quantification. Soc Neurosci Abstr 916.3.

Methods for calibration and quantitative measurement of the microscopic distribution of membrane proteins such as transporters. Methods such as these will become invaluable in constraining spatiotemporal models, and also provide for direct visualization of transporter localization in living brain slices.

Clements JD, Lester RA, Tong G, Jahr CE, Westbrook GL (1992): The time course of glutamate in the synaptic cleft. Science 258:1498–1501.

This paper introduced the use of antagonists as probes for the spatiotemporal profile of transmitter at the synapse.

Cobb SR, Buhl EH, Halasy K, Paulsen O, Somogyi P (1995): Synchronization of neuronal activity in hippocampus by individual GABAergic interneurons. Nature (London) 378:75–78.

Conti F, Melone M, De Biasi S, Minelli A, Brecha NC, Ducati A (1998): Neuronal and glial localization of GAT-1, a high-affinity gamma-aminobutyric acid plasma membrane transporter, in human cerebral cortex: with a note on its distribution in monkey cortex. J Comp Neurol 396:51–63.

Diamond JS, Jahr CE (1997): Transporters buffer synaptically released glutamate on a submillisecond time scale. J Neurosci 17:4672–4687.

Dingledine R, Korn SJ (1985): Gamma-aminobutyric acid uptake and the termination of inhibitory synaptic potentials in the rat hippocampal slice. J Physiol 366:387–409.

Draguhn A, Heinemann U (1996): Different mechanisms regulate IPSC kinetics in early postnatal and juvenile hippocampal granule cells. J Neurophysiol 76:3983–3993.

Frerking M, Borges S, Wilson M (1995): Variation in GABA mini amplitude is the consequence of variation in transmitter concentration. Neuron 15:885–895.

Gershenfeld N (1999): The Nature of Mathematical Modeling. Cambridge, UK: Cambridge University Press.

Hablitz JJ, Lebeda FJ (1985): Role of uptake in gamma-aminobutyric acid (GABA)-mediated responses in guinea pig hippocampal neurons. Cell Mol Neurobiol 5:353–371.

Halasy K, Somogyi P (1993): Distribution of GABAergic synapses and their targets in the dentate gyrus of rat: a quantitative immunoelectron microscopic analysis. J Hirnforsch 34:299–308.

Isaacson JS, Solis JM, Nicoll RA (1993): Local and diffuse synaptic actions of GABA in the hippocampus. Neuron 10:165–175.

A clear experimental demonstration of GABA spillover and crosstalk. In these studies, GABA is shown to spill over onto *excitatory* synapses, where it down-regulates glutamate release via $GABA_B$ receptor activation.

Jones MV, Westbrook GL (1995): Desensitized states prolong $GABA_A$ channel responses to brief agonist pulses. Neuron 15:181–191.

Jones MV, Sahara Y, Dzubay JA, Westbrook GL (1998): Defining affinity with the $GABA_A$ receptor. J Neurosci 18:8590–8604.

Jones MV, Jonas P, Sahara Y, Westbrook GL (2001): Microscopic kinetics and energetics distinguish $GABA_A$ receptor agonists from antagonists. Biophys J 81:2660–2670.

Experimental studies of nonstationary $GABA_A$ channel kinetics by using rapid solution exchange methods and the development of a kinetic model of $GABA_A$ receptor function.

Mager S, Naeve J, Quick M, Labarca C, Davidson N, Lester HA (1993): Steady states, charge movements, and rates for a cloned GABA transporter expressed in *Xenopus* oocytes. Neuron 10:177–188.

Mellor JR, Randall AD (2001): Synaptically released neurotransmitter fails to desensitize postsynaptic $GABA_A$ receptors in cerebellar cultures. J Neurophysiol 85:1847–1857.

Minelli A, Brecha NC, Karschin C, DeBiasi S, Conti F (1995): GAT-1, a high-affinity GABA plasma membrane transporter, is localized to neurons and astroglia in the cerebral cortex. J Neurosci 15:7734–7746.

Mozrzymas JW, Barberis A, Michalak K, Cherubini E (1999): Chlorpromazine inhibits miniature GABAergic currents by reducing the binding and by increasing the unbinding rate of $GABA_A$ receptors. J Neurosci 19:2474–2488.

Nicholson C, Sykova E (1998): Extracellular space structure revealed by diffusion analysis. Trends Neurosci 21:207–215.

Overstreet LS, Jones MV, Westbrook GL (2000): Slow desensitization regulates the availability of synaptic $GABA_A$ receptors. J Neurosci 20:7914–7921.

Perrais D, Ropert N (1999): Effect of zolpidem on miniature IPSCs and occupancy of postsynaptic $GABA_A$ receptors in central synapses. J Neurosci 19:578–588.

Roepstorff A, Lambert JD (1992): Comparison of the effect of the GABA uptake blockers, tiagabine and nipecotic acid, on inhibitory synaptic efficacy in hippocampal CA1 neurones. Neurosci Lett 146:131–134.

Roepstorff A, Lambert JD (1994): Factors contributing to the decay of the stimulus-evoked IPSC in rat hippocampal CA1 neurons. J Neurophysiol 72:2911–2926.

Rusakov DA, Kullmann DM (1998): Extrasynaptic glutamate diffusion in the hippocampus: ultrastructural constraints, uptake, and receptor activation. J Neurosci 18:3158–3170.

A thorough study of the microscopic geometry of tissue surrounding excitatory synapses, yielding estimates for volume fraction and tortuosity. Also includes a series of simulations to address the plausibility of crosstalk at excitatory synapses.

Scanziani M (2000): GABA spillover activates postsynaptic $GABA_B$ receptors to control rhythmic hippocampal activity. Neuron 25:673–681.

A demonstration of a possible physiological role for GABA spillover, with intriguing implications for information processing.

Schwartzkroin PA, Haglund MM (1986): Spontaneous rhythmic synchronous activity in epileptic human and normal monkey temporal lobe. Epilepsia 27:523–533.

Stiles JR, Bartol TM (2001): Monte Carlo methods for simulating realistic synaptic microphysiology using MCell. In DeSchutter E (ed): Computational Neuroscience. Realistic Modeling for Experimentalists. Boca Raton, FL: CRC Press LLC, pp 87–127.

Stiles JR, Van Helden D, Bartol TM, Jr., Salpeter EE, Salpeter MM (1996): Miniature endplate current rise times less than 100 microseconds from improved dual recordings can be modeled with passive acetylcholine diffusion from a synaptic vesicle. Proc Natl Acad Sci USA 93:5747–5752.

The paper is one of several in which the authors used Monte Carlo methods to simulate neuromuscular transmission. The book chapter is an invaluable and comprehensive resource for anyone interested in performing such simulations.

Thompson SM, Gahwiler BH (1992): Effects of the GABA uptake inhibitor tiagabine on inhibitory synaptic potentials in rat hippocampal slice cultures. J Neurophysiol 67:1698–1701.

Treiman DM (2001): GABAergic mechanisms in epilepsy. Epilepsia 42:8–12.

Velazquez JL, Carlen PL (1999): Synchronization of GABAergic interneuronal networks during seizure-like activity in the rat horizontal hippocampal slice. Eur J Neurosci 11:4110–4118.

INDEX

Transmembrane Transporters. Edited by Michael Quick

ISBNs: 0-471-06517 (Hardcover); 0-471-43404-3 (Electronic)